ESCOLA DE DOUTORAMENTO
INTERNACIONAL DA USC

Marta
Vizoso González

Tese de doutoramento

New molecular mechanisms and novel biomarkers associated with Extracellular Vesicles in Polycystic Kidney Disease: from preclinical models to patients

Santiago de Compostela, 2022

Programa de Doutoramento en Investigación e Desenvolvemento de Medicamentos

TESIS DE DOCTORADO

NEW MOLECULAR MECHANISMS AND NOVEL BIOMARKERS ASSOCIATED WITH EXTRACELLULAR VESICLES IN POLYCYSTIC KIDNEY DISEASE: FROM PRECLINICAL MODELS TO PATIENTS

Marta Vizoso González

ESCUELA DE DOCTORADO INTERNACIONAL DE LA UNIVERSIDAD DE SANTIAGO DE COMPOSTELA

PROGRAMA DE DOCTORADO EN INVESTIGACIÓN Y DESARROLLO DE MEDICAMENTOS

SANTIAGO DE COMPOSTELA / LUGO

2022

USC
UNIVERSIDADE
DE SANTIAGO
DE COMPOSTELA

AUTORIZACIÓN DEL AUTOR/A DE LA TESIS

D/Dña. **Marta Vizoso González**

Título de la tesis: **New molecular mechanisms and novel biomarkers associated with Extracellular Vesicles in Polycystic Kidney Disease: from preclinical models to patients**

Presento mi tesis, siguiendo el procedimiento adecuado al Reglamento y declaro que:

1) La tesis abarca los resultados de la elaboración de mi trabajo.
2) De ser el caso, en la tesis se hace referencia a las colaboraciones que tuvo este trabajo.
3) Confirmo que la tesis no incurre en ningún tipo de plagio de otros autores ni de trabajos presentados por mí para la obtención de otros títulos.
4) La tesis es la versión definitiva presentada para su defensa y coincide la versión impresa con la presentada en formato electrónico.

Y me comprometo a presentar el Compromiso Documental de Supervisión en el caso que el original no esté depositado en la Escuela.

En Santiago de Compostela. 18 de agosto de 2022.

Asdo. Marta Vizoso González

USC
UNIVERSIDADE
DE SANTIAGO
DE COMPOSTELA

DECLARACIÓN DEL A DIRECTOR/TUTOR DE LA TESIS

D/Dña. **Miguel Ángel García González**

En condición de: **Director/a**

Título de la tesis: **New molecular mechanisms and novel biomarkers associated with Extracellular Vesicles in Polycystic Kidney Disease: from preclinical models to patients**

INFORMA:

Que la presente tesis, se corresponde con el trabajo realizado por D/Dña **Marta Vizoso González**, bajo mi dirección/tutorización, y autorizo su presentación, considerando que reúne los resquisitos exigidos en el Reglamento de Estudios de Doctorado de la USC, y que como director/tutor de esta no incurre en las causas de abstención establecidas en la Ley 40/2015.

En Santiago de Compostela. 18 de agosto de 2022.

Asdo. Miguel Ángel García González

USC
UNIVERSIDADE
DE SANTIAGO
DE COMPOSTELA

DECLARACIÓN DEL DIRECTOR/TUTOR DE LA TESIS

D/Dña. **Alejandro Sánchez Barreiro**

En condición de: **Director y Tutor**

Título de la tesis: **New molecular mechanisms and novel biomarkers associated with Extracellular Vesicles in Polycystic Kidney Disease: from preclinical models to patients**

INFORMA:

Que la presente tesis, se corresponde con el trabajo realizado por D/Dña **Marta Vizoso González**, bajo mi dirección/tutorización, y autorizo su presentación, considerando que reúne los resquisitos exigidos en el Reglamento de Estudios de Doctorado de la USC, y que como director/tutor de esta no incurre en las causas de abstención establecidas en la Ley 40/2015.

En Santiago de Compostela. 18 de agosto de 2022.

Asdo. Alejandro Sánchez Barreiro

USC
UNIVERSIDADE
DE SANTIAGO
DE COMPOSTELA

Marta Vizoso González, autora de la presente tesis, declaro que no existe ningún conflicto de intereses.

Este trabajo ha sido financiado por una beca Predoctoral de la Xunta de Galicia del año 2017.

USC
UNIVERSIDADE
DE SANTIAGO
DE COMPOSTELA

USC
UNIVERSIDADE
DE SANTIAGO
DE COMPOSTELA

"*I don't have any particular recipe. It is the reason why doing research is challenging as well as attractive. It is like being lost in a jungle and trying to use all the knowledge that you can gather to come up with some new tricks, and with some luck, you might find a way out*."

MARYAM MIRZAKHANI, MATHEMATICIAN

USC
UNIVERSIDADE
DE SANTIAGO
DE COMPOSTELA

USC
UNIVERSIDADE
DE SANTIAGO
DE COMPOSTELA

A mis padres, porque sin vosotros no hubiese llegado hasta aquí.

USC
UNIVERSIDADE
DE SANTIAGO
DE COMPOSTELA

USC
UNIVERSIDADE
DE SANTIAGO
DE COMPOSTELA

AGRADECIMIENTOS

Este viaje comenzó hace mucho tiempo, siendo tan solo una niña curiosa a la que le descubrieron el mundo de la ciencia y que quería hacer el doctorado en Carolina del Norte. Hasta allí no me fui, pero si que, si me encuentro escribiendo estas líneas, es porque he conseguido mi objetivo de realizar el doctorado. Pero este trayecto no he estado sola, como dice La Vecina Rubia, la vida está formada por momentos y los míos tienen nombre de persona, de forma que al pensar en esta etapa se me llena la cabeza y los recuerdos de nombres que me han ido acompañando y que, sin ellos, estar aquí hubiese sido imposible.

Me gustaría empezar agradeciendo a mis directores. En primer lugar, gracias Miguel, por haber confiado en mi desde un primer momento y haber depositado la responsabilidad de avanzar con este proyecto. Me gustaría destacar que, precisamente gracias a ti, no soy la misma persona que entró en el laboratorio en el 2017, ambos sabemos que ha habido un tremendo de desarrollo tanto personal como profesional, de forma que considero que gracias a tus aportaciones ahora mismo siento que soy capaz de enfrentarme a las diferentes etapas y obstáculos que se me puedan ir presentando. Al igual que muchas gracias también a mi otro director, Alejandro, por enseñarme otra visión de este mundo y enseñarme el campo de la nanofarmacología, al igual que haber estado presente siempre que te he necesitado.

No puedo continuar por otro lugar que no sea mi laboratorio, donde tantas horas he pasado estos últimos años y que, gracias a todos los que forman parte de él, han hecho que lo sintiese como mi segunda casa. Primero a aquellos con los que he empezado pero que ya no están al terminar, gracias Vanesa por tu bondad y consejos, y gracias Adrián, porque es enorme lo que me has enseñado y eres un referente científico en mi vida. Gracias a María y a Noa, por enseñarme no solo a nivel profesional, si no en diferentes aspectos de la vida que esperar y como actuar, son largas las conversaciones que hemos tenido y el gran apoyo que me habéis brindado estos años. Gracias Laura, tu alegría y simpatía son contagiosas, pero tu ayuda y apoyo han sido un factor clave para que ahora mismo pueda estar escribiendo estas líneas. Gracias Raquel, no puedo no tener palabras bonitas y de agradecimiento para ti, tu forma de ser es maravillosa y siempre estás cuando más se necesita para echar una mano o dar palabras de ánimo. Laura y Raquel ha sido un placer haber coincido y compartido esta etapa con vosotras, sé que os queda lo más duro pero no tengo ninguna duda de que acabaremos celebrándolo por todo lo alto y riéndonos de todo lo que hemos pasado, sois muy especiales. Gracias Fernando por todas las palabras de ánimo que me has ofrecido, también estoy segura de que acabarás consiguiendo todo lo que te propongas. Pero en especial, mis mayores agradecimientos son para Ana, mi gran apoyo desde el principio y sé que no solo hasta aquí, si no que vas a formas parte de mi vida. Eres una persona con una fuerza envidiable que consigues transmitírnosla para que nosotros podamos atravesar los baches que se nos presentan, además de ser una profesional admirable. Eres una de las personas más especiales que he conocido y puedo decir claramente que sin ti hubiese tirado la toalla en algún momento, por eso y por tantas cosas que ambas sabemos, no puedo decir más que eres una verdadera amiga con todas las letras.

Al igual que gracias al servicio de Nefrología, por ofrecer su ayuda para que este proyecto haya podido salir adelante.

Pero no solo he tenido el laboratorio de Nefro, si no que me he sentido parte de mi laboratorio adoptivo, el laboratorio 3. Tamara y Nerea, gracias por apoyarme en todos los momentos durante este tiempo, tener paciencia para enseñarme todo lo que se y he podido aplicar, e

incluso, hasta por aprender de mi campo para ayudarme. No sólo me llevo dos compañeras más, me llevo dos buenas amigas de la que pocas hay. Tamara sé que ahora termina una etapa, pero créeme, vas a llegar hasta donde quieras porque eres una tremenda de profesional, con una calidad humana increíble, y me gustaría seguir viviéndolo contigo como hasta ahora que incluso hemos compartido el final de la nuestra etapa de predocs, compartiendo unos buenos agobios y animándonos mutuamente. Nerea eres maravillosa, confía en ti como hacemos los demás porque vales oro, sé que siempre que me pase algo vas a estar a mi lado escuchándome y apoyándome en todas mis decisiones como has hecho hasta ahora, te has convertido en alguien esencial en mi vida. Y por supuesto gracias a María, eres el ejemplo en el que todas deberíamos reflejarnos, gracias por todas las lecciones científicas que tanto me han aportado, tu tiempo y tu cariño, pero también gracias por las grandes conversaciones de feminismo y sororidad.

Gracias al servicio de proteómica, me habéis salvado con vuestra ayuda. Gracias Carmen, por tu ayuda en momentos más críticos para mí. Gracias María, por tu dedicación y conversaciones eternas sanadoras. Gracias Pili, transmites una energía increíble, siempre tan dispuesta a ayudar y a escuchar. Y, sobre todo, gracias Susana, no podría escribir en unas líneas todo lo que has hecho por mí, estoy eternamente agradecida, tu paciencia y ayuda son infinitas, has confiado en mi cuando ni yo me veía capaz y de una manera desinteresada, eres tremendamente admirable en todos los aspectos profesionales y personales.

También a otras personas del IDIS con las que he compartido estos años. En especial mención a Miriam, mi gran descubrimiento y compañera de batallas, eres una persona muy especial. Gracias también a Eloi, Ana y María (Lab 18), Alana, Sandra y Laura (Lab 7), Marinela (Lab 6), Carolina (Lab 17), Pablo, Roi, María y Víctor (Lab 16), Raquel (Lab 14), Lorena, Ángeles y Cris (Lab 10), Clara (Lab 9), María Jesús, porque en mayor o menor medida habéis formado parte de este camino tanto profesional como personalmente.

Pero una parte fundamental es mi familia, sin vosotros no sería quien soy. Gracias papá, porque sin ti no hubiese empezado esta etapa, y por todo tu cariño y apoyo diario. Gracias mamá, porque sin ti no lo hubiese conseguido, siempre has confiado en mí más que yo misma. Y gracias a mis hermanos, por su apoyo y confianza incondicional.

Y sobre todo, gracias a ti Chema, gracias por implicarte en lo que significa la investigación y la realización del doctorado, por tu vitalidad contagiosa, por creer en mi siempre, por apoyarme hasta en los momentos más duros, por comprenderme y animarme a partes iguales. Gracias por convertirte en un gran compañero de vida y demostrarme tanto cada día.

Muchas gracias a todos.

USC
UNIVERSIDADE DE SANTIAGO DE COMPOSTELA

RESUMO

A enfermidade renal poliquística (PKD) é un grupo heteroxéneo de trastornos monoxénicos caracterizados pola acumulación de quistes cheos de líquido no ril que causan insuficiencia renal crónica e enfermidade renal terminal, e tamén pode afectar a outros órganos como o fígado. As enfermidades quísticas son unha das principais causas da enfermidade renal crónica. A PKD engloba diferentes enfermidades, entre as que destaca a enfermidade renal poliquística autosómica dominante (ADPKD). A ADPKD ten unha incidencia de 1 de cada 500 a 1 de cada 1.000 nacidos vivos, e é causada o 85% das veces por mutacións no xene *PKD1*, que codifica a policistina-1 (PC1), mentres que o 15% restante é causada por mutacións no xene *PKD2*, que codifica a Policistina-2 (PC2). Tanto a PC1 como a PC2 son proteínas transmembrana, a PC1 actúa como mecanosensor na membrana plasmática das células epiteliais do túbulo renal e detecta alteracións e sinais do espazo extracelular, sendo un regulador crucial da conversión de sinais mecánicos en respostas intracelulares; mentres que a PC2 é unha canle iónica non selectiva permeable ao Ca^{2+}. Describíronse que estas proteínas están dispostas como un complexo heterotetramétrico que comprende unha PC1 e tres subunidades PC2 e aparecen predominantemente na membrana plasmática e no cilio primario. Non obstante, a fisiopatoloxía das policistinas aínda non está clara. Os mecanismos moleculares na formación dos quistes de ADPKD é un tema moi debatido que aínda non está claramente definido, entre as teorías máis compartidas está a teoría dos "two-hit", na que é necesaria unha segunda mutación somática no alelo non mutado; ou o modelo de dose, onde o inicio do quiste prodúcese porque a redución do nivel de proteína funcional é inferior ao nivel límite necesario para a súa correcta funcionalidade. Desde que se describiron os xenes e proteínas responsables da PKD, establecéronse múltiples modelos animais *in vitro* e *in vivo* para o estudo da PKD. Identificáronse e estudáronse diversos mecanismos implicados na ADPKD, incluíndo a proliferación, a apoptose, o metabolismo, a fibrose e a inflamación, entre outros. Non obstante, aínda se descoñece o mecanismo que leva ao inicio da formación de quistes. Do mesmo xeito, actualmente non existe unha terapia completamente eficaz para a PKD, só fármacos que retarden a progresión da enfermidade ou o tratamento de síntomas como a hipertensión, e finalmente a única opción é a terapia de substitución renal mediante diálise ou transplante. O crecente avance no coñecemento da fisiopatoloxía da ADPKD permitiu o desenvolvemento de novas dianas terapéuticas potenciais, entre as que se atopa a única terapia aprobada, o Tolvaptan, un antagonista selectivo do receptor da vasopresina tipo 2 (V2R). O Tolvaptan reduce o aumento do volume renal nun período de 3 anos e tamén retarda o deterioro da función renal. En cambio, ten efectos secundarios como poliuria, nicturia, sede e polidipsia, así como hepatotoxicidade. De forma que o tratamento con Tolvaptan só se recomenda actualmente para pacientes adultos con ADPKD con progresión rápida. Polo tanto, proponse que unha comprensión máis profunda da fisiopatoloxía da PKRAD levará ao descubrimento de novos tratamentos para evitar a necesidade de terapia de substitución renal en pacientes con ADPKD.

O seguimento da progresión da ADPKD baséase na medición da taxa de filtración glomerular (eGFR), normalmente mediante a medida da creatinina sérica. Non obstante, este parámetro ten unha especificidade e sensibilidade baixas e non predice a progresión da enfermidade. Actualmente existen tamén outros parámetros como as relacións xenotipo-fenotipo e a medición do volume renal total que axudan a definir mellor o deterioro da función renal. Polo tanto, a identificación de novos biomarcadores que permitan predecir se a enfermidade está a progresar en diferentes pacientes permitiría un prognóstico máis preciso e ofrecería un aumento significativo da calidade de vida dos pacientes. Unha opción podería ser

a través do perfil proteómico das Vesículas Extracelulares urinarias, xa que a urina proporciona unha fonte facilmente dispoñible de biofluídos e partículas derivadas das células renais. Ademais, a recollida de mostras non é invasiva e forma parte da práctica clínica habitual.

As vesículas extracelulares (VEs) constitúen un grupo heteroxéneo de estruturas limitadas por unha bicapa lipídica liberada polas células. Son secretadas pola maioría dos tipos celulares e, polo tanto, están presentes en todos os fluídos biolóxicos. As VEs presentan funcións fisiolóxicas polivalentes e están implicados na regulación das principais vías de sinalización e na comunicación intercelular. A carga da VE é específica do tipo celular e adoita estar afectada polo estado fisiolóxico ou patolóxico da célula. Esta carga da VE prodúcese durante a bioxénese da VE e pode incluír compoñentes celulares como ADN, ARN, lípidos, metabolitos e proteínas citosólicas e da superficie celular. Unha vez liberados no espazo extracelular, as VE poden chegar ás células receptoras e liberar o seu contido para producir respostas funcionais que afectan o seu estado fisiopatolóxico. O crecente interese pola composición dos VE tamén expuxo a posibilidade de utilizalos como biomarcadores da progresión de varios estados de enfermidade. O desenvolvemento de técnicas para illar e enriquecer EVs para definir a súa carga selectiva pode mellorar a sensibilidade á procura de tales biomarcadores. Existe unha gran variedade de técnicas de illamento de EV que se basean nas súas propiedades físicas e moleculares como a densidade, o tamaño, a carga e as proteínas da superficie EV para facilitar a súa purificación. Entre as técnicas de illamento máis utilizadas están: ultracentrifugación, ultrafiltración, cromatografía de exclusión por tamaño, inmunoafinidade e técnicas baseadas en axentes precipitantes. Non obstante, cada unha destas técnicas ten vantaxes e inconvenientes, polo que o gran reto que rodea ás VEs é atopar un método de illamento de referencia factible, preciso e fiable para analizar as VEs para investigación e aplicacións clínicas. Os principais fluídos biolóxicos nos que se identificaron e caracterizaron as VEs circulantes son o sangue (plasma ou soro), a urina, a saliva e o leite, entre outros.

As VE urinarias (uVE) identificáronse tanto en persoas sans como en pacientes con enfermidade renal, e son producidas e segregadas na urina por todo tipo de células renais de cada segmento da nefrona. A evidencia suxire que os uVEs son capaces de ser interiorizados por outras células e poden modular a súa función, o que indica a comunicación intra-nefrona ao longo do tracto urinario. Precisamente por estas características, teñen un excelente potencial como fonte de biomarcadores que poderían mellorar e complementar outras medicións clínicas. Os uVEs son facilmente accesibles de forma non invasiva, están dispoñibles en gran cantidade e son susceptibles de mostraxe frecuente. Ademais, como noutras enfermidades, é moi probable que o contido das vesículas urinarias se altere para reflectir a lesión renal e a progresión da enfermidade mediante a modulación das células veciñas, proporcionando así unha fonte distinta e rica en biomarcadores da enfermidade.

Por outra banda, descríbese amplamente que as VEs están fortemente glicosilados cunha variedade de glicosaminoglicanos (GAG) unidos a proteínas e lípidos da membrana das VEs, o que destaca a importancia dos patróns de glicosilación dos EV na súa captación e interacción coas células receptoras. Ademais diso, comprobouse que o patrón de glicación está alterado en relación a diferentes enfermidades, como as enfermidades renais.

Tendo en conta isto, proponse o estudo do compoñente glicosilado utilizando a ferramenta de recente desenvolvemento, ExoGAG, que permite o illamento dos GAG e a fracción unida a eles, como unha ferramenta prometedora na busca de biomarcadores en relación coa progresión da ADPKD.

Neste contexto, este traballo ten como obxectivos principais o estudo das vías de sinalización implicadas na cistoxénese para o desenvolvemento de novas estratexias terapéuticas mediante o estudo da proteómica diferencial de riles de *Wild type* e mutantes dun modelo murino ortólogo de ADPKD e o desenvolvemento dun nova ferramenta diagnóstica que tamén nos permite anticipar a evolución da enfermidade, mediante a caracterización da glicoproteína e da fracción vesicular unida aos GAGs. Ademais, compararase o potencial desta ferramenta como método de illamento de EVs con outros xa establecidos.

En primeiro lugar, realizouse a proteómica diferencial cuantitativa de *Wild type* e mutantes do modelo animal condicionado para a deleción de *Pkd1* ($Pkd1^{cond/cond}$; Tam-Cre). No primeiro enfoque, fíxose unha comparación dos riles de ratos sacrificados o día posnatal 30, momento no que a enfermidade está totalmente desenvolvida, demostrado polo alto índice de quistes, así como o número de quistes, o gran tamaño dos riles e o grave dano renal. Neste estudo atopáronse 152 proteínas expresadas de forma diferencial (DEP) de forma significativa e cun *fold change* superior a 2; dos cales 96 están *upregulados* nos mutantes e 56 *downregulados*. Estes resultados descubriron un gran número de proteínas nos mutantes no día 30 e que están relacionadas con varios procesos biolóxicos así como con diferentes compoñentes celulares, o que fai que o enfoque do estudo do complexo ADPKD, así como revalide o feito de que na actualidade, as vías principais e secundarias da cistoxénese aínda son difíciles de identificar. Por iso, para tentar atopar aquelas vías e proteínas relacionadas coas fases iniciais da cistoxénese, procedeuse á comparación de riles de *Wild type* e mutantes sacrificados o día posnatal 18, onde a enfermidade aínda non está claramente desenvolvida coa función renal practicamente intacta, pero onde xa se atopa un certo número de quistes. Neste caso, só se atoparon 14 DEPs, todos os cales estaban *downregulados* nos mutantes. As vías nas que se atopan estas proteínas están relacionadas co sistema inmunitario, o metabolismo e os procesos relacionados coa membrana celular, o que indica que estas vías xa están alteradas ao comezo da enfermidade.

Non obstante, para comparar os resultados obtidos nas diferentes condicións, decidiuse analizar de novo os resultados, pero, neste caso, combinando as bibliotecas proteómicas. Deste xeito, o número de proteínas identificadas aumentou, identificándose agora 2498 proteínas fronte ás 1283 proteínas identificadas na biblioteca do día 30 e as 971 identificadas nas do día 18. Con esta nova análise, observouse que os DEP identificados varían, con todo, aínda están implicados nas mesmas vías celulares. Nesta nova análise, no día 18 posnatal, atopáronse 15 DEP, 14 estaban *upregulados* e 1 *downregulados* nos mutantes. As proteínas *upreguladas* están relacionadas con procesos biolóxicos como a tradución e a regulación de quinasas e con compoñentes celulares como os ribosomas e a matriz extracelular. Pola contra, a proteína *downregulada* está relacionada co metabolismo. Por outra banda, atopáronse un total de 213 DEP no día posnatal 30, 156 foron regulados ao alza e 57 a baixa. Neste caso, as proteínas *upreguladas* estaban relacionadas coas vías citoesqueléticas, a adhesión celular, a activación de torrentes de sinalización e compoñentes como a membrana plasmática e a matriz extracelular. Por outra banda, e como se observou nas fases iniciais, as proteínas *downreguladas* están claramente relacionadas co metabolismo. Estes datos suxiren que en fases avanzadas de progresión da enfermidade, aumenta o número de proteínas desreguladas e as vías relacionadas. Do mesmo xeito, estes resultados reforzan a idea de que o crecemento do quiste pasa por dúas etapas principais: o inicio do quiste e a súa progresión. O que podemos observar é que hai vías que xa están alteradas nos estadios iniciais da enfermidade e que continúan alterando ao longo dela, como a vía translacional, a matriz extracelular ou o metabolismo. Ademais, só aparecen 3

proteínas (VIME, SPON1 e RBM3) desreguladas, neste caso *upreguladas* nos mutantes, desde os estadios iniciais e que permanecen alteradas co avance da enfermidade, o que as faría atractivas como posible diana terapéutica, xa que sería posible modular a súa expresión desde as primeiras fases.

En segundo lugar, desenvolvemos unha nova ferramenta, ExoGAG, que nos permite buscar novos biomarcadores diagnósticos ou pronósticos da enfermidade nunha mostra de urina. Este método baséase no illamento dos GAGs e da fracción asociada na mostra. A primeira análise con este método realizouse mediante a análise de mostras de urinas do modelo animal ortólogo de ADPKD utilizado previamente en diferentes estadios da enfermidade, desde a fase renal inicial ata a terminal, pasando por estadios avanzados. Na análise proteómica entre mostras de urina de *Wild type* e Mutantes, a fracción obtida mostrou unha serie de proteínas alteradas na enfermidade, entre as que destaca UROM, sendo a única atopada en menor abundancia en Mutantes e que decrece co transcurso da enfermiedad, e outras como ALBU ou AMBP, que aumentan. coa progresión da enfermidade. Ademais, estes resultados validáronse mediante a comparación e secuenciación do perfil proteico total das mostras illadas, que varía coa presenza da enfermidade así como coa súa evolución.

Esta análise foi replicada en mostras humanas de pacientes con ADPKD con mutacións tanto no xene *PKD1* como no xene *PKD2*. Observouse un perfil consistente de proteínas asociadas a GAG nas mostras de control. Non obstante, os nosos resultados revelaron que o patrón constante está alterado nos pacientes con ADPKD en función da función renal correlacionada coa creatinina sérica, sendo máis extremo nos estadios máis graves da enfermidade, pero comezando a alterarse nos estadios iniciais da enfermidade con niveis de creatinina relativamente baixos. Ademais, descubrimos que a variación no perfil dos pacientes era específica do tipo de enfermidade, como se pode ver entre o perfil dos pacientes con mutacións en *PKD1* e *PKD2* onde este patrón ten un cambio máis pronunciado desde respecto a fases iniciais da enfermidade. Como anteriormente, a secuenciación proteómica destas diferenzas no perfil proteico levou á identificación dunha serie de marcadores. A validación e cuantificación destes potenciais marcadores levou á identificación de UROM, CERU, AMBP e VTNC como biomarcadores potenciais da progresión da enfermidade. É interesante o comportamento da UROM, que diminúe en abundancia co avance da enfermidade mesmo antes dunha variación considerable da creatinina sérica. Mentres que CERU, AMBP e VTNC aumentan en fases avanzadas da enfermidade. Por outra banda, a combinación do estudo destes marcadores definidos pola relación dos que aumentan fronte a UROM aumenta o seu valor predictivo ante a progresión da enfermidade, e mesmo aumenta o valor diagnóstico, como ocorre, por exemplo, coa ratio UROM./AMBP.

En terceiro lugar, ExoGAG caracterizouse como un novo método de illamento para VE. O potencial como ferramenta de illamento de VEs foi descuberto despois de que a análise proteómica de illamento con ExoGAG revelase que a gran maioría das proteínas estaban relacionadas coas VEs. Ademais, a caracterización mediante microscopía electrónica e inmunofluorescencia confirmou a presenza destes VEs, que aparecían illados individualmente ou pertencentes a un complexo xunto coa Uromodulina. Xa se describiu o atrapamento de VEs por filamentos de Uromodulina, considerándose un contaminante para o estudo dos EV en urina, polo que se propón a súa depleción. Pero os resultados anteriormente comentados lévannos a pensar que o feito de que estas vesículas estean unidas á Uromodulina non é un feito aleatorio senón máis ben unha cuestión fisiolóxica, xa que co curso da enfermidade como a

ADPKD, o compoñente de Uromodulina diminúe, mostrando que desempeña un papel importante aínda descoñecido.

Posteriormente realizáronse diferentes comparacións co método máis utilizado para o illamento de EVs, a Ultracentrifugación, tendo en conta que o volume empregado en ExoGAG é dez veces menor que o da Ultracentrifugación. A análise de espectrometría de masas mostrou un alto rendemento e robustez no compoñente proteico illado por ExoGAG, sendo similar ao da Ultracentrifugación, ademais de mostrar que con ExoGAG, ademais do compoñente vesicular coñecido, illase un compoñente extracelular específico debido ao tipo de illamento producido pola fracción asociada.a GAGs. A caracterización do compoñente vesicular mediante Nanotracking Analysis (NTA) determinou unha alta eficiencia no que respecta ao número de partículas illadas con ExoGAG, obtendo VEs de tamaño similar aos illados por Ultracentrifugación. Ademais, a caracterización dos VEs illados con estes dous métodos coa tecnoloxía ExoView®, revelou que con ExoGAG se obtén un maior rendemento no illamento de VEs por mL de mostra de urina e que á súa vez o tipo de VE illado con este método determinada polo seu perfil de tetraspaninas (CD63, CD81 e CD9) é unha representación máis fiable dos VE na mostra de urina que a illada con Ultracentrifugación.

A aplicación de ExoGAG como método de illamento de VEs para buscar novos biomarcadores asociados á progresión de ADPKD revelou que o perfil de tetraspaninas aparece alterado desde o inicio da enfermidade. O compoñente CD63 aparece diminuído en comparación cos controis en todas as fases da enfermidade, mesmo en fases moi iniciais, tanto en pacientes con mutacións en *PKD1* como en *PKD2*. Por outra banda, o compoñente CD81 increméntase en pacientes con ADPKD en comparación cos controis, de xeito que nos pacientes con mutación en *PKD1* este compoñente aparece aumentado en todos os estadios da enfermidade mentres que en pacientes con mutación en *PKD2* diminúe ao longo da enfermidade, o que converteríao nun biomarcador con capacidade diagnóstica. Con estes resultados observamos non só que o perfil de tetraspanina cambia na ADPKD, senón tamén que pode ser específico do tipo de mutación causante, e o seu estudo pode ser proposto como candidato a novos biomarcadores para o diagnóstico e progresión da enfermidade. Por outra banda, a súa aplicación na validación no compoñente vesicular dos marcadores obtidos no compoñente proteico asociado a GAGs, UROM, CERU, AMBP e VTNC comprobou que só parte do compoñente de UROM e VTNC se correlaciona co observado previamente. Isto lévanos a pensar que non só o compoñente dos EV e a súa carga xoga un papel importante ao longo da enfermidade, senón que tamén existe un complexo formado por VEs e proteínas asociadas que é a parte que está realmente alterada e que xoga un papel fundamental no curso da enfermidade.

En resumo, identificáronse novas dianas e vías implicadas na fisiopatoloxía do ADPKD mediante a tecnoloxía de proteómica cuantitativa SWATH-MS. Do mesmo xeito que se identificaron aquelas vías que foron alteradas desde o inicio e ao longo da enfermidade, destacando o papel de VIME, SPON1 e RBM3 como posibles dianas terapéuticas, pola súa implicación dende as fases iniciais. Por outra banda, ExoGAG é un novo método analítico que separa o compoñente específico asociado aos GAGs da mostra. Esta fracción permitiunos identificar un patrón urinario de proteínas asociadas aos GAGs que se ve alterado na progresión da enfermidade. Todos estes datos mostraron os nosos resultados prometedores na busca de novos biomarcadores para o diagnóstico e prognóstico de enfermidades renais, como a ADPKD, así como para axudarnos a comprender mellor a fisiopatoloxía subxacente á enfermidade. Ademais, ExoGAG é unha nova ferramenta que nos permite un illamento

eficiente das Vesículas Extracelulares en comparación con outros métodos de uso habitual. O compoñente vesicular illado é específico para a asociación con GAG e non só illa os VEs, senón tamén un complexo formado por proteínas como a Uromodulina e estas Ves que parece estar alterados en relación coa ADPKD. Isto pode desenmascarar un novo mecanismo de sinalización dentro do ril que necesita máis estudos para comprender o mecanismo fisiopatolóxico subxacente.

USC
UNIVERSIDADE
DE SANTIAGO
DE COMPOSTELA

ABSTRACT

Polycystic kidney disease (PKD) is a group of monogenic disorders that result in renal cyst development, which cause chronic renal disease (CKD) and end-stage renal disease (ERSD), and other organs, such as the liver, may also be affected. PKD includes a number of different diseases including autosomal dominant polycystic kidney disease (ADPKD). ADPKD has an incidence of 1 in 500 to 1 in 1000 live births and is caused 85% of the time by mutations in the PKD1 gene, which encodes Polycystin-1 (PC1), while the remaining 15% is caused by mutations in the PKD2 gene, which encodes Polycystin-2 (PC2).

Since the genes and their encoded proteins were described, several *in vitro* and animal models were developed for the study of PKD and multiple molecular pathways were discovered and characterized. However, the central and key mechanism that trigger cyst formation remains unclear. In the same way, there is currently no fully efficient therapy for PKD, only drugs that slow the progression of the disease or treatment of symptoms such as hypertension, and finally the only option is renal replacement therapy by dialysis or transplantation. The increasing understanding of the pathophysiology of ADPKD has led to the development of new potential therapeutic targets, including the only approved therapy, Tolvaptan, a selective vasopressin type 2 receptor (V2R) antagonist. Tolvaptan reduces the increase in renal volume over 3 years, and also slows the deterioration of renal function. In contrast, Tolvaptan has side effects such as polyuria, nocturia, thirst and polydipsia, as well as hepatotoxicity.

Monitoring the progression of ADPKD is based on the measurement of the glomerular filtration rate (eGFR), usually by quantifying serum creatinine. However, this parameter has a low specificity and sensitivity and is not predictive of disease progression. Currently, there are also other parameters such as genotype-phenotype relationships and measurement of total renal volume that help to better define renal function decline. Therefore, the identification of new biomarkers that can predict disease progression in different patients would allow a more accurate prognosis and offer a significant increase in the quality of life of patients and their families. One option could be through the characterization of the proteomic profile of urinary Extracellular Vesicles, as urine provides a readily available source of biofluids and cell-derived particles. Moreover, sample collection is non-invasive and part of routine clinical practice.

Extracellular vesicles (EVs) are a heterogeneous group of structures bounded by a lipid bilayer released by most cell type and present in all biological fluids. EVs have exhibited versatile physiological functions and are involved in the regulation of major signaling and intercellular communication pathways. EV loading is cell type specific and is often affected by the physiological or pathological state of the cell. This EV cargo is produced during EV biogenesis and may include cellular components such as DNA, RNA, lipids, metabolites, and cytosolic and cell surface proteins. Once released into the extracellular space, EVs can reach the recipient cells and release their contents to produce functional responses that affect their pathophysiological state, as the intranephron communication carried out by urinary EVs. On the other hand, it is widely described that EVs are heavily glycosylated with a variety of glycosaminoglycans (GAGs) bound to proteins and lipids of the EV membrane.

In this context, the main objectives of this work are to study the signaling pathways involved in cystogenesis for the development of new therapeutic strategies by studying the differential proteomics of Wild Type and Mutant kidneys of an orthologous murine model of ADPKD and the development of a new diagnostic tool that will also allow us to anticipate the

evolution of the disease by characterizing the glycoprotein and vesicular fraction bound to GAGs. In addition, the potential of this tool as an EV isolation method will be compared with other established methods.

First, we performed a quantitative differential proteomics of Wild Type and Mutants of the animal model conditioned for *Pkd1* deletion ($Pkd1^{cond/cond}$; Tam-Cre) at two different points of disease development, at early and advanced stages. We identified novel molecular pathways and targets in PKD field, consistent with the fact that in advanced stages of disease progression the number of deregulated proteins and pathways increases. We highlight the appearance of 3 proteins (VIME, SPON1 and RBM3) that are deregulated from the initial stages and remain altered as the disease progresses, which would make them attractive as possible therapeutic targets, as it would be possible to modulate their expression from the early stages.

Secondly, we developed a new tool, ExoGAG, which allows us to search for new diagnostic or prognostic biomarkers of disease in a urine sample. This method is based on the isolation of GAGs and the associated fraction in the sample. A constant profile of GAG-associated proteins has been observed in control samples. However, our results revealed that the constant pattern is altered in ADPKD patients as a function of renal function correlated with serum creatinine, being more extreme in the more severe stages of the disease but starting to modify in early stages of the disease. Proteomic sequencing of these differences in protein profile led to the identification of a number of markers. Among them, the behavior of Uromodulin is interesting, which decreases in abundance with disease progression even before a considerable variation in serum creatinine. While Ceruloplasmin, protein AMBP and Vitronectin increase in advanced stages of the disease. On the other hand, the combination of the study of these markers defined by the ratio of those that increase against Uromodulin increases their predictive value in the face of disease progression.

Thirdly, the characterization of ExoGAG as a new method of EV isolation showed that in this isolation there are EVs found individually and others belonging to a complex together with Uromodulin. The previously results lead us to believe that the fact that these vesicles are bound to Uromodulin is not a random event but a physiological issue, as with the course of the disease like ADPKD the Uromodulin component decreases, showing that it plays an important yet unknown role. On the other hand, comparison with one of the most widely used methods for EVs isolation, ultracentrifugation, showed that ExoGAG is a high performance, efficient and robust method. In addition to demonstrating that the representation of EVs according to their tetraspanin profile isolated with ExoGAG is more reliable than that of the urine sample than those isolated with Ultracentrifugation.

The application of ExoGAG as a method of EV isolation to search for new biomarkers associated with ADPKD progression has revealed that from the onset of the disease, the profile of tetraspanins CD63, CD81 and CD9 appears altered and, in fact, it may be specific to the type of causative mutation, and its study could be proposed as a candidate for new biomarkers for the diagnosis and progression of the disease. Moreover, its application in the validation in the vesicular component of the markers obtained in the protein component associated with GAGs, UROM, CERU, AMBP and VTNC found that only part of the UROM and VTNC component correlates with what was previously observed. This leads us to think that not only the EV component and its load play an important role throughout the disease, but that there is also a complex formed by EVs and associated proteins that is the part that is really altered and plays a fundamental role in the course of the disease.

In summary, new targets and pathways involved in the pathophysiology of ADPKD have been identified using quantitative SWATH-MS proteomics technology. We also identified those pathways that are altered from the beginning and throughout the course of the disease, as well as highlighting the role of VIME, SPON1 and RBM3 as potential therapeutic targets, due to their involvement from the early stages of the disease. On the other hand, ExoGAG is a new analytical method that separates the specific component associated with GAGs from the sample. This fraction allowed us to identify a urinary pattern of GAG-associated proteins that is altered during disease progression. All these data showed our promising results in the search for new biomarkers for the diagnosis and prognosis of kidney diseases, such as Uromodulin, as well as to help us better understand the underlying pathophysiology of the ADPKD. In addition, ExoGAG is a new tool that allows us to efficiently isolate Extracellular Vesicles compared to other commonly used methods. The isolated vesicular component is specific for association with GAGs and not only isolates EVs, but also a complex formed by proteins as Uromodulin and these EVs appear to be altered in relation to ADPKD. This may unmask a new signaling mechanism within the kidney that needs further study to understand the underlying pathophysiological mechanism.

USC
UNIVERSIDADE
DE SANTIAGO
DE COMPOSTELA

USC
UNIVERSIDADE
DE SANTIAGO
DE COMPOSTELA

Table of contests

Resumo 17
Abstract 23
Abreviations 33
Introduction 37
1. Introduction 39
1.1 Function and physiology of the kidney 39
1.2 Kidney disease 40
1.2.1 Diagnosis and prognosis of renal disease 41
1.2.1.1 New diagnostic and prognostic biomarkers 42
1.3 Polycystic Kidney Disease 42
1.3.1 Autosomal Dominant Polycystic Kidney Disease 42
1.3.1.1 ADPKD Genes and Proteins 43
1.3.1.2 Initiation of cyst: Cystogenesis 45
1.3.1.3 Molecular pathogenesis of ADPKD 46
1.3.1.3.1 Polycystins and Ca^{2+} channel 47
1.3.1.3.2 Proliferation and apoptosis 48
1.3.1.3.3 Altered fluid secretion 48
1.3.1.3.4 Fibrosis and inflammation, role of extracellular matrix and epithelial-mesenchymal transition 48
1.3.1.3.5 Metabolism 49
1.3.1.3.6 Role of cilia 49
1.3.1.3.7 Wnt signaling 49
1.3.1.4 Therapies for ADPKD 50
1.3.1.5 Diagnosis of ADPKD 51
1.3.1.6 Prognosis and End-Stage Renal Disease in ADPKD 51
1.4 Extracellular Vesicles 53
1.4.1 Biogenesis of EV 53
1.4.1.1 Biogenesis of exosomes 54
1.4.1.2 Biogenesis of microvesicles 55
1.4.2 Composition of EV 56
1.4.2.1 Proteins 57
1.4.2.2 Nucleic acids 57
1.4.2.3 Lipids 57
1.4.3 EV-mediated intercellular communication 58
1.4.4 Biological roles of EVs and its applications 59

USC UNIVERSIDADE DE SANTIAGO DE COMPOSTELA

1.4.5 Isolation techniques 60
1.4.5.1 Ultracentrifugation 60
1.4.5.2 Ultrafiltration 61
1.4.5.3 Size Exclusion Chromatography 61
1.4.5.4 Asymmetrical Flow Field-Flow Fractionation 61
1.4.5.5 Precipitation based 62
1.4.5.6 Immunoaffinity 62
1.4.6 Characterization of EV 63
1.4.7 EVs in Kidney Disease 64
1.4.7.1. Urinary EVs 64
1.4.7.1.1. Removal of contaminating proteins 65
1.4.7.2 EVs as biomarkers of renal disease progression 65
1.4.7.2.1. EVs in ADPKD 66
1.4.8 Seeking for new biomarkers: Glycosylation and EVs 66
Objectives 69
2. Objectives 71
Material and Methods 73
3. Material and methods 75
3.1 Mouse model 75
3.1.1 Genotyping of mouse lines 75
3.1.2 Histology and Measurement of Cystic Index 75
3.1.3 Clinical Chemistry 76
3.1.4 Protein and RNA extractions 76
3.1.5 Mice urine sample collection 76
3.2 Human urine samples 76
3.3 ExoGAG isolation 77
3.4 Extracellular vesicle isolation 77
3.4.1 Ultracentrifugation 77
3.4.2 CD9 Immunoprecipitation 78
3.5 Proteomics 79
3.5.1 Protein digestion for proteomics. 79
3.5.2 Mass spectrometry by LC-MSMS 79
3.5.2.1 Qualitative analysis using a DDA (Dependent Data Analysis) method 79
3.5.2.2 Quantitative analysis by SWATH™ (Sequential Window Acquisition of All Theoretical Fragment Ion Mass Spectra) DIA (Data-independent acquisition) Method 80
3.5.2.2.1 Generation of the reference spectral libraries 80

3.5.2.2.2 Quantitative analysis by SWATH™ 80
3.5.2.3 Semi-quantitative analysis by spectral count using Scaffold software 81
3.5.3 Functional Analysis. 82
3.6 Gene expression analysis. 82
3.7 Electrophoresis and Western Blot analysis 83
3.7.1 Western blot 2D 84
3.8 Tissue Immunofluorescence 84
3.9 Extracellular Vesicle characterization 84
3.9.1 Transmission electron microscopy (TEM) 84
3.9.2 Immunofluorescence 84
3.9.3 Nanoparticle Tracking Analysis (NTA) 85
3.9.4 ExoView® assay 85
3.9.4.1 Fluorescence labelling of antibodies 86
3.10 Statistical analysis 86
Results 87
4. Results 89
4.1 Chapter 1. Identification of new signalling pathways involved in cystogenesis by quantitative differential proteomic study in Polycystic Kidney Disease mouse model 89
4.1.1 Kidney proteomic characterization by SWATH™ analysis 89
4.1.2 Quantitative proteomic analysis of significant deregulated proteins in ADPKD mice at postnatal day 30. 89
4.1.2.1 Protein-protein interaction and Pathway analysis 93
4.1.3 Quantitative proteomic analysis of significant deregulated proteins in ADPKD mice at postnatal day 18. 97
4.1.3.1 Protein-protein interaction and Pathway analysis 101
4.1.4 Quantitative proteomic analysis of significant deregulated proteins in ADPKD mice at postnatal days 18 and 30. 102
4.1.4.1 Proteomic approach at postnatal day 18 105
4.1.4.1.1 Protein-protein interaction and Pathway analysis 106
4.1.4.2 Proteomic approach at postnatal day 30 108
4.1.4.2.1 Protein-protein interaction and Pathway analysis 110
4.1.4.3 Comparative study between libraries 114
4.1.4.4 Comparative study of differential proteome of postnatal days 18 and 30... 116
4.1.4.5 Validation of target candidates 117
4.2 Chapter 2. New biomarkers in urine for diagnosis and prognosis of ADPKD. 121
4.2.1 Characterization of glycoprotein component of urine in a time course ADPKD mice. 121

4.2.1.1 Comparison between proteomic component of urine and isolated fraction with ExoGAG..... 123

4.2.1.2 Search for biomarkers of disease progression through differential comparison of Wild type and Mutants samples isolated with ExoGAG..... 124

4.2.2 Identification of biomarkers of disease by characterization of glycoprotein component of urine in ADPKD patients..... 126

4.2.2.1 Chracterization of the GAG associated proteins isolated fraction (ExoGAG pellet) in controls and patients..... 126

4.2.2.2 Identification of biomarkers in ADPKD patients by mass spectrometry sequencing..... 127

4.2.2.2.1 Validation of identified biomarkers by Western blot in ADPKD patients with mutation in *PKD2*..... 128

4.2.2.2.2 Validation of identified biomarkers by Western blot in ADPKD patients with mutation in *PKD1*..... 130

4.2.2.2.3 Quantification of biomarkers for possible use as disease markers..... 131

4.2.2.3 Characterization of the not isolated component with ExoGAG (ExoGAG supernatant)..... 133

4.2.2.3.1 Chracterization of the ExoGAG superanatant protein profile in controls and patients..... 133

4.2.2.3.2 Identification of biomarkers in ADPKD patients by mass spectrometry sequencing..... 134

4.2.2.3.3 Validation of identified biomarkers by Western Blot in ADPKD patients..... 135

4.2.2.4 Differential comparison between ExoGAG Pellet and Supernatant..... 137

4.2.2.4.1 Characterization of specific ExoGAG pellet proteins..... 137

4.2.2.4.2 Comparison of the behavior of biomarkers in ExoGAG pellet and supernatant..... 139

4.3 Chapter 3. Characterization of urine Extracellular Vesicles isolated by ExoGAG.. 141

4.3.1 Functional analysis of identified proteins in ExoGAG isolation..... 141

4.3.2 Image characterization of ExoGAG isolation..... 142

4.3.3 Comparison of ExoGAG and other Extracellular Vesicle isolation techniques. 144

4.3.4 Optimization and characterization of the ExoGAG isolation..... 146

4.3.5 Protein characterization by mass spectrometry of the differences between the component isolated with ExoGAG and ultracentrifugation techniques..... 147

4.3.5.1 Optimization of the protocol for mass spectrometry sequencing of ExoGAG isolation..... 147

4.3.5.2 Characterization and comparison by mass spectrometry of the component isolated with ExoGAG and ultracentrifugation..... 148

4.3.5.3 Characterization of the component isolated with ExoGAG according to the guideline of Extracellular Vesicle studies..... 152

4.3.5.4 Characterization of the origin of Extracellular Vesicles isolated with ExoGAG. 153
4.3.6 Characterisation of the vesicular profile of Extracellular Vesicles isolated with ExoGAG and comparison with those isolated by ultracentrifugation. 154
4.3.6.1 Quantification and size analysis using NanoTracking Analysis (NTA) 154
4.3.6.2 Quantification, size analysis and Tetraspanin characterization using ExoView® 156
4.3.7 Characterization of the vesicular profile of EVs associated with the onset and progression of autosomal dominant polycystic disease. 159
4.3.7.1 Characterization of the Tetraspanin profile of Extracellular Vesicles in patients with mutation in *PKD1* 159
4.3.7.2 Characterization of the Tetraspanin profile of Extracellular Vesicles in patients with mutation in *PKD2* 160
4.3.7.3 Comparison of the Tetraspanin profile of Extracellular Vesicles in patients with mutation in *PKD1* and *PKD2* 162
4.3.7.4 Characterization and validation of the possible biomarkers in the vesicular component of ExoGAG isolation in the progression of autosomal dominant polycystic disease. 163
Discussion 167
5. Discussion 169
5.1 identification of new signaling pathways involved in cystogenesis by quantitative differential proteomic study in Polycystic Kidney Disease mouse model 169
5.2 New biomarkers in urine for diagnosis and prognosis of ADPKD 173
5.3 Characterization of urine Extracellular Vesicles isolated by ExoGAG 179
Conclusions 185
6. Conclusions 187
Bibliography 189
Bibliography 191
Supplemental Material 227
1. Supplemental Figures 227
2. Supplemental Tables 230
Annexes 317
ANNEX 1: authorisation of the bioethics committee for human and experimental animal studies 319
1.1 Bioethics Committee authorization for human studies 319
1.2 Bioethics Committee authorization for studies on experimental animals 321

USC UNIVERSIDADE DE SANTIAGO DE COMPOSTELA

USC
UNIVERSIDADE
DE SANTIAGO
DE COMPOSTELA

ABREVIATIONS

A1AT: alpha-1-antitrypsin

ADPKD: Autosomal Dominant Polycystic Kidney Disease

AFF4: Asymmetrical Flow Field-Flow Fractionation

ARPKD: Autosomal Recessive Polycystic Kidney Disease

AMBP: Protein Alpha-1-microglobulin

ALBU: albumin

APOA4: Apolipoprotein A-IV

BUN: Blood Urea Nitrogen

CAH1: Carbonic anhydrase 1

CERU: Ceruloplasmin

CKD: chronic kidney disease

CREAT: serum creatinine

DAPI: 4′,6-diamidino-2-phenylindole

DBA: Dolichos Biflorus Agglutinin

DDA: Data Dependent Acquisition

DIA: Data Independent Acquisition

DEP: differentially expressed proteins

DPP4: Dipeptidyl peptidase 4

DTT: dithiothreitol

ECM: Extracellular Matrix

ESRD: End Stage Renal Disease

EVs: extracellular vesicles

FDR: false discovery rate

FIBB: Fibrinogen beta chain

GAG: glycosaminoglycan

USC
UNIVERSIDADE
DE SANTIAGO
DE COMPOSTELA

GAPDH: Glyceraldehyde-3-phosphate dehydrogenase

GFB: glomerular filtration barrier

GFR: glomerular filtration rate

GPI: glycosylphosphatidylinositol

IF: Immunofluorescence

ILV: Intraluminal Vesicles

IP: Immunoprecipitation

ISEV: International Society for Extracellular Vesicles

KDIGO: Kidney Disease: Improving Global Outcomes

KO: knockout

LG3BP: Galectin-3-binding protein

LUM: Lumican

MVB: Multivesicular Body

Mut: Mutant

NEP: Neprilysin

NTA: NanoTracking Analysis

SDS: sodium dodecyl sulfate

PBS: Phosphate buffered saline

PC1: Polycystin-1

PC2: Polycystin-2

PCA: Principal Component Analysis

PCP: Planar Cell Polarity

PCR: Polymerase chain reaction

pI: isoelectric point

PKD: polycystic kidney disease

RBM3: RNA-binding protein 3

RET4: Retinol-binding protein 4

RT: room temperature

RT-PCR: Reverse-transcription quantitative PCR

SEC: Size Exclusion Chromatography

SPON1: Spondin-1

TEM: Transmission electronic microscopy

TTHY: Transthyretin

TRFE: Serotransferrin

UC: Ultracentrifugation

uEV: urine Extracellular Vesicle

UF: Ultrafiltration

UMOD: Uromodulin

UROM: Uromodulin

VIME: Vimentin

VTNC: Vitronectin

WT: wild type

ZA2G: Zinc-alpha-2-glycoprotein

USC
UNIVERSIDADE
DE SANTIAGO
DE COMPOSTELA

USC
UNIVERSIDADE
DE SANTIAGO
DE COMPOSTELA

INTRODUCTION

USC
UNIVERSIDADE
DE SANTIAGO
DE COMPOSTELA

USC
UNIVERSIDADE
DE SANTIAGO
DE COMPOSTELA

1. INTRODUCTION

1.1 FUNCTION AND PHYSIOLOGY OF THE KIDNEY

The kidneys are paired organs that lie retroperitoneally on the posterior abdominal wall. The main function of the kidneys is the elimination of waste substances through the production of urine. The kidneys excrete about 1.5 litres of urine per day and they are capable of filtering 20% of the blood pumped by the heart (1,2). In addition to their excretory function, kidneys also perform endocrine (by secreting vitamin D, renin and erythropoietin), metabolic and blood pressure regulation (by activation of the renin-angiotensin-aldosterone axis), body water and thirst (by osmoregulation) functions. They also regulate oxygen supply to red blood cells, erythropoiesis, acid-base haemostasis, calcium and phosphate metabolism, potassium balance, and they are involved in the immune system and drug metabolism (2,3).

Anatomically, each kidney presents a superior and inferior pole, a convex border placed laterally, and a concave medial border with a marked depression, the hilum, which contains the renal vessels and the renal pelvis (1). The kidneys consist of a 1 cm thick outer part called cortex and an inner part called medulla made up of renal pyramids, the apices of which point towards the renal hilum. These apices end in minor calyces and these in turn end in major calyces, which merge into the renal pelvis from which the ureter arises (Figure 1, left) (4).

Each kidney is formed by functional units called nephrons; about one million nephrons in humans and 12-16,000 in mice (3). Structurally, each nephron consists of a filtering body, called the glomerulus, surrounded by Bowman's capsule, located in the cortex; and a long tubule divided into several segments. These segments are: the proximal tubule, the loop of Henle and the distal tubule which interconnect in the collecting tubules ending in the renal pelvis (Figure 1, right). (2).

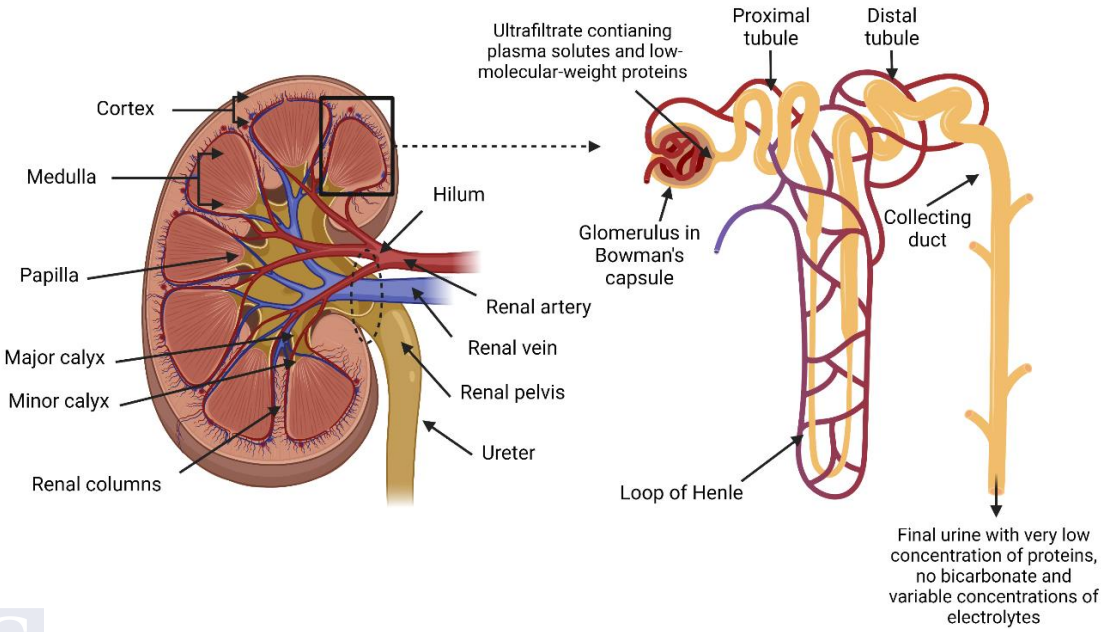

Figure 1. Anatomy of the kidney (left) and nephron (right). This figure was made using Biorender.

USC UNIVERSIDADE DE SANTIAGO DE COMPOSTELA

The renal artery, originating from the aorta, branches into afferent arterioles that carry blood to the capillaries that form part of the glomerulus. The filtration process is mediated by the glomerular filtration barrier (GFB) is in the glomerulus and consists of fenestrated endothelial cells, a basement membrane and a layer of highly epithelial cells called podocytes. Blood is filtered through GFB which is permeable to water and low molecular weight solutes. The filtrate passes into the proximal tubule where two-thirds of it is reabsorbed (5). Unfiltered blood leaves the glomerulus via the efferent arteriole.

In the proximal tubule, there are receptors able to reabsorb proteins and other components as vitamins or hormones. The loop of Henle oversees concentrating the urine and reabsorbing Ca^{2+} and Mg^{2+}, while K^{+} excretion is carried out in the distal and collecting tubule. Regulation of Na^{+} and Cl^{-}, essential in blood pressure control, takes place in almost the entire nephron (4,5).

Once the blood has been filtered in the glomerulus, it flows into the efferent arteriole and then through the peritubular capillaries and the vasa recta, forming a microvasculature around the nephron. The vasa recta are parallel to the loop of Henle and return ions and to the circulation. Finally, blood exits the kidney via the renal vein to the vena cava (5).

1.2 KIDNEY DISEASE

Kidney disease is defined as a heterogeneous group of pathological conditions affecting kidney structure and function. These alterations are associated with increased risk of kidney failure and complete loss of renal function or, even, development of complications in other organ systems, especially the cardiovascular system. The clinical presentation and progress of the renal disease are variable. Kidney disease can be classified as acute or chronic, dependent on duration, ≤3 months or >3 months, respectively. The association between acute kidney injury and chronic kidney disease is complex: acute kidney injury can lead to chronic kidney disease, and chronic kidney disease increases the risk of acute kidney injury (2,6).

Chronic kidney disease (CKD) has become one of the major public health problems in recent decades, affecting approximately 10% of the global adult population. However, a wide range of CKD prevalence has been observed in different studies, which has been related to clinical, environmental, geographical and socio-economic variables as well as to methodological differences. (6,7). Recent studies assign the prevalence in Spain at around 15% (6). By 2040, CKD is expected to become the fifth cause of death globally (8,9). The epidemiological significance of CKD is based on two fundamental aspects: the replacement treatment of advanced CKD by dialysis or kidney transplantation, although affecting only 1% of CKD patients; and the very significant increase in the risk of cardiovascular morbidity and mortality and total mortality (6).

There are many potential causes for chronic kidney diseases, including genetics, and non-genetic causes. There are causes that are common and well researched, such as diabetes, glomerulonephritis, and cystic kidney diseases, but relationship in CKD is not yet understood. Multiple genetic and environmental risk factors contribute to kidney diseases, making identification of the underlying pathophysiologic mechanisms difficult (8,9). For instance, despite a close association between CKD and hypertension, whether hypertension is a cause or a consequence of CKD is still controversial (8).

USC UNIVERSIDADE DE SANTIAGO DE COMPOSTELA

Consequence signs and symptoms of kidney failure develop progressive uremia, anemia, volume overload, electrolyte abnormalities, mineral and bone disorders, and acidemia that could cause premature death if left untreated. When renal failure is severe, the only life-sustaining treatment left is to renal replacement therapy, either in the form of chronic dialysis or kidney transplantation (8). Management of CKD is based on trying to preserve as much kidney function as possible before having to use renal replacement therapy (Figure 2).

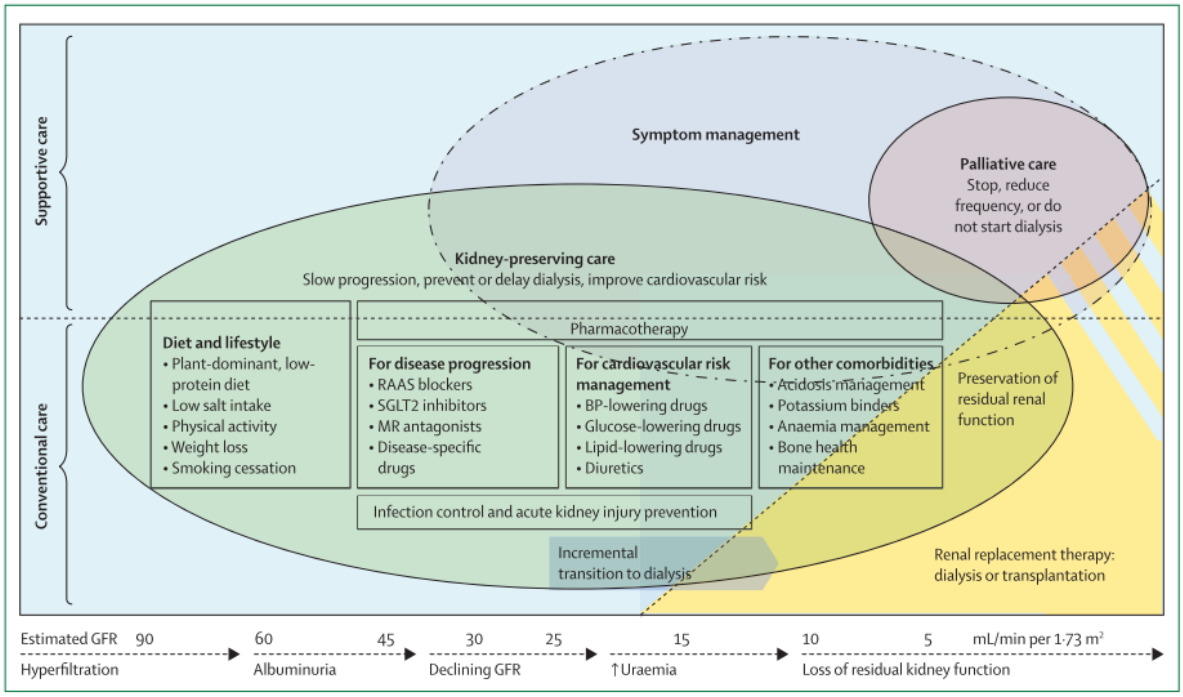

Figure 2. Management of throughout chronic kidney disease. This graph highlights the role of preservative management and its objectives (green area) within the overall conservative management of chronic kidney disease without dialysis (blue area), juxtaposing renal replacement therapy including dialysis and kidney transplantation (yellow area). Image taken from Kalantar-Zadeh, K., The Lancet, 2021 allowed by Elservier.

1.2.1 Diagnosis and prognosis of renal disease

Chronic kidney disease is defined as a reduction in kidney function, an estimated glomerular filtration rate (eGFR) of less than 60 mL/min per 1·73 m², or measurement of markers of kidney damage, such as albuminuria, hematuria, or abnormalities detected through laboratory testing, imaging (ultrasounds, computerized tomography or magnetic resonance), or from histopathological analysis of biopsied samples and that are present for at least 3 months by current international guidelines (8). Any of them have limited power in differential diagnosis, low specificity and sensitivity, and, especially, none is able to predict the outcome of the kidney disease in an accurate and efficient way.

The most used parameter for renal damage is the GFR. It could be measured indirectly by the renal clearance of exogenous filtration markers as inulin or endogenous filtration markers as creatinine or cystatin C (10). The endogenous filtration marker measure is a simple and cheap method that estimate the GFR through an algorithm as the CKD-EPI creatinine equation (10,11). Nowadays, The Kidney Disease: Improving Global Outcomes (KDIGO) 2012 guideline recommend the use of serum creatinine and albuminuria for evaluation and risk-stratum of CKD patients (12,13). However, creatinine levels are influenced by several non-

renal factors such as gender, age, muscle mass, metabolism, physical activity, diet, treatment, or hydration status (10).

As there are kidney diseases caused by genetic mutations, genetic diagnosis is also recommended. More than 600 genes have been associated in monogenic kidney diseases, being single-gene syndromes up to 50% of nondiabetic CKD in pediatric cohorts, and 30% in adult cohorts. Genetic diagnosis is used to inform clinical management of various nephropathies, allowing more precise diagnostics and better-informed choices for therapy and family counseling (9). In fact, in our NefroCHUS laboratory we carry out the genetic diagnosis of patients with suspected hereditary renal disease, always adapting to new sequencing technologies and taking into account the new genes that are associated with it.

1.2.1.1 New diagnostic and prognostic biomarkers

Over the last 15 years, there has been an explosion in the research of preclinical biomarkers of kidney disease. These biomarkers increase the estimation of kidney health by indicating injury type or the specific site of harm as tubulointerstitial injury, general inflammation, or repair. Plasma biomarkers are more frequently studied than urine biomarkers. The most common studied biomarkers in plasma are TNFR1 and TNFR2, related to inflammation; and FGF23, related to fibrosis. Whereas, urine KIM-1, related to tubular injury, and NGAL, associated with acute kidney injury are the most studied biomarkers. Although these biomarkers are highly sensitive and specific and have allowed an earlier diagnosis with promising results; none of them have been approved for clinical practice. These biomarkers could have the potential to indicate specific injury type or origin, so one biomarker would be insufficient and that leads to the study of a set of them in order to make clinical decisions. Larger and long-term studies are still needed (12,14).

1.3 POLYCYSTIC KIDNEY DISEASE

Polycystic kidney disease (PKD) is a heterogeneous group of monogenic disorders characterized by the accumulation of fluid-filled cysts in the kidney causing chronic renal failure and end stage renal disease (ESRD), also other organs could be affected, as liver. Previously described, cystic diseases are one of the main causes of CKD worldwide. PKD englobes different diseases including autosomal dominant polycystic kidney disease (ADPKD), autosomal recessive polycystic kidney disease (ARPKD), and atypical forms of PKD (15–17). ADPKD is caused by mutations in *PKD1* (18–20) and *PKD2* genes (21), meanwhile, ARPKD is caused by mutations in *PKDH1* (22–24), and recently discovered in *DZIP1L* (25). New genes associated with atypical forms of PKD have recently been discovered in an attempt to explain the genetic causes of the entire PKD phenotypic spectrum, among them are *GANAB* (26), *DNAJB11* (27), *ALG9* (28), *PMM2*(29), type 4A collagen gens (30) and more recently, *IFT140* (31) and *ALG5* (32).

1.3.1 Autosomal Dominant Polycystic Kidney Disease

Within this group of Polycystic Kidney diseases, the most common is ADPKD, with a incidence of 1 in 500 to 1 in 1000 live births worldwide, with no special propensity towards any race, geographical location or gender (15,16). However, calculating the prevalence of ADPKD has been challenging because of variable age-dependent penetrance and incomplete clinical ascertainment in the general population (33).

ADPKD is characterized by the extreme bilateral enlargement of kidneys due to the progressive expansion of fluid-filled cysts that are formed in uterine stage and over time enlarge

and destroy the normal renal structure and function that lead to End Stage Kidney Disease (ESKD), typically, at the age of 50-60s years (Figure 3) (34,35). The majority of patients develop the symptomatology at ages of 20-40s, but there have been sporadic cases that vary in onset in childhood ("early onset", before 15 years old) or even *in utero* ("very early onset") (36). Cysts derive from epithelial renal cells and predominantly originate from distal tubules and collecting duct but appear in all parts of the nephron (Figure 3) (15). Typical early symptoms of ADPKD include hypertension, polyuria, hematuria, flank pain and recurrent, refractory urinary tract infections. (34,37) ADPKD is a systemic disease because PKD genes are expressed in many tissues. ADPKD is associated with multiple extrarenal manifestations including symptomatic extrarenal cysts in liver, pancreas or spleen, and subarachnoid hemorrhage from intracranial aneurysms (36,38).

Due to the progressive advance of the disease and the hyperfiltration of healthy nephrons, renal function decline is usually not significant until ~60% of the normal kidney structure has been destroyed. After that point, loss of function accelerates leading to ESRD and the requirement for renal replacement therapy (RRT) by dialysis or transplantation (Figure 3) (39). Although both *PKD1* and *PKD2* mutations result in the development of similar pathophysiological features and cellular phenotypes, ADPKD patients with *PKD2* mutations typically show later onset of ESRD (79.9 years in compared to 53.1 years). This lag in onset of rapid functional decline with significant renal enlargement is of prognostic significance (40,41).

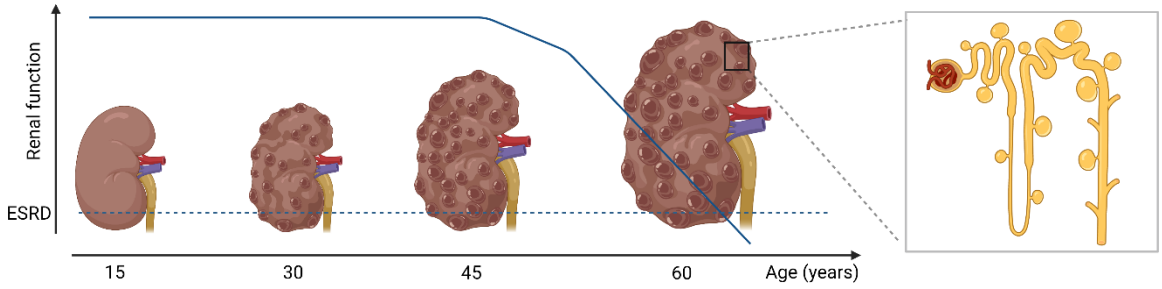

Figure 3. Pathogenesis of ADPKD. Cystogenesis and progression of cysts show a progressive growth throughout patient life. In early phases of disease, GFR (blue line) is compensated by intact nephrons hyperfiltration. However, with increasing renal volume, GRF decline leading to renal function loss and finally ESRD. On right, representation of the cysts across the nephron. This figure was made using Biorender.

1.3.1.1 ADPKD Genes and Proteins

ADPKD is a mendelian disease associated with autosomal dominant inheritance. It is caused by mutations in the *PKD1* (80-85% of cases) and PKD2 (15-20% of cases) genes. (40). *PKD1* is a complex gene mapping in chromosome 16 (16p13.3), (18–20), it has 46 exons and a size of 50kb with special features: it is highly enriched in GC with a large number of CpG dinucleotides (42), 70% of the gene sequenced is exactly repeated in 6 pseudogenes also located on chromosome 16 (43) and it contains a the largest polypyrimidine tract in human genome in intron 21 of 2.5 kb (44). On contrast, *PKD2* is located in chromosome 4 (4q21), it has 15 exons and a size of 68kb and has a simpler structure than *PKD1* (40) (Figure 4). There is compelling evidence from several groups worldwide to show that type and position of mutation has an effect on the disease phenotype, progression and severity, as proposed in PROPKD score (45–47).

USC
DE SANTIAGO DE COMPOSTELA

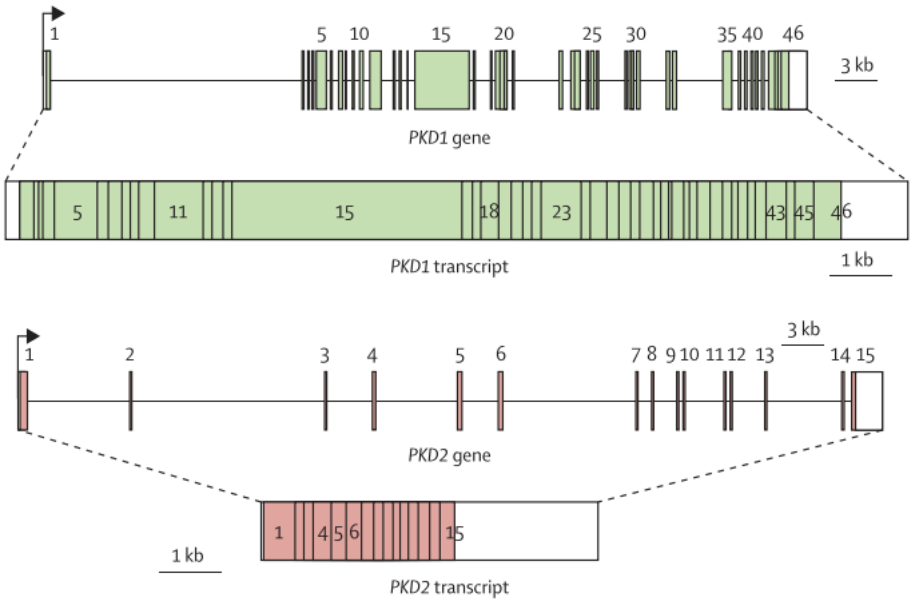

Figure 4. *PKD1* and *PKD2* genes and transcripts. Exons are numbered, the coding regions are shaded and untranslated regions are not shaded. Image taken from Torres,V., The Lancet, 2007 allowed by Elservier.

PKD1 gene encode for the protein Polycistin-1 (PC1), a large 4302 amino acid, 460 kDa 11-transmembrane domains with a long extracellular N-terminal domain and a short C-terminal domain (16,48) (Figure 5). PC-1 could act as a mechanosensory in the plasma membrane of renal tubule epithelial cells detecting alterations and signals in the extracellular space and a crucial regulator of the conversion of mechanical signals into intracellular responses (49). The long extracellular N-terminal domain contains many protein-protein interaction domains, including leucine-rich repeats, which may facilitate binding to ECM components such as collagens(50). PC1 is highly expressed in fetal maturing proximal and distal tubular and collecting duct epithelial cells and weak expressed in normal adult (51).

The protein encodes by *PKD2* is the Ca^{2+}-permeable non-selective ion cation channel Polycistin-2 (PC2), formed by 968 amino acids, ~110kDa, also known as TRPP2, since it belongs to the TRP (Transient Receptor Potential) family. PC2 structure consists in six transmembrane segments, a pore loop domain (separating the first two membrane segments) and an N- and C- terminal domains (52) (Figure 5).

PC1 is located in primary cilia, cytoplasmic vesicles, plasma membrane and cell adhesions. PC2 is found predominantly in endoplasmic reticulum, but also in plasma membrane, primary cilium and centrosome (53). PC1 and PC2 forms a receptor-channel complex implicated in Ca^{2+} pathway (54,55). Recent studies have reported that there is a heterotetrametric PC1-PC2 complex comprising one PC1 and three PC2 channel subunits. In fact, PC2 can function independently of PC1 in homomeric complexes formed by four PC2 in the primary cilium of renal epithelial cells to form a channel that is mainly permeant to monovalent cations (52,56,57). However, the physiological function of polycystins remains unclear (58).

USC
UNIVERSIDADE DE SANTIAGO DE COMPOSTELA

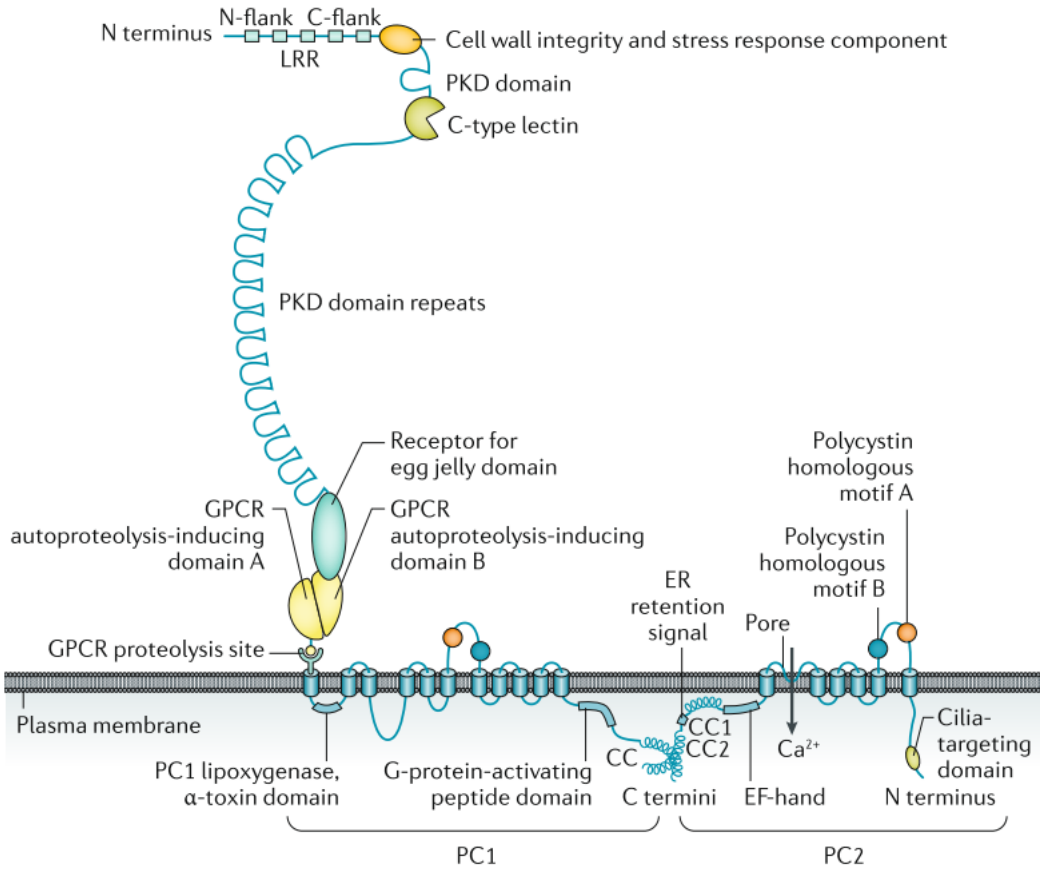

Figure 5. Structure of ADPKD proteins. Representation of structure and domains of Polycystin-1 (PC1) and Polycystin-2 (PC2). PC1 and PC2 are transmembrane proteins that form a complex that is localized to multiple subcellular locations, including the primary cilium. Image taken from Bergmann, C., Nature Reviews, 2018 allowed by Springer Nature.

1.3.1.2 Initiation of cyst: Cystogenesis

The molecular genetics of ADPKD cyst formation is a widely debated topic which has not been conclusively solved. The most widely recognized theory to explain the formation of cysts in human ADPKD is "two-hit" theory (59). This hypothesis proposes a complete loss of function of the protein caused by not only the germ-line mutation but also an additional somatic mutation in the normal allele (59–61). This theory considers that not only would numerous second hits need to occur to initiate cysts throughout the kidney but also that the kidney is more susceptible to second hits than other organs (62). This statement was demonstrated in studies with renal epithelial cysts from cystic fluid from patients, where a second pathogenic mutation either in *PKD1* or *PKD2* were found (60,63–65). Nevertheless, the mechanism and timing of this second-hit are currently unknown (66).

Moreover, there is a threshold and dosage model of cystogenesis. According to this hypothesis, PKD gene haplo-insufficiency, when one gene is defective and could not generate the encoded protein and the remaining copy produces reduced level of the proteins, would cause the initiation of cyst development throughout the kidney (67,68). This hypothesis suggests that cyst initiation and proliferation occurs when functional PC protein levels are below a specific threshold (35,68). This is consistent with the observation that homozygous for *PKD1* or *PKD2*

is incompatible with life and patients are heterozygous (35,68). Moreover, mutations in *PKD1* have worse prognosis than mutations in *PKD2* (41,47,69), and the *PKD1* truncated mutations were associated with the most severe polycystic severe phenotype (46,47). This could also be associated with intra-familial variability where family members although having the same mutation present differences in disease onset, severity and progression. In animal models, it was described that increasing or decreasing PC1 dosage can get worse or better renal phenotype, suggesting a central role of PC1 in cyst formation (70). In relation with this, it is also described the effect of several mutations in PC1 and PC2 trafficking and maturation, determining that dysfunctional maturation of PC complex underlie PKD pathology (71). So, it is suggested that gene dosage of 50% of *PKD1* is sufficient to initiate cyst formation and that this can be exacerbated by additional genetic or epigenetic factors including a somatic mutation ("second hit") in the *PKD1* or *PKD2* gene; modifier genes, environmental factors and/or renal fibrosis (72,73). In addition, a new microRNA-mediated mechanism has recently been described (74), such that expression of the unmutated allele would be repressed by the interaction of the 3'-UTR with miR-17. Therefore, even if there is only a mutation in one of the alleles, the other is more likely to be repressed, so that a polycystin dose of less than 50% is easily achieved.

Finally, a critical developmental window for cystogenesis has been identified suggesting that timing is also important in ADPKD severity, where, depending on the day of inactivation of the gene, there is a rapid onset of the disease phenotype or it is delayed (75,76).

1.3.1.3 Molecular pathogenesis of ADPKD

Since the genes and proteins causes of ADPKD were described, multiple *in vitro* and *in vivo* animal models were established for the study of PKD (15,38,77). A variety of mechanisms involved in ADPKD have been identified and studied. (38,66). However, the mechanism that leads to the initiation of cyst formation is still unknown. A schematic representation of some of the pathways involved can be found in Figure 6. The following is a description of some of the pathways involved in the pathogenesis of ADPKD.

USC UNIVERSIDADE DE SANTIAGO DE COMPOSTELA

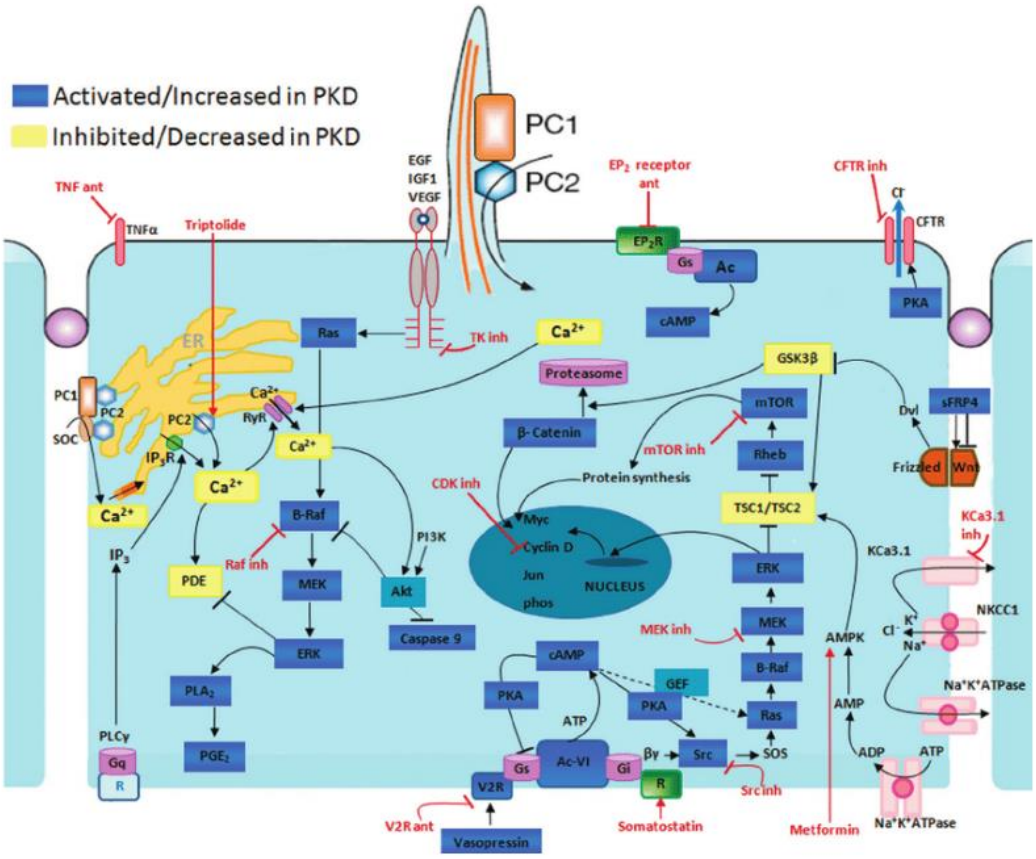

Figure 6. Altered pathways in ADPKD and potential therapeutic approaches. Agents with potential therapeutic approaches are represented in red; ant = antagonist; inh = inhibitor. Adenylate cyclase 6 (AC-VI); protein kinase B (AKT) ; AMP kinase (AMPK); v-raf murine sarcoma viral oncogene homolog B1 (B-raf); cyclin-dependent kinase (CDK); cystic fibrosis transmembrane conductance regulator (CFTR); epidermal growth factor (EGF); E-prostanoid receptor 2 (EP 2 R); extracellular signal-regulated protein kinase (ERK); glycogen synthase kinase 3 (GSK3); insulin-like growth factor 1 (IGF1); inositol 1,4,5- trisphosphate receptor (IP 3 R); mitogen-activated protein kinase (MAPK); mammalian target for rapamycin (mTOR); polycystin-1 (PC1); polycystin-2 (PC2); phosphodiesterase (PDE); prostaglandin E2 (PGE 2); phosphatidylinositol 3-kinase (PI3K); protein kinase A (PKA); phospholipase A2 (PLA 2); phospholipase C-γ2 (PLCγ); somatostatin sst2 receptor (R); ras homolog enriched in brain (Rheb); ryanodine receptor (RyR); secreted Frizzled-related protein 4 (sFRP4); tyrosine kinase (TK); tumor necro-sis factor-α (TNF-α); TSC = tuberous sclerosis proteins tuberin (TSC2) and hamartin (TSC1); vasopressin V2 receptor (V2R); vascular endothelial growth factor (VEGF). Image taken from Reiterová, J., Int. J. Mol. Sci, 2022 allowed by MDPI Open Access.

1.3.1.3.1 Polycystins and Ca^{2+} channel

Polycystins could be located in the endoplasmic reticulum. PC2, interacting with PC1, acts as a Ca^{2+} channel in the endoplasmic reticulum. C-terminus of PC2 also interacts with other calcium channels such as the inositol-3-phosphate receptor (IP3R) and can prolong IP3-dependent calcium release (78,79). Ca^{2+} is responsible for activating phosphodiesterase (PDE) that regulates the cAMP to AMP pathway and for inhibiting adenylate cyclase 6 (AC6) that regulates the ATP to cAMP pathway, thus controlling cAMP levels. Besides, this also activate the PI3K/Akt pathway, activated Akt can influence apoptosis, growth, proliferation, metabolism, angiogenesis, survival, protein synthesis and transcription (80). Activation of PI3K/Akt pathway may decrease the level of intracellular calcium, then PC2 is recruited to the plasma membrane where it forms complex with PC1 serving as an influx calcium channel (38,80).

1.3.1.3.2 Proliferation and apoptosis

In ADPKD, there is an increment both of cell proliferation and apoptosis. (81). Inactivation of *PKD1* and *PKD2* genes, decrease intracellular Ca^{2+} levels, leading to increased cAMP level (82). This increase of cAMP leads to an increase in protein kinase A (PKA) activity activating the MAPK/ERK pathway via Src and Ras/Raf/ERK, and this in turn activates the mTOR pathway (83). Both pathways activate the synthesis of proteins involved in the cell cycle and thus cell proliferation, leading to enlargement of cystic cells (53,82). In addition, the vasopressin 2 receptor (V2R) has been shown to be upregulated in PKD, which activates the formation of more cAMP via AC6 (79,84).

PC1 is responsible for inhibiting mTOR activity by modulating the TSC1/2 complex, so mutations in PC1 lead to an increase in mTOR (85). mTOR complex regulates cell growth and proliferation, together with actin cytoskeleton and apoptosis (38). On other hand, PC1 produces the resistance to apoptosis by activation PI3K by the interaction with the Carboxi-terminal tail (CTT) of PC1 to tuberin protecting the phosphorylation of Akt (38,80). Moreover, several PKD studies have shown increased activity of proteins with apoptotic activity as caspases and cytochrome c, as well as the *c-Myc* proto-oncogene and the *BCL-2* gene (86).

1.3.1.3.3 Altered fluid secretion

Increased fluid secretion is a factor in ADPKD cyst expansion and growth, which causes a dysregulation of the ion gradients that are present in normal renal nephrons. Unlike normal renal epithelium, where fluids are reabsorbed, in cystic epithelium they are secreted into the cyst lumen stimulated by cAMP. PKA, activated by cAMP, will phosphorylate the cystic fibrosis transmembrane conductance regulator (CFTR) channel, which facilitates Cl^- secretion (87). Also involved in secretion are the NKCC1 (Na^+-K^+-Cl^- cotransporter) channels that require K^+ efflux from KCa3.1 (activated by cAMP) to supply Cl^- to CFTR (88).

Reabsorption and passage of water across the epithelial plasma membrane in is mediated in part by aquaporins. PKA also phosphorylates Aquaporin-2 (AQP2) that goes to the apical membrane increasing water reabsorption and urine concentration (82).

1.3.1.3.4 Fibrosis and inflammation, role of extracellular matrix and epithelial-mesenchymal transition

Fibrosis is the accumulation of extracellular matrix (ECM) in the extracellular region of cells and it is a condition that tends to increase with cyst growth and progressive renal function decline (89). In advanced stages of the disease, large amounts of ECM (collagens, fibronectin, proteoglycans) are deposited between cysts throughout the enlarged kidney associated with interstitial inflammation (89).

One of the characteristics of fibrosis is the infiltration of inflammatory cells. Inflammation is one of the protective systems against foreign molecules, characteristic of the innate immune system response (89,90). Different studies showed that inflammatory pathways such as the JAK/STAT and NF-κB pathways were found to be activated in the disease (91). Phosphorylation of NF-κB by inflammatory cytokines (TNF-α, IL-1α and β, IL-6, Ccl3 y Ccl4) leads to its translocation to the nucleus to activate gene transcription (92,93). In the same way, some cytokines binding to their receptors activate JAK proteins, which phosphorylate STAT proteins leading to their translocation to the nucleus to activate gene transcription. The C-terminal tail of PC1 can amplify the signal of STAT proteins. This tail is upregulated in the presence of kidney damage or PKD, leading to increased expression of STAT proteins (94).

On the other hand, it has been observed that there is an increase in ECM proteins such as collagen (95); alterations in extracellular matrix turnover, which is carried out by matrix metalloproteinases (MMPs) and their inhibitors (TIMPs) (90); and an increase in proteins that act in cell-matrix interaction such as integrins and endothelial growth factor receptor (VEGFR) (89,96).

In PKD, there is an imbalance between cytokines and growth factors (90). Transforming growth factor beta (TGF-β) is considered the cytokine inducing the epithelial to mesenchymal transition (EMT) by phosphorylating SMAD2/3. SMAD2/3 inhibits GSK3β (glycogen synthase kinase 3 beta), which causes that SNAIL1 remains in the nucleus promoting the loss of epithelial markers, as E-caderin, and increasing mesenchymal markers, as collagen, fibronectin or vimentin (97).

1.3.1.3.5 Metabolism

Growing evidence of alterations in cell metabolism have been described in the past decade. ADPKD cells shift their mode of energy production from oxidative phosphorylation and fatty acid metabolism to alternative pathways, such as glycolysis (98–100). In addition, the polycystins seem to play regulatory roles in modulating mechanisms related to energy production and utilization, including AMP-activated protein kinase (AMPK) (101), PPARα (102), PPARγ co-activator 1 α (PGC1α), calcium signaling at mitochondria, mechanistic target of rapamycin complex 1 (mTORC1) (103), cAMP (104) and cystic fibrosis transmembrane conductance regulator (CFTR) as well as the expression of crucial components of the mitochondrial energy production apparatus (105). Moreover, new studies suggests that PC1 may link cell-matrix signaling to mitochondrial activity through the translocation of C-terminal cleavage product of PC1 (CTT) and play a direct role in regulating mitochondrial function and metabolism (106).

1.3.1.3.6 Role of cilia

PKD are cilia-related disorders or ciliopathies (107). All PC1 and PC2 proteins are localized, plus other cellular localizations, in apical and basal zones of primary cilium (15). The cilium seems to have a central role in cyst formation, deletion of the cilium leads to cyst formation (108). Surprisingly, in conditioned, cilia-deleted mice with mutations in the *Pkd1* or *Pkd2* genes, cyst growth has been shown to be reduced compared to models with mutations in only the *Pkd1* and *Pkd2* genes (109). Thus, cyst formation depends on the intact cilium when polycystins disappear (109,110) but cyst formation due to loss of the cilium is independent of polycystins (61).

1.3.1.3.7 Wnt signaling

The Wnt signaling pathway regulates essential biological functions. Wnt is implied in controlling proliferation, differentiation, motility, polarity, embryogenesis and organogenesis, among other (111). It is divided into two ways, the canonical Wnt/β-catenin pathway, and a β-catenin independent pathway that is responsible for planar cell polarity and tissue morphogenesis.

In the canonical pathway, Wnt binds to the Frizzled (Fz) receptor in the presence of low-density lipoprotein (LDL) receptor 5 or 6 (LRP5/6) and activates Dishevelled (Dvl) thereby inhibiting β-catenin proteolysis. Thus, it accumulates in the cytosol together with T cell factor (TCF) and translocate to the nucleus to transcriptionally activate Wnt genes (112,113). Carboxy-terminal part of PC1 inhibits the interaction between β-catenin and TCF. The

canonical Wnt pathway is activated in ADPKD patients. PC1 could affect the cystogenesis during embryogenesis by the influence on Wnt canonical pathway (38).

Noncanonical Wnt pathway plays role in determination of planar cellular polarity (PCP) and motility. In the non-canonical pathway, Wnt also binds to the Fz receptor and activates Dvl. Dvl regulates cytoskeleton rearrangement by activating RhoA (activates ROCK), Rac1 (activates JNK) or profilin. Proteins of the main PCP pathway are important in signal transduction where loss of PCP is frequently observed in cystic cells. By other hand, activation of the non- canonical pathway leads to an increase of Ca^{2+}. This pathway following with G-protein-dependent activation of phospholipase C. Wnt can bind to the extracellular domain of PC1 which leads whole cell currents and Ca^{2+} influx dependent on PC2 (38,114).

1.3.1.4 Therapies for ADPKD

The principal aim of the current PKD therapies is to reduce symptoms because there is no approved specific therapy. Although, some important advances have centered on reducing the growth of the cysts and slow the decline of kidney function. However, there is currently no effective treatment for ADPKD, only drugs that slow the progression of the disease, and finally renal replacement therapy (RRT) by dialysis or transplantation is the unique option. General recommendations in ADPKD are healthy diet and lifestyle, cardiovascular exercise and avoid smocking, with an strict control of hypertension (38)

Increasing knowledge of the pathophysiology of the ADPKD has laid the development of new potential therapeutic targets (Figure 6). Unfortunately, many of these therapeutic targets are involved not only in cyst formation, but also in numerous canonical physiological processes through the body that are important for cellular proliferation, growth, and repair, so drugs to these targets often present severe adverse effects that limit their utility or even these therapies could be very effective in animal models, but clinical studies reject them because of systemic adverse effects and toxicity (115). Some of the potential treatments being studied focus on inhibiting the increase in cAMP, and thus the growth of cysts, or act on the different pathways with which cAMP interacts. The unique approved therapy is Tolvaptan (Jinarc®), a selective vasopressin type 2 receptor (V2R) antagonist. It is based on the role of arginine vasopressin-mediated cAMP as a driver of fluid secretion. Tolvaptan reduces the increase in kidney volume in the 3-year study period, and also slows the decline in kidney function (38,116). In contrast, Tolvaptan presents secondary effects as polyuria, nycturia, thirst and polydipsia (115), as well as hepatotoxicity (117). Nowadays, Tolvaptan therapy is only recommended to ADPKD adult patients with rapid progression of the disease (38).

Another of the most advanced possible treatments is the use of somatostatin analogues, that binds to G protein-coupled receptors and inhibits intracellular cAMP production in liver and kidney. Although, there is no currently evidence that somatostatin analogues should be used in patients with polycystic renal disease, because the decline of the eGFR is not deaccelerated. However, they should come into account in patients with high volume polycystic liver to put off liver transplantation (38,115).

Other therapies that are under preclinical and clinical trials by targeting the following objectives (Figure 6) (38,115):

- cAMP pathway as Lixivaptan, a selective V2R antagonist with lower secondary effects than Tolvaptan

USC UNIVERSIDADE DE SANTIAGO DE COMPOSTELA

- CFTR and potassium channels
- Chloride channel TMEM16A by inhibitors
- EGF receptor pathway as Tasevatinib, a multikinase inhibitor
- AMP- Activator Protein Kinase as Metformin, that activates AMPK and inhibits CFTR by phosphorylation, or Statins
- MAPK Pathway-Raf Kinase by inhibitors as Sorafenib, another multi-kinase inhibitor.
- Dietary interventions and caloric restriction
- Metabolism with 2-Deoxyglucose, an inhibitor of the glycolytic pathway
- mTOR inhibitors
- Intracellular calcium and cell cycle regulation with calcimimetics or Cyclin Dependent Kinases inhibitors
- microRNA blockers as inhibitors of miR-17, miR-192 and miR-194

Deeper knowledge of the pathophysiology of ADPKD will hopefully bring new treatments to prevent the need for kidney replacement therapy in ADPKD patients.

1.3.1.5 Diagnosis of ADPKD

The diagnosis of ADPKD depends on the stage of the disease (35). First clinical manifestations are early-onset hypertension, abdominal pain, haematuria or urinary tract infections (15). When the disease is fully established, the diagnosis is based on the patient's history and physical examination, from a clinical point of view (16,118). However, providing a definitive diagnosis can be difficult as the disease can be mistaken with other diseases with similar symptoms. Therefore, other complementary tests are necessary, such as imaging or genetic tests (15).

Presymptomatic diagnosis usually is done in risk family members by abdominal imaging and the presence of bilateral cyst means affection of the disease. Ultrasonography is the most used imaging method due to its price, but computerized tomography (CT) and Magnetic Resonance Imaging (MRI) are more sensible, accurate and provide essential information for prognosis (15,119).

The problem with imaging techniques is that they are not sensitive enough for patients younger than 30 years where the cysts are smaller, or for patients with a family history of mild disease. Therefore, detection of mutations in these genes by genetic testing is the most appropriate diagnostic test (120). It has been described that the disease-causing mutation may be interacting with other PKD or ciliopathy genes modifying the phenotype and increasing the genetic complexity of the disease (35). For this reason, next-generation sequencing techniques are being used that allow the study of several genes simultaneously (121).

1.3.1.6 Prognosis and End-Stage Renal Disease in ADPKD

In ADPKD patients monitoring the renal functional decline using eGFR in standard practice, however predicting the rate of progression to ESRD remains a major clinical problem due to high clinical variability of ADPKD (34,37,122). The current state-of-art of assessment of prognosis is based in two approaches: genetic testing and measurement of total kidney volume.

USC UNIVERSIDADE DE SANTIAGO DE COMPOSTELA

On the other hand, genotype-phenotype correlation demonstrated that the gene and the type of mutation are key factors in the variability of ADPKD. Patients with mutations in *PKD1* present more rapid progression than those patients with mutations in *PKD2* (40,46,69). Moreover, the type of mutation is also critical where patients with *PKD1* truncated mutations are associated with worse renal prognosis than those with *PKD1* non-truncating mutations (46,69). Taking into account these predictive genetic factors with clinical information, a prognostic algorithm, the Predicting Renal Outcomes in Polycystic Kidney Disease (PROPKD) provides a stratification of risk in decline eGFR and progression to ESRD (34,45). However, this algorithm although is very specific has limited sensitivity (119)

On the other hand, the total kidney volume increases throughout the disease whereas a stable or slowly declining eGFR is caused by the hyperfiltration of surviving nephrons (123). The measurement of height-adjusted total kidney volume (htTKV) by MRI could predict of eGFR decline (124). However, this measurement by segmentation is not yet part of clinical routine.

These parameters, monitoring of serum creatinine, genotype-phenotype correlation and htTKV do not predict future changes in disease prognosis. The identification of new marker that could predict whether patients have a rapid or slower functional decline to ESRD, would allow for more accurate prognosis and offer a significant increase in quality of life for patients and family members (125). Besides, it would provide the time for treatment to slow disease progression and might measure efficacy of response to treatments. One opportunity may be through characterization of proteomic profiling of urinary Extracellular Vesicles, as urine provides a readily available source of biofluids and cell-derived particles. Additionally to preliminary results from our research group that have shown that Extracellular Vesicles play an important role in the course of the disease, which would make them an attractive resource for the search for biomarkers, even with the development by our laboratory of a new method of isolating them (patent registration WO 2017/042416 A1).

USC
UNIVERSIDADE DE SANTIAGO DE COMPOSTELA

1.4 EXTRACELLULAR VESICLES

Extracellular Vesicles (EVs) comprise a heterogeneous group of structures delimited by a lipidic bilayer released by cells and cannot replicate (126). They are secreted by most cell types, and therefore, they are present in all biological fluids. EVs have presented multipurpose physiological functions and are involved in the regulation of main routes of signaling and intercellular communication (127).

EVs could be classified according to their size and biogenesis in 3 main groups (Figure 7): exosomes, microvesicles and apoptotic bodies. Exosomes are the smallest population of EVs (measuring around 50-150 nm) and are released after fusion of multivesicular bodies (MVBs) with the plasma membrane (128). Microvesicles are a group of vesicular structures between 50-1000 nm that are generated by outward budding and fission of the plasma membrane and released into the extracellular space (129). And apoptotic bodies are the largest EVs with a size between 100nm to 5000nm that are released when plasma membrane blebbing occurs during apoptosis (127,130)

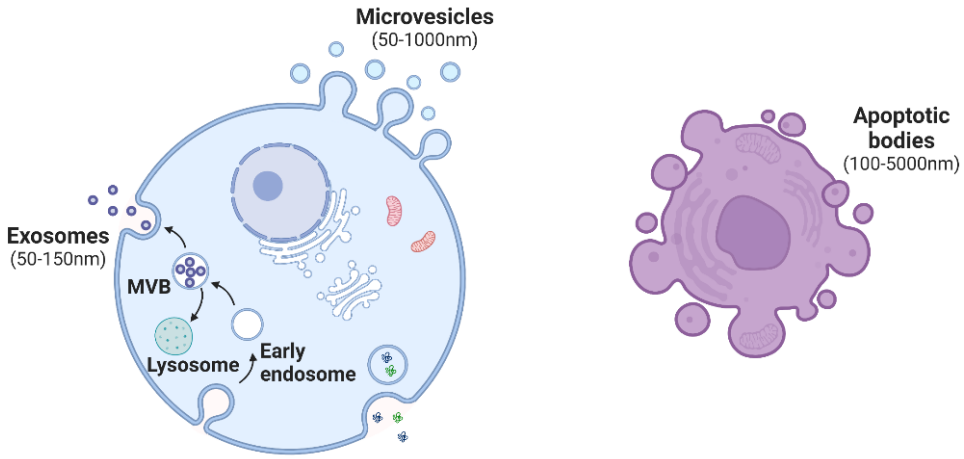

Figure 7. Biogenesis and release of Extracellular Vesicles. Exosomes are formed from the endosomal membrane invagination causing the formation of the early endosomes and then multivesicular bodies (MVB). The vesicles that reside in the MVBs fuse with the lysosome to degradation or fuse with the plasma membrane and release. Microvesicles are generated by evagination and direct fission of the plasma membrane and released into the extracellular space. Apoptotic bodies are released by blister generation during programmed cell death. This figure was made using Biorender.

However, since consensus among experts on the study of EVs on specific markers of EV subtype of particular biogenesis pathway remains difficult, change of classification of EVs urged. The following classification of EV subtypes is proposed by the International Society of Extracellular Vesicles that refer to: a) physical characteristics, such as size being “small EVs” < 200nm and “medium/large EVs” > 200nm, b) biochemical composition (CD63+/CD81+-EVs, Annexin A5-stained EVs, etc.); or c) descriptions of conditions or cell of origin as podocyte EVs, large oncosomes or apoptotic bodies (126).

1.4.1 Biogenesis of EV

Even though, exosomes and microvesicles have different processes of biogenesis at distinct sites in the cell, common intracellular mechanisms are involved in both entities’ biogenesis (Figure 7).

1.4.1.1 Biogenesis of exosomes

For the generation of exosomes, first of all an invagination of the plasma membrane is needed, forming a cup-shaped structure called the early endosome, with the contribution the trans-Golgi network. Early endosomes mature into late endosomes, and during this process accumulate intraluminal vesicles (IVs) in their lumen becoming into what is known as multivesicular endosome or body (MVBs) (128,131). The IVs that are formed by invagination into the early endosomal membrane sequester proteins and lipids that are specifically stored in the early endosomal membrane (132) (Figure 8). Finally, MVBs can fuse with lysosomes to be degraded or with the plasma membrane releasing the exosomes (128,131).

It has been shown that the formation of MVBs and ILVs may be mediated by the endosomal sorting complex required for transport (ESCRT) (Figure 8). This complex is a machinery composed of four separate ESCRT proteins (0, I, II and III) and accessory proteins such as ALIX and TSG101 that assist to facilitate the formation of MVBs (133). The ESCRT mechanism is initiated by the recognition of ubiquitinated proteins on the endosomal membrane through the ubiquitin-binding subunits of ESCRT-0. ESCRT-I and -II complexes are responsible for membrane deformation and then, interact with ESCRT-III, a complex involved in vesicle scission. After scission, the ESCRT-III complex is cleaved from the membrane of the MVBs by the vacuolar protein sorting-associated protein 4 (Vps4) (134,135).

Apart from this pathway dependent on the 4 ESCRT complexes, ESCRT-independent pathways of exosome biogenesis have been suggested (Figure 8). One of these pathways is ESCRT-III dependent through the interaction of the syndecan-syntenin complex with ALIX in the cytoplasm, an interaction that is involved in the recruitment of vesicular cargo and could directly recruit ESCRT-III (128,132,133,136,137). Moreover, there are other pathways of EVs biogenesis suggested completely ESCRT-independent through lipid and tetraspanin-dependent mechanisms. In this case, the main mediators of the biogenesis process are lipids such as ceramide, or tetraspanins such as CD63, CD81, CD82 or CD9. Thus, on the one hand, the key role of putative neutral sphingomyelinase (nSMase), which hydrolyze sphingomyelin into ceramide, and phospholipase D2, which allows hydrolysis of phosphatidylcholine into phosphatidic acid, has been demonstrated (137,138). Furthermore, tetraspanin CD63 was shown to be required for the formation of LVs and subsequent release of extracellular vesicles by ESCRT-independent invagination of the melanosome membrane (139).

The transport of MVBs to the plasma membrane for fusion and release of exosomes is like other intracellular vesicle transport mechanisms involving their interaction with the cytoskeleton and with different GTPases such as Rab family (Rab27a, Rab27b, Rab 35 and Rab11) (140,141) (Figure 9). The final step of exosome secretion is the fusion of MVBs with the plasma membrane, directed by several proteins including the Rab, Alix, TSG101 or the soluble N-ethylmaleimide-sensitive fusion attachment protein receptor (SNARE) to make the protein complex. The SNARE complex leads membrane fusion and exosome secretion. The accumulated MVBs are coupled to the plasma membrane via the trans-SNARE complex, consisting of V-SNAREs and T-SNAREs on endosomes and plasma membranes, respectively, leading to the release of exosomes into the extracellular environment (134,142) (Figure 9).

USC UNIVERSIDADE DE SANTIAGO DE COMPOSTELA

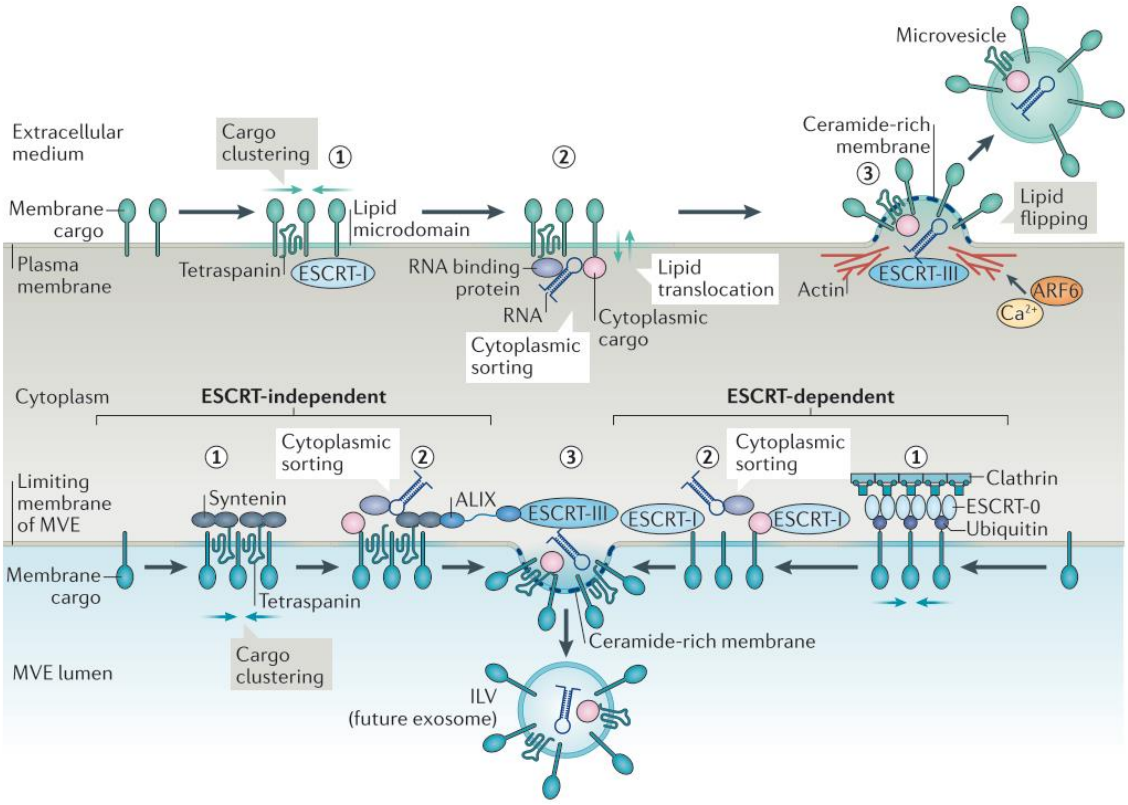

Figure 8. Biogenesis of Extracellular Vesicles. Image of biogenesis of Microvesicles and Exosomes. ESCRT-independent and some ESCRT-dependent pathways for exosome biogenesis are represented. Several sorting machineries are involved in the different steps: 1, lipids and membrane-associated proteins are clustered in discrete membrane microdomains; 2, these microdomains also participate in the recruitment of soluble components, such as cytosolic proteins and RNA species; 3 these clustered microdomains in cooperation with additional machineries encourages membrane budding and fission of the plasma membrane to the extracellular medium or the membrane of MVE towards the lumen of it. Transmembrane proteins sorted on exosomes and microvesicles keep the same topology as at the plasma membrane. ESCRT: endosomal sorting complex required for transport, ALIX: ALG-2 interacting protein X; ARF6: ADP-ribosylation factor 6, ILV: intraluminal Vesicle, MVE: multivesicular body. Image taken from Van Niel, G., Nature Reviews Molecular Cell Biology, 2018 allowed by Springer Nature.

1.4.1.2 Biogenesis of microvesicles

Microvesicles or ectosomes are originated from direct plasma membrane budding and fission (Figure 8 and Figure 9). (143). Notably, the molecular machineries of biogenesis are partly common to exosomes and microvesicles, including ESCRT proteins and the generation of ceramide (128), except for specific lipid species flipping between the faces of the budding membrane, which has been uniquely reported for microvesicle budding. The biogenesis of microvesicles requires molecular rearrangements in the plasma membrane, as changes in lipid components and protein composition as well as in Ca^{2+} levels. The asymmetry of lipid component is tightly regulated by the Ca^{2+} aminophospholipid translocases, as flippases that translocate phospholipids from the outside of the membrane to the inside, while flopases transfer phospholipids from the inside to the outside (128,144,145). The formation of these vesicles from the membrane is induced by the translocation of phosphatidylserine to the outer membrane; and this process is completed by the contraction of cytoskeletal structures through interactions between actin and myosin (144,146) (Figure 8 and Figure 9).

USC UNIVERSIDADE DE SANTIAGO DE COMPOSTELA

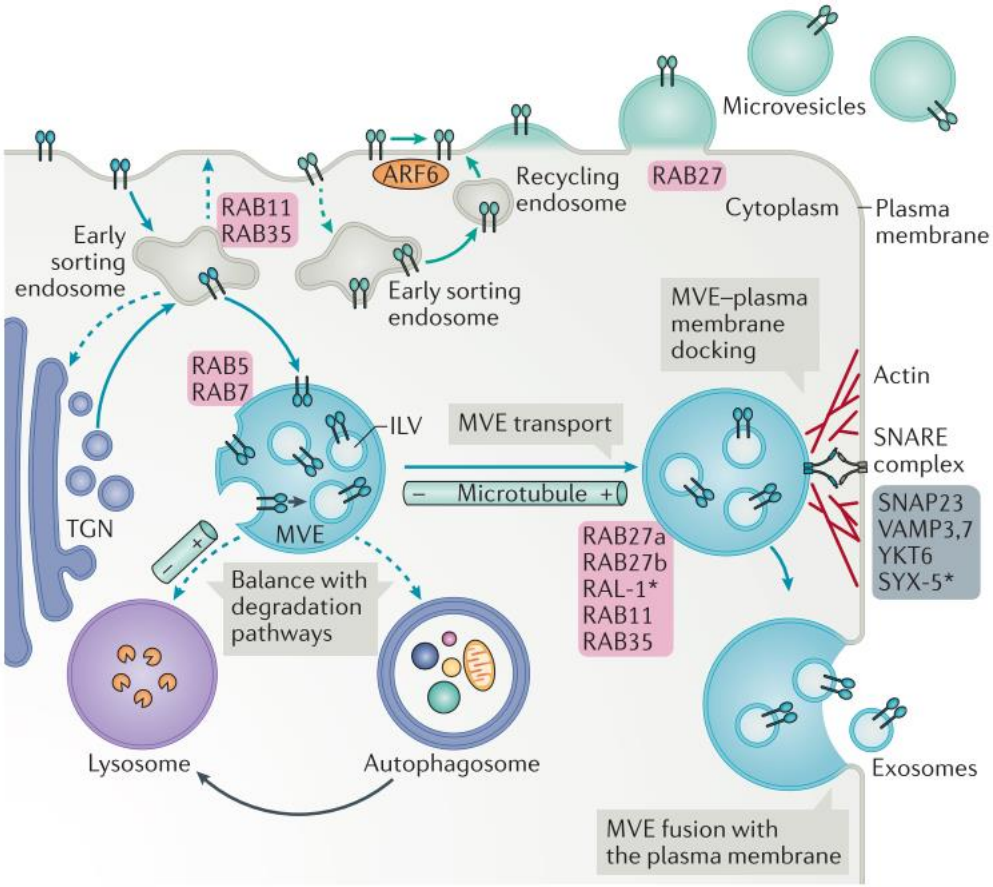

Figure 9. Intracellular trafficking routes in the biogenesis of Extracellular Vesicles. Cargoes are targeted to MVEs originate from endocytosis at the plasma membrane. Regressive transport towards the trans-Golgi network or recycling back to the plasma membrane will redirect cargoes from their targeting to the MVE. These processes are regulated by RAS-related protein (RAB) GTPases. MVEs that do not go to lysosomes or autophagosomes for degradation are transported along microtubules to the plasma membrane. At this step, docking and fusion are the two final processes required for exosome release that are mediated by RABs, actin and SNARE. ARF6: ADP-ribosylation factor 6; RAL-1: RAL (Ras-related GTPase) homolog; SNAP23: synaptosomal-associated protein 23; SYX-5: syntaxin 5; VAMP3: vesicle-associated membrane protein 3. Image taken from Van Niel, G., Nature Reviews Molecular Cell Biology, 2018 allowed by Springer Nature.

1.4.2 Composition of EV

The cargo of EVs is cell type specific and are often affected by the physiological or pathological state of the cell (147–149). This EV cargo is targeted during EV biogenesis, can include many components of a cell, such as DNA, RNA, lipids, metabolites, and cytosolic and cell surface proteins (Figure 10). Most studies on the biochemical composition of EVs involve the analysis of heterogeneous EVs populations due to the difficulties of different isolation methods to obtain pure vesicle subtypes. Therefore, the actual composition of each EV subtype is generally unknown (134,150). Studies on the composition of EVs have led to the creation of public databases that catalogue the components associated with EVs. These include Vesiclepedia (www.microvesicles.org/) (151), ExoCarta (www.exocarta.org) (152), EVAtlas (http://bioinfo.life.hust.edu.cn/EVAtlas/#/) (153) and EV track (https://evtrack.org/index.php) (154).

USC UNIVERSIDADE DE SANTIAGO DE COMPOSTELA

1.4.2.1 Proteins

The protein content of EVs has been studied extensively since they were described. Techniques allowing antibody-based detection of specific proteins as western blotting or immuno-Electron microscopy were first used, but the development of large-scale identification by proteomic analysis techniques allowed discovery of nonpredetermined proteins in EV preparations (134).

EVs are enriched in plasma membrane proteins as adhesion molecules, antigen presentation, membrane transport and glycoproteins as well as lumen proteins formed by cytoskeletal, cytosolic, signal transduction and proteins involved in vesicle trafficking and biogenesis and glycoproteins (134,155) (Figure 10). However, although protein profiles may be characteristic of different EV subgroups, there is no single marker that can uniquely identify EVs.

Among the proteins enriched in EVs, and often used as identification markers, are tetraspanins (CD9, CD63 and CD81), 14-3-3 proteins, major histocompatibility complex (MHC), heat shock proteins such as HSP70 or HSP90, TSG101, syntenin-1 and the ESCRT-III binding protein ALIX (156). The tetraspanins CD9, CD63 and CD81 were initially considered to be exosome-specific markers. However, it has been shown that these proteins are also abundantly expressed on the cell surface and are therefore present in other types of EVs that are generated by direct plasma membrane budding and do not have an endocytic origin (157).

A refinement of analysis and purification techniques in these years should allow us to clarify the protein composition of each EV type, which is certainly important to further understand their function.

1.4.2.2 Nucleic acids

Also, a diverse composition of genetic material is found in EVs. In some cases, DNA has been found, in genomic and mitochondrial DNA forms (133,158). On the other hand, EVs are mainly enriched with mRNAs and other RNAs as microRNAs, small RNAs, long-chain non-coding RNAs (lncRNAs), nuclear small RNAs (snRNAs), ribosomic RNA (RNAr) or transfer RNA (RNAt) (134,159). Different studies show that microRNAs play an important role in target cell gene regulation and in various biological processes as well as it has been described as a possible disease biomarker (134,160,161).

1.4.2.3 Lipids

Few studies have analyzed the lipid composition of EVs, but they have been found to reflect the plasma membrane lipid profile of the cell of origin. (134). However, an enrichment in glycosphingolipids, ceramide, sphingomyelin, cholesterol, and phosphatidylserine, which play important roles in the formation of EVs, has also been described (162) (Figure 10).

USC
UNIVERSIDADE DE SANTIAGO DE COMPOSTELA

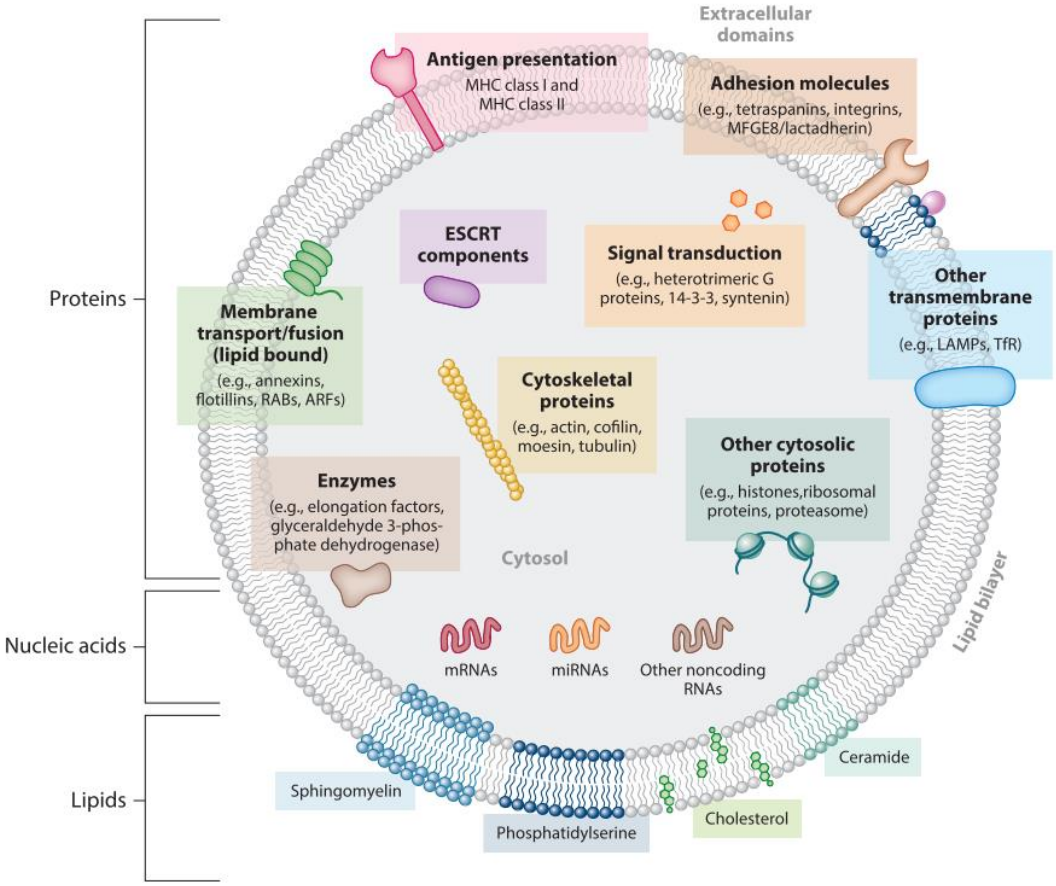

Figure 10. Overall composition of Extracellular Vesicles. Schematic representation of the composition and membrane orientation of EVs. ARF, ADP ribosylation factor; ESCRT, endosomal sorting complex required for transport; LAMP, lysosome-associated membrane protein; MHC, major histocompatibility complex; MFGE8, milk fat globule-epidermal growth factor-factor VIII; RAB, Ras-related proteins in brain; TfR, transferrin receptor. Image taken from Colombo, M. Annual Review of Cell and Developmental Biology, 2014 allowed by Annual Reviews.

1.4.3 EV-mediated intercellular communication

Once released into the extracellular space, EVs could reach recipient cells and deliver their contents to produce functional responses that will affect their physiological or pathological status (163). First, EVs mediated intercellular communication requires docking at the plasma membrane of the recipient cell. The mode of EV interaction and transfer of the cargo could be by activation of surface receptors and signaling, vesicle internalization or their fusion with target cells (128). The main interaction of EVs with recipient cells is depicted in Figure 11. This process is complex and dependent of EV origin and type of the recipient cell.

Target cell specificity is likely to be determined by specific interactions between surface EV and receptors at the plasma membrane of the recipient cells (164–166). Numerous intermediaries of these interactions are known, including tetraspanins (167), integrins (166), intercellular adhesion molecules (ICAMs) (168), lectins, proteoglycans and extracellular matrix (ECM) components (128) (Figure 11).

Once they have bound to recipient cells, EVs may be internalized by clathrin-mediated or clathrin-independent endocytosis, such as macropinocytosis and phagocytosis (169,170) as well

as through endocytosis via caveolae and lipid rafts (126) (Figure 11). The fate of EVs is also related to the presence of specific structures at the plasma membrane of the target cell. One feature that contributes to EV internalization is the lipid composition of the plasma membrane of recipient cells, for example, the disruption of lipid raft by cholesterol depletion reduces uptake of EVs (171).

After uptake, EVs could follow the endocytic pathway and reach MVBs, which, in most cases, are directed to digestion by lysosomal pathway (172). In some cases, EVs may escape degradation by fusion with the membrane of the MVB and releasing their contents into the cytoplasm (128).

Once the vesicular cargo is internalized and is not destined for degradation, information transfer take place. Several studies have shown that the interaction of EVs with target cells can activate various responses and processes, such as immune response (164) or gene expression (173) regulation.

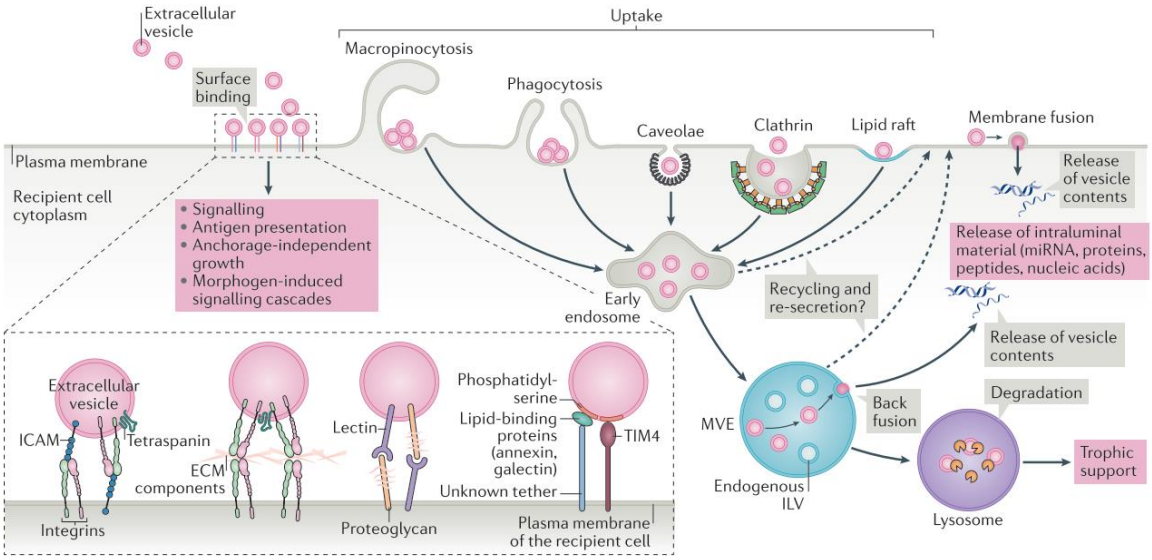

Figure 11. Interaction of extracellular vesicles in recipient cells. In the recipient cell, EVs will bind to the cell surface and can undergo various fates. Depending on the cell type, they can remain bound to the surface and can begin intracellular signaling pathways. EVs may also be internalized by multiple pathways as the canonical endosomal pathway, whereby they reach multivesicular endosomes (MVEs), in which the internalized vesicles are likely to mix with endogenous intraluminal vesicles (ILVs). Fusion of vesicles and the recycling of their contents to fuel the metabolism of the recipient cell. Extracellular vesicles docked at the plasma membrane can release their intraluminal contents into the cytoplasm. ECM: extracellular matrix; ICAM: intercellular adhesion molecule; TIM4: T cell immunoglobulin mucin receptor 4. Image taken from Van Niel, G., Nature Reviews Molecular Cell Biology, 2018 allowed by Springer Nature.

1.4.4 Biological roles of EVs and its applications

EVs are involved in several physiological contexts and pathological states, including blood coagulation, inflammation, neuronal transmission and tumorigenesis (174). In this context, several studies on the biological role of EVs in various human pathologies have emerged that EV hold great potential for clinical application. One of these functions is related to their ability to interact with target cells and release their contents into these cells, which gives EVs an important functional role in cellular communication and targeted delivery as therapeutic

vehicles (131). In addition to this role in cellular communication, EVs have emerged as a new diagnostic and prognostic avenue in the arrest and monitoring of diseases (175).

The increasing interest in EVs composition has also exposed the possibility to use them as biomarkers to follow the progression of various pathological states. For example, for tumor and metastasis progression or for neurodegenerative diseases (176). The development of techniques to enrich this disease EVs to define their selective cargo can improve the sensitivity to search such biomarkers (177). The main biological fluids in which circulating EVs have been identified are blood (plasma or serum), urine, saliva, milk, amniotic and cerebrospinal fluid, tears, among others (134). In addition, EVs, unlike other classical biomarkers, allow a minimally invasive analysis, without the need for biopsies, allowing sequential sampling too (175,178).

Another emerging application is the use of EVs as vectors for the delivery of defined compounds to modulate cell functions in an *in vivo* context. EVs present the advantages that are biocompatible, can be immunologically inert and could be patient-derived (128). Several clinical trials are ongoing to test the therapeutic potential of EVs in the immunotherapy-based treatment of lung cancer and melanoma (179). Other assays are based on EVs manipulation to load in this vesicles a particular cargo such as mRNAs, miRNAs, proteins or drugs in order to specifically target to a cell of interest (131,180).

1.4.5 Isolation techniques

There are a wide variety of EV isolation techniques that rely on physical and molecular properties as density, size, charge and surface proteins of EVs to facilitate their purification. However, nowadays, the great challenge surrounding EVs is to find a gold-standard method that will be feasible, accurate and reliable to analyze EVs for research and clinical applications (181). In this thesis, we will discuss the main used methods (Figure 12)

1.4.5.1 Ultracentrifugation

Ultracentrifugation (UC) (Figure 12A and B) is the most widely used technique for EV isolation and is based on sedimentation of solutes at high centrifugation force (126). There is no unique protocol for UC and they use different rotor types, washing steps, centrifugal forces and times and all of this may influence the yield and purity of the isolated vesicles (182,183). In general term, the established consensus is to perform a first 400-2,000×g centrifugation to remove cells and cell debris, followed by an optional centrifugation at 10,000-12,000×g to obtain larger vesicles. After that, another UC is performed at 100,000×g for a range of 70-90 min to obtain a pellet of EVs that can be resuspended, washed and centrifuged again at 100,000×g (184). The advantages of this method are that it is a simple and relatively low-cost procedure. Nonetheless, it is a low recovery method because added rounds of UC yield extra amounts of EVs (185). Other disadvantage is that centrifugation at such high speeds could lead to aggregation and co-precipitation of soluble proteins which would decrease the purity of the EVs obtained or even the rupture or fusion of EVs (186). In addition, the high disadvantages of this technique are that the results obtained depend on the type of biological material, the specific type of rotor and the centrifugation time, which makes comparisons between different experiments difficult (187).

A variation of this isolation method is the density gradient UC (Figure 12B), which is used to increase the separation efficiency of the particles according to their flotation density. Gradient ultracentrifugation is based on the size and density of the vesicles. The most used

solvents are sucrose and iodixanol. This type of technique allows isolation of EVs with higher purity than differential ultracentrifugation, avoiding contaminating proteins. However, both ultracentrifugation methods remains difficult to transfer to clinical practice due to the time required for EV isolation and the need for specific equipment, such as the ultracentrifuge (181,188).

1.4.5.2 Ultrafiltration

Another popular technique for EV isolation based on particle size is ultrafiltration (UF) (Figure 12C). The purpose is the separation of particles on the basis of their size or molecular weight (189). UF uses membranes with a defined molecular weight ranging from 10 to 100 kDa (kiloDaltons). This technique is mostly used to isolate EVs from relatively dilute samples, such as urine and cell cultures; or concentrating EVs that have been isolated by other methods such as UC or Size Exclusion Chromatography (190,191). The range of particles passing through a given pore size does not allow fractionation of the different types of EVs or ensure separation of contaminating proteins, and the membrane pores may even become clogged. Nevertheless, it is a fast and easy method to isolate EVs compared to UC (191).

1.4.5.3 Size Exclusion Chromatography

Size Exclusion Chromatography (SEC) technique has become popular in recent years. The principle of this type of liquid chromatography, SEC, is the separation of particles in solution according to their molecular size or hydrodynamic radius (Figure 12D). The isolation of EVs using this technique is based on the differential elution profiles of particles of different sizes passing through a porous polymer, which constitutes the stationary phase (also known as gel filtration matrix or resin), and which passes through the mobile phase of the SEC column. Small particles are slowed down as they enter the polymer pores, so they elute later than larger particles. In contrast, larger molecules will have less access to the internal pore volume than smaller molecules and therefore elute earlier. The advantages of this technique are that it is fast and does not damage the integrity of EVs. However, while SEC has been effective in removing most HDL and relatively small proteins from plasma, its major drawback is the co-isolation of other lipoproteins which share the same size range as EVs (192). In addition, it was observed that SEC isolated relatively smaller EVs than those obtained by UC, resulting in different proteomes. To overcome some of the limitations of SEC and to improve the purity of the isolated EVs, some studies have combined the use of this methodology with other techniques such as UC and UF (193), which would slow down the isolation process.

1.4.5.4 Asymmetrical Flow Field-Flow Fractionation

Field flow fractionation (FFF) is an emerging size-based technique for the separation of EVs. Asymmetrical Flow Field-Flow Fractionation (AF4) is the most widely used FFF-derived technique where the separation of macromolecules is based on their diffusion coefficients (Figure 12E). The laminar flow profile transports the EVs from the channel to the detectors. Size-based fractionation is achieved by a cross-flow transverse to a laminar flow profile that separates the EVs based on their size at the accumulation wall (194). The crossflow can be modified and optimized even between runs to improve separation efficiency, which makes this system more flexible compared to SEC. One of the advantages of AF4 for the separation of EVs is the gentle fractionation, so that the particles do not deteriorate. However, EVs obtained by AF4 are diluted and may require an extra pre-concentration step before further studies (181).

USC DE SANTIAGO DE COMPOSTELA

1.4.5.5 Precipitation based

Precipitation techniques can also be used for the isolation of EVs because they separate vesicles from other compounds based on their solubility. Most of these systems are based on the use of exclusion polymers such as PEG (polyethylene glycol) (Figure 12F). The recovery of EVs with these methods can be high, but without much purity, as they precipitate all soluble particles present in the starting sample. Several commercial kits based on precipitation agents are available as ExoQuick® (System Biosciences), ExoPrep® (HansaBioMed), miRCURY Exosome Isolation Kit (Exiqon) and ExoGAG®(195) (discovered and registered by our laboratory -WO 2017/042416 A1- and marketed by NasasBiotech). The EV isolation procedure with these technologies is simple, fast and scalable and does not require additional equipment for isolation, which makes this method very attractive for clinical research. However, its main disadvantages are the variable contamination of the sample with protein and lipoprotein complexes, as well as viral and other particles, which means that the isolated EVs are not pure; and the difficulty of separate the polymers from the sample (196).

1.4.5.6 Immunoaffinity

Affinity-based isolation methods use selective and specific interactions between proteins or receptors on the EV membrane and their corresponding ligands, such as antibodies. To develop an affinity-based isolation technique, ligands are immobilized or conjugated on a variety of solid media, such as magnetic beads or polymeric materials (agarose beads) (Figure 12G). The most commonly used antibodies target tetraspanins proteins commonly enriched on the surfaces of EVs, such as CD9, CD63 and CD81, alone or in combination (197). One of the main advantages of immunoaffinity, besides the selective isolation of EVs in general, is the possibility to isolate EVs from different cell types. This method is simple and fast. However, a highly specific antibody is needed, and this marker must be as stable as possible in different physiological situations because EVs are highly dynamic. In addition, a pan-EV marker has not been found yet, so the EV preparations obtained in this case are always a biased EV subpopulation expressing the marker(s) used for isolation (181).

As developed in this section, multiple techniques for EV isolation and purification are available. However, none of these technologies could be easily implemented in clinical routine due to disadvantages that present each one. This highlights the importance of finding a simple and efficient technology for EV isolation that will be easily transferable to clinical practice.

USC UNIVERSIDADE DE SANTIAGO DE COMPOSTELA

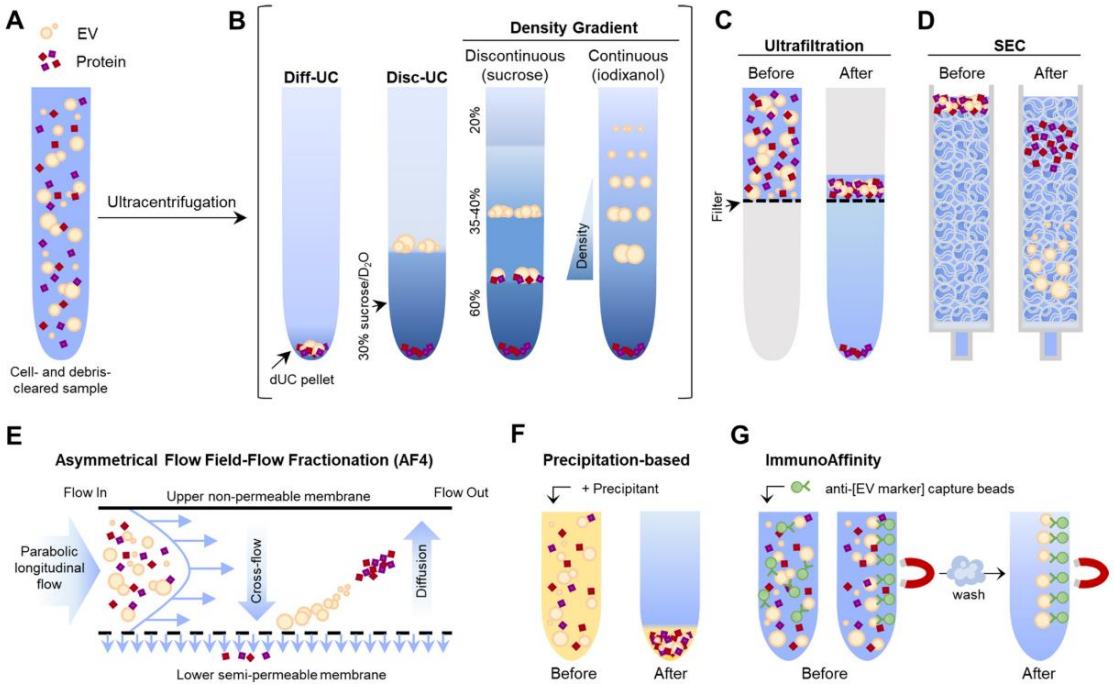

Figure 12. Graphical summary of mainly used EV isolation methods. A) The starting containing EVs and proteins in suspension. B) Ultracentrifugation renders an EV pellet that also contains proteins (dUC pellet), which can be further purified by discontinuous ultracentrifugation (disc-UC), like in sucrose, or by density gradient (DG) ultracentrifugation to separate EVs by their density. Ultrafiltration (C), size-exclusion chroma- tography (SEC; D) and asymmetrical flow filed-flow fractionation (AF4; E) separate molecules by their size. C) Ultrafiltration allows the separation of molecules according to the molecular weight cutoff (size) of the filter pore used. D) In SEC, the first to elute are the molecules bigger than the matrix pores (EVs), while smaller particles within the fractionation range (proteins) get slowed down by entering the matrix bead pores and so elute later on. E) In AF4, a cross-flow (field) perpendicular to the longitudinal laminar flow forces particles towards the semipermeable membrane. F) Precipitation-based isolation relies on the addition of precipitants to concentrate all particles in one pellet. G) Immunoaffinity isolation is based on EV capture using a specific antibody that recognizes an EV-specific marker, coupled to beads that can be separated by centrifugation or magnetically. Image taken from Monguió-Tortajada, M., Cellular and Molecular Life Science, 2019 allowed by Springer Nature.

1.4.6 Characterization of EV

Once the EVs have been isolated, it is important to evaluate and confirm the EVs isolated by the method used to isolate these particles. To do that, The International Society for Extracellular Vesicles (ISEV) recommends that the EV sample could be characterized by three criteria: quantitative measure of the source from which the EVs are obtained (number of secreting cells, volume of biofluid used, etc.); abundance of VEs in the sample (total number of particles and/or protein or lipid content) and presence of VE-associated components and co-isolated non-vesicular components (126).

Particle number can be determined using light scattering technologies, such as nanoparticle tracking analysis (NTA), which measures particle concentration and size based on their Brownian motion (198); by flow cytometry (199), by transmission electron microscopy (TEM) or cryo-ME (200) or by surface plasmon resonance (SPR) (201), among others. Something to have in mind is that particle quantification using light scattering systems, SPR, and similar techniques often leads to an overestimation of the number of VEs, as these techniques are not specific for VEs and also detect co-isolated particles, including lipoproteins and other protein aggregates (202).

Regarding the characterization based on the detection of markers associated with EVs, it has been described that the protein composition differs in the different subtypes of EVs obtained depending on the isolation method used (203), which makes it difficult to propose specific and pan- markers of EVs. However, the ISEV proposes 3 essential categories that should be analyzed to demonstrate the presence of EVs in a sample (126):

- Transmembrane or GPI-anchoring proteins, associated with the plasma membrane and/or endosomes, which demonstrate the presence of the lipid bilayer present in VEs. Among these proteins are the tetraspanins (CD9, CD81, CD63, CD82); complement binding proteins such as CD55 and CD59; integrins or proteoglycans including syndecans.
- Cytosolic proteins that are actively incorporated into VEs and that can bind to transmembrane proteins, demonstrating the presence of lipid bilayer structures that enclose intracellular material. Among them would be proteins of the ESCRT-I/II/III complex such as TSG101 and its accessory proteins such as ALIX or Vps4A/B; flotillin-1 and 2 (FLOT1/2) or heat shock proteins such as HSC70, HSP90AB1 and HSP70.
- Proteins that are not associated with vesicular components and that are normally co-isolated with VEs. Their presence would help assess the degree of purity of the isolate. In biological fluids such as plasma or serum, the presence of lipoprotein contaminants (204) and albumin, among others, stands out. Thus, apolipoproteins A1/2 and B (APOA1/2, APOB) and albumin could be used as negative controls for VEs. In urine samples, uromodulin usually coprecipitates with Ves (205), so it could also be used as a negative marker.

The most common techniques used to detect the markers associated with EVs are: Western Blot, which consists of an analytical technique that allows the identification of specific proteins present in the sample under study (206); ELISA systems (enzyme-linked immunosorbent assay) that allow capturing, detecting, characterizing and quantifying VEs (207); flow cytometry designed to detect populations of VEs (208) or mass spectometry that would allow the analysis of several proteins at the same time (209).

1.4.7 EVs in Kidney Disease

1.4.7.1. Urinary EVs

Analysis of urine is routinely used in clinical practice (210). In fact, urine is the second most used biofluid for clinical diagnostics after blood. One advantage is that it can be easily and frequently collected in a non-invasive manner and in large quantities (211).

The presence of EVs in urine (uEVs) was first documented by Wiggins *et al* in 1986 in the electron microscopy images of a pellet of a 100000g ultracentrifugation in normal urine (212). But it was not until 2004 that sufficient attention began to be paid to them, following the publication of Pisitkun *et al*, where they characterized the uEV component by mass spectrometry (213). This initial characterization of the proteome of uEVs and the variation of the molecular composition in pathological situations revealed the potential as a new source of biomarker (214).

uEVs have been identified in both healthy and patients with renal disease (215,216). They are produced and secreted into the urine by all types of renal cells from every segment of the nephron, including the podocytes (217,218), mesangial cells (219) and epithelial cells from

proximal tubule (220,221), distal tubule epithelial (222), and collecting duct (223). Evidence suggests that uEVs are able to be internalized by other cells and may modulate their function, indicating an intra-nephron communication along the urinary track (222). It has been described that EVs could be internalized by proximal tubular epithelial cells through cilia (224). Renal EVs have been shown to enable signaling in the kidney to support homeostasis, differentiation, innate immunity (Hiemstra et al., 2014) and nephron function (216,218,225,226) . In addition, it is suggested that a subset of uEVs enters the urine from the circulation (227) by smaller membrane-pores of ~6nm in healthy state or larger perturbed membrane-pores in pathological conditions (228). Alternatively, it is possible that uEVs include non-vesicular circulating proteins because they are endocytosed from the blood by renal tubular cells (229), and then released to the urinary space in the EVs.

The study of uEVs rather than the bulk urine reduces the complexity of the urinary proteome as well as enabled the detection of low concentration molecules related to EVs. The protein composition of EVs has been extensively studied indicating that only the 0.6-3% of the protein in urine is associated with uEVs (230,231), and that the 66% of identified proteins in EVs are not identified in bulk urine (232,233). This means that characterization of isolated EVs enriches low abundance proteins that may be important for diagnostic or prognostic. In fact, the use of new generation mass spectrometry instruments has extended the uEV proteome to over 3000 proteins, enabling deeper analysis of EV biology and identification of additional biomarker candidates (234,235).

1.4.7.1.1. Removal of contaminating proteins

A major challenge to effective EV separation is the highly abundant urinary glycoprotein uromodulin, which forms long polymers that can entrap small EVs (213,236). Uromodulin is a glycoprotein exclusively produced by renal epithelial cells of the thick ascending limb of Henle's loop. After undergoing an intracellular maturation process, it is cleavage and release into the tubule fluid and, subsequently, the urine. Uromodulin has the capacity of polymerize and form a mesh-like structure (205,237,238). Trapped EVs will then co-pellet with uromodulin at low centrifugation speeds and reduce the yield of serial centrifugation recovery. Several approaches have been shown to release entrapped vesicles such as addition of the reducing agent dithiothreitol (DTT), the detergent 3-[(3-Cholamidopropyl) dimethylammonio]- 1-propanesulfonate (CHAPS) or alkaline buffers. (205,236,239,240).

1.4.7.2 EVs as biomarkers of renal disease progression

As EVs play a key role in inter- communication in both healthy and disease states, derive from all segments of the nephron and are reflective of the pathological state of the origin cell, (216,241–243) they hold excellent potential as a source of biomarkers that could refine and complement other clinical measurements. Current biomarkers for kidney disease, such as the estimated glomerular filtration rate (eGFR) based on serum creatinine, are insensitive and non-specific biomarkers and may not always accurately reflect the changes produced in early stages and throughout the disease (216,241). uEVs are easily accessible non-invasively, available in large quantities and susceptible to frequent longitudinal sampling. Moreover, similar to other disease conditions, it is highly likely that the urinary vesicle content is altered to reflect renal injury and disease progression through modulation of neighboring cells, and thus would provide a distinct and rich source of disease biomarkers (216,242,244–246).

USC UNIVERSIDADE DE SANTIAGO DE COMPOSTELA

Standard analytical methods and high-throughput omics have been applied in urinary EV biomarker investigation, leading to the discovery of numerous potential EV-based biomarkers for a variety of diseases. Early studies focused mainly on urogenital diseases and they were able to identified protein, mRNA, miRNA, lipid and metabolite biomarkers for prostate, bladder, and renal cancers (247–251). In fact, two RNAs associated with prostate, PCA3, and TMPRSS2:ERG, were identified in uEVs (252) that enable the creation of a prostate cancer diagnostic test (253). The potential of urinary exosomes as biomarkers of disease has already been demonstrated in other kidney-related diseases such as cystinuria (254), diabetic nephropathy (255), glomerulonephritis (256), renal fibrosis/CKD (257), lupus nephritis (258), and in the diagnosis and prognosis the tubulopathies Gitelman's and Bartter's syndromes (259). For example, studies in CKD patients with kidney fibrosis have identified a down-regulation of miR-29 and miR-200, miRNAs implied in the fibrotic responses, in EVs from patients at later stages of fibrosis compared to patients with milder fibrosis (260,261).

1.4.7.2.1. EVs in ADPKD

In ADPKD, there is a clinical need to identify patients with a risk of rapdigly progressing to End Stage Renal Disease (ESRD). To this end, studies have been carried out to analyze the content of EVs, especially proteins, in search of possible markers of progression. It is thanks to them that it has been discovered that proteins such as β-microglobulin (B2M) and monocyte chemotactic protein-1 (MCP1), plakins and some mediators of the complement system (262) can be altered in ADPKD patients and they can be useful in conjunction with conventional markers of disease progression (263,264). Urinary EVs have also been isolated from ADPKD patients in different stages of the disease comparing the protein content to control samples and with other causes of CKD (224,262,265). Alterations are not only seen at the protein level but also at the miRNA level, it has been described that several miRNAs of the miR-192/miR-194-2 and miR-30 families are deregulated in ADPKD uEVs (266).

Therefore, it was the necessity of deeper research in the search for new biomarkers that would allow identification and stratification of ADPKD patients at risk of progressing to ESRD rapidly compared to those with a slower rate of progression might be identified from their urinary EV protein profiles.

1.4.8 Seeking for new biomarkers: Glycosylation and EVs

It is widely described that EVs are heavily glycosylated with a variety of glycans linked to proteins and lipids of the EV membrane, enriched in specific glycoconjugates (267–269). Several studies have highlighted the importance of the glycosylation patterns of EVs in their uptake and interaction with recipient cells (270,271).

Glycosaminoglycans (GAGs) are large non-ramified polysaccharides made from repeated sequences of disaccharides, formed by one amino sugar (D-galactosamine or D-glucosamine) and uronic acid (such as L-glucuronic or L-iduronic acids). GAGs appear linked by N-glycosidic or O-glycosidic bonds to proteins and lipids forming glycoproteins as proteoglycans and glycolipids (272). Proteoglycans work as structural and mechanical support, attachment surface to ECM. Proteoglycans are implied in signal transduction, cytokine, inflammatory regulation and as in intercellular communication (269,273). The glycation pattern has been found to be altered in relation to different diseases, such as infections and cancer; it has also been found to be altered in relation to kidney disease (273,274).

USC
UNIVERSIDADE
DE SANTIAGO
DE COMPOSTELA

Taking this into account, we propose the study of the glycosylated component using the newly developed tool, ExoGAG, which allows the isolation of GAGs and the fraction bound to them, as a promising tool in the search for biomarkers in relation to the progression of Autosomal Dominant Polycystic Kidney Disease.

USC
UNIVERSIDADE
DE SANTIAGO
DE COMPOSTELA

USC
UNIVERSIDADE
DE SANTIAGO
DE COMPOSTELA

OBJECTIVES

USC
UNIVERSIDADE
DE SANTIAGO
DE COMPOSTELA

USC
UNIVERSIDADE
DE SANTIAGO
DE COMPOSTELA

2. OBJECTIVES

1. Elucidate the molecular biology of ADPKD in order to define the pathways involved in the pathophysiology of the disease, because a variety of mechanism involved have been identified but the key mechanism involved in the cystogenesis is still unknown. Moreover, the increase in the knowledge of the pathophysiology of the ADPKD could develop new potential therapeutic targets. To achieve this goal, we propose:

A. Compare the differential proteome of *Wild type* and polycystic kidneys of an orthologous ADPKD mouse model by the quantitative SWATH-MS analysis.
B. Comparison of the molecular mechanism that are altered in the onset and progression of the cyst by the proteomic analysis carried out at two different stages of the disease, early and severe stage.
C. Validation by other transcriptomics and proteomics techniques of targets with potential therapeutic interest.

2. Up to date, the parameters used in the monitorization of renal disease have limited power in differential diagnosis, low specificity and sensitivity and none is able to predict the outcome of the disease in an accurate and efficient way. So, we propose the identification of new biomarkers that could improve diagnosis and provide insights in the prognosis of the renal disease by:

A. Development of ExoGAG, a new diagnostic and prognostic tool that is based in the specific isolation of the fraction bound to Glycosaminoglycans.
B. Application of this new tool in the monitorization and characterization of the course of disease in urine samples of both murine model and patients with ADPKD.
C. Analysis of the fraction isolated with this new tool by mass spectrometry to identify possible biomarkers
D. Validation by other proteomic techniques of this potential biomarkers.

3. An emerging field in the source of biomarkers is the study of Extracellular Vesicles. However, although there are a wide variety of Extracellular Vesicles isolation techniques, the great challenge is to find a gold-standard accurate and reliable method for research and able to be applied in clinical routine. To this end we propose:

A. Use of the newly developed tool ExoGAG in the isolation of the GAG-associated fraction in the isolation of Extracellular Vesicles.
B. Characterization of the vesicular component isolated with this new isolation method and its comparison with other commonly used methods of extracellular vesicle isolation, such as ultracentrifugation.
C. Application in the discovery of new biomarkers associated with Extracellular Vesicles in ADPKD

USC UNIVERSIDADE DE SANTIAGO DE COMPOSTELA

USC
UNIVERSIDADE
DE SANTIAGO
DE COMPOSTELA

MATERIAL AND METHODS

USC
UNIVERSIDADE
DE SANTIAGO
DE COMPOSTELA

USC
UNIVERSIDADE
DE SANTIAGO
DE COMPOSTELA

3. MATERIAL AND METHODS

3.1 MOUSE MODEL

The mouse line used in the present thesis is *Pkd1*$^{cond/cond}$*; Tam-Cre* or *Pkd1*-CKO, developed by our laboratory. A PKD mouse line inbreed in C57BL/6 strain that is a homozygous *Pkd1* conditional knockout with the Cr-LoxP system and induced promotor of tamoxifen. (75,92,275). Mice were dwelling in pathogen-free facility (SPF) and all studies were performed according to University of Santiago and ethical committee established conditions. The experiments were conducted strictly following the protocols approved by the Ethical Committee of University of Santiago de Compostela, in the centre CEBEGA (code: #15010/2020/002, ANNEX 1.2).

We consider *Pkd1*$^{cond/cond}$ Tam-Cre^{-} mouse as Wild Types (also designated as WT) and *Pkd1*$^{cond/cond}$ Tam-Cre^{+} as mutants (also Mut or KO), both genotypes were confirmed by PCR. *Pkd1* suppression was always performed on postnatal days 10 and 11 with a single intraperitoneal injection of tamoxifen (10 mg/40g) (Sigma® No. T5648) per day to the lactating mother. Tamoxifen stock was prepared by dissolving it in corn oil (Sigma-Aldrich® No. C8267) at 65º for 2 hours with shaking and protected from light.

The animals were euthanized at postnatal day 18 (p18), day 22 (p22), day 30 (p30) and day 45 (p45). In case of availability, a Wild Type and Mutant of the same littermate were selected.

All the experiments with the mice until the processing of the samples were carried out by people with the required qualifications and training.

3.1.1 Genotyping of mouse lines

For genotyping, DNA was extracted from a piece of finger incubated at 56°C overnight with lysis buffer (50mM Tris pH8, 100mM NaCl and 0.5% Tween 20) and proteinase K (Roche, #03115801001) at a dilution of 1:100. Proteinase K activity was blocked by heating samples at 95°C for 10 minutes. DNA was stored at 4°C.

The set of primers, PCR mix and the thermocycler (Veriti^{TM} 96-Well Thermal Cycler Applied Biosystems, #9902) programs used were the following for each case:

- *Pkd1*^{cond} *(Pkd1 flox)* (275): 6.25 µL of Biomix (Bioline), 5 µL de Q 5M, 2.15 µL de H_2O mQ, 0.3 µL of F4 *primer* (5‘-CCT GCC TTG CTC TAC TTT CC-3‘), 0.3 µL of R5 *primer* (5‘-AGG GCT TTT CTT GCT GGT CT-3‘) and 1 µL of DNA.
- *Cre*(75)*:* 5 µL of Biomix (Bioline), 1 µL de Q 5M, 2.1 µL de H_2O mQ, 0.2 µL of Forward *primer* (5’-ATT GCT GTC ACT TGG TCG TGG C- 3’); 0.2 µL of Reverse *primer (*5’-GGA AAA TGC TTC TGT CCG TTT GC- 3’) and 1.5 µL of DNA.

PCR products were separated by 1.6-2% agarose gel electrophoresis loading 7 µL of PCR product mixed with 2µL of loading dye (Bioline®, BIO-33026). Voltage was settled depending on the size of the gel (90-110V). Gels were visualized in the ChemiDoc^{TM} Imaging System (Bio-Rad®).

3.1.2 Histology and Measurement of Cystic Index

After mice euthanize, the right kidneys of mice were immediately fixed in paraformaldehyde (4% paraformaldehyde buffered solution, pH=7.4; Labbox® #FORM-D0P-

10K) overnight at 4ºC. Then, tissues were washed again with distilled water for 2 hours and dehydrated though 50% ethanol for 2 hours and kept in 70% ethanol at 4ºC. Finally, kidneys were embedded in paraffin and longitudinally sectioned at 4.5 µm for histological analysis.

Kidney sections were stained for Haematoxylin-Eosin using the standard protocol and visualized under a loupe Leica DMD 108 (Leica®). For microscopic images, an Olympus BX51 microscope connected to an Olympus Camera DP70 were used. The quantification of cystic index and number of cyst was calculated with Automatic Cyst Recognition software tool called CystAnalyser® (276), developed by our group.

3.1.3 Clinical Chemistry

Blood was collected before sacrifice and serum was obtained using SB vacutainer® SST II Advance tubes, after settling down for 30min and centrifugated at 2000g 10 minutes. Serum Blood Urean Nitrogen (BUN) was measured using the ADVIA 2400 Chemistry System (Siemens Healthineers®) from de Biochemical Unit of Clinical University Hospital of Santiago de Compostela.

3.1.4 Protein and RNA extractions

At sacrificed points, left kidneys were stored at -80ºC. The whole kidney was ground in liquid nitrogen using a liquid nitrogen-cooled mortar (DD BioLab®, No. 088763). Then, the tissue was divided in two halves, one assigned to protein extraction and the other to RNA extraction.

Protein extractions were performed with RIPA lysis buffer (10Mm TRIS, 5mM EDTA, 150mM NaCl, 0.1%SDS, 1% TRITON X-100 and 1% sodium deoxycholate) with 1% protease and phosphatase inhibitors (Sigma® #P8340 y #P0044). The lysate was followed by a centrifugation at 14000g for 30 minutes at 4ºC. The supernatant was then recollected and stored at -80ºC.

On the other hand, RNA isolation was performed using TRIzol protocol (TRI Reagent, Sigma® No. T9424), as described by the manufacturer. Where chloroform (Sigma® No. C2432) worked as denaturing agent for the cells and isopropanol (Sigma® No. 650447) was the precipitating agent for RNA. The precipitate was diluted in DEPC water (Ambion®, No. AM9920), which also contains 1% SUPERaseIn RNase Inhibitor (Thermo Fisher®, No. AM2694).

3.1.5 Mice urine sample collection

Urine was collected from each animal housed in a metabolic cage (3600M021, Tecniplast®) for a 12-h period (from 8pm to 8am). Mice were fed and hydrated *ad libitum*. Urine was collected and centrifugated at 200g for 10 min at 4ºC to eliminate remains of powdered chow. Then, urine was again centrifugated at 2000g for 10 min at 4ºC to separate cell component. All samples were stored at -80ºC until further processing.

3.2 HUMAN URINE SAMPLES

Patients were collected from our database of families with several renal diseases. Most of them are from the Nephrology consulting room of Clinical University Hospital of Santiago de Compostela, but we also received some cases from other areas of Galicia and Spain. They were diagnosed by biochemical, clinical and genetic criteria and received the medication indicated for each disease.

Second morning urine from patients and healthy donors were collecting in a 100 ml sterile urine container and processed within 3 hours of collection. Samples were centrifugated at 2000g for 10 min at 4ºC to separate cellular component. All samples were stored at -80ºC until further processing.

The study was approved by the Ethics Committee of our Institution and all the participants provided written informed consent (Code: #2018/611, ANNEX 1.1).

3.3 EXOGAG ISOLATION

ExoGAG reagent (Nasasbiotech®) is the commercial reagent of the patent developed by our laboratory P201531297 (PCT/ES2016/070637, WO 2017/042416 A1). It is based in a cationic colorant and its affinity to negative charges, especially to Glycosaminoglycans (GAGs), which allow the isolation of the fraction associated to GAGs in a sample.

The procedure carried out for the isolation with ExoGAG as Figure 13. Previous incubation, the urine sample needed to be centrifugated at 2000g for 10 min at 4ºC to separate cellular debris. Then, the optimization of the protocol allowed us that the sample was incubated in a 1:1 proportion with ExoGAG during at least 15 min at 4ºC, instead of 1:2 that was recommended by the company. After incubation, the mix was centrifugated at 16000g for 15 min at 4ºC. Next, we kept the supernatant fraction and resuspended the pellet in the corresponding buffer for the next experiments: for proteomics and western blot, we resuspended in 5% SDS buffer; for extracellular vesicle characterization, we resuspended in Milli-Q water.

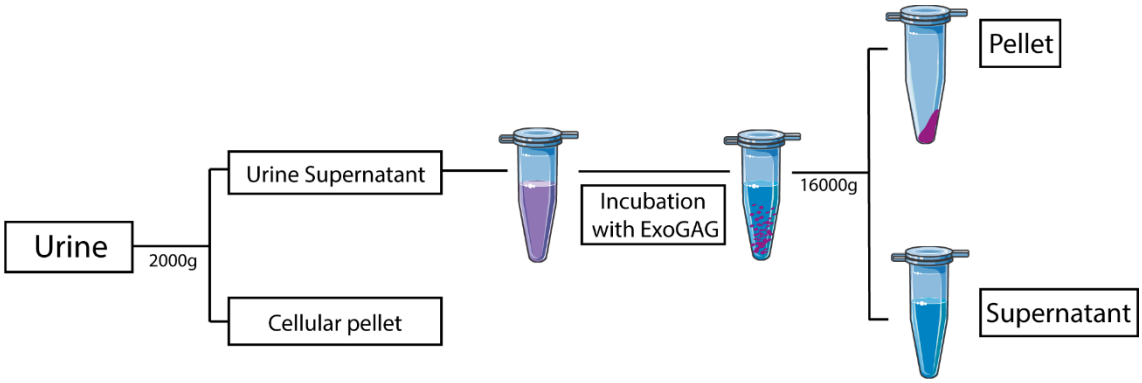

Figure 13. Schematic representation of ExoGAG isolation protocol. In a first step, we centrifugate the urine at 2000g to separate the cellular component. Then, the urine supernatant is incubated with ExoGAG and centrifugate at 16000g. After this last step, both pellet and supernatant are valuable.

3.4 EXTRACELLULAR VESICLE ISOLATION

3.4.1 Ultracentrifugation

Isolation of Extracellular Vesicles by ultracentrifugation (126) was carried out in the Beckman Coulter OptimaTM-100XP centrifuge using the SW41Ti swing-bucket rotor and 13.2 mL tubes (Thinwall Polypropylene Tubes, 14 x 89 mm; #331362 Beckman Coulter); with an acceleration and deceleration brake profile of 9, and a k-factor: 124. The protocol used consisted of a variation of that of (205,232) without depletion of Uromodulin. The procedure carried out for the isolation of VEs was as follows (Figure 14): a) 30 mL of urine sample needed to be centrifugated at 2000g for 10 min at 4ºC to separate cellular part, b) then the supernatant was separated in the ultracentrifuged tubes and centrifugated at 17,000 g for 15 minutes at 4 ºC was

carried out to eliminate possible cell debris and larger vesicles; c) the supernatant was transferred to another centrifugation tube, and ultracentrifuged at 100,000 g for 90 minutes at 4 ºC; d) the supernatant was carefully removed by decantation and saved for later studies; On contrast, the pellet was resuspended in PBS, grouping those tubes that belonged to the same type of sample; e) it was ultracentrifuged again at 100,000 g for 90 minutes at 4 ºC; f) finally, the extracellular vesicle pellet was carefully resuspended in 100 µL of RIPA lysis buffer or 100 µL of PBS, depending on the subsequent study.

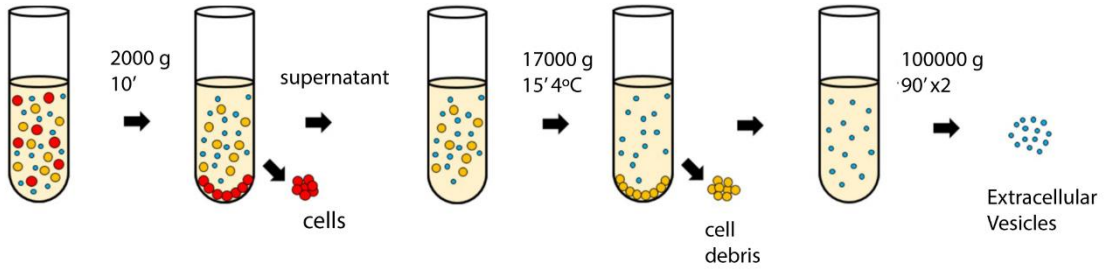

Figure 14. Schematic representation of Ultracentrifugation isolation. In a first step, we centrifugate the urine at 2000g to separate the cellular component. The following process consist in a serial of high-speed centrifugations to first remove cell debris to finally get the Extracellular Vesicles.

3.4.2 CD9 Immunoprecipitation

For this isolation method, 2 mL of sample, both total urine and pellet and supernatant of 2 mL of urine precipitated with ExoGAG as well as 2 mL of supernatant from ultracentrifugation were always used as a starting point. Two independent immunoprecipitations per sample were performed in 1mL eppendorfs and finally pooled. 2ug of CD9 antibody (Santa Cruz Biotechnology Inc® #sc13118) was added to each 1mL of sample in each eppendorf and incubated on a rotating wheel at 4°C. Next day, 20µL of sepharose sferes (Protein A/G PLUS-Agarose, Santa Cruz Biotechnology Inc® #sc-2003) were added and incubated for 2 hours on a rotating wheel at room temperature (Figure 15). After this time, the samples were washed three times with MiliQ water, centrifugating for 2 minutes at 2500g and discarding the supernatant, in order to obtain the sepharose spheres bound to the CD9 antibodies which are bound to the EVs. Finally, samples were resuspended in Laemmli Loading Buffer (25% Tris-Base at 0.5 M, 0.4% SDS pH 6.8, 20% glycerol, 0.2% 2-ß-mercaptoethanol and 0.001% bromophenol blue (Merck, Germany) and boiled at 95°C for 5 minutes. Then, samples were centrifugated at 2500g to eliminate the Sepharose spheres and thus obtain the supernatant containing the protein lysate of the vesicles of interest.

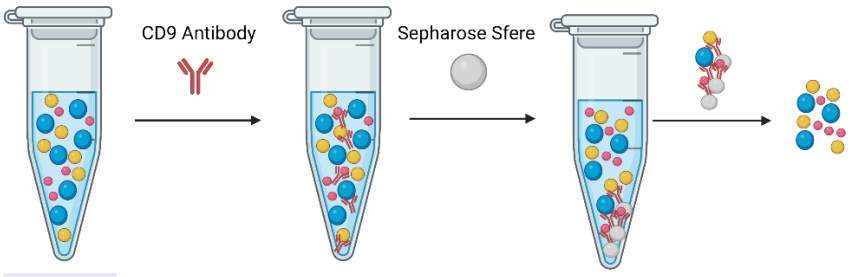

Figure 15. Schematic representation of Immunoprecipitation with CD9 isolation. First, one incubation with CD9 antibody overnight is required following an incubation of 2 hour with Sepharose spheres. After a briefly centrifugation and boil, we obtain the Extracellular Vesicles bind to CD9 antibody.

3.5 PROTEOMICS

3.5.1 Protein digestion for proteomics.

We used different amount of protein depends of the assay: In Chapter 1, we used 100 µg of the total protein from p18 and p30 kidneys; In Chapter 2, we used 20 µg of the total protein from mice and human urine quantified by similar method to Lowry protein assay (Bio-Rad® No. 5000112), for protein analysis. In Chapter 3, for comparison between ExoGAG and ultracentrifugation isolation, we used the whole isolated sample from 3 mL of urine in the case of ExoGAG and 30 mL of urine for ultracentrifugation. Proteins were diluted in loading-buffer (25% Tris-Base at 0.5 M, 0.4% SDS pH 6.8, 20% glycerol, 0.2% 2-ß-mercaptoethanol and 0.001% bromophenol blue (Merck, Germany), after boiling for 5 minutes.

SDS-PAGE gels were used to concentrate the samples into a single band about 3-4 mm thick, just after "stacking" part. By other hand, if we wanted to know the proteins belonged to a specific band, we let the gel run until they were properly separated. In this work, 10% acrylamide gels were used with 1.5M Tris-Base pH 8.8, 10% SDS (Sigma-Aldrich®), 10% APS (Sigma-Aldrich®) and 1% TEMED (Bio-Rad®). For visualizing the bands, the gels are stained with QC-Colloidal Coomassie reagent (Bio-Rad®) according to the manufacturer's maximum sensitivity protocol. The bands of the different samples are then cut with a scalpel for subsequent in-gel digestion following the standard Shevchenko protocol, with minor modifications (277–279).

The bands were washed three times with 50 mM NH_4HCO_3 (Sigma-Aldrich®) and 50% methanol (Scharlau®) for 10 minutes and dehydrated in acetonitrile, previously to vacuum drying. Then, proteins were reduced in 10 mM dithiothreitol (Sigma-Aldrich®) in 10 mM NH_4HCO_3 (Sigma-Aldrich®) at 56°C for 30 min and alkylated with 55 mM iodoacetamide (Sigma-Aldrich®) in 50 mM $NH_4HCO_3$for 20 min in the dark. Lastly, the gel pieces were again washed and dehydrated. Porcine trypsin (Promega®) was added at a final concentration of 20 ng/µl in 20 mM NH_4HCO_3 overnight at 37ºC to make a protein digestion.

The generated peptides were extracted by three 20 min incubations with 60% acetonitrile and 0.5% formic acid, pooled and dried under vacuum in a SpeedVac to be stored at -20ºC until use.

3.5.2 Mass spectrometry by LC-MSMS

Mass spectrometry analyses were performed using a Triple TOF 6600 (Sciex®), which allows both qualitative and quantitative analysis using the recently developed SWATH™ acquisition method (Sciex®) in conjunction with a nanoHPLC, Eksigent Technologies nanoLC 400 (Sciex®).

3.5.2.1 Qualitative analysis using a DDA (Dependent Data Analysis) method

In this technique the digested peptides were resuspended in 20 µl of mobile phase A (2% ACN (acetonitrile), 0.1%, formic acid), by sonication for 10 min. 4 µl of each sample were injected into a loop (5 µl/min) where the peptide mixture was properly resuspended in mobile phase A (95% H2O, 0.1% formic acid). The peptides were passed to a reverse phase precolumn based on YMC TRIART C18 silica, 5 x 0.5 mm, 3 mm particle size and 120Å pore size (YMC Technologies) where possible contaminants that may damage the column were removed. This pre-column is connected online to a Chrom XP C18, 150 x 0.30 mm, 3 mm particle size and 120Å pore size capture column (Eksigent, ABSciex®) where peptides are separated by polarity

at a rate of 5 µL/min. The elution gradient of the peptides ranges from 2% to 90% mobile phase B. Peptides were separated using a 90-minute gradient.

Data acquisition was performed on a quadrupole-TOF mass spectrometer, 6600 (SCIEX®) using a data dependent workflow (DDA) operating with the software Analyst TF 1.7.1 (SCIEX®). A 250 ms survey scan was performed from 400 to 1250 m/z followed by MS/MS experiments from 100 to 1500 m/z (25 ms of acquisition time) for a total cycle time of 2.8 s. The fragmented precursors were added to the dynamic exclusion list for 15 s, any ion with charge +1 was excluded from the MS/MS analysis. After MS/MS acquisition, the files were processed with ProteinPilot™ 5.0.1 software (SCIEX) using the Paragon™ algorithm for database searching and Progroup™ for data clustering. Searches were conducted using a mouse or human-specific, database, the UniProt Swiss-Prot database for Mouse or Human. It is necessary to specify iodoacetamide cysteine-alkylation and trypsin digestion. The false discovery rate (FDR) was set to 1 for peptides and proteins with a confidence score above 99%. (280)

3.5.2.2 Quantitative analysis by SWATH™ (Sequential Window Acquisition of All Theoretical Fragment Ion Mass Spectra) DIA (Data-independent acquisition) Method

3.5.2.2.1 Generation of the reference spectral libraries

To perform a *sequential window acquisition of all theoretical mass spectra* (SWATH™), it is necessary to build a MS/MS spectral library; this process is usually done by starting from peptide mixtures (sample pools) for each experimental sample group. This information allows us to obtain the chromatographic elution traces of a group of ions and the specific fragments for each confidence peptide. It also contains additional information such as charge state and relative intensity, which can be used to assess the confidence with which each peptide is identified. The quality of the library is a very important factor for the quantification process.

The library was generated using the previously DDA method described but using a shorter gradient, a 40 min gradient.

3.5.2.2.2 Quantitative analysis by SWATH™

The SWATH–MS acquisition was performed using a DIA (*data-independent acquisition*) method. In this case, we used 4 groups (p18 WT, p18 KO, p30 WT, p30 KO) with 3 biological replicates per group and 3 technical replicates per sample. Each sample (4 µg) was analyzed using an LC-MS system with an LC gradient as described for the spectral library construction but using a SWATH-MS acquisition method. For each set of samples, the width of the 100 variable windows was adjusted according to the ionic density found in the library DDA runs using a Sciex SWATH variable window spreadsheet. Thus, the SWATH method was based on a cycle of repetitions that consisted of the acquisition of 100 TOF MS/MS scans (limited to 400 to 1500 m/z, high sensitivity mode and 50 ms acquisition time) of isolation windows of sequential overlapping precursor variables with widths (1 m/z overlap) covering the 400 to 1250 m/z mass range with a previous TOF MS scan (400 to 1500 m/z, 50 ms acquisition time) for each cycle. Total cycle time was 6.3 s. For each set of samples, the width of the 100 variable windows was optimized according to the ion density found in the peptide/protein library previously created by DDA method.

For processing the SWATH data from the micro-LC MS/MS equipment, PeakView software (version 2.2) with SWATH Acquisition MicroApp (version 2.0) was used.

Specifically, PeakView attributed a score and an FDR to each peptide in relation to the micro-LC MS/MS data and the SWATH library. The retention times from the peptides that were selected for each protein were realigned in each run according to the iRT peptides spiked in each sample and eluted along the whole-time axis. The extracted ion chromatograms were then generated for each selected fragment ion; the peak areas for the peptides were obtained by summing the peak areas from the corresponding fragment ions. Areas under curve are then extracted from all those proteins that fulfill the following conditions: at least 10 peptides with an FDR <1%; in addition, each of these peptides must have at least 7 transitions (fragments). When all these requirements are met, the area extracted is specific and the quantitative value is very accurate. It is the area for each protein that ultimately became the absolute quantifiable value (arbitrary units) and upon which relative abundance values were calculated for each protein in the proteome.

The integrated peak areas (processed ".mrkvw" files from PeakView) were directly exported to MarkerView software (AB SCIEX®) for relative quantitative analysis. MarkerView data alignment compensates for minor variations in both mass and retention time values, ensuring that identical compounds in different samples are accurately compared to each other. The first step to perform with the areas is the normalization of areas of the data to eliminate possible variations between samples of the same group, done by total sum areas algorithm. Once the normalization is done, the program allows Principal Component Analysis (PCAs), in which it is possible to see how the samples are separated according to the values of the protein areas. This analysis shows the presence of differential proteins that allow the separation of the groups as well as the uniformity between replicates.

Finally, the Student's t-test statistical analysis (MarkerView) provides the p-values and fold change values for the proteins between the different groups. The results can be exported to Excel spreadsheets, where the p-value, mean, median, fold change and log fold change data are displayed. To analyze the differential proteins between groups, these data were processed manually and a p-value < 0.05 and a fold change > 2 were set as criteria for a statistically significant protein(278,279).

3.5.2.3 Semi-quantitative analysis by spectral count using Scaffold software

The gel band protein Quantification was performed using a Spectral count method. Protein Pilot was searched with a fragment ion mass tolerance of 0,100 Da and a parent ion tolerance of 0,050 Da. MS/MS were normalized between samples using Scaffold 5.0 by the sum of the unweighted spectral counts for each sample method in order to define a sample specific scaling factor and then this was applied to all proteins in all the samples. Therefore Scaffold (version Scaffold 5.0.0, Proteome Software Inc., Portland, OR) was used to validate MS/MS based peptide and protein identifications. Peptide identifications were accepted if they could be established at greater than 95,0% probability by the Percolator posterior error probability calculation (281). Protein identifications were accepted if they could be established at greater than 99,0% probability and contained at least 2 identified peptides. Protein probabilities were assigned by the Protein Prophet algorithm (282). Proteins that contained similar peptides and could not be differentiated based on MS/MS analysis alone were grouped to satisfy the principles of parsimony. Proteins sharing significant peptide evidence were grouped into clusters.

USC UNIVERSIDADE DE SANTIAGO DE COMPOSTELA

3.5.3 Functional Analysis.

Different functional analysis was performed using differentially expressed proteins (DEPs) with the aim to evaluate the most relevant interaction networks, related pathways or cellular components and other associated proteins or pathways. The functional analysis was performed using the open access software FunRich (http://funrich.org/index.html), which is a tool for functional enrichment analysis. Besides, to perform the protein-protein interaction analysis and, also, functional enrichment analysis between the identified proteins, we used the STRING database (https://string-db.org). These tools were based on the characterization of Gene Ontology Terms Enrichment. We also used the statistical analysis program GraphPad 9 to obtain the so-called volcano plots representing the significant proteins of each group analyzed and the tool Heatmapper (http://www.heatmapper.ca/expression/) for the creation of heatmaps.

3.6 GENE EXPRESSION ANALYSIS.

To confirm the findings obtained in the quantitative mass spectrometry assays, we decided to analyze the expression levels of the genes coding for the identified proteins in the different groups of mice. For this experiment we used a total of 24 kidney samples, 12 coming from p18 mice and 12 from p30 mice. Within each group, 6 samples were from Wild Type phenotypes and 6 samples from mutants.

One microgram of total kidney RNA was treated with DNase I (Invitrogen®, No. 18068015). Then, reverse transcription was performed with SuperScript® III First-Strand Synthesis System kit (Invitrogen®, No. 18080051), and gene expression analysis by quantitative real-time PCR using FastStart Universal SYBR GREEN Master (ROX) (Roche® No. 04913914001) in a Mx3005P system (Agilent Technologies®). The primers used for this study were designed with Primer3Plus (https://www.bioinformatics.nl/cgi-bin/primer3plus/primer3plus.cgi) and are based on cDNA reference sequences published in Ensembl genome browser (https://www.ensembl.org/index.html), considering that the amplified region consisted of the end of one exon and the beginning of the next and was between 80-130 bp in size. The primer pairs were checked to ensure that they were specific and did not amplify other regions of the DNA using the UCSC in-Silico PCR online tool (Mouse, Dec. 2011 version (GRGm38/mm10); www.genome.ucsc.edu/cgi-bin/hgPcr).

The full sequences of all primers used in the study are the following:

Protein	Gene		Primer sequence (5'-3')
HPRT	**Hprt**	Forward	5'-CAATGCAAACTTTGCTTTCCC-3'
		Reverse	5'-TCCTTTTCACCAGCAAGCTTG-3'
VIME	**Vim**	Forward	5'-CGAGAGAAATTGCAGGAGGA-3'
		Reverse	5'-AGACGTGCCAGAGAAGCATT-3'
SPON1	**Spon1**	Forward	5'-GGAAGCAGCTACCGAGTGAC-3'
		Reverse	5'-AGGTGCCTGCATGATCTTCT-3'
RBM3	**Rbm3**	Forward	5'-CGAGTTGATCATGCAGGAAA-3'
		Reverse	5'-CCTGGTCTCCACCACCTCTA-3'

The following program was used for all complete PCR reactions: a denaturation step with 30 s at 95 °C; 45 cycles of 30 s at 95 °C, 1 min at 60 °C and 30 s at 72 °C; followed by a cooling step. Each sample was run in triplicate in each experiment. The results were analyzed through

the absolute quantification method. Consequently, a standard curve with known concentrations was used in the assay and, in addition, each sample was normalized to a constantly expression gene. In this study, the *Hprt* gene was used as the housekeeping gene.

3.7 ELECTROPHORESIS AND WESTERN BLOT ANALYSIS

Total protein content was determined using a similar method to Lowry protein assay (Bio-Rad® #5000112) and the same amount of protein (40µg in Chapter 1 and 20µg in Chapter 2) was incubated with Laemmli Loading Buffer (25% Tris-Base at 0.5 M, 0.4% SDS pH 6.8, 20% glycerol, 0.2% 2-ß-mercaptoethanol and 0.001% bromophenol blue (Merck, Germany) and boiled at 95°C for 5 minutes and separated in 10% or 12 % SDS-PAGE gel under reducing conditions.

For total protein staining, the gel was incubated with Oriole (Bio-Rad® #1610496) for 90 minutes. The stained gels were scanned using a Typhoon fluorescence scanner (GE Healthcare).

For continue to Western Blot analysis, proteins were transferred to nitrocellulose membranes (Bio-Rad® #1620115) in wet transfer at 300mA for an hour and a half. To avoid non-specific binding, membranes were blocked for 1 hour at room temperature using SuperBlock Blocking Buffer (Thermo Fisher® #37515). Thereafter, membranes were incubated overnight at 4°C with primary antibodies. Next day, they were washed in 0.3% Tween-20 in PBS and were incubated for 1 hour at room temperature with the HRP-linked secondary antibodies. Signals were developed with the SuperSignal™ West Pico PLUS Chemiluminescent Substrate kit (Thermo Fisher® #34580) or Pierce™ ECL Western Blotting Substrate kit (Thermo Fisher® #32109) prior to visualization in the ChemiDoc™ Imaging System (Bio-Rad®). Protein bands were quantified using ImageJ® Lab software (v 4.0.1). Levels of the proteins were corrected for GAPDH, used as housekeeping.

The following primary antibodies were used for Western Blot:

- In Chapter 1: anti-VIME (1:500-1:1000, Santa Cruz Biotechnology Inc® #sc-6260), anti-SPON1 (1:500, Santa Cruz Biotechnology Inc® #sc-390182), anti-RBM3 (1:500, Santa Cruz Biotechnology Inc® #sc-390139) and anti-GAPDH (1:10000, Millipore®, #mab374)
- In Chapter 2: anti- DPP4 (1:250, Santa Cruz Biotechnology Inc® #sc52642), anti-LUM (1:250, Santa Cruz Biotechnology Inc® #sc166871), anti-NEP (1:250, Santa Cruz Biotechnology Inc® #sc46656), anti-CAH1 (1:250; Santa Cruz Biotechnology Inc® #sc 393490), anti-LGALS3BP (1:250, Santa Cruz Biotechnology Inc® #sc374541), anti-CERU (1:500, Santa Cruz Biotechnology Inc® #sc365205), anti-FIBB (1:250, Santa Cruz Biotechnology Inc® #sc271035), anti-APOAIV (1:250, Santa Cruz Biotechnology Inc® #sc374543), anti-AMBP (1:250- 1:1000, Santa Cruz Biotechnology Inc® #sc81948), anti-A1AT (1:250; Santa Cruz Biotechnology Inc® #sc166018), anti-UROM (1:10000, Biomedical-BTI), anti-ALBU (1:500-1:2000, Santa Cruz Biotechnology Inc® #sc271605), anti-VTNC (1:250; Santa Cruz Biotechnology Inc® #sc74484)
- In Chapter 3: anti-ALIX, (1:500, Santa Cruz Biotechnology Inc® #sc53538), anti-CD81(1:500, Santa Cruz Biotechnology Inc® #sc166029), anti-SYNTENIN-1(1:250, Santa Cruz Biotechnology Inc® #sc100336), anti-UROM (1:10000, Biomedical-BTI).

USC UNIVERSIDADE DE SANTIAGO DE COMPOSTELA

Secondary antibodies Goat anti-Rabbit IgG HRP (Thermo Fisher® #31460) or Goat anti-Mouse IgG HRP (Thermo Fisher® #31430) were used where appropiated.

3.7.1 Western blot 2D

Isoelectric focusing (IEF) was performed in pH 3-10 immobilized pH gradient (IPG) strips of 7cm (Bio-Rad® #1632000). 20µg of protein were re-suspended in 250µL of DeStreak™ Buffer (Bio-Rad® #17-6003-19) with ampholytes (0.1% servalyte 3-10 and 2-4, 0.05% servalyte 9-11, SERVA), and subjected to solubilization during 1 hour a RT. After solubilization, the mixture was centrifuged at 18000g for 15 minutes and discarded the pellet. Samples were load to each trip and submitted to active rehydration at 50V during 12h before IEF. IEF was performed in a Protean IEF Cell focusing unit (BioRad) until 20000 V/total h reached. After IEF, the IPG strips were equilibrated for 15 min in 4M urea, 2M thiourea, 50mM Tris pH 6.8, 2% SDS, 12mM DTT and 30% glycerol with 1% DTT and 15 min in 4M urea, 2M thiourea, 50mM Tris pH 6.8, 2% sodium dodecyl sulphate (SDS), 12mM dithiothreitol (DTT) and 30% glycerol with 4% iodoacetamide (all reagents from Sigma-Aldrich).

Second dimension was performed in 10-12% SDS-PAGE and continue with Western Blot as previously described.

3.8 TISSUE IMMUNOFLUORESCENCE

For immunofluorescence, sodium citrate buffer pH=6 (Agilent Dako® #S2369) was used for antigen retrieval and tissue was blocked with antibody diluent (Agilent Dako® #K8006). Sections were then washed three times with PBS for 5 minutes and incubated with primary antibodies: anti-VIME (1:500, Santa Cruz Biotechnology Inc® #sc-6260) and DBA-rhodamine labelled (1:100, Vector Laboratories®#FL-1031). Alexa-Fluor 488 goat anti-mouse (Thermo Fisher® , #A28175) was the secondary antibody. Finally, tissues were incubated with DAPI (ThermoFisher Scientific® #D1306).

3.9 EXTRACELLULAR VESICLE CHARACTERIZATION

3.9.1 Transmission electron microscopy (TEM)

Transmission Electron Microscopy (TEM) is one of the most used imaging methods for the study of EVs. Due to its high resolution, it allows individual morphology and size to be determined. In this thesis, the TEM was carried out in the Microscopy Service of the University of Santiago de Compostela (USC). First, the pellet obtained by the isolation with ExoGAG was resuspended in PBS. Then, 5 µL of pellet or supernatant of ExoGAG were spotted on carbon film-coated electron microscopy grids (Formvar, Gilder-Grids). Subsequently, they were contrasted with a phosphotungstic acid solution. Images were acquired at 200 kV on a JEOL 2010 microscope.

3.9.2 Immunofluorescence

We started with the isolation of 500 µL of urine with ExoGAG, which we resuspend in 1 mL of PBS.

For the labelling of Extracellular Vesicles, we added 5 µL of Vybrant™ DiD labelling solution (V22887, Invitrogen®), which is a lipophilic fluorophore that intercalates into the lipid bilayer, and incubated at room temperature for 15 minutes in dark. After that, we washed the sample by centrifugated it at 16000g for 15 minutes at 4ºC and resuspended in 1mL of PBS. Then, we fixed the sample with 1mL of 4% of Paraformaldehyde for 20 minutes and permeabilized with 1mL 0.25% Triton X100 for 20 minutes. The sample was blocked with

antibody diluent (Agilent Dako® #K8006) for 1 hour in a wheel. Then, the sample was incubated with anti-UROM (1:250, Biomedical-BTI) primary antibody overnight at 4ºC in a wheel. Alexa-Fluor 488 goat anti-rabbit (Thermo Fisher®, #A-11008) was the secondary antibody and was incubated for 1 hour at room temperature in a wheel. We washed the sample by centrifugated it at 16000g for 15 minutes at 4ºC and resuspended in 1mL of PBS. Finally, we resuspended in 20 µL of PBS and 20 µL of mounting medium and put in the slide. Images were taken on a Leica TCS SP8 confocal microscope.

3.9.3 Nanoparticle Tracking Analysis (NTA)

Nanoparticle Tracking Analysis (NTA) allows rapid determination of the size and number of particles by light scattering and Brownian motion of the suspended particles (283). The pure urine and the pellet and supernatant of ExoGAG as well as Ultracentrifugation ones were diluted in miliQ water and injected using a 1mL syringe (BD, Plastipak) in the Malvern NanoSight NS300 (v3.3 Malvern Panaytical) equipment according to the manufacturer's instructions. As a negative control, milliQ water was used. The measurements were made with the SOP-Standard measurement as follows: each sample analysis was performed for 60 seconds making three measurements using the NanoSight automatic analysis setup, the syringe pump speed to 40, the chamber level was selected between 8 to 12 and the detection threshold in 11.

3.9.4 ExoView® assay

ExoView® (NanoView Bioscience) is a new fully automated tool that provides multi-level and comprehensive measurements of the EV size, particle number, as well as phenotype characterization and colocalization of different biomarkers by single vesicle fluorescence. The core of this technology lies in the specific immunocapture of EVs, specifically via an antibody-functionalized microarray chip. Captured particles can be measured in two ways: count and multiplexed marker expression by immuno- fluorescence or count and size by interferometry (284,285). We performed the analysis in ExoView R100 and R200 and using ExoView® Tetraspanin kit assays (NANEV-TETRA-C, Human-tetraspanin). In this case, the chips were sculpted with capture antibodies against Tetraspanins such as CD81, CD63 and CD9.

The protocol was followed according to the manufacturer's instructions. After tempering all reagents and chips used to room temperature, the chips were pre-scanned to measure the background signal. 50 µL of each the samples diluted in incubation buffer were added carefully to different chips and incubated overnight without shaking. Next day, we washed with solution A for 3 minutes under agitation. To observe the protein cargo inside the EVs, the captured EVs were fixed on the chip with solution C for 10 minutes, and then the EV membrane was permeabilized with solution D for 10 minutes under agitation, if we only wanted to analyze membrane proteins these steps were omitted. Then we washed again with solution A for 3 minutes under agitation. The fluorophore-labelled antibodies were then diluted in blocking solution. The fluorophore-labelled antibodies used were: provided Tetraspanin antibodies CF488-anti-CD9, CF647-anti-CD63 and CF555-anti-CD81 for Tetraspanin profile; and labelled antibodies DyLight755-anti-UROM, AF647-anti-AMBP, AF488-anti-CERU, AF594-anti-VTNC for biomarker characterization. 250 µL/chip of the fluorescently labelled antibody mixture (0.6 µL/antibody chip in the case of detection of membrane proteins, and 1.5 µL/antibody chip to detect proteins inside EVs) were incubated in the dark for one hour with gentle agitation. After incubation with the different antibodies, we washed with solution A and B for 3 minutes under agitation. Finally, the chips were then washed with distilled water and dried at room temperature. Once dried, they were scanned for interferometric and fluorescence imaging. Results were analyzed in the software provided with the ExoView® Software Suite,

adjusting the fluorescence cut-offs individually to restrict the number of detected particles on MIgG capture spots.

3.9.4.1 Fluorescence labelling of antibodies

Prior to characterization by ExoView®, antibodies to the proteins of interest were labelled with different fluorophore conjugation kits depending on the excitation field. We used the following primary antibodies: anti-CERU (Santa Cruz Biotechnology Inc® #sc365205), anti-AMBP (Santa Cruz Biotechnology Inc® #sc81948), anti-UROM (Santa Cruz Biotechnology Inc® # sc-271022), and anti-VTNC (Santa Cruz Biotechnology Inc® #sc74484).

Alexa Fluor® 488 - Lightning-Link® (AB236553, Abcam), Alexa Fluor® 594 - Lightning-Link® (AB269822, Abcam), Alexa Fluor® 647 - Lightning-Link® (AB269823, Abcam) and DyLight® 755-Lightning-Link® (AB201805, Abcam) fast conjugation kits were used according to manufacturer provided protocol. First of all, we needed an antibody concentration of 1 mg/mL, to achieve this we concentrated the antibodies using centrifugation filtration units (Amicon® Ultra-0.5 mL 10K, Merck Millipore) according to the manufacturer's recommendations. 1 µL of Modifier reagent was added for every 10 µL of antibody (10 µg) and gently shaken. Then, the mixture was transferred to the lyophilized conjugation mixture vial and carefully resuspended and incubated in the dark at room temperature for 15 minutes. After this incubation time, 1 µL of Quencher reagent was added for every 10 µL of antibody initially used.

3.10 STATISTICAL ANALYSIS

Data are presented as mean ± SEM for all cases (bar or point plots). First, normal distribution was confirmed by the Kolmogorov–Smirnov test. For comparisons between two groups two-tailed Student's t test was used to determine significance of differences. For multiple comparisons, One-Way ANOVA analysis was performed. P-values less than 0.05 were considered statistically significant (*). Furthermore, ** corresponds to p-values < 0.01 and *** to p-values < 0.001. All data sets were analyzed with GraphPad Prism® Software (version 9.0).

The proteomic statistical analysis was performed using Markerview software in the SWATH analysis or Scaffold in the semi quantitative analysis by spectral count. All the information about the analysis was found in the proteomic section.

USC UNIVERSIDADE DE SANTIAGO DE COMPOSTELA

RESULTS

USC
UNIVERSIDADE
DE SANTIAGO
DE COMPOSTELA

USC
UNIVERSIDADE
DE SANTIAGO
DE COMPOSTELA

4. RESULTS

4.1 CHAPTER 1. IDENTIFICATION OF NEW SIGNALLING PATHWAYS INVOLVED IN CYSTOGENESIS BY QUANTITATIVE DIFFERENTIAL PROTEOMIC STUDY IN POLYCYSTIC KIDNEY DISEASE MOUSE MODEL

4.1.1 Kidney proteomic characterization by SWATH™ analysis

In this thesis, we perform a differential comparison between the proteome Wild Types (WT) and mutants (KO or Mut, interchangeably) mice kidneys from an ADPKD orthologous murine model (*Pkd1*$^{cond/cond}$*; Tam-Cre* mouse) with the objective to uncover new molecular pathways and therapeutic targets for renal cystogenesis.

Liquid chromatography coupled to tandem mass spectrometry (LC-MS/MS) was the most used and common technology for the characterization of complex proteomes, as well as biomarker researching or drug screening (278,286). A new technology called SWATH-MS (*Sequential Window Acquisition of all Theoretical fragment-ion spectra-Mass Spectrometry*) offers reproducibly, reliability and high-throughput quantification of up to thousands of proteins per biological sample and perform simultaneously a big number of assays. So, this next-generation proteomics SWATH-MS technology allows quantify proteome and identify protein abundance. For SWATH-MS measurement, the samples are digested with trypsin and next are analyzed by liquid chromatography coupled to a tandem mass chromatography working in the so-called Data-Independent Acquisition (DIA) mode (more details in Material and Methods) (278,279).

4.1.2 Quantitative proteomic analysis of significant deregulated proteins in ADPKD mice at postnatal day 30.

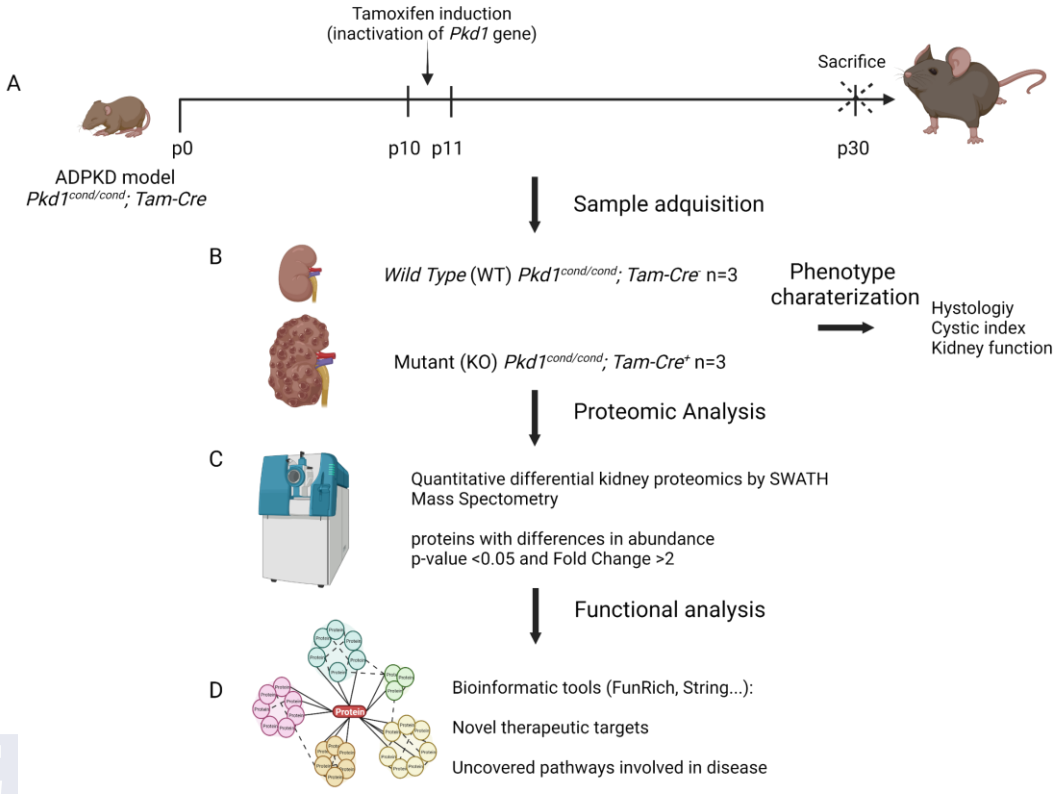

Figure 16 Illustrated workflow scheme. (A) First, we used an ADPKD mouse model (*Pkd1*$^{cond/cond}$*; Tam-Cre* mice, inactivating *Pkd1* gene at day 10-11) to obtain cystic (Cre^{+}) and no-cystic (Cre^{-}) kidneys at postnatal day

30 to be phenotypically studied (B). (C) Next, the total protein was extracted, quantified and trypsin digested. After digestion using LC-MS/MS we made a SWATH-MS analysis to obtain the differential kidney proteome. (D) Finally, we performed a functional analysis using bioinformatic tools to find novel therapeutic targets and pathways involved in the cystogenesis process.

Previous studies showed that early inactivation of the *Pkd1* gene (before p12) triggers rapid development of polycystic disease (75). To draw a direct comparison with our studies (278), mice were induced with tamoxifen to inactivate the *Pkd1* gene at postnatal days 10-11 and sacrificed at the age of 30 days (p30) (Figure 16). The cystic kidney characterization by hematoxylin-eosin stained shown a severe cystic phenotype in mutants at day 30 (Figure 17A-C) with a significantly increase in the kidney weight (Figure 17D). However, the renal damage measured by the BUN level appeared not statistically significative (Figure 17E).

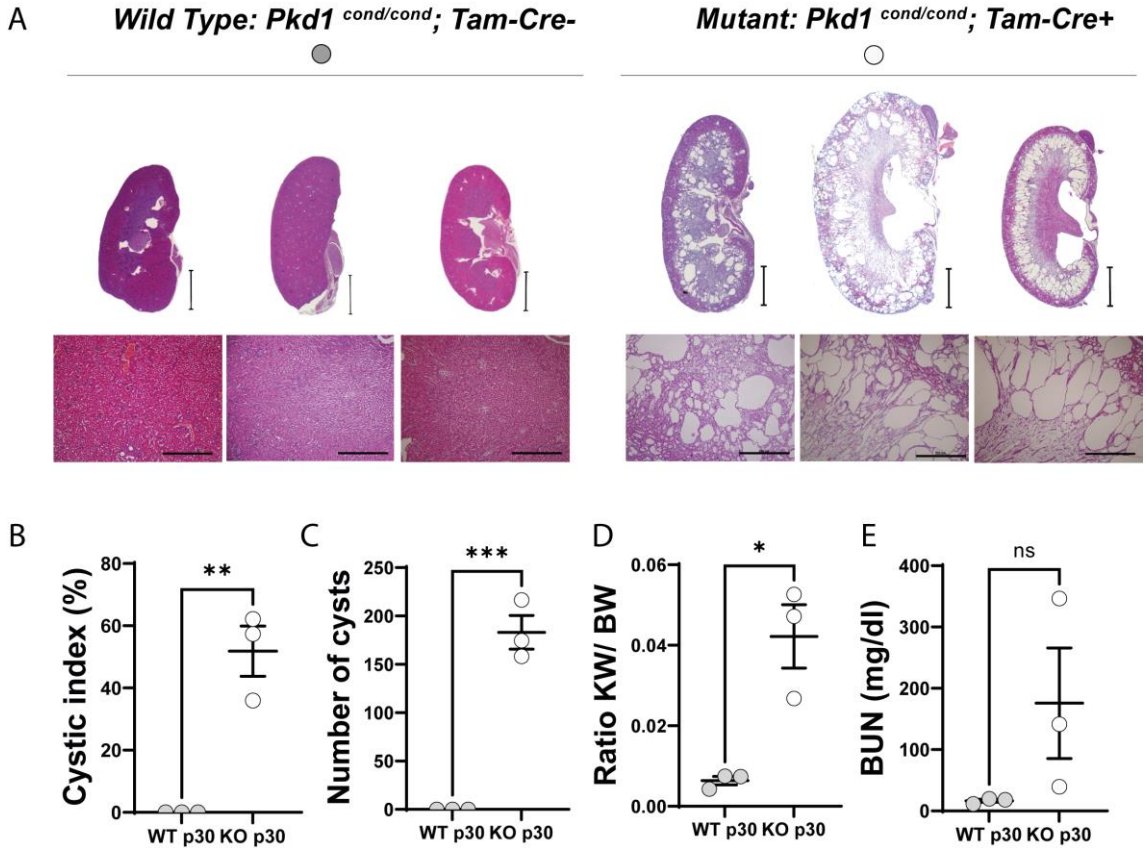

Figure 17. Characterization of the cystic kidney phenotype at day 30. (A) Representative macroscopic and microscopic images of hematoxylin-eosin stained from kidneys of Wild Type and Mutant mice sacrificed at day 30. Scale bar, 2mm (upper panel) and 100µm (lower panel). A *n* of 3 samples per group were used. (B, C) Renal cystic index and number of cysts of the different phenotypes. (D) Kidney weight to body weight ratios and (E) Blood Urea Nitrogen (BUN) concentrations of distinct groups. Bars represent means ± SEM in all cases. $p<0.05$ by Student's *t*-test (two-tail) was considered as a significant result: ns represent not significative; * $p<0.05$; ** $p<0.01$; *** $p<0.001$.

For the proteomic approach, we used kidneys of mice sacrificed at postnatal day 30 and a *n* of 3 per group, because it is a consanguineous model. We used a pool of samples of each condition to create the spectral library, obtaining a number of 1283 identified proteins with a critical FDR < 1%. Once the library and the SWATH^{TM} method were created, each sample was analyzed individually by mass spectrometry. This method performs a massive targeted search of all the peptides present in the library, allowing the quantification of all proteins in all

conditions. In our analysis a total of 695 differentially expressed proteins (DEPs) were significantly found. Unsupervised multivariate statistical analysis using Principal Component Analysis (PCA) was performed to compare the obtained data across the samples. In this case, PCA demonstrates that samples separated and grouped regarding their genotype (Figure 18). Although it is worth noting the greater variability between mutant samples than *Wild Type* samples. Proteins showing a significant difference in abundance with a two-fold increase or decrease and an adjusted p-value significant between Mutant and Wild Type samples are shown in Figure 18, with its respectively fold-changed and adjusted p-value observed. It is important to note that our criteria for considering that one protein was deregulated was a p-value < 0.05 and a Fold Change > 2 or < 0.5. In total, 152 proteins accomplished these characteristics: 96 being more abundant in KO and 56 in WT. We considered these data as upregulated or more enriched in mutant or downregulated or less enriched in mutant. Graphically, these variations can be observed through of volcano plots, which were generated by plotting the log 2 of fold change for all proteins identified against their - log 10 of p-value (Figure 19). Moreover, significant differences among protein abundance levels can be visualized and clustering in the heatmap with individualized values across the different samples according to the areas of the spectral library, using heat map analysis (Figure 20). In this case, we can observe that all proteins identified had a similar behavior among samples of the same group. The heatmap and PCA data demonstrated reproducibility among the triplicates sample as all samples from each group closely clustered in both analyses.

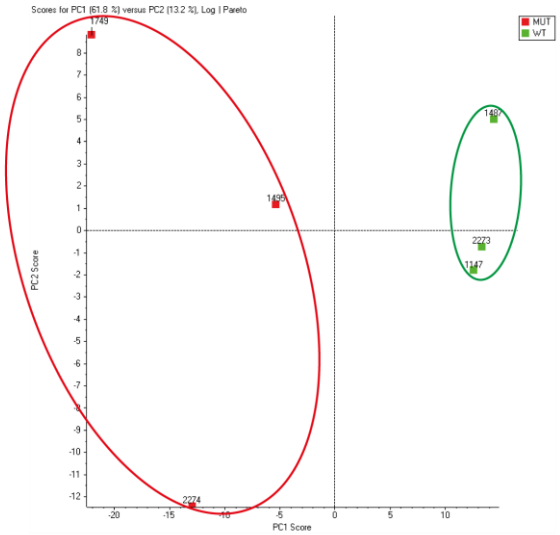

Figure 18. Unsupervised PCA where red and green circles represent Mutant and Wild Type samples, respectively.

USC
UNIVERSIDADE DE SANTIAGO DE COMPOSTELA

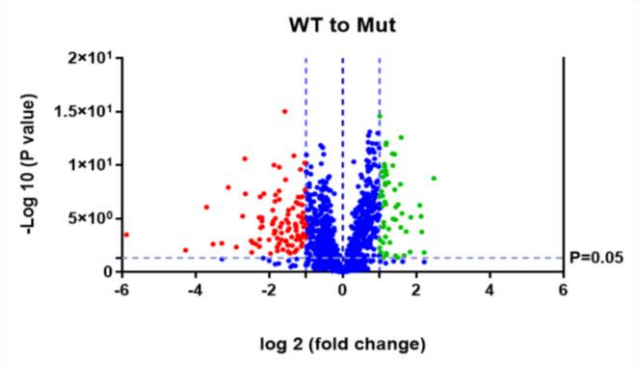

Figure 19. Volcano plot showing proteins with significance differences of protein abundance and fold change >2. X-axis shows log2 of fold change and y-axis shows -log10 of p-value. Red dots mark upregulated proteins in Mutants and green dots mark downregulated.

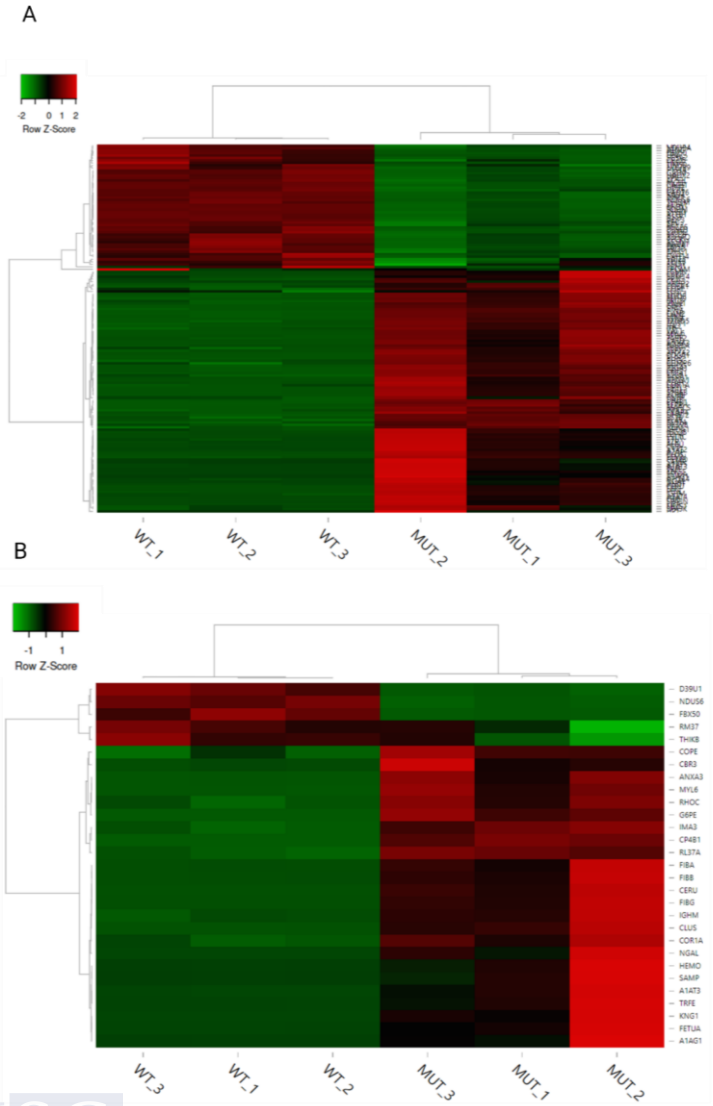

Figure 20. Heatmap figures of unsupervised cluster analysis with a fold change > 2 (A) and, most enriched, with a fold change > 4 (B). Color gradient is determined by the Row-Z-Score, where red represent increase and green decrease of protein abundance.

4.1.2.1 Protein-protein interaction and Pathway analysis

To establish the function related to the differentially expressed proteins identified by SWATH-MS analysis, we used bioinformatic tools as String (287) and FunRich (288).

Therefore, protein–protein or cluster analysis based on String software was performed to investigate possible protein–protein interactions. Overall, our DEPs obtained in the quantitative analysis showed numerous interactions and proteins clusters (Figure 21). When we analyzed upregulated proteins in Mutant samples, we observed three main independent clusters (Figure 21A). Moreover, the functional analysis, specifically the cellular component, allowed us to see that one cluster was formed by extracellular matrix related proteins, other with cytoskeleton and the third one with cytosolic ribosomal proteins (Figure 21A). On the other hand, downregulated proteins not clustered so well, it seemed like a central cluster with ramifications (Figure 21B). The cellular component analysis showed that the central cluster was formed by mitochondrial proteins and the ramifications by basolateral membrane proteins (Figure 21B).

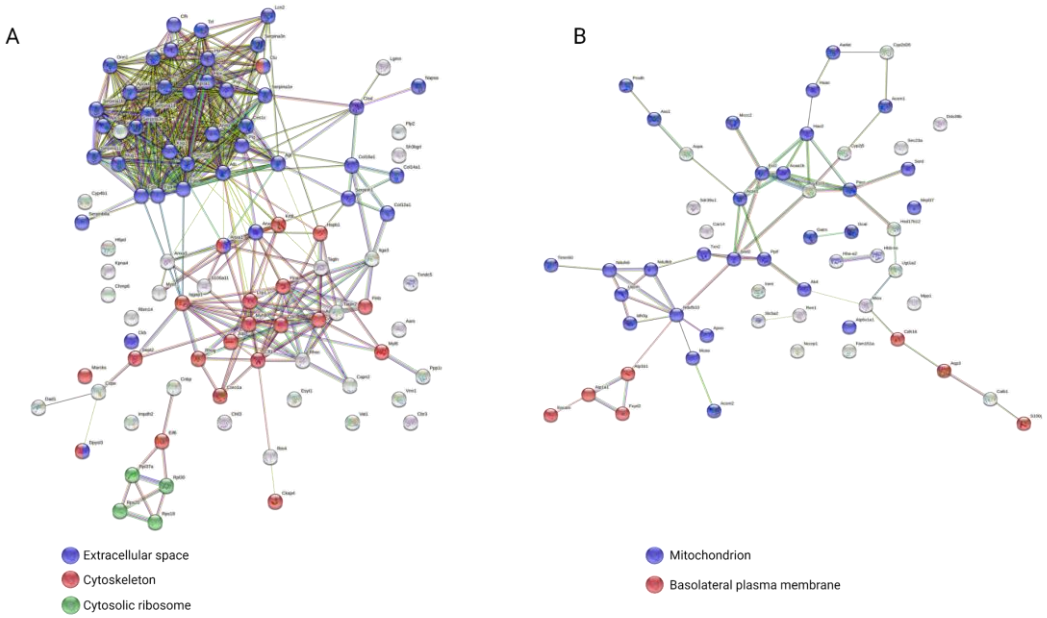

Figure 21. Cellular component of protein clusters according to String at postnatal day 30. Enrichment functional analysis of cellular component showing principal clusters of upregulated (A) and downregulated (B) proteins.

To delve further into the functional analysis of proteins, we analyzed the Gene Ontology terms (GO terms) and pathways using String and FunRich tools.

Most enriched Biological Process terms of deregulated proteins are shown in Figure 22 and Figure 23. For upregulated proteins in KO group, according to String, most enriched terms were associated with cellular process, response to stimulus, metabolism and development (Figure 22A). If we considered most enriched features attending to the background dataset, we observed terms as uropod organization, wound repairing, immune system and cytoskeleton (Figure 22B). Analysis of biological process with FunRich tool obtained similar results with most enriched terms associated with immune system, cytoskeleton and wound repairing (Figure 22C). On contrast, downregulated proteins were clearly related to metabolism according to String

database both of percentage of features as well as related to background dataset (Figure 23A and B). However, using FunRich analysis, other terms as development and response to different ions appear also enriched (Figure 23C).

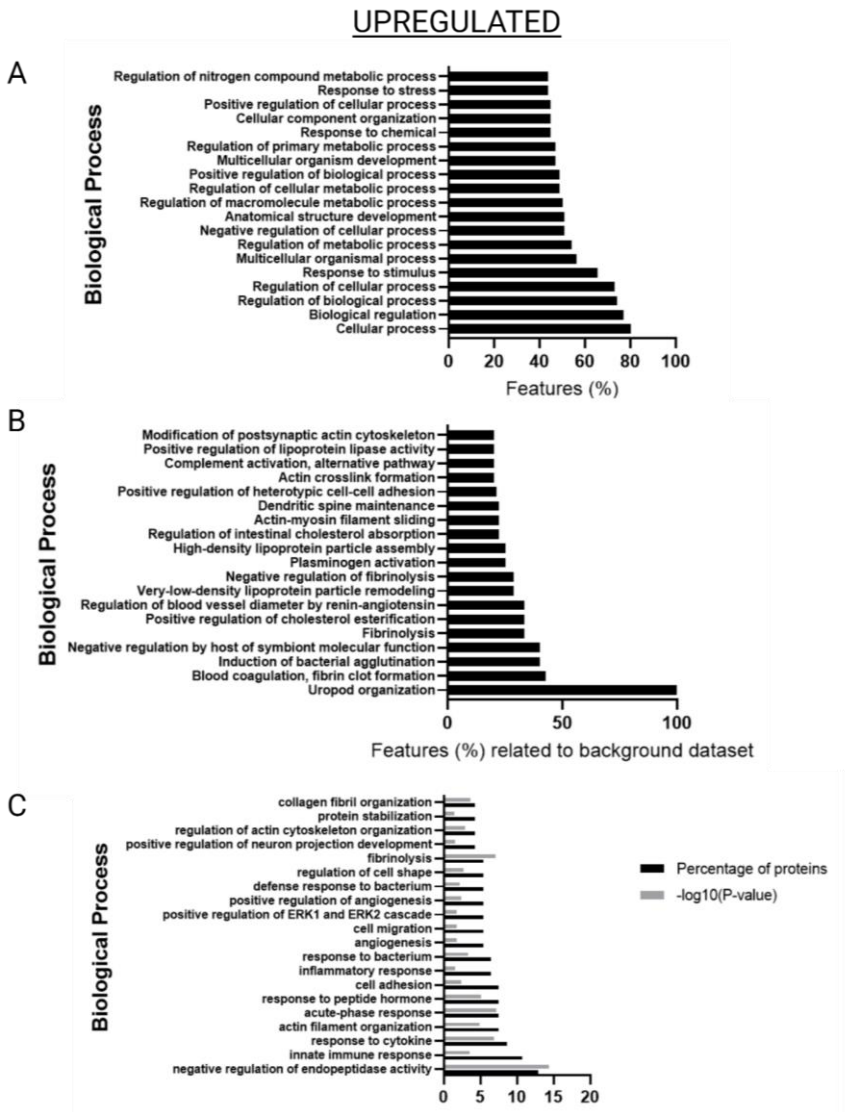

Figure 22. Functional enrichment analysis of Biological Process GO terms of upregulated proteins at postnatal day 30. String functional enrichment analysis according to the percentage of features or related to background dataset for upregulated proteins (A and B, respectively). (C) FunRich functional analysis. The highest FDR and *p-value* top 20 features are shown.

USC UNIVERSIDADE DE SANTIAGO DE COMPOSTELA

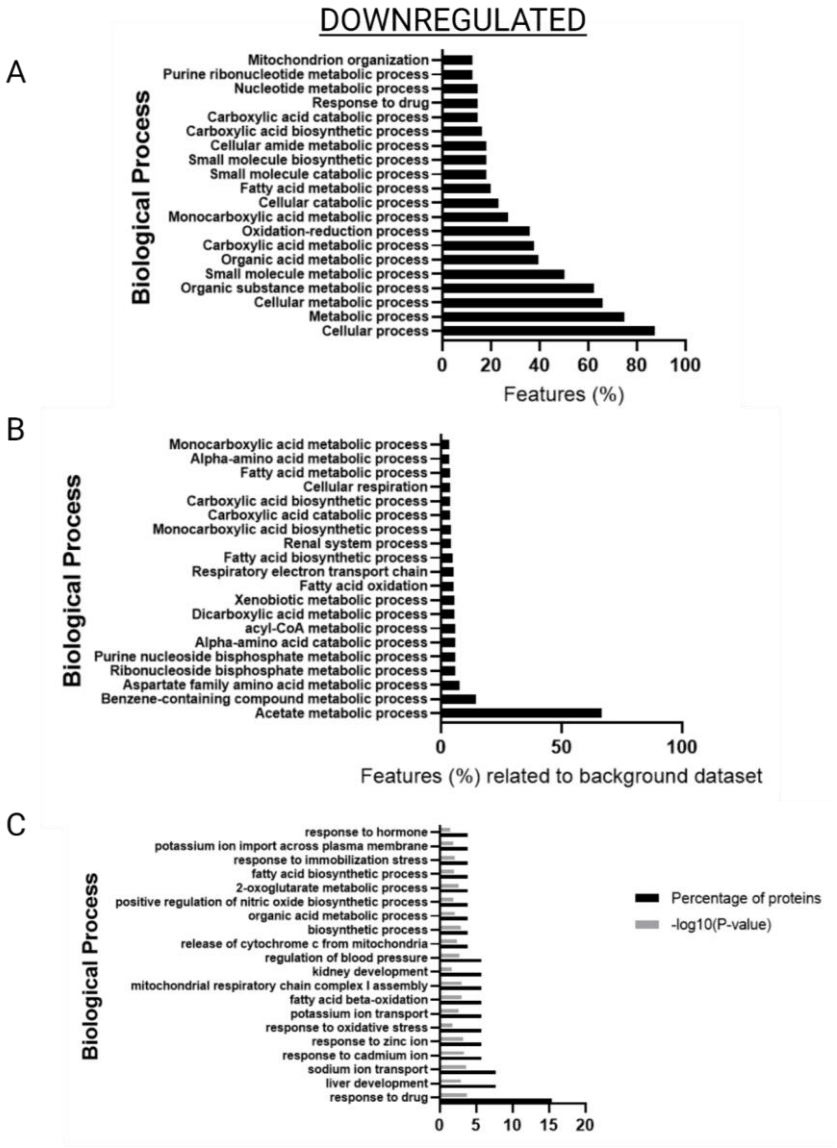

Figure 23. Functional enrichment analysis of Biological Process GO terms of downregulated proteins at postnatal day 30. String functional enrichment analysis according to the percentage of features or related to background dataset for downregulated proteins (A and B, respectively). (C) FunRich functional analysis. The highest FDR and *p-value* top 20 features are shown.

On the other hand, we also performed an analysis of cellular component (Figure 24 and Figure 25). For upregulated proteins, most enriched components were associated with organelles, extracellular region and membrane (Figure 24A). If we considered most enriched features attending to the background dataset, we observed terms as fibrinogen complex and cytoskeleton related proteins, and blood microparticles (Figure 24B). Analysis of cellular component with FunRich tool obtained similar results with most enriched terms associated with extracellular space, plasma membrane and cytoskeleton (Figure 24C). On contrast, downregulated proteins were clearly related to mitochondrion, as well as membrane, according to String database both of percentage of features as well as related to background dataset (Figure 25A and B). Moreover, according to FunRich analysis, these terms appeared also enriched (Figure 25C).

USC DE SANTIAGO DE COMPOSTELA

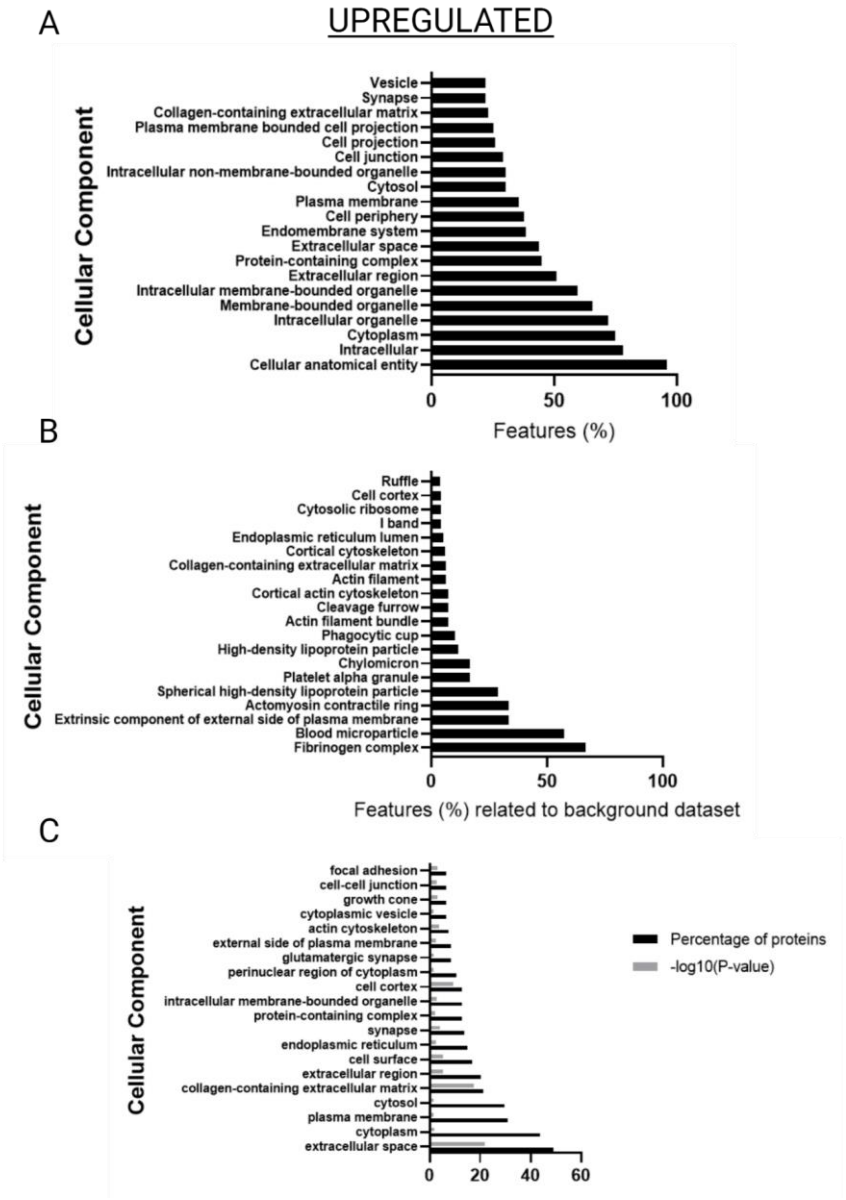

Figure 24. Functional enrichment analysis of Cellular Component GO terms of upregulated proteins at postnatal day 30. String functional enrichment analysis according to the percentage of features or related to background dataset for upregulated proteins (A and B, respectively). (C) FunRich functional analysis. The highest FDR and *p-value* top 20 features are shown.

USC
UNIVERSIDADE DE SANTIAGO DE COMPOSTELA

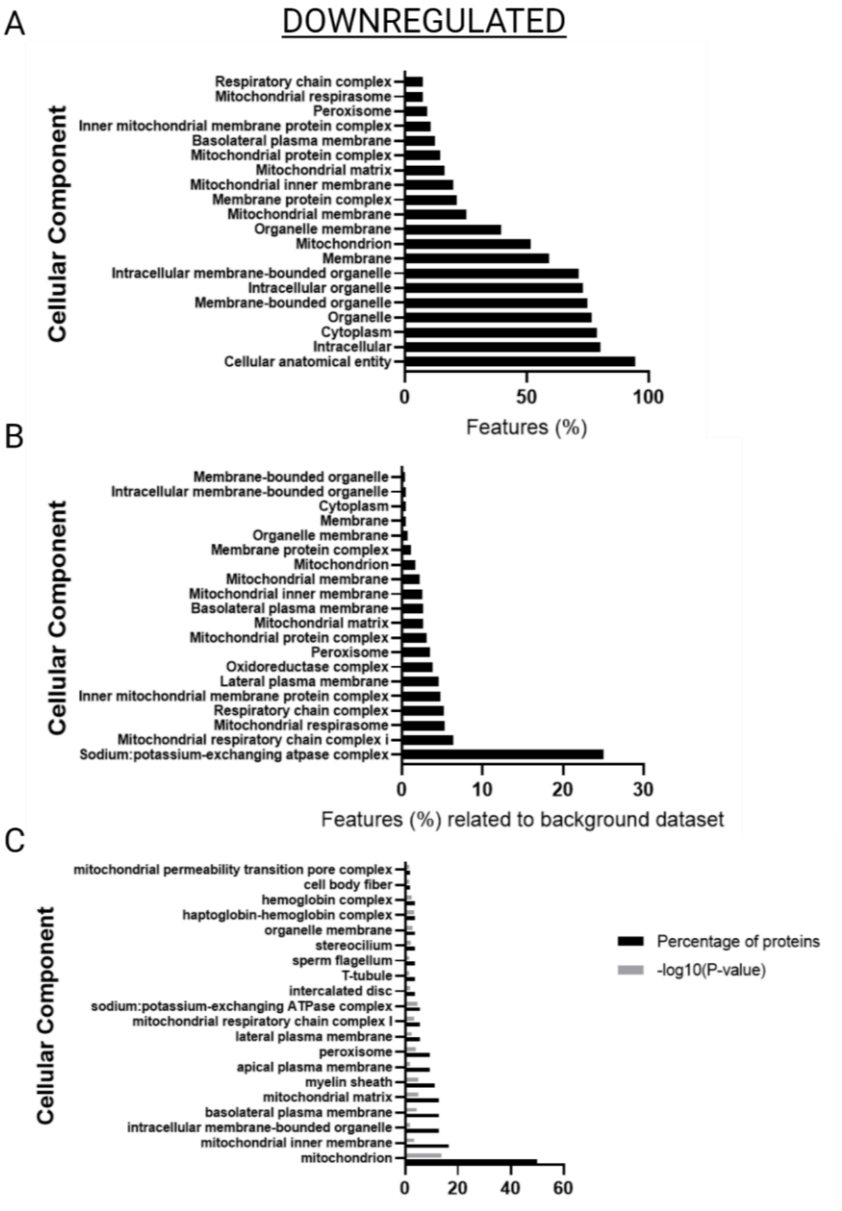

Figure 25. Functional enrichment analysis of Cellular Component GO terms of downregulated proteins at postnatal day 30. String functional enrichment analysis according to the percentage of features or related to background dataset for downregulated proteins (A and B, respectively). (C) FunRich functional analysis. The highest FDR and *p-value* top 20 features are shown.

4.1.3 Quantitative proteomic analysis of significant deregulated proteins in ADPKD mice at postnatal day 18.

Due to the high number of DEPs and involved pathways identified, we decided to perform the same differential comparison between the proteome Wild Types (WT) and mutants (KO or Mut, interchangeably) mice kidneys from ADPKD *Pkd1*$^{cond/cond}$*; Tam-Cre* mouse but in an early stage of the disease with mild phenotype, day 18. The aim is to analyze targets and pathways that are more related to cyst initiation than to cyst progression, it means, those altered in early stages (Figure 26).

USC
UNIVERSIDADE DE SANTIAGO DE COMPOSTELA

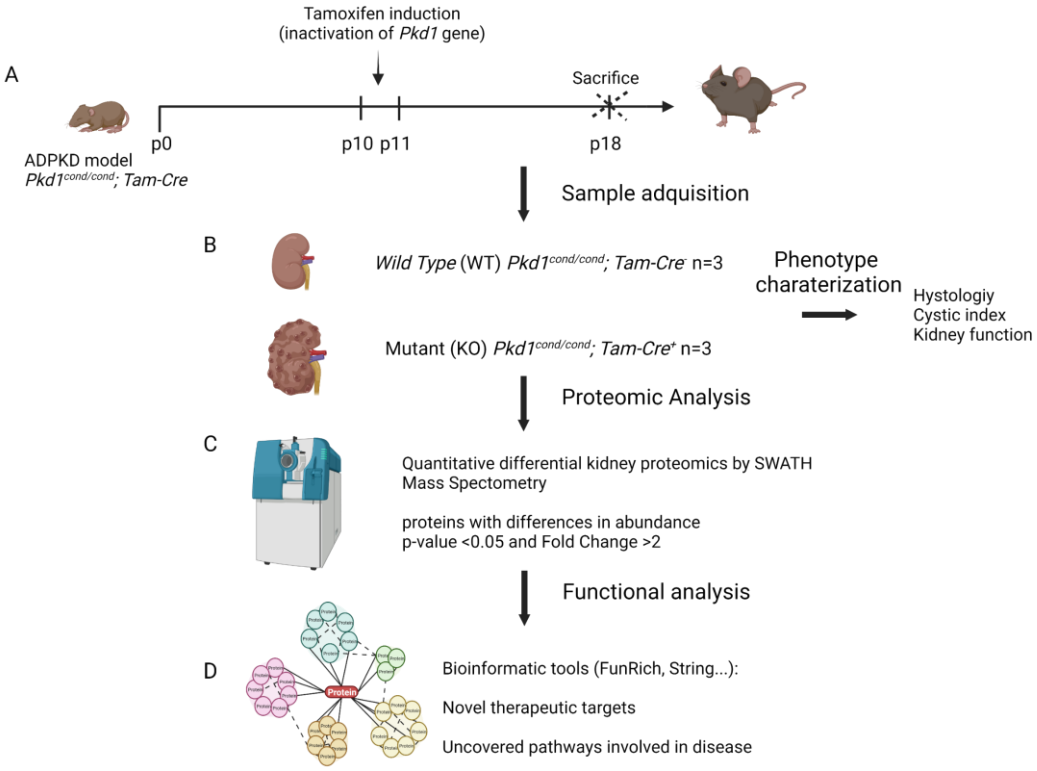

Figure 26. Illustrated workflow scheme. (A) First, we used an ADPKD mouse model (*Pkd1*$^{cond/cond}$; *Tam-Cre* mice, inactivating *Pkd1* gene at day 10-11) to obtain cystic (Cre^{+}) and no-cystic (Cre^{-}) kidneys at postnatal day 18. (B) All kidneys were phenotypically studied to characterized the WT and KO kidneys(B). (C) Next, the total protein was extracted, quantified and trypsin digested. After digestion using LC-MS/MS we made a SWATH-MS analysis to obtain the differential kidney proteome. (D) Finally, we performed a functional analysis using bioinformatic tools to find novel therapeutic targets and pathways involved in the renal cystogenesis process.

The cystic kidney characterization by hematoxylin-eosin stained shown a beginner cystic phenotype in mutants at day 18 (Figure 27A-C) with a not significantly increase in the kidney weight (Figure 27D). However, the KO samples present a significative renal damage measured by the BUN (Figure 27E).

USC
UNIVERSIDADE DE SANTIAGO DE COMPOSTELA

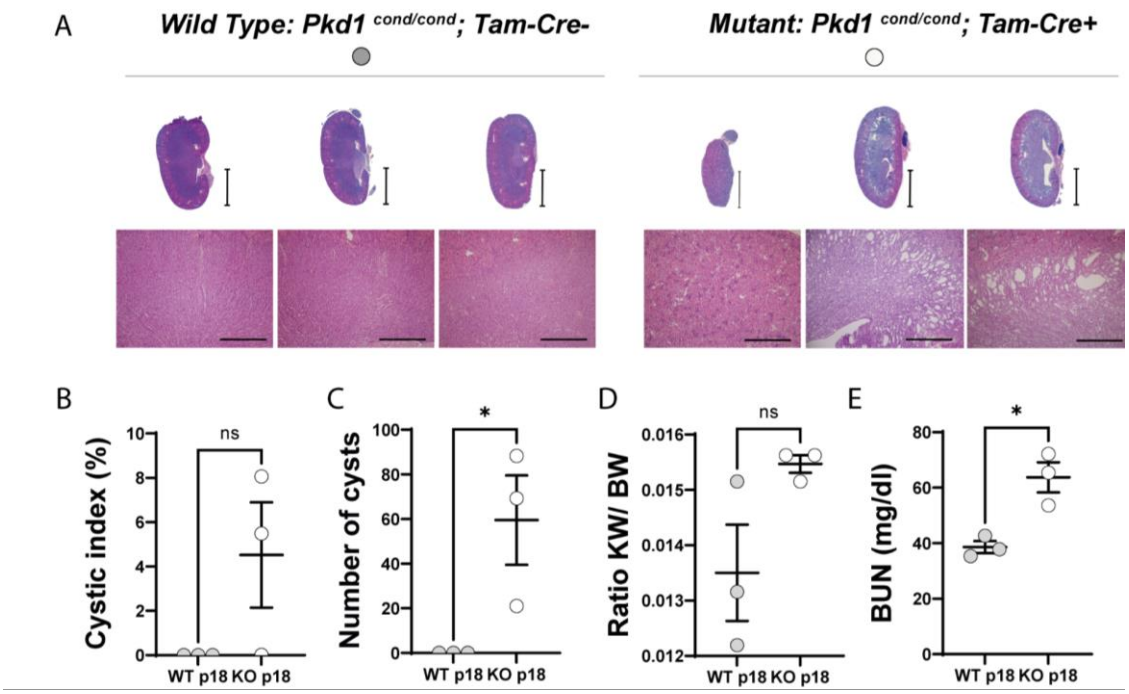

Figure 27. Characterization of the cystic kidney phenotype at day 18. (A) Representative macroscopic and microscopic images of hematoxylin-eosin stained from kidneys of Wild Type and Mutant mice sacrificed at day 18. Scale bar, 2mm (upper panel) and 100µm (lower panel). A *n* of 3 samples per group were used. (B, C) Renal cystic index and number of cysts of the different phenotypes. (D) Kidney weight to body weight ratios and (E) Blood Urea Nitrogen (BUN) concentrations of distinct groups. Bars represent means ± SEM in all cases. $p<0.05$ by Student's *t*-test (two-tail) was considered as a significant result: ns represent not significative; * $p<0.05$; ** $p<0.01$; *** $p<0.001$.

For the proteomic approach, we used three kidneys per group of mice sacrificed at postnatal day 18. We used a pool of samples of each condition to create the spectral library, obtaining a number of 971 identified proteins with a critical FDR < 1%. Once the library and the SWATH™ method were created, each sample was analyzed individually by mass spectrometry. In this analysis, a total of 159 DEPs were significantly found. PCA analysis was performed to compare the obtained data across the samples and demonstrated that samples separated and grouped correctly (Figure 28). Proteins showing a significant difference in abundance with a two-fold increase or decrease and an adjusted p-value significant between Mutant and Wild Type samples are shown in Supplementary Table 2 with its respectively fold-changed and adjusted p-value observed. In total, 14 proteins accomplished these characteristics and, in this case, all of them were downregulated in KO samples. Volcano plot showed graphically these variations (Figure 29). Moreover, using heat map analysis, we could observe differences among protein abundance and how these values clustered (Figure 30) between groups. In this case, we observed that all proteins identified had a similar behavior among the same group samples. Again, the heatmap and PCA data showed reproducibility among the triplicates sample as tightly clustered samples from each group in both analyses.

USC
UNIVERSIDADE DE SANTIAGO DE COMPOSTELA

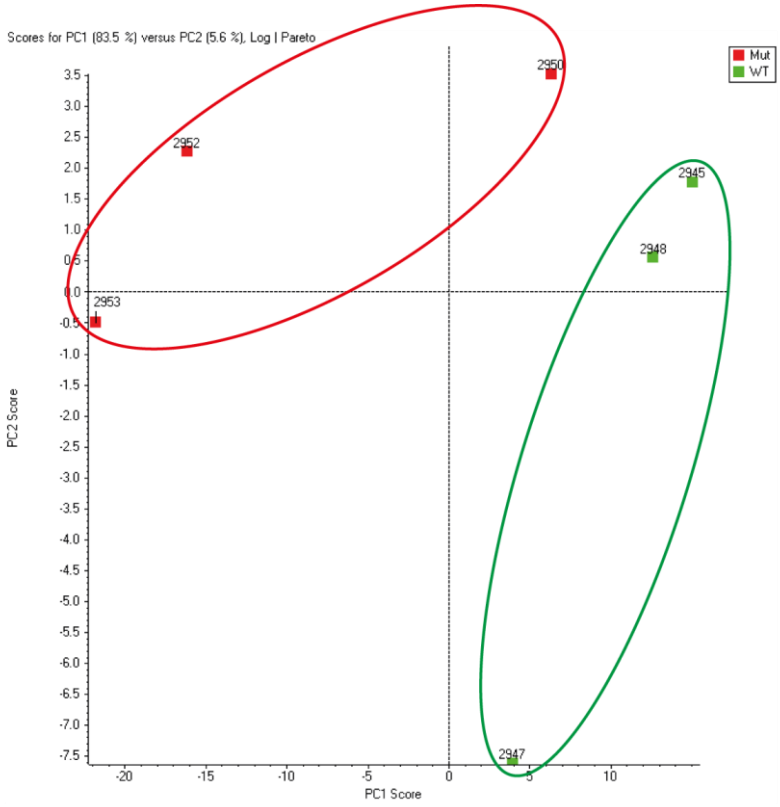

Figure 28. Unsupervised PCA where red and green circles represent Mutant and Wild Type samples, respectively.

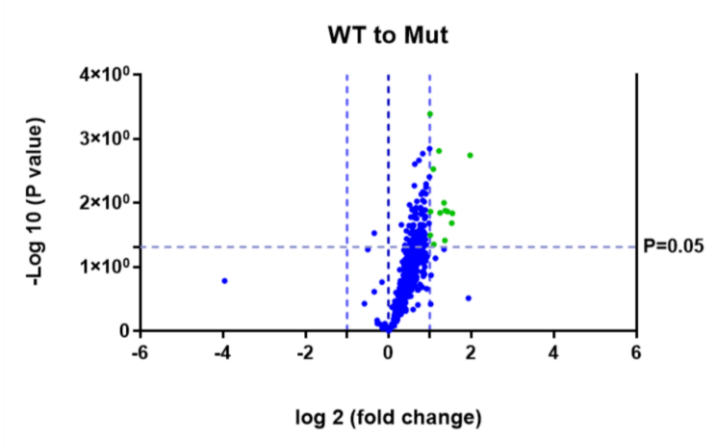

Figure 29. Volcano plot showing proteins with significance differences of protein abundance and fold change >2. X-axis shows log2 of fold change and y-axis shows -log10 of p-value. Green dots mark downregulated proteins in Mutants.

USC UNIVERSIDADE DE SANTIAGO DE COMPOSTELA

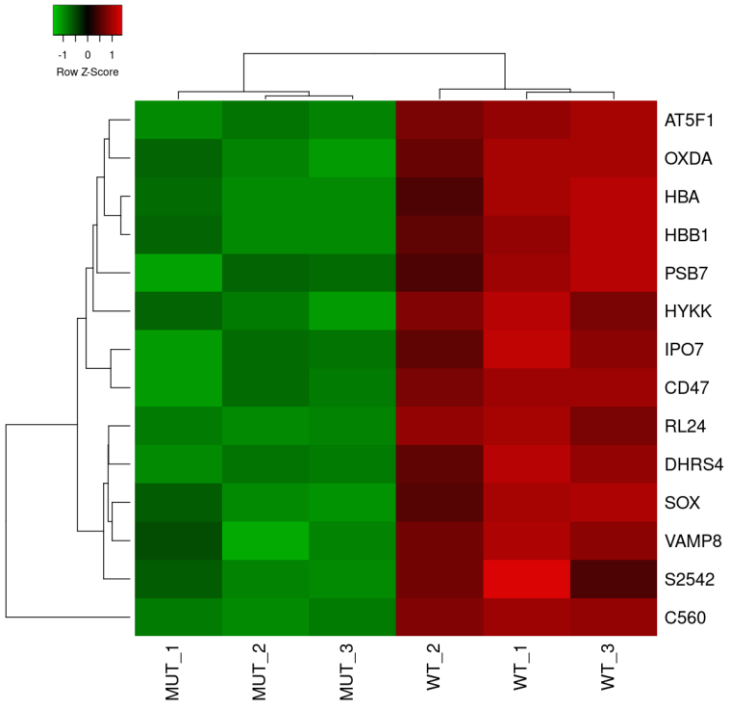

Figure 30. Heatmap figure of unsupervised cluster analysis with a fold change > 2. Color gradient is determined by the Row-Z-Score, where red represent increase and green decrease of protein abundance.

4.1.3.1 Protein-protein interaction and Pathway analysis

Protein–protein or cluster analysis based on String software was also made to explore possible protein–protein interactions. In this case, our downregulated DEPs obtained in the quantitative analysis showed three small clusters of proteins (Figure 31). However, due to the little number of proteins, String software was not able to stablish the GO terms analysis. On the other hand, FunRich tool allowed us to identify several biological process and cellular component of these proteins (Figure 32). Identified biological process terms are related to immune system, metabolism and membrane processes (Figure 32A). If we observed the cellular component terms, we noted that are related to mitochondrion and other organelles as peroxisomes and ribosomes (Figure 32B).

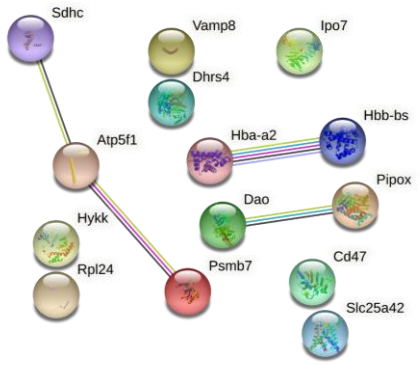

USC
UNIVERSIDADE DE SANTIAGO DE COMPOSTELA

Figure 31. Protein clusters according to String of differential expressed proteins at postnatal day 18.

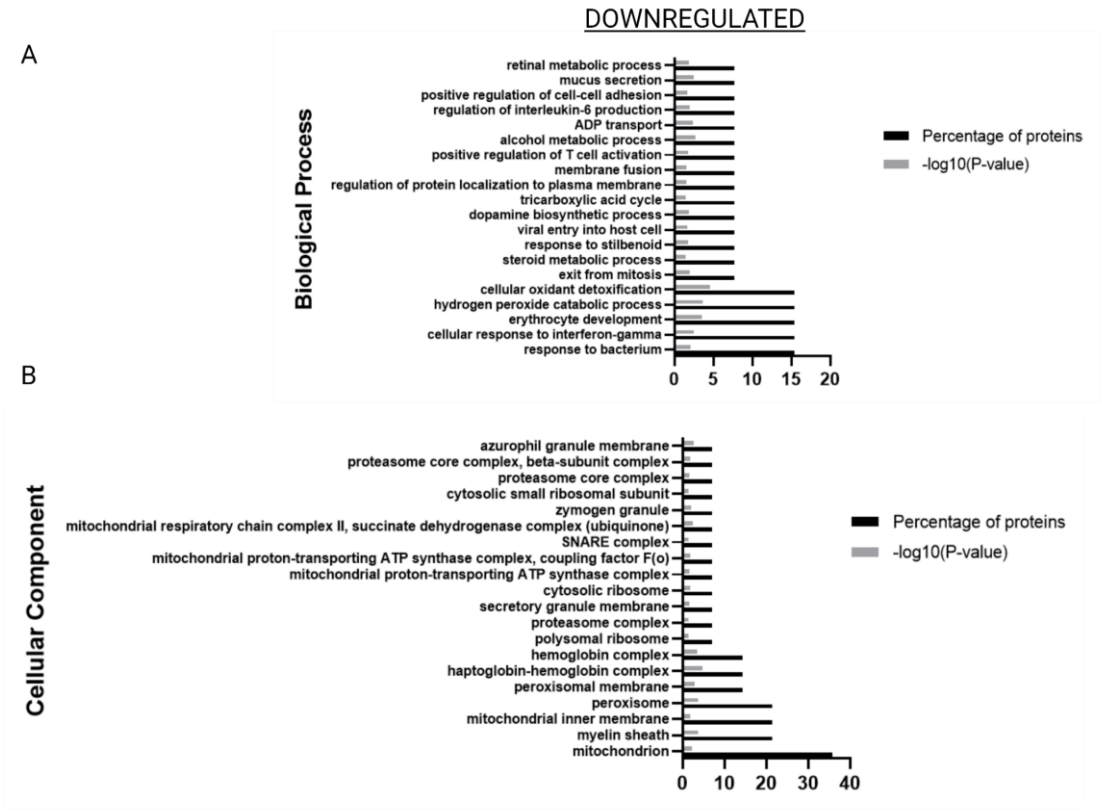

Figure 32. Functional enrichment analysis using FunRich software at postnatal day 18. FunRich functional enrichment of biological process and cellular component GO terms for downregulated proteins (A and B, respectively). The highest FDR and *p-value* top 20 features are shown.

4.1.4 Quantitative proteomic analysis of significant deregulated proteins in ADPKD mice at postnatal days 18 and 30.

Next, in order to improve the library and the data obtained in the proteomics on postnatal days 18 and 30, we decided to analyze all the samples together and thus generate a common library. In addition, as in this case all comparisons will be made between the different groups, both postnatal 18 and 30 days, in this approach that all samples will be analyzed in the same process and the results will be more comparative.

So, the final workflow scheme is represented in the Figure 33. The aim is to analyze targets and pathways that are related to cyst initiation and are continued deregulated in cyst progression. Targets will be validated by another transcriptomic and proteomic techniques.

USC UNIVERSIDADE DE SANTIAGO DE COMPOSTELA

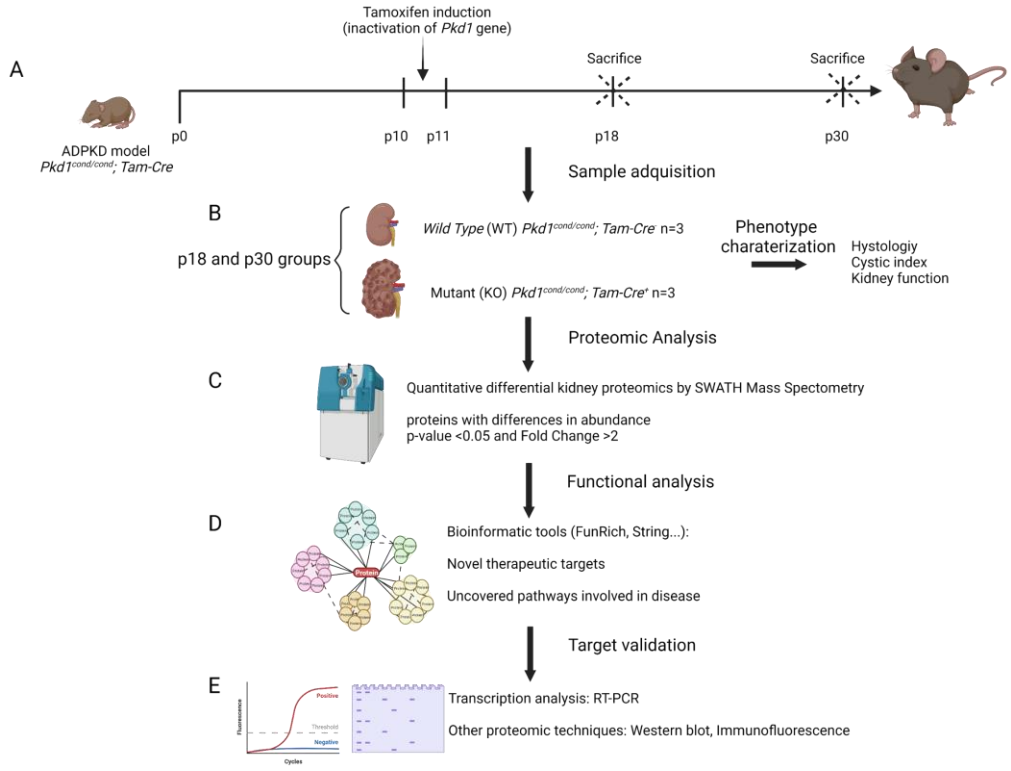

Figure 33. Illustrated workflow scheme. (A) First, we used an ADPKD mouse model (*Pkd1*$^{cond/cond}$*; Tam-Cre* mice, inactivating *Pkd1* gene at day 10-11) to obtain cystic and no-cystic kidneys at postnatal day 18 and day 30 to be phenotypically studied (B). (C) Next, the total protein was extracted, quantified and trypsin digested. After digestion using LC-MS/MS we made a SWATH-MS analysis to obtain the differential kidney proteome. (D) We performed a functional analysis using bioinformatic tools to find novel therapeutic targets and pathways involved in the cystogenesis process. (E) Finally, we validated the possible targets by other transcriptomic and proteomic techniques.

Phenotype characterization of all groups is shown in Figure 34. The cystic kidney characterization by hematoxylin-eosin stained shown more severe cystic phenotype in mutants at day 30 than at day 18 (Figure 34A-C). While at postnatal day 18 the cystic index was not significantly elevated, at day 30 it was, as well as the number of cysts also increased (Figure 34C and D). Same happened with the kidney weight, with the significantly increase in the kidney weight at day 30 (Figure 34E). However, the renal damage measured by the BUN level appeared significative at day 18 but not significative at day 30, maybe due to the data dispersion (Figure 34F).

USC
UNIVERSIDADE
DE SANTIAGO
DE COMPOSTELA

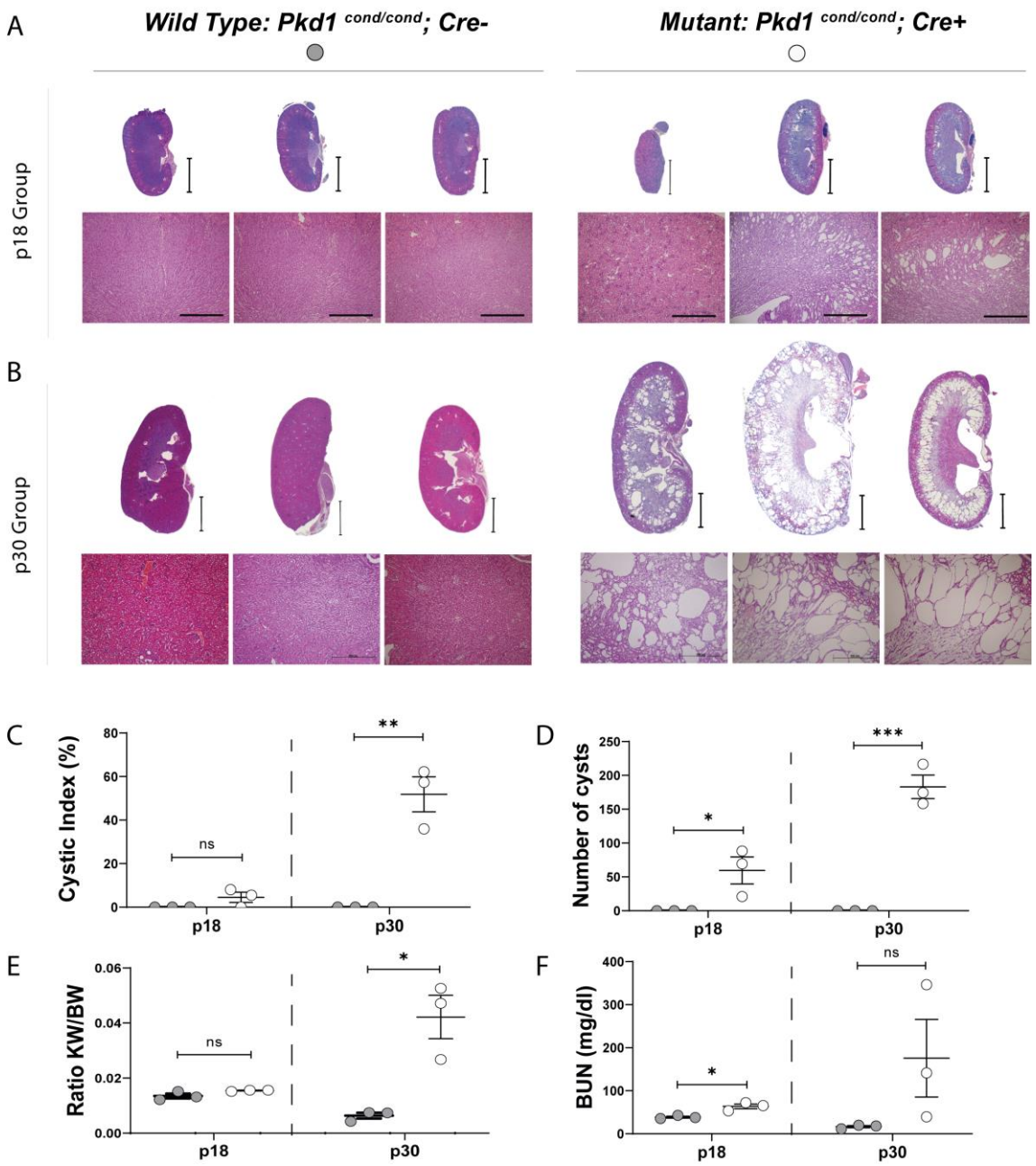

Figure 34. Characterization of the cystic kidney phenotype at day 18 and day 30. Representative macroscopic and microscopic images of hematoxylin-eosin stained from kidneys of Wild Type and Mutant mice sacrificed at day 18 (A) and day 30 (B). Scale bar, 2mm (upper panel) and 100µm (lower panel). A *n* of 3 samples per group were used. (C, D) Renal cystic index and number of cysts of the different phenotypes. (E) Kidney weight to body weight ratios and (F) Blood Urea Nitrogen (BUN) concentrations of different groups. Bars represent means ± SEM in all cases. $p<0.05$ by Student's *t*-test (two-tail) was considered as a significant result: ns represent not significative; * $p<0.05$; ** $p<0.01$; *** $p<0.001$.

For the proteomic approach, we used kidneys of Wild Type and Mutant mice sacrificed at postnatal days 18 and 30 and a *n* of 3 per group. We used a pool of samples of each condition (postnatal 18 or 30 days) and group (WT or KO) to create the spectral library, obtaining a number of 2498 identified proteins with a critical FDR < 1%, a greater number of proteins compared with those obtained in separately libraries. Once the library and the SWATH™ method were created, each sample was analyzed individually by mass spectrometry. PCA was

performed to compare the obtained data across the samples. In this case, PCA demonstrates that samples separated and grouped correctly, although p18 samples were less separated than p30 samples, probably due to mild cystic phenotype in these early stages (Figure 35).

Then, we performed the differential proteomic analysis between Mutant and Wild Type samples in each group (at postnatal day 18 and day 30).

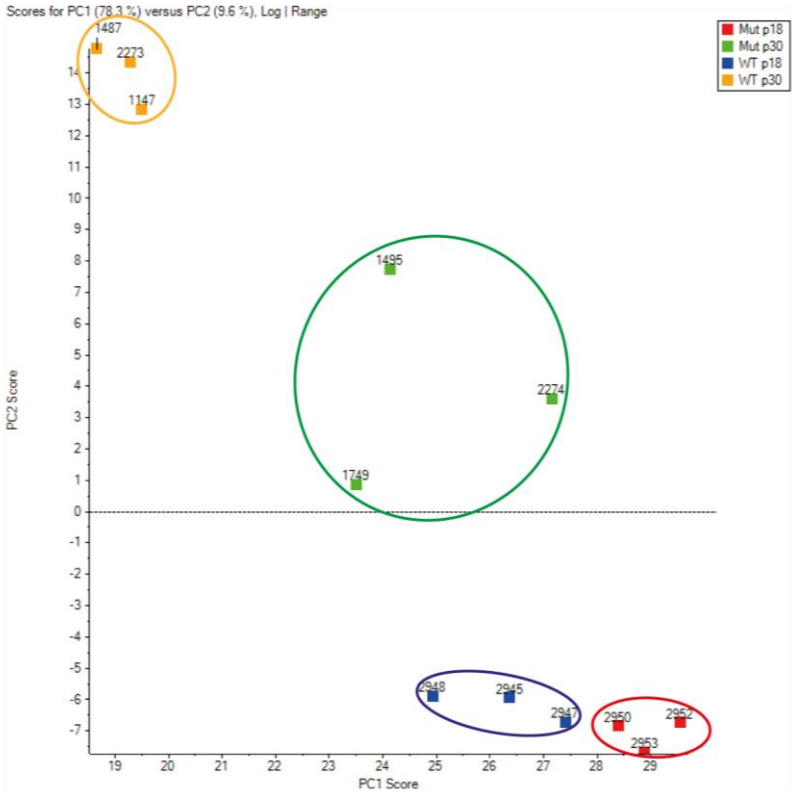

Figure 35. Unsupervised PCA. Blue and red circles represent Wild Type and Mutant postnatal day 18 samples, respectively; and yellow and green circles represent Wild Type and Mutant postnatal day 30 samples, respectively.

4.1.4.1 Proteomic approach at postnatal day 18

In our analysis a total of 248 differentially expressed proteins (DEPs) were significantly found. Proteins showing a significant difference in abundance with a two-fold increase or decrease and an adjusted p-value significant between Mutant and Wild Type samples are shown in Supplementary Table 3 with its respectively fold-changed and adjusted p-value observed. In total, 15 proteins accomplished these characteristics and, in this case, only one of them was downregulated in KO samples. Volcano plot showed graphically these variations (Figure 36). Furthermore, we could observe abundance differences and clustering among proteins in heat map analysis (Figure 37). In this case, we were able to see that all DEPs with fold change more than 2 had a similar behavior among samples corresponding to each group. Once again, the heatmap and PCA data showed reproducibility among the triplicates sample as tightly clustered samples from each group in both analyses.

USC UNIVERSIDADE DE SANTIAGO DE COMPOSTELA

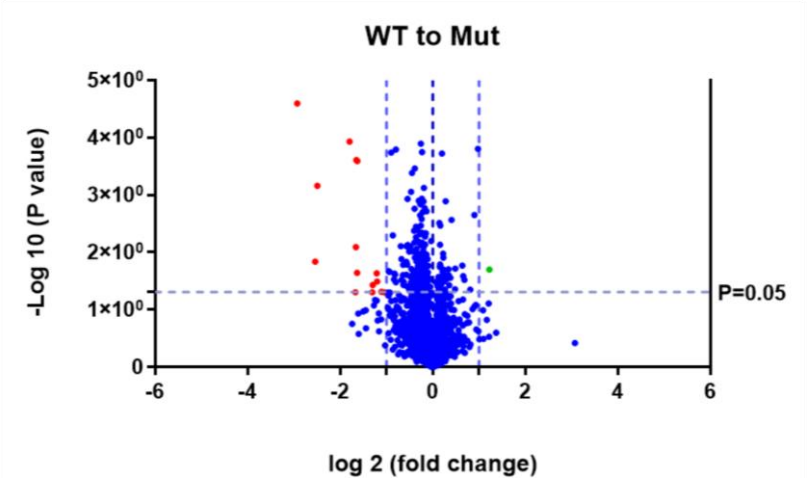

Figure 36. Volcano plot showing proteins with significance differences of protein abundance and fold change >2. X-axis shows log2 of fold change and y-axis shows -log10 of p-value. Red dots mark upregulated proteins and green dots mark downregulated proteins and in Mutants.

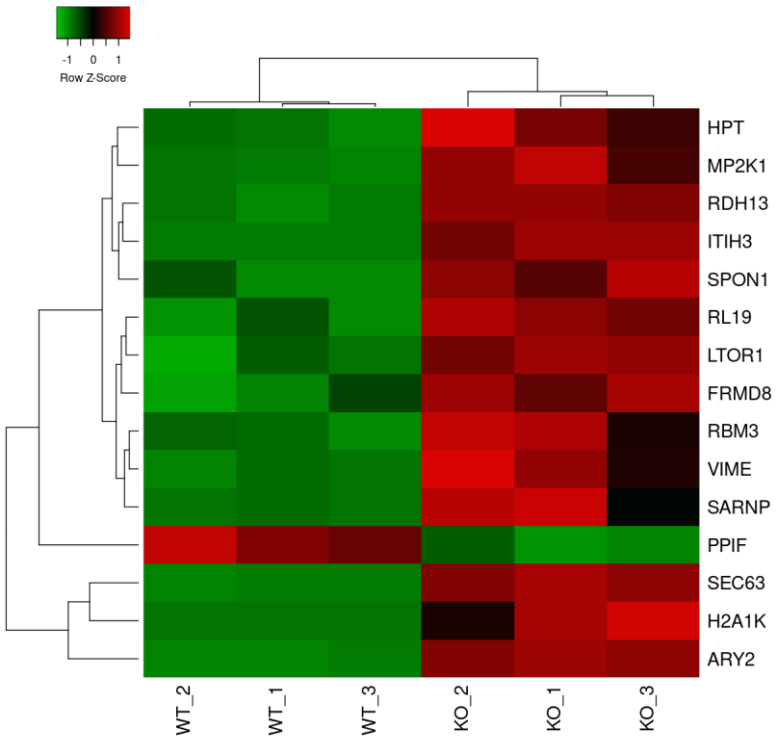

Figure 37. Heatmap figure of unsupervised cluster analysis with a fold change > 2. Color gradient is determined by the Row-Z-Score, where red represent increase and green decrease of protein abundance.

4.1.4.1.1 Protein-protein interaction and Pathway analysis

Protein–protein or cluster analysis based on String software was also made to explore possible protein–protein interactions. In this case, the analysis was only possible in upregulated DEPs obtained in the quantitative analysis, because downregulated was only one. The result showed that there were no cluster in these proteins (Figure 38). Moreover, due to the little number of proteins, String software was not able to stablish the GO terms analysis. On the other hand, FunRich tool allowed us to identify several biological process and cellular

component of these proteins (Figure 39). Identified biological process terms are related to translation, development and kinase pathway (Figure 39A). If we observed the cellular component terms, we noted that are related to extracellular matrix, ribosomes and cytoskeleton (Figure 39B). On contrast, the only downregulated protein was related to metabolism and necrotic process (Figure 40A); and regarding to cellular component was related to mitochondrion (Figure 40B).

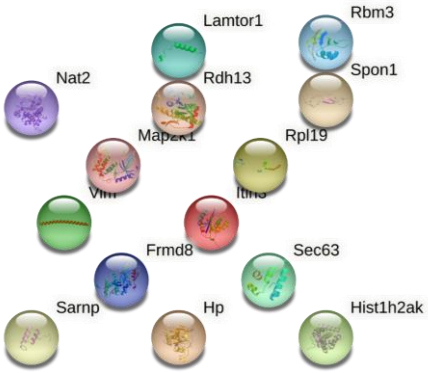

Figure 38. Protein clusters according to String of upregulated proteins at postnatal day 18.

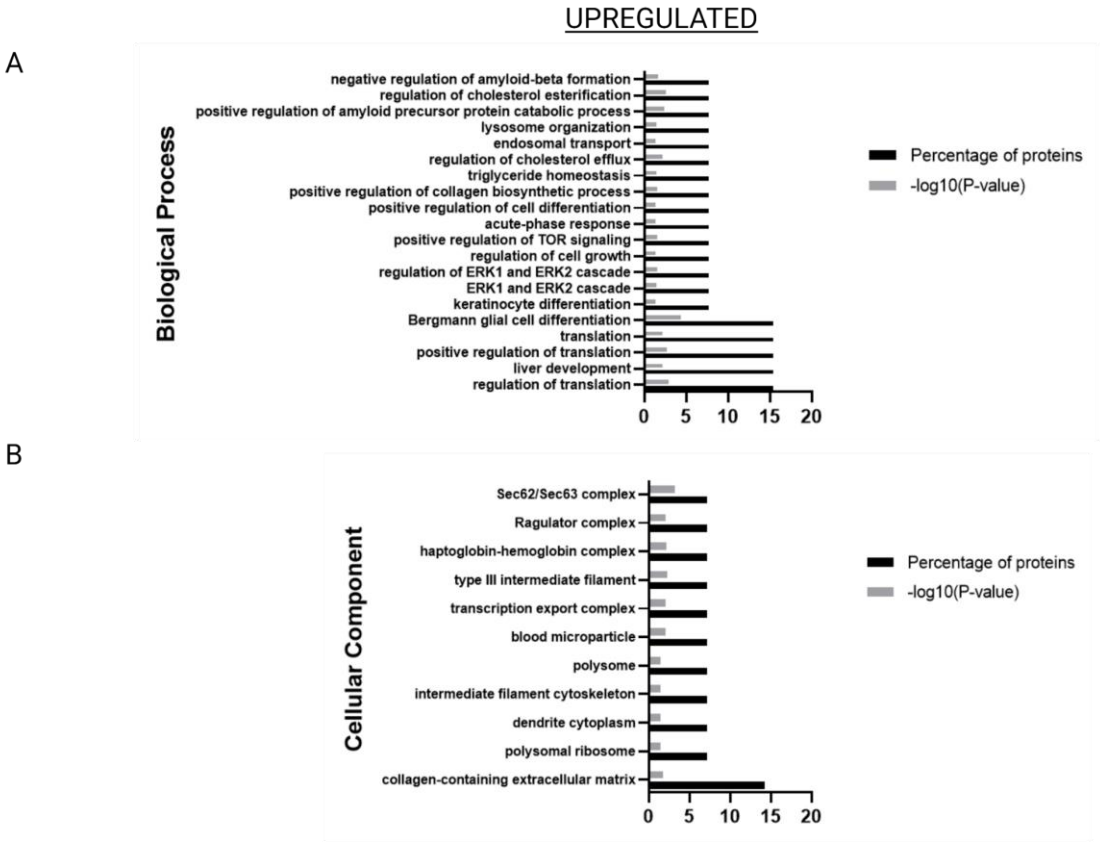

Figure 39. Functional enrichment analysis using FunRich software at postnatal day 18. FunRich functional enrichment of biological process and cellular component GO terms for upregulated proteins (A and B, respectively). The highest FDR and *p-value* features are shown.

USC
DE SANTIAGO
DE COMPOSTELA

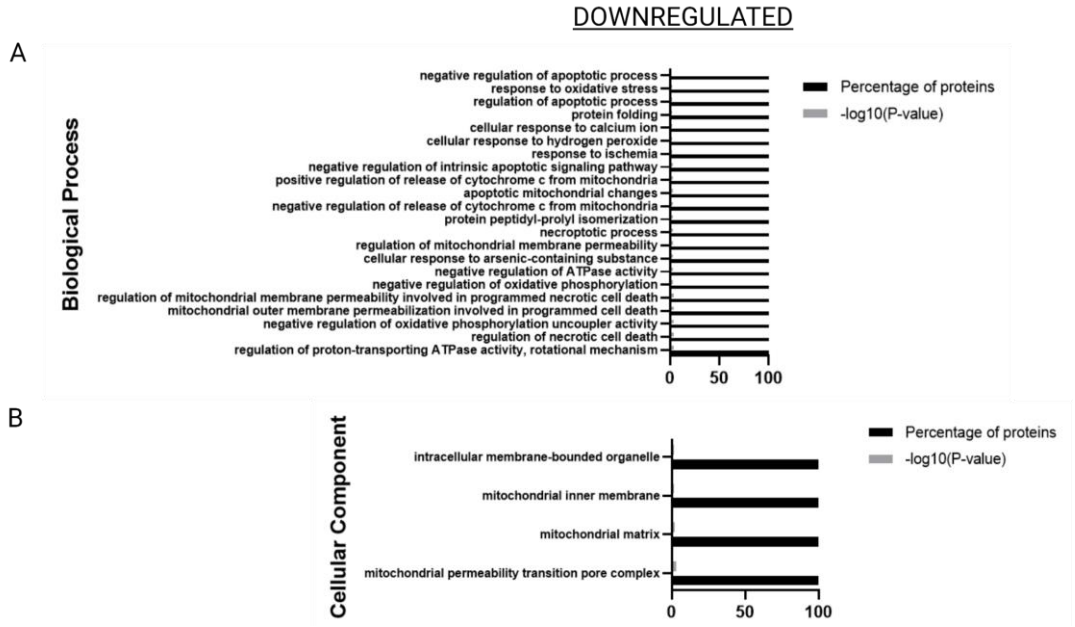

Figure 40. Functional enrichment analysis using FunRich software at postnatal day 18. FunRich functional enrichment of biological process and cellular component GO terms for downregulated protein (A and B, respectively). The highest FDR and *p-value* features are shown.

4.1.4.2 Proteomic approach at postnatal day 30

In this analysis a number of 914 DEPs were significantly found. Proteins showing a significant difference in abundance with a two-fold increase or decrease and an adjusted p-value significant between Mutant and Wild Type samples are shown in Supplementary Table 4 with its respectively fold-changed and adjusted p-value observed. In total, 213 proteins accomplished these characteristics, being 156 proteins upregulated and 57 proteins downregulated in Mutants. Graphically we used a Volcano plot to show these variations (Figure 41).

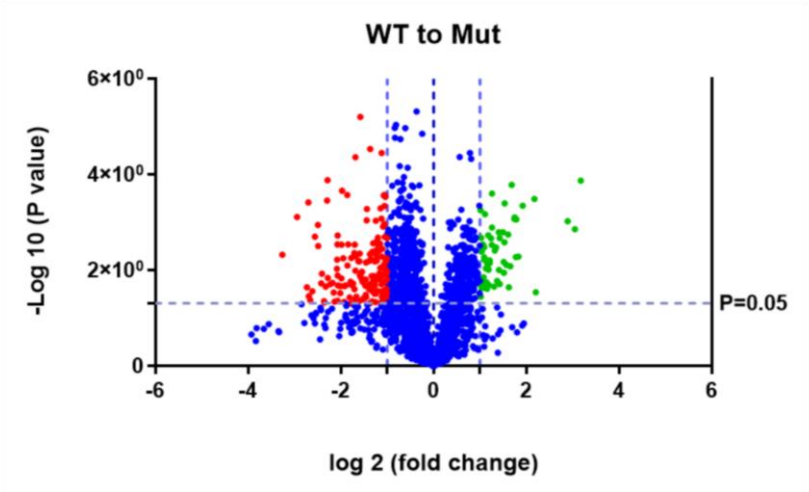

Figure 41. Volcano plot showing proteins with significance differences of protein abundance and fold change >2. X-axis shows log2 of fold change and y-axis shows -log10 of p-value. Red dots mark upregulated proteins and green dots mark downregulated proteins and in Mutants.

Furthermore, heat map analysis is shown in Figure 42, where significant differences among protein abundance levels can be visualized. Over again, we could notice that all proteins identified had a similar behavior among samples of the same group. The heatmap and PCA data demonstrated reproducibility among the triplicates sample so that all samples from each group closely clustered in both analyses.

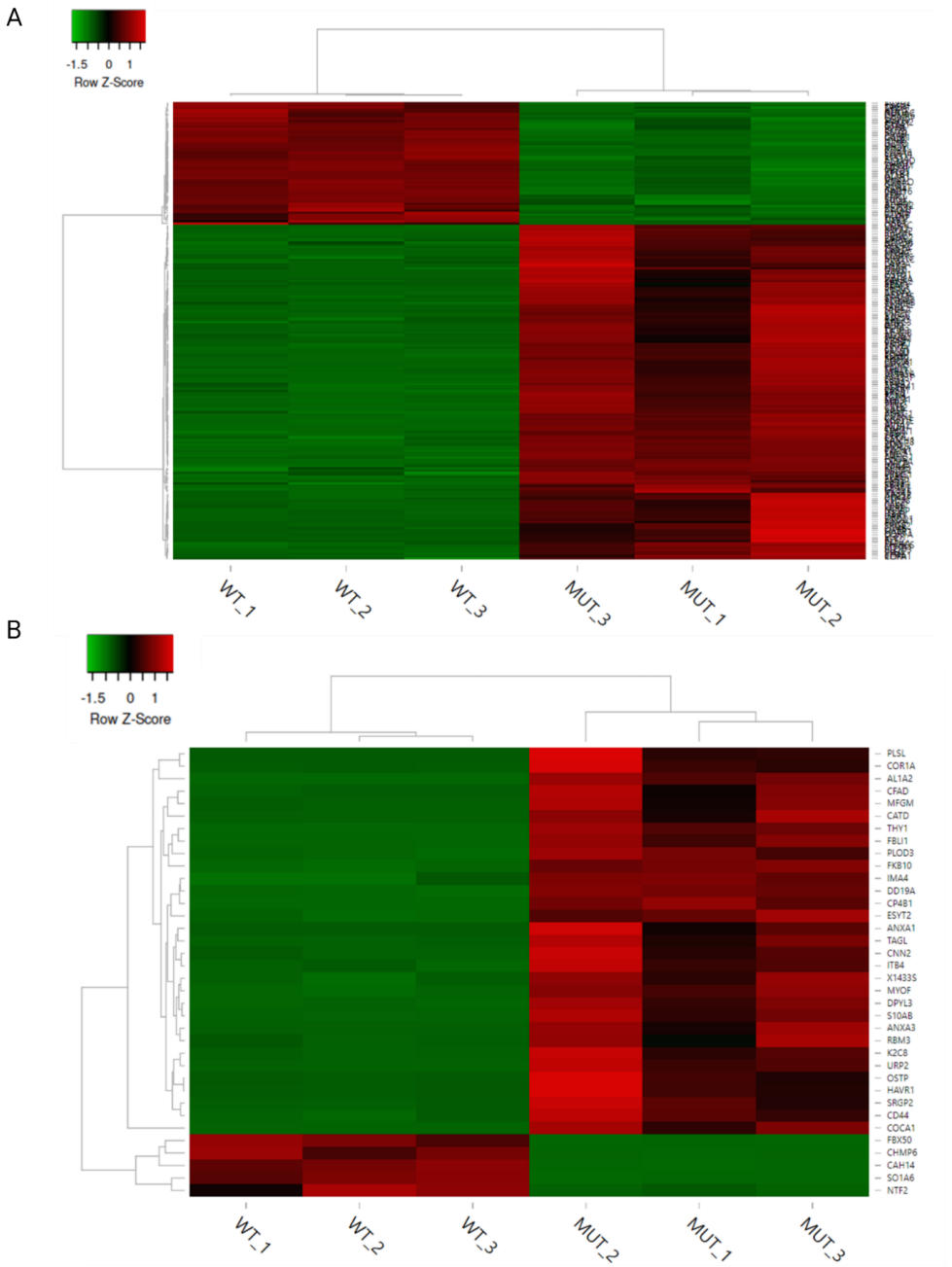

Figure 42. Heatmap figures of unsupervised cluster analysis with a fold change > 2 (A) and, most enriched, with a fold change > 4 (B). Color gradient is determined by the Row-Z-Score, where red represent increase and green decrease of protein abundance.

USC
UNIVERSIDADE DE SANTIAGO DE COMPOSTELA

4.1.4.2.1 Protein-protein interaction and Pathway analysis

Protein–protein or cluster analysis based on String software was also performed in this data set. Overall, in this case, the cluster analysis of our DEPs didn't show many independent clusters (Figure 43). When we analyzed upregulated proteins in Mutant samples, we observed a main cluster with several extensions (Figure 43A). Moreover, the functional analysis, particularly the cellular component, allowed us to see that the main cluster was formed by proteins related to membrane, then one part of the cluster was formed by extracellular region related proteins and the other part with cytoskeleton (Figure 43A). On the other hand, downregulated proteins clustered also in a main cluster with two differenced arms and a small cluster (Figure 43B). The cellular component analysis showed that one arm of the cluster was formed by mitochondrial proteins and the other arm by plasma membrane region proteins (Figure 43B).

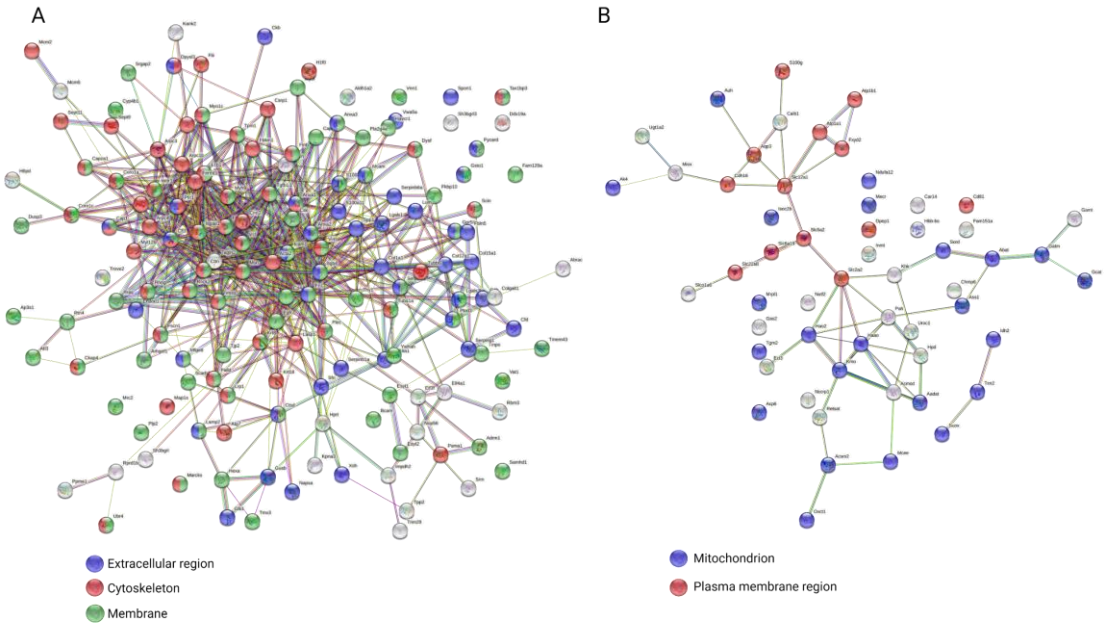

Figure 43. Cellular component of protein clusters according to String at postnatal day 30. Enrichment functional analysis of cellular component of principal clusters of proteins with significant differential increase (A) and decrease (B) protein abundance in mutants.

Most enriched Biological Process terms of DEPs are shown in Figure 44 and Figure 45. For upregulated proteins in KO group, according to String, most enriched terms were associated with cellular process, response to stimulus and development (Figure 44A). If we considered most enriched features attending to the background dataset, we observed terms as uropod organization, wound repairing, metabolism and cytoskeleton more increased (Figure 44B). Analysis of biological process with FunRich tool obtained similar results with most enriched terms associated with cytoskeleton, development and cell-cell adhesion and migration (Figure 44C). On contrast, downregulated proteins were evidently related to metabolism according to String database both of percentage of features as well as related to background dataset (Figure 45A and B). Moreover, using FunRich analysis, other terms as response to stimulus and different ions appear also enriched (Figure 45C).

USC UNIVERSIDADE DE SANTIAGO DE COMPOSTELA

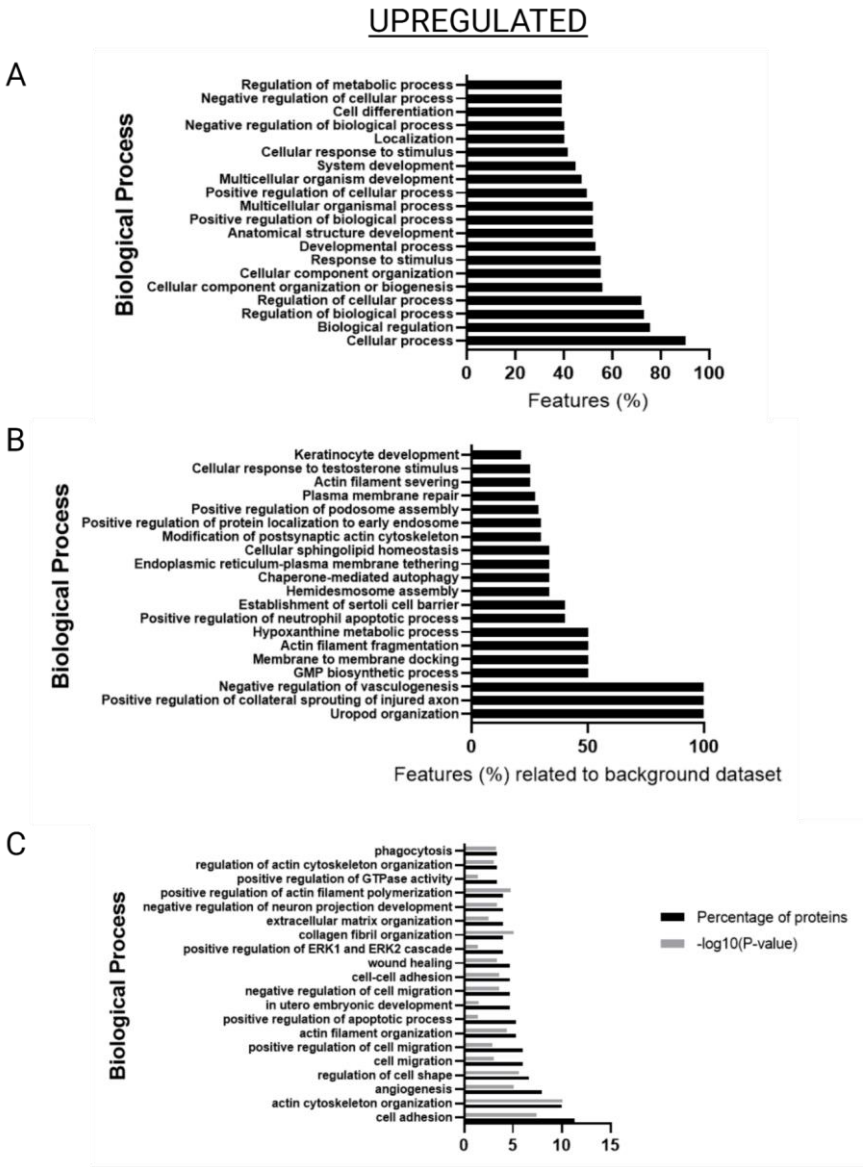

Figure 44. Functional enrichment analysis of Biological Process GO terms of upregulated proteins at postnatal day 30. String functional enrichment analysis according to the percentage of features or related to background dataset for upregulated proteins (A and B, respectively). (C) FunRich functional analysis. The highest FDR and *p-value* top 20 features are shown.

USC
UNIVERSIDADE DE SANTIAGO DE COMPOSTELA

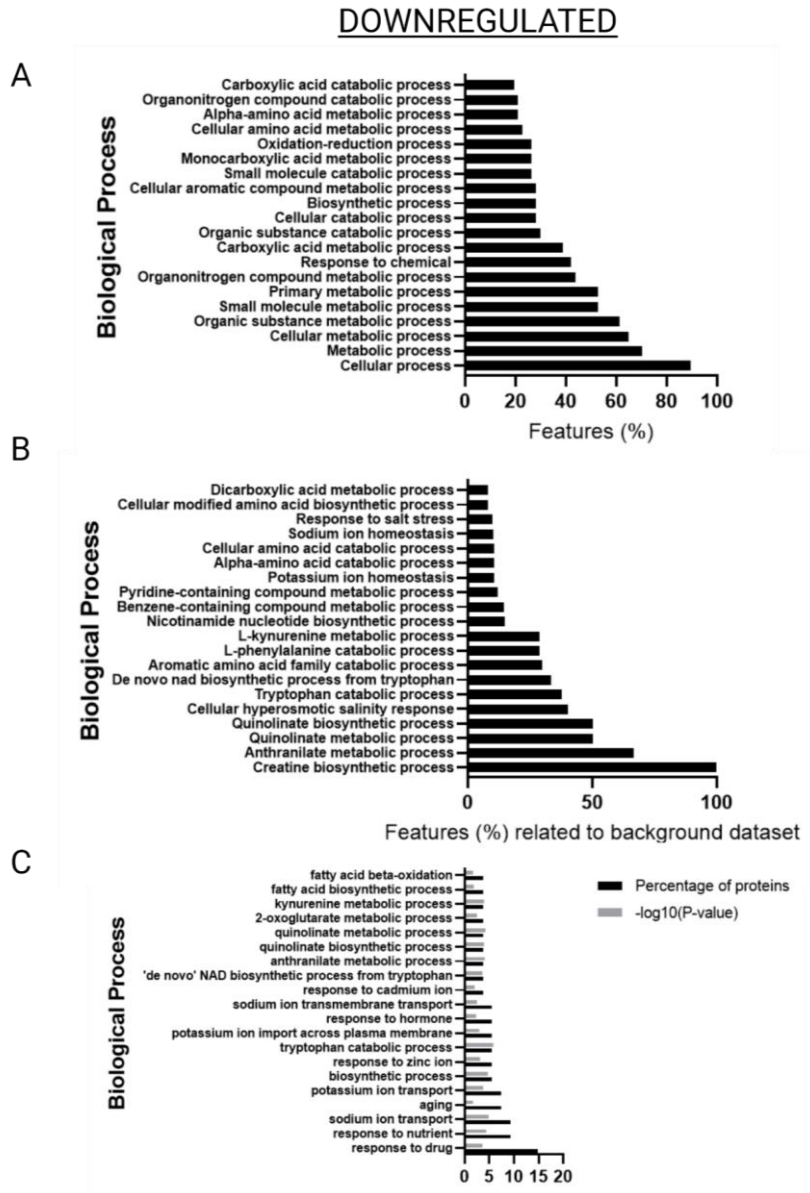

Figure 45. Functional enrichment analysis of Biological Process GO terms of downregulated proteins at postnatal day 30. String functional enrichment analysis according to the percentage of features or related to background dataset for downregulated proteins (A and B, respectively). (C) FunRich functional analysis. The highest FDR and *p-value* top 20 features are shown.

On the other hand, we also performed an analysis of cellular component (Figure 46 and Figure 47). For upregulated proteins, most enriched components were associated with cytoplasm, organelles and membrane (Figure 46A). If we considered most enriched features attending to the background dataset, we observed terms mostly related to cytoskeleton (Figure 46B). Analysis of cellular component with FunRich tool obtained similar results with most enriched terms associated with cytoplasm, plasma membrane, extracellular space and cytoskeleton (Figure 46). On contrast, downregulated proteins were distinctly related to mitochondrion, as well as membrane, according to String database both of percentage of features as well as related to background dataset (Figure 47A and B). Moreover, according to FunRich analysis, these terms appeared also enriched as well as other terms as exosome related terms (Figure 47C).

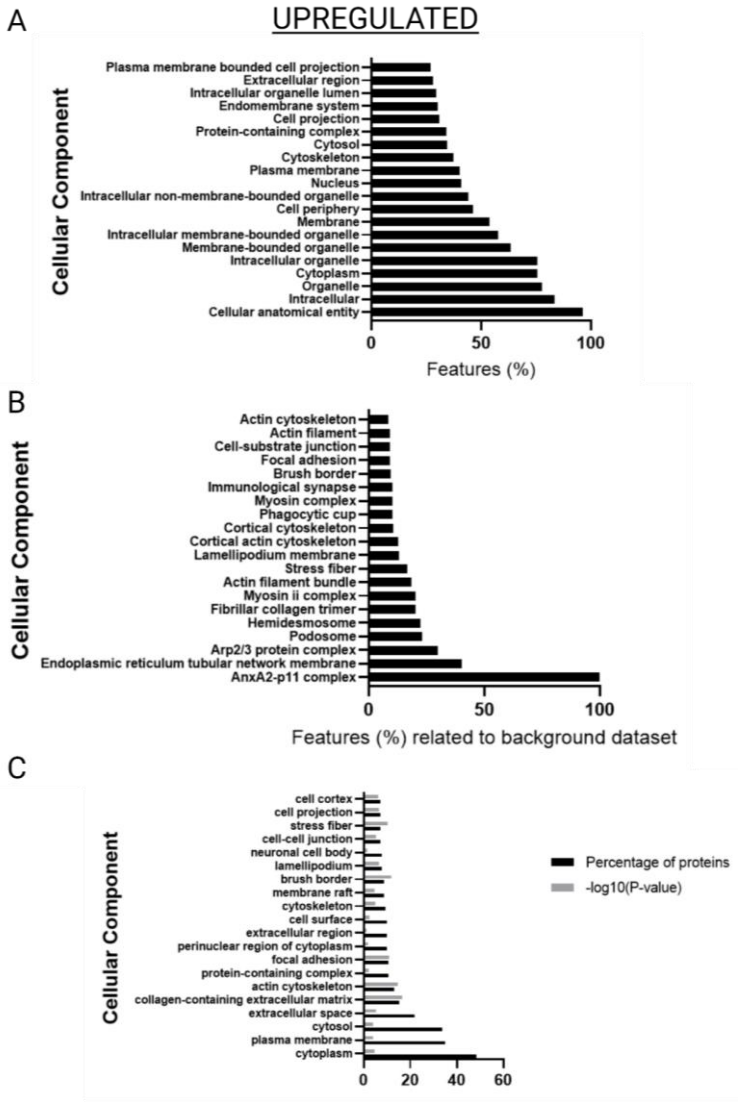

Figure 46. Functional enrichment analysis of Cellular Component GO terms of upregulated proteins at postnatal day 30. String functional enrichment analysis according to the percentage of features or related to background dataset for upregulated proteins (A and B, respectively). (C) FunRich functional analysis. The highest FDR and *p-value* top 20 features are shown.

USC
UNIVERSIDADE DE SANTIAGO DE COMPOSTELA

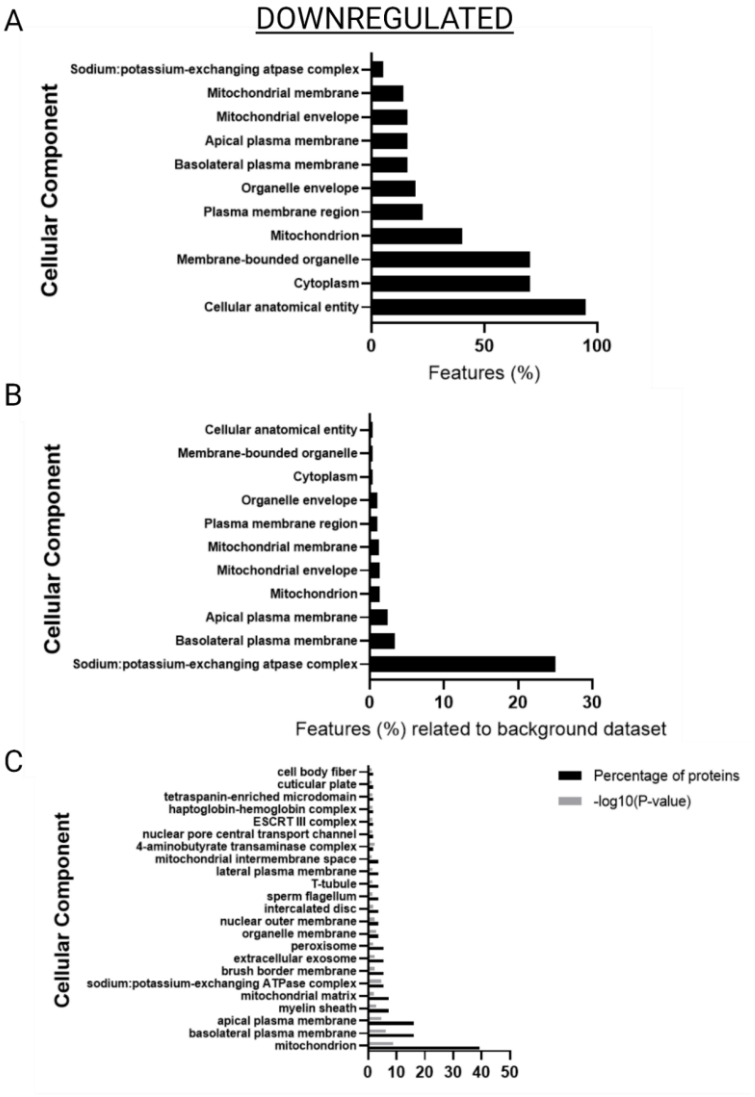

Figure 47. Functional enrichment analysis of Cellular Component GO terms of downregulated proteins at postnatal day 30. String functional enrichment analysis according to the percentage of features or related to background dataset for downregulated proteins (A and B, respectively). (C) FunRich functional analysis. The highest FDR and *p-value* top 20 features are shown.

4.1.4.3 Comparative study between libraries

After that, we decided to compare the result obtained by the different libraries to distinguish those primary pathways of cystogenesis from those secondary to it. We compared the DEPs with a fold change > 2 of the libraries done only with samples from postnatal 18 or 30 days and the library generated with the combination of both days (Figure 48). We observed that a postnatal day 18 no proteins were shared between libraries in both upregulated and downregulated proteins. In fact, surprisingly, while in the library only from postnatal day 18 there are only downregulated proteins in KO, in the joint library most of them are upregulated in KO samples. When we analyzed what happened at postnatal day 30, we noted that only 38 upregulated proteins were shared between libraries, what meant a 40% of only day 30 library and almost 25% of the joint library; and 26 downregulated proteins were shared between libraries, a 45% of each library.

USC
DE SANTIAGO
DE COMPOSTELA

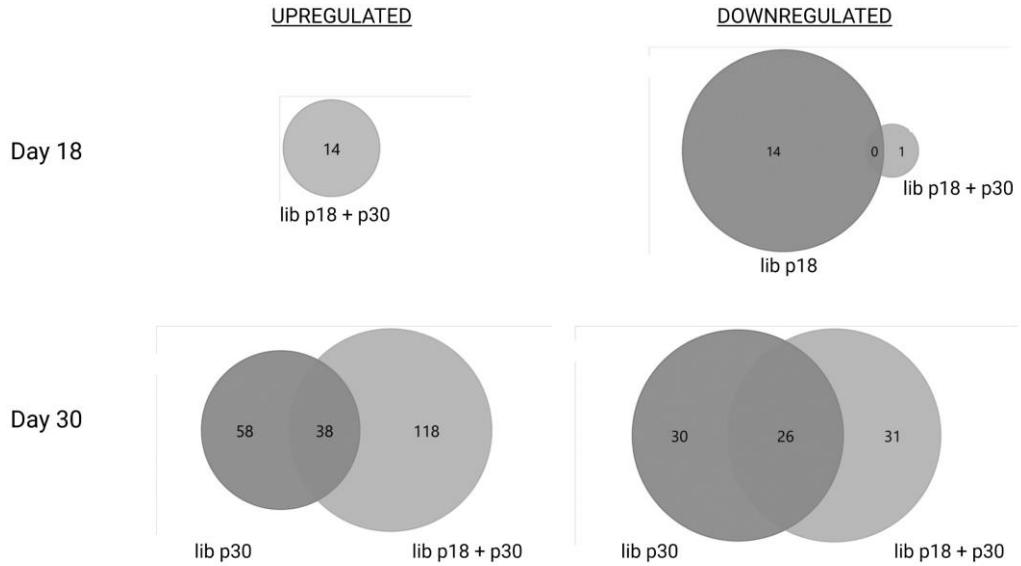

Figure 48. Venn diagrams of results of different libraries. Comparison of DEPs with a fold change > 2 between p18 and p30 alone libraries and the p18+p30 joint library.

However, due to the low overlap between the DEPs with a fold change > 2, we decided to compare the pathways in which they are involved in order to obtain more valuate information. This could only be done at postnatal day 30, because we found both upregulated and downregulated proteins. For this we decided to do FunRich analysis. As we could see in Figure 49 and Figure 50, virtually all of the most enriched pathways are shared both in terms of biological processes and in the cellular component.

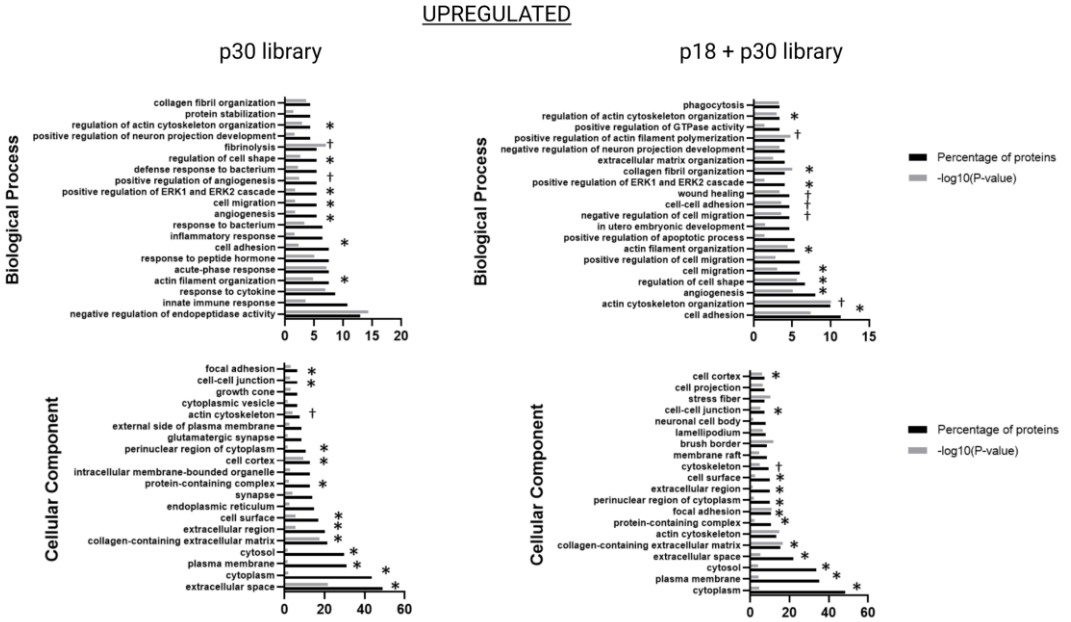

Figure 49. Comparison of pathways involved in upregulated proteins according to FunRich. GO enrichment of protein significantly upregulated according to FunRich showing 20 most enriched biological process and cellular component with p-value <0,05 by hypergeometric test. * Means equal GO term † means similar GO term.

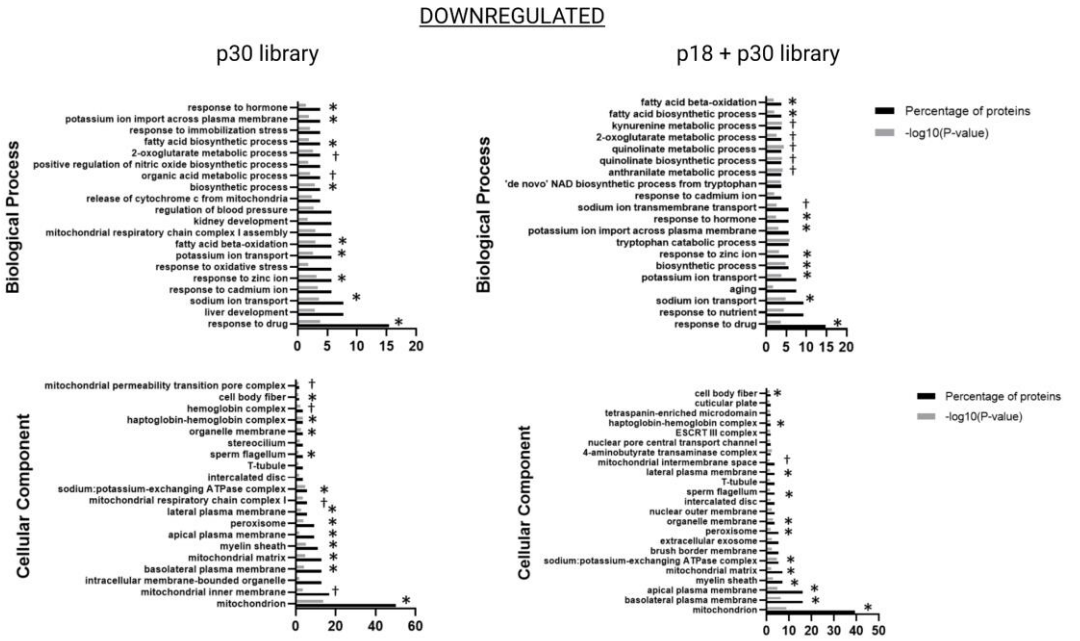

Figure 50. Comparison of pathways involved in downregulated proteins according to FunRich. GO enrichment of protein significantly downregulated according to FunRich showing 20 most enriched biological process and cellular component with p-value <0,05 by hypergeometric test. * Means equal GO term † means similar GO term.

4.1.4.4 Comparative study of differential proteome of postnatal days 18 and 30.

Finally, we decided to see if there was any protein that started to be altered at postnatal day 18 and continue altered in more severe stages at postnatal day 30, to study those proteins that are constant throughout the process of cystogenesis. For this purpose, we compare differential proteome of day 18 and day 30 using the joint library. Only 3 proteins were shared among all DEPs with a fold change > 2 (Figure 51A and B). To revalidate this result, we compared the normalized summatory of areas of the SWATH analysis of these three proteins and we observed how all of them were upregulated in KO samples (Figure 51B). In summary, Vimentin, Spondin-1 and RNA-binding protein 3 are the only proteins that were altered in early and advanced stages of the disease.

USC
UNIVERSIDADE DE SANTIAGO DE COMPOSTELA

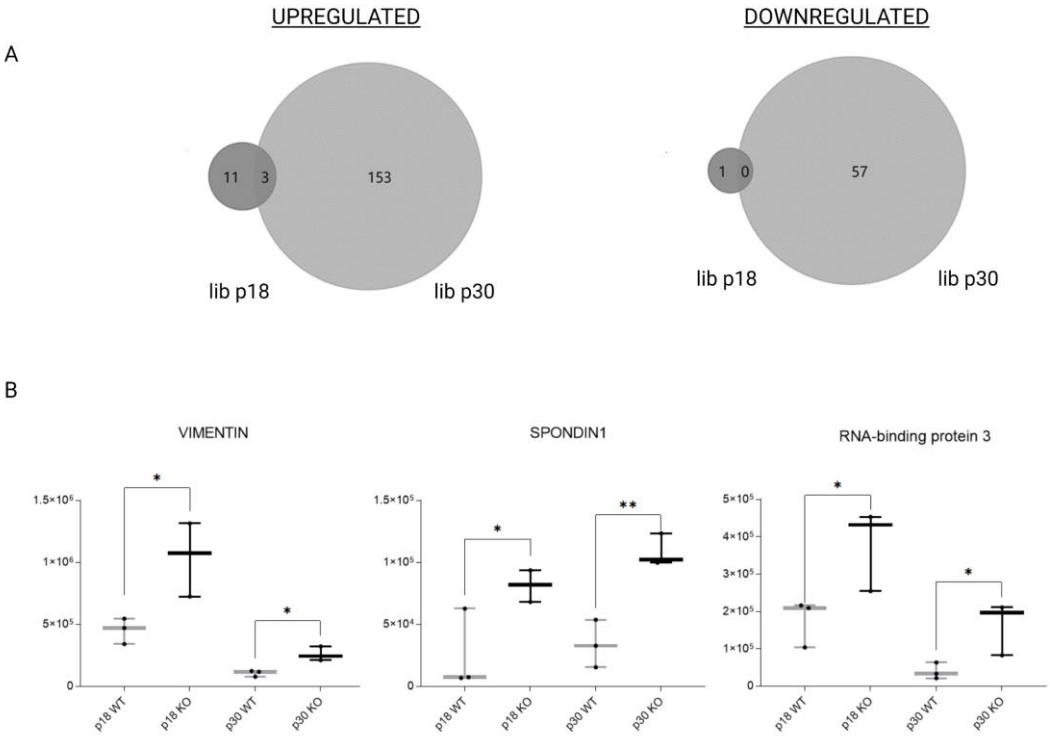

Figure 51. Comparison of differential proteome of postnatal day 18 and day 30. A) Venn diagrams showed shared upregulated and downregulated proteins between each day. B) Box and whiskers plot of normalized summatory spectral areas of SWATH analysis of the three shared proteins between postnatal day 18 and day 30, minimum to maximum and all points are represented. Statistical analysis was performed using Student's t-test comparing conditions inside each group. $p<0.05$ by Student's *t*-test (two-tail) was considered as a significant result: ns represent not significative; * $p<0.05$; ** $p<0.01$.

Table 1. Proteins significatively altered with a fold change > 2 in postnatal day 18 (p18) and day 30 (p30) in the differential comparison between *Wild Type* and Mutants. FC means Fold Change

Entry Name	UniProt Name	Name		FC p18	FC p30
P20152	VIME_MOUSE	Vimentin	↑	2,29	2,44
Q8VCC9	SPON1_MOUSE	Spondin-1	↑	3,18	3,2
O89086	RBM3_MOUSE	RNA-binding protein 3	↑	2,16	4,2

4.1.4.5 Validation of target candidates

The three proteins altered in postnatal day 18 and day 30 were selected for validation using other methodology approaches: transcriptomic with RT-qPCR and proteomic using *Western Blot.* Validation was performed using others six independent samples of each group.

Gene expression analysis by RT-PCR showed that only Vimentin is significatively overexpressed which correlated with the increased of protein abundance in KO samples (Figure 52A), although Spondin-1 showed a tendency to be overexpressed but not significantly (Figure 52B). On the other hand, RNA-binding protein 3 was no significatively altered at postnatal day 18, in contrast, it was downregulated at postnatal day 30, the opposite situation as the protein abundance by SWATH analysis (Figure 52C).

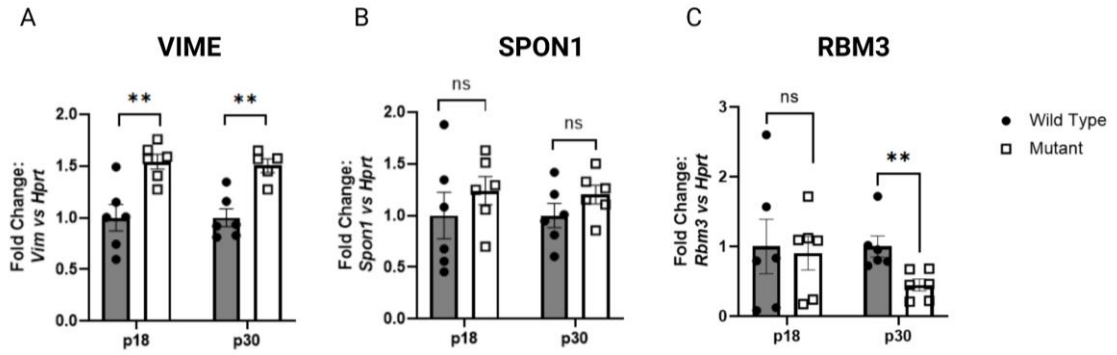

Figure 52. Validation of possible targets by RT-qPCR. Gene expression of Vimentin (A), Spondin-1 (B) and RNA-binding protein (C). A number of 6 samples were used for each group. *Hprt* expression was used as housekeeping. Bars represent means ± SEM. Student`s t-test with two-tail was used and a value of P<0.05 was considered significant. ns: not significant (p≥0.05), * p<0.05, ** p<0.01.

Moreover, we performed the validation analysis using Western blot as other proteomic approach. In this case, all three (Vimentin, Spondin-1 and RNA-binding protein 3) were validated as upregulated at postnatal day 30. However, none of them are validated at postnatal day 18, even without seeing any trend (Figure 53 and Supplementary Figure 1).

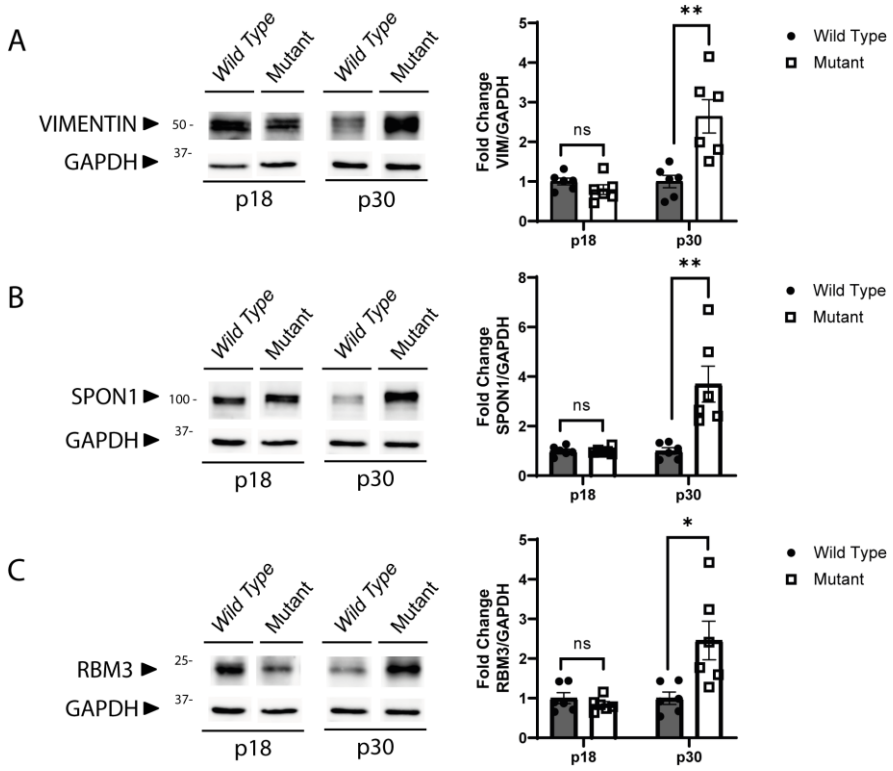

Figure 53. Validation of possible targets by Western Blot. The protein abundance of the three possible targets of our quantitative proteomic SWATH MS data were validated by Western Blot (WB) analysis: (A) Vimentin, (B) Spondin-1 and (C) RNA-binding protein 3. GAPDH was used as housekeeping. Bars represent means ± SEM. Student`s t-test with two-tail was used and a value of P<0.05 was considered significant. * p<0.05, ** p<0.01. Full WBs are shown in Supplemental Figure 1.

To further investigate why these proteins were not validated by *Western Blot* at day 18 of development, we performed the 2-diamensional *Western Blot*. By this approach, we were able

to distinguish the different isoforms and post-translational modifications, not possible in a 1D-PAGE gel. For all 3 proteins (Figure 54A, B and C), we could see the majority spot corresponding to the protein without modification and different spots between WT and Mut that indicate that this proteins have a lot of different modifications that make more difficult to quantified it by *Western Blot* 1D.

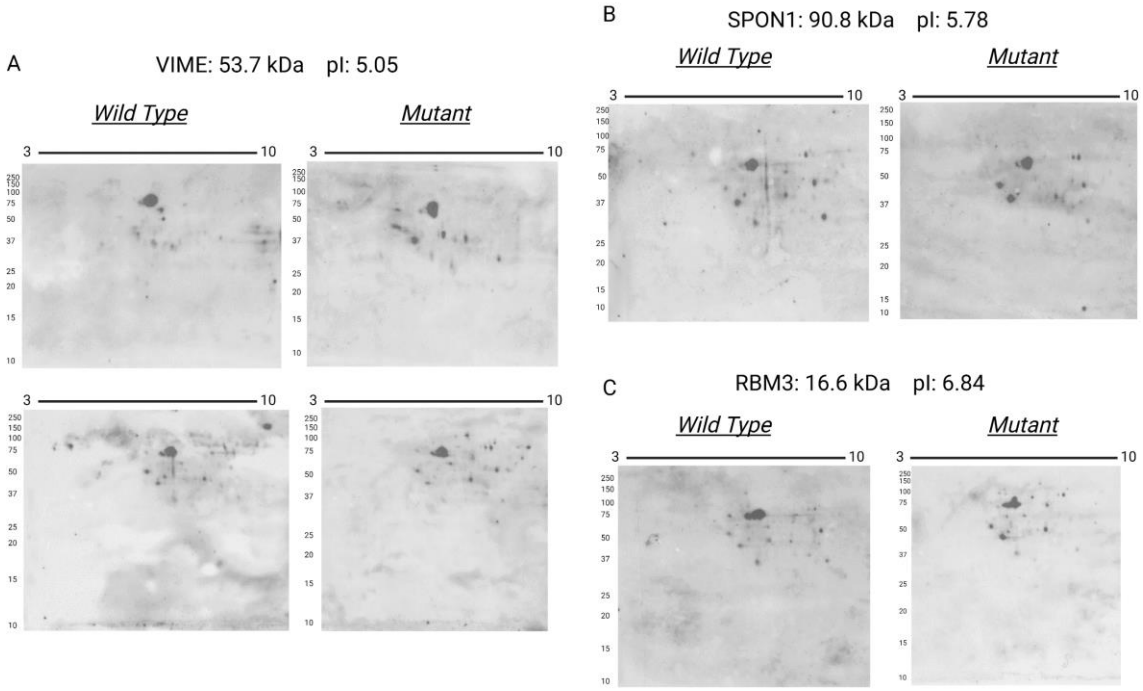

Figure 54. **Validation of possible targets at postnatal day 18 by *Western Blot* 2D.** Vimentin (A), Spondin-1 (B) and RNA-binding protein 3 (C) analysis by 2 dimensions *Western Blot*, separated by a isoelectric point from 3 to 10.

Furthermore, to obtain more information and observe what happen *in vivo*, we performed an immunofluorescence assay. We started studying Vimentin, because it was the only that was validated by RT-PCR and seemed to be altered by *Western Blot* 2D and we combined with stained the collecting duct cyst with DBA, which are the most prominent and big cyst in our mouse model as well as in ADPKD. As we could see in Figure 55, Vimentin behaved in two ways. On one side, as filaments with orientation that follow the orientation of the tubules of the nephron. This occurred from the papilla and along the entire medullary zone. These filaments were thin in *Wild type* samples, and wider and thickened in cystic individuals. On the other side, there was staining in the more cortical area of the nephron, where Vimentin surrounds the tubule, what appeared stained in both *Wild Type* and mutant samples. In both postnatal day 18 and day 30 mutant samples, we observed the cortical cysts stained green, these were smaller in diameter than the DBA cysts. Similarly, the tubular cells constituting these cysts were usually not as flattened as those belonging to DBA cysts. DBA cysts are predominantly found in the medulla, so they do not coincide with the cysts stained with Vimentin. However, we could observe some cysts that appear to be stained by both antibodies. Generally, Vimentin seemed to behave differentially between mutant and *Wild type* samples from early stages of disease.

USC UNIVERSIDADE DE SANTIAGO DE COMPOSTELA

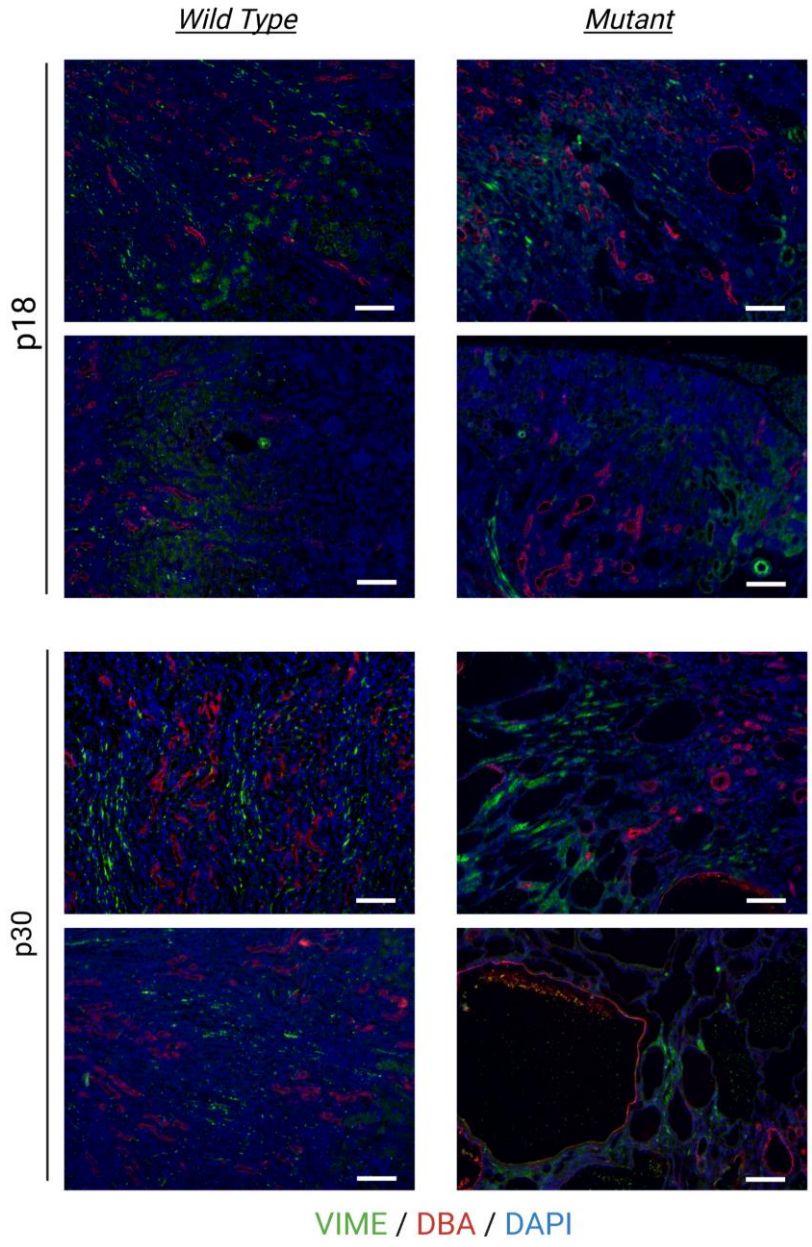

Figure 55.Validation of Vimentin at postnatal days 18 and 30 by Immunofluorescence. Immunofluorescence staining of Vimentin in green, collecting duct marker DBA in red and nuclei marker DAPI in blue. Scale bar 100 µm.

Overall, SWATH-MS proteomic data provided us interesting new targets and molecular pathways for future works and possible new therapeutic approaches for ADPKD. We identified those pathways that are altered early in and throughout the course of the disease, as well as possible targets for their modulation among which we highlight Vimentin, Spondin-1 and RNA-binding protein 3 due to its alteration at all stages of the disease.

USC UNIVERSIDADE DE SANTIAGO DE COMPOSTELA

4.2 CHAPTER 2. NEW BIOMARKERS IN URINE FOR DIAGNOSIS AND PROGNOSIS OF ADPKD.

Currently, the most used parameter to detect and follow-up renal function is the measure of creatinine. Both its measurement in blood, which together with the CKD-EPI equation allows us to estimate the glomerular filtration rate (GFR), and its measurement in urine together with the measurement of albumin allows us to estimate the albumin-to-creatinine ratio to know the amount of protein secreted that indicates a possible renal damage. However, this is a late biomarker and could not reflect early stages of disease. Besides, genetic diagnosis could also help to predict the prognosis of the disease as a genetic scoring alone (47) or together with clinical data as a PROPKD score (45). Nevertheless, all these data do not reflect the real status of the kidney function neither its evolution throughout the outcome of the disease. Because of that, the research of novel biomarkers is required.

We decided to focus our biomarker research on urine because it is a non-invasive liquid biopsy. Nevertheless, urine is a complex sample, and detection of potential biomarkers there have never been an easy task. This is especially difficult because urine may reflect variations from the whole urinary system, and also the whole body, and may content residuals from processes that are not always restricted to kidney (289). In this regard, isolation of the urine protein content associated to natural components would be useful. It is known that Glycosaminoglycans (GAGs) are altered related to diseases (289–291). GAGs could be associated with proteins forming proteoglycans that are part of the glycocalyx and the extracellular matrix, that are key points to maintain the correct function of the kidney (292,293).

In order to specifically isolate the fraction associated to GAGs, we developed a new method, ExoGAG, taking advantage of a cationic colorant that is able to create specific complexes with negatively charged sulfated GAGs, precipitating them and allowing the study of the fraction that is bound to them. Our new technique, which is further explained in methods, is protected by patent application P201531297 (PCT/ES2016/070637).

4.2.1 Characterization of glycoprotein component of urine in a time course ADPKD mice.

For this purpose, we perform a differential comparison between *Wild Types* (WT) and mutants (KO or Mut, interchangeably) mice urine samples from an ADPKD orthologous murine model (*Pkd1*$^{cond/cond}$*; Tam-Cre* mouse) with the objective to discover possible biomarkers that are altered across the disease (Figure 56). For this purpose, we collected a 12-hour urine samples from postnatal days 22, 30 and 45 of the same WT and Mut individual to perform a time course study.

USC UNIVERSIDADE DE SANTIAGO DE COMPOSTELA

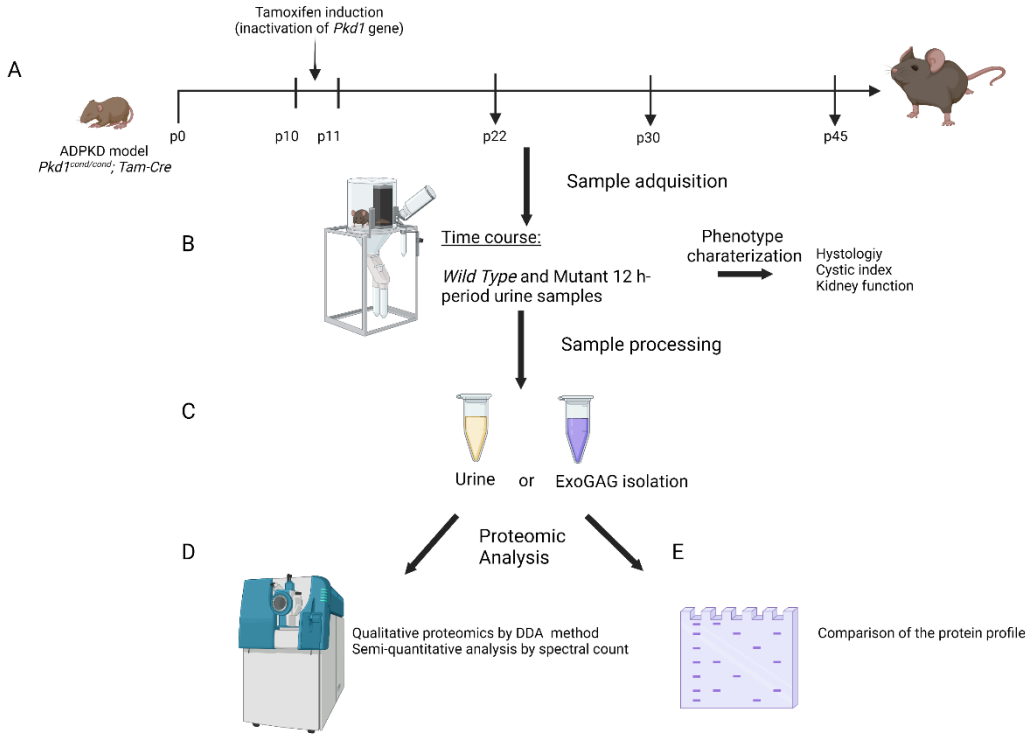

Figure 56. Illustrated workflow scheme. (A) First, we used an ADPKD mouse model (*Pkd1*$^{cond/cond}$; *Tam-Cre* mice, inactivating *Pkd1* gene at day 10-11) to obtain *Wild type* and Mutant mice. (B) We performed a *time course* collection of urines at postnatal days 22, 30 and 45. (C) Next, the urine was processed or isolated with ExoGAG, for the protein extracted and quantified. (D) A DDA analysis and a semi-quantitative analysis by Spectral count were made to obtain the whole urine or ExoGAG proteome. (E) Finally, we compared the whole protein profile isolated by ExoGAG throughout the progression of the disease.

Mice were induced with tamoxifen to inactivate the *Pkd1* gene at postnatal days 10-11. To draw a direct comparison with our studies (92,278) and the proteomic approach of this thesis on the Chapter 1, we collected urine from mice at the age of 22 (p22), 30 (p30) and 45 (p45) days. We were not able to collect urine at the same age of 18 days for the 12-hour period due to the small size of the mice for being in the metabolic cage. Phenotype characterization of all groups is shown in Figure 57. The cystic kidney characterization by hematoxylin-eosin stained shown more severe cystic phenotype in mutants at day 30 and 45 than at day 22 (Figure 57A-C). Cystic index and number of cysts were significatively increased in mutants in all postnatal days (Figure 57D and E). However, the appearance of cysts did not imply an increase in kidney size or impairment of renal function as measured by BUN at postnatal day 22, whereas already from postnatal day 30 there was an increase in kidney size and significant renal damage (Figure 57F and G).

USC UNIVERSIDADE DE SANTIAGO DE COMPOSTELA

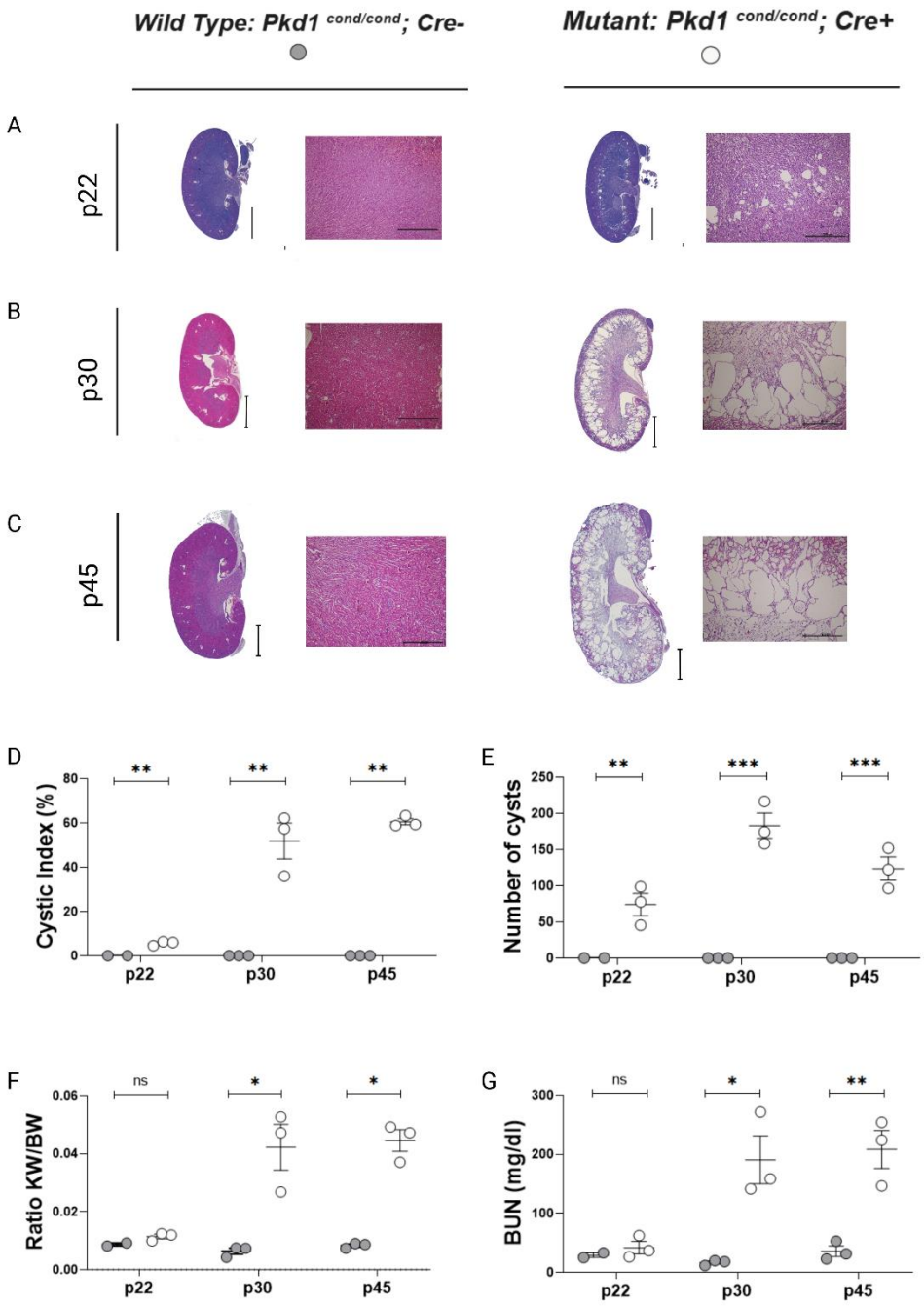

Figure 57. Characterization of the cystic kidney phenotype at day 22, day 30 and day 45. Representative macroscopic and microscopic images of hematoxylin-eosin stained from kidneys of Wild Type and Mutant mice sacrificed at day 22 (A), day 30 (B) and day 45 (C). Scale bar, 2mm (left panel) and 100µm (right panel). A *n* of 3 samples per group were used. (D, E) Renal cystic index and number of cysts of the different phenotypes. (F) Kidney weight to body weight ratios and (G) Blood Urea Nitrogen (BUN) concentrations of different groups. Bars represent means ± SEM in all cases. $p<0.05$ by Student's *t*-test (two-tail) was considered as a significant result: ns represent not significative; * $p<0.05$; ** $p<0.01$; *** $p<0.001$.

USC UNIVERSIDADE DE SANTIAGO DE COMPOSTELA

4.2.1.1 Comparison between proteomic component of urine and isolated fraction with ExoGAG

First of all, we started with a proteomic analysis of urine and the isolated fraction with ExoGAG of *Wild Type* and Mutant at days 30 and 45. We could not performed it with day 22

samples due to the small amount of proteins. A total of 20µg of each sample were sequenced and analized by Qualitative DDA method. A mean of 200 proteins were identified in the isolated fraction with ExoGAG, in contrast to a mean of 100 proteins in the whole urine (Figure 58A). The analysis of the cellular component with FunRich tool showed that both urine and ExoGAG proteins were related to same components, however they were more enriched with ExoGAG isolation (Figure 58B). All these data confirm that using ExoGAG we could performed a deeper and more sensitive analysis.

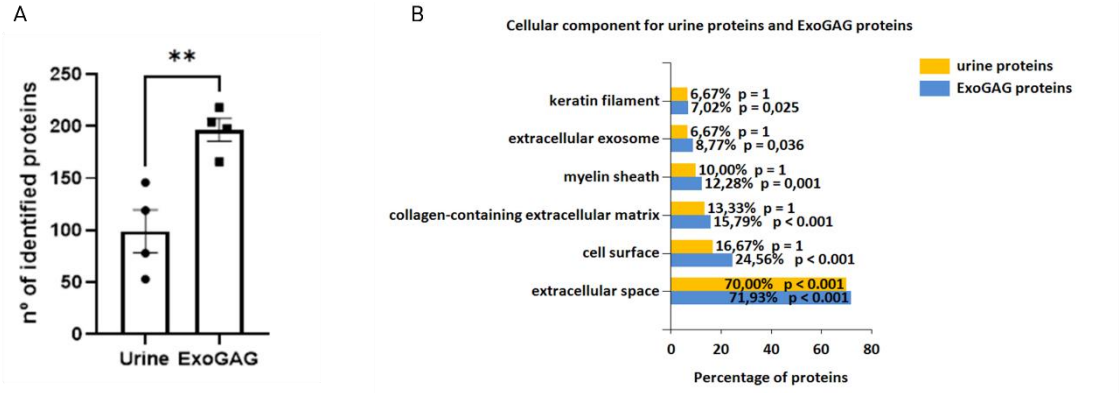

Figure 58. Comparison between proteomic qualitative analysis of urine and isolation with ExoGAG of p30 and p45 mice urine samples. A. Number of identified proteins of each sample. B. FunRich cellular component analysis for urine and ExoGAG isolated proteins. A *n* of 4 samples were used. The significative, with a p-value <0,05, involved cellular component terms for ExoGAG proteins were shown.

4.2.1.2 Search for biomarkers of disease progression through differential comparison of Wild type and Mutants samples isolated with ExoGAG

Next, to elucidate if there were differences in proteins or protein abundance both between *Wild Type* and Mutants and throughout the course of the disease, we made a differential comparison among WT and KO p30 and WT and KO p45 samples by a semi-quantitative analysis by spectral count using Scaffold software (Supplementary Table 5, 6, 7 and 8). The principal differential proteins are shown in Table 2. In this study we did not consider pheromone proteins because these are related to maturity more than disease. Notably, only one protein, UROM (Uromodulin), decreases in abundance with disease progression. Three proteins, AMYP (Pancreatic alpha-amylase), EGF (Pro-epidermal growth factor) and NAPSA (Napsin-A) are much more enriched in *Wild type*. In addition, most of the proteins that increase with disease progression are more enriched in Mutants and increase in abundance throughout the disease.

Table 2. Summary list of principal proteins with differences in abundance between *Wild type* and Mutant samples and throughout the disease. Semi-quantitative analysis is based in Total Spectral Count. *Maximal Total spectral count: >500 √√√√√, 250-500 √√√√, 100-250 √√√, 50-100 √√, 25-50 √, 1-25 √, 0 -.*

Protein Name	Uniprot Name	WT	Mut	Disease progression
Uromodulin	UROM_MOUSE	√√√√√	√√	↓
Pancreatic alpha-amylase	AMYP_MOUSE	√√√√√	√	-
Pro-epidermal growth factor	EGF_MOUSE	√√√√√	√	-
Napsin-A	NAPSA_MOUSE	√√√√	√	-
Albumin	ALBU_MOUSE	√√√√	√√√√	↑

Complement C3	CO3_MOUSE	√	√√√√√	↑
Hemopexin	HEMO_MOUSE	√	√√√√	↑
Protein AMBP	AMBP_MOUSE	√	√√√√	↑
Ceruloplasmin	CERU_MOUSE	√	√√√	↑
Angiotensinogen	ANGT_MOUSE	√	√√√	↑
Apolipoprotein A-IV	APOA4_MOUSE	-	√√√	↑
Fibrinogen alpha chain	FIBA_MOUSE	-	√√	↑
Fibrinogen beta chain	FIBB_MOUSE	-	√√	↑
Fibrinogen gamma chain	FIBG_MOUSE	-	√√	↑

Knowing that there were differences in protein abundances, we decided to see if there were differences in the protein profile. For this, we compared *Wild type* and Mutant urine samples isolated with ExoGAG at postnatal day 22, 30 and 45 by staining the whole protein content with Oriole (BioRad®). At postnatal day 22, there were little amount of protein, but enough to see that no major differences were discernible between WT and KO samples (Figure 59A). However, at postnatal day 30 (Figure 59B), we started to observed difference in relative abundance of different bands, as we could see in the bands at 100, 55 and 20 kDa. These differences were more severe if we compared WT and KO at postnatal day 45 (Figure 59C), where even there were more differential bands as the 43 or 30 kDa. In fact, we could observed that even among the different days in *Wild type* there was a change at protein pattern, probably due to the development status of the kidney.

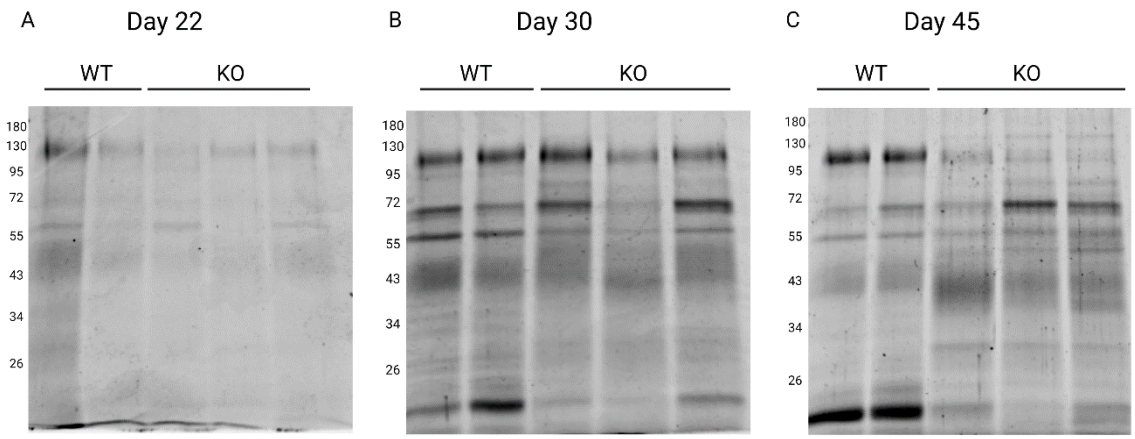

Figure 59. Urinary pattern of proteins associated to GAGs in mice urine. Urine collected from mice at age 22 (A), 30 (B) and 45 (C) and isolated with ExoGAG. SDS-PAGE gels stained with Oriole (BioRad®) showed that different pattern among WT and KO samples and during the disease progression.

Therefore, we cut the gel bands in order to sequence all these bands and validate the proteomic data obtained in the whole sample (Supplementary Figure 2). The results showed that the relative abundance of proteins as UROM (2 and 3 bands of p45 samples), ALBU (band 4 of p30 and p45 samples), AMYP (band 6 of at p45 samples) and AMBP (band 8 of p45 samples) correlated with previous obtained data. All these data show that this method allows us to identify potential biomarkers of progression of the disease.

USC
UNIVERSIDADE DE SANTIAGO DE COMPOSTELA

4.2.2 Identification of biomarkers of disease by characterization of glycoprotein component of urine in ADPKD patients.

Taking into account our previous data in an animal model, we decided to find out if it happened also in humans. For this purpose, we analysed second morning urine from patients and healthy donors as is described in Figure 60. We selected patients with truncated mutations in *PKD1* or *PKD2* genes, because truncating mutations manifest a more rapid and severe progression of the disease.

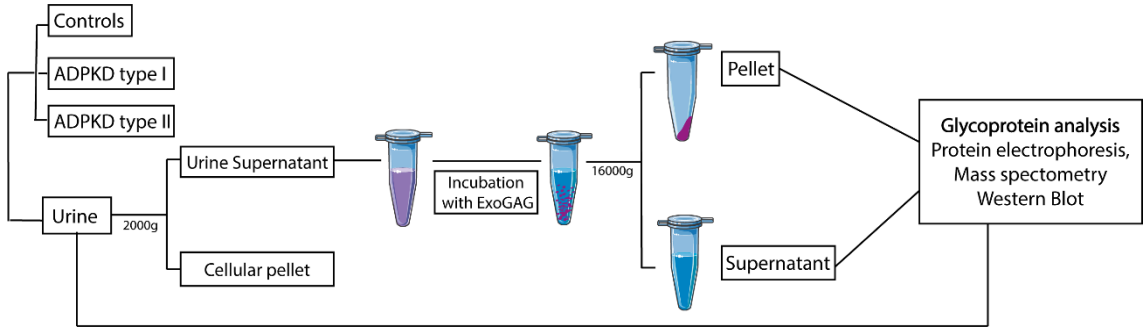

Figure 60. Workflow scheme of urine isolation with ExoGAG. Urine collected from ADPKD patients and healthy donors were incubated with ExoGAG, isolating the fraction bound to GAGs. Glycoprotein analysis were performed in pellet, supernatant and urine.

4.2.2.1 Chracterization of the GAG associated proteins isolated fraction (ExoGAG pellet) in controls and patients

Firsrt of all, we decided to characterized the GAG associated proteins isolated fraction (ExoGAG pellet). We observed a constant fingerprint of GAG associated proteins in control samples (Figure 61A) staining with the whole protein staining with Oriole (BioRad®). However, our results revealed that the constant pattern was altered in PKD patients (Figure 61B and C). This alteration depends on renal function correlated with serum creatinine, being more extreme in the most severe stages of the disease (high levels of creatinine) but beginning to be altered at initial stages of the disease with relatively low creatinine levels. Moreover, the variation of the profile in patients was characteristic of the disease, as can be observed between patients with mutations in *PKD1* (Figure 61B), and patients with mutations in *PKD2* (Figure 61C), where this pattern had more pronounced change.

USC UNIVERSIDADE DE SANTIAGO DE COMPOSTELA

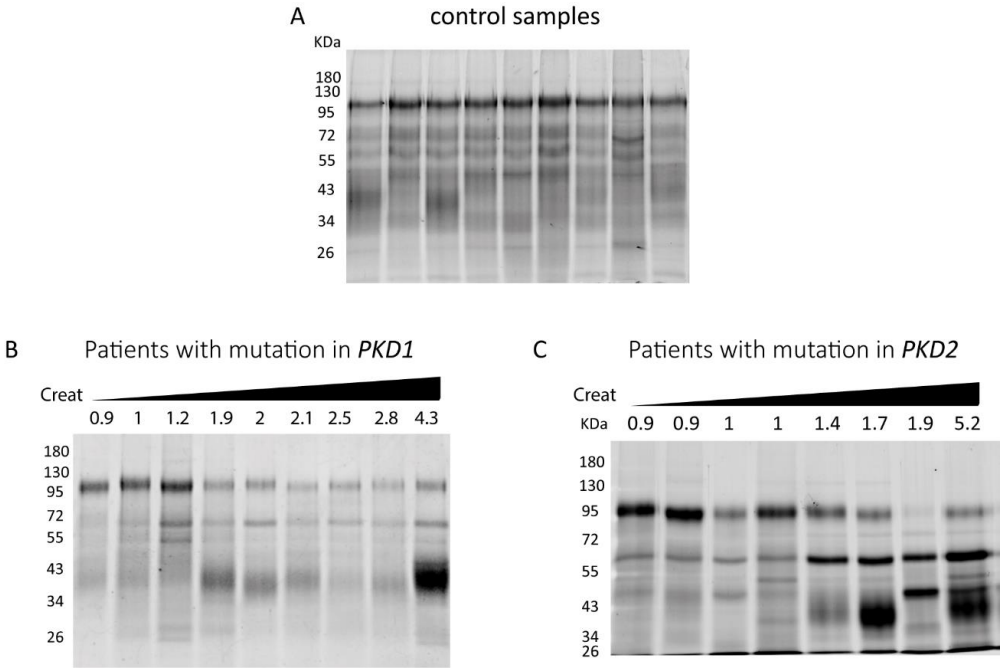

Figure 61. Protein analysis of ExoGAG pellet. Whole protein component of urine samples precipitated with ExoGAG from controls (A), patients with ADPKD type I (B) and patients with ADPKD type II (C) staining with Oriole (BioRad®). Patients were ordered according to the increase in serum creatinine (Creat).

4.2.2.2 Identification of biomarkers in ADPKD patients by mass spectrometry sequencing

To identify new biomarkers and understand the changes produced by the disease, we cut the more differential bands for mass spectrometry sequencing and analysis by qualitative DDA method and semi-quantitative analysis by spectral count (Supplementary Figure 3 and Supplementary Table 9,10,11,12,13,14,15,16,17,18,19 and 20). This analysis were performed using ExoGAG pellets from patients with mutations in *PKD2* because of its more noticeable variations.

The principal differential proteins are shown in Table 3. Remarkably, as we observed with mice urine, only one protein, UROM, decreases in abundance with disease progression. Moreover, ALBU, APOA4, CERU, FIBA, FIBB, FIBG and AMBP that were upregulated in mice appeared also increased throughout the disease.

Table 3. Summary list of principal proteins with differences in abundance throughout the disease in ExoGAG pellet in *PKD2* patients.

Protein name	Uniprot name	Disease progression
Uromodulin	UROM_HUMAN	↓
Albumin	ALBU_HUMAN	↑
Alpha-1-antitrypsin	A1AT_HUMAN	↑
Apolipoprotein A-IV	APOA4_HUMAN	↑
Carbonic anhydrase 1	CAH1_HUMAN	↑
Ceruloplasmin	CERU_HUMAN	↑
Dipeptidyl peptidase 4	DPP4_HUMAN	↑
Galectin-3-binding protein	LG3BP_HUMAN	↑

USC UNIVERSIDADE DE SANTIAGO DE COMPOSTELA

Fibrinogen alpha chain	FIBA_HUMAN	↑
Fibrinogen beta chain	FIBB_HUMAN	↑
Fibrinogen gamma chain	FIBG_HUMAN	↑
Pro-epidermal growth factor	EGF_HUMAN	↑
Protein AMBP	AMBP_HUMAN	↑
Serotransferrin	TRFE_HUMAN	↑
Vitronectin	VTNC_HUMAN	↑

4.2.2.2.1 Validation of identified biomarkers by Western blot in ADPKD patients with mutation in *PKD2*

Then, we decided to validate these possible biomarkers in other patients with mutation in *PKD2* by other techniques as Western Blot. First, we tested the protein fingerprint of the samples we used. Once again, the pattern was altered related to the disease progression (Figure 62A). Afterwards, Western Blot analysis revealed that 9 of these 16 proteins were validated (Figure 62). UROM decreased in abundance in the 100 kDa band with disease progression (Figure 62B) and ALBU, A1AT, APOA4, CERU, LG3BP, FIBB, AMBP and VTNC increased (Figure 62C, D, E, F, G, H, I and J). The increase was most reflected in samples from patients with high creatinine levels. Although ALBU, CERU, AMBP and VTNC (Figure 62C, F, I and J) began to show an increase in lower creatinine levels. A schematic representation of the semi-quantitative mass spectrometry results of these validated proteins is shown in Table 4, where we could observe that almost all proteins appear in all weights.

USC UNIVERSIDADE DE SANTIAGO DE COMPOSTELA

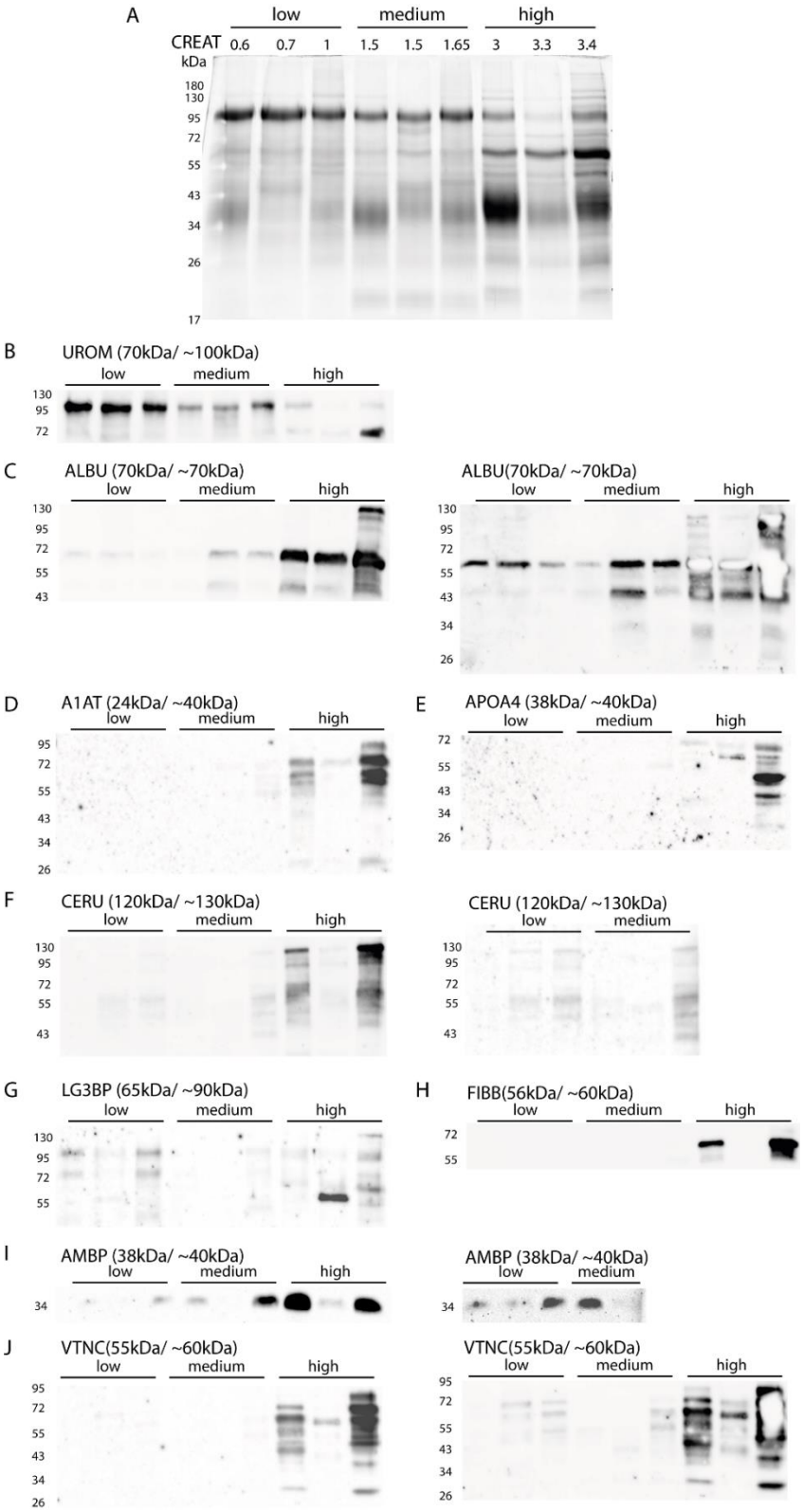

Figure 62. Validation of possible targets by Western Blot in patients with mutation in *PKD2*. On the top, the whole protein component of urine samples precipitated with ExoGAG of patients with mutation in *PKD2* staining with Oriole (BioRad®). The protein abundance of the possible biomarkers of our semi-quantitative proteomic data were validated by Western Blot: UROM (B), ALBU (C), A1AT (D), APOA4 (E), CERU (F), LG3BP (G),FIBB (H), AMBP (I), VTNC (J). Low means creatinine levels <1.1, Medium means creatinine levels between 1.2-2 and High means creatinine levels >2.

Table 4. Schematic representation of the maximum protein abundance per band by semi-quantitative analysis in ExoGAG pellets. Semi-quantitative analysis is based in Total Spectral Count. *Maximal Total spectral count: >1000 √√√√√*, 500-1000 *√√√√*, 100-500 *√√√*, 50-100 *√√*, 1-50 *√*, 0 -.

kDa	UROM	ALBU	A1AT	APOA4	CERU	LG3BP	FIBB	AMBP	VTNC
130-95	√√√√√	√√√	√	-	√	√√	-	√	√
95-72	√	√√√	√	-	√	√	√	√	√√
72-55	√√√	√√√√√	√√√	-	√	√	√√	√√	√√√
55	√√	√√√	√	-	√	√	√	√√	√
55-34	√√	√√√	√	√√	√	√	√√	√√√√	√
34-26	√	√√	√	√	√	-	√	√√	√

4.2.2.2.2 Validation of identified biomarkers by Western blot in ADPKD patients with mutation in *PKD1*

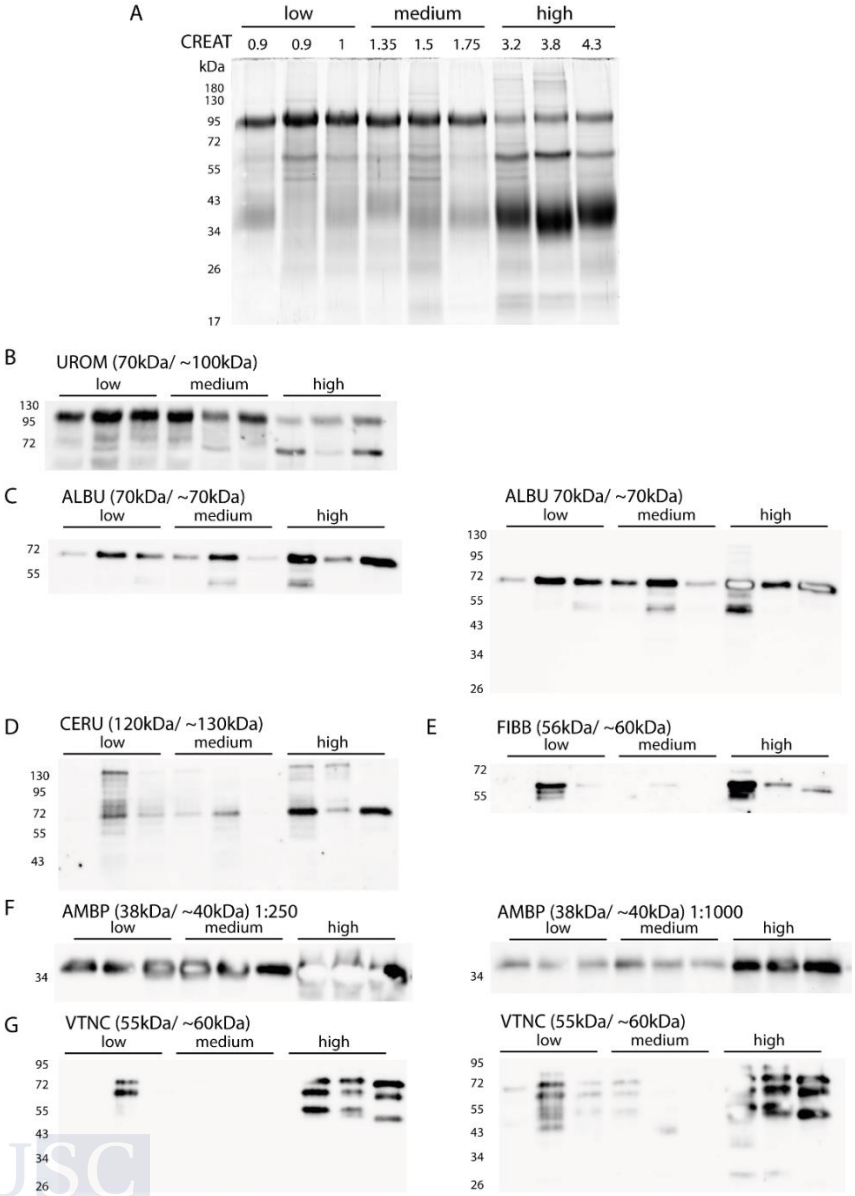

Figure 63. Validation of possible targets by Western Blot in patients with mutation in *PKD1*. On the top, the whole protein component of urine samples precipitated with ExoGAG of patients with mutation in *PKD1*

staining with Oriole (BioRad®). The protein abundance of the possible biomarkers of our semi-quantitative proteomic data were validated by Western Blot: UROM (B), ALBU (C), CERU (D), FIBB (E), AMBP (F), VTNC (G). Low means creatinine levels <1.1, Medium means creatinine levels between 1.2-2 and High means creatinine levels >2.

We studied too how these markers behaved in patients with mutations in *PKD1* (Figure 63). As before, we tested the protein fingerprint of the samples we used, and we saw again how the fingerprint was altered related to the disease progression (Figure 63A). Over again, UROM decreased in the 100 kDa band with the disease (Figure 63B) and ALBU, CERU, FIBB, AMBP and VTCN increased (Figure 63C, D, E, F and G). Although there was a sample with low creatinine that acted similar as the high creatinine. Moreover, it seemed that there were more AMBP in *PKD1* than in *PKD2* because we need to dilute the antibody to not saturated the image.

4.2.2.2.3 Quantification of biomarkers for possible use as disease markers

Considering the results of validations obtained for both *PKD2* and *PKD1* mutation patients, we could conclude that the markers that seemed to correlate best with the disease progression were UROM, CERU, AMBP and VTNC.

For patients with mutation in *PKD2*, densitometry analysis revealed that decreased of UROM correlated significatively with the increased of creatinine, even in medium values of creatinine (Figure 64A). AMBP showed a small growth at medium creatinine, especially if we take into account the value corrected for total protein, with the trend of a large increase in high creatinine values (Figure 64C). CERU and VTNC seemed constant in low and medium creatinine or, even, with a tiny trend of decreased in medium, but with a trend to raise in high creatinine (Figure 64B and D).

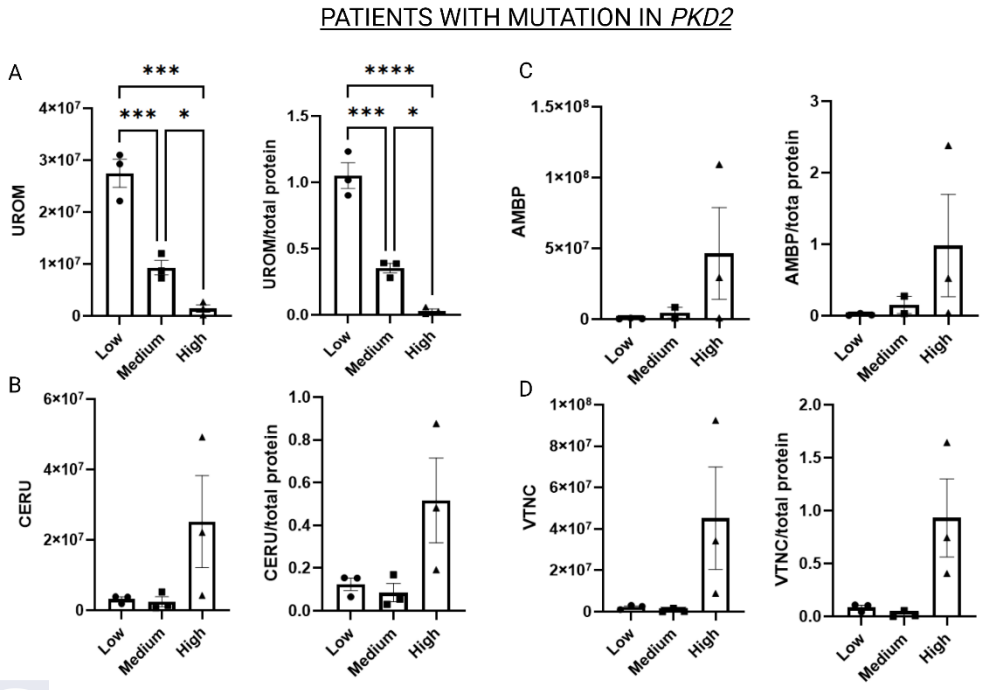

Figure 64. Densitometry analysis of Western Blot of possible targets in patients with mutation in *PKD2*. Densitometry of UROM (A), CERU (B), AMBP (C) and VTNC (D) bands and the ratio with the whole protein of the same sample obtained by Oriole staining (BioRad®) used as housekeeping. Bars represent means ± SEM. Ordinary

One-way ANOVA with multiple comparations was used and a value of P<0.05 was considered significant. Only significative comparisons are shown: * p<0.05, ** p<0.01, *** p<0.001, **** p<0.0001.

In contrast, for patients with mutation in *PKD1*, densitometry analysis revealed that UROM showed a decreasing trend with increasing creatinine levels, being significant only between the early and late stages (Figure 65A). AMBP showed a significatively increased in high creatinine in relation to low and medium ones (Figure 65C). In this case, CERU presented the tendency to decrease at medium levels of creatinine, but it did not increase in high respecting to low values (Figure 65B). And VTNC, again, seemed a tiny trend of decrease in medium, but with a significatively raised in high creatinine (Figure 65D).

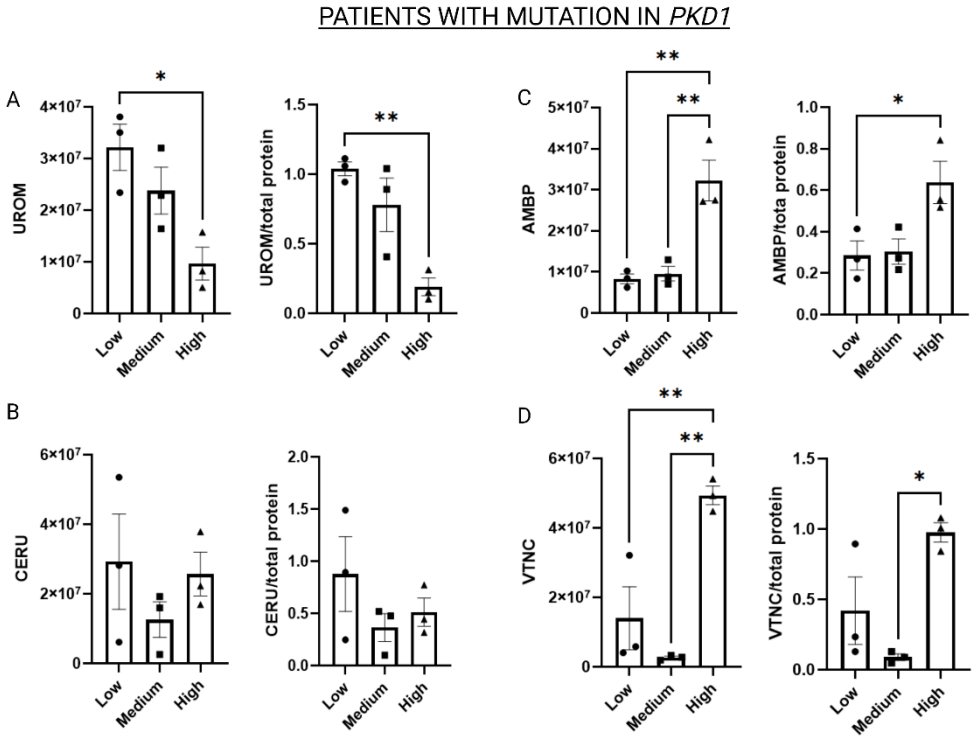

Figure 65. Densitometry analysis of Western Blot of possible targets in patients with mutation in *PKD1*. Densitometry of UROM (A), CERU (B), AMBP (C) and VTNC (D) bands and the ratio with the whole protein of the same sample obtained by Oriole staining (BioRad®) used as housekeeping. Bars represent means ± SEM. Ordinary One-way ANOVA with multiple comparations was used and a value of P<0.05 was considered significant. Only significative comparisons are shown: * p<0.05, ** p<0.01, *** p<0.001, **** p<0.0001.

Then, in order to try to improve the marker anticipation capacity, we studied the ratio between the markers that tend to appear (CERU, AMBP and VTNC) and disappear as UROM. In patients with mutation in *PKD2*, the UROM/CERU ratio showed a tendency, although not significant, to anticipate changes in serum creatinine increase (Figure 66A). In contrast, in *PKD1* patients, the UROM/CERU ratio did not improve the detection (Figure 66D). The ratio UROM/AMBP displayed very high values in *PKD2* patients with low creatinine with a drastic drop in medium and high creatinine levels (Figure 66B). Instead, the UROM/AMBP ratio in *PKD1* mutation patients shows a progressive decrease trend from medium creatinine values (Figure 66E). The UROM/VTNC ratio shows in both types of patients the same opposite trend in mean creatinine values (Figure 66C and F). All these data show that the markers do not only depend on the functional state of the kidney but also behave in a specific way in the different forms of the disease.

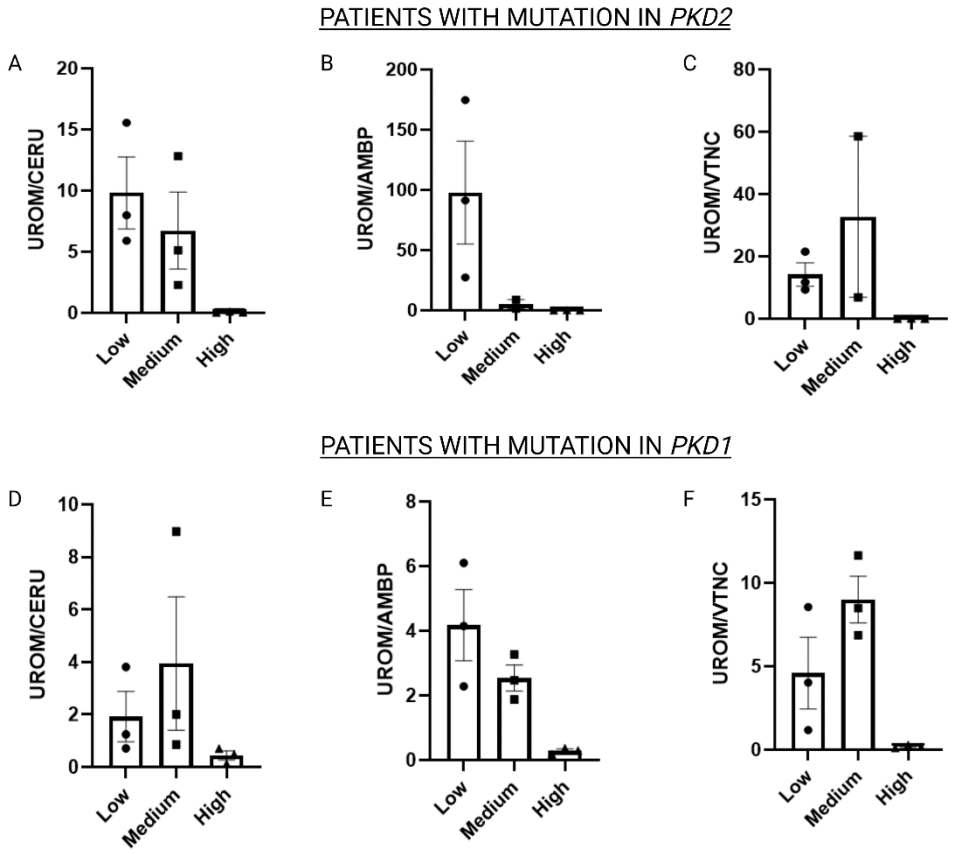

Figure 66. Ratio of the densitometry analysis of CERU, AMBP and VTNC to UROM for patients with mutations in *PKD2* and *PKD1*. Bars represent means ± SEM. Ordinary One-way ANOVA with multiple comparations was used and a value of P<0.05 was considered significant. Only significative comparisons are shown.

4.2.2.3 Characterization of the not isolated component with ExoGAG (ExoGAG supernatant)

4.2.2.3.1 Chracterization of the ExoGAG superanatant protein profile in controls and patients

Once the component isolated in the ExoGAG pellet (P) was characterized, we proceeded to compare it with that which was not isolated in the supernatant (S) and with the total urine (U) (Figure 67). As we could observed, the ExoGAG isolation enrich in a component of its own, quite different from what remains in the supernatant. The sum of the profile observed in the pellet and in the supernatant results in the profile of the whole urine, which is logical, although the profile of the supernatant is more similar to the profile of the whole urine. Again, we observed a constant fingerprint in control samples when we looked at the components separately (Figure 67A). However, the constant pattern was altered in PKD patients (Figure 67B and C). In addition to the alteration in the ExoGAG pellet, we also observed an alteration in the supernatant and in the urine itself corresponding to the course of the disease. This alteration depend on renal function correlated with serum creatinine, being more extreme in the most severe stages of the disease, but beginning to be altered at initial stages with relatively low creatinine levels. All over again, the variation of the profile in patients was characteristic of the disease, as can be observed between ADPKD type I (Figure 67B) and ADPKD type II (Figure 67C), where again shown a more pronounced change.

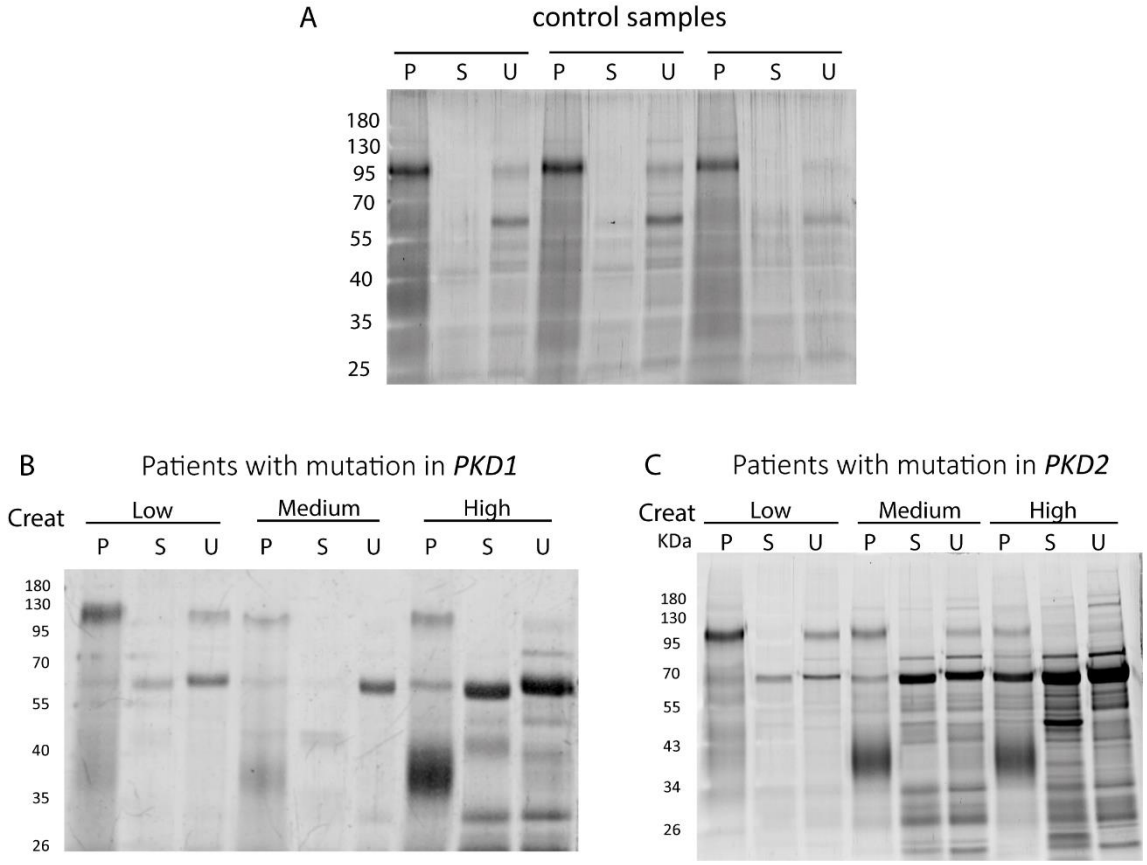

Figure 67. **Protein analysis of ExoGAG pellet, ExoGAG supernatant and whole urine sample.** Whole protein component of isolated fraction of ExoGAG (P), its supernatant (S) and the whole urine samples controls (A), patients with ADPKD type I (B) and patients with ADPKD type II (C). All were stained with Oriole (BioRad®). Patients were ordered according to the increase in serum creatinine (Creat) levels. Low means creatinine levels <1.1, Medium means creatinine levels between 1.2-2 and High means creatinine levels >2.

4.2.2.3.2 Identification of biomarkers in ADPKD patients by mass spectrometry sequencing

Again, the variation in the protein profile in supernatants was more severe in patients with mutations in *PKD2* (Figure 68). Subsequent, to identify new differential proteins and understand the changes produced by the disease, we cut the more differential bands for mass spectrometry sequencing and analysis by qualitative DDA method and semi-quantitative analysis by spectral count (Supplementary Figure 4 and Supplementary Table 21, 22, 23, 24, 25, 26, 27, 28 and 29).

USC UNIVERSIDADE DE SANTIAGO DE COMPOSTELA

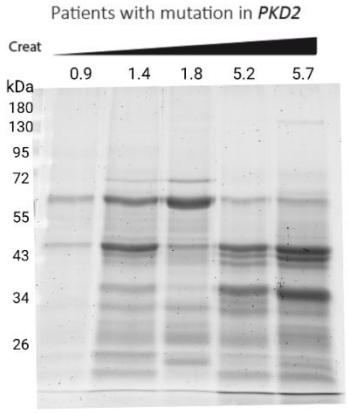

Figure 68. Protein analysis of ExoGAG supernatants of patients with mutation in *PKD2*. Whole protein component of ExoGAG supernatant staining with Oriole (BioRad®). Patients were ordered according to the increase in serum creatinine (Creat) levels.

The principal differential proteins are shown in Table 5. In this case, we only found proteins that increase in abundance throughout the disease. The proteins ALBU, and AMBP were also upregulated and tested as biomarkers in ExoGAG pellet.

Table 5. Summary list of principal proteins with differences in abundance throughout the disease of ExoGAG supernatants in PKD2 patients.

Protein Name	Uniprot Name	Disease progression
Albumin	ALBU_HUMAN	↑
Alpha-1-acid glycoprotein 1	A1AG1_HUMAN	↑
Keratin, type II cytoskeletal 1	K2C1_HUMAN	↑
Keratin, type I cytoskeletal 10	K1C10_HUMAN	↑
Retinol-binding protein 4	RET4_HUMAN	↑
Serotransferrin	TRFE_HUMAN	↑
Transthyretin	TTHY_HUMAN	↑
Protein AMBP	AMBP_HUMAN	↑
Zinc-alpha-2-glycoprotein	ZA2G_HUMAN	↑

4.2.2.3.3 Validation of identified biomarkers by Western Blot in ADPKD patients

As we made previously in ExoGAG pellet, we decided to validate the differential proteins in other patients with mutation in *PKD2* by Western Blot. We used the supernatant of the same samples that we validated in ExoGAG pellet previously. First, we tested the protein fingerprint of the samples we used and once again, the pattern was altered related to the disease progression (Figure 69A), but not so accused in medium levels of creatinine. Then, Western Blot analysis revealed that 6 of these 9 proteins were validated (Figure 69). All of them increased with the disease progression with the increase most pronounced in samples from patients with high creatinine levels. Although RET4, TTHY, AMBP and ZA2G began to show an increase in lower creatinine levels (Figure 69C, D, F and G). A schematic representation of the semi-quantitative mass spectrometry results of these validated proteins is shown in Table 6, where we could observe that almost all proteins appear in all weights, except RET4.

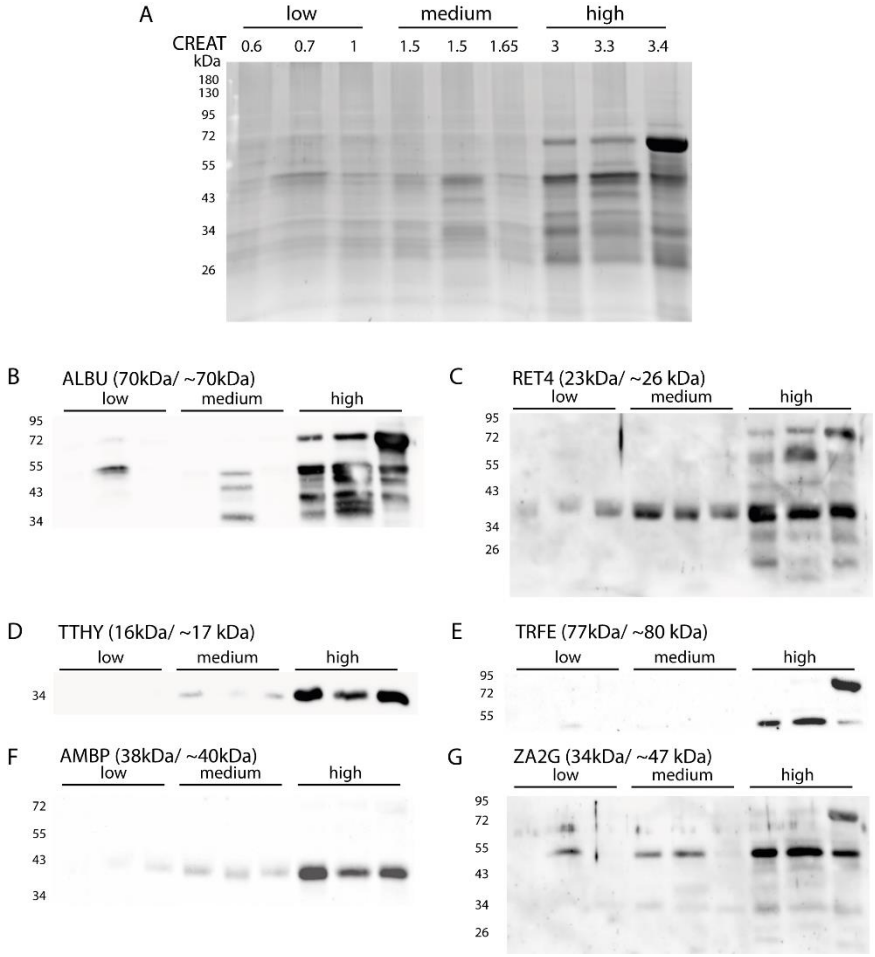

Figure 69. Validation of possible targets in ExoGAG supernatants by Western Blot in patients with mutation in *PKD2*. On the top, the whole protein component of ExoGAG supernatants of patients with mutation in *PKD2* staining with Oriole (BioRad®). The protein abundance of the possible biomarkers of our semi-quantitative proteomic data were validated by Western Blot. Low means creatinine levels <1.1, Medium means creatinine levels between 1.2-2 and High means creatinine levels >2.

Table 6. Schematic representation of the maximum protein abundance per band by semi-quantitative analysis in ExoGAG supernatants. Semi-quantitative analysis is based in Total Spectral Count. Maximal Total spectral count: >1000 √√√√√, 500-1000 √√√√, 100-500 √√√, 50-100 √√, 1-50 √, 0 -.

kDa	ALBU	RET4	TTHY	TRFE	AMBP	ZA2G
130-95	√√√	-	√	√	-	-
95	√√√	-	√	√	√	-
95-72	√√√	-	√	√√√	√	-
72-55	√√√√√	-	√	√√√	√	√
55	√√√√√	-	√	√√√	√	√
55-43	√√√√	-	√	√√	√	√√√
40-30	√√√√	-	√	√√√	√√√	√
30-26	√√√√	-	√	√√√	√√	√
25-20	√√√√	√√√	√	√√	√	√

USC UNIVERSIDADE DE SANTIAGO

As before, we decided to study how these markers behaved in patients with mutations in *PKD1* (Figure 70). We used the supernatant of the same samples that we validated in ExoGAG

pellet previously. Another time, we tested the protein fingerprint of the samples we used, and the fingerprint was altered related to the disease progression, but again with less change in medium levels of creatinine (Figure 70A). Over again, all of them increased with the disease progression with the increase most pronounced in samples from patients with high creatinine levels (Figure 70B, C, D, E and F).

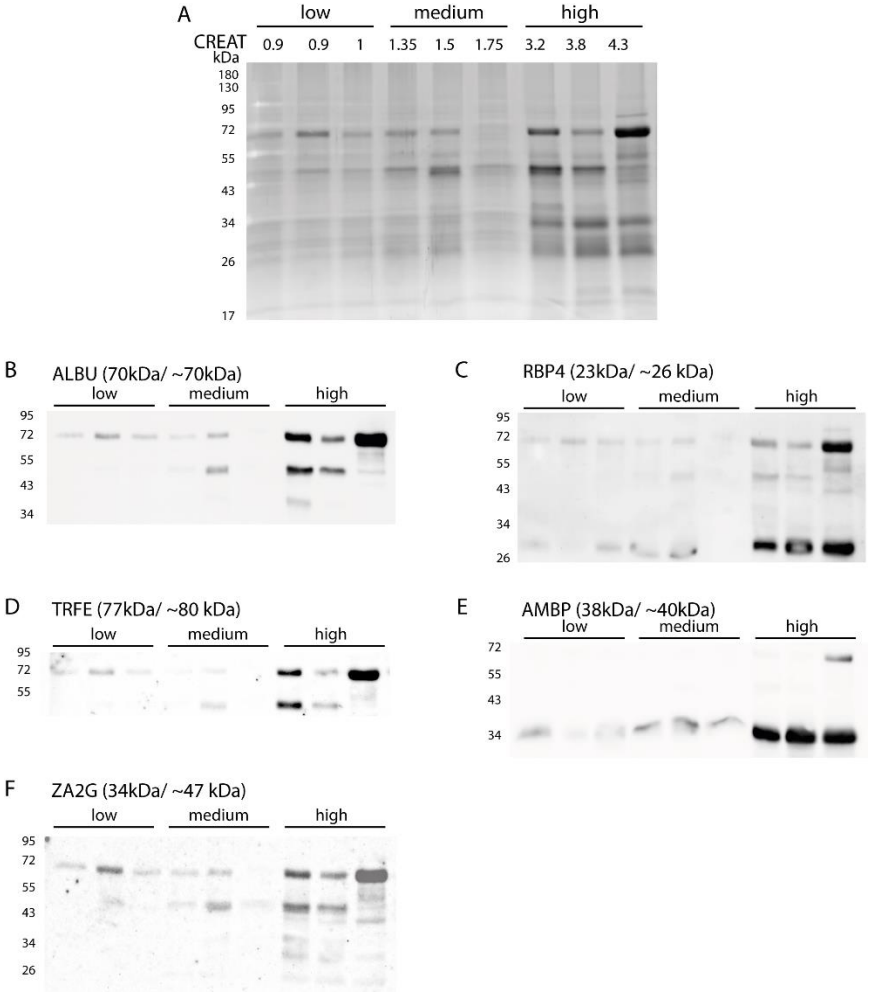

Figure 70. Validation of possible targets in ExoGAG supernatants by Western Blot in patients with mutation in *PKD1*. On the top, the whole protein component of ExoGAG supernatants of patients with mutation in *PKD1* staining with Oriole (BioRad®). The protein abundance of the possible biomarkers of our semi-quantitative proteomic data were validated by Western Blot. Low means creatinine levels <1.1, Medium means creatinine levels between 1.2-2 and High means creatinine levels >2.

4.2.2.4 Differential comparison between ExoGAG Pellet and Supernatant

4.2.2.4.1 Characterization of specific ExoGAG pellet proteins

As we observe there were common markers in both sample types (pellet and supernatant), we decided to investigate if some biomarker were any specifically found in the ExoGAG pellets. We discovered that CAH1, DPP4, LUM and NEP were only sequenced in ExoGAG pellet samples (Table 7). We validated them by Western Blot in ExoGAG pellet samples of patients with mutations in *PKD2* (Figure 71) and *PKD1* (Figure 72). DPP4, LUM and NEP were validated in both types of mutations. However, the behavior was different, in *PKD2* samples they tend to increase in abundance in high creatinine levels only, but in *PKD1*

USC DE COMPOSTELA

samples this marker appeared in lower levels of creatinine with a less pronounced increase in high creatinine levels.

Table 7. List of proteins that appeared only sequenced in ExoGAG pellet samples

Protein Name	Uniprot Name	Disease progression
Carbonic anhydrase 1	CAH1_HUMAN	↑
Dipeptidyl peptidase 4	DPP4_HUMAN	-
Lumican	LUM_HUMAN	↑
Neprilysin	NEP_HUMAN	-

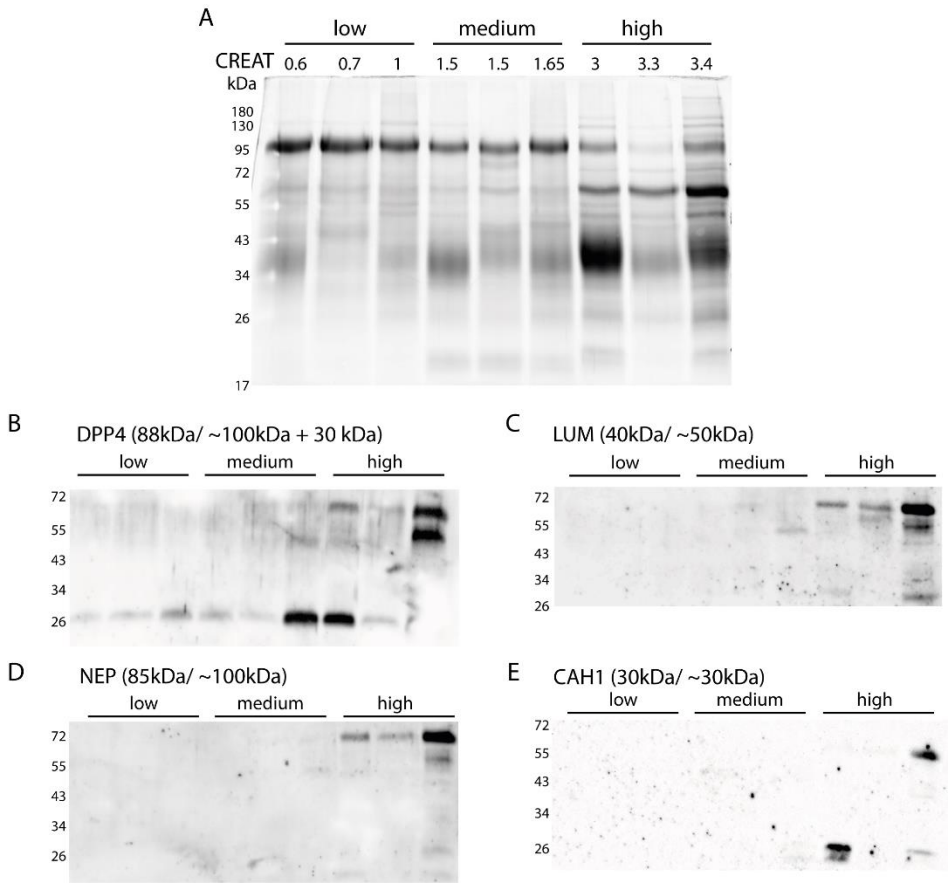

Figure 71. Validation of targets that appear only in ExoGAG pelle by Western Blot in patients with mutation in *PKD2*. On the top, the whole protein component of urine samples precipitated with ExoGAG of patients with mutation in *PKD2* staining with Oriole (BioRad®). Low means creatinine levels <1.1, Medium means creatinine levels between 1.2-2 and High means creatinine levels >2.

USC UNIVERSIDADE DE SANTIAGO DE COMPOSTELA

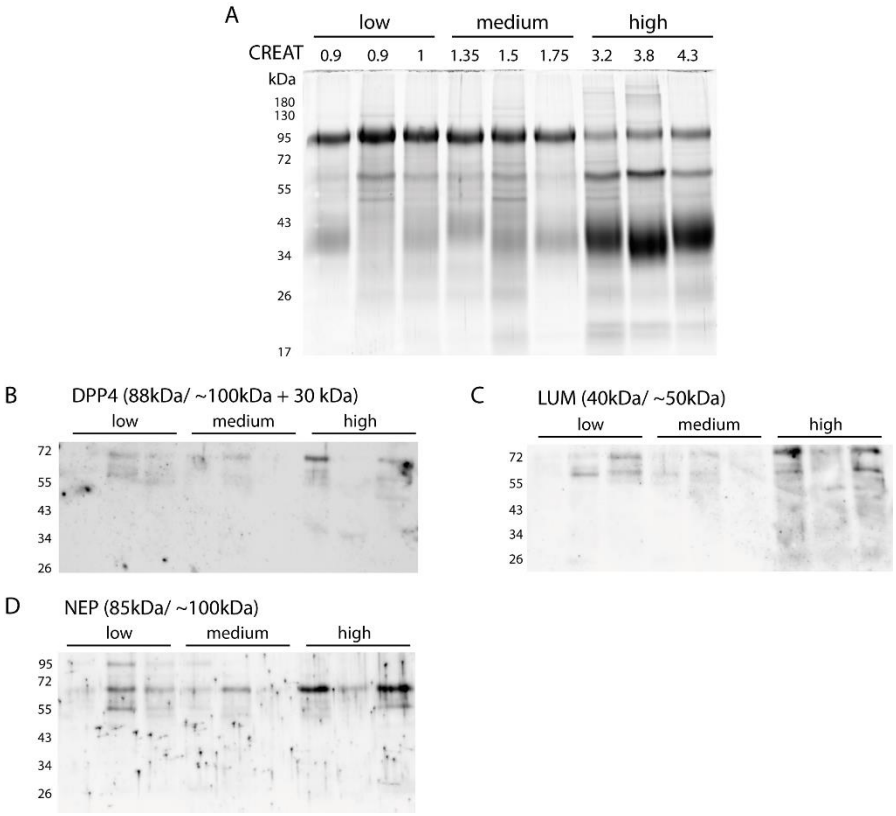

Figure 72. Validation of targets that appear only in ExoGAG pellet by Western Blot in patients with mutation in *PKD1*. On the top, the whole protein component of urine samples precipitated with ExoGAG of patients with mutation in *PKD1* staining with Oriole (BioRad®). Low means creatinine levels <1.1, Medium means creatinine levels between 1.2-2 and High means creatinine levels >2.

4.2.2.4.2 Comparison of the behavior of biomarkers in ExoGAG pellet and supernatant

As we previously described, AMBP was found in both in ExoGAG pellet and supernatant, with disease progression marker features. Other interesting issue is to see how is the behavior of the other markers found in the ExoGAG pellet in supernatants. We found that CERU and VTNC appeared but with a tremendously low amount per total spectral count analysis, so we considered that almost non-existent in these samples. However, we noticed that UROM was sequenced in almost all bands of ExoGAG supernatant. So, we studied how UROM behaved in different sample types (ExoGAG pellet, Supernatant and the whole urine) in *PKD1* and *PKD2* patients. As we could observed in Figure 73, the UROM behavior depends on the type of sample. In ExoGAG pellets, we enriched UROM component in contrast to the whole urine and the UROM component of the ExoGAG supernatants looked like splits or degradation of the whole protein.

USC UNIVERSIDADE DE SANTIAGO DE COMPOSTELA

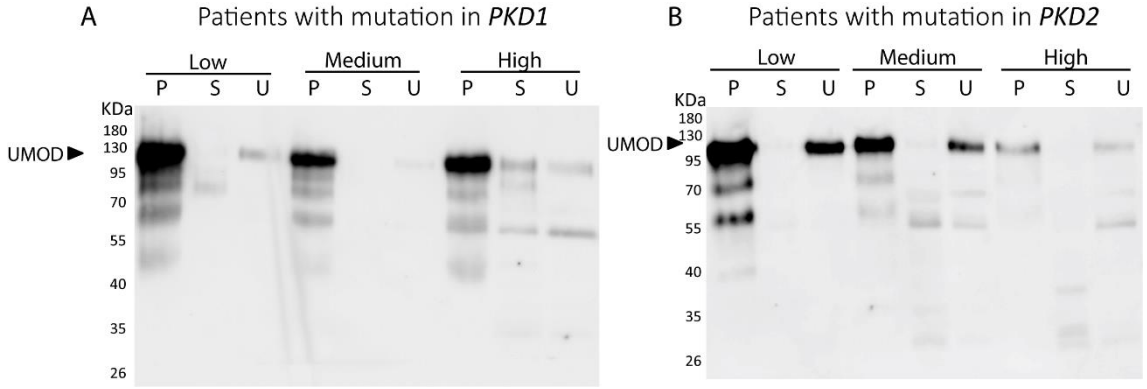

Figure 73. **Validation of Uromodulin in ExoGAG pellet, ExoGAG supernatant and whole urine by Western Blot.** Validation of UROM in patients with mutation in *PKD1* (A) and *PKD2* (B). Uromodulin is enriched in ExoGAG pellets (P) in contrast to the whole urine (U) and in ExoGAG supernatants (S) seems like splits or degradation of the whole protein.

In summary, ExoGAG is a new analytical tool that separates specific component of the sample. This fraction allowed us to identify a urinary pattern of proteins associated to GAGs that it is altered in the disease progression, highlighting the biomarker Uromodulin with a predictive value for disease progression that anticipates pathological changes in serum creatinine levels, together with their combination with the study of other markers such as CERU, AMBP or VTNC which increases their sensitivity. All these data showed our promising results in searching for new biomarkers for diagnosis and prognosis of kidney diseases, at least in ADPKD.

USC
UNIVERSIDADE DE SANTIAGO DE COMPOSTELA

4.3 Chapter 3. Characterization of urine Extracellular Vesicles isolated by ExoGAG.

Glycosaminoglycans and the related proteins (proteoglycans) are associated with and part of Extracellular Vesicles (EVs), in fact, they are key factors for biogenesis and internalization processes (294–296). EVs are membrane-enclosed heterogeneous structures that are secreted by all cells and have many different physiological and pathophysiological roles as being part of cell-to-cell communication. In the past few years, the study of extracellular vesicles became a topic of interest in biomedical research (296).

Urinary EVs have been identified in both healthy donors and patients with renal disease. They are produced and secreted into urine by all types of renal epithelial cells across each segment of the nephron (242,297). They demonstrated to be important in facilitating signaling to support nephron function and kidney homeostasis. As EVs play a role in inter and intracellular communication in both healthy and disease states, it provide a significant potential as a source of biomarkers and an aid to understanding renal physiology (216,242).

On the other hand, Uromodulin has been considered an artifact associated with EVs, and it is proposed that for the study of EVs, uromodulin should be depleted (205,239). In the previous chapter we have described how this protein is involved in disease progression using ExoGAG precipitation. Thus, ExoGAG provides us a great opportunity to study the urinary EV fraction associated to the specific precipitation of GAGs and its components fraction, and validate the hypothesis that Uromodulin play an important role as part of an important biological complex.

4.3.1 Functional analysis of identified proteins in ExoGAG isolation.

We performed the functional analysis of the identified proteome of ExoGAG pellet and supernatant of *Chapter 2* using FunRich tool. Functional analysis of cellular component of ExoGAG pellet revealed that the majority component of ExoGAG pellet was Exosomes, one kind of EVs, with almost 70% of the identified proteins belonging to this category (Figure 74A). In contrast, for ExoGAG supernatant, the percentage of proteins belonging to this category was reduced to 50% and the most enriched component was Extracellular (Figure 74A). Extracellular matrix and other organelle components were also more enriched in ExoGAG pellet (Figure 74A).

We found that around 40% of proteins were shared between pellet and supernatant (Figure 74B). When we analyzed the differential component between pellet and supernatant, we observed that the Exosome component was even more enriched in ExoGAG pellet (67%), decreased to 37% in proteins found only in supernatant samples (Figure 74C). Moreover, we decided to compare our mass spectrometry results with Vesiclepedia dataset (http://www.microvesicles.org/), a compendium of molecular data identified in different EVs (151) and Urine Vesiclepedia, the results of experiments regarded only to urine samples. 97% of identified proteins in ExoGAG pellet were shared with Vesiclepedia and 91% with Urine Vesiclepedia (Figure 74D). On the other hand, approximately the 80% of identified proteins in ExoGAG supernatant were in common with Vesiclepedia and Urine Vesiclepedia (Figure 74E). So, we could conclude that we were isolating an EV component with ExoGAG.

USC UNIVERSIDADE DE SANTIAGO DE COMPOSTELA

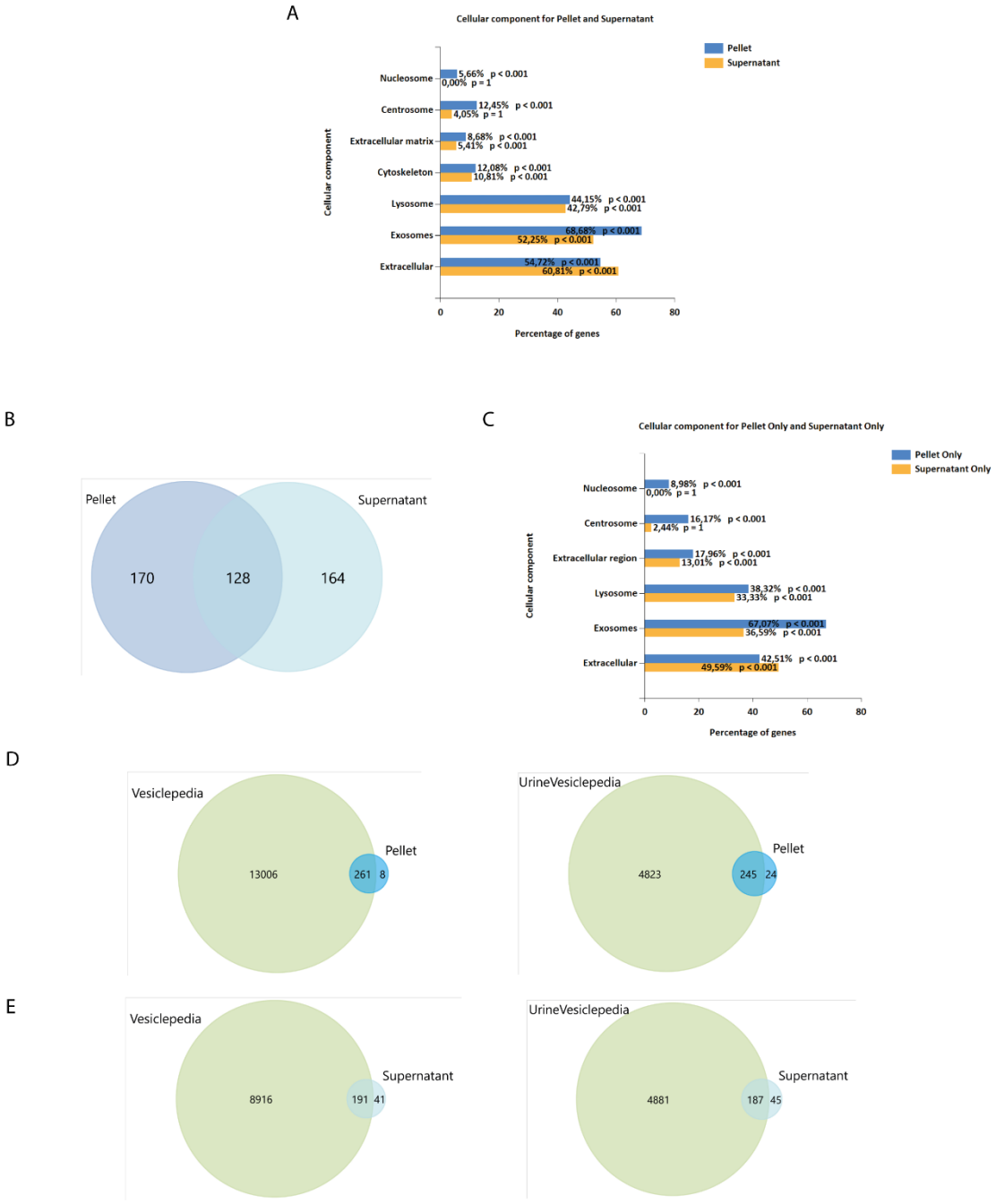

Figure 74. ExoGAG pellet and ExoGAG supernatant proteins characterization. (A) FunRich enrichment analysis of cellular component of identified proteins in pellet (blue) and supernatant (yellow). (B) Venn Diagram showing the shared proteins of pellet and supernatant and proteins that only belonged to pellet or supernatant. (C) FunRich enrichment analysis of cellular component of identified proteins only in pellet (blue) and only in supernatant (yellow). (D) Venn diagram displaying the identified proteins in ExoGAG pellet that are shared with Vesiclepedia and Urine Vesiclepedia. (E) Venn diagram displaying the identified proteins in ExoGAG supernatant that are shared with Vesiclepedia and Urine Vesiclepedia. The significative involved cellular component terms for ExoGAG pellet were shown.

4.3.2 Image characterization of ExoGAG isolation.

First, we characterized the vesicles isolated with ExoGAG by Transmission Electron Microscopy. As we could see in Figure 75A, in the ExoGAG pellet we obtained two kinds of vesicles, ones that appeared as a complex and others that appeared individually. In contrast,

when we characterized ExoGAG supernatant we only found independent EV (Figure 75B). The size of the EVs was variable, from more than 200nm to less than 50nm.

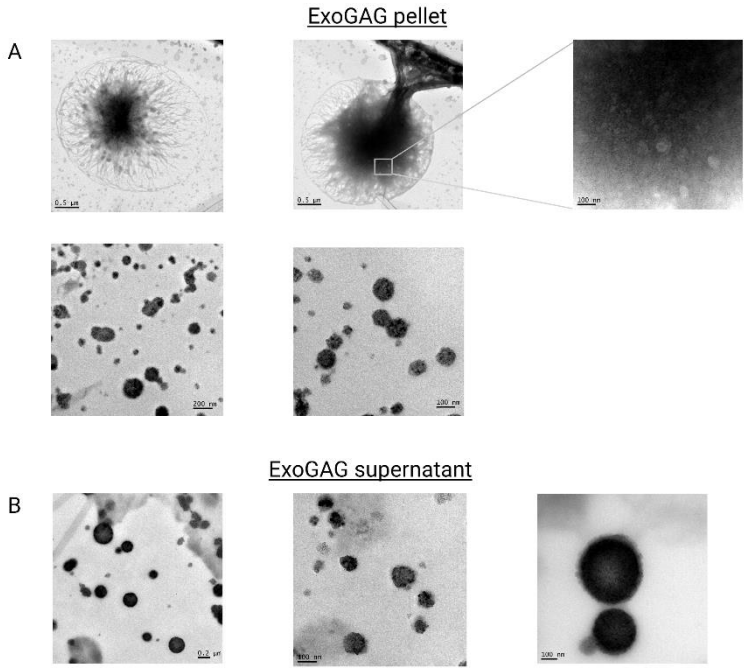

Figure 75. Representative transmission electronic images (TEM) of ExoGAG pellet (A) and supernatant (B). (A) EVs that form part of a complex or individually EVs are found in ExoGAG pellet. (B) Remaining EVs in the ExoGAG supernatant.

After saw this result, we wanted to validate if these complexes were formed by EVs and Uromodulin. As it was previously described, Uromodulin formed long polymeric filaments that entrapped abundant EVs (205,239). The immunofluorescence of DiD, a lipophilic marker for membranes, and Uromodulin revealed that both colocalize and this means that Uromodulin form part of these complexes with extracellular vesicles (Figure 76). In addition to being part of these complexes, it was also observed that there are isolated Uromodulin-positive EVs. In fact, as we saw in TEM, we observed that with ExoGAG isolation we obtained these complexes and EVs that stood alone (Figure 75 and Figure 76).

USC
UNIVERSIDADE DE SANTIAGO DE COMPOSTELA

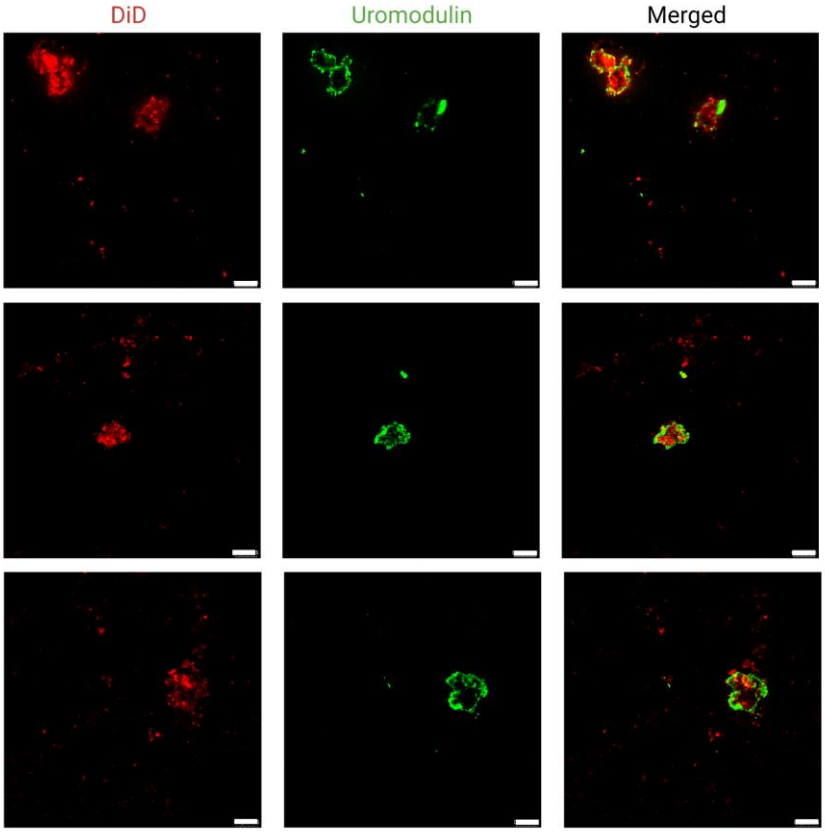

Figure 76. **Immunofluorescence of ExoGAG pellet.** Red marks DiD lipophilic fluorescent stain for labelling membranes, in this case, Extracellular Vesicle membranes. Green marks Uromodulin, one of the most abundant glycoprotein of the urine. Scale bar 25µm

4.3.3 Comparison of ExoGAG and other Extracellular Vesicle isolation techniques.

All this data led us to believe that we were isolating Extracellular Vesicles, so we decided to compare this new isolation method with other commonly used methods. We compared our method with ultracentrifugation, one of the most used techniques that is an intermediate recovery and specificity method for EVs isolation, and immunocapture with CD9, that is a low recovery but high specificity method (126). In Figure 77, we shown a summary of the types of samples obtained after the corresponding isolations methods as well as the initial volumes from which they have been taken as a starting point. It is important to note the difference between the volume needed for Ultracentrifugation isolation and what we need for ExoGAG isolation.

USC
UNIVERSIDADE DE SANTIAGO DE COMPOSTELA

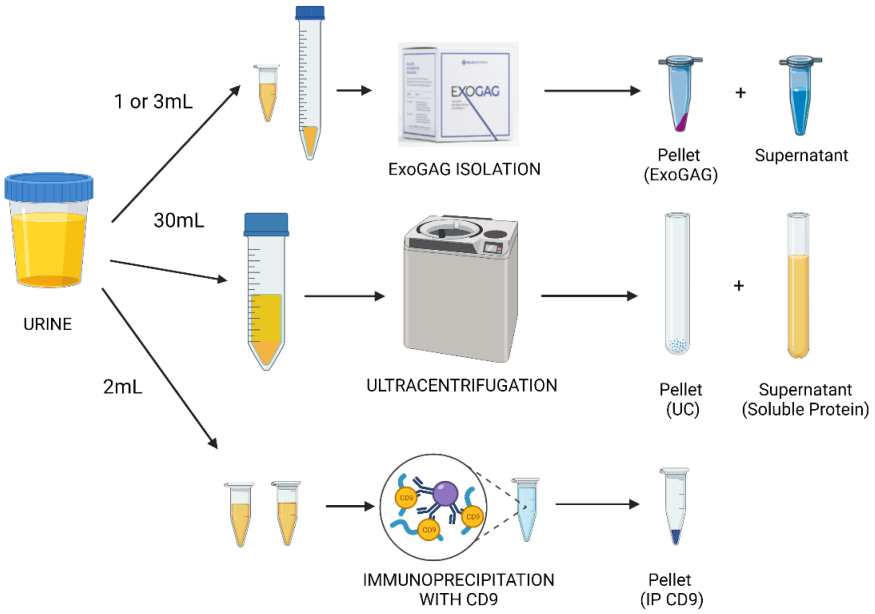

Figure 77. Schematic representation of EVs isolation techniques used. Starting volume as well as type of sample that we could obtain are also represented.

We first made a Uromodulin component characterization. We compared the Uromodulin obtained by the immunoprecipitation with CD9 isolation, the ExoGAG isolation and the immunoprecipitation with Uromodulin itself, therefore we were able to compared not only the isolation by immunoprecipitation of the total sample, but also the isolation of each of the components of the ExoGAG isolation (Figure 78A). As we used 2 ml of sample for the immunoprecipitations, we tried to replicate the same in the ExoGAG isolation but this was only possible in pellet samples, in the supernatant samples and total urine only 200 µL of sample were used, a ratio of 10 times less sample amount. The first thing that was observed is that in all cases the ExoGAG pellet component was the most enrichment in Uromodulin and that in the Supernatant it was not appreciated. The next most enriched one to the same level as above is UMOD immunoprecipitation in total urine. Also noteworthy was the presence of uromodulin in the CD9 immunoprecipitation of total urine, which demonstrates, together with the uromodulin obtained in the immunoprecipitation of the pellet, that part of the vesicles which were CD9 positive were also associated with or carry uromodulin (Figure 78A).

When we analyzed other EV-specific markers, we observed that they behave differently depending on the type of isolation. In the case of internal vesicle markers such as ALIX, it is only found in the 2mL ExoGAG pellet sample, or SYNTENIN-1, that appeared in immunoprecipitation with CD9 from urine. However, another membrane marker, CD81, appeared in all samples immunoprecipitated with CD9 but in none of the ExoGAG samples (Figure 78B).

The next comparison we made was with ultracentrifugation method. In this first approach we compared not only the isolations separately, but also the components not isolated by each technique, the isolation with another of them, both with immunoprecipitation with CD9 and ExoGAG (Figure 78C). Only ultracentrifugation and ExoGAG pellets were positive for both

markers. Although SYNTENIN-1 was also positive for isolation with ExoGAG from the ultracentrifugation supernatant and for isolation by immunoprecipitation with CD9 per se and for ExoGAG supernatant (Figure 78C). This again showed that the behavior of the markers was dependent on the type of isolation.

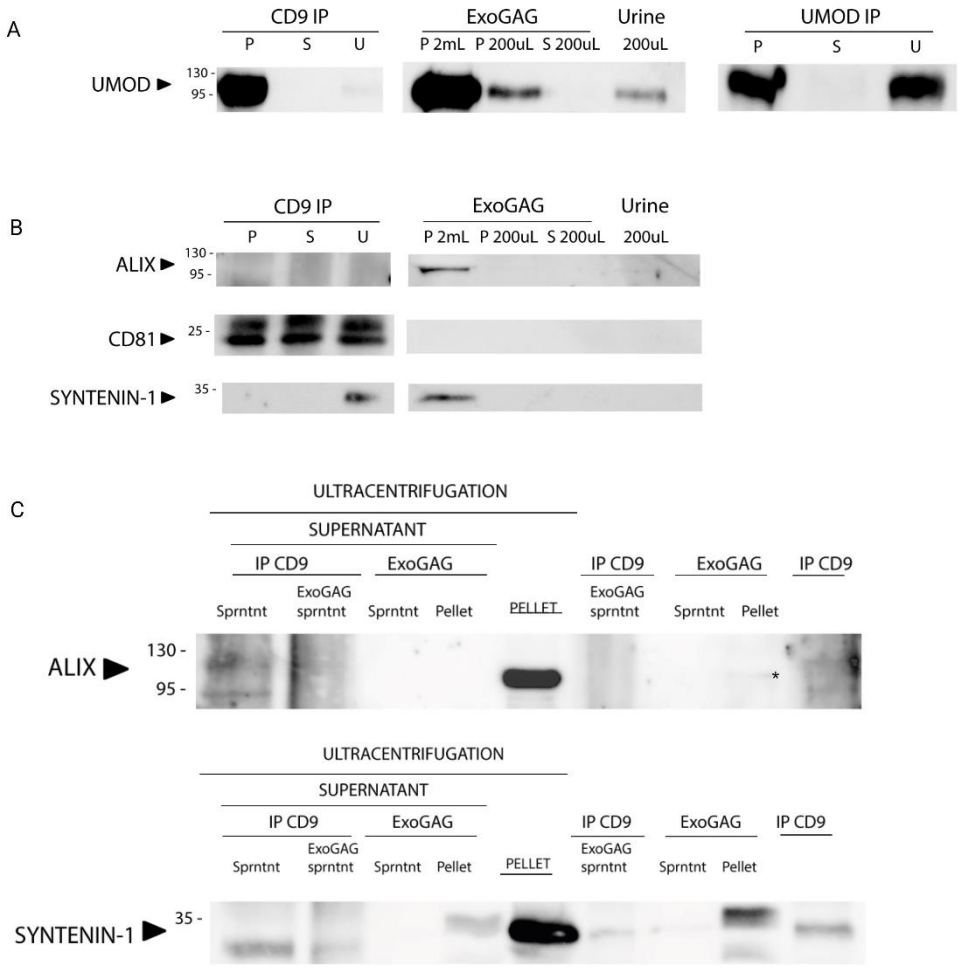

Figure 78. Comparative study among types of EV isolation. (A) Uromodulin levels comparation among the immunoprecipitation with the EV marker CD9 of the pellet (P) and supernatant (S) of ExoGAG and urine (U), pellet (P) and supernatant (S) of ExoGAG isolation, the total urine and the immunoprecipitation with UMOD of the pellet (P) and supernatant (S) of ExoGAG and urine (U). (B) EV markers (ALIX, CD81 and SYNTENIN-1) evaluation among the immunoprecipitation with the EV marker CD9 of the pellet (P) and supernatant (S) of ExoGAG and urine, pellet (P) and supernatant (S) of ExoGAG isolation and the whole urine (U). (C) EV markers (ALIX and SYNTENIN-1) among Ultracentrifugation, ExoGAG isolation and immunoprecipitation with CD9. Inside Ultracentrifugation, we performed ExoGAG isolation of supernatant as well as immunoprecipitation with CD9 of supernatant and previous ExoGAG supernatant of ultracentrifugation supernatant. Inside ExoGAG, we performed immunoprecipitation with CD9 of the supernatant of ExoGAG isolation. * marks the band of ALIX in the pellet of ExoGAG.

4.3.4 Optimization and characterization of the ExoGAG isolation.

Once we had characterized the presence of extracellular vesicles, we decided to find out what is the optimal starting sample volume for the ExoGAG isolation. The presence of ALIX and SINTENIN-1 markers appeared from a volume of 1mL of urine. However, we have a clearest detection using 3 mL of urine (Figure 79A). Therefore, we characterized the presence of these markers from 3 ml of urine in different control samples, and we observed ALIX, CD81

and SINTENIN-1 in all samples, but with a non-homogeneous level that seems to be sample-dependent as well as isolation-dependent (Figure 79B).

To see if this variation in detection is characteristic of ExoGAG isolation, we used different proportions of soluble protein to see if this ratio affects isolation performance. Therefore, using the pellet isolated with ultracentrifugation as a control, we resuspended it in different ratios of soluble protein and re-precipitated it with ExoGAG. No differences were observed in the level of marker obtained when the ratio of soluble protein in the sample increased. It was even possible to observe again that these markers are present both in the isolation by ultracentrifugation and in ExoGAG isolation (Figure 79C).

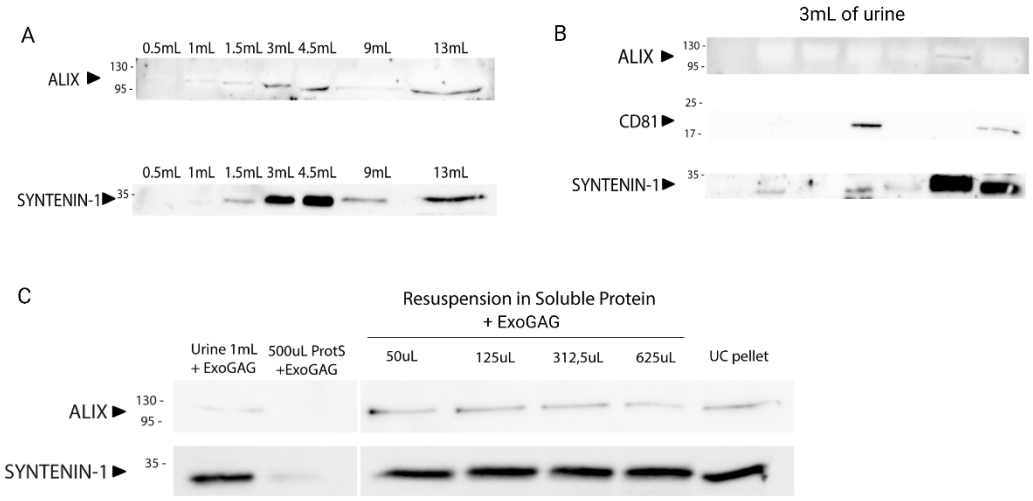

Figure 79. Optimization and characterization of the ExoGAG isolation protocol. (A) EV markers (ALIX and SYNTENIN-1) in different volumes of urine precipitated with ExoGAG. (B) EV markers (ALIX, CD81 and SYNTENIN-1) in the precipitation of 3 ml of urine of control samples. (C) Validation of the ExoGAG isolation with different proportion of soluble protein in the sample.

4.3.5 Protein characterization by mass spectrometry of the differences between the component isolated with ExoGAG and ultracentrifugation techniques

Mass spectrometry is a technique that allow protein fingerprint identification at once. Moreover, this technique has a great advantage over the typically antibody-based methods, such as Western Blot, because it offers greater specificity, reproducibility and typical limits of quantification lower than fmol range. It also removes some of the antibody specificity issues as peptides unique to each protein are measured (298).

Knowing the benefits that mass spectrometry can offer us, we decided to use it to try to complement the detection of vesicle-associated markers in ExoGAG isolation.

4.3.5.1 Optimization of the protocol for mass spectrometry sequencing of ExoGAG isolation

We tested different ways of sample preparation for mass spectrometric sequencing because we know that we have majority proteins in our samples such as Uromodulin and that this can affect the sensitivity of the identification of the minoritary proteins present in the sample.

USC DE COMPOSTELA

The approaches we used were:

- Sequencing directly (Direct). In this case, it was sequenced just after the isolation with ExoGAG. The sample was concentrated on a gel band and cut out for further trypsin digestion and mass spectrometry sequencing.
- ExoGAG pellet precipitation with the methanol-chloroform protocol (Precipitated). Methanol-chloroform protein precipitation was performed to eliminate possible buffer contaminants prior to in gel concentration for trypsin digestion and mass spectrometry sequencing.
- Sequencing of the sample by banding (Bands). In this case, the sample was loaded onto the gel and allowed to separate all the proteins by weight. The entire gel was then cut into four bands that cover the entire sample, trypsin digested and mass spectrometry sequenced.

The best sequencing approach was the banding method as it identified 3 times more proteins than direct sequencing and almost twice as many as methanol-chloroform precipitation (Figure 80).

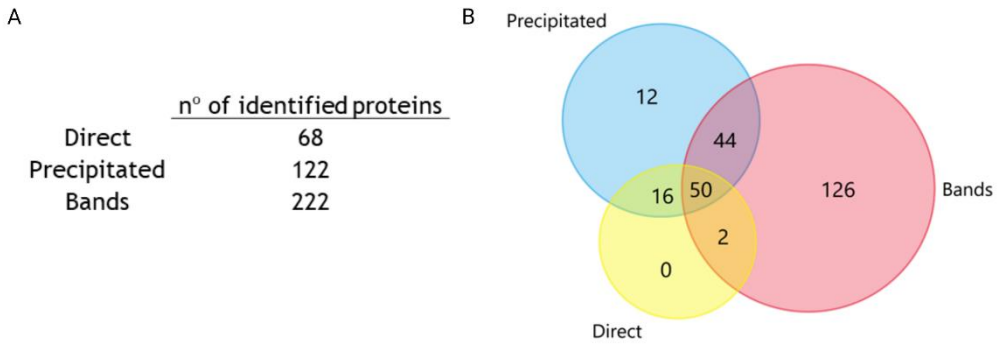

Figure 80. Optimization of the protocol for mass spectrometry sequencing by Qualitative DDA method of ExoGAG isolation. (A) Number of identified proteins according to each type of sequencing method. (B) Venn diagram showing the common and different proteins of each method.

4.3.5.2 Characterization and comparison by mass spectrometry of the component isolated with ExoGAG and ultracentrifugation

Using the same sample isolated by ExoGAG and UC, mass spectrometry sequencing was performed to analyze and compare protein component isolated by both methods. For ExoGAG isolation, 3mL of urine were used and for UC isolation, 30mL of the same urine sample was used (10 times more volume) (Figure 81A). A mean of 630 proteins were identified in ExoGAG isolation in contrast to 745 identified proteins in UC, despite the huge volume difference there was no significative difference in the number of identified proteins between both methods, what mean that ExoGAG has a good yield with 10 times less volume (Figure 81B).

Next, we decided to compare the percentage of shared proteins among samples isolated with the same technique. If we compared samples two by two and taking all identified proteins by the two samples like a whole set, the percentage mean of shared proteins for ExoGAG is 55%, a bit more than the 52,8% found in UC samples (Figure 81C). However, if we compared the identified proteins of samples individually (left samples related to down samples), the

shared percentage increased to 72% of ExoGAG and 70% of UC isolation (Figure 81D), meaning robustness in techniques. Finally, 303 proteins were shared in all ExoGAG samples and 318 in UC samples (Figure 81E), some less than half of mean identified proteins.

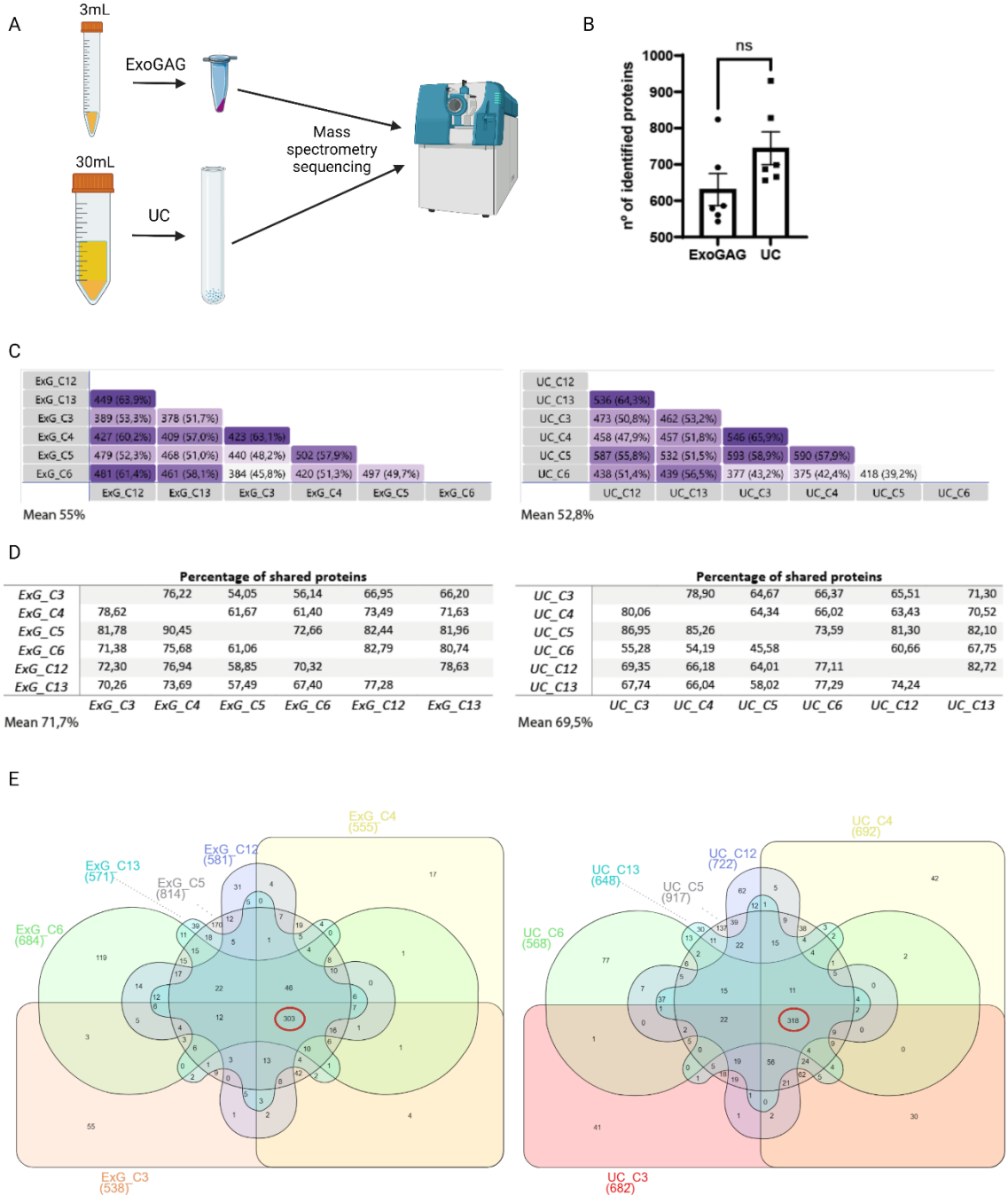

Figure 81. Characterization of identified proteins isolated by ExoGAG or UC by mass spectrometry. (A) Schematic representation of sequenced samples. (B) Comparison between the number of identified proteins in ExoGAG or Ultracentrifugation. (C) Percentage of shared proteins in samples isolated by same technique, left ExoGAG and right Ultracentrifugation, and compared identified proteins by two samples as a unique set. (D) Percentage of shared proteins in samples isolated by same technique, left ExoGAG and right Ultracentrifugation, and compared identified proteins by sample, left to down. (E) Venn diagram of identified proteins of each

sample, left ExoGAG where 303 were shared by all samples and right Ultracentrifugation where 318 where shared by all samples. Bars represent means ± SEM. p<0.05 by T-student test (two tail) was considered significative result: ns represents not significative.

More than 50% of identified proteins are common between ExoGAG and UC, 58% for ExoGAG dataset and 52% for UC (Figure 82A) (Supplementary Table 30). These decreased to 42% and 40%, respectively, if we considered only the shared proteins for all samples (Figure 82B) (Supplementary Table 30). Using the bioinformatic tool FunRich to analyze the cellular component of these identified protein sets (Figure 82C), we found that exosomes was the most enriched component for ExoGAG and UC shared proteins, followed by cytoplasm, plasma membrane and organelles as lysosomes, nucleus or mitochondrion. The set of identified proteins only by UC was more enriched in cytoplasm, exosomes and organelles than those identified only in ExoGAG, in fact it seemed that identified proteins only by UC had a similar pattern as ExoGAG and UC shared proteins, less in the extracellular component that was most enriched component in only identified proteins in ExoGAG. The same pattern was observed when we analyzed the cellular component of the shared proteins in all samples, even the differences were more pronounced (Figure 82D). In this case, almost all proteins of ExoGAG and UC shared proteins and only UC proteins were related to exosomes, followed, again, by proteins related to cytoplasm, plasma membrane and organelles as lysosomes, nucleus or mitochondrion. In contrast, those only identified proteins in ExoGAG were related mostly to extracellular components. This means that ExoGAG isolation allow us to obtain exosome component, but with an important component of extracellular fraction.

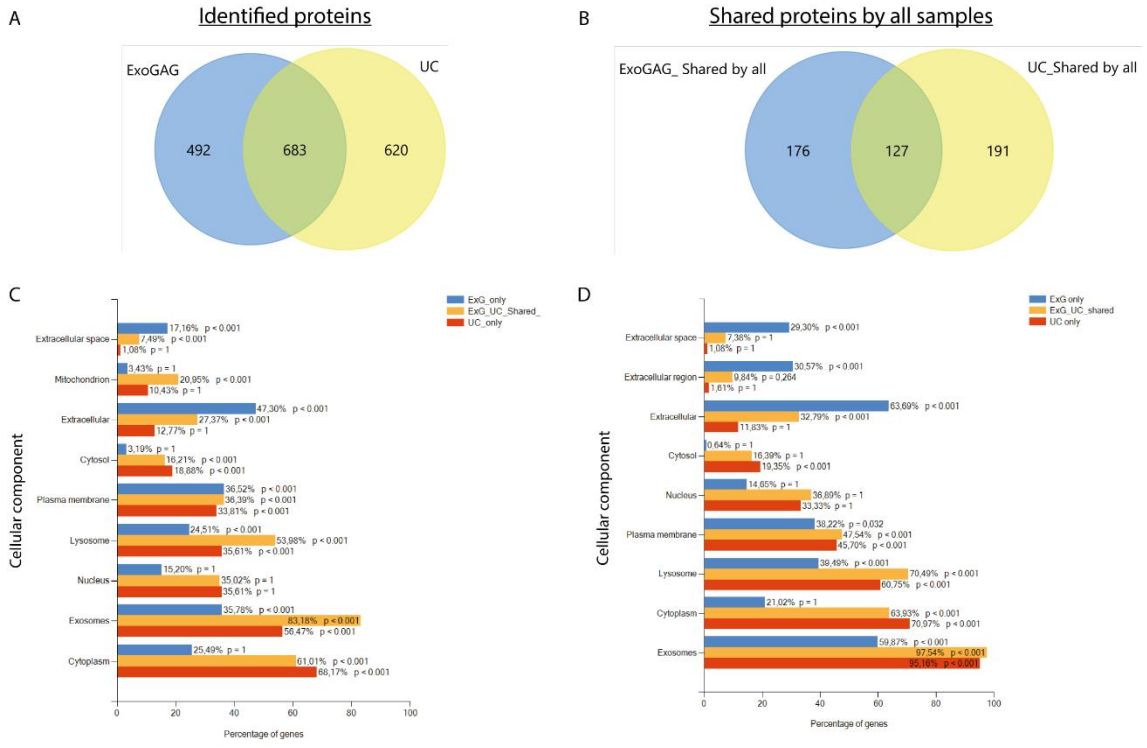

Figure 82. Comparison of identified proteins isolated by ExoGAG or UC by mass spectrometry. Venn diagram of common identified proteins in ExoGAG and UC (A) and shared proteins by all samples (B). FunRich analysis for cellular component of only identified proteins by ExoGAG isolation (blue), shared ExoGAG and UC proteins (yellow) and only identified proteins by UC only proteins (red) (C) and shared proteins by all samples(D).

Then, we decided to compare mass spectrometry results with Vesiclepedia dataset (151)(Figure 83) (Supplementary Table 30). A huge percentage of proteins, 97%, of both ExoGAG and UC identified proteins were shared with Vesiclepedia dataset (Figure 83A). However, these percentage decreased if we considered the urine Vesiclepedia, the Vesiclepedia experiments regarded only to urine samples, 86% shared with ExoGAG and 90% with UC identified proteins. Moreover, when we studied the shared proteins by all samples, we observed how almost 100% of ExoGAG proteins and 100% of UC proteins were shared with Vesiclepedia and urine Vesiclepedia (Figure 83B). In fact, if we considered top 100 proteins described in Vesiclepedia or urine Vesiclepedia, more than 90% were shared with ExoGAG and UC identified proteins (Figure 83C). Nevertheless, these percentages decreased tremendously if we chose the shared proteins by all samples and compared to Vesiclepedia dataset, to 34% in ExoGAG proteins and to 56% of UC proteins (Figure 83D top). In contrast, these percentages raised up again with urine Vesiclepedia dataset, more than 70% in ExoGAG and more than 80% in UC shared proteins by all samples (Figure 83D bottom). To further investigate what happened to these proteins that were not shared with Vesiclepedia or urine Vesiclepedia, we compared those ExoGAG or UC proteins that were not shared with urine Vesiclepedia because they englobed not shared with Vesiclepedia too, using FunRich tool. Related to cellular component, ExoGAG proteins were more enriched in extracellular and plasma membrane components, and UC proteins were more related to mitochondrion and actin linked components (Figure 83E). The site of expression of these proteins were in a similar percentage in serum component, however, interesting twice ExoGAG proteins were expressed in urine more than UC proteins (Figure 83F). All these data demonstrate that ExoGAG is a good EV isolation method with consistent data compared to the current state of art of EV research.

USC
UNIVERSIDADE DE SANTIAGO DE COMPOSTELA

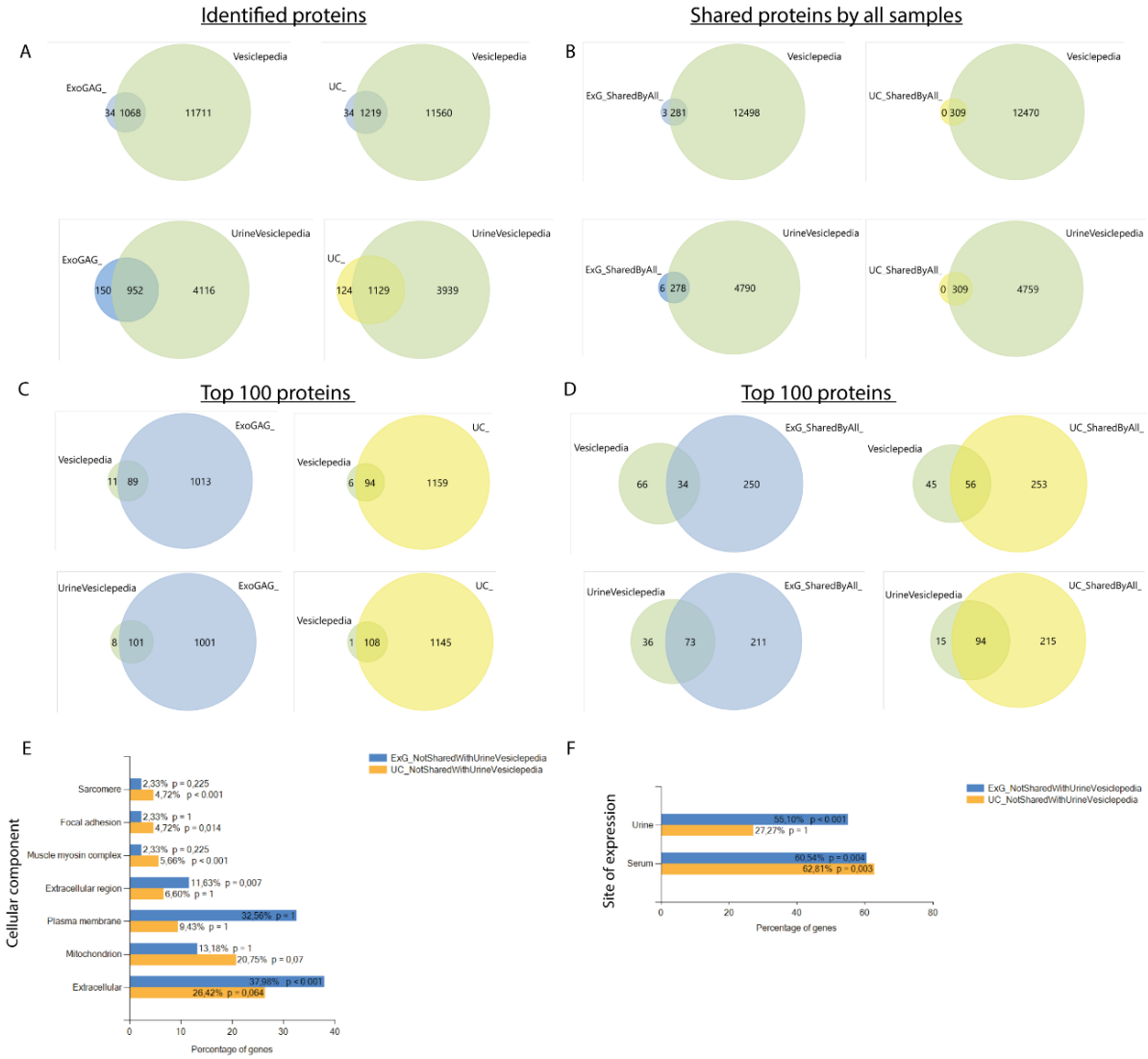

Figure 83. Analysis by comparison of identified proteins isolated by ExoGAG or UC by mass spectrometry with Vesiclepedia dataset. Comparison between all ExoGAG and UC identified proteins (A) and shared proteins by all samples (B) to Vesiclepedia and Urine Vesiclepedia datasets using FunRich software. C and D, respectively, analysis of 100 top proteins of Vesiclepedia and Urine Vesiclepedia contrasted to ExoGAG and UC identified proteins and shared proteins by all samples. (E) FunRich analysis for cellular component for ExoGAG (blue) and UC (yellow) not present proteins in Urine Vesiclepedia. (F) FunRich analysis for site of expression for ExoGAG (blue) and UC (yellow) not present proteins in Urine Vesiclepedia.

4.3.5.3 Characterization of the component isolated with ExoGAG according to the guideline of Extracellular Vesicle studies.

An schematic illustration of identified proteins in ExoGAG isolation (Supplementary Table 30) according to MISEV18 guideline of proteomic characterization is represented in Figure 84 (126). For this purpose, mass spectrometry is an optimum method due to the capacity of allowing the characterization of many proteins at once. Three categories of markers that must be found to demonstrate the presence of EVs (Categories 1 and 2) and the purity from common contaminants (Category 3), unless there are no universal "negative controls". Analysis of proteins of category 4 is required when declaring small EVs, and of category 5 to support functional assays. The categories are:

- Category 1. Transmembrane or GPI-anchored proteins to demonstrate the presence of a lipid bilayer as plasma membrane or endosome. This category is divided in: 1a, non-tissue specific markers as *CD63* or *CD81*; or 1b, tissue specific ones such as *TSPAN8* for epithelial cells or *THY1* for mesenchymal stem cells.
- Category 2. Cytosolic or periplasmic proteins that show the encapsulation of intracellular material. This category englobes: 2a, proteins with lipid or membrane protein attachment capacity as *TSG101* or *PDCD6IP* (most known as ALIX); and 2b, other promiscuously proteins associated with EVs as *ACTS* or *GAPDH*.
- Category 3. Purity controls that include the most common non-EV structures co-isolated contaminants, however there is no stablished threshold of the abundance of these proteins. This category is divided in: 3a, serum/plasma and lipoproteins as *APOA1* or *ALB*; 3b, protein-protein/protein-nuclei acid aggregates or ribosomal proteins as *UMOD* or *RL17*.
- Category 4. Proteins present in other organelles and intracellular compartments not plasma membrane or endosomes, this category is important for claiming specificity of small EVs. This englobes proteins related to: 4a, nucleus as *LMNA* or *HIST1H*; 4b, mitochondrion; 4c, secretory pathway as *CANX* or *HSP90B1*; and 4d, other as cytoskeleton *ACTN1* or *ACTN4*.
- Category 5. Soluble proteins recovery with EVs by binding to specific or promiscuous receptors on the EV surface with functional activities. This category is divided in: 5a, cytokines and growth factors as *PDGFD* or *EGF*; and 5b, adhesion and extracellular matrix as *FN1* or *LGALS3BP*.

Again, these results give evidences of the frat value of our isolation method using ExoGAG.

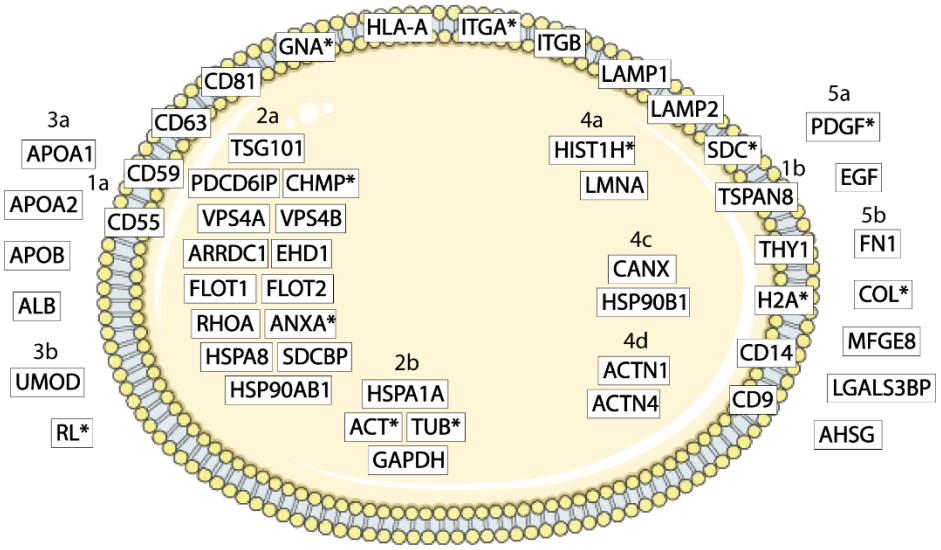

Figure 84. Schematic representation of identified proteins by mass spectrometry analysis in ExoGAG isolation according to MISEV18 guidelines. Category 1, transmembrane or GPI-anchored proteins; Category 2, cytosolic or periplasmic proteins; Category 3, purity controls; Category 4, proteins present in other organelles or intracellular components; Category 5, soluble proteins recovery with EVs.

4.3.5.4 Characterization of the origin of Extracellular Vesicles isolated with ExoGAG.

We analyzed the origin of the vesicles we found in the isolation with ExoGAG. Urine contains a mixture of EVs that were originated from different part of kidneys, although the relative contributions of each part to the total population of urine EVs has not yet been

concluded. The markers we considered for each part of the nephron were those listed in the publication by Urinary Task Force of the International Society of Extracellular Vesicles (297). With ExoGAG we are able to isolate EVs belonging to each of the different segments of the nephron according to the identification of segment-specific markers as we could see in Figure 85.

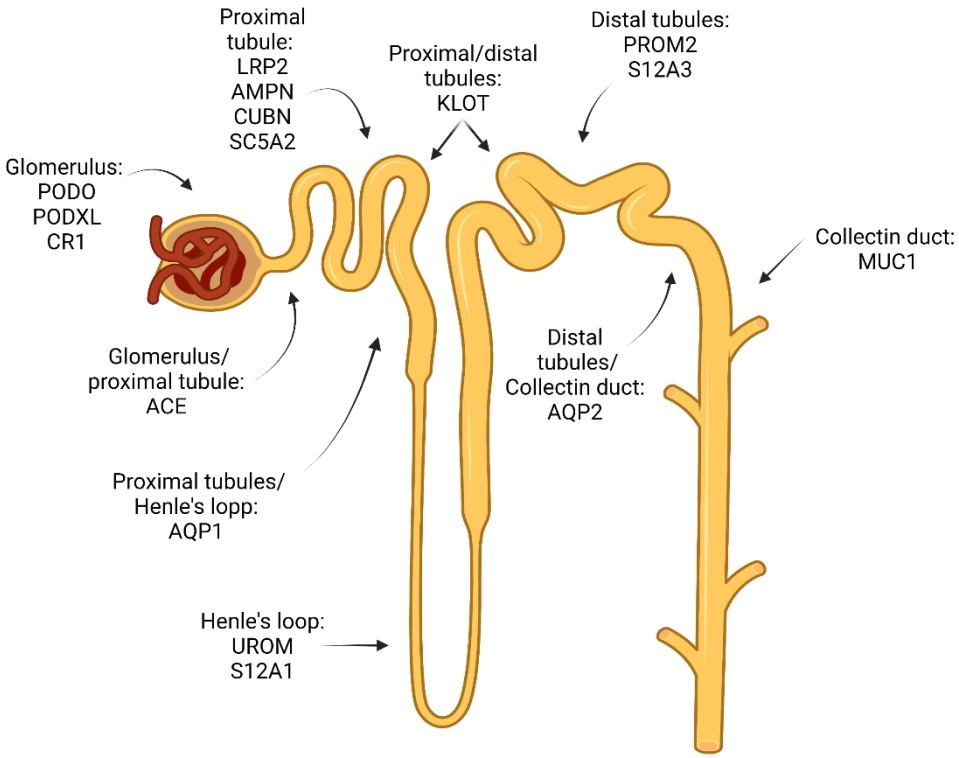

Figure 85. Illustrated representation of identified Extracellular Vesicle markers specific to different segments of the nephron according to Urinary Task Force of the International Society of Extracellular Vesicles by mass spectrometry analysis in ExoGAG.

4.3.6 Characterisation of the vesicular profile of Extracellular Vesicles isolated with ExoGAG and comparison with those isolated by ultracentrifugation.

In addition to the identification of the EV markers as well as the protein component associated with each of the isolation methods, we also decided to analyse the vesicular component obtained by isolation with ExoGAG or ultracentrifugation.

4.3.6.1 Quantification and size analysis using NanoTracking Analysis (NTA)

EVs isolated from 3mL for ExoGAG or 30 mL for Ultracentrifugation isolation of the same urine were characterized using NTA for quantification and size measurement. We analysed the pellet and supernatant for ExoGAG and UC as well as the pure urine sample (Figure 86A).

When we compared the ExoGAG isolation with the ultracentrifugation isolation and the urine sample itself, we observed that the ultracentrifugation isolation sample was more enriched in terms of particle number, although one has to take into account the volume from which it started, 10 times more than for ExoGAG (Figure 86B). The mean size of the isolated particles ranged from just over 200 nm for the UC samples, 200 nm for the ExoGAG isolates and less

than 200 nm for the urine sample. These mean sizes show no significant differences between samples (Figure 86B). Even if we look at the size mode, we see how these differences were even diminished and in all samples, it was slightly less than 150nm (Figure 86B).

We then characterised in the same method how the vesicles isolated in the pellet behaved compared to those not isolated in the supernatant. In both types of isolation (ExoGAG and UC) we obtain more particles per mL of isolated sample (pellet) than those remaining in the supernatant (Figure 86C and D). However, interestingly, the size of EVs that were not isolated with ExoGAG (supernatant) tended to be larger than those isolated, with a mean and mode of 250nm (Figure 86C). In contrast to those that were not isolated by UC, where in this case they were smaller with a mean of less than 150nm and a mode of 100nm (Figure 86D).

Based on the data obtained by the NTA using ExoGAG isolation method we obtain a good yield in the isolation of the EVs as well as isolating a component quite similar in size to those isolated by UC.

USC
UNIVERSIDADE
DE SANTIAGO
DE COMPOSTELA

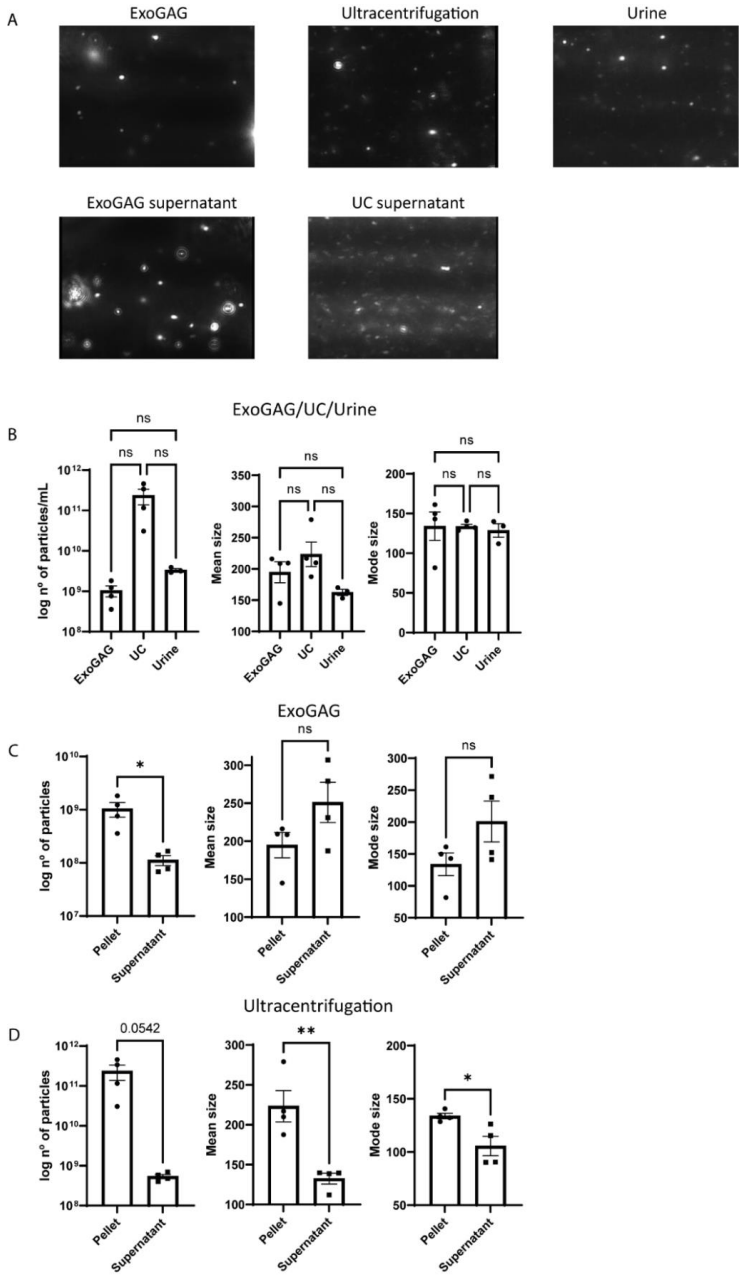

Figure 86. Study of the Extracellular Vesicles number and size of ExoGAG isolation, Ultracentrifugation and the urine without isolation by NTA (NanoTracking Analysis®). (A) Representative image of the NTA capture video of ExoGAG isolation (pellet) and its supernatant, Ultracentrifugation and its supernatant and the urine. (B) Comparison of number of particles per mL and mean and mode size of ExoGAG, Ultracentrifugation and urine. (C) Differences between ExoGAG pellet and supernatant in number of particles per mL and mean and mode size. (D) Variations between Ultracentrifugation pellet and supernatant in number of particles per mL and mean and mode size. Bars represent means ± SEM. Ordinary One-way ANOVA for was used for multiple comparations and T-student test (two tail) for comparisons between two groups and a value of $P<0.05$ was considered significant. ns represents not significative, * $p<0.05$, ** $p<0.01$.

4.3.6.2 Quantification, size analysis and Tetraspanin characterization using ExoView®

ExoView® is a new tool that provides comprehensive measurements of the size, particle number, phenotype and colocalization of different biomarkers by single vesicle fluorescence analysis based on the immunocapture by and immunodetection of specific markers.

For this analysis, EVs were isolated with ExoGAG or Ultracentrifugation of the same urine sample and they were analysed by ExoView®. In this case, the analysis was performed using the tetraspanin CD63, CD81 and CD9 antibodies for capture of EVs and the same labelled antibodies, CD63 in red, CD81 in green and CD9 in blue for immunodetection. We analysed the pellet and supernatant for ExoGAG and UC isolation as well as the pure urine sample (Figure 87A).

For the quantification of total particles by ExoView® we took into account the corrected dilution we performed against the original sample, i.e. for the ExoGAG pellet we previously concentrated 10 times which we then diluted for the analysis, and for the ultracentrifugation we concentrated 300 times. Therefore, we could perfectly compare the total number of particles with the starting urine sample as we were relativising against the original sample. Clearly, we could observe that with ExoGAG we isolated much more particles per ml of urine than with ultracentrifugation with CD63 as well as CD81 and CD9 captured antibodies (Figure 87B). Even more particles remain in the supernatant of ExoGAG than have been isolated by UC (Figure 87B). For the mean particle size measured by ExoView®, there were no differences among samples (Figure 87C).

But in addition to the number of particles and their size, what we are also interested in characterising is the type of EV population we are isolating. For this purpose, we characterized the number of particles positive for the Tetraspanin CD63, CD81 and CD9. The Tetraspanin profile in the urine samples and those isolated with ExoGAG was practically identical, the UC profile was quite similar but already varied a little in the percentage of CD63 and CD9 and what varied considerably is the profile of Tetraspanin that we left unisolated in the ExoGAG supernatant (Figure 87D and E). These data are disaggregated in Figure 87D where, although there were no significant differences, we observed the tendency for there to be fewer CD63 particles in UC and more in the ExoGAG supernatant while it is similar in the urine and ExoGAG samples; the CD81 component is quite similar among all sample types; and the CD9 component decreases a little in the ExoGAG samples, decreases more in the UC samples and quite a bit more in the ExoGAG supernatant.

The results of the ExoView® analysis showed that not only we are able to perform a better isolation with ExoGAG, but also that the vesicular component we were isolating corresponds better to that of the urine.

USC
UNIVERSIDADE DE SANTIAGO DE COMPOSTELA

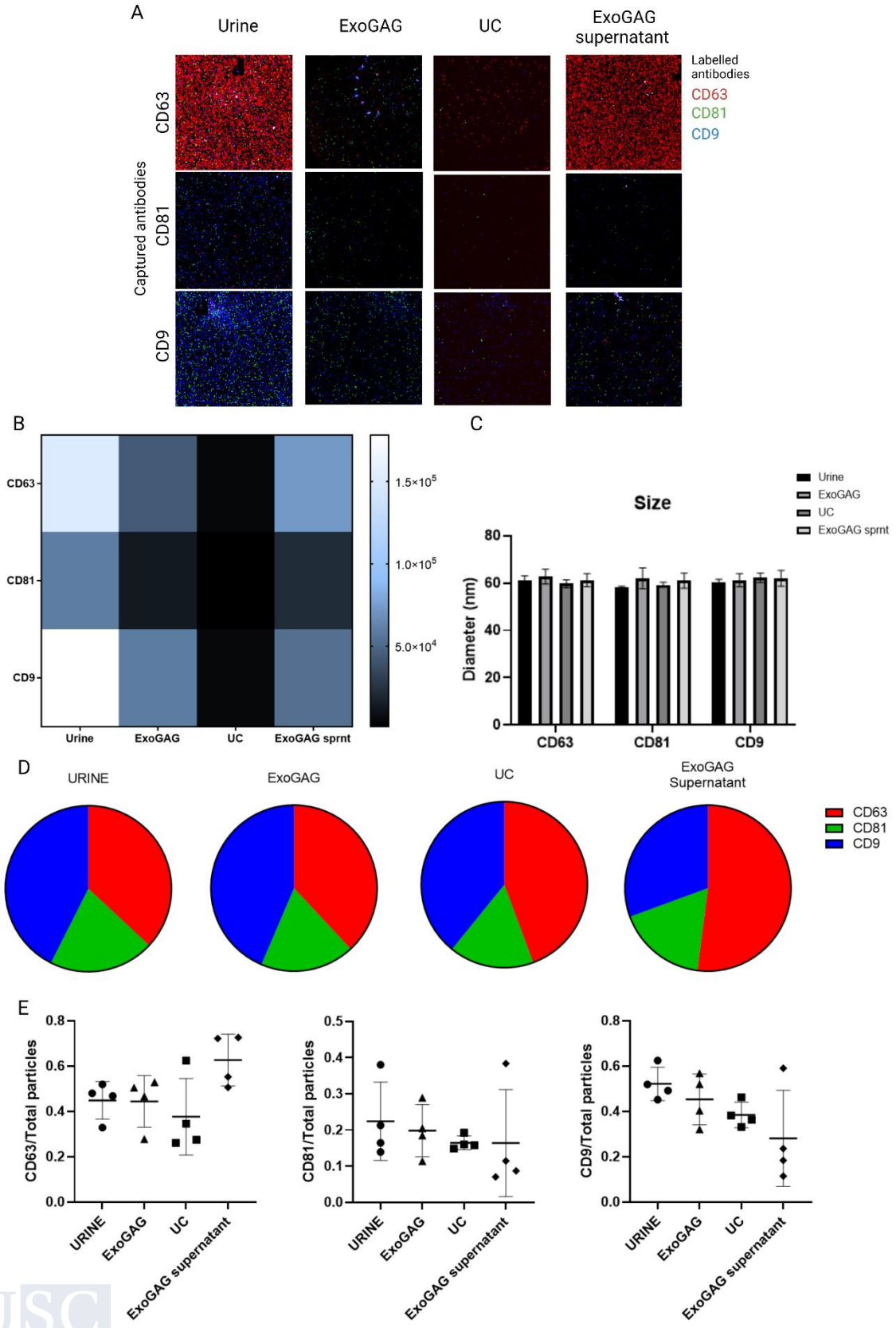

Figure 87. Characterization of the Extracellular Vesicles of urine, ExoGAG isolation, Ultracentrifugation and not isolated Vesicles with ExoGAG by ExoView ® technology. (A) Representative images of the

immunofluorescence in each type of sample. (B) Representation of the total number of particles captured by CD63, CD81 and CD9 for each type of sample. The heatmap showed differences across urine without isolation, ExoGAG and Ultracentrifugation isolation and ExoGAG supernatant. (C) EV size distribution taking into account capture antibody and sample type. (D) Tetraspanin profile (CD63 in red, CD81 in green and CD9 in blue) of urine, ExoGAG and Ultracentrifugation isolation and ExoGAG supernatant. (E) Number of positive particles for CD63, CD81 and CD9 adjusted by the total captured particles for each type of sample. Ordinary One-way ANOVA with multiple comparations was used and a value of $P<0.05$ was considered significant. Only significative comparisons are shown.

4.3.7 Characterization of the vesicular profile of EVs associated with the onset and progression of autosomal dominant polycystic disease.

Once we have demonstrated and characterized the isolated vesicular component by the ExoGAG method, we decided to apply it to the study of ADPKD to understand the underlying molecular mechanisms as well as to search for vesicle-associated biomarkers.

4.3.7.1 Characterization of the Tetraspanin profile of Extracellular Vesicles in patients with mutation in *PKD1*

For this analysis, EVs were isolated with ExoGAG from controls and patients with mutation in *PKD1* in different stages of the disease measured by the serum creatinine level, as we also performed in Chapter 2. In this case, the analysis was performed using the Tetraspanin CD63, CD81 and CD9 antibodies for capture of EVs and the same labelled antibodies, CD63 in red, CD81 in green and CD9 in blue for immunodetection. (Figure 88A).

The first thing we analysed is whether the number of particles captured varies with the different stages of the disease, but we can see that although there is some dispersion, there is no difference in the total number of particles captured (Figure 88B).

However, what we wanted to study is whether the Tetraspanin profile that we saw previously was similar in the control samples changes with the disease. For this purpose, we characterized the number of particles positive for the Tetraspanin CD63, CD81 and CD9. As can be seen, the Tetraspanin profile varied from the beginning of the disease (low creat), where a decrease of the CD63 component and an increase of the CD81 component could be observed, while the CD9 component remains similar. This profile is also seen in medium and high creatinine, but there is a small decrease in CD9 vesicles in medium creatinine (Figure 88C). The dispersion of the data can be seen at in Figure 88D where, although there were no significant differences, we observed the tendency to be fewer CD63 particles in patients with mutation in *PKD1* since the beginning of the disease; the percentage of CD81 particles is also increased in patients with *PKD1* mutation; and the CD9 component decreases a little in the medium creatinine samples, but generally did not change with the onset of the disease.

USC
UNIVERSIDADE DE SANTIAGO DE COMPOSTELA

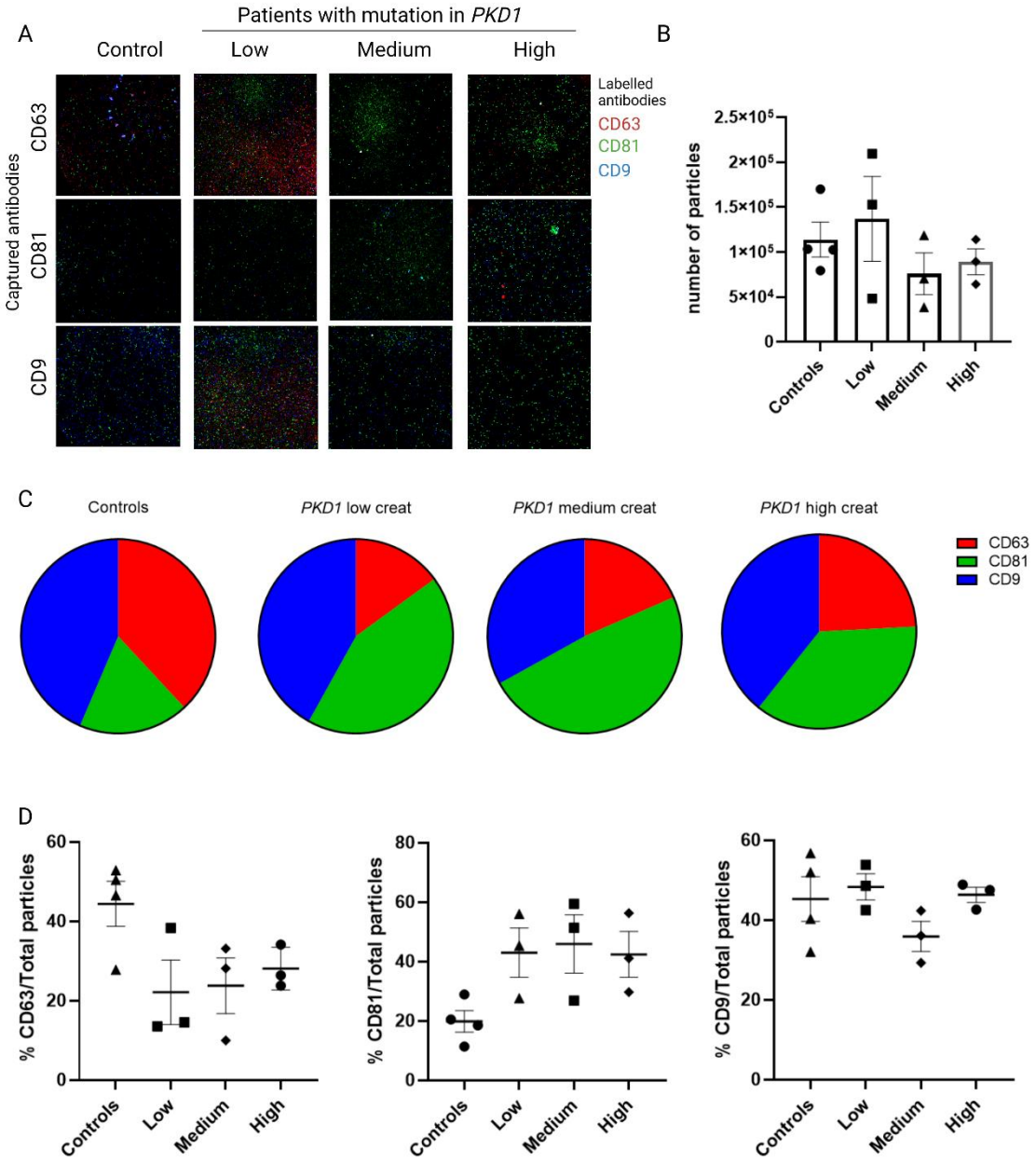

Figure 88. Characterization of the Tetraspanin profile of Extracellular Vesicles in patients with mutation in *PKD1*, with renal damage according to serum creatinine value. (A) Representative images of the immunofluorescence in samples of controls and patients with mutation in *PKD1*, with renal damage measured by serum creatinine, divided in low, medium and high levels of creatinine. (B) Representation of the total number of particles captured by CD63, CD81 and CD9 for each type of sample. (C) Tetraspanin profile (CD63 in red, CD81 in green and CD9 in blue) of controls and patients with mutation in *PKD1* in different stages of the disease. (D) Percentage of positive particles for CD63, CD81 and CD9 adjusted by the total captured particles for each type of sample. Ordinary One-way ANOVA with multiple comparations was used and a value of $P<0.05$ was considered significant. Only significative comparisons are shown.

4.3.7.2 Characterization of the Tetraspanin profile of Extracellular Vesicles in patients with mutation in *PKD2*

In addition to the study in patients with PKD1 mutations, we also analysed patients whose disease is caused by PKD2 mutations.

For this analysis, EVs were isolated with ExoGAG from controls and patients with mutation in *PKD2* in different stages of the disease measured by the serum creatinine level. In this case, again, the analysis was performed using the Tetraspanin CD63, CD81 and CD9 antibodies for capture of EVs and the same labelled antibodies, CD63 in red, CD81 in green and CD9 in blue for immunodetection (Figure 89A).

In reference to the number of particles captured, although there was the tend to decrease in patients, there was no difference in the total number of particles captured (Figure 89B).

However, what we wanted to study if the Tetraspanin profile changed between control and patients or changed related to the different stages of the disease. For this purpose, we characterized the number of particles positive for the Tetraspanin CD63, CD81 and CD9. As can be seen, the Tetraspanin profile varied from the beginning of the disease (low creat), where a decrease of the CD63 component and an increase of the CD81 component could be observed, while the CD9 component remains similar. In patients with mutation in *PKD2*, this profile also presented a tiny decreased in CD81 and a tiny increased in CD9 component in medium and high creatinine in respect of low create (Figure 89C). The dispersion of the data can be seen at in Figure 89D where, although there were no significant differences, we observed the tendency for there to be fewer CD63 particles in patients with mutation in *PKD2* since the beginning of the disease; the percentage of CD81 particles increased in low creatinine but tend to decrease with the rise of creatinine levels in patients with *PKD2* mutation.; and the CD9 component decreases a little in the low creatinine samples and present a small increased correlating throughout the disease, but generally did not change excessively.

USC
UNIVERSIDADE
DE SANTIAGO
DE COMPOSTELA

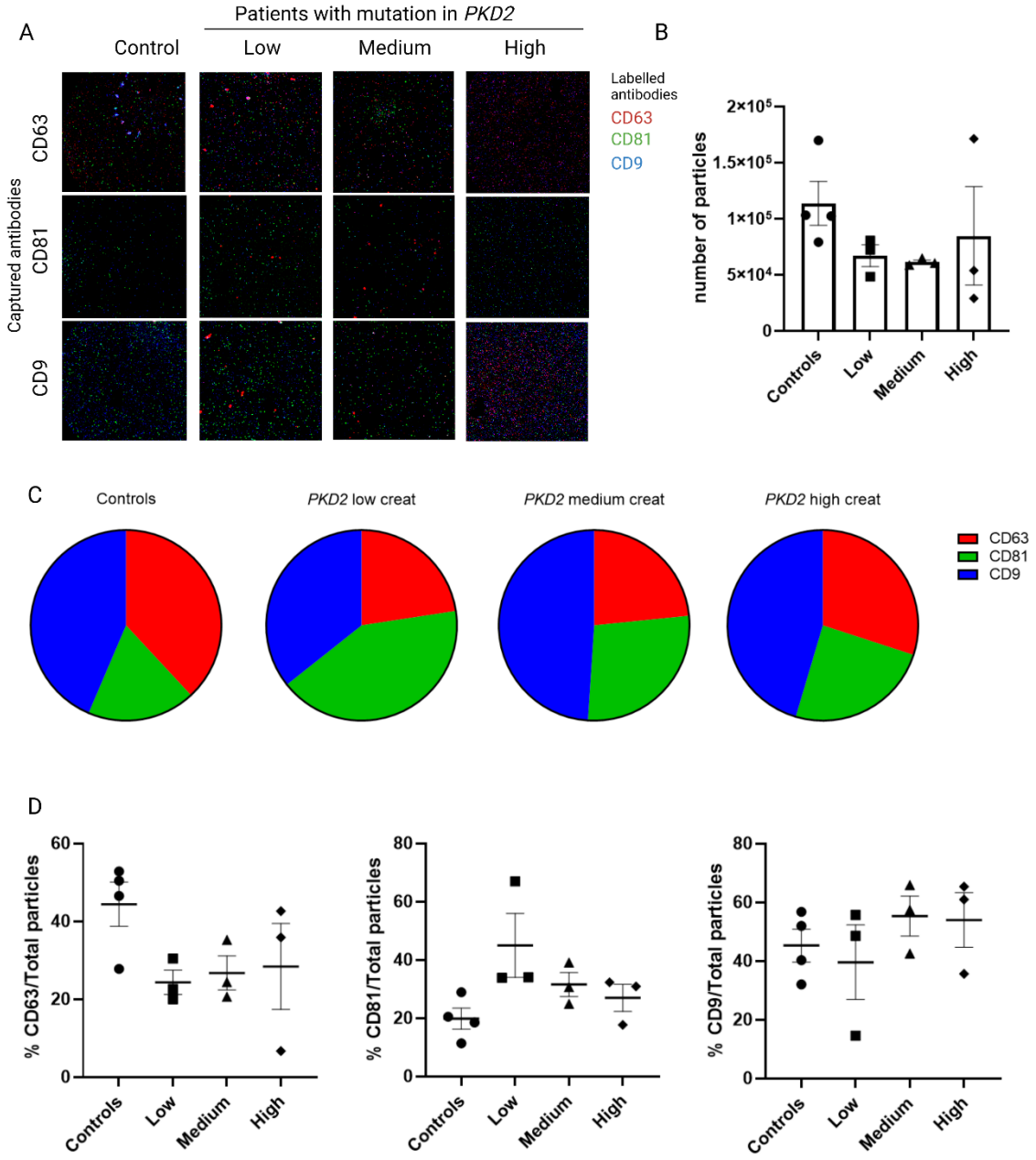

Figure 89. Characterization of the Tetraspanin profile of Extracellular Vesicles in patients with mutation in *PKD2*, with renal damage according to serum creatinine value. (A) Representative images of the immunofluorescence in samples of controls and patients with mutation in *PKD2*, with renal damage measured by serum creatinine, divided in low, medium and high levels of creatinine. (B) Representation of the total number of particles captured by CD63, CD81 and CD9 for each type of sample. (C) Tetraspanin profile (CD63 in red, CD81 in green and CD9 in blue) of controls and patients with mutation in *PKD1* in different stages of the disease. (D) Percentage of positive particles for CD63, CD81 and CD9 adjusted by the total captured particles for each type of sample. Ordinary One-way ANOVA with multiple comparations was used and a value of $P<0.05$ was considered significant. Only significative comparisons are shown.

4.3.7.3 Comparison of the Tetraspanin profile of Extracellular Vesicles in patients with mutation in *PKD1* and *PKD2*

Once we had the analysis separately, we wanted to check if the changes were due to the presence of the disease or if they were characteristic of each ADPKD gene mutated, so we

compared the Tetraspanin profile of patients with PKD1 mutation versus those with PKD2 mutation.

As for the total number of particles captured (Figure 90A), we could see that there were no differences between samples from PKD1 and PKD2 patients, although there was a tendency for *PKD1* patients with low creatinine levels to have more particles than *PKD2* patients.

The percentage of CD63 positive particles remained constant between patients (Figure 90B). However, the percentage of CD81 and CD9 particles tended to vary between *PKD1* and *PKD2* mutated patients. The number of CD81 particles was lower in *PKD2*-mutated patients at low and medium creatinine levels than in *PKD1*-mutated patients, although at high creatinine levels there was no difference in the number of CD81-positive EVs (Figure 90C). In the CD9 positive component, differences were only observed at medium creatinine levels where there was a predisposition for *PKD1* mutation patients to have less CD9 positive than in *PKD2* and at all other creatinine levels (Figure 90D).

With these results we have observed not only that the Tetraspanin profile changes when ADPKD occurs, but also that this may be specific to the type of causative mutation.

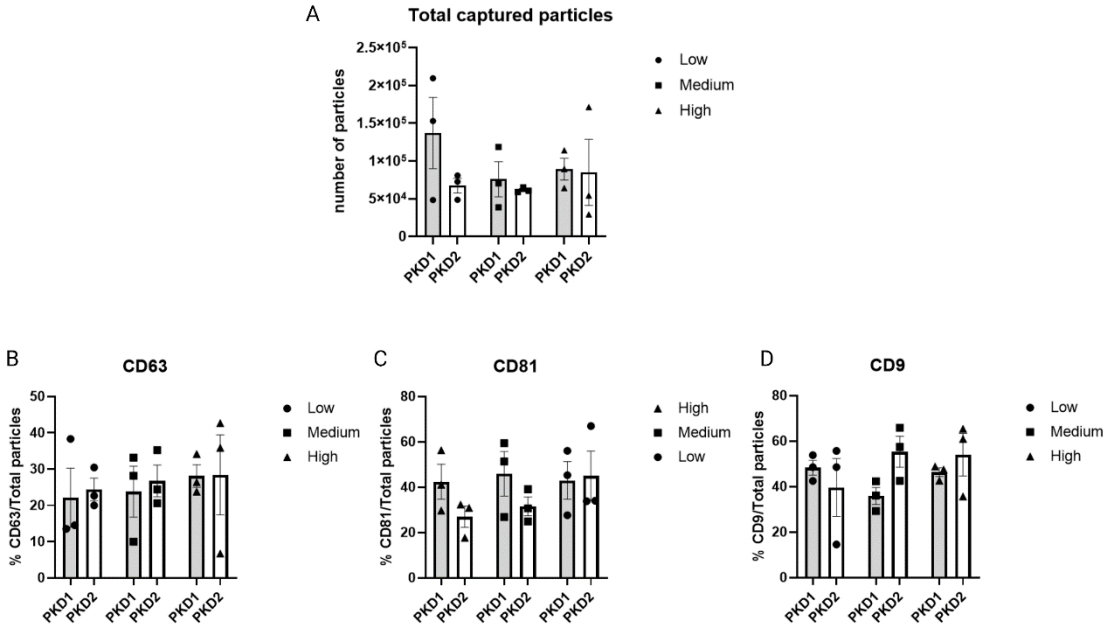

Figure 90. Comparison of total captured particles and Tetraspanin profile between patients with mutation in *PKD1* and *PKD2*. Multiple unpaired t test was used and a value of P<0.05 was considered significant. Only significative comparisons are shown.

4.3.7.4 Characterization and validation of the possible biomarkers in the vesicular component of ExoGAG isolation in the progression of autosomal dominant polycystic disease.

We then decided to study whether the biomarkers we had found in the ExoGAG isolation of the glycoprotein component were found in the EVs. For this we again used the ExoView® platform. In this analysis, EVs were isolated with ExoGAG from patients with mutation in *PKD1* and *PKD2* in different stages of the disease measured by the serum creatinine

level. In this case, again, the analysis was performed using the Tetraspanin CD63, CD81 and CD9 antibodies for capture of EVs and the immunodetected with UROM in violet (far-red), AMBP in red, VTNC in green and CERU in blue labelled antibodies (Figure 91A).

The total number of particles captured, appeared to be similar in samples from patients with PKD1 and PKD2 mutation independently of the capture antibody (Figure 91B) (Supplementary Figure 5).

To characterize the number of positive EVs for the possible biomarkers, what we did was to calculate the percentage of positive vesicles for each of them (UROM, AMBP, VTNC and CERU) in the total number of particles captured, in this way we had a parameter of normalisation between each condition. In the case of Uromodulin (Figure 91C), we observed a tendency for the number of positive EVs to decrease over the course of the disease, especially for *PKD2* samples, which corresponds to what was observed in the study of the glycoprotein component. Although these differences were not as clear in PKD1 samples and less so between medium and high creatinine samples. Another marker that tends to correlate with previous data is Vitronectin (Figure 91F), where it could be observed that the number of VTNC-positive particles tends to increase with increasing creatinine levels. However, the results obtained in the characterisation of the glycoprotein component were not observed for the AMBP Protein and Ceruloplasmin markers. For the AMBP protein (Figure 91D), the opposite is observed for the glycoprotein component, in this case the number of AMBP positive vesicles decreases with the course of the disease, especially in the *PKD1* samples, where this decrease is already observed from mean creatinine levels. Moreover, for CERU (Figure 91E), what we observed was that there was no variation in the number of positive EVs throughout the disease, while what we observed was a decrease in medium creatinine samples in *PKD1* and an increase in high creatinine in *PKD2*.

This leads us to think that not only the component of the Extracellular Vesicles and their cargo play an important role throughout the disease, but also that there is a complex formed by EVs and associated proteins that is the part really altered and plays a fundamental role in the course of the disease.

USC UNIVERSIDADE DE SANTIAGO DE COMPOSTELA

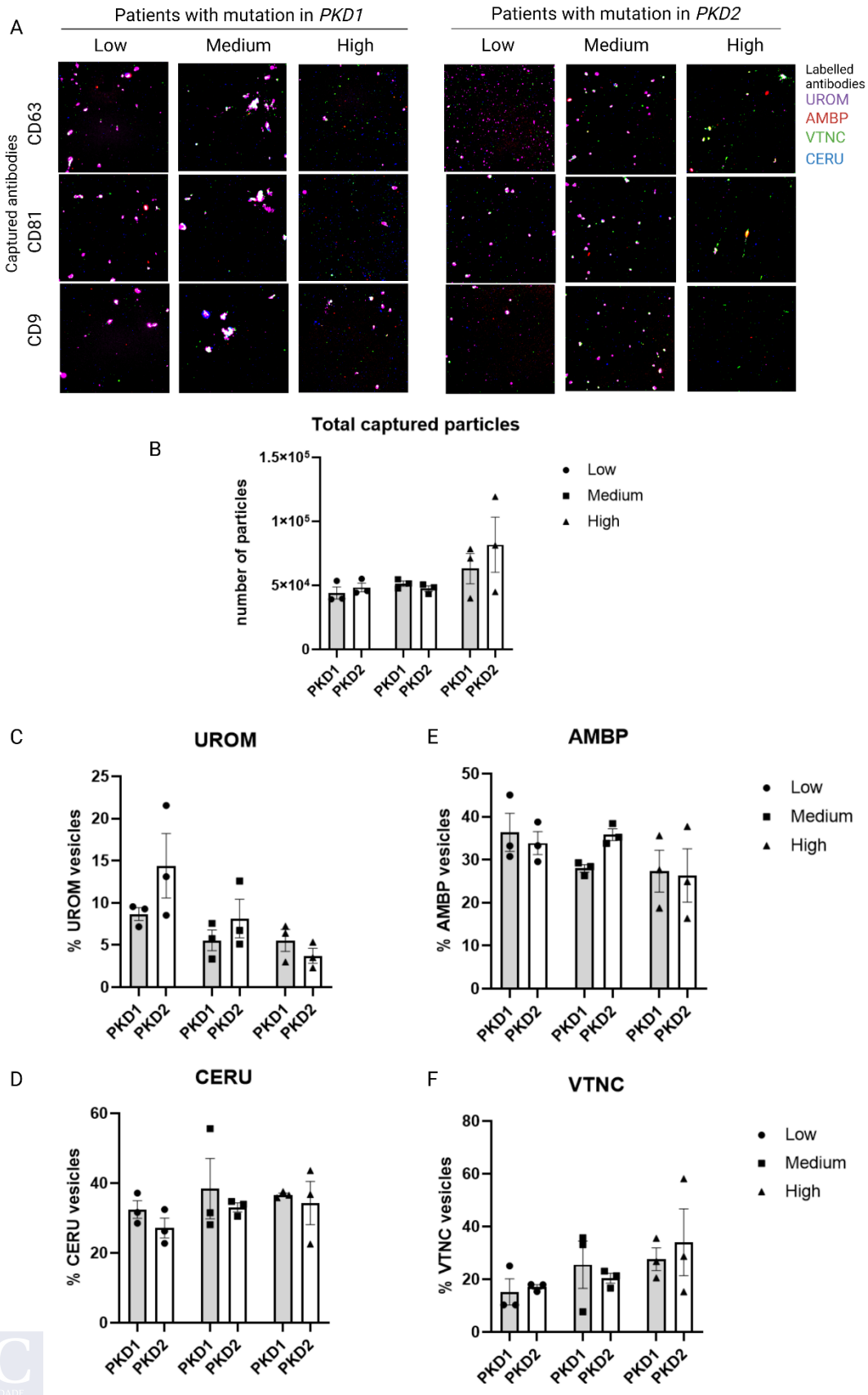

Figure 91. Validation of the possible targets in the Extracellular Vesicle component in patients with mutation in *PKD1* and *PKD2* throughout the disease. EVs were captured by Tetraspanin CD63, CD81 and CD9

and immunodetecting with UROM (DyLighy 755, far-red), AMBP (Alexa Fluor 647, red), CERU (Alexa Fluor 488, blue) and VTNC (Alexa Fluor 594, green). (A) Representative images of the immunofluorescence in samples of patients with truncated mutation in *PKD1*(left) and *PKD2* (right), with renal damage measured by serum creatinine, divided in low, medium and high levels of creatinine. (B) Representation of the total number of particles captured by CD63, CD81 and CD9 for each type of sample. Percentage of Uromodulin (C), Ceruloplasmin (D), Protein AMBP (E) and Vitronectin (F) positive vesicles adjusted by the total captured particles for each type of sample. Ordinary One-way ANOVA with multiple comparations was used and a value of $P<0.05$ was considered significant. Only significative comparisons are shown.

USC
UNIVERSIDADE DE SANTIAGO DE COMPOSTELA

DISCUSSION

USC
UNIVERSIDADE
DE SANTIAGO
DE COMPOSTELA

USC
UNIVERSIDADE
DE SANTIAGO
DE COMPOSTELA

5. DISCUSSION

5.1 IDENTIFICATION OF NEW SIGNALING PATHWAYS INVOLVED IN CYSTOGENESIS BY QUANTITATIVE DIFFERENTIAL PROTEOMIC STUDY IN POLYCYSTIC KIDNEY DISEASE MOUSE MODEL

The pathophysiology of Autosomal Dominant Polycystic Kidney Disease is associated with high number of molecular mechanisms. Indeed, it is not known whether the alteration of these pathways is the cause of cystogenesis or a consequence of it. Furthermore, the therapies in use act by palliating some of the symptoms or delaying the progression of the disease. Currently, there is no effective therapy capable of eliminating cysts. So, an emerging interest in understanding molecular pathways and developing new therapeutic strategies is increasing (15,38). The purpose of present work was characterized the proteomic changes in polycystic kidneys and provided new insights in the pathophysiology and possible biomarkers and therapeutic targets into ADPKD.

Therefore, we performed the differential comparison between the proteomes of *Wild Type* and Mutant kidneys from an ADPKD orthologous mouse model (75,275) by the high throughput quantitative SWATH method in different stages of the disease. The first approach, to draw a direct comparison with our previous studies (278), we performed a differential quantitative proteomic study of the *Wild type* and mutant kidneys of mice euthanized at postnatal day 30, time at which the disease is fully developed in this animal model, as demonstrated by the results of histological characterization in cystic index and number of cysts, as well as in the KW/BW ratio and with establishment of renal damage with increasing BUN value. In this study, we found 152 significant DEPs with a fold change greater than 2, with 96 of them upregulated in mutants and 56 downregulated. These results uncovered plenty of upregulated and downregulated proteins found in the quantitative analysis in mutants at day 30 of development and were related to several biological processes as well as different cellular component, which makes the approach to the study of the ADPKD complex as well as revalidates the fact that to this day of development the main and secondary pathways of cystogenesis are still hard to identify (15,77). To try to elucidate the molecular mechanisms related to the onset of cystogenesis we decided to perform the study at an earlier time, at postnatal day 18, where the disease is not yet fully developed, with relatively less cystic index as well as number of cysts and with the renal function measured by BUN practically unchanged. Taking only this condition into account, the study showed that only 14 significant DEPs met the criteria of having a fold change >2. In this case, all these proteins are downregulated in the mutants and are related to the immune system, metabolism and plasma membrane-related processes. These pathways are already described by other authors as being altered in ADPKD (34,38). There are even some studies where the metabolic (299) and inflammatory (300) pathways are seen to be altered in early stages of the disease.

However, it is known that in the SWATH analysis one of the most important issue is the library (301–303), therefore we considered that in order to be able to compare the results obtained on each of the stages of the disease, it is necessary to combine the proteomic libraries and perform the analysis as a whole. In this way, we obtained a combined spectral library of 2498 proteins with an FDR<1%, much higher than when we studied the separate libraries where 1283 proteins were obtained in the postnatal day 30 library and 971 in the postnatal day 18 library. Moreover, we think that by increasing the number of samples and conditions for the generation of the library we obtain a better performance in the identification of proteins that

fulfil the inclusion criteria that each protein, consists of at least 10 peptides identified with the FDR<1% and that each one of these peptides presents at least 7 fragments. This conclusion is also supported by independent studies where the generation of the library is key in obtaining mass spectrometric results (304,305). In fact, when comparing the results obtained in the library of each condition or the library of the set of conditions, it can be seen that not all DEPs with a fold change >2 were shared, which indicates that the results of the identified proteins are library-specific. However, the altered pathways that have been identified in each of the analyses are the same, which shows that although the same targets are not specifically obtained, the altered pathways in the disease are identified. To solve these library dependency problems, recent studies show promising results in the use of library free acquisition methods where the depth, range and complexity of quantitative proteomics studies are increased (306–308).

In this analysis, a total of 15 significantly DEP proteins with a fold change >2 were found at postnatal day 18 between *Wild type* and Mutants. In this case, 14 of them were upregulated in Mutant and only 1 downregulated, contrary to what was found in the postnatal day 18 independent library, where only down-regulated proteins are found, this may be due to the fact that few DEPs are identified and that increasing the number of proteins in the library by almost 3-fold and for statistical reasons leads to these differences in significantly deregulated proteins. Upregulated proteins are related to biological processes such as translation and regulation of kinases pathway and to the cellular components as extracellular matrix and ribosomes, while downregulated proteins are related to metabolism and are found in the mitochondria, the latter being the same pathways that had already been found in the postnatal day 18 library study. On the other hand, a total of 213 significantly DEP proteins with a fold change >2 were found at postnatal day 30, being 156 upregulated and 57 downregulated. Upregulated proteins have been shown to be involved biological processes as cytoskeletal pathways, cell-cell adhesion, cell migration, as well as activation of cell signaling cascades, and in cellular components as cytoskeleton, plasma membrane and extracellular matrix. In contrast, downregulated proteins were evidently related to metabolism together with response to different ions, so these proteins were related to cellular component as the mitochondrion and membrane. The pathways that we are seeing that are altered in the pathophysiology of ADPKD have been described previously (15,38). These data suggest that in advanced stages of disease progression the number of proteins and related pathways deregulated increased. In the same way, these results reinforce the idea of cyst growth passes with two big stages: cyst initiation and cyst progression (77). What we can observe is that there are pathways that are already altered in the initial stages of the disease and this continue to be altered throughout the disease. This is the case of the upregulation of the translational pathway which can be a consequence activation of transcription factors leading to the activation of protein synthesis that are related for example to proliferation and apoptosis (82,309), or due to the activation of the MAPK kinase cascade which in turn is involved in the regulation of the cytoskeleton, a pathway which is also altered (38), even the extracellular matrix is already deregulated in these very early stages where there does not seem to be much progression of the cysts, which has been described as being associated with (89); or the downregulation of the metabolism since initial stages of the disease (98).

In addition to the fact that there are pathways that are already altered in the early stages and continue in the most severe stages, there are three proteins (Vimentin, Spondin-1 and RNA-binding protein 3) that, in our study, appear upregulated in the differential analysis in the mutants at postnatal day 18 and continue at postnatal day 30, which would make them attractive as a possible therapeutic target as it would be possible to modulate their expression from the

early stages. Moreover, as described in other articles studying the transcriptomics of the disease (310,311) and in the results of this thesis, there is a difference in the proteins that are altered in early or advanced stages of the disease, so it is important to act when these proteins are deregulated. Furthermore, the renal plasticity described in ADPKD has to be taking into account where complete reversal of the disease occurs when genes are re-expressed in early stages of the disease and the secondary pathogenic mechanisms, as the fibrosis, have not occurred, seeing that in later stages the disease is partially reversed or even only slows the progression of the disease, it is stage-specific of the ADPKD (312,313). This, open the same for the therapeutic window with other drugs, where they will be more effective for treatment if they are administered in the early stages.

Vimentin (VIME) is a member of the type III intermediate filaments found in various non-epithelial cell types, especially in mesenchymal cells, so it is a marker of the epithelial-mesenchymal transition. VIME is attached to the nucleus, endoplasmic reticulum, and mitochondria, either laterally or terminal; and is involved in motility, maintenance of cell shape, and endurance of mechanical stress (314). Studies have already found increased VIME in patients with advanced ADPKD at both histological (315) and serum levels (316).

Spondin-1 is an extracellular-matrix protein related to cell-adhesion, member of the thrombospondin family. It was reported that SPON1 promotes the growth of neural axon cells while inhibiting the migration of neural crest cells (317). Other studies showed that SPON1 triggers focal adhesion kinase 1 (Fak) and tyrosine-protein kinase Src signaling and promotes distant metastasis in osteosarcoma (318). Another study reported that SPON1 promotes tumor invasion and metastasis in liver cancer (319). Its involvement in the ADPKD may be related to its function in the extracellular matrix.

RNA-binding protein 3 (RBM3) is a member of the highly conserved RNA binding proteins that participate in cellular processes by binding to mRNA of target genes. Moreover, it acts as a cold shock response protein to protect cells from hypothermia-induced death. Under normal physiological conditions, RBM3 is essential for cell survival and proliferation (320,321). The major functions of RBM3 comprise regulation of post-transcriptional, translational changes and microRNA synthesis. Enhances phosphorylation of translation initiation factors and active polysome formation (321,322). The RNA-binding family of proteins has been shown to play an important role in kidney diseases (323).

Due to the importance of these targets, the validations have been carried out by other techniques, starting with transcriptomic validation by RT-qPCR. Gene expression analysis showed that only Vimentin is significatively overexpressed which correlated with the increased of protein abundance in mutants, although Spondin-1 showed a tendency to be overexpressed but not significantly. On the other hand, RNA-binding protein 3 was no significatively altered at postnatal day 18, in contrast, it was downregulated at postnatal day 30, the opposite situation as the protein abundance by SWATH analysis. The RT-qPCR allows validation of proteins detected by proteomics but not invalidation, as they are not complementary techniques. RT-qPCR analyses gene expression while proteomics studies proteins. Therefore, not finding differences in gene expression do not mean that they do not exist at the protein level (324), but the fact that there are differences at the gene level implies that there are differences at the protein level. In fact, it may be the case that the level of protein regulates the level of gene expression through negative feedback, where increased protein abundance leads to inhibition of gene expression, as is the case with circadian proteins (325).

Therefore, we also validate by other techniques such as *Western Blot*. In this case, the results at postnatal day 30 agrees with those obtained by mass spectrometry, however, none of them are validated by western blot at postnatal day 18. In order to see if this is due to same issue that make difficult to identify the correct protein we perform a Western Blot 2D and this show us that the proteins have post-translational modifications that are not possible to see in the Western Blot 1D. Even in the validation by immunofluorescence of vimentin is evident that this protein plays an essential role in the physiology of ADPKD as it appears colocalized with the cysts from the early stages.

In summary, we identified novel targets and pathways involved in physiopathology of ADPKD by quantitative proteomic SWATH-MS technology. We were also able to identify those pathways that are altered early in and throughout the course of the disease, as well as possible targets for their modulation. We emphasized the novel therapeutic opportunity presented by the regulation of Vimentin, Spondin-1 and RNA-binding protein 3, because of their deregulation from the early stages and the pathological function they play. Nevertheless, there is necessity to confirm this in future preclinical studies as well as more functional studies to characterize the exact role of our target candidates in PKD. In conclusion, this work has identified a new mechanism and opportunity for future research in ADPKD physiopathology, leading to possible new therapeutic approaches of the disease.

USC
UNIVERSIDADE
DE SANTIAGO
DE COMPOSTELA

5.2 NEW BIOMARKERS IN URINE FOR DIAGNOSIS AND PROGNOSIS OF ADPKD

Chronic kidney disease (CKD) has become one of the major public health problems in recent decades, affecting approximately 10% of the global adult population, or even, recent studies calculate that in Spain the rate increases to 15% (6,7), making it likely to become the fifth leading cause of death worldwide by 2040 (9). There are many potential causes for chronic kidney diseases, including genetics, and non-genetic causes. In particular, ADPKD is the fourth leading global cause for kidney failure, triggering the 5 to 10% of ESRD (326). Management of CKD is based on trying to preserve as much kidney function as possible before having to use renal replacement therapy, but finally the only life-sustaining treatment of severe renal failure is renal replacement therapy both by dialysis or kidney transplantation (8). In addition to the damage caused to patients' lives, it is also a problem for health services and their finances due to the high cost of the latest treatments for ESRD (327). Thus, early detection of kidney injury in risk population would be an invaluable tool in order to manage this group of patients and to control the incidence of kidney disease.

Despite there are different tools and biomarkers, as the most used measurement of GFR by serum creatinine parameter (8), that are being used in the clinical practice, there is still a lack in specificity and sensitivity, making it difficult to classify some of the patients and, none of them is able to predict the outcome of the disease throughout time. Although specifically in the case of ADPKD, as it is a genetic disease, the use of genetic diagnosis can be of help in trying to predict the progression of the disease, although it is not yet fully sensitive and accurate, due to the high variability, even, between patients with the same mutation or family history (45,47). Furthermore, it has been shown that the measurement of total kidney volume (htTKV) can also be a relatively good predictor, but it is a very expensive test that is difficult to implement in routine clinical practice (124). Because of that, the research of new biomarkers is necessary.

For this purpose, we decided to search for new biomarkers in urine, as it is a non-invasive method that is implemented in the clinical routine on a regular basis, besides it is the most direct fluid that could reflect changes in renal homeostasis and kidney function at any level. We developed an isolation method in relation to glycosaminoglycans (ExoGAG) to characterize the fraction bound to them in the urine, thus reducing the complexity of the sample such as urine and also characterizing a component known to be susceptible to change in the presence of disease as the renal disease (273,274), as, for example, the alteration of GAGs in diabetic nephropathy has already been described (328,329).

We started with an analysis of the mouse model established and studied previously in Chapter 1, for which we collected urine from different stages of the disease, specifically at days 22 as early stage, 30 as advance stage and 45 as end-stage of renal disease, defined by parameters such as histology, cystic index or renal function by BUN quantification, in order to carry out a time course of the disease. The first thing to mention is that it was impossible to collect urine at postnatal day 18, the same time as that studied in the differential proteomics study, due to the small size of the mice and the small amount of urine they produce, so we had to wait until postnatal day 22 to be able to perform the first valid urine collection in early stages of cystic disease. First, a comparison was made between the proteome obtained in the pure urine sample and the same sample isolated with ExoGAG, where twice as many proteins were identified in those samples isolated with ExoGAG, demonstrating that with this method we obtain a component that allows a deeper and more sensitive analysis of the sample. This may be due to the fact that with this isolation what we are doing is enriching the sample and eliminating from this component those proteins that are in the majority and mask the detection

of other more minority proteins, such as the major urinary proteins (MUPs), major proteins in the urine of mice that function as pheromones (330).

Differential proteomics analysis of urine samples isolated with ExoGAG between *Wild Types* and Mutants and over the course of the disease shows a number of proteins that are altered and could be possible biomarkers of disease. It is noteworthy that only one protein, Uromodulin, was found in lower abundance in the mutants and its abundance decreased over the course of the disease. A set of three proteins, AMYP, EFG and NAPSA were found in higher abundance in the *Wild Type* samples but unchanged over the course of the disease, but most of the proteins were found to be enriched in the mutants and increased in abundance over the course of the disease. Within this last category, it is worth mentioning the fibrinogen cluster, which has recently been described as being associated with the cystic hepatic manifestation (PLD, Polycystic Liver Disease) of polycystic kidney disease by means of differential proteomic analysis of *Wild Type* and Mutant livers carried out by our group in the same animal model (278). The validation of these results of possible biomarkers was carried out by comparing the protein profile isolated with ExoGAG between *Wild type* and Mutant samples where clear differences were observed both in the profile obtained with total protein staining, beginning to see clear differences at postnatal day 30 but clearly distinct at day 45, and in the sequencing results of the independent bands where there are variations in the abundance of proteins such as UROM, ALBU, AMYP or AMPB.

This analysis was replicated with human urine samples from controls and ADPKD patients with mutations in the *PKD1* and *PKD2* gene. We observed a constant fingerprint of GAG associated proteins in control samples. However, our results revealed that the constant pattern was altered in PKD patients dependently on renal function correlated with serum creatinine, being more extreme in the most severe stages of the disease (high levels of creatinine) but beginning to be altered at initial stages of the disease with relatively low creatinine levels. Moreover, we found that the variation of the profile in patients was specific of the type of the disease, as can be observed between the profile of patients with mutations in *PKD1* and *PKD2* where this pattern had more pronounced change from earlier stages. This new ExoGAG method allows us to characterise the protein profile associated with GAGs from a small sample volume and in a relatively short time, where this profile is homogeneous in a normal population and is altered in renal patients, even in patients with renal function not yet impaired. This application of ExoGAG could be evaluated in other renal pathologies as well as other aetiologies.

The characterization of the differences observed in the profile of GAG-associated proteins by mass spectrometry leads to the identification of a series of possible biomarkers that show a specific behavior throughout the disease. Within this set, it is worth noting again that only one protein, Uromodulin, decreases with disease progression, the same protein found in the mouse urine study. In addition, other markers have been found that are also shared with the results of the mouse urine study, such as Albumin, Apolipoprotein-IV, Ceruloplasmin, the fibrinogen component and the AMBP protein. The fact that we found a number of biomarkers shared between the animal model and humans revalidates the idea that they are indeed altered in the progression of PKD, as well as demonstrating the robustness and reproducibility of the ExoGAG method. Moreover, most of these interested markers have already been described in association with CKD, measure directly in serum or urine samples: Uromodulin (12,331–334), Albumin (335,336), A1AT (332,333,337), APOA4 (338–340), Ceruloplasmin (333,341–343), DPP4 (344), Galectin-3 binding protein (345), Fibrinogens (333,346,347), Protein AMBP (348–350) or TRFE (351).

Validation of proteins identified by mass spectrometry that vary with disease course by Western Blot found that UROM, ALBU, A1AT, APOA4, CERU, LG3BP, FIBB, AMBP and VTNC were validated in patients with mutation in *PKD2*, while UROM, ALBU, CERU, FIBB, AMBP and VTNC were validated in patients with mutation in *PKD1*. However, as we mentioned before, the non-validation by Western Blot does not mean the invalidation of the results of mass spectrometry. Mass spectrometry, in this case, is based on the quantification of the number of peptides sequenced and the spectral obtained by each peptide (spectral count), so that the greater number of spectra, mean the greater abundance of the protein, while in the Western blot a specific antibody detection is performed and it may be possible that the proteins identified by mass spectrometry suffer some modification that are not able to recognize the antibodies used. Among the proteins that are validated in both *PKD2* and *PKD1* mutated patients and that best match the variation in the profile observed in the total protein are UROM, CERU, AMBP and VTNC. In addition to the validation of Albumin, a parameter that is already implemented in the clinical routine for its study as a marker of renal function (352–354), isolated with this method we also see that it correlates with the increase in serum creatinine and is one of the main responsible for the change in the protein profile associated with GAGs. In fact, it can be observed how in the band of its weight around 70kDa there are also associated many other proteins that do not have that weight, but which seem to form a complex that does not break down in reducing and denaturing conditions as occurs in the case of Ceruloplasmin or Vitronectin, in both types of patients.

Uromodulin (UROM), also known as Tamm-Horsfall protein, is the most abundant urinary protein in physiological conditions, and it is exclusively produced by epithelial cells in the kidney tubule, mostly in the thick ascending limb of Henle's loop (TAL) and lesser by epithelial cells of early part of the distal tubule (237). Glycosylation accounts for about 30% of the molecular weight of mature protein, although the functions of post-translational modifications are not yet fully understood (355). Uromodulin is found in urine as a filamentous-polymer with an average length of ~2.5μm that forms a matrix-like structure, due to its zona pellucida domain that allows protein polymerization, after the cleaved of the glycosylphosphatidylinositol-anchored precursor (356,357). Among the physiological functions that are known, although not yet entirely clear, are the following: protection against urinary tract infections by binding to the surface proteins of bacterium and preventing them from adhering to the urinary epithelium (355,356,358,359); protection against kidney stones (355); renal salt (sodium (360), calcium (361) and magnesium (362)) transport and homeostasis and then regulation of blood pressure (355,357,359); and modulating inflammation, even acting at the systemic level beyond the kidney (355,359). Previously it has already been mentioned that there are studies involving a decrease in Uromodulin with the appearance of CKD (12,331–334,357). Urinary levels of uromodulin reflect tubular mass and function and are positively correlated with eGFR (355,359), and some of these studies are in ADPKD patient cohorts (264,363). Moreover, it is one of the causes recently described as being implicated in tubulointerstitial fibrosis (364), pathway involved in the progression of ADPKD (89). Furthermore, in recent years, the correlation of serum uromodulin with the progression of CKD has been studied, which is able to detect early stages of CKD progression (365,366), even in the measurement of renal function in ADPKD patients (367).

Ceruloplasmin (CERU) is a blue coloured plasma glycoprotein that binds most of circulating copper (368). Moreover, it also play a role in iron homeostasis and facilitate iron transport in diverse tissues, as kidney, by oxidizing ferrous iron to ferric form to be able to bind

ferric iron carrier transferrin (369). CERU is mainly found as a soluble serum protein originating from the liver, but it is also found as a glycosylphosphatidylinositol (GPI)-linked protein in astrocytes and the kidney (370). Homeostasis of iron is essential and plays a role in the physiology of oxygen transport, for example, leading to anemia; these pathways are clearly described as altered in CKD (371,372). Due to that, CERU is altered related to CKD stages (333,341–343).

Protein AMBP, or α-1-microglobulin/bikunin precursor, is a complex glycoprotein secreted in plasma that is cleaved by a furin-like protease to the two mature molecules with no structural or functional relationship (373): α-1-microglobulin, member of the superfamily of lipocalins that plays a role in immune regulation (374); and bikunin, a serine protease inhibitor of the Kunitz superfamily that participates in many physiological and pathological processes as endothelial cell growth or extracellular matrix stabilization (373,375). Although, sometimes Protein AMBP forms dimmers to protect from cleavage (373). Studies show how this protein is altered in relation to CKD (348–350,376). Even the cleavage form of alpha-1-microglobulin has been studied in relation to the progression of kidney disease and as a marker of tubular damage (377,378).

Vitronectin (VTNC) is an adhesive glycoprotein that play key roles in the attachment of cells to the matrix and participate in regulation of cell differentiation, proliferation and morphogenesis (379). VTNC is synthesized and secreted mainly by hepatocytes found in serum, but it also appears in other tissues as the kidney (379,380). Vitronectin interact with glycosaminoglycans and proteoglycans and is recognized by certain members of the integrin family and serves as a cell-to-substrate adhesion molecule (379,380). These extracellular matrix and cell adhesion pathways have already been described as altered in ADPKD (89). Altered VTNC concentration has been linked to the progression of CKD through its role in fibrosis (380,381). This protein was found also in the cystic fluid proteome of ADPKD (382).

Quantification of these biomarkers, UROM, CERU, AMBP and VTNC, isolated and characterized by ExoGAG shows that all are altered in advanced stages of the disease, except CERU in patients with mutation in *PKD1*. Interestingly, the only one that shows a significant change in not yet pathological serum creatinine levels is Uromodulin, especially in *PKD2* patients, although in *PKD1* patients there is a trend that will probably become significant as the sample size increases, making it a very attractive biomarker for its predictive power for disease progression, and may become a sensitive marker obtained in a less invasive way than the serum analysis. This is something interesting, the fact that between patients with different mutations it behaves differently, since it is also known that in patients with *PKD1* mutation the disease progresses faster than in *PKD2* patients (46,47), which could be used as a marker not only of the disease progression but also of the type of progression. In addition, the behavior of CERU and VTNC should also be mentioned, especially in patients with *PKD1* mutation, where the concentrations of these markers decrease in intermediate stages of the disease compared to the initial ones and then rise in the more advanced stages. This shows us that changes predictive of disease progression are already occurring in the intermediate stages of the disease, which we are being able to identify thanks to ExoGAG. In addition, we proceeded to study the ratios between the markers that increased against the decreased of Uromodulin. These ratio values vary depending on the type of mutation, showing as a clear example the UROM/AMBP ratio with low serum creatinine levels in patients with *PKD2* mutation around a value of 100, while in the same conditions in patients with *PKD1* mutation the value is around 4, it means that there is more AMBP in patients with mutation in *PKD1* than in *PKD2*, at least in initial stages.

Although genetic diagnosis is recommended in cases of familial suspicion, this would help to stratify patients with suspected ADPKD in a rapid manner, and to start the therapeutic approach as quickly as possible. Therefore, all these results show us that the study of isolation with the ExoGAG method provides us a great understanding of the changes produced by the disease, and we can get to know possible biomarkers or combination of them that would help us in clinical practice, being more sensitive than the current ones, as they would help in the characterization of the prognosis of the disease and even in the possible diagnosis, as they behave in a specific way depending on the type of mutation that produces the disease.

But the application of the ExoGAG method has not only been studied in its isolation of the GAG-associated component, but also of what it does not isolate directly and remains in the supernatant. In this case it was also observed that there was a constant protein profile in a healthy population that is altered in the presence of ADPKD. Their sequencing by mass spectrometry also revealed the presence of certain markers, which in this case all increased in abundance as the disease progressed. The markers ALBU, RBP4, TRFE, AMBP and ZA2G were validated in both *PKD1* and *PKD2* mutated patients, together with TTHY in the latter. This also identifies a new application of ExoGAG in the search for biomarkers. In addition to the previously described ALBU and AMBP markers, RBP4(383–385), TRFE (386,387) and ZA2G (388–390) have also been described as altered throughout to kidney disease.

With the study of the isolated and non-isolated components by ExoGAG, we can see that there are proteins that appear in both components in a fairly high level, as is the case of AMBP or ALBU; others that only appear in the isolated pellet, as is the case of DPP4 (344,391), LUM (390,392), NEP (393,394) or CAH1 (395), which are also related to the progression of kidney disease and which, interestingly, we see as a part of that complex that we see in the 70 kDa albumin band; or it may be the case that they appear in both components but much more enriched in the pellet while in the supernatant they are practically undetectable, as is the case of CERU and VTNC. An interesting example is what happens with Uromodulin, in ExoGAG pellets, we enriched UROM component in contrast to the whole urine and the UROM component of the ExoGAG supernatants looked like splits or degradation of the whole protein. This indicates that we are really dealing with two distinctly different types of samples.

In summary, ExoGAG is a new analytical method that separates the specific component associated to GAGs of the sample. This fraction allowed us to identify a urinary pattern of proteins associated to GAGs that it is altered in the disease progression. All these data showed our promising results in searching for new biomarkers for diagnosis and prognosis of kidney diseases, at least in ADPKD, as well as to help us better understand the underlying pathophysiology of the disease.

USC
UNIVERSIDADE DE SANTIAGO DE COMPOSTELA

USC
UNIVERSIDADE
DE SANTIAGO
DE COMPOSTELA

5.3 Characterization of urine Extracellular Vesicles isolated by ExoGAG

Currently, the great challenge surrounding EVs is to find a gold-standard method that will be achievable, accurate, trustworthy and reproducible to analyze EVs for research and above all that it has an application in clinical routine (126,181,396,397). This thesis proposes a new isolation method, ExoGAG, which is based on the precipitation of Extracellular Vesicles by isolation of the GAG-associated fraction from a complex sample.

The first thing that led us to think that we were looking at a new isolation method was the functional analysis result of proteins identified in the ExoGAG isolation, this reveals that most of the proteins are associated with exosomes rather than those identified in the non-isolated component of the ExoGAG supernatant, especially if we take into account those differential proteins between pellet and supernatant. Of the proteins identified, 97% are described in the Vesiclepedia database (151,398). These data led us to believe that a vesicular component was being isolated by the ExoGAG method.

As has been done in other new vesicle isolation methods (196,236,399,400), the first step is to confirm the presence of these EVs. This could be validated in a first approach by electron microscopy (TEM) and immunofluorescence, where we observed EVs that some are lonely and others are part of a complex of vesicles. These complexes are formed by the aggregation of vesicles together with at least one polymerized Uromodulin filaments, as confirmed by Uromodulin immunodetection. The entrapment of vesicles by Uromodulin filaments has already been described (269,401,402), and in fact, for the study of EVs in urine, the depletion of Uromodulin is proposed, since it is considered a contaminating factor of the sample and is not related to the study of EVs (126,214,401,403,404). But the results discussed in the previous chapter lead us to believe that the fact that these vesicles are bound to Uromodulin is not a random occurrence but a physiological question, as with the course of the disease as ADPKD the Uromodulin component decreases, showing that it plays an important yet unknown role. Even a preliminary study has begun to characterize the EVs trapped by the Uromodulin filaments isolated in the first low force centrifugation of ultracentrifugation (236), with subsequent depletion of the uromodulin fragment; our study also took into account the depletion of Uromodulin after isolation but significant EVs were lost so this was not included in the process (data not shown). In addition of characterization by imaging techniques, the presence of EV markers was also validated by Western Blot immunodetection as well as by comparison with other isolation techniques (405), such as ultracentrifugation and CD9 immunoprecipitation. The results show the better presence of biomarkers in ultracentrifugation and ExoGAG isolation, with the latter having 30 times less volume. The comparison with immunoprecipitation shows that the type of marker depends on the isolation (406,407), with the presence of membrane ones in IP while intracellular ones appear in ExoGAG.

Optimization of the isolation protocol with ExoGAG showed that it is only needed 1 or 1.5mL of urine to detect these EVs markers by immunodetection, but with an optimal volume of 3mL to obtain a strong signal. However, these markers are sample-dependent, so that not all this markers can be identified in all the individual samples in the optimal volume by this method, as already described, there is no universal marker, as existing markers are highly variable and sample-dependent (126). It was demonstrated that this is not due to the amount of soluble protein present in the sample, which would involve that more soluble protein conduces to less EVs precipitated, however that EVs are isolated equally regardless of the percentage of soluble protein.

Once the presence of ExoGAG was validated as a method of EV isolation, it was compared to the most widely used method to date, ultracentrifugation, as were recommended by authors as Sodar et al(405). The first approach was carried out by mass spectrometric sequencing of the same sample isolated with the ExoGAG method and Ultracentrifugation. For this purpose, the ExoGAG isolation was carried out with 10 times less volume, with only 3mL of urine in contrast to 30mL used in Ultracentrifugation. Even with this difference in volume, there was no significant difference in the number of proteins identified in each of the isolations, which means a high isolation yield with ExoGAG from a much smaller sample volume. In addition, a robust isolation method was shown, with an average of 72% of common proteins between control samples, similar to that observed with ultracentrifugation, with just over half of the identified proteins being common to all samples. On the other hand, around 50% of the proteins identified are common between the isolation by ExoGAG and Ultracentrifugation, which indicates that common but also specific populations are isolated in each technique (406,407). Functional analysis(405) of cellular component reveals that most of the common component between the techniques is related to Exosomes, while the Ultracentrifugation specific one is more related to cytoplasmic components, and the ExoGAG specific one is much more enriched in the extracellular component. Practically all the proteins identified by both methods are already included in the Vesiclepedia dataset (151). Those identified proteins not described in the Vesiclepedia urine experiments demonstrate the previously described, because those isolated by ExoGAG belong to the extracellular component and the plasma membrane while those by Ultracentrifugation are related to cytoplasmic components such as the mitochondria. Interestingly, those isolated by ExoGAG are more related to urine than those isolated by Ultracentrifugation. The fact that with ExoGAG, in addition to the exosomal component, a specific extracellular component is being isolated, corresponds to the fact that with this method a component related to GAGs is being isolated, which are present in the extracellular region both in the membranes and in the extracellular matrix as well as in the secreted proteins such as uromodulin, which has already been shown to form part of the complex with EVs that is isolated with ExoGAG (269,273).

Mass spectrometric analysis also allowed us to characterize the markers associated with EVs according to the MISEV18 guidelines (126), due to its ability to detect all the proteins in a sample at the same time. As the protein composition of EVs may differ under different conditions as well as according to the subtype and location of the EVs (203), which makes it impossible to propose a universal EV marker, this guide for the characterization of the EVs obtained proposes the detection of 3 essential categories to demonstrate the presence of vesicular populations. Of these categories, the presence of EVs is determined by the presence of categories 1 and 2, which encompass membrane or cytosolic proteins, respectively. Regarding the need for detection of these categories, with ExoGAG isolation we can conclude that we found a large number of markers that indicate the presence of EVs. On the other hand, category 3 determines the purity controls, that is those structures that are isolated together with the EVs that are considered to be contaminants of the sample as they are not considered to be part of the vesicles per se. With ExoGAG we obtain certain proteins related to this category, although it is clear that there is no threshold for the abundance of these markers (126), something that we cannot know with qualitative detection by mass spectrometry. However, it is worth noting the detection of Albumin and Uromodulin. Regarding to the first, the results obtained in the previous chapter show that, together with this protein, which increases in abundance with disease progression, there are others that also change in abundance with disease progression, which demonstrates that functionally they have a biological role. On the other

hand, as previously mentioned, Uromodulin forms complexes with the vesicles that have always been considered an impediment to the isolation of the EVs, which is why it has been depleted for the release of the associated EVs. However, it has already been demonstrated in the previous chapter that this protein also plays an important role, as its abundance decreases significantly with the progression of the ADPKD disease and is also dependent on the type of causative mutation. Therefore, we propose that the fact of considering contaminants is something to be careful with, since if physiologically they are interacting, they will have a biological role. This is something that has happened even with the consideration of EVs, as they were initially considered cellular debris until it was shown how important a role they play in cellular intercommunication (408,409). In addition to these categories that are considered as mandatory in the characterization of EVs by the MISEV18 guideline there are also proposed other categories as category 4, for specificity of small vesicles that are not parts from other intracellular compartments or organelles, and category 5, which are soluble proteins that bind to EV receptors and exhibit functional activities. With ExoGAG we isolated proteins related to the nucleus or the secretory pathway, indicating that there is not full purity in the small EVs. But we, again, also found secreted proteins that bind to the EVs. This correlates with what we obtain using the ExoGAG isolation, where of the component associated with GAGs, where there are secreted proteins that can be associated with different receptors in the cell membrane as well as EVs (273). In addition, this mass spectrometry analysis also allowed us to identify markers from all segments of the nephron (214), which indicates that EVs belonging to all parts of the nephron are being isolated.

In addition to the characterization of EV markers, it is also necessary to determine the abundance of isolated EVs (126). For this purpose, we will use the Nanotracking Analysis (NTA), already described for this function (198,202,283), and compare the results obtained with ExoGAG with those obtained with Ultracentrifugation, as recommended by Sódar et al, 2017 (405). The characterization of the vesicular component using the NTA in terms of yield in the number of particles isolated by each method as well as their size showed that in the isolation by Ultracentrifugation there are more particles per mL of isolated sample, although even so it is not a significant difference and more considering that the volume is ten times smaller in the isolation by ExoGAG. Moreover, the same number of particles per mL of isolated sample with ExoGAG are obtained as are observed per mL of pure urine, so the performance of this new method is fairly good allowing using a small sample volume, something quite advantageous compared to the Ultracentrifugation method. In addition, there are no differences in the mean and mode of sizes of the particles isolated by any of the isolation methods, as well as that of the starting urine sample, which implies that the same subtype of EVs in terms of size is isolated. When comparing the yield of each of the techniques, in both cases we see how more particles per mL are obtained after isolation by both ExoGAG and Ultracentrifugation. However, there are differences in the sizes in the not isolated phase, the EVs not isolated by ExoGAG are larger than those isolated, while those not isolated by Ultracentrifugation are smaller than those isolated. The latter can be explained by the fact that in the isolation protocol by Ultracentrifugation, a first centrifugation is carried out where the largest EVs must be eliminated, while those that are not capable of precipitating in the 100,000g centrifugation are much smaller (410). with an average of 130nm. Instead, those not isolated with ExoGAG may be another different population of EVs that are not so associated with GAG or that are not part of these complexes with Uromodulin.

USC UNIVERSIDADE DE SANTIAGO DE COMPOSTELA

In addition, we characterize the isolation of EVs by ExoGAG and Ultracentrifugation with the new ExoView® tool, which allows the quantification of the abundance of isolated EVs as well as the characterization of different markers associated, in this first approach the Tetraspanin CD63, CD81 and CD9, by single vesicle fluorescence analysis (411). The results obtained by the analysis with the new ExoView® technique have shown us, again, that with ExoGAG we have a higher yield in isolation per mL of starting sample than with Ultracentrifugation. In addition, the vesicular component regarding the characterization of the CD63, CD81 and CD9 markers is more similar between the urine and the ExoGAG isolation than the Ultracentrifugation isolation. This means that with ExoGAG we isolate a reliable representation of the EVs that are in the urine, while in the isolation by Ultracentrifugation there is a preference where fewer CD81 and CD9 EVs are isolated. Additionally, where the greatest differences are really seen is in the EVs not isolated with ExoGAG, where there are more CD63 particles and less CD9 than in the isolated ones. This agrees with our other results, where we see that there are different subtypes of EVs between the isolated and non-isolated ones, such as the fact of isolating EVs in complex with Uromodulin.

With all these results, the vesicular component that is isolated with ExoGAG is demonstrated and characterized, so we decided to apply it to the study of ADPKD progression for the search of new biomarkers and to know the underlying molecular mechanisms. Tetraspanins are known to be altered when there is a pathology (412–414), but this alteration in ADPKD has not yet been described. Therefore, the first thing we characterized with Exoview® was the profile of tetraspanins CD63, CD81 and CD9 in patients with mutation in *PKD1* and *PKD2* throughout different stages of the disease. The first thing to say is that the number of EVs isolated with ExoGAG and captured by CD63, CD81 and CD9 antibodies does not vary with the onset or progression of the disease, contrary to what has been described by Ding. H et al. in a study of EVs in patients with ADPKD isolated with Ultracentrifugation (415). The results revealed that only with the presence of the pathology without the appearance of renal damage, this profile is altered. The CD63 component is constantly decreased compared to the control in all stages of the disease, both in patients with mutation in *PKD1* and in those with *PKD2*, therefore it can be a good marker of the presence of the disease. The CD81 component is increased compared to the control, however, the behavior differs between patients with the different mutations, in patients with *PKD1* mutation this component is increased throughout the disease, while in *PKD2*, CD81 decreases with kidney damage. Therefore, we could consider the study of the behavior of this CD81 marker not only as an identification of the disease but also to help distinguish the causative gene and thus try to predict the progression of the disease. On the other hand, the CD9 component, despite showing some oscillation, behaves quite similarly between the control samples and those of the patients. With these results we have observed not only that the Tetraspanin profile changes in ADPKD, but also that this may be specific to the type of causative mutation, its study could be proposed as a candidate for new biomarkers for the diagnosis and progression of the disease.

Moreover, an attempt was made to validate the results obtained in Chapter 2, to see if the alterations in the observed biomarkers, Uromodulin (215), Ceruloplasmin (342), Protein AMBP(416) and Vitronectin (380), that have already been found in different studies in the urinary EVs, are due to their alteration in the isolated vesicular component. Only the Uromodulin and Vitronectin markers correlate, Uromodulin decreasing and Vitronectin increasing, to a small level with what was observed in the study of the protein component associated with GAGs. This leads us to think that not only the component of the Extracellular

Vesicles and their cargo play an important role throughout the disease, but also that there is a complex formed by EVs and associated proteins that is the part really altered and plays a fundamental role in the course of the disease.

In summary, ExoGAG is a new tool that allows us an effective isolation of Extracellular Vesicles compared to other commonly used methods. The isolated vesicular component is specific for the association with GAGs and not only isolates EVs, but also a complex formed by proteins such as Uromodulin and these EVs seems that are altered in relation to ADPKD. This may unmask a new signalling mechanism within the kidney that needs further study to understand the underlying pathophysiological mechanism.

USC
UNIVERSIDADE
DE SANTIAGO
DE COMPOSTELA

USC
UNIVERSIDADE
DE SANTIAGO
DE COMPOSTELA

CONCLUSIONS

USC
UNIVERSIDADE
DE SANTIAGO
DE COMPOSTELA

USC
UNIVERSIDADE
DE SANTIAGO
DE COMPOSTELA

6. CONCLUSIONS

1. Differential proteomics between *Wild Type* and Mutant kidneys in a murine model of ADPKD, by quantitative mass spectrometric analysis using SWATH technology, revealed multiple new pathways and targets involved in the disease, increasing the understanding of the molecular mechanisms involved in PKD.

2. The results of the proteomic analysis are dependent on the reference spectral library. The combination of the different study conditions generates a much wider library, leading to the identification of different DEPs, but involved in the same pathways altered in the disease.

3. The number of altered pathways and targets increases with the progression of the disease, demonstrating the division into two phases, cystogenesis and cyst progression. Among the pathways altered in early stages are upregulated those related to biological processes, such as translation and regulation of kinases in the extracellular matrix and ribosomes, and downregulated metabolism pathway. Besides, among the altered pathways in more advanced stages of the disease, those related to the cytoskeleton, plasma membrane and extracellular matrix such as cell-cell adhesion and activation of signalling cascades are upregulated, while downregulation of the metabolic pathway is still important.

4. Vimentin, Spondin-1 and RNA-binding protein 3 are the only proteins that appear altered in the early stages and remain altered throughout the disease. Therefore, its regulation is proposed as a new possible therapeutic opportunity for the treatment of ADPKD from early stages of the disease.

5. We have developed ExoGAG, a new rapid and cost-efficient tool for the detection and characterisation of pathological states in liquid biopsy, based on the isolation of GAGs and the associated fractions.

6. The application of ExoGAG in urine has allowed us to identify a constant proteomic profile in the GAG-associated fraction in samples from controls. This pattern is altered in the urine of individuals with ADPKD in a renal function-dependent manner in both the murine model and in patients with mutations in the PKD genes. Moreover, we found that the variation of the profile in patients was specific of the type of the disease.

7. The protein characterization of the differences observed in the profile of GAG-associated proteins by ExoGAG leads to the identification of possible biomarker or combination of biomarkers for diagnosis and prognosis of the kidney diseases. Among these new biomarkers, Uromodulin shows up, with a predictive value for disease progression that anticipates pathological changes in serum creatinine levels. Moreover, their combination with other biomarkers such as CERU, VTNC or AMBP increases the sensitivity even in the diagnosis of the pathology.

8. ExoGAG is a new method for the isolation of Extracellular Vesicles based on their precipitation as part of the GAG-associated fraction. In addition, ExoGAG provides effective and cost-efficient isolation of EVs compared to other isolation methods such as ultracentrifugation, starting from a very low sample volume.

USC
UNIVERSIDADE
DE SANTIAGO
DE COMPOSTELA

9. The application of ExoGAG to the study of EVs in the ADPKD revealed that Tetraspanin profile (CD63, CD81 and CD9) changes throughout the disease, even in a manner dependent on the specific type of causative mutation. It is therefore proposed to its study as a candidate for new biomarkers for the diagnosis and progression of the disease.

10. The isolated EV component is specific for the association with GAGs and not only isolates EVs, but also a complex formed by proteins such as Uromodulin that are altered in relation to ADPKD. The deep study of these complexes formed by EVs and secreted proteins may uncover a new signalling mechanism within the kidney.

USC
UNIVERSIDADE
DE SANTIAGO
DE COMPOSTELA

BIBLIOGRAPHY

USC
UNIVERSIDADE
DE SANTIAGO
DE COMPOSTELA

USC
UNIVERSIDADE
DE SANTIAGO
DE COMPOSTELA

BIBLIOGRAPHY

1. Sampaio FJB. Renal anatomy. Endourologic considerations. Urol Clin North Am. 2000;27(4):585–607.
2. Eckardt KU, Coresh J, Devuyst O, Johnson RJ, Köttgen A, Levey AS, et al. Evolving importance of kidney disease: From subspecialty to global health burden. Lancet. 2013;382(9887):158–69.
3. Mcmahon AP. Development of the Mammalian Kidney. Curr Top Dev Biol. 2016;117(1):31–64.
4. de Boer A, Hoogduin JM, Blankestijn PJ, Li X, Luijten PR, Metzger GJ, et al. 7 T renal MRI: challenges and promises. Magn Reson Mater Physics, Biol Med [Internet]. 2016 Jun 1;29(3):417–33. Available from: https://link.springer.com/article/10.1007/s10334-016-0538-3
5. Herzlinger D, Hurtado R. Patterning the Renal Vascular Bed Doris. Semin Cell Dev Biol. 2014;36:50–6.
6. Gorostidi M, Sánchez-Martínez M, Ruilope LM, Graciani A, de la Cruz JJ, Santamaría R, et al. Prevalencia de enfermedad renal crónica en España: impacto de la acumulación de factores de riesgo cardiovascular. Nefrología. 2018 Nov;38(6):606–15.
7. Brück K, Stel VS, Gambaro G, Hallan S, Völzke H, Ärnlöv J, et al. CKD prevalence varies across the European general population. J Am Soc Nephrol. 2016 Jul 1;27(7):2135–47. Available from: https://jasn.asnjournals.org/content/27/7/2135
8. Kalantar-Zadeh K, Jafar TH, Nitsch D, Neuen BL, Perkovic V. Chronic kidney disease. Lancet. 2021;398(10302):786–802. Available from: http://dx.doi.org/10.1016/S0140-6736(21)00519-5
9. Conference Participants K, Köttgen A, Cornec-Le Gall E, Halbritter J, Kiryluk K, Mallett AJ, et al. Genetics in chronic kidney disease: conclusions from a Kidney Disease: Improving Global Outcomes (KDIGO) Controversies Conference. Kidney Int [Internet]. 2022 [cited 2022 Aug 4];101:1126–41. Available from: www.kidney-international.org
10. Webster AC, Nagler E V., Morton RL, Masson P. Chronic Kidney Disease. Lancet [Internet]. 2017;389(10075):1238–52. Available from: http://dx.doi.org/10.1016/S0140-6736(16)32064-5
11. Delanaye P, Mariat C. The applicability of eGFR equations to different populations. Nat Rev Nephrol [Internet]. 2013;9(9):513–22. Available from: http://dx.doi.org/10.1038/nrneph.2013.143
12. Liu C, Debnath N, Mosoyan G, Chauhan K, Vasquez-Rios G, Soudant C, et al.

USC UNIVERSIDADE DE SANTIAGO DE COMPOSTELA

Systematic Review and Meta-Analysis of Plasma and Urine Biomarkers for CKD Outcomes. J Am Soc Nephrol [Internet]. 2022 [cited 2022 Aug 4];33. Available from: https://doi.org/10.1681/ASN.2022010098

13. Levin A, Stevens PE. Summary of KDIGO 2012 CKD Guideline: behind the scenes, need for guidance, and a framework for moving forward. Kidney Int [Internet]. 2014 Jan 1 [cited 2022 Aug 4];85(1):49–61. Available from: http://www.kidney-international.org/article/S0085253815561747/fulltext

14. Lopez-Giacoman S. Biomarkers in chronic kidney disease, from kidney function to kidney damage. World J Nephrol. 2015;4(1):57.

15. Bergmann C, Guay-woodford LM, Harris PC, Horie S, Peters DJM, Torres VE. Polycystic kidney disease. Nat Rev Dis Prim [Internet]. 2018; Available from: http://dx.doi.org/10.1038/s41572-018-0047-y

16. Igarashi P, Somlo S. Genetics and Pathogenesis of Polycystic Kidney Disease. J Am Soc Nephrol. 2002;13(9):2384–98.

17. Cordido A, Vizoso-gonzalez M, Garcia-gonzalez MA. Molecular pathophysiology of autosomal recessive polycystic kidney disease. Int J Mol Sci. 2021;22(12).

18. Reeders ST, Keith T, Green P, Germino GG, Barton NJ, Lehmann OJ, et al. Regional localization of the autosomal dominant polycystic kidney disease locus. Genomics. 1988;3(2):150–5.

19. Germino GG, Weinstat-Saslow D, Himmelbauer H, Gillespie GAJ, Somlo S, Wirth B, et al. The gene for autosomal dominant polycystic kidney disease lies in a 750-kb CpG-rich region. Genomics. 1992;13(1):144–51.

20. Somlo S, Wirth B, Germino GG, Weinstat-Saslow D, Gillespie GAJ, Himmelbauer H, et al. Fine genetic localization of the gene for autosomal dominant polycystic kidney disease (PKD1) with respect to physically mapped markers. Genomics. 1992;13(1):152–8.

21. Mochizuki T, Wu G, Hayashi T, Xenophontos SL, Veldhuisen B, Saris JJ, et al. PKD2, a gene for polycystic kidney disease that encodes an integral membrane protein. Science (80-). 1996;272(5266):1339–42.

22. Onuchic LF, Furu L, Nagasawa Y, Hou X, Eggermann T, Ren Z, et al. PKHD1, the polycystic kidney and hepatic disease 1 gene, encodes a novel large protein containing multiple immunoglobulin-like plexin-transcription-factor domains and parallel beta-helix 1 repeats. Am J Hum Genet. 2002;70(5):1305–17.

23. Lens XM, Onuchic LF, Wu G, Hayashi T, Daoust M, Mochizuki T, et al. An Integrated Genetic and Physical Map of the Autosomal Recessive Polycystic Kidney Disease Region. Genomics. 1997 May 1;41(3):463–6.

24. Ward CJ, Hogan MC, Rossetti S, Walker D, Sneddon T, Wang X, et al. The gene mutated in autosomal recessive polycystic kidney disease encodes a large, receptor-like protein. Nat Genet. 2002;30(3):259–69.

25. Lu H, Galeano MCR, Ott E, Kaeslin G, Kausalya PJ, Kramer C, et al. Mutations in DZIP1L, which encodes a ciliary-transition-zone protein, cause autosomal recessive polycystic kidney disease. Nat Genet [Internet]. 2017;49(7):1025–34. Available from: http://dx.doi.org/10.1038/ng.3871

26. Porath B, Gainullin VG, Cornec-Le Gall E, Dillinger EK, Heyer CM, Hopp K, et al. Mutations in GANAB, Encoding the Glucosidase IIα Subunit, Cause Autosomal-Dominant Polycystic Kidney and Liver Disease. Am J Hum Genet [Internet]. 2016 Jun 2 [cited 2022 Aug 5];98(6):1193–207. Available from: http://www.cell.com/article/S0002929716301380/fulltext

27. Cornec-Le Gall E, Olson RJ, Besse W, Heyer CM, Gainullin VG, Smith JM, et al. Monoallelic Mutations to DNAJB11 Cause Atypical Autosomal-Dominant Polycystic Kidney Disease. Am J Hum Genet [Internet]. 2018 May 3 [cited 2022 Aug 5];102(5):832–44. Available from: http://www.cell.com/article/S0002929718301022/fulltext

28. Besse W, Chang AR, Luo JZ, Triffo WJ, Moore BS, Gulati A, et al. *ALG9* Mutation Carriers Develop Kidney and Liver Cysts. J Am Soc Nephrol [Internet]. 2019 Aug 8;ASN.2019030298. Available from: http://www.jasn.org/lookup/doi/10.1681/ASN.2019030298

29. Rubio Cabezas O, Flanagan SE, Stanescu H, García-Martínez E, Caswell R, Lango-Allen H, et al. Polycystic Kidney Disease with Hyperinsulinemic Hypoglycemia Caused by a Promoter Mutation in Phosphomannomutase 2. J Am Soc Nephrol [Internet]. 2017 [cited 2022 Aug 5];28:2529–39. Available from: www.jasn.org

30. Gulati A, Sevillano AM, Praga M, Gutierrez E, Alba I, Dahl NK, et al. Collagen IV Gene Mutations in Adults With Bilateral Renal Cysts and CKD. Kidney Int Reports [Internet]. 2020;5(1):103–8. Available from: https://doi.org/10.1016/j.ekir.2019.09.004

31. Senum SR, Li Y (Sabrina) M, Benson KA, Joli G, Olinger E, Lavu S, et al. Monoallelic IFT140 pathogenic variants are an important cause of the autosomal dominant polycystic kidney-spectrum phenotype. Am J Hum Genet. 2022;109(1):136–56.

32. Lemoine H, Raud L, Audre M, Gall EC, Lemoine H, Raud L, et al. Monoallelic pathogenic ALG5 variants cause atypical polycystic kidney disease and interstitial fibrosis Authors ARTICLE Monoallelic pathogenic ALG5 variants cause atypical polycystic kidney disease and interstitial fibrosis. Am J Hum Genet. 2022;109:1484–99.

33. Lanktree MB, Haghighi A, Guiard E, Iliuta IA, Song X, Harris PC, et al. Prevalence

USC UNIVERSIDADE DE SANTIAGO DE COMPOSTELA

estimates of polycystic kidney and liver disease by population sequencing. J Am Soc Nephrol. 2018 Oct 1;29(10):2593–600.

34. Cornec-Le Gall E, Alam A, Perrone RD. Autosomal dominant polycystic kidney disease. Vol. 393, The Lancet. Lancet Publishing Group; 2019. p. 919–35.

35. Cordido A, Besada-Cerecedo L, García-González MAMAMA. The Genetic and Cellular Basis of Autosomal Dominant Polycystic Kidney Disease—A Primer for Clinicians. Front Pediatr. 2017 Dec;5(5):279.

36. Torres VE, Harris PC, Pirson Y. Autosomal dominant polycystic kidney disease. Vol. 369, Lancet. Elsevier B.V.; 2007. p. 1287–301.

37. Woon C, Bielinski-Bradbury A, O'Reilly K, Robinson P. A systematic review of the predictors of disease progression in patients with autosomal dominant polycystic kidney disease. BMC Nephrol [Internet]. 2015 Aug 15 [cited 2022 Aug 5];16(1):1–16. Available from: https://bmcnephrol.biomedcentral.com/articles/10.1186/s12882-015-0114-5

38. Reiterová J, Tesař V. Autosomal Dominant Polycystic Kidney Disease: From Pathophysiology of Cystogenesis to Advances in the Treatment. Int J Mol Sci. 2022 Mar 1;23(6).

39. Wilson PD, Goilav B. Cystic disease of the kidney. Annu Rev Pathol. 2007;2:341–68.

40. Cornec-Le Gall E, Audrézet MP, Renaudineau E, Hourmant M, Charasse C, Michez E, et al. PKD2-Related Autosomal Dominant Polycystic Kidney Disease: Prevalence, Clinical Presentation, Mutation Spectrum, and Prognosis. Am J Kidney Dis. 2017;70(4):476–85.

41. Harris PC, Hopp K. The mutation, a key determinant of phenotype in ADPKD. J Am Soc Nephrol. 2013;24(6):868–70.

42. Burn TC, Connors TD, Dackowski WR, Petry LR, Van Raay TJ, Millholland JM, et al. Analysis of the genomic sequence for the autosomal dominant polycystic kidney disease (PKD1) gene predicts the presence of a leucine-rich repeat: The AMERICAN pkd1 consortium (apkd1 consortium). Hum Mol Genet. 1995;4(4):575–82.

43. Bogdanova N, Markoff A, Gerke V, McCluskey M, Horst J, Dworniczak B. Homologues to the first gene for autosomal dominant polycystic kidney disease are pseudogenes. Genomics. 2001;74(3):333–41.

44. Van Raay TJ, Burn TC, Connors TD, Petry LR, Germino GG, Kilnger KW. A 2.5 kb Polypyrimidine Tract in the PKD1 Gene Contains at Least 23 H-DNA-Forming Sequences. 1996;1(4):317–27.

45. Gall EC Le, Audrézet MP, Rousseau A, Hourmant M, Renaudineau E, Charasse C, et al.

USC UNIVERSIDADE DE SANTIAGO

The PROPKD score: A new algorithm to predict renal survival in autosomal dominant polycystic kidney disease. J Am Soc Nephrol [Internet]. 2016 Mar 1 [cited 2022 Jul 16];27(3):942–51. Available from: https://jasn.asnjournals.org/content/27/3/942

46. Gall EC Le, Audrézet MP, Chen JM, Hourmant M, Morin MP, Perrichot R, et al. Type of PKD1 mutation influences renal outcome in ADPKD. J Am Soc Nephrol [Internet]. 2013 May 31 [cited 2022 Jul 19];24(6):1006–13. Available from: /pmc/articles/PMC3665389/

47. Heyer CM, Sundsbak JL, Abebe KZ, Chapman AB, Torres VE, Grantham JJ, et al. Predicted mutation strength of nontruncating PKD1 mutations AIDS genotype-phenotype correlations in autosomal dominant polycystic kidney disease. J Am Soc Nephrol [Internet]. 2016 [cited 2022 Jul 16];27(9):2872–84. Available from: https://pubmed.ncbi.nlm.nih.gov/26823553/

48. Hughes J, Ward CJ, Peral B, Aspinwall R, Clark K, Millán JLS, et al. The polycystic kidney disease 1 (PKD1) gene encodes a novel protein with multiple cell recognition domains. Nat Genet. 1995;10(2):151–60.

49. Chapin HC, Caplan MJ. The cell biology of polycystic kidney disease. J Cell Biol. 2010;191(4):701–10.

50. Mekahli D, Parys JB, Bultynck G, Missiaen L, De Smedt H. Polycystins and cellular Ca2+ signaling. Cell Mol Life Sci. 2013;70(15):2697–712.

51. Paul BM, Vanden Heuvel GB. Kidney: polycystic kidney disease. Wiley Interdiscip Rev Dev Biol [Internet]. 2014 Nov 1 [cited 2022 Aug 6];3(6):465–87. Available from: https://onlinelibrary.wiley.com/doi/full/10.1002/wdev.152

52. Grieben M, Pike ACW, Shintre CA, Venturi E, El-Ajouz S, Tessitore A, et al. Structure of the polycystic kidney disease TRP channel Polycystin-2 (PC2). Nat Struct Mol Biol [Internet]. 2017;24(2):114–22. Available from: http://dx.doi.org/10.1038/nsmb.3343

53. Torres VE, Harris PC. Autosomal dominant polycystic kidney disease: The last 3 years. Kidney Int [Internet]. 2009;76(2):149–68. Available from: http://dx.doi.org/10.1038/ki.2009.128

54. Qian F, Germino FJ, Cai Y, Zhang X, Somlo S, Germino GG. PKD1 interacts with PKD2 through a probable coiled-coil domain. Nat Genet. 1997;15:57–61.

55. Hanaoka K, Qian F, Boletta A, Bhunia AK, Piontek K, Tsiokas L, et al. Co-assembly of polycystin-1 and -2 produces unique cation-permeable currents. Nature. 2000;408(6815):990–4.

56. Qiang Su1, * FH, * XG, Jianlin Lei2, Shengqiang Yu3, Tingliang Wang1,4 QZ, Changlin Mei3, Yigong Shi1 4†. Structure of the human PKD1/PKD2 complex. Science (80-). 2018;

USC UNIVERSIDADE DE SANTIAGO DE COMPOSTELA

57. Wang Z, Ng C, Liu X, Wang Y, Li B, Kashyap P, et al. The ion channel function of polycystin-1 in the polycystin-1/polycystin-2 complex. EMBO Rep. 2019;1–18.

58. Douguet D, Patel A, Honoré E. Structure and function of polycystins: insights into polycystic kidney disease. Nat Rev Nephrol. 2019;15(7):412–22.

59. Pei Y. A "two-hit" model of cystogenesis in autosomal dominant polycystic kidney disease? Trends Mol Med. 2001;7(4):151–6.

60. Watnick T, Torres VE, Gandolph MA, Qian F, Onuchic LF, Klinger KW, et al. Somatic Mutation in Individual Liver Cysts Supports a Two-Hit Model of Cystogenesis in Autosomal Dominant Polycystic Kidney Disease. Mol Cell. 1998;2:247–51.

61. Lee SH, Somlo S. Cyst growth, polycystins, and primary cilia in autosomal dominant polycystic kidney disease. Kidney Res Clin Pract [Internet]. 2014;33(2):73–8. Available from: http://dx.doi.org/10.1016/j.krcp.2014.05.002

62. Lantinga-van Leeuwen IS, Dauwerse JG, Baelde HJ, Leonhard WN, van de Wal A, Ward CJ, et al. Lowering of Pkd1 expression is sufficient to cause polycystic kidney disease. Hum Mol Genet. 2004;13(24):3069–77.

63. Nauli SM, Rossetti S, Kolb RJ, Alenghat FJ, Consugar MB, Harris PC, et al. Loss of polycystin-1 in human cyst-lining epithelia leads to ciliary dysfunction. J Am Soc Nephrol. 2006;17(4):1015–25.

64. Qian F, Watnick TJ, Onuchic LF, Germino GG. The molecular basis of focal cyst formation in human autosomal dominant polycystic kidney disease type I. Cell. 1996;87(6):979–87.

65. Janssen MJ, Waanders E, Te Morsche RHM, Xing R, Dijkman HBPM, Woudenberg J, et al. Secondary, somatic mutations might promote cyst formation in patients with autosomal dominant polycystic liver disease. Gastroenterology [Internet]. 2011;141(6):2056-2063.e2. Available from: http://dx.doi.org/10.1053/j.gastro.2011.08.004

66. Saigusa T, Darwin Bell P. Molecular pathways and therapies in autosomal-dominant polycystic kidney disease. Physiology. 2015;30(3):195–207.

67. Eccles MR, Stayner CA. Polycystic kidney disease - Where gene dosage counts. F1000Prime Rep. 2014 Apr 1;6.

68. Hopp K, Ward CJ, Hommerding CJ, Nasr SH, Tuan HF, Gainullin VG, et al. Functional polycystin-1 dosage governs autosomal dominant polycystic kidney disease severity. J Clin Invest. 2012;122(11):4257–73.

69. Hwang YH, Conklin J, Chan W, Roslin NM, Liu J, He N, et al. Refining genotype-phenotype correlation in autosomal dominant polycystic kidney disease. J Am Soc

USC DE SANTIAGO

Nephrol. 2016;27(6):1861–8.

70. Fedeles S V., Gallagher AR, Somlo S. Polycystin-1: A master regulator of intersecting cystic pathways. Trends Mol Med [Internet]. 2014;20(5):251–60. Available from: http://dx.doi.org/10.1016/j.molmed.2014.01.004

71. Cai Y, Fedeles S V., Dong K, Anyatonwu G, Onoe T, Mitobe M, et al. Altered trafficking and stability of polycystins underlie polycystic kidney disease. J Clin Invest. 2014 Dec 1;124(12):5129–44.

72. Ali H, Hussain N, Naim M, Zayed M, Al-Mulla F, Kehinde EO, et al. A novel PKD1 variant demonstrates a disease-modifying role in trans with a truncating PKD1 mutation in patients with Autosomal Dominant Polycystic Kidney Disease. BMC Nephrol. 2015;16(1):1–7.

73. Harris PC, Rossetti S. Molecular diagnostics for autosomal dominant polycystic kidney disease. Nat Rev Nephrol. 2010;6(4):197–206.

74. Lakhia R, Ramalingam H, Chang C-M, Cobo-Stark P, Biggers L, Flaten A, et al. PKD1 and PKD2 mRNA cis-inhibition drives polycystic kidney disease progression. 2022;1–14. Available from: https://doi.org/10.1101/2022.02.23.479396

75. Piontek K, Menezes LF, Garcia-Gonzalez MA, Huso DL, Germino GG. A critical developmental switch defines the kinetics of kidney cyst formation after loss of Pkd1. Nat Med. 2007;13(12):1490–5.

76. Lantinga-van leeuwen IS, Leonhard WN, van der Wal A, Breuning MH, de Heer E, Peters DJM. Kidney-specific inactivation of the Pkd1 gene induces rapid cyst formation in developing kidneys and a slow onset of disease in adult mice. Hum Mol Genet. 2007;16(24):3188–96.

77. Happé H, Peters DJM. Translational research in ADPKD: Lessons from animal models. Nat Rev Nephrol [Internet]. 2014;10(10):587–601. Available from: http://dx.doi.org/10.1038/nrneph.2014.137

78. Li Y, Santoso NG, Yu S, Woodward OM, Qian F, Guggino WB. Polycystin-1 interacts with inositol 1,4,5-trisphosphate receptor to modulate intracellular Ca2+ signaling with implications for polycystic kidney disease. J Biol Chem. 2009;284(52):36431–41.

79. Torres VE, Harris PC. Strategies targeting cAMP signaling in the treatment of polycystic kidney disease. J Am Soc Nephrol. 2014;25(1):18–32.

80. Boca M, Distefano G, Qian F, Bhunia AK, Germino GG, Boletta A. Polycystin-1 induces resistance to apoptosis through the phosphatidylinositol 3-kinase/Akt signaling pathway. J Am Soc Nephrol. 2006;17(3):637–47.

81. Lee EJ. Cell proliferation and apoptosis in ADPKD. Adv Exp Med Biol. 2016;933:25–

USC UNIVERSIDADE DE SANTIAGO DE COMPOSTELA

34.

82. Janssens P, Weydert C, De Rechter S, Wissing KM, Liebau MC, Mekahli D. Expanding the role of vasopressin antagonism in polycystic kidney diseases: From adults to children? Pediatr Nephrol. 2017;

83. Shibazaki S, Yu Z, Nishio S, Tian X, Thomson RB, Mitobe M, et al. Cyst formation and activation of the extracellular regulated kinase pathway after kidney specific inactivation of Pkd1. Hum Mol Genet. 2008;17(11):1505–16.

84. Gattone VH, Wang X, Harris PC, Torres VE. Inhibition of renal cystic disease development and progression by a vasopressin V2 receptor antagonist. Nat Med. 2003;9(10):1323–6.

85. Boletta A. Emerging evidence of a link between the polycystins and the mTOR pathways. Pathogenetics. 2009;2(1):1–16.

86. Harris PC, Torres VE. Genetic mechanisms and signaling pathways in autosomal dominant polycystic kidney disease. J Clin Invest. 2014;124(6):2315–24.

87. Hanaoka K, Guggino WB. cAMP regulates cell proliferation and cyst formation in autosomal polycystic kidney disease cells. J Am Soc Nephrol. 2000;11(7):1179–87.

88. Ghata J, Cowley BD. Polycystic kidney disease. Compr Physiol. 2017;7(3):945–75.

89. Norman J. Fibrosis and progression of Autosomal Dominant Polycystic Kidney Disease (ADPKD). Biochim Biophys Acta - Mol Basis Dis [Internet]. 2011;1812(10):1327–36. Available from: http://dx.doi.org/10.1016/j.bbadis.2011.06.012

90. Mun H, Park JH. Inflammation and fibrosis in ADPKD. Adv Exp Med Biol. 2016;933:35–44.

91. Song X, Di Giovanni V, He N, Wang K, Ingram A, Rosenblum ND, et al. Systems biology of autosomal dominant polycystic kidney disease (ADPKD): Computational identification of gene expression pathways and integrated regulatory networks. Hum Mol Genet. 2009;18(13):2328–43.

92. Cordido A, Nunez-Gonzalez L, Martinez-Moreno JM, Lamas-Gonzalez O, Rodriguez-Osorio L, Perez-Gomez MV, et al. Tweak signaling pathway blockade slows cyst growth and disease progression in autosomal dominant polycystic kidney disease. J Am Soc Nephrol. 2021;32(8):1913–32.

93. Ta MHT, Harris DCH, Rangan GK. Role of interstitial inflammation in the pathogenesis of polycystic kidney disease. Nephrology. 2013;18(5):317–30.

94. Weimbs T, Olsan EE, Talbot JJ. Regulation of STATs by polycystin-1 and their role in polycystic kidney disease. Jak-Stat. 2013;2(2):e23650.

USC

95. Liu B, Li C, Liu Z, Dai Z, Tao Y. Increasing extracellular matrix collagen level and MMP activity induces cyst development in polycystic kidney disease. BMC Nephrol. 2012 Dec;13(109):1–8.

96. Lee K, Boctor S, Barisoni LMC, Gusella GL. Inactivation of integrin-β1 prevents the development of polycystic kidney disease after the loss of polycystin-1. J Am Soc Nephrol. 2015;26(4):888–95.

97. Cruz-Solbes AS, Youker K. Epithelial to mesenchymal transition (EMT) and endothelial to mesenchymal transition (EndMT): Role and implications in kidney fibrosis. Results Probl Cell Differ. 2017;60:345–72.

98. Magistroni R, Boletta A. Defective glycolysis and the use of 2-deoxy-d-glucose in polycystic kidney disease: from animal models to humans. J Nephrol. 2017;30(4):511–9.

99. Padovano V, Podrini C, Boletta A, Caplan MJ. Metabolism and mitochondria in polycystic kidney disease research and therapy. Nat Rev Nephrol. 2018;

100. Riwanto M, Kapoor S, Rodriguez D, Edenhofer I, Segerer S, Wüthrich RP. Inhibition of aerobic glycolysis attenuates disease progression in polycystic kidney disease. PLoS One. 2016 Jan;11(1).

101. Takiar V, Nishio S, Seo-Mayer P, King JD, Li H, Zhang L, et al. Activating AMP-activated protein kinase (AMPK) slows renal cystogenesis. Proc Natl Acad Sci U S A. 2011;108(6):2462–7.

102. Lakhia R, Yheskel M, Flaten A, Quittner-Strom EB, Holland WL, Patel V. PPARα agonist fenofibrate enhances fatty acid β-oxidation and attenuates polycystic kidney and liver disease in mice. Am J Physiol - Ren Physiol. 2018;314(1):F122–31.

103. Belibi F, Ravichandran K, Zafar I, He Z, Edelstein CL. mTORC1/2 and rapamycin in female Han:SPRD rats with polycystic kidney disease. Am J Physiol - Ren Physiol. 2011;300(1):236–45.

104. Magenheimer BS, St. John PL, Isom KS, Abrahamson DR, De Lisle RC, Wallace DP, et al. Early embryonic renal tubules of wild-type and polycystic kidney disease kidneys respond to cAMP stimulation with cystic fibrosis transmembrane conductance regulator/Na+,K+,2Cl- Co-transporter-dependent cystic dilation. J Am Soc Nephrol. 2006;17(12):3424–37.

105. Podrini C, Rowe I, Pagliarini R, Costa ASH, Chiaravalli M, Meo I Di, et al. Dissection of metabolic reprogramming in polycystic kidney disease reveals coordinated rewiring of bioenergetic pathways. Commun Biol |. 2018;1:194.

106. Lin C-C, Kurashige M, Liu Y, Terabayashi T, Ishimoto Y, Wang T, et al. A cleavage product of Polycystin-1 is a mitochondrial matrix protein that affects mitochondria

morphology and function when heterologously expressed. Sci Rep [Internet]. 2018;8(1):2743. Available from: http://www.nature.com/articles/s41598-018-20856-6

107. Gerth-Kahlert C, Koller S. Ciliopathies. Klin Monbl Augenheilkd. 2018;235(3):264–72.

108. Landis DE, Henke SJ, Yoder. Cilia and Polycystic Kidney Disease. Polycystic Kidney Dis Transl Mech into Ther. 2018;1–273.

109. Ma M, Tian X, Igarashi P, Pazour GJ, Somlo S. Loss of cilia suppresses cyst growth in genetic models of autosomal dominant polycystic kidney disease. Nat Genet. 2013;45(9):1004–12.

110. Ma M, Gallagher AR, Somlo S. Ciliary mechanisms of cyst formation in polycystic kidney disease. Cold Spring Harb Perspect Biol. 2017;9(11).

111. Steinhart Z, Angers S. Wnt signaling in development and tissue homeostasis. Development. 2018;145(11):1–8.

112. Clevers H. Wnt/β-Catenin Signaling in Development and Disease. Cell. 2006;127(3):469–80.

113. Richards T, Modarage K, Dean C, McCarthy-Boxer A, Hilton H, Esapa C, et al. Atmin modulates Pkhd1 expression and may mediate Autosomal Recessive Polycystic Kidney Disease (ARPKD) through altered non-canonical Wnt/Planar Cell Polarity (PCP) signalling. Biochim Biophys Acta - Mol Basis Dis. 2019 Feb 1;1865(2):378–90.

114. Lancaster MA, Gleeson JG. Cystic kidney disease: The role of Wnt signaling. Trends Mol Med [Internet]. 2010;16(8):349–60. Available from: http://dx.doi.org/10.1016/j.molmed.2010.05.004

115. Bais T, Gansevoort RT, Meijer E. Drugs in Clinical Development to Treat Autosomal Dominant Polycystic Kidney Disease. Drugs [Internet]. 2022;82(10):1095–115. Available from: https://doi.org/10.1007/s40265-022-01745-9

116. Torres VE, Chapman AB, Devuyst O, Gansevoort RT, Grantham JJ, Higashihara E, et al. Tolvaptan in Patients with Autosomal Dominant Polycystic Kidney Disease. N Engl J Med. 2012;367(25):2407–18.

117. Blair HA. Tolvaptan: A Review in Autosomal Dominant Polycystic Kidney Disease. Drugs [Internet]. 2019;79(3):303–13. Available from: https://doi.org/10.1007/s40265-019-1056-1

118. Pei Y. Diagnostic approach in autosomal dominant polycystic kidney disease. Clin J Am Soc Nephrol. 2006;1(5):1108–14.

119. Naranjo J, Furlano M, Torres F, Hernandez J, Pybus M, Ejarque L, et al. Comparative analysis of tools to predict rapid progression in autosomal dominant polycystic kidney disease. Clin Kidney J. 2022;15(5):912–21.

USC DE COMPOSTELA

120. Garcia-Gonzalez MA, Jones JG, Allen SK, Palatucci CM, Batish SD, Seltzer WK, et al. Evaluating the clinical utility of a molecular genetic test for polycystic kidney disease. Mol Genet Metab. 2007;92(1–2):160–7.

121. Renkema KY, Stokman MF, Giles RH, Knoers NVAM. Next-generation sequencing for research and diagnostics in kidney disease. Nat Rev Nephrol [Internet]. 2014;10(8):433–44. Available from: http://dx.doi.org/10.1038/nrneph.2014.95

122. Rangan GK, Tchan MC, Tong A, Wong ATY, Nankivell BJ. Recent advances in autosomal-dominant polycystic kidney disease. Intern Med J. 2016;46(8):883–92.

123. Grantham JJ, Chapman AB, Torres VE. Volume progression in autosomal dominant polycystic kidney disease: the major factor determining clinical outcomes. Clin J Am Soc Nephrol. 2006;1(1):148–57.

124. Chapman AB, Bost JE, Torres VE, Guay-woodford L, Bae KT, Landsittel D, et al. Kidney Volume and Functional Outcomes in Autosomal Dominant Polycystic Kidney Disease. Clin J Am Soc Nephrol. 2012;(26):479–86.

125. Rizk D, Jurkovitz C, Veledar E, Bagby S, Baumgarten DA, Rahbari-Oskoui F, et al. Quality of life in autosomal dominant polycystic kidney disease patients not yet on dialysis. Clin J Am Soc Nephrol. 2009;4(3):560–6.

126. Théry C, Witwer KW, Aikawa E, Alcaraz MJ, Anderson JD, Andriantsitohaina R, et al. Minimal information for studies of extracellular vesicles 2018 (MISEV2018): a position statement of the International Society for Extracellular Vesicles and update of the MISEV2014 guidelines. J Extracell Vesicles. 2018 Jan 1;7(1).

127. Yáñez-Mó M, Siljander PR-MRM, Andreu Z, Zavec AB, Borràs FE, Buzas EI, et al. Biological properties of extracellular vesicles and their physiological functions. J Extracell vesicles [Internet]. 2015;4(2015):27066. Available from: http://www.ncbi.nlm.nih.gov/pubmed/25979354

128. Van Niel G, D'Angelo G, Raposo G. Shedding light on the cell biology of extracellular vesicles. Nat Rev Mol Cell Biol [Internet]. 2018;19(4):213–28. Available from: http://dx.doi.org/10.1038/nrm.2017.125

129. Tricarico C, Clancy J, Souza-schorey CD. Biology and Biogenesis of Shed Microvesicles. Small GTPases. 2016;1248(August).

130. Mathieu M, Martin-Jaular L, Lavieu G, Théry C. Specificities of secretion and uptake of exosomes and other extracellular vesicles for cell-to-cell communication. Vol. 21, Nature Cell Biology. Nature Publishing Group; 2019. p. 9–17.

131. Kalluri R, LeBleu VS. The biology, function, and biomedical applications of exosomes. Science (80-). 2020;6977(February).

USC UNIVERSIDADE DE SANTIAGO DE COMPOSTELA

132. Pegtel DM, Gould SJ. Exosomes. 2019;

133. Teng F, Fussenegger M. Shedding Light on Extracellular Vesicle Biogenesis and Bioengineering. 2020;2003505:1–17.

134. Colombo M, Raposo G, Théry C. Biogenesis, Secretion, and Intercellular Interactions of Exosomes and Other Extracellular Vesicles. Annu Rev Cell Dev Biol. 2014 Oct 11;30(1):255–89.

135. Hill CP, Babst M. Biochimica et Biophysica Acta Structure and function of the membrane deformation AAA ATPase Vps4 ☆. BBA - Mol Cell Res [Internet]. 2012;1823(1):172–81. Available from: http://dx.doi.org/10.1016/j.bbamcr.2011.08.017

136. Colombo M, Moita C, van Niel G, Kowal J, Vigneron J, Benaroch P, et al. Analysis of ESCRT functions in exosome biogenesis, composition and secretion highlights the heterogeneity of extracellular vesicles. J Cell Sci. 2013;(October).

137. Ghossoub R, Lembo F, Rubio A, Gaillard CB, Bouchet J, Vitale N, et al. Syntenin-ALIX exosome biogenesis and budding into multivesicular bodies are controlled by ARF6 and PLD2. Nat Commun. 2014;

138. Trajkovic K, Hsu C, Chiantia S, Rajendran L, Wenzel D, Wieland F, et al. Ceramide Triggers Budding of Exosome Vesicles into Multivesicular Endosomes. Science (80-). 2008;319(February).

139. van Niel G, Charrin S, Simoes S, Romao M, Rochin L, Saftig P, et al. The Tetraspanin CD63 Regulates Endosomal Sorting during Melanogenesis. 2011;708–21.

140. Hessvik NP, Llorente A. Current knowledge on exosome biogenesis and release. Cell Mol Life Sci. 2018;75(2):193–208.

141. Ostrowski M, Carmo NB, Krumeich S, Fanget I, Raposo G, Savina A, et al. Rab27a and Rab27b control different steps of the exosome secretion pathway. Nat Cell Biol [Internet]. 2009;12(1):19–30. Available from: http://dx.doi.org/10.1038/ncb2000

142. Fader CM, Sánchez DG, Mestre MB, Colombo MI. Biochimica et Biophysica Acta TI-VAMP / VAMP7 and VAMP3 / cellubrevin : two v-SNARE proteins involved in speci fi c steps of the autophagy / multivesicular body pathways. BBA - Mol Cell Res [Internet]. 2009;1793(12):1901–16. Available from: http://dx.doi.org/10.1016/j.bbamcr.2009.09.011

143. Doyle LM, Wang MZ. Overview of Extracellular Vesicles, Their Origin, Composition, Purpose, and Methods for Exosome Isolation and Analysis. Cells. 2019;8.

144. Piccin A, Murphy WG, Smith OP. Circulating microparticles : pathophysiology and clinical implications. 2007;157–71.

145. Al-nedawi K, Meehan B, Micallef J, Lhotak V, May L, Guha A, et al. Intercellular

USC DE SANTIAGO DE COMPOSTELA

transfer of the oncogenic receptor EGFRvIII by microvesicles derived from tumour cells. 2008;10(5).

146. Muralidharan-chari V, Clancy J, Plou C, Romao M, Chavrier P. Article ARF6-Regulated Shedding of Tumor Cell-Derived Plasma Membrane Microvesicles. Curr Biol [Internet]. 2009;19(22):1875–85. Available from: http://dx.doi.org/10.1016/j.cub.2009.09.059

147. Minciacchi VR, Freeman MR, Di D. Extracellular vesicles in cancer: Exosomes, microvesicles and the emerging role of large oncosomes. Semin Cell Dev Biol [Internet]. 2015;1–11. Available from: http://dx.doi.org/10.1016/j.semcdb.2015.02.010

148. Kalra H, Drummen GPC, Mathivanan S. Focus on extracellular vesicles: Introducing the next small big thing. Int J Mol Sci. 2016;17(2).

149. Fais S. Exosomes : the future of biomarkers in medicine. 2013;7:769–78.

150. Théry C, Zitvogel L, Amigorena S. Exosomes: Composition, biogenesis and function. Nat Rev Immunol. 2002;2(8):569–79.

151. Pathan M, Fonseka P, Chitti S V., Kang T, Sanwlani R, Van Deun J, et al. Vesiclepedia 2019: A compendium of RNA, proteins, lipids and metabolites in extracellular vesicles. Nucleic Acids Res [Internet]. 2019 Jan 8 [cited 2022 Jan 16];47(D1):D516–9. Available from: https://click.endnote.com/viewer?doi=10.1093%2Fnar%2Fgky1029&token=WzMyNzE5ODMsIjEwLjEwOTMvbmFyL2dreTEwMjkiXQ.e6AxngMrsjeSD4Sk8JkL03giam4

152. Keerthikumar S, Chisanga D, Ariyaratne D, Al Saffar H, Anand S, Zhao K, et al. ExoCarta: A Web-Based Compendium of Exosomal Cargo. J Mol Biol [Internet]. 2016;428(4):688–92. Available from: http://dx.doi.org/10.1016/j.jmb.2015.09.019

153. Liu C, Xie G, Miao Y, Xia M, Wang Y, Lei Q, et al. EVAtlas : a comprehensive database for ncRNA expression in human extracellular vesicles. 2022;50(August 2021):111–7.

154. Consotrium E-T. EV-TRACK : transparent reporting and centralizing knowledge in extracellular vesicle research. Nat Methods. 2017;14(3):228–32.

155. Gurung S, Perocheau D, Touramanidou L, Baruteau J. The exosome journey : from biogenesis to uptake and intracellular signalling. Cell Commun Signal [Internet]. 2021;1–19. Available from: https://doi.org/10.1186/s12964-021-00730-1

156. Zaborowki MP, Balaj L, Breakefield XO, Lai CP. Extracellular Vesicles : Composition , Biological Relevance , and Methods of Study. Bioscience. 2015;XX(X):1–15.

157. Andreu Z, Yáñez-Mó M. Tetraspanins in extracellular vesicle formation and function. Front Immunol. 2014;5(SEP):1–13.

158. Kawamura Y, Yamamoto Y, Sato T, Ochiya T. Extracellular vesicles as trans-genomic agents : Emerging roles in disease and evolution. 2017;(4).

USC UNIVERSIDADE DE SANTIAGO DE COMPOSTELA

159. Zhang J, Li S, Li L, Li M, Guo C, Yao J, et al. Exosome and Exosomal MicroRNA : Trafficking , Sorting , and Function. Genomics, Proteomics Bioinforma. 2015;

160. Alvarez ML. Isolation of urinary exosomes for RNA biomarker discovery using a simple, fast, and highly scalable method. Methods Mol Biol. 2014;1182:145–70.

161. Cintio M, Polacchini G, Scarsella E, Montanari T, Stefanon B, Colitti M. Microrna milk exosomes: From cellular regulator to genomic marker. Animals. 2020;10(7):1–19.

162. Skotland T, Sagini K, Sandvig K, Llorente A. An emerging focus on lipids in extracellular vesicles. Adv Drug Deliv Rev [Internet]. 2020; Available from: https://doi.org/10.1016/j.addr.2020.03.002

163. Mulcahy LA, Pink RC, Raul D, Carter F, Ann L, Pink RC, et al. Routes and mechanisms of extracellular vesicle uptake. J Extracell Vesicles. 2017;3078(February).

164. Mallegol J, van Niel G, Lebreton C, Lepelletier Y, Candalh C, Dugave C, et al. T84-Intestinal Epithelial Exosomes Bear MHC Class II/Peptide Complexes Potentiating Antigen Presentation by Dendritic Cells. Gastroenterology. 2007;1866–76.

165. Chivet M, Javalet C, Laulagnier K, Blot B, Fiona J. Exosomes secreted by cortical neurons upon glutamatergic synapse activation specifically interact with neurons. 2014;3078(May 2017).

166. Hoshino A, Costa-Silva B, Shen TL, Rodrigues G, Hashimoto A, Tesic Mark M, et al. Tumour exosome integrins determine organotropic metastasis. Nature [Internet]. 2015;527(7578):329–35. Available from: http://dx.doi.org/10.1038/nature15756

167. Rana S, Yue S, Stadel D, Zöller M. Toward tailored exosomes : The exosomal tetraspanin web contributes to target cell selection. Int J Biochem Cell Biol [Internet]. 2012;44(9):1574–84. Available from: http://dx.doi.org/10.1016/j.biocel.2012.06.018

168. Morelli AE, Larregina AT, Shufesky WJ, Sullivan MLG, Stolz DB, Papworth GD, et al. Endocytosis , intracellular sorting , and processing of exosomes by dendritic cells. 2004;104(10):3257–66.

169. Feng D, Zhao W, Ye Y, Bai X, Liu R, Chang L, et al. Cellular Internalization of Exosomes Occurs Through Phagocytosis. 2010;(1):675–87.

170. Tian T, Zhu Y, Zhou Y, Chem JB. Exosome Uptake through Clathrin-mediated Endocytosis and Macropinocytosis and Mediating miR-21 Delivery. 2014;

171. Escrevente C, Keller S, Altevogt P, Costa J. Interaction and uptake of exosomes by ovarian cancer cells. BMC Cancer. 2011 Mar 27;11.

172. Tian T, Wang Y, Wang H, Zhu Z, Xiao Z. Visualizing of the Cellular Uptake and Intracellular Trafficking of Exosomes by Live-Cell Microscopy. J Cell Biochem. 2010;496(March):488–96.

USC DE COMPOSTELA

173. Valadi H, Ekström K, Bossios A, Sjöstrand M, Lee JJ, Lötvall JO. Exosome-mediated transfer of mRNAs and microRNAs is a novel mechanism of genetic exchange between cells. Nat Cell Biol. 2007;9(6):654–9.

174. Cicero A Lo, Stahl PD. Extracellular vesicles shuffling intercellular messages : for good or for bad. Curr Protoc cell Biol. 2015;

175. Barile L, Vassalli G. Exosomes : Therapy delivery tools and biomarkers of diseases. Pharmacol Ther [Internet]. 2017;174:63–78. Available from: http://dx.doi.org/10.1016/j.pharmthera.2017.02.020

176. Fais S, Driscoll LO, Borras FE, Buzas E, Camussi G, Cappello F, et al. Evidence-Based Clinical Use of Nanoscale Extracellular Vesicles in Nanomedicine. ACS Nano. 2016;

177. Torrano V, Royo F, Loizaga-iriarte A, Unda M, Falco JM, Carracedo A. Vesicle-MaNiA : extracellular vesicles in liquid biopsy and cancer. ScienceDirect. 2016;47–53.

178. Simeone P, Bologna G, Lanuti P, Pierdomenico L, Guagnano MT, Pieragostino D, et al. Extracellular Vesicles as Signaling Mediators and Disease Biomarkers across Biological Barriers. 2020;1–27.

179. Ciferri MC, Quarto R. Extracellular Vesicles as Biomarkers and Therapeutic Tools : From Pre-Clinical to Clinical Applications. 2021;1–14.

180. Mizrak A, Bolukbasi MF, Ozdener GB, Brenner GJ, Madlener S, Erkan EP, et al. Genetically Engineered Microvesicles Carrying Suicide mRNA / Protein Inhibit Schwannoma Tumor Growth. Mol Ther [Internet]. 2009;21(1):101–8. Available from: http://dx.doi.org/10.1038/mt.2012.161/nature06264

181. Monguió-Tortajada M, Gálvez-Montón C, Bayes-Genis A, Roura S, Borràs FE. Extracellular vesicle isolation methods: rising impact of size-exclusion chromatography. Cell Mol Life Sci [Internet]. 2019; Available from: https://doi.org/10.1007/s00018-019-03071-y

182. Kuo WP. Impact of biofluid viscosity on size and sedimentation efficiency of the isolated microvesicles. 2012;3(May):1–7.

183. Livshits MA, Khomyakova E, Evtushenko EG, Laz VN. Isolation of exosomes by differential centrifugation : Theoretical analysis of a commonly used protocol. 2015;(May):1–14.

184. Théry C, Amigorena S, Raposo G, Clayton A. Isolation and characterization of exosomes from cell culture supernatants and biological fluids. Curr Protoc cell Biol [Internet]. 2006 Apr;Chapter 3:Unit 3.22. Available from: http://www.ncbi.nlm.nih.gov/pubmed/18228490

185. Baranyai T, Herczeg K, Onódi Z, Voszka I, Módos K. Isolation of Exosomes from Blood

USC UNIVERSIDADE DE SANTIAGO DE COMPOSTELA

Plasma : Qualitative and Quantitative Comparison of Ultracentrifugation and Size Exclusion Chromatography Methods. 2015;1–13.

186. Linares R, Tan S, Gounou C, Arraud N, Alain R, Arraud N, et al. High-speed centrifugation induces aggregation of extracellular vesicles. 2015;3078(March 2017).

187. Stam J, Bartel S, Bischoff R, Wolters JC. Isolation of extracellular vesicles with combined enrichment methods. J Chromatogr B [Internet]. 2021;1169(February):122604. Available from: https://doi.org/10.1016/j.jchromb.2021.122604

188. Momen-heravi F. Isolation of Extracellular Vesicles by Ultracentrifugation. 2017;1660:25–32.

189. Xu R, Simpson RJ, Greening DW. Chapter 7 A Protocol for Isolation and Proteomic Characterization Centrifugal Ultrafiltration. 2017;1545.

190. Merchant ML, Powell DW, Wilkey DW, Cummins TD, Deegens JK, Rood IM, et al. Microfiltration isolation of human urinary exosomes for characterization by MS. 2010;84–96.

191. He L, Zhu D, Wang J, Wu X. A highly efficient method for isolating urinary exosomes. 2019;83–90.

192. Askeland A, Borup A, Ostegaard O, Olsen J V, Lund SM, Christiansen G, et al. Mass-Spectrometry Based Proteome Comparison of Extracellular Vesicle Isolation Methods : Comparison of ME-kit, Size-Exclusion Chromatography, and High-Speed Centrifugation. Biomedicines. 2020;8:256.

193. Wei R, Zhao L, Kong G, Liu X, Zhu S, Zhang S, et al. Combination of Size-Exclusion Chromatography and Ultracentrifugation Improves the Proteomic Profiling of Plasma-Derived Small Extracellular Vesicles. 2020;1–11.

194. Sitar S, Kejžar A, Pahovnik D, Kogej K, Tušek-Žnidarič M, Lenassi M, et al. Size Characterization and Quantification of Exosomes by Asymmetrical-Flow Field-Flow Fractionation. Anal Chem. 2015;87(18):9225–33.

195. Herrero C, Fuente A De, Casas-arozamena C, Abalo A, Colás E, Moreno-bueno G, et al. Extracellular vesicle based biomarkers as liquid biopsy in endometrial cancer. Cancers (Basel). 2019;1–15.

196. Konoshenko MY, Lekchnov EA, Vlassov A V, Laktionov PP. Isolation of Extracellular Vesicles : General Methodologies and Latest Trends. 2018;2018.

197. Görgens A. Systematic Methodological Evaluation of a Multiplex Bead-Based Flow Cytometry Assay for Detection of Extracellular Vesicle Surface Signatures. 2018;9(June).

198. Vestad B, Llorente A, Neurauter A, Phuyal S, Kierulf B, Kierulf P, et al. Size and concentration analyses of extracellular vesicles by nanoparticle tracking analysis: a variation study. J Extracell Vesicles. 2017 Dec 1;6(1).

199. Suárez H, Gámez-Valero A, Reyes R, López-Martín S, Rodríguez MJ, Carrascosa JL, et al. A bead-assisted flow cytometry method for the semi-quantitative analysis of Extracellular Vesicles. Sci Rep. 2017;7(1):1–11.

200. Cizmar P, Yuana Y. Detection and Characterization of Extracellular Vesicles by Transmission and Cryo-Transmission Electron Microscopy. 2017;1660:221–32.

201. Wang Q, Zou L, Yang X, Liu X, Nie W, Zheng Y, et al. Biosensors and Bioelectronics Direct quanti fi cation of cancerous exosomes via surface plasmon resonance with dual gold nanoparticle-assisted signal ampli fi cation. Biosens Bioelectron [Internet]. 2019;135(April):129–36. Available from: https://doi.org/10.1016/j.bios.2019.04.013

202. Gleadle J, McNicholas K, Li J, Michael M, Rojas-Canales D. Nanoparticle tracking analysis of urine to detect exosomes can be confounded by albuminuria. J Am Soc Nephrol. 2018;29(6):1784.

203. Jeon H, Kang S, Id ML. Effects of different separation methods on the physical and functional properties of extracellular vesicles. 2020;(i):1–15. Available from: http://dx.doi.org/10.1371/journal.pone.0235793

204. Sódar BW, Kittel Á, Pálóczi K, Vukman K V, Osteikoetxea X, Szabó-taylor K, et al. Low-density lipoprotein mimics blood plasma-derived exosomes and microvesicles during isolation and detection. Nat Publ Gr [Internet]. 2016;(January):1–12. Available from: http://dx.doi.org/10.1038/srep24316

205. Fernández-Llama P, Khositseth S, Gonzales PA, Star RA, Pisitkun T, Knepper MA. Tamm-Horsfall protein and urinary exosome isolation. Kidney Int. 2010 Apr;77(8):736–42.

206. Kowal EJK, Ter-ovanesyan D, Regev A, Church GM. Extracellular Vesicle Isolation and Analysis by Western Blotting. 2017;1660:143–52.

207. Logozzi M, Raimo R Di, Mizzoni D, Fais S. Immunocapture-based ELISA to characterize and quantify exosomes in both cell culture supernatants and body fluids [Internet]. 1st ed. Vol. 645, Extracellular vesicles. Elsevier Inc.; 2020. 155–180 p. Available from: http://dx.doi.org/10.1016/bs.mie.2020.06.011

208. Nolan JP, Duggan E. Analysis of Individual Extracellular Vesicles by Flow Cytometry. 2017;1678.

209. Bandu R, Oh JW, Kim KP. Mass spectrometry-based proteome pro fi ling of extracellular vesicles and their roles in cancer biology. Exp Mol Med [Internet]. 2019; Available from: http://dx.doi.org/10.1038/s12276-019-0218-2

USC UNIVERSIDADE DE SANTIAGO DE COMPOSTELA

210. Magiorkinis E, Diamantis A. The Fascinating Story of Urine Examination: From Uroscopy to the Era of Microscopy and Beyond. Diagn Cytopathol. 2008;36(4):245–51.

211. Harpole M, Davis J, Espina V. Current state of the art for enhancing urine biomarker discovery. Expert Rev Proteomics. 2016;13(6):609–26.

212. Wiggins RC, Glatfelter A, Kshirsagar B, Brukman J. Procoagulant activity in normal human urine associated with subcellular particles. kid. 1986;29.

213. Pisitkun T, Shen R, Knepper MA. Identification and proteomic profiling of exosomes in human urine. 2004;101(36).

214. Erdbrügger U, Blijdorp CJ, Bijnsdorp I V., Borràs FE, Burger D, Bussolati B, et al. Urinary extracellular vesicles: A position paper by the Urine Task Force of the International Society for Extracellular Vesicles. J ofExtracellular Vesicles [Internet]. 2021 May 1 [cited 2021 Aug 9];10(7). Available from: https://pubmed.ncbi.nlm.nih.gov/34035881/

215. Pomatto MAC, Gai C, Bussolati B, Camussi G. Extracellular Vesicles in Renal Pathophysiology. Front Mol Biosci. 2017;

216. Morrison EE, Bailey MA, Dear JW. Renal extracellular vesicles: from physiology to clinical application. J Physiol. 2016;594(20):5735–48.

217. Prunotto M, Farina A, Lane L, Pernin A, Schifferli J, Hochstrasser DF, et al. Proteomic analysis of podocyte exosome-enriched fraction from normal human urine. J Proteomics [Internet]. 2013;82:193–229. Available from: http://dx.doi.org/10.1016/j.jprot.2013.01.012

218. Lv LL, Feng Y, Tang TT, Liu BC. New insight into the role of extracellular vesicles in kidney disease. J Cell Mol Med. 2019;23(2):731–9.

219. Wu XM, Gao Y Bin, Cui FQ, Zhang N. Exosomes from high glucose-treated glomerular endothelial cells activate mesangial cells to promote renal fibrosis. Biol Open. 2016;5(4):484–91.

220. Viñas JL, Spence M, Gutsol A, Knoll W, Burger D, Zimpelmann J, et al. Receptor-Ligand Interaction Mediates Targeting of Endothelial Colony Forming Cell-derived Exosomes to the Kidney after Ischemic Injury. Sci Rep. 2018;8(1):1–12.

221. Jella KK, Yu L, Yue Q, Friedman D, Duke BJ, Alli AA. Exosomal GAPDH from proximal tubule cells regulate ENaC activity. PLoS One. 2016;

222. Gildea JJ, Seaton JE, Victor KG, Reyes CM, Bigler Wang D, Pettigrew AC, et al. Exosomal transfer from human renal proximal tubule cells to distal tubule and collecting duct cells. Clin Biochem [Internet]. 2014;47(15):89–94. Available from: http://dx.doi.org/10.1016/j.clinbiochem.2014.06.018

223. Dang VD, Jella KK, Ragheb RRT, Denslow ND, Allik AA. Lipidomic and proteomic analysis of exosomes from mouse cortical collecting duct cells. FASEB J. 2017;31(12):5399–408.

224. Hogan MC, Manganelli L, Woollard JR, Masyuk AI, Masyuk T V., Tammachote R, et al. Characterization of PKD Protein-Positive Exosome-Like Vesicles. J Am Soc Nephrol. 2009;

225. Oosthuyzen W, Scullion KM, Ivy JR, Morrison EE, Hunter RW, Starkey Lewis PJ, et al. Vasopressin Regulates Extracellular Vesicle Uptake by Kidney Collecting Duct Cells. J Am Soc Nephrol. 2016;

226. Hiemstra TF, Charles PD, Gracia T, Hester SS, Gatto L, Al-Lamki R, et al. Human Urinary Exosomes as Innate Immune Effectors. J Am Soc Nephrol. 2014;

227. Erozenci LA, Böttger F, Bijnsdorp I V., Jimenez CR. Urinary exosomal proteins as (pan-)cancer biomarkers: insights from the proteome. FEBS Lett. 2019;593(13):1580–97.

228. Longmire M, Choyke PL. Clearance properties of nano-sized particles and molecules as imaging agents: considerations and caveats. Nanomedicine. 2008;3:703–17.

229. Londono I, Bendayan M. Glomerular handling of native albumin in the presence of circulating modified albumins by the normal rat kidney. Am J Physiol - Ren Physiol. 2005;289(6 58-6).

230. Zhou H, Yuen PST, Pisitkun T, Gonzales PA, Yasuda H, Dear JW, et al. Collection, storage, preservation, and normalization of human urinary exosomes for biomarker discovery. Kidney Int. 2006;

231. Bryzgunova OE, Zaripov MM, Skvortsova TE, Lekchnov EA, Grigor'eva AE, Zaporozhchenko IA, et al. Comparative study of extracellular vesicles from the urine of healthy individuals and prostate cancer patients. PLoS One. 2016;11(6):1–17.

232. Gonzales PA, Pisitkun T, Hoffert JD, Tchapyjnikov D, Star RA, Kleta R, et al. Large-scale proteomics and phosphoproteomics of urinary exosomes. J Am Soc Nephrol [Internet]. 2009 Feb [cited 2022 Jul 22];20(2):363–79. Available from: https://pubmed.ncbi.nlm.nih.gov/19056867/

233. Hildonen S, Skarpen E, Halvorsen TG, Reubsaet L. Isolation and mass spectrometry analysis of urinary extraexosomal proteins. Sci Rep [Internet]. 2016;6(November):1–14. Available from: http://dx.doi.org/10.1038/srep36331

234. Bijnsdorp I V., Maxouri O, Kardar A, Schelfhorst T, Piersma SR, Pham T V., et al. Feasibility of urinary extracellular vesicle proteome profiling using a robust and simple, clinically applicable isolation method. J Extracell Vesicles. 2017;6(1).

235. Dhondt B, Geeurickx E, Tulkens J, Van Deun J, Vergauwen G, Lippens L, et al.

USC UNIVERSIDADE DE SANTIAGO DE COMPOSTELA

Unravelling the proteomic landscape of extracellular vesicles in prostate cancer by density-based fractionation of urine. J Extracell Vesicles [Internet]. 2020;9(1). Available from: https://doi.org/10.1080/20013078.2020.1736935

236. Musante L, Bontha SV, La Salvia S, Fernandez-Piñeros A, Lannigan J, Le TH, et al. Rigorous characterization of urinary extracellular vesicles (uEVs) in the low centrifugation pellet - a neglected source for uEVs. Sci Rep. 2020;10(1):1–14.

237. Tokonami N, Takata T, Beyeler J, Ehrbar I, Yoshifuji A, Christensen EI, et al. Uromodulin is expressed in the distal convoluted tubule, where it is critical for regulation of the sodium chloride cotransporter NCC. Kidney Int [Internet]. 2018;1–15. Available from: https://doi.org/10.1016/j.kint.2018.04.021

238. Chen CY, Hogan MC, Ward CJ. Purification of exosome-like vesicles from urine. Methods Enzymol. 2013;524:225–41.

239. Musante L, Saraswat M, Duriez E, Byrne B, Ravidà A, Domon B, et al. Biochemical and physical characterisation of urinary nanovesicles following CHAPS treatment. PLoS One [Internet]. 2012 [cited 2020 Jan 16];7(7):37279. Available from: www.plosone.org

240. Puhka M, Nordberg ME, Valkonen S, Rannikko A, Kallioniemi O, Siljander P, et al. KeepEX, a simple dilution protocol for improving extracellular vesicle yields from urine. Eur J Pharm Sci [Internet]. 2017;98:30–9. Available from: http://dx.doi.org/10.1016/j.ejps.2016.10.021

241. Erdbrügger U, Le TH. Extracellular Vesicles in Renal Diseases: More than Novel Biomarkers? J Am Soc Nephrol. 2016;27(1):12–26.

242. Gonzales PA, Pisitkun T, Hoffert JD, Tchapyjnikov D, Star RA, Kleta R, et al. Large-Scale Proteomics and Phosphoproteomics of Urinary Exosomes. J Am Soc Nephrol. 2009;

243. Lv L-L, Feng Y, Wen Y, Wu W-J, Ni H-F, Li Z-L, et al. Exosomal CCL2 from Tubular Epithelial Cells Is Critical for Albumin-Induced Tubulointerstitial Inflammation. J Am Soc Nephrol [Internet]. 2018 [cited 2021 Mar 4];29:919–35. Available from: www.jasn.org

244. Kamińska A, Platt M, Kasprzyk J, Kuśnierz-Cabala B, Gala-Błądzińska A, Woźnicka O, et al. Urinary Extracellular Vesicles: Potential Biomarkers of Renal Function in Diabetic Patients. J Diabetes Res. 2016;2016.

245. Peake PW, Pianta TJ, Succar L, Fernando M, Pugh DJ, McNamara K, et al. A comparison of the ability of levels of urinary biomarker proteins and exosomal mRNA to predict outcomes after renal transplantation. PLoS One. 2014;9(6):11–4.

246. Dear JW, Street JM, Bailey MA. Urinary exosomes: A reservoir for biomarker discovery and potential mediators of intrarenal signalling. Vol. 13, Proteomics. 2013. p. 1572–80.

247. Bijnsdorp I V., Geldof AA, Lavaei M, Piersma SR, van Moorselaar RJA, Jimenez CR. Exosomal ITGA3 interferes with non-cancerous prostate cell functions and is increased in urine exosomes of metastatic prostate cancer patients. J Extracell Vesicles. 2013;2(1):22097.

248. Chen CL, Lai YF, Tang P, Chien KY, Yu JS, Tsai CH, et al. Comparative and targeted proteomic analyses of urinary microparticles from bladder cancer and hernia patients. J Proteome Res. 2012;11(12):5611–29.

249. Clos-Garcia M, Loizaga-Iriarte A, Zuñiga-Garcia P, Sánchez-Mosquera P, Rosa Cortazar A, González E, et al. Metabolic alterations in urine extracellular vesicles are associated to prostate cancer pathogenesis and progression. J Extracell Vesicles [Internet]. 2018;7(1). Available from: https://doi.org/10.1080/20013078.2018.1470442

250. Dhondt B, Van Deun J, Vermaerke S, de Marco A, Lumen N, De Wever O, et al. Urinary extracellular vesicle biomarkers in urological cancers: From discovery towards clinical implementation. Int J Biochem Cell Biol [Internet]. 2018;99(2010):236–56. Available from: https://doi.org/10.1016/j.biocel.2018.04.009

251. Leiblich A. Recent Developments in the Search for Urinary Biomarkers in Bladder Cancer. Curr Urol Rep. 2017;18(12).

252. Nilsson J, Skog J, Nordstrand A, Baranov V, Mincheva-Nilsson L, Breakefield XO, et al. Prostate cancer-derived urine exosomes: A novel approach to biomarkers for prostate cancer. Br J Cancer [Internet]. 2009;100(10):1603–7. Available from: http://dx.doi.org/10.1038/sj.bjc.6605058

253. McKiernan J, Donovan MJ, O'Neill V, Bentink S, Noerholm M, Belzer S, et al. A novel urine exosome gene expression assay to predict high-grade prostate cancer at initial biopsy. JAMA Oncol. 2016;2(7):882–9.

254. Bourderioux M, Nguyen-Khoa T, Chhuon C, Jeanson L, Tondelier D, Walczak M, et al. A new workflow for proteomic analysis of urinary exosomes and assessment in cystinuria patients. J Proteome Res. 2015;14(1):567–77.

255. Abe H, Sakurai A, Ono H, Hayashi S, Yoshimoto S, Ochi A, et al. Urinary exosomal mRNA of WT1 as diagnostic and prognostic biomarker for diabetic nephropathy. J Med Investig. 2018;65(3–4):208–15.

256. Morikawa Y, Takahashi N, Kamiyama K, Nishimori K, Nishikawa Y, Morita S, et al. Elevated Levels of Urinary Extracellular Vesicle Fibroblast-Specific Protein 1 in Patients with Active Crescentic Glomerulonephritis. Nephron. 2019;141(3):177–87.

257. Yu Y, Bai F, Qin N, Liu W, Sun Q, Zhou Y, et al. Non-proximal renal tubule-derived urinary exosomal miR-200b as a biomarker of renal fibrosis. Nephron. 2018;139(3):269–82.

USC UNIVERSIDADE DE SANTIAGO DE COMPOSTELA

258. Tangtanatakul P, Klinchanhom S, Sodsai P, Sutichet T, Promjeen C, Avihingsanon Y, et al. Down-regulation of let-7a and miR-21 in urine exosomes from lupus nephritis patients during disease flare. Asian Pacific J Allergy Immunol. 2019;37(4):189–97.

259. Corbetta S, Raimondo F, Tedeschi S, Syrèn M-L, Rebora P, Savoia A, et al. Urinary exosomes in the diagnosis of Gitelman and Bartter syndromes. Nephrol Dial Transplant. 2015;67(4):588–92.

260. Krause M, Samoylenko A, Vainio SJ. Exosomes as renal inductive signals in health and disease, and their application as diagnostic markers and therapeutic agents. Front Cell Dev Biol. 2015;3(OCT):1–13.

261. Lv LL, Cao Y, Liu D, Xu M, Liu H, Tang RN, et al. Isolation and quantification of MicroRNAs from urinary exosomes/microvesicles for biomarker discovery. Int J Biol Sci. 2013;9(10):1021–31.

262. Salih M, Demmers JA, Bezstarosti K, Leonhard WN, Losekoot M, Van Kooten C, et al. Proteomics of urinary vesicles links plakins and complement to polycystic kidney disease. J Am Soc Nephrol [Internet]. 2016 [cited 2020 Jan 23];27(10):3079–92. Available from: www.jasn.org

263. Messchendorp AL, Meijer E, Boertien WE, Engels GE, Casteleijn NF, Spithoven EM, et al. Urinary Biomarkers to Identify Autosomal Dominant Polycystic Kidney Disease Patients With a High Likelihood of Disease Progression. Kidney Int Reports [Internet]. 2018;3(2):291–301. Available from: https://doi.org/10.1016/j.ekir.2017.10.004

264. Petzold K, Poster D, Krauer F, Spanaus K, Andreisek G, Nguyen-Kim TDL, et al. Urinary biomarkers at early ADPKD disease stage. PLoS One. 2015;10(4):1–15.

265. Hogan MC, Bakeberg JL, Gainullin VG, Irazabal M V., Harmon AJ, Lieske JC, et al. Identification of biomarkers for PKD1 using urinary exosomes. J Am Soc Nephrol. 2015 Jul 1;26(7):1661–70.

266. Magayr TA, Song X, Streets AJ, Vergoz L, Chang L, Valluru MK, et al. Global microRNA profiling in human urinary exosomes reveals novel disease biomarkers and cellular pathways for autosomal dominant polycystic kidney disease. Kidney Int [Internet]. 2020;98(2):420–35. Available from: https://doi.org/10.1016/j.kint.2020.02.008

267. Batista BS, Eng WS, Pilobello KT, Hendricks-Muñoz KD, Mahal LK. Identification of a conserved glycan signature for microvesicles. J Proteome Res. 2011 Oct 7;10(10):4624–33.

268. Gerlach JQ, Griffin MD. Getting to know the extracellular vesicle glycome. Mol Biosyst. 2016;12(4):1071–81.

269. Brown CJ, Gaunitz S, Wang Z, Strindelius L, Jacobson SC, Clemmer DE, et al.

USC DE SANTIAGO DE COMPOSTELA

Glycoproteomic Analysis of Human Urinary Exosomes. Anal Chem. 2020;92(21):14357–65.

270. Liang Y, Eng WS, Colquhoun DR, Dinglasan RR, Graham DR, Mahal LK. Complex N-linked glycans serve as a determinant for exosome/microvesicle cargo recruitment. J Biol Chem. 2014 Nov 21;289(47):32526–37.

271. Williams C, Pazos R, Royo F, González E, Roura-Ferrer M, Martinez A, et al. Assessing the role of surface glycans of extracellular vesicles on cellular uptake. Sci Rep. 2019;9(1):1–14.

272. Tzanakakis G, Kovalszky I, Heldin P, Nikitovic D. Proteoglycans / Glycosaminoglycans : From Basic Research to Clinical Practice. 2014;2014:2–4.

273. Reily C, Stewart TJ, Renfrow MB, Novak J. Glycosylation in health and disease. Nat Rev Nephrol [Internet]. 2019;15(6):346–66. Available from: http://dx.doi.org/10.1038/s41581-019-0129-4

274. Adua E, Anto EO, Roberts P, Kantanka OS, Aboagye E, Wang W. The potential of N-glycosylation profiles as biomarkers for monitoring the progression of Type II diabetes mellitus towards diabetic kidney disease. J Diabetes Metab Disord. 2018;17(2):233–46.

275. Piontek KB, Huso DL, Grinberg A, Liu L, Bedja D, Zhao H, et al. A functional floxed allele of Pkd1 that can be conditionally inactivated in vivo. J Am Soc Nephrol. 2004;15(12):3035–43.

276. Cordido A, Cernadas E, Fernández-Delgado M, García-González MA. CystAnalyser: A new software tool for the automatic detection and quantification of cysts in polycystic kidney and liver disease, and other cystic disorders. PLoS Comput Biol. 2020 Oct 22;16(10).

277. Shevchenko A, Wilm M, Vorm O, Jensen ON, Podtelejnikov A V., Neubauer G, et al. A strategy for identifying gel-separated proteins in sequence databases by MS alone. Biochem Soc Trans. 1996;24(3):893–6.

278. Cordido A, Vizoso-Gonzalez M, Nuñez-Gonzalez L, Molares-Vila A, Chantada-Vazquez MDP, Bravo SB, et al. Quantitative Proteomic Study Unmasks Fibrinogen Pathway in Polycystic Liver Disease. Biomedicines [Internet]. 2022 Feb 1 [cited 2022 May 27];10(2). Available from: https://pubmed.ncbi.nlm.nih.gov/35203500/

279. Chantada-Vazquez MP, Garcia Vence M, Senra A, Núñez C, Bravo SB. Chapter 7. Vol. 2259. 2021. 105–137 p.

280. Shilov I V., Seymourt SL, Patel AA, Loboda A, Tang WH, Keating SP, et al. The paragon algorithm, a next generation search engine that uses sequence temperature values sequence temperature values and feature probabilities to identify peptides from tandem mass spectra. Mol Cell Proteomics. 2007;6(9):1638–55.

USC UNIVERSIDADE DE SANTIAGO DE COMPOSTELA

281. Käll L, Storey JD, Noble WS. Non-parametric estimation of posterior error probabilities associated with peptides identified by tandem mass spectrometry. Bioinformatics. 2008;24(16):42–8.

282. Nesvizhskii AI, Keller A, Kolker E, Aebersold R. A statistical model for identifying proteins by tandem mass spectrometry. Anal Chem. 2003;75(17):4646–58.

283. Oosthuyzen W, Sime NEL, Ivy JR, Turtle EJ, Street JM, Pound J, et al. Quantification of human urinary exosomes by nanoparticle tracking analysis. Authors J Physiol C [Internet]. 2013 Dec 1 [cited 2021 Mar 4];591(23):5833–42. Available from: http://doi.wiley.com/10.1113/jphysiol.2013.264069

284. Park S, Moon HY. Urinary extracellular vesicle as a potential biomarker of exercise-induced fatigue in young adult males. Eur J Appl Physiol [Internet]. 2022 Jul 4 [cited 2022 Jul 31]; Available from: https://link.springer.com/10.1007/s00421-022-04995-3

285. Mizenko RR, Brostoff T, Rojalin T, Koster HJ, Swindell HS, Leiserowitz GS, et al. Tetraspanins are unevenly distributed across single extracellular vesicles and bias sensitivity to multiplexed cancer biomarkers. J Nanobiotechnology [Internet]. 2021 Dec 1 [cited 2022 Jul 7];19(1). Available from: https://pubmed.ncbi.nlm.nih.gov/34419056/

286. Chang RYK, Etheridge N, Nouwens AS, Dodd PR. SWATH analysis of the synaptic proteome in Alzheimer's disease. Neurochem Int [Internet]. 2015;87:1–12. Available from: http://dx.doi.org/10.1016/j.neuint.2015.04.004

287. von Mering C, Huynen M, Jaeggi D, Schmidt S, Bork P, Snel B. STRING: A database of predicted functional associations between proteins. Nucleic Acids Res. 2003;31(1):258–61.

288. Fonseka P, Pathan M, Chitti S V., Kang T, Mathivanan S. FunRich enables enrichment analysis of OMICs datasets. J Mol Biol [Internet]. 2021;433(11):166747. Available from: https://doi.org/10.1016/j.jmb.2020.166747

289. Han X, Sanderson P, Nesheiwat S, Lin L, Yu Y, Zhang F, et al. Structural analysis of urinary glycosaminoglycans from healthy human subjects. Glycobiology [Internet]. 2020 [cited 2022 Jul 16];30(3):143. Available from: /pmc/articles/PMC7415306/

290. Gatto F, Volpi N, Nilsson H, Nookaew I, Maruzzo M, Roma A, et al. Glycosaminoglycan Profiling in Patients' Plasma and Urine Predicts the Occurrence of Metastatic Clear Cell Renal Cell Carcinoma. Cell Rep [Internet]. 2016 [cited 2022 Jul 16];15(8):1822–36. Available from: http://dx.doi.org/10.1016/j.celrep.2016.04.056

291. Erturk E, Kiernan M, Schoen SR. Clinical association with urinary glycosaminoglycans and urolithiasis. Urology. 2002;59(4):495–9.

292. Genovese F, Manresa AA, Leeming DJ, Karsdal MA, Boor P. The extracellular matrix in the kidney: a source of novel non-invasive biomarkers of kidney fibrosis? Fibrogenes

Tissue Repair 2014 71 [Internet]. 2014 Mar 28 [cited 2022 Jul 16];7(1):1–14. Available from: https://fibrogenesis.biomedcentral.com/articles/10.1186/1755-1536-7-4

293. Khramova A, Boi R, Fridén V, Granqvist AB, Nilsson U, Tenstad O, et al. Proteoglycans contribute to the functional integrity of the glomerular endothelial cell surface layer and are regulated in diabetic kidney disease. Sci Reports 2021 111 [Internet]. 2021 Apr 19 [cited 2022 Jul 16];11(1):1–12. Available from: https://www.nature.com/articles/s41598-021-87753-3

294. Cerezo-Magaña M, Bång-Rudenstam A, Belting M. The pleiotropic role of proteoglycans in extracellular vesicle mediated communication in the tumor microenvironment. Vol. 62, Seminars in Cancer Biology. Academic Press; 2020. p. 99–107.

295. Royo F, Cossío U, Ruiz De Angulo A, Llop J, Falcon-Perez JM. Modification of the glycosylation of extracellular vesicles alters their biodistribution in mice. Nanoscale. 2019;11(4):1531–7.

296. Buzás EI, Tóth E, Sódar BW, Szabó-Taylor K. Molecular interactions at the surface of extracellular vesicles [Internet]. Vol. 40, Seminars in Immunopathology. 2018 [cited 2022 Jul 22]. p. 453–64. Available from: https://doi.org/10.1007/s00281-018-0682-0

297. Erdbrügger U, Blijdorp CJ, Bijnsdorp I V., Borràs FE, Burger D, Bussolati B, et al. Urinary extracellular vesicles: A position paper by the Urine Task Force of the International Society for Extracellular Vesicles. J Extracell Vesicles. 2021 May 1;10(7).

298. Jayasena T, Poljak A, Braidy N, Zhong L, Rowlands B, Muenchhoff J, et al. Application of Targeted Mass Spectrometry for the Quantification of Sirtuins in the Central Nervous System. Sci Reports 2016 61 [Internet]. 2016 Oct 20 [cited 2022 Jul 28];6(1):1–11. Available from: https://www.nature.com/articles/srep35391

299. Menezes LF, Zhou F, Patterson AD, Piontek KB, Krausz KW, Gonzalez FJ, et al. Network Analysis of a Pkd1-Mouse Model of Autosomal Dominant Polycystic Kidney Disease Identifies HNF4α as a Disease Modifier. PLoS Genet. 2012;8(11).

300. Menon V, Rudym D, Chandra P, Miskulin D, Perrone R, Sarnak M. Inflammation, oxidative stress, and insulin resistance in polycystic kidney disease. Clin J Am Soc Nephrol. 2011;6(1):7–13.

301. Zhong CQ, Wu R, Chen X, Wu S, Shuai J, Han J. Systematic Assessment of the Effect of Internal Library in Targeted Analysis of SWATH-MS. J Proteome Res. 2019;19(1):477–92.

302. Isaksson M, Karlsson C, Laurell T, Kirkeby A, Heusel M. MSLibrarian: Optimized Predicted Spectral Libraries for Data-Independent Acquisition Proteomics. J Proteome Res. 2022;21(2):535–46.

USC UNIVERSIDADE DE SANTIAGO DE COMPOSTELA

303. Schubert OT, Gillet LC, Collins BC, Navarro P, Rosenberger G, Wolski WE, et al. Building high-quality assay libraries for targeted analysis of SWATH MS data. Nat Protoc. 2015;10(3):426–41.

304. Zhong CQ, Wu R, Chen X, Wu S, Shuai J, Han J. Systematic Assessment of the Effect of Internal Library in Targeted Analysis of SWATH-MS. J Proteome Res. 2020;19(1):477–92.

305. Njoku K, Chiasserini D, Geary B, Pierce A, Jones ER, Whetton AD, et al. Comprehensive library generation for identification and quantification of endometrial cancer protein biomarkers in cervico-vaginal fluid. Cancers (Basel). 2021;13(15).

306. Joanna Bons, Jacob Rose, Amy O'Broin BS. Chapter 20 - Advanced mass spectrometry-based methods for protein molecular-structural biologists,. Adv Protein Mol Struct Biol Methods,. 2022;

307. Mehta D, Scandola S, Uhrig RG. BoxCar and Library-Free Data-Independent Acquisition Substantially Improve the Depth, Range, and Completeness of Label-Free Quantitative Proteomics. Anal Chem. 2022;

308. Bons J, Rose J, Zhang R, Burton JB, Carrico C, Verdin E, et al. In-depth Analysis of the Sirtuin 5-regulated Mouse Brain Acylome using Library-free Data-Independent Acquisitions. bioRxiv [Internet]. 2022 Aug 6 [cited 2022 Aug 13];2022.08.06.503046. Available from: https://www.biorxiv.org/content/10.1101/2022.08.06.503046v1

309. Harris PC, Torres VEVE. Polycystic kidney disease. Annu Rev Med. 2009;60:321–37.

310. Malas TB, Leonhard WN, Bange H, Granchi Z, Hettne KM, Van Westen GJP, et al. Prioritization of novel ADPKD drug candidates from disease-stage specific gene expression profiles. EBioMedicine. 2020;51.

311. Menezes LF, Lin CC, Zhou F, Germino GG. Fatty Acid Oxidation is Impaired in An Orthologous Mouse Model of Autosomal Dominant Polycystic Kidney Disease. EBioMedicine [Internet]. 2016;5:183–92. Available from: http://dx.doi.org/10.1016/j.ebiom.2016.01.027

312. Dong K, Zhang C, Tian X, Coman D, Hyder F, Ma M, et al. Renal plasticity revealed through reversal of polycystic kidney disease in mice. Nat Genet. 2021;53(12):1649–63.

313. Boletta A. Reversing polycystic kidney disease. Nat Genet. 2021;53(12):1623–4.

314. Challa AA, Stefanovic B. A Novel Role of Vimentin Filaments: Binding and Stabilization of Collagen mRNAs. Mol Cell Biol. 2011;31(18):3773–89.

315. Chea SW, Lee KB. TGF-β mediated epithelial-mesenchymal transition in autosomal dominant polycystic kidney disease. Yonsei Med J. 2009;50(1):105–11.

316. Leierer J, Perco P, Hofer B, Eder S, Dzien A, Kerschbaum J, et al. Coregulation analysis

USC DE SANTIAGO DE COMPOSTELA

of mechanistic biomarkers in autosomal dominant polycystic kidney disease. Int J Mol Sci. 2021;22(13).

317. Burstyn-Cohen T, Frumkin A, Xu YT, Scherer SS, Klar A. Accumulation of F-spondin in injured peripheral nerve promotes the outgrowth of sensory axons. J Neurosci. 1998;18(21):8875–85.

318. Chang H, Dong T, Ma X, Zhang T, Chen Z, Yang Z, et al. Spondin 1 promotes metastatic progression through Fak and Src dependent pathway in human osteosarcoma. Biochem Biophys Res Commun [Internet]. 2015;464(1):45–50. Available from: http://dx.doi.org/10.1016/j.bbrc.2015.05.092

319. Huo Y, Yang J, Zheng J, Xu D, Yang M, Tao L, et al. Increased SPON1 promotes pancreatic ductal adenocarcinoma progression by enhancing IL-6 trans-signalling. Cell Prolif. 2022;55(5):1–14.

320. Zargar R, Urwat U, Malik F, Shah RA, Bhat MH, Naykoo NA, et al. Molecular characterization of RNA binding motif protein 3 (RBM3) gene from Pashmina goat. Res Vet Sci [Internet]. 2015;98:51–8. Available from: http://dx.doi.org/10.1016/j.rvsc.2014.11.016

321. Zhang L, Zhang Y, Shen D, Chen Y, Feng J, Wang X, et al. RNA Binding Motif Protein 3 Promotes Cell Metastasis and Epithelial–Mesenchymal Transition Through STAT3 Signaling Pathway in Hepatocellular Carcinoma. J Hepatocell Carcinoma. 2022;Volume 9(April):405–22.

322. Dresios J, Aschrafi A, Owens GC, Vanderklish PW, Edelman GM, Mauro VP. Cold stress-induced protein Rbm3 binds 60S ribosomal subunits, alter microRNA levels, and enhances global protein synthesis. Proc Natl Acad Sci U S A. 2005;102(6):1865–70.

323. Seufert L, Benzing T, Ignarski M, Müller RU. RNA-binding proteins and their role in kidney disease. Nat Rev Nephrol. 2022;18:153–70.

324. Borghouts C, Tittmann H, Delis N, Kirchenbauer M, Brill B, Groner B. The intracellular delivery of a recombinant peptide derived from the acidic domain of PIAS3 inhibits STAT3 transactivation and induces tumor cell death. Mol Cancer Res. 2010;8(4):539–53.

325. Malik A, Nalluri S, De A, Beligala D, Geusz ME. The Relevance of Circadian Clocks to Stem Cell Differentiation and Cancer Progression. NeuroSci. 2022;3(2):146–65.

326. Chebib FT, Torres VE. Autosomal Dominant Polycystic Kidney Disease: Core Curriculum 2016. Vol. 176, American Journal of Kidney Diseases. 2016. 792–810 p.

327. Honeycutt AA, Segel JE, Zhuo X, Hoerger TJ, Imai K. Medical Costs of CKD in the Medicare Population. J Am Soc Nephrol. 2013;1478–83.

USC UNIVERSIDADE DE SANTIAGO DE COMPOSTELA

328. Junior A, Muro P De, Capobianco G, Formato M. Significance of urinary glycosaminoglycans / proteoglycans in the evaluation of type 1 and type 2 diabetes complications. J Diabetes Complications [Internet]. 2016;1–7. Available from: http://dx.doi.org/10.1016/j.jdiacomp.2016.10.013

329. Lee S, Choi ME. Urinary biomarkers for early diabetic nephropathy : beyond albuminuria. Pediatr Nephrol. 2015;1063–75.

330. Beynon RJ, Hurst JL. Multiple roles of major urinary proteins in the house mouse , Mus domesticus. Biochem Soc Trans. 2003;31:142–6.

331. Prajczer S, Heidenreich U, Pfaller W, Kotanko P, Lhotta K, Jennings P. Evidence for a role of uromodulin in chronic kidney disease progression. Nephrol Dial Transplant. 2010;(January):1896–903.

332. Pontillo C, Jacobs L, Staessen JA, Schanstra JP, Rossing P, Heerspink HJL, et al. A urinary proteome-based classifier for the early detection of decline in glomerular filtration. Nephrol Dial Transplant. 2017;(July 2016):1510–6.

333. Cañadas-Garre M, Anderson K, McGoldrick J, Maxwell AP, McKnight AJ. Proteomic and metabolomic approaches in the search for biomarkers in chronic kidney disease. Journal of Proteomics. 2018;

334. Puthumana J, Thiessen-Philbrook H, Xu L, Coca SG, Garg AX, Himmelfarb J, et al. Biomarkers of inflammation and repair in kidney disease progression. J Clin Invest. 2021;131(3).

335. Methven S, MacGregor M, Traynor J, Hair MPhil M, O'Reilly D, Deighan C. Comparison of Urinary Albumin and Urinary Total Protein as Predictors of Patient Outcomes in CKD. Am J Kidney Dis [Internet]. 2011;57:21–8. Available from: http://dx.doi.org/10.1016/j.ypat.2011.08.010

336. Narva AS, Briggs M. The National Kidney Disease Education Program : Improving Understanding , Detection , and Management of CKD. YAJKD [Internet]. 2009;53(3):S115–20. Available from: http://dx.doi.org/10.1053/j.ajkd.2008.05.038

337. Smith A, Imperio VL, Sio G De, Ferrario F, Scalia C. ␣ -1-Antitrypsin detected by MALDI imaging in the study of glomerulonephritis : Its relevance in chronic kidney disease progression. Proteomics. 2016;1759–66.

338. Rauniyar N, Yu X, Cantley J, Voss E, Belcher J, Colangelo C. Quantification of Urinary Protein Biomarkers of Autosomal Dominant Polycystic Kidney Disease by Parallel Reaction Monitoring. PROTEOMICS – Clin Appl. 2018;1–25.

339. Romanova Y, Laikov A, Markelova M, Khadiullina R, Makseev A, Hasanova M, et al. Proteomic Analysis of Human Serum from Patients with Chronic Kidney Disease.

Biomolecules. 2020;257.

340. Cheng C, Chen J. Serum ApoA4 levels predicted the progression of renal impairment in T2DM. Eur J Clin Invest. 2018;

341. Jerebtsova M, Saraf SL, Lin X, Lee G, Adjei EA, Kumari N, et al. Identification of ceruloplasmin as a biomarker of chronic kidney disease in urine of sickle cell disease patients by proteomic analysis. Vol. 93, American Journal of Hematology. Wiley-Liss Inc.; 2018. p. E45–7.

342. Gudehithlu KP, Hart P, Joshi A, Garcia-Gomez I, Cimbaluk DJ, Dunea G, et al. Urine exosomal ceruloplasmin: a potential early biomarker of underlying kidney disease. Clin Exp Nephrol [Internet]. 2019;23(8):1013–21. Available from: https://doi.org/10.1007/s10157-019-01734-5

343. Kawano H, Muto S, Ohmoto Y. Exploring urinary biomarkers in autosomal dominant polycystic kidney disease. Clin Exp Nephrol [Internet]. 2015;968–73. Available from: http://dx.doi.org/10.1007/s10157-014-1078-7

344. Benetti A, Martins FL, Sene LB, Shimizu MHM, Seguro AC, Luchi WM, et al. Urinary DPP4 correlates with renal dysfunction , and DPP4 inhibition protects against the reduction in megalin and podocin expression in experimental CKD. Am J Ren Physiol. 2021;285–96.

345. Ding H, Shen Y, Lin C, Qin L, He S, Dai M, et al. Urinary galectin-3 binding protein (G3BP) as a biomarker for disease activity and renal pathology characteristics in lupus nephritis. Arthritis Res Ther [Internet]. 2022;1–10. Available from: https://doi.org/10.1186/s13075-022-02763-4

346. Wang H, Zheng C, Lu Y, Jiang Q, Yin R, Zhu P, et al. Article Urinary Fibrinogen as a Predictor of Progression of CKD. Clin J Am Soc Nephrol. 2017;12.

347. Gupta J, Mitra N, Kanetsky PA, Devaney J, Wing MR, Reilly M, et al. Article Association between Albuminuria , Kidney Function , and Inflammatory Biomarker Profile in CKD in CRIC. Clin J Am Soc Nephrol. 2012;7(15).

348. Drinkwater JJ, Peters K, Davis WA, Turner AW, Bringans SD, Lipscombe RJ, et al. Journal of Diabetes and Its Complications Assessment of biomarkers associated with rapid renal decline in the detection of retinopathy and its progression in type 2 diabetes : The Fremantle Diabetes Study Phase II. J Diabetes Complications [Internet]. 2021;35(4):107853. Available from: https://doi.org/10.1016/j.jdiacomp.2021.107853

349. Kalantari S, Rutishauser D, Samavat S, Nafar M, Mahmudieh L. Urinary Prognostic Biomarkers and Classification of IgA Nephropathy by High Resolution Mass Spectrometry Coupled with Liquid Chromatography. PLoS One. 2013;8(12):1–11.

350. Makridakis M, Kont G, Petra E, Stroggilos R, Lygirou V, Filip S, et al. Multiplexed

USC UNIVERSIDADE DE SANTIAGO DE COMPOSTELA

MRM-based protein quantification of putative prognostic biomarkers for chronic kidney disease progression in plasma. Sci Rep [Internet]. 2020;1–12. Available from: http://dx.doi.org/10.1038/s41598-020-61496-z

351. Maeda H, Sogawa K, Sakaguchi K, Abe S, Sagikaza W, Mochinuki S, et al. Urinary albumin and transferrin as early diagnostic markers of chronic kidney disease. J veretinary Med Sci. 2015;

352. Peralta CA, Shlipak MG, Judd S, Cushman M, Mcclellan W, Zakai NA, et al. Detection of Chronic Kidney Disease With Creatinine , Cystatin C , and Association With Progression to End-Stage Renal Disease and Mortality. JAMA. 2011;305(15):1545–52.

353. Verhave JC, Gansevoort RT, Hillege H, Bakker S, Zeeuw D, Jong P. An elevated urinary albumin excretion predicts de novo development of renal function impairment in the general population. Kidney Int. 2004;66:18–21.

354. Sumida K, Nadkarni G, Grams ME, Sang Y, Ballew S, Polkinghorne K, et al. Conversion of Urine Protein – Creatinine Ratio or Urine Dipstick Protein to Urine Albumin – Creatinine Ratio for Use in Chronic Kidney Disease Screening and Prognosis. Ann Intern Med. 2020;

355. Schaeffer C, Devuyst O, Rampoldi L. Uromodulin : Roles in Health and Disease. Annu Rev Physiol. 2021;83:477–501.

356. Weiss GL, Stanisich JJ, Sauer MM, Lin C-WW, Eras J, Zyla DS, et al. Architecture and function of human uromodulin filaments in urinary tract infections. Science (80-). 2020;369(6506):1005–10.

357. Lafavers KA, Micanovic R, Sabo AR, Maghak LA, El-achkar TM. Evolving Concepts in Uromodulin Biology, Physiology, and Its Role in Disease: a Tale of Two Forms. Hypertension. 2022;70:1–10.

358. Beenken A, Al-Awqati Q. Uromodulin fights UTI with sugars. Kidney Int [Internet]. 2021 Feb [cited 2021 Mar 4]; Available from: https://doi.org/10.1016/j.kint.2020.12.035

359. Kipp A, Olinger E. What Does Uromodulin Do ? 2021;16:150–3.

360. Torffvit O, Hultén UL. Urinary Excretion Rate of Tamm-Horsfall Protein Is Related to Salt Intake in Humans. Nephron Physiol. 2004;97:31–7.

361. Wolf MTF, Wu XR, Huang CL. Uromodulin upregulates TRPV5 by impairing caveolin-mediated endocytosis. Kidney Int. 2013;84(1):130–7.

362. Nie M, Bal PDMS, Liu PDJ, Yang PDZ, Rivera PDC, Wu X, et al. Uromodulin regulates renal magnesium homeostasis through the ion channel transient receptor potential melastatin 6 (TRPM6). 2018;6.

363. Devuyst O, Olinger E, Rampoldi L. Uromodulin: From physiology to rare and complex

USC DE SANTIAGO DE COMPOSTELA

kidney disorders. Nat Rev Nephrol [Internet]. 2017;13(9):525–44. Available from: http://dx.doi.org/10.1038/nrneph.2017.101

364. Melchinger H, Calderon-gutierrez F, Obeid W, Xu L, Shaw MM, Luciano RL, et al. Article Urine Uromodulin as a Biomarker of Kidney Tubulointerstitial Fibrosis. 2022;17.

365. Risch L, Lhotta K, Meier D, Medina-escobar P, Nydegger UE. The serum uromodulin level is associated with kidney function. Clin Chem Lab Med. 2014;52(12):1755–61.

366. Steubl D, Block M, Herbst V, Nockher WA, Schlumberger W, Kemmner S, et al. Urinary uromodulin independently predicts end-stage renal disease and rapid kidney function decline in a cohort of chronic kidney disease patients. Medicine (Baltimore). 2019;98(21):e15808.

367. Nur H, Funda C, Can S, Ramazan C, Gultekin C, Fevzi S. Serum uromodulin levels , MR imaging findings , and their relationship with eGFR - based CKD staging in ADPKD patients. Int Urol Nephrol [Internet]. 2021;53(7):1383–9. Available from: https://doi.org/10.1007/s11255-020-02730-5

368. Healy J, Tipton K. Ceruloplasmin and what it might do. J Neural Transm. 2007;777–81.

369. Jiang B, Liu G, Zheng J, Chen M, Maimaitiming Z, Chen M, et al. Hephaestin and ceruloplasmin facilitate iron metabolism in the mouse kidney. Nat Publ Gr. 2016;1–11.

370. Mostad EJ, Prohaska JR. Glycosylphosphatidylinositol-linked ceruloplasmin is expressed in multiple rodent organs and is lower following dietary copper deficiency. Exp Biol Med. 2015;298–308.

371. Honda H, Ganz T. Iron Metabolism in Chronic Kidney Disease Patients. 2019;198:103–11.

372. Panwar B, Gutiérrez OM. Disorders of Iron Metabolism and Anemia in Chronic Kidney Disease. Semin Nephrol [Internet]. 2016;36(4):252–61. Available from: http://dx.doi.org/10.1016/j.semnephrol.2016.05.002

373. Tyagi S, Salier J, Lal SK. The Liver-Specific Human ⎵ 1 -Microglobulin / Bikunin Precursor (AMBP) Is Capable of Self-Association. Act Biochem Biophys. 2002;399(1):66–72.

374. Bo A, Lödgbeg L, Berggärd T, Osmark P, Lindqvist A. a 1 -Microglobulin : a yellow-brown lipocalin. Biochim Biophys Acta. 2000;1482:172–84.

375. Zhuo L, Yoneda M, Zhao M, Yingsung W, Yoshida N, Kitagawa Y, et al. Defect in SHAP-Hyaluronan Complex Causes Severe. J Biol Chem. 2001;276:7963–9.

376. Glorieux G, Mullen W, Duranton F, Filip S, Gayrard N, Husi H, et al. New insights in molecular mechanisms involved in chronic kidney disease using high-resolution plasma proteome analysis. Nephrol Dial Transplant. 2015;(July):1842–52.

USC UNIVERSIDADE DE SANTIAGO DE COMPOSTELA

377. Greenberg JH, Abraham AG, Xu Y, Schelling JR, Feldman HI, Sabbisetti VS, et al. Urine Biomarkers of Kidney Tubule Health , Injury , and In fl ammation are Associated with Progression of CKD in Children. 2021;2664–77.

378. Robles NR, Lopez Gomez J, Garcia Pino G, Valladares J, Hernandez Gallego R, Cerezo I. Alpha-1-microglobulin: Prognostic value in chronic kidney disease. Med Clínica (English Ed. 2021 Oct 22;157(8):368–70.

379. Preissner KT, Seiffert D. Role of vitronectin and its receptors in haemostasis and vascular remodeling. Thromb Res. 1998;89(1):1–21.

380. Carreras-Planella L, Cucchiari D, Cañas L, Juega J, Franquesa M, Bonet J, et al. Urinary vitronectin identifies patients with high levels of fibrosis in kidney grafts. J Nephrol [Internet]. 2021;34(3):861–74. Available from: https://doi.org/10.1007/s40620-020-00886-y

381. Hassan EA, Khaleel FM. Serum vitronectin and related molecules in chronic kidney disease. Medico-Legal Updat. 2020;20(2):339–47.

382. Lai X, Bacallao RL, Blazer-Yost BL, Hong D, Mason SB, Witzmann FA. Characterization of the renal cyst fluid proteome in autosomal dominant polycystic kidney disease (ADPKD) patients. Proteomics - Clin Appl. 2008;2(7–8):1140–52.

383. Díaz de León-Martínez L, Ortega-Romero M, Gavilán-García A, Barbier OC, Carrizalez-Yáñez L, Van-Brusel E, et al. Correction to: Assessment of biomarkers of early kidney damage and exposure to pollutants in artisanal mercury mining workers from Mexico (Environmental Science and Pollution Research, (2022), 29, 9, (13333-13343), 10.1007/s11356-021-16628-x). Environ Sci Pollut Res. 2022;29(9):13344.

384. Jeon HJ, Shin DH, Oh J, Kee YK, Park JY, Ko K, et al. Urinary Retinol-Binding Protein 4 is Associated With Renal Function and Rapid Renal Function Decline in Kidney Transplant Recipients. Transplant Proc. 2022 Mar 1;54(2):362–6.

385. Nanayakkara N. Evaluating serum RBP4 as an auxiliary biomarker for CKDu diagnosis. Res Sq. 2022;

386. Kang M, Kwon S, Lee W, Kim Y, Bae E, Lee J, et al. Soluble transferrin receptor can predict all-cause mortality regardless of anaemia and iron storage status. Sci Rep [Internet]. 2022 Dec 13;12(1):11911. Available from: https://www.nature.com/articles/s41598-022-15674-w

387. Hou Y-P, Wang C, Mao X-Y, Zhang M-Z, Li B. Roxadustat regulates iron metabolism in dialysis-dependent and non-dialysis-dependent chronic kidney disease patients: A meta-analysis. J Formos Med Assoc [Internet]. 2022 Jul; Available from: https://linkinghub.elsevier.com/retrieve/pii/S0929664622002479

388. Chan GC-K, Than WH, Kwan BC-H, Lai K-B, Chan RC-K, Teoh JY-C, et al. Adipose

USC DE SANTIAGO DE COMPOSTELA

and serum zinc alpha-2-glycoprotein (ZAG) expressions predict longitudinal change of adiposity, wasting and predict survival in dialysis patients. Sci Rep. 2022 Dec;12(1).

389. Sörensen-Zender I, Rong S, Haller H, Schmitt R. The Therapeutic Potential of Zinc-Alpha2-Glycoprotein (AZGP1) in Fibrotic Kidney Disease. Int J Mol Sci. 2022 Jan 1;23(2).

390. Vivekanandan-Giri A, Slocum JL, Buller CL, Basrur V, Ju W, Pop-Busui R, et al. Urine Glycoprotein Profile Reveals Novel Markers for Chronic Kidney Disease. Int J Proteomics. 2011;2011:1–18.

391. Nistala R, Savin V. Diabetes, hypertension, and chronic kidney disease progression: Role of DPP4. Am J Physiol - Ren Physiol. 2017;312(4):F661–70.

392. Schaefer L, Raslik I, Gröne H, Schönherr E, Macakova K, Ugorcakova J, et al. Small proteoglycans in human diabetic nephropathy: discrepancy between glomerular expression and protein accumulation of decorin, biglycan, lumican, and fibromodulin. FASEB J. 2001;15(3):559–61.

393. Kaltenecker CC, Domenig O, Kopecky C, Antlanger M, Poglitsch M, Berlakovich G, et al. Critical Role of Neprilysin in Kidney Angiotensin Metabolism. Circ Res. 2020;127(5):593–606.

394. Judge P, Haynes R, Landray MJ, Baigent C. Neprilysin inhibition in chronic kidney disease. Nephrol Dial Transplant. 2015;30(5):738–43.

395. Mafra D, Cozzolino SMF. Erythrocyte zinc and carbonic anhydrase levels in nondialyzed chronic kidney disease patients. Clin Biochem. 2004;37(1):67–71.

396. Clemmens H, Lambert DW. Extracellular vesicles: Translational challenges and opportunities. Biochem Soc Trans. 2018;46(5):1073–82.

397. Ramirez MI, Amorim MG, Gadelha C, Milic I, Welsh JA, Freitas VM, et al. Technical challenges of working with extracellular vesicles. Nanoscale. 2018;10(3):881–906.

398. Keerthikumar S, Gangoda L, Gho YS, Mathivanan S. Bioinformatics tools for extracellular vesicles research. Methods Mol Biol. 2017;1545:189–96.

399. Crescitelli R, Lässer C, Lötvall J. Isolation and characterization of extracellular vesicle subpopulations from tissues. Nat Protoc. 2021;16(3):1548–80.

400. Lv C yan, Ding W jun, Wang Y li, Zhao Z yi, Li J hui, Chen Y, et al. A PEG-based method for the isolation of urinary exosomes and its application in renal fibrosis diagnostics using cargo miR-29c and miR-21 analysis. Int Urol Nephrol [Internet]. 2018;50(5):973–82. Available from: https://doi.org/10.1007/s11255-017-1779-4

401. Fernández-Llama P, Khositseth S, Gonzales PA, Star RA, Pisitkun T, Knepper MA. Tamm-Horsfall protein and urinary exosome isolation. Kidney Int [Internet]. 2010 Apr

USC UNIVERSIDADE DE SANTIAGO DE COMPOSTELA

2 [cited 2022 Jul 22];77(8):736–42. Available from: http://www.kidney-international.org/article/S0085253815543378/fulltext

402. Gonzalez-Begne M, Lu B, Han X, Hagen FK, Hand AR, Melvin JE, et al. Proteomic analysis of human parotid gland exosomes by multidimensional protein identification technology (MudPIT). J Proteome Res. 2009 Mar 6;8(3):1304–14.

403. Musante L, Saraswat M, Duriez E, Byrne B, Ravidà A, Domon B, et al. Biochemical and physical characterisation of urinary nanovesicles following CHAPS treatment. PLoS One [Internet]. 2012 Jul 12 [cited 2021 Dec 16];7(7). Available from: https://pubmed.ncbi.nlm.nih.gov/22808001/

404. Liu Z, Cauvi DM, Bernardino EMA, Lara B, Lizardo RE, Hawisher D, et al. Isolation and characterization of human urine extracellular vesicles. Cell Stress Chaperones. 2018;23(5):943–53.

405. Sódar BW, Kovács Á, Visnovitz T, Pállinger É, Vékey K, Pocsfalvi G, et al. Best practice of identification and proteomic analysis of extracellular vesicles in human health and disease. Expert Rev Proteomics [Internet]. 2017;14(12):1073–90. Available from: http://dx.doi.org/10.1080/14789450.2017.1392244

406. Van Deun J, Mestdagh P, Sormunen R, Cocquyt V, Vermaelen K, Vandesompele J, et al. The impact of disparate isolation methods for extracellular vesicles on downstream RNA profiling. J Extracell Vesicles. 2014;3(1).

407. Gardiner C, Vizio D Di, Sahoo S, Théry C, Witwer KW, Wauben M, et al. Techniques used for the isolation and characterization of extracellular vesicles: Results of a worldwide survey. J Extracell Vesicles. 2016;5(1).

408. Bang C, Thum T. Exosomes: New players in cell-cell communication. Int J Biochem Cell Biol [Internet]. 2012;44(11):2060–4. Available from: http://dx.doi.org/10.1016/j.biocel.2012.08.007

409. Morelli AE. Exosomes: From Cell Debris to Potential Biomarkers in Transplantation. Transplantation. 2017;101(10):2275–6.

410. Musante L, Tataruch-Weinert D, Kerjaschki D, Henry M, Meleady P, Holthofer H. Residual urinary extracellular vesicles in ultracentrifugation supernatants after hydrostatic filtration dialysis enrichment. J Extracell Vesicles. 2017 Dec 1;6(1).

411. Breitwieser K, Koch LF, Tertel T, Proestler E, Burgers LD, Lipps C, et al. Detailed Characterization of Small Extracellular Vesicles from Different Cell Types Based on Tetraspanin Composition by ExoView R100 Platform. 2022;

412. Hemler ME. Targeting of tetraspanin proteins - Potential benefits and strategies. Nat Rev Drug Discov. 2008;7(9):747–58.

413. Schröder J, Lüllmann-Rauch R, Himmerkus N, Pleines I, Nieswandt B, Orinska Z, et al. Deficiency of the Tetraspanin CD63 Associated with Kidney Pathology but Normal Lysosomal Function. Mol Cell Biol. 2009;29(4):1083–94.

414. Titu S, Grapa CM, Mocan T, Balacescu O, Irimie A. Tetraspanins: Physiology, colorectal cancer development, and nanomediated applications. Cancers (Basel). 2021;13(22):1–17.

415. Ding H, Li LX, Harris PC, Yang J, Li X, H D, et al. Extracellular vesicles and exosomes generated from cystic renal epithelial cells promote cyst growth in autosomal dominant polycystic kidney disease. Nat Commun [Internet]. 2021 Dec 1 [cited 2021 Oct 30];12(1):1–18. Available from: https://doi.org/10.1038/s41467-021-24799-x

416. Fujita K, Kume H, Matsuzaki K, Kawashima A, Ujike T, Nagahara A, et al. Proteomic analysis of urinary extracellular vesicles from high Gleason score prostate cancer. Sci Rep. 2017;7(February):1–9.

USC
UNIVERSIDADE DE SANTIAGO DE COMPOSTELA

USC
UNIVERSIDADE
DE SANTIAGO
DE COMPOSTELA

SUPPLEMENTAL MATERIAL

1. SUPPLEMENTAL FIGURES

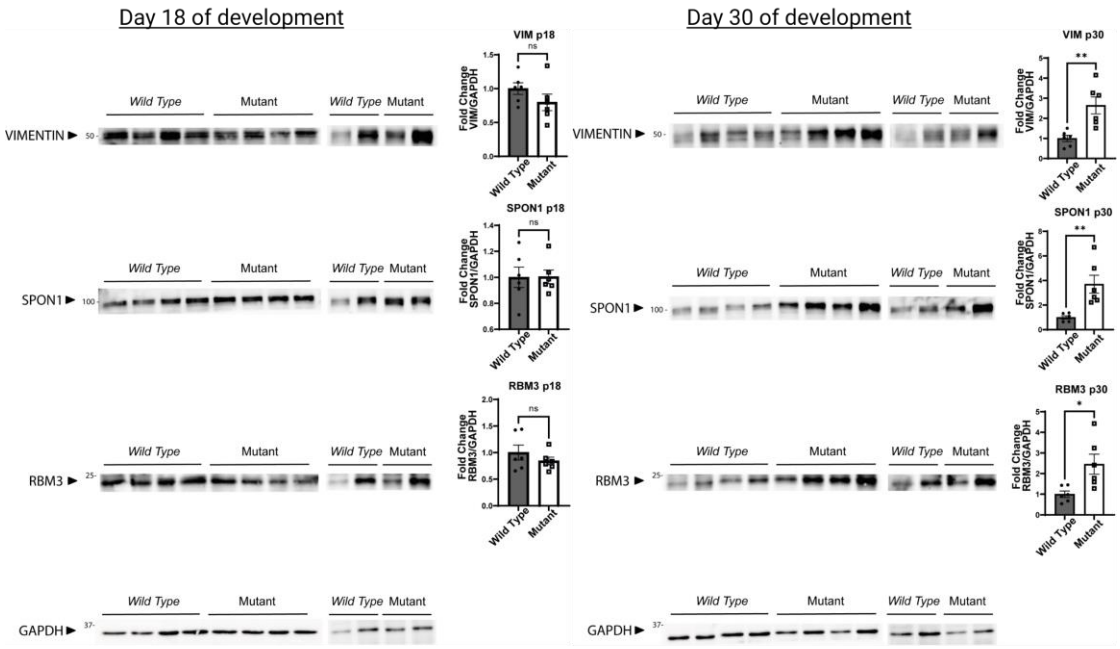

Supplementary Figure 1. Full Western Blots of protein validations. Full WBs are shown of shared proteins at postnatal day 18 and day 30: Vimentin, Spondin-1 and RNA-binding protein 3. GAPDH was used as housekeeping. Bars represent means ± SEM. Student`s t-test with two-tail was used and a value of P<0.05 was considered significant. * p<0.05, ** p<0.01

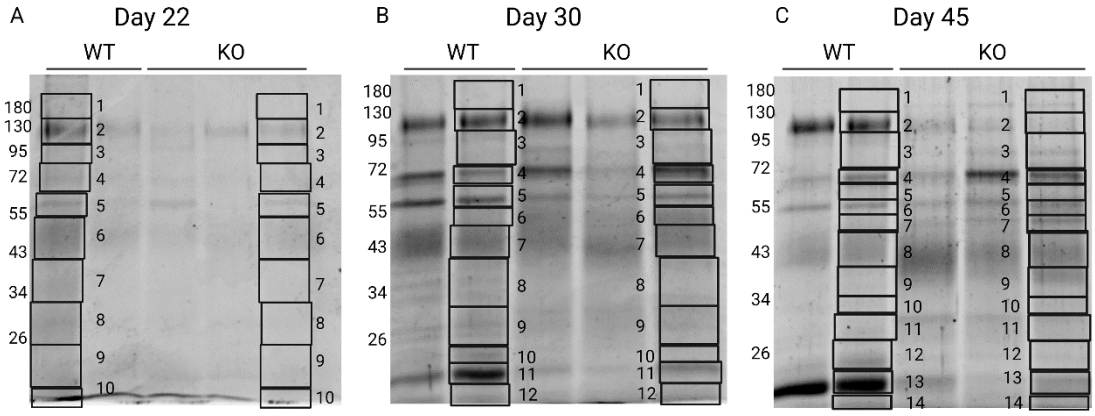

Supplementary Figure 2. Schematic representation of sequenced bands by mass spectrometry of *Wild Type* and Mutant urine samples of mice at postnatal day 22, 30 and 45.

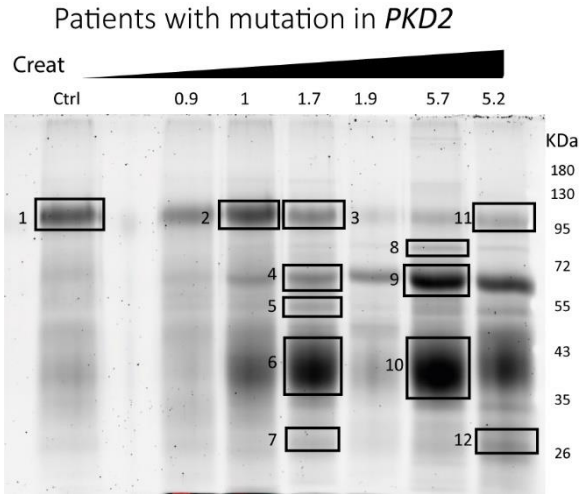

Supplementary Figure 3. Schematic representation of sequenced bands by mass spectrometry of ExoGAG pellet of patients with mutation in *PKD2*. Results in Supplementary Tables.

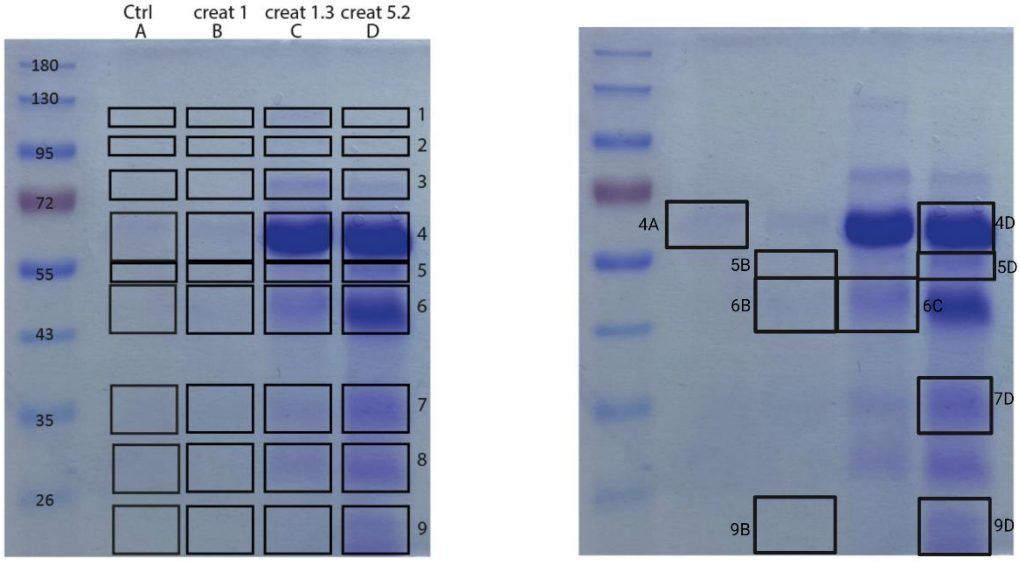

Supplementary Figure 4. Schematic representation of sequenced bands by mass spectrometry of ExoGAG supernatants of patients with mutation in *PKD2*. Left, completed scheme of mass spectrometry sequenced bands and right, most representative bands for identified biomarkers. Staining with Colloidal Coomassie. Results in Supplementary Tables.

USC
UNIVERSIDADE DE SANTIAGO DE COMPOSTELA

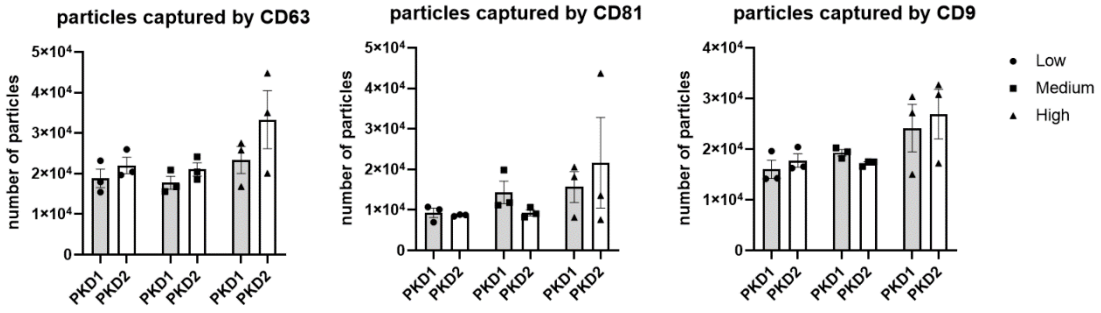

Supplementary Figure 5. Number of particles captured by each Tetraspanin in samples of patients with mutation in *PKD1* and *PKD2*, with renal damage according to serum creatinine value.

USC
UNIVERSIDADE DE SANTIAGO DE COMPOSTELA

2. SUPPLEMENTAL TABLES

Supplementary Table 1. Proteins list with two-fold increase or decrease abundance and an adjusted p-value <0,05 (according to parametric Student`s t-test) comparing Mutant and Wild Type polycystic kidneys at postnatal day 30.

Entry Name	UniProt Name	Name	p-value		Fold Change Mut to WT
P11672	NGAL_MOUSE	Neutrophil gelatinase-associated lipocalin	3,23E-04	↑	58,82
P12246	SAMP_MOUSE	Serum amyloid P-component	9,27E-03	↑	19,3
O89053	COR1A_MOUSE	Coronin-1A	8,45E-07	↑	13,01
Q8K354	CBR3_MOUSE	Carbonyl reductase [NADPH] 3	2,46E-03	↑	11,51
Q60605	MYL6_MOUSE	Myosin light polypeptide 6	2,05E-03	↑	9,76
P61514	RL37A_MOUSE	60S ribosomal protein L37a	1,23E-08	↑	8,62
P29699	FETUA_MOUSE	Alpha-2-HS-glycoprotein	4,68E-03	↑	7,42
Q8VCM7	FIBG_MOUSE	Fibrinogen gamma chain	6,06E-06	↑	6,59
Q64462	CP4B1_MOUSE	Cytochrome P450 4B1	2,63E-11	↑	6,31
Q62159	RHOC_MOUSE	Rho-related GTP-binding protein RhoC	5,00E-08	↑	6,25
O35343	IMA3_MOUSE	Importin subunit alpha-3	1,20E-03	↑	5,61
P01872	IGHM_MOUSE	Immunoglobulin heavy constant mu	1,44E-02	↑	5,55
Q91X72	HEMO_MOUSE	Hemopexin	1,87E-03	↑	5,45
Q60590	A1AG1_MOUSE	Alpha-1-acid glycoprotein 1	2,36E-03	↑	5,15
Q61147	CERU_MOUSE	Ceruloplasmin	8,02E-06	↑	4,83
O08677	KNG1_MOUSE	Kininogen-1	4,24E-03	↑	4,81
Q921I1	TRFE_MOUSE	Serotransferrin	8,94E-04	↑	4,79
O35639	ANXA3_MOUSE	Annexin A3	9,54E-08	↑	4,75
Q8K0E8	FIBB_MOUSE	Fibrinogen beta chain	7,32E-05	↑	4,69
Q06890	CLUS_MOUSE	Clusterin	1,73E-05	↑	4,58
E9PV24	FIBA_MOUSE	Fibrinogen alpha chain	8,29E-06	↑	4,57
O89079	COPE_MOUSE	Coatomer subunit epsilon	5,78E-05	↑	4,54
Q8CFX1	G6PE_MOUSE	GDH/6PGL endoplasmic bifunctional protein	4,75E-08	↑	4,42
Q00896	A1AT3_MOUSE	Alpha-1-antitrypsin 1-3	9,67E-04	↑	4
Q61646	HPT_MOUSE	Haptoglobin	1,90E-02	↑	3,9
Q61233	PLSL_MOUSE	Plastin-2	3,28E-05	↑	3,77
P10107	ANXA1_MOUSE	Annexin A1	1,61E-06	↑	3,74
Q04447	KCRB_MOUSE	Creatine kinase B-type	1,88E-05	↑	3,71
Q8VDD5	MYH9_MOUSE	Myosin-9	9,82E-11	↑	3,64
O55135	IF6_MOUSE	Eukaryotic translation initiation factor 6	2,62E-04	↑	3,63
Q62470	ITA3_MOUSE	Integrin alpha-3	1,38E-04	↑	3,61
P37804	TAGL_MOUSE	Transgelin	2,46E-07	↑	3,58
P07724	ALBU_MOUSE	Albumin	1,53E-04	↑	3,56
P18242	CATD_MOUSE	Cathepsin D	9,63E-06	↑	3,55
P50543	S10AB_MOUSE	Protein S100-A11	6,25E-08	↑	3,55
P20918	PLMN_MOUSE	Plasminogen	4,73E-03	↑	3,43
P0C0A3	CHMP6_MOUSE	Charged multivesicular body protein 6	1,08E-02	↑	3,42
Q80X19	COEA1_MOUSE	Collagen alpha-1(XIV) chain	6,99E-04	↑	3,42
P63087	PP1G_MOUSE	Serine/threonine-protein phosphatase PP1-gamma catalytic subunit	2,20E-03	↑	3,32
Q60854	SPB6_MOUSE	Serpin B6	2,62E-08	↑	3,31

USC UNIVERSIDADE DE SANTIAGO DE COMPOSTELA

P07356	ANXA2_MOUSE	Annexin A2	1,64E-07	↑	3,31
P39061	COIA1_MOUSE	Collagen alpha-1(XVIII) chain	1,57E-10	↑	3,3
Q62465	VAT1_MOUSE	Synaptic vesicle membrane protein VAT-1 homolog	5,91E-05	↑	3,24
P01027	CO3_MOUSE	Complement C3	9,89E-04	↑	3,17
P53996	CNBP_MOUSE	Cellular nucleic acid-binding protein	2,21E-04	↑	3,16
Q69ZN7	MYOF_MOUSE	Myoferlin	2,75E-05	↑	3,14
Q00898	A1AT5_MOUSE	Alpha-1-antitrypsin 1-5	7,91E-03	↑	3,08
Q8BTM8	FLNA_MOUSE	Filamin-A	9,75E-16	↑	2,98
P19324	SERPH_MOUSE	Serpin H1	2,33E-09	↑	2,94
Q91WP6	SPA3N_MOUSE	Serine protease inhibitor A3N	1,33E-03	↑	2,93
Q61247	A2AP_MOUSE	Alpha-2-antiplasmin	1,19E-03	↑	2,92
P61804	DAD1_MOUSE	Dolichyl-diphosphooligosaccharide--protein glycosyltransferase subunit DAD1	1,30E-05	↑	2,89
P01867	IGG2B_MOUSE	Ig gamma-2B chain C region	1,35E-04	↑	2,81
P11859	ANGT_MOUSE	Angiotensinogen	3,20E-03	↑	2,8
O09043	NAPSA_MOUSE	Napsin-A	4,15E-06	↑	2,8
P14602	HSPB1_MOUSE	Heat shock protein beta-1	1,20E-02	↑	2,79
Q8C2Q3	RBM14_MOUSE	RNA-binding protein 14	3,05E-03	↑	2,79
P62270	RS18_MOUSE	40S ribosomal protein S18	2,64E-05	↑	2,79
Q9R1Q7	PLP2_MOUSE	Proteolipid protein 2	1,66E-06	↑	2,77
Q61838	PZP_MOUSE	Pregnancy zone protein	8,40E-05	↑	2,75
P60867	RS20_MOUSE	40S ribosomal protein S20	1,73E-02	↑	2,69
P07759	SPA3K_MOUSE	Serine protease inhibitor A3K	5,30E-04	↑	2,62
P24547	IMDH2_MOUSE	Inosine-5'-monophosphate dehydrogenase 2	3,33E-03	↑	2,59
Q60847	COCA1_MOUSE	Collagen alpha-1(XII) chain	1,06E-06	↑	2,55
Q9Z0K8	VNN1_MOUSE	Pantetheinase	1,37E-11	↑	2,51
P22599	A1AT2_MOUSE	Alpha-1-antitrypsin 1-2	1,36E-02	↑	2,46
Q8BGQ7	SYAC_MOUSE	Alanine--tRNA ligase, cytoplasmic	3,22E-05	↑	2,44
O35744	CHIL3_MOUSE	Chitinase-like protein 3	4,39E-05	↑	2,43
P06909	CFAH_MOUSE	Complement factor H	1,31E-04	↑	2,41
Q60598	SRC8_MOUSE	Src substrate cortactin	6,79E-05	↑	2,41
Q9JKF1	IQGA1_MOUSE	Ras GTPase-activating-like protein IQGAP1	2,99E-07	↑	2,4
Q99P72	RTN4_MOUSE	Reticulon-4	9,81E-04	↑	2,4
P06728	APOA4_MOUSE	Apolipoprotein A-IV	7,85E-03	↑	2,38
P23953	EST1C_MOUSE	Carboxylesterase 1C	3,76E-04	↑	2,33
P62889	RL30_MOUSE	60S ribosomal protein L30	7,70E-04	↑	2,32
Q8BMK4	CKAP4_MOUSE	Cytoskeleton-associated protein 4	9,89E-08	↑	2,31
P42208	SEPT2_MOUSE	Septin-2	4,26E-07	↑	2,3
A6X935	ITIH4_MOUSE	Inter alpha-trypsin inhibitor, heavy chain 4	5,91E-06	↑	2,3
P18760	COF1_MOUSE	Cofilin-1	1,00E-07	↑	2,22
P07309	TTHY_MOUSE	Transthyretin	8,35E-04	↑	2,22
Q3U7R1	ESYT1_MOUSE	Extended synaptotagmin-1	2,61E-10	↑	2,22
Q91W90	TXND5_MOUSE	Thioredoxin domain-containing protein 5	7,49E-06	↑	2,18
Q00897	A1AT4_MOUSE	Alpha-1-antitrypsin 1-4	4,04E-03	↑	2,18
P11679	K2C8_MOUSE	Keratin, type II cytoskeletal 8	2,15E-05	↑	2,17
Q9JJU8	SH3L1_MOUSE	SH3 domain-binding glutamic acid-rich-like protein	5,22E-07	↑	2,15

USC UNIVERSIDADE DE SANTIAGO DE COMPOSTELA

P28665	MUG1_MOUSE	Murinoglobulin-1	2,06E-03	↑	2,15
P84096	RHOG_MOUSE	Rho-related GTP-binding protein RhoG	4,91E-04	↑	2,15
P26645	MARCS_MOUSE	Myristoylated alanine-rich C-kinase substrate	8,95E-08	↑	2,14
Q9WVA4	TAGL2_MOUSE	Transgelin-2	2,83E-06	↑	2,11
O89017	LGMN_MOUSE	Legumain	2,62E-04	↑	2,1
Q62188	DPYL3_MOUSE	Dihydropyrimidinase-related protein 3	1,07E-05	↑	2,1
P68033	ACTC_MOUSE	Actin, alpha cardiac muscle 1	6,08E-05	↑	2,09
Q80X90	FLNB_MOUSE	Filamin-B	6,48E-11	↑	2,04
O08529	CAN2_MOUSE	Calpain-2 catalytic subunit	2,07E-08	↑	2,03
Q00623	APOA1_MOUSE	Apolipoprotein A-I	5,72E-04	↑	2,01
Q02257	PLAK_MOUSE	Junction plakoglobin	3,48E-05	↑	2,01
G3X9C2	FBX50_MOUSE	F-box only protein 50	1,71E-09	↓	0,18
Q8VCH0	THIKB_MOUSE	3-ketoacyl-CoA thiolase B, peroxisomal	1,51E-02	↓	0,22
P52503	NDUS6_MOUSE	NADH dehydrogenase [ubiquinone] iron-sulfur protein 6, mitochondrial	1,81E-04	↓	0,23
Q5M8N4	D39U1_MOUSE	Epimerase family protein SDR39U1	6,35E-06	↓	0,23
Q921S7	RM37_MOUSE	39S ribosomal protein L37, mitochondrial	5,81E-07	↓	0,23
Q9QXN5	MIOX_MOUSE	Inositol oxygenase	7,61E-06	↓	0,28
Q9WVT6	CAH14_MOUSE	Carbonic anhydrase 14	1,35E-02	↓	0,28
Q9Z1N5	DX39B_MOUSE	Spliceosome RNA helicase Ddx39b	1,65E-04	↓	0,3
Q78JN3	ECI3_MOUSE	Enoyl-CoA delta isomerase 3, peroxisomal	2,88E-02	↓	0,31
P97493	THIOM_MOUSE	Thioredoxin, mitochondrial	3,27E-06	↓	0,33
P12658	CALB1_MOUSE	Calbindin	2,60E-13	↓	0,33
O54749	CP2J5_MOUSE	Cytochrome P450 2J5	6,79E-05	↓	0,34
Q923I7	SC5A2_MOUSE	Sodium/glucose cotransporter 2	6,35E-09	↓	0,34
Q78JT3	3HAO_MOUSE	3-hydroxyanthranilate 3,4-dioxygenase	4,89E-07	↓	0,35
Q99KR7	PPIF_MOUSE	Peptidyl-prolyl cis-trans isomerase F, mitochondrial	4,44E-02	↓	0,36
Q91VA0	ACSM1_MOUSE	Acyl-coenzyme A synthetase ACSM1, mitochondrial	8,29E-07	↓	0,37
P50518	VATE1_MOUSE	V-type proton ATPase subunit E 1	1,30E-05	↓	0,37
P99028	QCR6_MOUSE	Cytochrome b-c1 complex subunit 6, mitochondrial	2,99E-02	↓	0,37
Q9D964	GATM_MOUSE	Glycine amidinotransferase, mitochondrial	2,01E-08	↓	0,38
Q9DCZ4	MIC26_MOUSE	MICOS complex subunit Mic26	9,63E-12	↓	0,38
Q9D1I5	MCEE_MOUSE	Methylmalonyl-CoA epimerase, mitochondrial	1,07E-05	↓	0,39
Q9WUR9	KAD4_MOUSE	Adenylate kinase 4, mitochondrial	1,12E-10	↓	0,39
O88338	CAD16_MOUSE	Cadherin-16	8,64E-12	↓	0,39
O70503	DHB12_MOUSE	Very-long-chain 3-oxoacyl-CoA reductase	1,77E-03	↓	0,41
Q8QZW3	F151A_MOUSE	Protein FAM151A	9,53E-05	↓	0,42
P16460	ASSY_MOUSE	Argininosuccinate synthase	4,23E-09	↓	0,42
Q04646	ATNG_MOUSE	Sodium/potassium-transporting ATPase subunit gamma	8,01E-10	↓	0,44
Q01405	SC23A_MOUSE	Protein transport protein Sec23A	2,62E-02	↓	0,44
Q8R3P0	ACY2_MOUSE	Aspartoacylase	1,79E-02	↓	0,44
Q64442	DHSO_MOUSE	Sorbitol dehydrogenase	8,04E-13	↓	0,44
Q9NYQ2	HAOX2_MOUSE	Hydroxyacid oxidase 2	3,52E-10	↓	0,44
P70691	UD12_MOUSE	UDP-glucuronosyltransferase 1-2	1,27E-12	↓	0,44

USC UNIVERSIDADE DE SANTIAGO DE COMPOSTELA

Q3ULD5	MCCB_MOUSE	Methylcrotonoyl-CoA carboxylase beta chain, mitochondrial	4,62E-07	↓	0,45
P70404	IDHG1_MOUSE	Isocitrate dehydrogenase [NAD] subunit gamma 1, mitochondrial	5,07E-04	↓	0,45
Q99MZ7	PECR_MOUSE	Peroxisomal trans-2-enoyl-CoA reductase	4,78E-09	↓	0,45
Q9CQJ8	NDUB9_MOUSE	NADH dehydrogenase [ubiquinone] 1 beta subcomplex subunit 9	7,32E-09	↓	0,45
P97816	S100G_MOUSE	Protein S100-G	2,68E-07	↓	0,45
Q8VDN2	AT1A1_MOUSE	Sodium/potassium-transporting ATPase subunit alpha-1	1,49E-10	↓	0,45
P14094	AT1B1_MOUSE	Sodium/potassium-transporting ATPase subunit beta-1	8,37E-11	↓	0,46
Q9WU79	PROD_MOUSE	Proline dehydrogenase 1, mitochondrial	5,11E-05	↓	0,46
Q9DCS9	NDUBA_MOUSE	NADH dehydrogenase [ubiquinone] 1 beta subcomplex subunit 10	2,29E-05	↓	0,46
P40936	INMT_MOUSE	Indolethylamine N-methyltransferase	1,88E-03	↓	0,47
P70290	EM55_MOUSE	55 kDa erythrocyte membrane protein	6,23E-05	↓	0,47
O88986	KBL_MOUSE	2-amino-3-ketobutyrate coenzyme A ligase, mitochondrial	1,31E-09	↓	0,47
Q9D880	TIM50_MOUSE	Mitochondrial import inner membrane translocase subunit TIM50	4,85E-02	↓	0,47
Q8K0L3-2	ACSM2_MOUSE	Isoform 2 of Acyl-coenzyme A synthetase ACSM2, mitochondrial	7,47E-08	↓	0,47
Q99NB1	ACS2L_MOUSE	Acetyl-coenzyme A synthetase 2-like, mitochondrial	4,06E-10	↓	0,48
Q8CIM7	CP2DQ_MOUSE	Cytochrome P450 2D26	8,22E-07	↓	0,48
Q9WVM8	AADAT_MOUSE	Kynurenine/alpha-aminoadipate aminotransferase, mitochondrial	2,96E-08	↓	0,48
Q99JW5	EPCAM_MOUSE	Epithelial cell adhesion molecule	1,53E-02	↓	0,49
Q9WUR2	ECI2_MOUSE	Enoyl-CoA delta isomerase 2	2,77E-02	↓	0,49
Q8R2N1	AQP3_MOUSE	Aquaporin-3	3,52E-02	↓	0,49
P02088	HBB1_MOUSE	Hemoglobin subunit beta-1	1,00E-03	↓	0,5
P09671	SODM_MOUSE	Superoxide dismutase [Mn], mitochondrial	2,66E-15	↓	0,5
P06281	RENI1_MOUSE	Renin-1	5,49E-03	↓	0,5
P01942	HBA_MOUSE	Hemoglobin subunit alpha	9,01E-08	↓	0,5

Supplementary Table 2. Proteins list with two-fold increase or decrease abundance and an adjusted p-value <0,05 (according to parametric Student`s t-test) comparing Mutant and Wild Type polycystic kidneys at postnatal day 18

Entry Name	UniProt Name	Name	p-value		Fold Change Mut to WT
Q9CZB0	C560_MOUSE	Succinate dehydrogenase cytochrome b560 subunit, mitochondrial	1,81E-03	↓	0,25
Q61735	CD47_MOUSE	Leukocyte surface antigen CD47	1,46E-02	↓	0,34
Q9EPL8	IPO7_MOUSE	Importin-7	2,07E-02	↓	0,35
Q5U5V2	HYKK_MOUSE	Hydroxylysine kinase	1,37E-02	↓	0,37
P02088	HBB1_MOUSE	Hemoglobin subunit beta-1	1,32E-02	↓	0,39
P70195	PSB7_MOUSE	Proteasome subunit beta type-7	3,86E-02	↓	0,39
P01942	HBA_MOUSE	Hemoglobin subunit alpha	1,00E-02	↓	0,39
P18894	OXDA_MOUSE	D-amino-acid oxidase	1,43E-02	↓	0,42
Q9CQQ7	AT5F1_MOUSE	ATP synthase F(0) complex subunit B1, mitochondrial	1,55E-03	↓	0,43
O70404	VAMP8_MOUSE	Vesicle-associated membrane protein 8	4,48E-02	↓	0,47
Q99LB2	DHRS4_MOUSE	Dehydrogenase/reductase SDR family member 4	2,98E-03	↓	0,47

Q9D826	SOX_MOUSE	Peroxisomal sarcosine oxidase	1,37E-02	↓	0,49
Q8R0Y8	S2542_MOUSE	Mitochondrial coenzyme A transporter SLC25A42	3,20E-02	↓	0,50
Q8BP67	RL24_MOUSE	60S ribosomal protein L24	4,09E-04	↓	0,50

Supplementary Table 3. Proteins list with two-fold increase or decrease abundance and an adjusted p-value <0,05 (according to parametric Student`s t-test) comparing Mutant and Wild Type polycystic kidneys at postnatal day 18.

Entry Name	UniProt Name	Name	p-value		Fold Change Mut to WT
P50295	ARY2_MOUSE	Arylamine N-acetyltransferase 2	2,52E-05	↑	7,60
Q8CGP7	H2A1K_MOUSE	Histone H2A type 1-K	1,45E-02	↑	5,81
Q8VHE0	SEC63_MOUSE	Translocation protein SEC63 homolog	6,92E-04	↑	5,63
Q61704	ITIH3_MOUSE	Inter-alpha-trypsin inhibitor heavy chain H3	1,16E-04	↑	3,47
Q8VCC9	SPON1_MOUSE	Spondin-1	4,97E-02	↑	3,18
P31938	MP2K1_MOUSE	Dual specificity mitogen-activated protein kinase kinase 1	8,11E-03	↑	3,16
Q61646	HPT_MOUSE	Haptoglobin	2,27E-02	↑	3,10
Q8CEE7	RDH13_MOUSE	Retinol dehydrogenase 13	2,54E-04	↑	3,09
Q9D1J3	SARNP_MOUSE	SAP domain-containing ribonucleoprotein	4,96E-02	↑	2,47
Q9CQ22	LTOR1_MOUSE	Ragulator complex protein LAMTOR1	3,72E-02	↑	2,46
P84099	RL19_MOUSE	60S ribosomal protein L19	2,31E-02	↑	2,31
P20152	VIME_MOUSE	Vimentin	3,21E-02	↑	2,29
O89086	RBM3_MOUSE	RNA-binding protein 3	4,88E-02	↑	2,16
Q3UFK8	FRMD8_MOUSE	FERM domain-containing protein 8	4,98E-02	↑	2,07
Q99KR7	PPIF_MOUSE	Peptidyl-prolyl cis-trans isomerase F, mitochondrial	1,99E-02	↓	0,43

Supplementary Table 4. Proteins list with two-fold increase or decrease abundance and an adjusted p-value <0,05 (according to parametric Student`s t-test) comparing Mutant and Wild Type polycystic kidneys at postnatal day 30.

Entry Name	UniProt Name	Name	p-value		Fold Change Mut to WT
Q60847	COCA1_MOUSE	Collagen alpha-1(XII) chain	4,76E-03	↑	9,59
Q62148	AL1A2_MOUSE	Retinal dehydrogenase 2	7,71E-04	↑	7,68
P21956	MFGM_MOUSE	Lactadherin	2,26E-02	↑	6,64
Q61576	FKB10_MOUSE	Peptidyl-prolyl cis-trans isomerase FKBP10	3,85E-04	↑	6,49
O89053	COR1A_MOUSE	Coronin-1A	3,49E-02	↑	6,44
Q61233	PLSL_MOUSE	Plastin-2	4,24E-02	↑	6,32
P03953	CFAD_MOUSE	Complement factor D	2,75E-02	↑	6,12
Q71FD7	FBLI1_MOUSE	Filamin-binding LIM protein 1	1,99E-03	↑	5,89
P01831	THY1_MOUSE	Thy-1 membrane glycoprotein	1,13E-03	↑	5,63
Q9R0E1	PLOD3_MOUSE	Procollagen-lysine,2-oxoglutarate 5-dioxygenase 3	3,13E-03	↑	5,60
P18242	CATD_MOUSE	Cathepsin D	1,87E-02	↑	5,36
Q8K1B8	URP2_MOUSE	Fermitin family homolog 3	1,18E-02	↑	5,30
Q5QNS5	HAVR1_MOUSE	Hepatitis A virus cellular receptor 1 homolog	4,45E-02	↑	5,14
P10923	OSTP_MOUSE	Osteopontin	4,73E-02	↑	5,10
P11679	K2C8_MOUSE	Keratin, type II cytoskeletal 8	2,19E-02	↑	5,02
Q64462	CP4B1_MOUSE	Cytochrome P450 4B1	3,51E-04	↑	4,90
Q61655	DD19A_MOUSE	ATP-dependent RNA helicase DDX19A	1,31E-04	↑	4,87

O35344	IMA4_MOUSE	Importin subunit alpha-4	1,46E-02	↑	4,85
P37804	TAGL_MOUSE	Transgelin	1,97E-02	↑	4,68
P15379	CD44_MOUSE	CD44 antigen	1,84E-02	↑	4,54
Q91Z67	SRGP2_MOUSE	SLIT-ROBO Rho GTPase-activating protein 2	2,92E-02	↑	4,45
P10107	ANXA1_MOUSE	Annexin A1	4,54E-02	↑	4,39
P50543	S10AB_MOUSE	Protein S100-A11	9,36E-03	↑	4,23
Q62188	DPYL3_MOUSE	Dihydropyrimidinase-related protein 3	6,04E-03	↑	4,23
Q3TZZ7	ESYT2_MOUSE	Extended synaptotagmin-2	2,89E-03	↑	4,20
Q69ZN7	MYOF_MOUSE	Myoferlin	1,88E-03	↑	4,20
O89086	RBM3_MOUSE	RNA-binding protein 3	4,31E-02	↑	4,20
O70456	1433S_MOUSE	14-3-3 protein sigma	1,29E-02	↑	4,19
A2A863	ITB4_MOUSE	Integrin beta-4	2,08E-02	↑	4,18
Q08093	CNN2_MOUSE	Calponin-2	3,02E-02	↑	4,03
O35639	ANXA3_MOUSE	Annexin A3	2,15E-02	↑	4,02
Q04447	KCRB_MOUSE	Creatine kinase B-type	1,49E-02	↑	3,96
P16045	LEG1_MOUSE	Galectin-1	2,92E-03	↑	3,95
Q8BMK4	CKAP4_MOUSE	Cytoskeleton-associated protein 4	2,18E-04	↑	3,93
Q99P72	RTN4_MOUSE	Reticulon-4	5,65E-03	↑	3,85
Q60854	SPB6_MOUSE	Serpin B6	4,60E-02	↑	3,80
Q91VW3	SH3L3_MOUSE	SH3 domain-binding glutamic acid-rich-like protein 3	2,15E-02	↑	3,78
P08207	S10AA_MOUSE	Protein S100-A10	2,08E-02	↑	3,73
Q922F4	TBB6_MOUSE	Tubulin beta-6 chain	2,68E-04	↑	3,63
Q8VDD5	MYH9_MOUSE	Myosin-9	7,98E-03	↑	3,61
P12265	BGLR_MOUSE	Beta-glucuronidase	2,88E-03	↑	3,59
P10833	RRAS_MOUSE	Ras-related protein R-Ras	3,70E-02	↑	3,51
Q07797	LG3BP_MOUSE	Galectin-3-binding protein	1,73E-02	↑	3,46
Q9DBS1	TMM43_MOUSE	Transmembrane protein 43	4,95E-02	↑	3,45
P07356	ANXA2_MOUSE	Annexin A2	2,01E-02	↑	3,42
P11087	CO1A1_MOUSE	Collagen alpha-1(I) chain	5,56E-03	↑	3,42
Q91YH5	ATLA3_MOUSE	Atlastin-3	1,89E-02	↑	3,33
Q9Z0U1	ZO2_MOUSE	Tight junction protein ZO-2	4,39E-03	↑	3,28
Q62465	VAT1_MOUSE	Synaptic vesicle membrane protein VAT-1 homolog	2,49E-02	↑	3,26
Q9QXS1	PLEC_MOUSE	Plectin	2,93E-03	↑	3,25
P97290	IC1_MOUSE	Plasma protease C1 inhibitor	4,03E-02	↑	3,23
Q8BTM8	FLNA_MOUSE	Filamin-A	4,33E-05	↑	3,21
Q8CFX1	G6PE_MOUSE	GDH/6PGL endoplasmic bifunctional protein	1,02E-02	↑	3,21
O09043	NAPSA_MOUSE	Napsin-A	4,16E-02	↑	3,20
Q8VCC9	SPON1_MOUSE	Spondin-1	5,14E-03	↑	3,20
P11276	FINC_MOUSE	Fibronectin	3,58E-02	↑	3,17
P13597	ICAM1_MOUSE	Intercellular adhesion molecule 1	6,53E-03	↑	3,07
P01029	CO4B_MOUSE	Complement C4-B	4,41E-02	↑	3,04
P62737	ACTA_MOUSE	Actin, aortic smooth muscle	6,50E-03	↑	3,03
Q9DCR2	AP3S1_MOUSE	AP-3 complex subunit sigma-1	4,50E-03	↑	3,01
Q9D7X3	DUS3_MOUSE	Dual specificity protein phosphatase 3	1,27E-02	↑	3,01
Q64449	MRC2_MOUSE	C-type mannose receptor 2	6,27E-06	↑	2,99
Q9WV32	ARC1B_MOUSE	Actin-related protein 2/3 complex subunit 1B	1,38E-02	↑	2,97
Q3UW53	NIBAN_MOUSE	Protein Niban	1,11E-02	↑	2,93
P41241	CSK_MOUSE	Tyrosine-protein kinase CSK	1,59E-02	↑	2,92
P97310	MCM2_MOUSE	DNA replication licensing factor MCM2	1,08E-02	↑	2,91
Q3THE2	ML12B_MOUSE	Myosin regulatory light chain 12B	1,76E-02	↑	2,88

P29416	HEXA_MOUSE	Beta-hexosaminidase subunit alpha	4,02E-02	↑	2,87
Q01279	EGFR_MOUSE	Epidermal growth factor receptor	3,88E-02	↑	2,84
O35114	SCRB2_MOUSE	Lysosome membrane protein 2	2,10E-02	↑	2,78
P05784	K1C18_MOUSE	Keratin, type I cytoskeletal 18	3,25E-02	↑	2,76
Q9WVH9	FBLN5_MOUSE	Fibulin-5	1,57E-02	↑	2,75
Q99KC8	VMA5A_MOUSE	von Willebrand factor A domain-containing protein 5A	6,89E-03	↑	2,74
Q9CSU0	RPR1B_MOUSE	Regulation of nuclear pre-mRNA domain-containing protein 1B	3,64E-02	↑	2,74
Q00519	XDH_MOUSE	Xanthine dehydrogenase/oxidase	8,99E-04	↑	2,71
Q8R2Y2	MUC18_MOUSE	Cell surface glycoprotein MUC18	5,23E-04	↑	2,71
Q9Z0K8	VNN1_MOUSE	Pantetheinase	6,44E-03	↑	2,62
Q9R1Q7	PLP2_MOUSE	Proteolipid protein 2	2,00E-02	↑	2,61
P60843	IF4A1_MOUSE	Eukaryotic initiation factor 4A-I	2,49E-02	↑	2,61
Q8C052	MAP1S_MOUSE	Microtubule-associated protein 1S	2,28E-02	↑	2,61
Q61033	LAP2A_MOUSE	Lamina-associated polypeptide 2, isoforms alpha/zeta	4,90E-02	↑	2,59
Q62219	TGFI1_MOUSE	Transforming growth factor beta-1-induced transcript 1 protein	4,65E-03	↑	2,59
Q61553	FSCN1_MOUSE	Fascin	2,92E-05	↑	2,58
P19324	SERPH_MOUSE	Serpin H1	5,91E-03	↑	2,55
P58771	TPM1_MOUSE	Tropomyosin alpha-1 chain	1,32E-02	↑	2,52
Q9D906	ATG7_MOUSE	Ubiquitin-like modifier-activating enzyme ATG7	2,16E-02	↑	2,52
Q4KML4	ABRAL_MOUSE	Costars family protein ABRACL	2,70E-02	↑	2,50
Q9WVA4	TAGL2_MOUSE	Transgelin-2	4,50E-02	↑	2,50
P68369	TBA1A_MOUSE	Tubulin alpha-1A chain	4,09E-03	↑	2,50
Q9JJU8	SH3L1_MOUSE	SH3 domain-binding glutamic acid-rich-like protein	1,76E-02	↑	2,49
Q9WUM4	COR1C_MOUSE	Coronin-1C	2,74E-03	↑	2,46
P20152	VIME_MOUSE	Vimentin	1,32E-02	↑	2,44
Q8BVQ5	PPME1_MOUSE	Protein phosphatase methylesterase 1	1,59E-02	↑	2,43
Q9DBG9	TX1B3_MOUSE	Tax1-binding protein 3	3,08E-02	↑	2,42
Q9R069	BCAM_MOUSE	Basal cell adhesion molecule	6,49E-03	↑	2,41
P84096	RHOG_MOUSE	Rho-related GTP-binding protein RhoG	2,06E-02	↑	2,40
P97315	CSRP1_MOUSE	Cysteine and glycine-rich protein 1	1,44E-02	↑	2,39
P10922	H10_MOUSE	Histone H1.0	2,79E-02	↑	2,39
P17047	LAMP2_MOUSE	Lysosome-associated membrane glycoprotein 2	1,65E-02	↑	2,38
Q9D6Z1	NOP56_MOUSE	Nucleolar protein 56	4,64E-02	↑	2,38
P70460	VASP_MOUSE	Vasodilator-stimulated phosphoprotein	9,27E-04	↑	2,37
P00493	HPRT_MOUSE	Hypoxanthine-guanine phosphoribosyltransferase	3,10E-02	↑	2,37
Q9ET54	PALLD_MOUSE	Palladin	4,69E-03	↑	2,36
Q3U7R1	ESYT1_MOUSE	Extended synaptotagmin-1	5,63E-03	↑	2,34
P70336	ROCK2_MOUSE	Rho-associated protein kinase 2	6,34E-03	↑	2,34
Q61210	ARHG1_MOUSE	Rho guanine nucleotide exchange factor 1	3,66E-03	↑	2,33
Q80X90	FLNB_MOUSE	Filamin-B	2,47E-03	↑	2,33
Q8C1B7	SEP11_MOUSE	Septin-11	2,76E-03	↑	2,32
Q61792	LASP1_MOUSE	LIM and SH3 domain protein 1	1,42E-02	↑	2,32
Q60605	MYL6_MOUSE	Myosin light polypeptide 6	2,69E-02	↑	2,31
P26645	MARCS_MOUSE	Myristoylated alanine-rich C-kinase substrate	2,09E-03	↑	2,30
Q9D154	ILEUA_MOUSE	Leukocyte elastase inhibitor A	1,49E-02	↑	2,28
P23780	BGAL_MOUSE	Beta-galactosidase	1,36E-02	↑	2,28
P39061	COIA1_MOUSE	Collagen alpha-1(XVIII) chain	4,00E-03	↑	2,28
P47713	PA24A_MOUSE	Cytosolic phospholipase A2	1,17E-02	↑	2,25

USC UNIVERSIDADE DE SANTIAGO DE COMPOSTELA

P18760	COF1_MOUSE	Cofilin-1	1,50E-02	↑	2,23
Q64727	VINC_MOUSE	Vinculin	2,79E-03	↑	2,22
Q62318	TIF1B_MOUSE	Transcription intermediary factor 1-beta	8,91E-03	↑	2,22
P47753	CAZA1_MOUSE	F-actin-capping protein subunit alpha-1	5,06E-04	↑	2,21
P40124	CAP1_MOUSE	Adenylyl cyclase-associated protein 1	8,35E-04	↑	2,18
Q8BX02	KANK2_MOUSE	KN motif and ankyrin repeat domain-containing protein 2	4,93E-02	↑	2,18
O35206	COFA1_MOUSE	Collagen alpha-1(XV) chain	1,96E-02	↑	2,18
Q9ESD7	DYSF_MOUSE	Dysferlin	2,79E-02	↑	2,17
P26041	MOES_MOUSE	Moesin	3,54E-05	↑	2,17
Q9EPB4	ASC_MOUSE	Apoptosis-associated speck-like protein containing a CARD	3,58E-02	↑	2,16
P49718	MCM5_MOUSE	DNA replication licensing factor MCM5	1,28E-02	↑	2,16
Q60604	ADSV_MOUSE	Adseverin	4,54E-02	↑	2,16
P68510	1433F_MOUSE	14-3-3 protein eta	5,17E-03	↑	2,16
Q64514	TPP2_MOUSE	Tripeptidyl-peptidase 2	3,56E-03	↑	2,16
Q91ZX7	LRP1_MOUSE	Prolow-density lipoprotein receptor-related protein 1	2,85E-02	↑	2,15
Q64674	SPEE_MOUSE	Spermidine synthase	1,22E-03	↑	2,12
P51885	LUM_MOUSE	Lumican	4,14E-02	↑	2,12
Q9JJ28	FLII_MOUSE	Protein flightless-1 homolog	2,73E-04	↑	2,10
Q8K297	GT251_MOUSE	Procollagen galactosyltransferase 1	7,81E-03	↑	2,10
Q9WTI7	MYO1C_MOUSE	Unconventional myosin-Ic	2,62E-02	↑	2,09
E9Q634	MYO1E_MOUSE	Unconventional myosin-Ie	1,10E-03	↑	2,09
O88342	WDR1_MOUSE	WD repeat-containing protein 1	4,56E-04	↑	2,08
Q8K209	AGRG1_MOUSE	Adhesion G-protein coupled receptor G1	1,10E-03	↑	2,08
Q60710	SAMH1_MOUSE	Deoxynucleoside triphosphate triphosphohydrolase SAMHD1	2,69E-04	↑	2,08
O08848	RO60_MOUSE	60 kDa SS-A/Ro ribonucleoprotein	2,91E-02	↑	2,07
O08529	CAN2_MOUSE	Calpain-2 catalytic subunit	2,01E-03	↑	2,07
Q9JKF1	IQGA1_MOUSE	Ras GTPase-activating-like protein IQGAP1	1,74E-02	↑	2,07
Q05793	PGBM_MOUSE	Basement membrane-specific heparan sulfate proteoglycan core protein	1,05E-02	↑	2,06
Q8BXZ1	TMX3_MOUSE	Protein disulfide-isomerase TMX3	2,94E-04	↑	2,06
Q80UG5	SEPT9_MOUSE	Septin-9	6,71E-03	↑	2,05
Q9R1P4	PSA1_MOUSE	Proteasome subunit alpha type-1	9,32E-03	↑	2,05
P62962	PROF1_MOUSE	Profilin-1	5,65E-03	↑	2,04
O09131	GSTO1_MOUSE	Glutathione S-transferase omega-1	3,66E-02	↑	2,03
Q60598	SRC8_MOUSE	Src substrate cortactin	5,98E-03	↑	2,03
Q9DCH4	EIF3F_MOUSE	Eukaryotic translation initiation factor 3 subunit F	1,18E-02	↑	2,02
Q9JM76	ARPC3_MOUSE	Actin-related protein 2/3 complex subunit 3	2,42E-02	↑	2,02
P24547	IMDH2_MOUSE	Inosine-5'-monophosphate dehydrogenase 2	1,56E-02	↑	2,01
Q9JKV1	ADRM1_MOUSE	Proteasomal ubiquitin receptor ADRM1	5,69E-03	↑	2,01
Q8C522	ENDD1_MOUSE	Endonuclease domain-containing 1 protein	3,01E-02	↑	2,01
P59999	ARPC4_MOUSE	Actin-related protein 2/3 complex subunit 4	1,08E-02	↑	2,01
A2AN08	UBR4_MOUSE	E3 ubiquitin-protein ligase UBR4	2,12E-03	↑	2,01
Q9WVT6	CAH14_MOUSE	Carbonic anhydrase 14	1,35E-04	↓	0,11
P0C0A3	CHMP6_MOUSE	Charged multivesicular body protein 6	1,39E-03	↓	0,12
G3X9C2	FBX50_MOUSE	F-box only protein 50	9,48E-04	↓	0,13
P61971	NTF2_MOUSE	Nuclear transport factor 2	2,88E-02	↓	0,22
Q99J94	SO1A6_MOUSE	Solute carrier organic anion transporter family member 1A6	3,23E-04	↓	0,22
P49429	HPPD_MOUSE	4-hydroxyphenylpyruvate dioxygenase	4,48E-04	↓	0,26

UBC UNIVERSIDADE BEIRA

Q8VC12	HUTU_MOUSE	Urocanate hydratase	5,19E-03	↓	0,28
P35762	CD81_MOUSE	CD81 antigen	8,59E-04	↓	0,29
P97493	THIOM_MOUSE	Thioredoxin, mitochondrial	5,33E-03	↓	0,29
Q9QXN5	MIOX_MOUSE	Inositol oxygenase	7,88E-04	↓	0,30
P12658	CALB1_MOUSE	Calbindin	8,45E-04	↓	0,30
Q99N96	RM01_MOUSE	39S ribosomal protein L1, mitochondrial	1,65E-04	↓	0,31
Q64FW2	RETST_MOUSE	All-trans-retinol 13,14-reductase	8,25E-03	↓	0,32
O88909	S22A8_MOUSE	Solute carrier family 22 member 8	2,28E-02	↓	0,33
P16331	PH4H_MOUSE	Phenylalanine-4-hydroxylase	1,79E-03	↓	0,33
Q04646	ATNG_MOUSE	Sodium/potassium-transporting ATPase subunit gamma	7,68E-03	↓	0,34
Q9DCC7	ISC2B_MOUSE	Isochorismatase domain-containing protein 2B	4,00E-04	↓	0,35
Q9D964	GATM_MOUSE	Glycine amidinotransferase, mitochondrial	2,62E-03	↓	0,35
Q9WVM8	AADAT_MOUSE	Kynurenine/alpha-aminoadipate aminotransferase, mitochondrial	1,13E-02	↓	0,35
Q923I7	SC5A2_MOUSE	Sodium/glucose cotransporter 2	6,76E-03	↓	0,35
O88338	CAD16_MOUSE	Cadherin-16	1,60E-03	↓	0,35
Q9D687	S6A19_MOUSE	Sodium-dependent neutral amino acid transporter B(0)AT1	1,95E-02	↓	0,37
Q91WN4	KMO_MOUSE	Kynurenine 3-monooxygenase	2,12E-03	↓	0,37
Q8QZW3	F151A_MOUSE	Protein FAM151A	9,85E-03	↓	0,38
Q9WUR9	KAD4_MOUSE	Adenylate kinase 4, mitochondrial	1,60E-03	↓	0,38
Q8BP40	PPA6_MOUSE	Lysophosphatidic acid phosphatase type 6	1,67E-02	↓	0,39
O88986	KBL_MOUSE	2-amino-3-ketobutyrate coenzyme A ligase, mitochondrial	3,34E-03	↓	0,39
O35969	GAMT_MOUSE	Guanidinoacetate N-methyltransferase	3,87E-03	↓	0,40
P11862	GAS2_MOUSE	Growth arrest-specific protein 2	2,19E-02	↓	0,40
P14094	AT1B1_MOUSE	Sodium/potassium-transporting ATPase subunit beta-1	1,28E-03	↓	0,42
Q8VDN2	AT1A1_MOUSE	Sodium/potassium-transporting ATPase subunit alpha-1	2,51E-04	↓	0,42
P40936	INMT_MOUSE	Indolethylamine N-methyltransferase	2,94E-03	↓	0,42
Q8R2N1	AQP3_MOUSE	Aquaporin-3	2,16E-03	↓	0,42
P16460	ASSY_MOUSE	Argininosuccinate synthase	6,19E-03	↓	0,43
P70691	UD12_MOUSE	UDP-glucuronosyltransferase 1-2	7,14E-03	↓	0,43
Q9D1I5	MCEE_MOUSE	Methylmalonyl-CoA epimerase, mitochondrial	2,03E-02	↓	0,44
Q8R086	SUOX_MOUSE	Sulfite oxidase, mitochondrial	9,79E-03	↓	0,44
Q9DCG6	PBLD1_MOUSE	Phenazine biosynthesis-like domain-containing protein 1	1,86E-03	↓	0,44
P55014	S12A1_MOUSE	Solute carrier family 12 member 1	9,22E-03	↓	0,44
Q78JT3	3HAO_MOUSE	3-hydroxyanthranilate 3,4-dioxygenase	7,36E-03	↓	0,45
P97816	S100G_MOUSE	Protein S100-G	2,45E-02	↓	0,45
P21981	TGM2_MOUSE	Protein-glutamine gamma-glutamyltransferase 2	1,78E-02	↓	0,45
Q78JN3	ECI3_MOUSE	Enoyl-CoA delta isomerase 3, peroxisomal	9,14E-03	↓	0,46
P54071	IDHP_MOUSE	Isocitrate dehydrogenase [NADP], mitochondrial	6,74E-04	↓	0,46
Q64442	DHSO_MOUSE	Sorbitol dehydrogenase	6,06E-03	↓	0,47
Q9D0K2	SCOT1_MOUSE	Succinyl-CoA:3-ketoacid coenzyme A transferase 1, mitochondrial	3,31E-03	↓	0,47
Q8K0L3	ACSM2_MOUSE	Acyl-coenzyme A synthetase ACSM2, mitochondrial	2,32E-02	↓	0,47
Q9NYQ2	HAOX2_MOUSE	Hydroxyacid oxidase 2	5,36E-03	↓	0,47
Q9DCS3	MECR_MOUSE	Enoyl-[acyl-carrier-protein] reductase, mitochondrial	1,40E-02	↓	0,47
P97328	KHK_MOUSE	Ketohexokinase	2,91E-03	↓	0,48

USC UNIVERSIDADE DE SANTIAGO DE COMPOSTELA

P14246	GTR2_MOUSE	Solute carrier family 2, facilitated glucose transporter member 2	1,78E-02	↓	0,48
Q7TMF3	NDUAC_MOUSE	NADH dehydrogenase [ubiquinone] 1 alpha subcomplex subunit 12	4,04E-03	↓	0,49
P31428	DPEP1_MOUSE	Dipeptidase 1	2,34E-02	↓	0,49
P61922	GABT_MOUSE	4-aminobutyrate aminotransferase, mitochondrial	2,10E-03	↓	0,49
P02088	HBB1_MOUSE	Hemoglobin subunit beta-1	3,57E-02	↓	0,49
Q9JLZ3	AUHM_MOUSE	Methylglutaconyl-CoA hydratase, mitochondrial	1,94E-02	↓	0,49
Q8R519	ACMSD_MOUSE	2-amino-3-carboxymuconate-6-semialdehyde decarboxylase	5,55E-04	↓	0,50

Supplementary Table 5. Protein list of all identified proteins by qualitative mass spectrometry analysis in ExoGAG isolated fraction of postnatal day 30 *Wild Type* urine sample.

Entry Name	UniProt Name	Protein Name	Peptides(95%)	%Cov(95)	Total spectrum count
P01132	EGF_MOUSE	Pro-epidermal growth factor	210	46,34	882
P11589	MUP2_MOUSE	Major urinary protein 2	130	83,89	868
P00688	AMYP_MOUSE	Pancreatic alpha-amylase	158	74,80	595
Q91X17	UROM_MOUSE	Uromodulin	83	44,08	551
P03953	CFAD_MOUSE	Complement factor D	101	71,04	414
P07724	ALBU_MOUSE	Albumin	74	62,50	298
P00687	AMY1_MOUSE	Alpha-amylase 1	55	43,05	262
P28825	MEP1A_MOUSE	Meprin A subunit alpha	47	36,81	183
O09043	NAPSA_MOUSE	Napsin-A	41	42,00	161
Q06890	CLUS_MOUSE	Clusterin	37	46,43	144
P04939	MUP3_MOUSE	Major urinary protein 3	35	61,96	129
Q921I1	TRFE_MOUSE	Serotransferrin	30	38,88	90
Q5FW60	MUP20_MOUSE	Major urinary protein 20	19	56,35	86
A2ARV4	LRP2_MOUSE	Low-density lipoprotein receptor-related protein 2	36	8,13	80
P15947	KLK1_MOUSE	Kallikrein-1	21	47,89	69
P13020	GELS_MOUSE	Gelsolin	20	21,92	66
P06869	UROK_MOUSE	Urokinase-type plasminogen activator	14	34,87	58
P13634	CAH1_MOUSE	Carbonic anhydrase 1	17	58,24	54
P02816	PIP_MOUSE	Prolactin-inducible protein homolog	15	56,16	52
Q9DBV4	MXRA8_MOUSE	Matrix remodeling-associated protein 8	13	25,11	36
Q91X72	HEMO_MOUSE	Hemopexin	9	17,39	32
Q60932	VDAC1_MOUSE	Voltage-dependent anion-selective channel protein 1	10	32,09	32
P01898	HA10_MOUSE	H-2 class I histocompatibility antigen, Q10 alpha chain	12	37,54	31
Q00897	A1AT4_MOUSE	Alpha-1-antitrypsin 1-4	12	20,58	31
P20918	PLMN_MOUSE	Plasminogen	12	14,04	29
Q8BPB5	FBLN3_MOUSE	EGF-containing fibulin-like extracellular matrix protein 1	8	10,55	29
P22599	A1AT2_MOUSE	Alpha-1-antitrypsin 1-2	11	19,85	29
P97449	AMPN_MOUSE	Aminopeptidase N	15	16,56	28
P07758	A1AT1_MOUSE	Alpha-1-antitrypsin 1-1	12	24,70	28
P63260	ACTG_MOUSE	Actin, cytoplasmic 2	14	24,27	26
Q61592	GAS6_MOUSE	Growth arrest-specific protein 6	10	16,17	25
P20060	HEXB_MOUSE	Beta-hexosaminidase subunit beta	8	12,87	25
Q9R1E6	ENPP2_MOUSE	Ectonucleotide pyrophosphatase/phosphodiesterase family member 2	11	13,69	24
P49183	DNAS1_MOUSE	Deoxyribonuclease-1	10	14,79	23

USC UNIVERSIDADE DE SANTIAGO DE COMPOSTELA

Q07456	AMBP_MOUSE	Protein AMBP	6	21,49	22
P11087	CO1A1_MOUSE	Collagen alpha-1(I) chain	4	1,17	22
Q9JIL4	NHRF3_MOUSE	Na(+)/H(+) exchange regulatory cofactor NHE-RF3	10	19,85	21
P51910	APOD_MOUSE	Apolipoprotein D	6	27,51	21
P02535	K1C10_MOUSE	Keratin, type I cytoskeletal 10	10	17,89	21
O09164	SODE_MOUSE	Extracellular superoxide dismutase [Cu-Zn]	7	33,07	19
Q02596	GLCM1_MOUSE	Glycosylation-dependent cell adhesion molecule 1	9	36,42	19
Q61847	MEP1B_MOUSE	Meprin A subunit beta	13	18,75	19
O89020	AFAM_MOUSE	Afamin	11	17,27	19
P09803	CADH1_MOUSE	Cadherin-1	7	9,39	16
Q61147	CERU_MOUSE	Ceruloplasmin	9	9,71	15
P04104	K2C1_MOUSE	Keratin, type II cytoskeletal 1	7	7,54	15
P55288	CAD11_MOUSE	Cadherin-11	2	3,27	14
P07759	SPA3K_MOUSE	Serine protease inhibitor A3K	8	22,25	13
P09470	ACE_MOUSE	Angiotensin-converting enzyme	6	5,11	13
P51655	GPC4_MOUSE	Glypican-4	6	11,49	13
Q60928	GGT1_MOUSE	Glutathione hydrolase 1 proenzyme	5	10,74	13
Q07797	LG3BP_MOUSE	Galectin-3-binding protein	5	12,31	13
Q9D7Z6	CLCA1_MOUSE	Calcium-activated chloride channel regulator 1	6	6,90	13
O35206	COFA1_MOUSE	Collagen alpha-1(XV) chain	5	5,05	12
Q9DBH5	LMAN2_MOUSE	Vesicular integral-membrane protein VIP36	5	13,97	12
Q02819	NUCB1_MOUSE	Nucleobindin-1	5	11,55	12
P11679	K2C8_MOUSE	Keratin, type II cytoskeletal 8	3	6,94	12
Q9CZ52	ANTR1_MOUSE	Anthrax toxin receptor 1	3	6,41	12
Q9DBX3	SUSD2_MOUSE	Sushi domain-containing protein 2	5	6,83	11
P26040	EZRI_MOUSE	Ezrin	7	10,58	11
Q61391	NEP_MOUSE	Neprilysin	7	8,40	11
Q8K2I4	MANBA_MOUSE	Beta-mannosidase	5	6,26	11
Q91V98	CD248_MOUSE	Endosialin	4	4,57	11
Q9ESD1	PRSS8_MOUSE	Prostasin	4	9,36	11
Q61646	HPT_MOUSE	Haptoglobin	3	10,09	11
Q922U2	K2C5_MOUSE	Keratin, type II cytoskeletal 5	3	3,79	11
Q9R045	ANGL2_MOUSE	Angiopoietin-related protein 2	5	7,50	10
P17182	ENOA_MOUSE	Alpha-enolase	4	16,13	10
Q08189	TGM3_MOUSE	Protein-glutamine gamma-glutamyltransferase E	3	4,47	10
P16125	LDHB_MOUSE	L-lactate dehydrogenase B chain	4	11,38	10
P70269	CATE_MOUSE	Cathepsin E	2	4,53	10
P21956	MFGM_MOUSE	Lactadherin	6	14,25	10
P46412	GPX3_MOUSE	Glutathione peroxidase 3	7	34,51	9
Q8BHC0	LYVE1_MOUSE	Lymphatic vessel endothelial hyaluronic acid receptor 1	3	9,43	9
Q9WVH9	FBLN5_MOUSE	Fibulin-5	3	7,37	9
Q6GU68	ISLR_MOUSE	Immunoglobulin superfamily containing leucine-rich repeat protein	3	7,94	9
O09114	PTGDS_MOUSE	Prostaglandin-H2 D-isomerase	8	32,80	9
P01837	IGKC_MOUSE	Immunoglobulin kappa constant	2	25,23	9
O08677-2	KNG1_MOUSE	Isoform LMW of Kininogen-1	2	4,63	8
P61110	ANRE_MOUSE	Kidney androgen-regulated protein	3	19,83	8
P52480	KPYM_MOUSE	Pyruvate kinase PKM	4	8,85	8
P63101	1433Z_MOUSE	14-3-3 protein zeta/delta	3	13,88	7
Q9DAK9	PHP14_MOUSE	14 kDa phosphohistidine phosphatase	4	40,32	7
Q61543	GSLG1_MOUSE	Golgi apparatus protein 1	2	2,04	7
P10126	EF1A1_MOUSE	Elongation factor 1-alpha 1	2	7,58	7

O88968	TCO2_MOUSE	Transcobalamin-2	3	5,58	7
P26041	MOES_MOUSE	Moesin	5	8,15	7
Q80YX1	TENA_MOUSE	Tenascin	3	1,56	7
O08709	PRDX6_MOUSE	Peroxiredoxin-6	6	22,32	6
P70441	NHRF1_MOUSE	Na(+)/H(+) exchange regulatory cofactor NHE-RF1	4	13,80	6
P14152	MDHC_MOUSE	Malate dehydrogenase, cytoplasmic	3	12,57	6
Q8VI78	PLA1A_MOUSE	Phospholipase A1 member A	3	9,65	6
Q91Y97	ALDOB_MOUSE	Fructose-bisphosphate aldolase B	4	11,81	6
P21614	VTDB_MOUSE	Vitamin D-binding protein	3	7,14	6
O35448	PPT2_MOUSE	Lysosomal thioesterase PPT2	1	4,64	6
Q8VED5	K2C79_MOUSE	Keratin, type II cytoskeletal 79	1	2,26	6
P62259	1433E_MOUSE	14-3-3 protein epsilon	2	8,24	6
P01027	CO3_MOUSE	Complement C3	2	1,62	5
Q61096	PRTN3_MOUSE	Myeloblastin	2	8,66	5
P30275	KCRU_MOUSE	Creatine kinase U-type, mitochondrial	2	7,42	5
Q99LJ1	FUCO_MOUSE	Tissue alpha-L-fucosidase	2	4,87	5
Q02013	AQP1_MOUSE	Aquaporin-1	3	9,66	5
P63017	HSP7C_MOUSE	Heat shock cognate 71 kDa protein	1	1,86	5
Q8R0I0	ACE2_MOUSE	Angiotensin-converting enzyme 2	2	2,24	5
P19221	THRB_MOUSE	Prothrombin	1	1,29	5
P62984	RL40_MOUSE	Ubiquitin-60S ribosomal protein L40	3	24,22	5
P97384	ANX11_MOUSE	Annexin A11	4	7,75	4
P10649	GSTM1_MOUSE	Glutathione S-transferase Mu 1	3	10,55	4
O70570	PIGR_MOUSE	Polymeric immunoglobulin receptor	3	3,76	4
Q8BM88	CATO_MOUSE	Cathepsin O	2	5,77	4
Q80Z19	MUC2_MOUSE	Mucin-2 (Fragments)	3	1,16	4
Q08761	PROS_MOUSE	Vitamin K-dependent protein S	2	3,11	4
Q9WVJ9	FBLN4_MOUSE	EGF-containing fibulin-like extracellular matrix protein 2	2	4,97	4
Q91WR8	GPX6_MOUSE	Glutathione peroxidase 6	2	9,50	4
O88322	NID2_MOUSE	Nidogen-2	2	2,28	4
P04186	CFAB_MOUSE	Complement factor B	3	5,52	4
Q60930	VDAC2_MOUSE	Voltage-dependent anion-selective channel protein 2	3	9,83	4
P11276	FINC_MOUSE	Fibronectin	2	0,89	4
Q01768	NDKB_MOUSE	Nucleoside diphosphate kinase B	1	11,18	4
Q8K426	RETNG_MOUSE	Resistin-like gamma	2	18,80	4
Q8K1H9	OBP2A_MOUSE	Odorant-binding protein 2a	1	5,11	4
P12658	CALB1_MOUSE	Calbindin	1	4,21	4
Q9QWR8	NAGAB_MOUSE	Alpha-N-acetylgalactosaminidase	1	2,65	4
Q6IFX2	K1C42_MOUSE	Keratin, type I cytoskeletal 42	4	8,19	4
Q01341	ADCY6_MOUSE	Adenylate cyclase type 6	1	1,29	4
P16858	G3P_MOUSE	Glyceraldehyde-3-phosphate dehydrogenase	1	2,10	4
Q3UV17	K22O_MOUSE	Keratin, type II cytoskeletal 2 oral	1	1,52	4
Q9D3H2	OBP1A_MOUSE	Odorant-binding protein 1a	1	4,91	4
Q80XI7	VOME_MOUSE	Vomeromodulin	2	3,72	3
Q03265	ATPA_MOUSE	ATP synthase subunit alpha, mitochondrial	2	3,98	3
Q4KML4	ABRAL_MOUSE	Costars family protein ABRACL	2	30,86	3
P35441	TSP1_MOUSE	Thrombospondin-1	2	1,71	3
Q9CQ60	6PGL_MOUSE	6-phosphogluconolactonase	2	12,45	3
P28843	DPP4_MOUSE	Dipeptidyl peptidase 4	2	3,03	3
P35700	PRDX1_MOUSE	Peroxiredoxin-1	1	5,03	3
P47738	ALDH2_MOUSE	Aldehyde dehydrogenase, mitochondrial	1	1,73	3
P23780	BGAL_MOUSE	Beta-galactosidase	1	2,16	3

Q91VW3	SH3L3_MOUSE	SH3 domain-binding glutamic acid-rich-like protein 3	2	19,35	3
O89023	TPP1_MOUSE	Tripeptidyl-peptidase 1	1	3,74	3
Q9R0E2	PLOD1_MOUSE	Procollagen-lysine,2-oxoglutarate 5-dioxygenase 1	2	3,57	3
A2AEP0	OBP1B_MOUSE	Odorant-binding protein 1b	2	8,77	3
Q9QZZ6	DERM_MOUSE	Dermatopontin	1	5,47	3
Q60590	A1AG1_MOUSE	Alpha-1-acid glycoprotein 1	1	4,35	3
P63082	VATL_MOUSE	V-type proton ATPase 16 kDa proteolipid subunit	1	11,61	3
Q5SSE9	ABCAD_MOUSE	ATP-binding cassette sub-family A member 13	1	0,26	3
P16406	AMPE_MOUSE	Glutamyl aminopeptidase	2	2,22	2
Q9WUU7	CATZ_MOUSE	Cathepsin Z	2	6,21	2
Q9JLB4	CUBN_MOUSE	Cubilin	2	0,66	2
P08228	SODC_MOUSE	Superoxide dismutase [Cu-Zn]	2	15,58	2
Q9JHE3	ASAH2_MOUSE	Neutral ceramidase	1	1,72	2
Q8CIF4	BTD_MOUSE	Biotinidase	1	2,31	2
Q8C6C9	LEG1H_MOUSE	Protein LEG1 homolog	1	3,56	2
Q9Z2L6	MINP1_MOUSE	Multiple inositol polyphosphate phosphatase 1	1	2,29	2
Q91V08	CLC2D_MOUSE	C-type lectin domain family 2 member D	1	5,80	2
Q9R0B9	PLOD2_MOUSE	Procollagen-lysine,2-oxoglutarate 5-dioxygenase 2	1	1,90	2
P40142	TKT_MOUSE	Transketolase	1	1,93	2
Q8CFZ5	S22AC_MOUSE	Solute carrier family 22 member 12	1	1,81	2
P08226	APOE_MOUSE	Apolipoprotein E	1	2,89	2
P11859	ANGT_MOUSE	Angiotensinogen	1	1,89	2
O08997	ATOX1_MOUSE	Copper transport protein ATOX1	1	11,76	2
P21460	CYTC_MOUSE	Cystatin-C	1	12,14	2
O54990	PROM1_MOUSE	Prominin-1	2	3,00	2
P01869	IGH1M_MOUSE	Ig gamma-1 chain C region, membrane-bound form	2	5,60	2
Q9Z0Z4	HEPH_MOUSE	Hephaestin	1	1,04	2
P99029	PRDX5_MOUSE	Peroxiredoxin-5, mitochondrial	1	5,24	2
P12023	A4_MOUSE	Amyloid-beta A4 protein	2	2,60	2
Q8VHY0	CSPG4_MOUSE	Chondroitin sulfate proteoglycan 4	2	0,95	2
Q7TMS5	ABCG2_MOUSE	Broad substrate specificity ATP-binding cassette transporter ABCG2	1	1,52	1
P12246	SAMP_MOUSE	Serum amyloid P-component	1	2,68	1
Q9QZF2	GPC1_MOUSE	Glypican-1	1	2,51	1
Q5SWY8	SC5AA_MOUSE	Sodium/glucose cotransporter 5	1	1,85	1
P23953	EST1C_MOUSE	Carboxylesterase 1C	1	1,99	1
P01843	LAC1_MOUSE	Ig lambda-1 chain C region	1	16,19	1
Q61207	SAP_MOUSE	Prosaposin	1	1,80	1
Q8BYF6	SC5A8_MOUSE	Sodium-coupled monocarboxylate transporter 1	1	1,64	1
Q8BND5	QSOX1_MOUSE	Sulfhydryl oxidase 1	1	1,47	1
Q9QWL7	K1C17_MOUSE	Keratin, type I cytoskeletal 17	4	8,31	
P27046	MA2A1_MOUSE	Alpha-mannosidase 2	2	1,83	
P01668	KV3AG_MOUSE	Ig kappa chain V-III region PC 7210	2	30,91	
O88338	CAD16_MOUSE	Cadherin-16	2	2,65	
P04938	MUP11_MOUSE	Major urinary protein 11	125	77,35	
Q61598	GDIB_MOUSE	Rab GDP dissociation inhibitor beta	1	2,47	
P01631	KV2A7_MOUSE	Ig kappa chain V-II region 26-10	1	11,50	
Q9ET22	DPP2_MOUSE	Dipeptidyl peptidase 2	1	1,98	
Q61282	PGCA_MOUSE	Aggrecan core protein	1	0,47	
Q9R098	HGFA_MOUSE	Hepatocyte growth factor activator	3	2,91	

Q3V1M1	IGS10_MOUSE	Immunoglobulin superfamily member 10	1	0,50
P97501	FMO3_MOUSE	Dimethylaniline monooxygenase [N-oxide-forming] 3	1	1,12
Q9EP95	RETNA_MOUSE	Resistin-like alpha	1	13,51
Q9DC51	GNAI3_MOUSE	Guanine nucleotide-binding protein G(i) subunit alpha-3	1	3,11
Q9D7R7	PEPC_MOUSE	Gastricsin	1	3,06
Q9D2U9	H2B3A_MOUSE	Histone H2B type 3-A	1	11,90
Q9CY00	TT30B_MOUSE	Tetratricopeptide repeat protein 30B	2	1,36
Q8R1M2	H2AJ_MOUSE	Histone H2A.J	1	6,98
Q8BU03	PWP2_MOUSE	Periodic tryptophan protein 2 homolog	1	1,20
Q61581	IBP7_MOUSE	Insulin-like growth factor-binding protein 7	1	5,69
Q5NCF2	TPPC1_MOUSE	Trafficking protein particle complex subunit 1	1	9,66
Q3URD3	SLMAP_MOUSE	Sarcolemmal membrane-associated protein	1	1,18
Q01721	GAS1_MOUSE	Growth arrest-specific protein 1	1	3,21
P35459	LY6D_MOUSE	Lymphocyte antigen 6D	2	11,02
P16110	LEG3_MOUSE	Galectin-3	1	2,27
P09036	ISK1_MOUSE	Serine protease inhibitor Kazal-type 1	1	8,75
P04945	KV6AB_MOUSE	Ig kappa chain V-VI region NQ2-6.1	2	14,81
P02340	P53_MOUSE	Cellular tumor antigen p53	1	2,56
P01878	IGHA_MOUSE	Ig alpha chain C region	1	4,36
O09159	MA2B1_MOUSE	Lysosomal alpha-mannosidase	2	1,28
D3Z7H8	CILP2_MOUSE	Cartilage intermediate layer protein 2	1	0,86
P31428	DPEP1_MOUSE	Dipeptidase 1	1	2,20
O88188	LY86_MOUSE	Lymphocyte antigen 86	1	5,56
P61971	NTF2_MOUSE	Nuclear transport factor 2	1	6,30
Q8VCS0	PGRP2_MOUSE	N-acetylmuramoyl-L-alanine amidase	1	2,07
Q8C3K6	SC5A1_MOUSE	Sodium/glucose cotransporter 1	1	1,65
P00920	CAH2_MOUSE	Carbonic anhydrase 2	1	3,85
Q9D2G2	ODO2_MOUSE	Dihydrolipoyllysine-residue succinyltransferase component of 2-oxoglutarate dehydrogenase complex, mitochondrial	1	1,76
Q8K419	LEG4_MOUSE	Galectin-4	1	4,29
Q64442	DHSO_MOUSE	Sorbitol dehydrogenase	1	2,52
P56383	AT5G2_MOUSE	ATP synthase F(0) complex subunit C2, mitochondrial	1	4,79
O88343	S4A4_MOUSE	Electrogenic sodium bicarbonate cotransporter 1	1	0,65

Supplementary Table 6. Protein list of all identified proteins by qualitative mass spectrometry analysis in ExoGAG isolated fraction of postnatal day 30 Mutant urine sample.

Entry Name	UniProt Name	Protein Name	Peptides(95%)	%Cov(95)	Total spectrum count
P11589	MUP2_MOUSE	Major urinary protein 2	65	69,44	295
P07724	ALBU_MOUSE	Albumin	106	62,50	279
Q921I1	TRFE_MOUSE	Serotransferrin	64	51,79	69
Q91X17	UROM_MOUSE	Uromodulin	76	40,50	52
Q06890	CLUS_MOUSE	Clusterin	41	48,44	41
Q91X72	HEMO_MOUSE	Hemopexin	40	50,43	34

P15947	KLK1_MOUSE	Kallikrein-1	7	27,97	31
Q5FW60	MUP20_MOUSE	Major urinary protein 20	5	27,62	30
P03953	CFAD_MOUSE	Complement factor D	31	57,92	30
P04939	MUP3_MOUSE	Major urinary protein 3	9	41,85	27
Q07456	AMBP_MOUSE	Protein AMBP	26	39,26	24
P11087	CO1A1_MOUSE	Collagen alpha-1(I) chain	3	1,17	24
Q00897	A1AT4_MOUSE	Alpha-1-antitrypsin 1-4	9	16,71	23
P28825	MEP1A_MOUSE	Meprin A subunit alpha	38	36,68	17
P04104	K2C1_MOUSE	Keratin, type II cytoskeletal 1	9	10,68	16
P02535	K1C10_MOUSE	Keratin, type I cytoskeletal 10	10	15,61	16
O09114	PTGDS_MOUSE	Prostaglandin-H2 D-isomerase	4	23,81	15
P13020	GELS_MOUSE	Gelsolin	35	24,49	14
P23953	EST1C_MOUSE	Carboxylesterase 1C	1	1,99	13
P04186	CFAB_MOUSE	Complement factor B	8	7,88	12
Q02596	GLCM1_MOUSE	Glycosylation-dependent cell adhesion molecule 1	20	36,42	11
P01027	CO3_MOUSE	Complement C3	85	44,02	10
Q8C6C9	LEG1H_MOUSE	Protein LEG1 homolog	17	25,82	9
Q922U2	K2C5_MOUSE	Keratin, type II cytoskeletal 5	2	3,79	8
P01132	EGF_MOUSE	Pro-epidermal growth factor	36	22,10	7
Q61646	HPT_MOUSE	Haptoglobin	24	37,75	7
O08677-2	KNG1_MOUSE	Isoform LMW of Kininogen-1	7	16,44	7
Q8BHC0	LYVE1_MOUSE	Lymphatic vessel endothelial hyaluronic acid receptor 1	3	8,18	7
Q9D3H2	OBP1A_MOUSE	Odorant-binding protein 1a	3	18,40	7
P09803	CADH1_MOUSE	Cadherin-1	5	8,37	6
P07361	A1AG2_MOUSE	Alpha-1-acid glycoprotein 2	2	8,70	6
A2AEP0	OBP1B_MOUSE	Odorant-binding protein 1b	3	18,13	6
Q8VED5	K2C79_MOUSE	Keratin, type II cytoskeletal 79	1	2,26	6
P00688	AMYP_MOUSE	Pancreatic alpha-amylase	50	49,21	5
P07759	SPA3K_MOUSE	Serine protease inhibitor A3K	12	21,77	5
P21614	VTDB_MOUSE	Vitamin D-binding protein	7	10,50	5
O09043	NAPSA_MOUSE	Napsin-A	22	23,87	5
O88322	NID2_MOUSE	Nidogen-2	2	2,28	5
P11672	NGAL_MOUSE	Neutrophil gelatinase-associated lipocalin	2	8,00	5
P00687	AMY1_MOUSE	Alpha-amylase 1	73	57,93	4
P11276	FINC_MOUSE	Fibronectin	5	2,26	4
P49183	DNAS1_MOUSE	Deoxyribonuclease-1	7	12,32	4
Q03401	CRIS1_MOUSE	Cysteine-rich secretory protein 1	2	8,61	4
Q06318	UTER_MOUSE	Uteroglobin	1	10,42	4
E9PV24	FIBA_MOUSE	Fibrinogen alpha chain	10	12,42	3
P11859	ANGT_MOUSE	Angiotensinogen	5	9,01	3
Q8K0E8	FIBB_MOUSE	Fibrinogen beta chain	5	7,69	3
P13634	CAH1_MOUSE	Carbonic anhydrase 1	4	23,37	3
Q6IFX2	K1C42_MOUSE	Keratin, type I cytoskeletal 42	3	6,19	3
Q9WTR5	CAD13_MOUSE	Cadherin-13	2	3,08	3

USC UNIVERSIDADE DE SANTIAGO DE COMPOSTELA

P21460	CYTC_MOUSE	Cystatin-C	1	12,14	3
P08228	SODC_MOUSE	Superoxide dismutase [Cu-Zn]	1	7,14	3
Q8BND5	QSOX1_MOUSE	Sulfhydryl oxidase 1	6	7,62	3
P62984	RL40_MOUSE	Ubiquitin-60S ribosomal protein L40	2	17,19	3
Q61147	CERU_MOUSE	Ceruloplasmin	26	25,45	2
P20918	PLMN_MOUSE	Plasminogen	12	14,04	2
Q8VCM7	FIBG_MOUSE	Fibrinogen gamma chain	9	21,56	2
P19221	THRB_MOUSE	Prothrombin	4	5,18	2
P63260	ACTG_MOUSE	Actin, cytoplasmic 2	10	21,60	2
P29699	FETUA_MOUSE	Alpha-2-HS-glycoprotein	4	9,85	2
P01837	IGKC_MOUSE	Immunoglobulin kappa constant	6	57,01	2
Q9DBV4	MXRA8_MOUSE	Matrix remodeling-associated protein 8	2	4,75	2
P10493	NID1_MOUSE	Nidogen-1	6	5,46	1
Q80Z19	MUC2_MOUSE	Mucin-2 (Fragments)	4	1,57	1
Q91V98	CD248_MOUSE	Endosialin	3	3,27	1
Q9QZZ6	DERM_MOUSE	Dermatopontin	1	5,47	1
Q8K1H9	OBP2A_MOUSE	Odorant-binding protein 2a	1	5,11	1
P28665	MUG1_MOUSE	Murinoglobulin-1	20	13,96	
Q9D7Z6	CLCA1_MOUSE	Calcium-activated chloride channel regulator 1	26	25,96	
Q61838	PZP_MOUSE	Pregnancy zone protein	14	9,30	
Q07797	LG3BP_MOUSE	Galectin-3-binding protein	11	19,93	
O70570	PIGR_MOUSE	Polymeric immunoglobulin receptor	10	13,49	
Q61592	GAS6_MOUSE	Growth arrest-specific protein 6	9	14,24	
A2ARV4	LRP2_MOUSE	Low-density lipoprotein receptor-related protein 2	8	1,80	
P08730	K1C13_MOUSE	Keratin, type I cytoskeletal 13	10	17,62	
Q00896	A1AT3_MOUSE	Alpha-1-antitrypsin 1-3	10	17,96	
O54990	PROM1_MOUSE	Prominin-1	7	11,42	
Q3UZZ4	OLFM4_MOUSE	Olfactomedin-4	6	13,27	
P02816	PIP_MOUSE	Prolactin-inducible protein homolog	8	56,16	
P97449	AMPN_MOUSE	Aminopeptidase N	5	7,45	
Q9ESB3	HRG_MOUSE	Histidine-rich glycoprotein	6	10,29	
Q08761	PROS_MOUSE	Vitamin K-dependent protein S	5	9,18	
P01898	HA10_MOUSE	H-2 class I histocompatibility antigen, Q10 alpha chain	6	19,08	
Q61847	MEP1B_MOUSE	Meprin A subunit beta	6	8,66	
Q60928	GGT1_MOUSE	Glutathione hydrolase 1 proenzyme	4	7,92	
Q8BPB5	FBLN3_MOUSE	EGF-containing fibulin-like extracellular matrix protein 1	7	9,53	
A6X935	ITIH4_MOUSE	Inter alpha-trypsin inhibitor, heavy chain 4	4	4,35	
P46412	GPX3_MOUSE	Glutathione peroxidase 3	4	21,24	
Q9DBH5	LMAN2_MOUSE	Vesicular integral-membrane protein VIP36	3	8,10	
P09470	ACE_MOUSE	Angiotensin-converting enzyme	3	2,36	
O89020	AFAM_MOUSE	Afamin	3	5,92	
O35206	COFA1_MOUSE	Collagen alpha-1(XV) chain	4	2,71	
P12246	SAMP_MOUSE	Serum amyloid P-component	6	21,43	

USC UNIVERSIDADE DE SANTIAGO DE COMPOSTELA

Q9CR35	CTRB1_MOUSE	Chymotrypsinogen B	4	11,41
Q9R045	ANGL2_MOUSE	Angiopoietin-related protein 2	3	3,85
P97497	SHBG_MOUSE	Sex hormone-binding globulin	2	5,21
P23090	GAG_MLVDU	Gag polyprotein	3	7,37
P20060	HEXB_MOUSE	Beta-hexosaminidase subunit beta	3	5,60
P01878	IGHA_MOUSE	Ig alpha chain C region	3	5,81
Q8R121	ZPI_MOUSE	Protein Z-dependent protease inhibitor	2	4,91
O88968	TCO2_MOUSE	Transcobalamin-2	2	5,58
P70412	CUZD1_MOUSE	CUB and zona pellucida-like domain-containing protein 1	2	4,62
Q9WVH9	FBLN5_MOUSE	Fibulin-5	3	6,70
P06909	CFAH_MOUSE	Complement factor H	2	1,62
P07146	TRY2_MOUSE	Anionic trypsin-2	3	12,20
P01869	IGH1M_MOUSE	Ig gamma-1 chain C region, membrane-bound form	2	5,60
P63017	HSP7C_MOUSE	Heat shock cognate 71 kDa protein	2	3,71
O09159	MA2B1_MOUSE	Lysosomal alpha-mannosidase	2	3,55
Q9JIL4	NHRF3_MOUSE	Na(+)/H(+) exchange regulatory cofactor NHE-RF3	2	4,62
Q9CQ60	6PGL_MOUSE	6-phosphogluconolactonase	3	15,56
P21956	MFGM_MOUSE	Lactadherin	3	6,48
Q9DBX3	SUSD2_MOUSE	Sushi domain-containing protein 2	2	2,44
P0DOG8	GGAG_MLVAV	Glyco-Gag protein	3	6,08
Q61391	NEP_MOUSE	Neprilysin	1	1,47
P52480	KPYM_MOUSE	Pyruvate kinase PKM	2	3,77
P01029	CO4B_MOUSE	Complement C4-B	2	1,32
Q60932	VDAC1_MOUSE	Voltage-dependent anion-selective channel protein 1	2	7,10
Q80YX1	TENA_MOUSE	Tenascin	2	0,95
P51910	APOD_MOUSE	Apolipoprotein D	2	6,35
Q8K3J9	GPC5C_MOUSE	G-protein coupled receptor family C group 5 member C	2	5,23
Q91WP6	SPA3N_MOUSE	Serine protease inhibitor A3N	3	8,13
P51655	GPC4_MOUSE	Glypican-4	2	4,49
O35988	SDC4_MOUSE	Syndecan-4	3	14,14
Q61129	CFAI_MOUSE	Complement factor I	2	2,82
P57780	ACTN4_MOUSE	Alpha-actinin-4	1	1,32
Q8R0I0	ACE2_MOUSE	Angiotensin-converting enzyme 2	2	2,24
P26040	EZRI_MOUSE	Ezrin	1	1,54
Q9CZ52	ANTR1_MOUSE	Anthrax toxin receptor 1	1	1,60
P28843	DPP4_MOUSE	Dipeptidyl peptidase 4	1	1,84
P45700	MA1A1_MOUSE	Mannosyl-oligosaccharide 1,2-alpha-mannosidase IA	1	1,68
P51885	LUM_MOUSE	Lumican	1	3,25
P31428	DPEP1_MOUSE	Dipeptidase 1	2	3,90
Q61703	ITIH2_MOUSE	Inter-alpha-trypsin inhibitor heavy chain H2	1	1,59
Q9R0B9	PLOD2_MOUSE	Procollagen-lysine,2-oxoglutarate 5-dioxygenase 2	1	1,90
Q9ET22	DPP2_MOUSE	Dipeptidyl peptidase 2	1	1,98

P21765	GPX5_MOUSE	Epididymal secretory glutathione peroxidase	2	10,41
Q6GU68	ISLR_MOUSE	Immunoglobulin superfamily containing leucine-rich repeat protein	1	3,04
P01633	KV5A1_MOUSE	Ig kappa chain V19-17	1	6,04
Q9Z1R3	APOM_MOUSE	Apolipoprotein M	1	3,68
Q61282	PGCA_MOUSE	Aggrecan core protein	1	0,47
P01631	KV2A7_MOUSE	Ig kappa chain V-II region 26-10	1	11,50
P35441	TSP1_MOUSE	Thrombospondin-1	1	0,94
P06330	HVM51_MOUSE	Ig heavy chain V region AC38 205.12	1	16,10
Q8R3G9	TSN8_MOUSE	Tetraspanin-8	1	5,96
P01592	IGJ_MOUSE	Immunoglobulin J chain	2	16,35
P04938	MUP11_MOUSE	Major urinary protein 11	64	62,98
P06869	UROK_MOUSE	Urokinase-type plasminogen activator	2	5,54
Q9JHE3	ASAH2_MOUSE	Neutral ceramidase	1	1,72
Q8VI78	PLA1A_MOUSE	Phospholipase A1 member A	1	2,19
Q8R1M8	MPTX_MOUSE	Mucosal pentraxin	1	4,57
Q8BHL4	RAI3_MOUSE	Retinoic acid-induced protein 3	1	3,65
Q61702	ITIH1_MOUSE	Inter-alpha-trypsin inhibitor heavy chain H1	1	1,32
Q02013	AQP1_MOUSE	Aquaporin-1	1	3,35
Q01768	NDKB_MOUSE	Nucleoside diphosphate kinase B	1	11,18
Q00493	CBPE_MOUSE	Carboxypeptidase E	1	2,10
P57096	PSCA_MOUSE	Prostate stem cell antigen	1	8,13
P16675	PPGB_MOUSE	Lysosomal protective protein	1	1,69
P03977	KV3A4_MOUSE	Ig kappa chain V-III region 50S10.1	1	16,22
P01843	LAC1_MOUSE	Ig lambda-1 chain C region	1	16,19
P01636	KV5A4_MOUSE	Ig kappa chain V-V region MOPC 149	1	12,04
O88593	PGRP1_MOUSE	Peptidoglycan recognition protein 1	1	6,59
Q61696	HS71A_MOUSE	Heat shock 70 kDa protein 1A	1	1,87
P11679	K2C8_MOUSE	Keratin, type II cytoskeletal 8	1	2,45
Q05793	PGBM_MOUSE	Basement membrane-specific heparan sulfate proteoglycan core protein	1	0,24
Q99LJ1	FUCO_MOUSE	Tissue alpha-L-fucosidase	1	2,43
Q6GQW0	BTBDB_MOUSE	Ankyrin repeat and BTB/POZ domain-containing protein BTBD11	1	0,81
P20029	BIP_MOUSE	Endoplasmic reticulum chaperone BiP	1	1,83
P18761	CAH6_MOUSE	Carbonic anhydrase 6	2	8,52
Q60963	PAFA_MOUSE	Platelet-activating factor acetylhydrolase	1	2,73
Q61096	PRTN3_MOUSE	Myeloblastin	1	3,54
Q9R1E6	ENPP2_MOUSE	Ectonucleotide pyrophosphatase/phosphodiesterase family member 2	1	1,28
P01680	KV4A1_MOUSE	Ig kappa chain V-IV region S107B	1	8,53
O09164	SODE_MOUSE	Extracellular superoxide dismutase [Cu-Zn]	1	3,98
O88188	LY86_MOUSE	Lymphocyte antigen 86	1	5,56
Q60590	A1AG1_MOUSE	Alpha-1-acid glycoprotein 1	2	11,59

P14152	MDHC_MOUSE	Malate dehydrogenase, cytoplasmic	1	2,39
Q9WUU7	CATZ_MOUSE	Cathepsin Z	1	2,94
P84750	KVM5_MOUSE	Ig kappa chain V region Mem5 (Fragment)	1	5,78
Q02819	NUCB1_MOUSE	Nucleobindin-1	1	2,18
P62631	EF1A2_MOUSE	Elongation factor 1-alpha 2	1	2,38
P07744	K2C4_MOUSE	Keratin, type II cytoskeletal 4	1	2,29
G5E8Q8	AGRF5_MOUSE	Adhesion G protein-coupled receptor F5	1	0,67
P06151	LDHA_MOUSE	L-lactate dehydrogenase A chain	1	3,01
P32261	ANT3_MOUSE	Antithrombin-III	1	1,93
Q8VCG4	CO8G_MOUSE	Complement component C8 gamma chain	1	5,45
P04945	KV6AB_MOUSE	Ig kappa chain V-VI region NQ2-6.1	1	14,81
Q9WTS4	TEN1_MOUSE	Teneurin-1	1	0,29
P03976	KV2A5_MOUSE	Ig kappa chain V-II region 17S29.1	1	11,50
Q9D7Q1	CHIT1_MOUSE	Chitotriosidase-1	1	2,37
P01729	LV2B_MOUSE	Ig lambda-2 chain V region MOPC 315	1	6,98
P16125	LDHB_MOUSE	L-lactate dehydrogenase B chain	1	2,69
Q8R5I6	GSTM4_MOUSE	Glutathione S-transferase Mu 4	1	4,13
P97384	ANX11_MOUSE	Annexin A11	1	1,79
Q9D2L5	CPXM2_MOUSE	Inactive carboxypeptidase-like protein X2	1	1,18
Q9QXC1	FETUB_MOUSE	Fetuin-B	1	2,32
P01821	HVM45_MOUSE	Ig heavy chain V region MC101	1	5,17
P16858	G3P_MOUSE	Glyceraldehyde-3-phosphate dehydrogenase	1	2,10
Q80UF9-2	OTOP3_MOUSE	Isoform 2 of Proton channel OTOP3	1	1,17

Supplementary Table 7. Protein list of all identified proteins by qualitative mass spectrometry analysis in ExoGAG isolated fraction of postnatal day 45 *Wild type* urine sample.

Entry Name	UniProt Name	Protein Name	Peptides(95%)	%Cov(95)	Total spectrum count
P11589	MUP2_MOUSE	Major urinary protein 2	223	87,22	1301
P11588	MUP1_MOUSE	Major urinary protein 1	207	90,00	1215
B5X0G2	MUP17_MOUSE	Major urinary protein 17	184	84,44	1053
Q91X17	UROM_MOUSE	Uromodulin	99	42,06	570
P01132	EGF_MOUSE	Pro-epidermal growth factor	125	38,37	457
P00688	AMYP_MOUSE	Pancreatic alpha-amylase	83	68,11	294
P03953	CFAD_MOUSE	Complement factor D	54	57,92	230
P07724	ALBU_MOUSE	Albumin	46	50,82	181
P28825	MEP1A_MOUSE	Meprin A subunit alpha	31	31,59	138
P00687	AMY1_MOUSE	Alpha-amylase 1	28	26,22	136
O09043	NAPSA_MOUSE	Napsin-A	30	31,74	131
P04939	MUP3_MOUSE	Major urinary protein 3	30	56,52	102
Q5FW60	MUP20_MOUSE	Major urinary protein 20	19	43,09	98
Q06890	CLUS_MOUSE	Clusterin	27	35,27	80

A2ARV4	LRP2_MOUSE	Low-density lipoprotein receptor-related protein 2	27	5,88	58
P63260	ACTG_MOUSE	Actin, cytoplasmic 2	17	37,33	49
Q9JIL4	NHRF3_MOUSE	Na(+)/H(+) exchange regulatory cofactor NHE-RF3	20	29,67	48
P15947	KLK1_MOUSE	Kallikrein-1	13	27,97	46
Q921I1	TRFE_MOUSE	Serotransferrin	11	16,93	38
Q61847	MEP1B_MOUSE	Meprin A subunit beta	16	21,59	35
P06869	UROK_MOUSE	Urokinase-type plasminogen activator	9	21,02	33
P97449	AMPN_MOUSE	Aminopeptidase N	16	16,36	32
Q60928	GGT1_MOUSE	Glutathione hydrolase 1 proenzyme	11	22,18	27
P26040	EZRI_MOUSE	Ezrin	11	18,94	27
P26043	RADI_MOUSE	Radixin	8	13,04	25
P02816	PIP_MOUSE	Prolactin-inducible protein homolog	8	50,00	24
P49183	DNAS1_MOUSE	Deoxyribonuclease-1	10	14,79	23
P26041	MOES_MOUSE	Moesin	7	12,82	21
P70441	NHRF1_MOUSE	Na(+)/H(+) exchange regulatory cofactor NHE-RF1	8	24,23	20
Q61391	NEP_MOUSE	Neprilysin	7	9,07	19
Q61592	GAS6_MOUSE	Growth arrest-specific protein 6	9	14,39	18
O09164	SODE_MOUSE	Extracellular superoxide dismutase [Cu-Zn]	8	31,87	17
P09470	ACE_MOUSE	Angiotensin-converting enzyme	5	4,57	16
P51910	APOD_MOUSE	Apolipoprotein D	5	26,98	16
Q61147	CERU_MOUSE	Ceruloplasmin	6	7,07	15
Q60932	VDAC1_MOUSE	Voltage-dependent anion-selective channel protein 1	5	12,16	15
Q9R1E6	ENPP2_MOUSE	Ectonucleotide pyrophosphatase/phosphodiesterase family member 2	9	9,05	14
P13634	CAH1_MOUSE	Carbonic anhydrase 1	3	11,88	14
Q00897	A1AT4_MOUSE	Alpha-1-antitrypsin 1-4	5	11,62	13
P04104	K2C1_MOUSE	Keratin, type II cytoskeletal 1	5	5,97	13
Q8CFZ5	S22AC_MOUSE	Solute carrier family 22 member 12	6	11,39	12
Q02596	GLCM1_MOUSE	Glycosylation-dependent cell adhesion molecule 1	6	29,14	11
P48758	CBR1_MOUSE	Carbonyl reductase [NADPH] 1	6	21,66	10
P09803	CADH1_MOUSE	Cadherin-1	4	7,58	10
Q91Y97	ALDOB_MOUSE	Fructose-bisphosphate aldolase B	4	13,74	10
O09114	PTGDS_MOUSE	Prostaglandin-H2 D-isomerase	6	30,69	10
P02535	K1C10_MOUSE	Keratin, type I cytoskeletal 10	6	11,40	10
Q9DBV4	MXRA8_MOUSE	Matrix remodeling-associated protein 8	3	7,92	10
P20060	HEXB_MOUSE	Beta-hexosaminidase subunit beta	2	2,99	10
P01898	HA10_MOUSE	H-2 class I histocompatibility antigen, Q10 alpha chain	3	11,38	9
Q91XE4	ACY3_MOUSE	N-acyl-aromatic-L-amino acid amidohydrolase (carboxylate-forming)	2	5,66	9
Q8BPB5	FBLN3_MOUSE	EGF-containing fibulin-like extracellular matrix protein 1	4	8,52	8
Q8VCA0	S22AJ_MOUSE	Solute carrier family 22 member 19	4	8,35	8
Q07456	AMBP_MOUSE	Protein AMBP	4	17,77	8
Q62468	VILI_MOUSE	Villin-1	5	6,53	7

USC UNIVERSIDADE DE SANTIAGO DE COMPOSTELA

P51655	GPC4_MOUSE	Glypican-4	4	10,77	7
P21956	MFGM_MOUSE	Lactadherin	3	10,15	7
P16858	G3P_MOUSE	Glyceraldehyde-3-phosphate dehydrogenase	2	8,71	7
Q922U2	K2C5_MOUSE	Keratin, type II cytoskeletal 5	2	3,79	7
P20918	PLMN_MOUSE	Plasminogen	2	2,59	7
O89020	AFAM_MOUSE	Afamin	4	7,07	6
Q9DBX3	SUSD2_MOUSE	Sushi domain-containing protein 2	5	6,58	6
P07759	SPA3K_MOUSE	Serine protease inhibitor A3K	3	9,09	6
Q02013	AQP1_MOUSE	Aquaporin-1	3	9,66	6
Q8K2I4	MANBA_MOUSE	Beta-mannosidase	2	2,16	6
P13020	GELS_MOUSE	Gelsolin	3	3,59	6
Q5SWY8	SC5AA_MOUSE	Sodium/glucose cotransporter 5	2	3,52	6
P10126	EF1A1_MOUSE	Elongation factor 1-alpha 1	2	7,58	6
P16125	LDHB_MOUSE	L-lactate dehydrogenase B chain	1	2,69	6
P61110	ANRE_MOUSE	Kidney androgen-regulated protein	1	9,92	6
P99029	PRDX5_MOUSE	Peroxiredoxin-5, mitochondrial	2	9,05	5
P01027	CO3_MOUSE	Complement C3	4	3,13	5
P46412	GPX3_MOUSE	Glutathione peroxidase 3	3	14,60	5
P16406	AMPE_MOUSE	Glutamyl aminopeptidase	2	2,22	5
P63017	HSP7C_MOUSE	Heat shock cognate 71 kDa protein	2	3,71	5
P14152	MDHC_MOUSE	Malate dehydrogenase, cytoplasmic	3	9,58	5
Q9ESD1	PRSS8_MOUSE	Prostasin	2	6,14	5
Q8BYF6	SC5A8_MOUSE	Sodium-coupled monocarboxylate transporter 1	3	3,44	5
Q60866	PTER_MOUSE	Phosphotriesterase-related protein	2	6,02	5
P70269	CATE_MOUSE	Cathepsin E	2	4,53	5
O88968	TCO2_MOUSE	Transcobalamin-2	3	5,58	5
Q9CZ52	ANTR1_MOUSE	Anthrax toxin receptor 1	1	1,60	5
O35448	PPT2_MOUSE	Lysosomal thioesterase PPT2	2	7,62	5
P10649	GSTM1_MOUSE	Glutathione S-transferase Mu 1	2	6,42	4
Q8VI78	PLA1A_MOUSE	Phospholipase A1 member A	2	4,83	4
P54818	GALC_MOUSE	Galactocerebrosidase	2	3,66	4
P35441	TSP1_MOUSE	Thrombospondin-1	2	1,71	4
P21614	VTDB_MOUSE	Vitamin D-binding protein	1	3,15	4
Q5SX39	MYH4_MOUSE	Myosin-4	1	0,62	4
Q8BHC0	LYVE1_MOUSE	Lymphatic vessel endothelial hyaluronic acid receptor 1	1	2,83	4
Q9DBH5	LMAN2_MOUSE	Vesicular integral-membrane protein VIP36	1	2,51	4
P63082	VATL_MOUSE	V-type proton ATPase 16 kDa proteolipid subunit	1	11,61	4
Q7TMS5	ABCG2_MOUSE	Broad substrate specificity ATP-binding cassette transporter ABCG2	1	1,52	4
Q9Z2J0	S23A1_MOUSE	Solute carrier family 23 member 1	0	0,00	4
Q8R0I0	ACE2_MOUSE	Angiotensin-converting enzyme 2	2	2,24	3
Q02819	NUCB1_MOUSE	Nucleobindin-1	2	4,57	3
P31725	S10A9_MOUSE	Protein S100-A9	2	23,01	3
P35700	PRDX1_MOUSE	Peroxiredoxin-1	1	5,03	3

P11087	CO1A1_MOUSE	Collagen alpha-1(I) chain	3	1,17	3
O35206	COFA1_MOUSE	Collagen alpha-1(XV) chain	1	0,95	3
O08677-2	KNG1_MOUSE	Isoform LMW of Kininogen-1	1	2,32	3
P28843	DPP4_MOUSE	Dipeptidyl peptidase 4	1	1,84	3
Q8VED5	K2C79_MOUSE	Keratin, type II cytoskeletal 79	1	2,26	3
P17182	ENOA_MOUSE	Alpha-enolase	1	3,92	3
Q62217	SEM5A_MOUSE	Semaphorin-5A	1	1,02	3
P01837	IGKC_MOUSE	Immunoglobulin kappa constant	1	7,48	3
Q9D687	S6A19_MOUSE	Sodium-dependent neutral amino acid transporter B(0)AT1	1	1,89	3
P62984	RL40_MOUSE	Ubiquitin-60S ribosomal protein L40	2	17,19	2
Q6A4L0	S22AD_MOUSE	Solute carrier family 22 member 13	2	3,81	2
Q01768	NDKB_MOUSE	Nucleoside diphosphate kinase B	2	19,08	2
Q01721	GAS1_MOUSE	Growth arrest-specific protein 1	2	11,66	2
P01869	IGH1M_MOUSE	Ig gamma-1 chain C region, membrane-bound form	2	5,60	2
Q9JII6	AK1A1_MOUSE	Aldo-keto reductase family 1 member A1	2	5,54	2
P09411	PGK1_MOUSE	Phosphoglycerate kinase 1	2	8,39	2
Q9QZF2	GPC1_MOUSE	Glypican-1	1	2,51	2
Q60590	A1AG1_MOUSE	Alpha-1-acid glycoprotein 1	1	4,35	2
Q91WR8	GPX6_MOUSE	Glutathione peroxidase 6	1	5,43	2
P21460	CYTC_MOUSE	Cystatin-C	1	12,14	2
Q8K426	RETNG_MOUSE	Resistin-like gamma	1	10,26	2
P19221	THRB_MOUSE	Prothrombin	1	1,29	2
Q91X72	HEMO_MOUSE	Hemopexin	1	1,96	2
Q8VCR7	ABHEB_MOUSE	Protein ABHD14B	1	5,24	2
P07146	TRY2_MOUSE	Anionic trypsin-2	1	8,13	2
Q9JI44	DMAP1_MOUSE	DNA methyltransferase 1-associated protein 1	1	1,71	2
Q99JW2	ACY1_MOUSE	Aminoacylase-1	1	3,43	2
P11276	FINC_MOUSE	Fibronectin	1	0,40	2
P16675	PPGB_MOUSE	Lysosomal protective protein	1	1,69	2
Q5SSE9	ABCAD_MOUSE	ATP-binding cassette sub-family A member 13	1	0,18	1
Q9JLB4	CUBN_MOUSE	Cubilin	1	0,36	1
Q61207	SAP_MOUSE	Prosaposin	1	1,80	1
Q06318	UTER_MOUSE	Uteroglobin	1	10,42	1
P62806	H4_MOUSE	Histone H4	1	11,65	1
P55292	DSC2_MOUSE	Desmocollin-2	1	1,11	1
P08228	SODC_MOUSE	Superoxide dismutase [Cu-Zn]	1	7,14	1
P01843	LAC1_MOUSE	Ig lambda-1 chain C region	1	16,19	1
O54990	PROM1_MOUSE	Prominin-1	1	1,73	1
Q61096	PRTN3_MOUSE	Myeloblastin	1	3,54	1
Q99N23	CAH15_MOUSE	Carbonic anhydrase 15	1	3,09	1
Q9JHE3	ASAH2_MOUSE	Neutral ceramidase	1	1,72	1
P55288	CAD11_MOUSE	Cadherin-11	1	1,26	1
Q8K1H9	OBP2A_MOUSE	Odorant-binding protein 2a	1	5,11	1

Q08761	PROS_MOUSE	Vitamin K-dependent protein S	1	1,93	1
O88188	LY86_MOUSE	Lymphocyte antigen 86	2	9,26	
Q9ET22	DPP2_MOUSE	Dipeptidyl peptidase 2	1	1,98	
Q9QWL7	K1C17_MOUSE	Keratin, type I cytoskeletal 17	2	4,62	
Q91ZX6	SENP2_MOUSE	Sentrin-specific protease 2	1	1,70	
Q91WR5	AK1CL_MOUSE	Aldo-keto reductase family 1 member C21	1	2,48	
Q8VCS0	PGRP2_MOUSE	N-acetylmuramoyl-L-alanine amidase	1	2,07	
Q71RI9	KAT3_MOUSE	Kynurenine--oxoglutarate transaminase 3	1	2,64	
Q64442	DHSO_MOUSE	Sorbitol dehydrogenase	1	2,52	
Q61581	IBP7_MOUSE	Insulin-like growth factor-binding protein 7	1	5,69	
Q5NC05	TTF2_MOUSE	Transcription termination factor 2	1	0,88	
P81183	IKZF2_MOUSE	Zinc finger protein Helios	1	1,90	
P51855	GSHB_MOUSE	Glutathione synthetase	1	3,59	
P24452	CAPG_MOUSE	Macrophage-capping protein	1	3,69	
F8VQB6	MYO10_MOUSE	Unconventional myosin-X	1	0,44	
P20263	PO5F1_MOUSE	POU domain, class 5, transcription factor 1	1	3,41	
P06797	CATL1_MOUSE	Procathepsin L	1	2,69	
Q9CQH0	PDZ1I_MOUSE	PDZK1-interacting protein 1	1	9,65	
O88576	S6A18_MOUSE	Sodium-dependent neutral amino acid transporter B(0)AT3	1	1,14	
Q91ZI0	CELR3_MOUSE	Cadherin EGF LAG seven-pass G-type receptor 3	1	0,24	
Q9QYB1	CLIC4_MOUSE	Chloride intracellular channel protein 4	1	4,74	
Q8CGK7	GNAL_MOUSE	Guanine nucleotide-binding protein G(olf) subunit alpha	1	2,89	
P62880	GBB2_MOUSE	Guanine nucleotide-binding protein G(I)/G(S)/G(T) subunit beta-2	2	7,06	
B9EJA2-4	CTTB2_MOUSE	Isoform 4 of Cortactin-binding protein 2	1	0,68	
Q6P5H2	NEST_MOUSE	Nestin	1	0,48	

Supplementary Table 8. **Protein list of all identified proteins by qualitative mass spectrometry analysis in ExoGAG isolated fraction of postnatal day 45 mutant urine sample.**

Entry Name	UniProt Name	Protein Name	Peptides(95%)	%Cov(95)	Total spectrum count
P07724	ALBU_MOUSE	Albumin	90	67,43	328
P01027	CO3_MOUSE	Complement C3	95	47,93	262
P03953	CFAD_MOUSE	Complement factor D	47	64,48	149
Q07456	AMBP_MOUSE	Protein AMBP	40	59,03	136
Q91X72	HEMO_MOUSE	Hemopexin	33	48,70	120
Q61147	CERU_MOUSE	Ceruloplasmin	38	35,82	91
P07759	SPA3K_MOUSE	Serine protease inhibitor A3K	23	35,65	89
P07758	A1AT1_MOUSE	Alpha-1-antitrypsin 1-1	21	39,23	80
P06728	APOA4_MOUSE	Apolipoprotein A-IV	27	66,58	77
Q06890	CLUS_MOUSE	Clusterin	24	37,50	76
P22599	A1AT2_MOUSE	Alpha-1-antitrypsin 1-2	21	38,01	75

P11859	ANGT_MOUSE	Angiotensinogen	20	31,66	65
Q00897	A1AT4_MOUSE	Alpha-1-antitrypsin 1-4	20	35,84	64
Q921I1	TRFE_MOUSE	Serotransferrin	24	32,28	59
P04186	CFAB_MOUSE	Complement factor B	20	26,94	49
Q91WP6	SPA3N_MOUSE	Serine protease inhibitor A3N	18	39,95	48
P63260	ACTG_MOUSE	Actin, cytoplasmic 2	20	53,07	48
Q8C6C9	LEG1H_MOUSE	Protein LEG1 homolog	14	28,19	48
Q03734	SPA3M_MOUSE	Serine protease inhibitor A3M	13	27,03	48
P11591	MUP5_MOUSE	Major urinary protein 5	5	20,00	45
P17742	PPIA_MOUSE	Peptidyl-prolyl cis-trans isomerase A	17	60,98	44
Q8VCM7	FIBG_MOUSE	Fibrinogen gamma chain	16	33,72	43
P13020	GELS_MOUSE	Gelsolin	21	31,15	42
P01029	CO4B_MOUSE	Complement C4-B	24	15,88	38
Q8K0E8	FIBB_MOUSE	Fibrinogen beta chain	18	34,10	35
E9PV24	FIBA_MOUSE	Fibrinogen alpha chain	17	20,79	35
Q9ESB3	HRG_MOUSE	Histidine-rich glycoprotein	13	22,48	35
P00687	AMY1_MOUSE	Alpha-amylase 1	12	28,38	32
Q9D7Z6	CLCA1_MOUSE	Calcium-activated chloride channel regulator 1	19	22,02	31
P00688	AMYP_MOUSE	Pancreatic alpha-amylase	11	24,80	30
P20918	PLMN_MOUSE	Plasminogen	15	15,52	29
Q91X17	UROM_MOUSE	Uromodulin	14	18,85	29
O08677-2	KNG1_MOUSE	Isoform LMW of Kininogen-1	12	35,42	29
P21614	VTDB_MOUSE	Vitamin D-binding protein	9	17,02	28
P13634	CAH1_MOUSE	Carbonic anhydrase 1	12	59,39	26
Q9QZZ6	DERM_MOUSE	Dermatopontin	9	28,36	26
P97298	PEDF_MOUSE	Pigment epithelium-derived factor	10	32,37	25
Q02596	GLCM1_MOUSE	Glycosylation-dependent cell adhesion molecule 1	7	29,14	25
Q9WVH9	FBLN5_MOUSE	Fibulin-5	7	12,95	23
P19221	THRB_MOUSE	Prothrombin	9	14,72	22
Q61704	ITIH3_MOUSE	Inter-alpha-trypsin inhibitor heavy chain H3	11	16,76	22
P02816	PIP_MOUSE	Prolactin-inducible protein homolog	8	45,21	22
Q9DBD0	ICA_MOUSE	Inhibitor of carbonic anhydrase	11	16,14	20
P51885	LUM_MOUSE	Lumican	7	22,78	18
Q8BND5	QSOX1_MOUSE	Sulfhydryl oxidase 1	7	11,10	17
P02535	K1C10_MOUSE	Keratin, type I cytoskeletal 10	8	15,44	17
Q00623	APOA1_MOUSE	Apolipoprotein A-I	7	23,86	17
P29699	FETUA_MOUSE	Alpha-2-HS-glycoprotein	7	28,70	16
Q5FW60	MUP20_MOUSE	Major urinary protein 20	2	11,05	16
Q9DBV4	MXRA8_MOUSE	Matrix remodeling-associated protein 8	5	12,67	14
Q61702	ITIH1_MOUSE	Inter-alpha-trypsin inhibitor heavy chain H1	8	11,47	13
P23953	EST1C_MOUSE	Carboxylesterase 1C	7	15,70	13
P06683	CO9_MOUSE	Complement component C9	6	13,87	13
Q05793	PGBM_MOUSE	Basement membrane-specific heparan sulfate proteoglycan core protein	6	2,27	13

USC UNIVERSIDADE DE SANTIAGO DE COMPOSTELA

P01132	EGF_MOUSE	Pro-epidermal growth factor	6	6,57	12
P46412	GPX3_MOUSE	Glutathione peroxidase 3	6	29,20	12
Q9CQ60	6PGL_MOUSE	6-phosphogluconolactonase	5	35,02	12
O09114	PTGDS_MOUSE	Prostaglandin-H2 D-isomerase	8	35,98	11
P11672	NGAL_MOUSE	Neutrophil gelatinase-associated lipocalin	7	21,00	11
P01837	IGKC_MOUSE	Immunoglobulin kappa constant	4	41,12	10
Q61247	A2AP_MOUSE	Alpha-2-antiplasmin	3	7,33	10
O09131	GSTO1_MOUSE	Glutathione S-transferase omega-1	2	7,92	10
P04104	K2C1_MOUSE	Keratin, type II cytoskeletal 1	4	5,49	10
Q922U2	K2C5_MOUSE	Keratin, type II cytoskeletal 5	4	5,00	10
P32261	ANT3_MOUSE	Antithrombin-III	5	15,91	9
A6X935	ITIH4_MOUSE	Inter alpha-trypsin inhibitor, heavy chain 4	5	5,84	9
Q07797	LG3BP_MOUSE	Galectin-3-binding protein	4	11,79	9
Q9Z1Q5	CLIC1_MOUSE	Chloride intracellular channel protein 1	4	21,16	9
P10493	NID1_MOUSE	Nidogen-1	4	4,82	9
Q61646	HPT_MOUSE	Haptoglobin	3	9,22	9
P04939	MUP3_MOUSE	Major urinary protein 3	2	10,87	9
P29788	VTNC_MOUSE	Vitronectin	6	15,27	8
Q60590	A1AG1_MOUSE	Alpha-1-acid glycoprotein 1	5	27,54	8
Q6GU68	ISLR_MOUSE	Immunoglobulin superfamily containing leucine-rich repeat protein	4	10,28	8
P21460	CYTC_MOUSE	Cystatin-C	4	32,14	8
P07361	A1AG2_MOUSE	Alpha-1-acid glycoprotein 2	5	24,64	8
Q61703	ITIH2_MOUSE	Inter-alpha-trypsin inhibitor heavy chain H2	5	7,82	7
P30412	PPIC_MOUSE	Peptidyl-prolyl cis-trans isomerase C	3	18,87	7
Q00724	RET4_MOUSE	Retinol-binding protein 4	4	20,40	7
P11679	K2C8_MOUSE	Keratin, type II cytoskeletal 8	4	6,94	7
P06909	CFAH_MOUSE	Complement factor H	3	3,08	7
P10923	OSTP_MOUSE	Osteopontin	2	3,06	7
Q60847	COCA1_MOUSE	Collagen alpha-1(XII) chain	3	1,06	6
P63017	HSP7C_MOUSE	Heat shock cognate 71 kDa protein	6	8,82	6
Q9CQI6	COTL1_MOUSE	Coactosin-like protein	5	23,94	6
P07309	TTHY_MOUSE	Transthyretin	4	41,50	6
P01898	HA10_MOUSE	H-2 class I histocompatibility antigen, Q10 alpha chain	4	16,00	6
Q9JII6	AK1A1_MOUSE	Aldo-keto reductase family 1 member A1	3	12,00	6
Q9WUU7	CATZ_MOUSE	Cathepsin Z	2	6,21	6
P07146	TRY2_MOUSE	Anionic trypsin-2	2	12,20	6
P18419	SVS4_MOUSE	Seminal vesicle secretory protein 4	2	33,63	6
Q08761	PROS_MOUSE	Vitamin K-dependent protein S	4	8,00	5
P49182	HEP2_MOUSE	Heparin cofactor 2	4	7,53	5
P19001	K1C19_MOUSE	Keratin, type I cytoskeletal 19	4	8,93	5
O09043	NAPSA_MOUSE	Napsin-A	2	5,73	5
Q06318	UTER_MOUSE	Uteroglobin	2	18,75	5
P62806	H4_MOUSE	Histone H4	1	9,71	5
Q9QUN9	DKK3_MOUSE	Dickkopf-related protein 3	2	8,60	5

Q6IFX2	K1C42_MOUSE	Keratin, type I cytoskeletal 42	3	6,19	5
Q8VED5	K2C79_MOUSE	Keratin, type II cytoskeletal 79	2	3,58	5
P12246	SAMP_MOUSE	Serum amyloid P-component	4	16,96	4
P08228	SODC_MOUSE	Superoxide dismutase [Cu-Zn]	3	23,38	4
Q9DBH5	LMAN2_MOUSE	Vesicular integral-membrane protein VIP36	3	8,66	4
P08226	APOE_MOUSE	Apolipoprotein E	3	12,22	4
Q02819	NUCB1_MOUSE	Nucleobindin-1	3	7,41	4
P63101	1433Z_MOUSE	14-3-3 protein zeta/delta	2	9,80	4
O09051	GUC2B_MOUSE	Guanylate cyclase activator 2B	2	25,47	4
P81117	NUCB2_MOUSE	Nucleobindin-2	2	7,14	4
P35230	REG3B_MOUSE	Regenerating islet-derived protein 3-beta	3	17,71	4
P14211	CALR_MOUSE	Calreticulin	2	4,33	4
O70570	PIGR_MOUSE	Polymeric immunoglobulin receptor	2	2,72	4
O08709	PRDX6_MOUSE	Peroxiredoxin-6	2	8,04	4
P01887	B2MG_MOUSE	Beta-2-microglobulin	1	7,56	4
O54990	PROM1_MOUSE	Prominin-1	3	5,07	3
P18761	CAH6_MOUSE	Carbonic anhydrase 6	2	11,99	3
P57780	ACTN4_MOUSE	Alpha-actinin-4	2	2,41	3
P70412	CUZD1_MOUSE	CUB and zona pellucida-like domain-containing protein 1	2	6,27	3
Q9DAK9	PHP14_MOUSE	14 kDa phosphohistidine phosphatase	2	25,00	3
Q61592	GAS6_MOUSE	Growth arrest-specific protein 6	2	3,56	3
P01635	KV5A3_MOUSE	Ig kappa chain V-V region K2 (Fragment)	2	20,00	3
P28665	MUG1_MOUSE	Murinoglobulin-1	2	1,29	3
P49183	DNAS1_MOUSE	Deoxyribonuclease-1	2	6,69	3
Q9D3H2	OBP1A_MOUSE	Odorant-binding protein 1a	2	14,11	3
P45700	MA1A1_MOUSE	Mannosyl-oligosaccharide 1,2-alpha-mannosidase IA	2	3,66	3
Q8VCG4	CO8G_MOUSE	Complement component C8 gamma chain	2	12,38	3
Q8BPB5	FBLN3_MOUSE	EGF-containing fibulin-like extracellular matrix protein 1	2	4,06	3
Q80XI7	VOME_MOUSE	Vomeromodulin	3	6,77	3
P97290	IC1_MOUSE	Plasma protease C1 inhibitor	1	2,18	3
Q80YX1	TENA_MOUSE	Tenascin	2	0,95	2
Q8BFR5	EFTU_MOUSE	Elongation factor Tu, mitochondrial	1	2,43	2
Q9WVJ9	FBLN4_MOUSE	EGF-containing fibulin-like extracellular matrix protein 2	2	8,13	2
Q8R121	ZPI_MOUSE	Protein Z-dependent protease inhibitor	2	4,91	2
O88322	NID2_MOUSE	Nidogen-2	2	2,21	2
Q07235	GDN_MOUSE	Glia-derived nexin	2	6,04	2
P01843	LAC1_MOUSE	Ig lambda-1 chain C region	2	27,62	2
Q923D2	BLVRB_MOUSE	Flavin reductase (NADPH)	2	12,62	2
P56480	ATPB_MOUSE	ATP synthase subunit beta, mitochondrial	2	4,73	2
O88968	TCO2_MOUSE	Transcobalamin-2	2	5,58	2
P30933	SVS5_MOUSE	Seminal vesicle secretory protein 5	2	22,95	2
P82198	BGH3_MOUSE	Transforming growth factor-beta-induced protein ig-h3	1	1,90	2
Q99LJ1	FUCO_MOUSE	Tissue alpha-L-fucosidase	1	2,43	2

USC UNIVERSIDADE DE SANTIAGO DE COMPOSTELA

Q91V98	CD248_MOUSE	Endosialin	1	1,31	2
P07214	SPRC_MOUSE	SPARC	1	4,64	2
P09803	CADH1_MOUSE	Cadherin-1	1	1,58	2
P15947	KLK1_MOUSE	Kallikrein-1	1	8,43	2
P30275	KCRU_MOUSE	Creatine kinase U-type, mitochondrial	1	2,39	2
P28825	MEP1A_MOUSE	Meprin A subunit alpha	1	1,21	2
Q9Z1T2	TSP4_MOUSE	Thrombospondin-4	1	1,56	2
P35441	TSP1_MOUSE	Thrombospondin-1	1	0,94	2
A2AEP0	OBP1B_MOUSE	Odorant-binding protein 1b	2	17,54	1
P39061	COIA1_MOUSE	Collagen alpha-1(XVIII) chain	1	0,96	1
P55288	CAD11_MOUSE	Cadherin-11	1	1,26	1
Q3UV17	K22O_MOUSE	Keratin, type II cytoskeletal 2 oral	2	2,69	1
Q80Z19	MUC2_MOUSE	Mucin-2 (Fragments)	1	0,37	1
Q01721	GAS1_MOUSE	Growth arrest-specific protein 1	1	3,21	1
P51910	APOD_MOUSE	Apolipoprotein D	1	6,35	1
P16125	LDHB_MOUSE	L-lactate dehydrogenase B chain	1	2,69	1
Q8K1H9	OBP2A_MOUSE	Odorant-binding protein 2a	1	5,11	1
P04938	MUP11_MOUSE	Major urinary protein 11	56	69,61	
Q8BH35	CO8B_MOUSE	Complement component C8 beta chain	4	7,64	
P01668	KV3AG_MOUSE	Ig kappa chain V-III region PC 7210	2	30,91	
P62984	RL40_MOUSE	Ubiquitin-60S ribosomal protein L40	2	17,19	
P01869	IGH1M_MOUSE	Ig gamma-1 chain C region, membrane-bound form	2	5,60	
P01631	KV2A7_MOUSE	Ig kappa chain V-II region 26-10	3	17,70	
P84244	H33_MOUSE	Histone H3.3	2	10,29	
P01867	IGG2B_MOUSE	Ig gamma-2B chain C region	2	6,44	
P06684	CO5_MOUSE	Complement C5	1	0,77	
O09010	LFNG_MOUSE	Beta-1,3-N-acetylglucosaminyltransferase lunatic fringe	1	2,91	
Q9QWL7	K1C17_MOUSE	Keratin, type I cytoskeletal 17	4	8,31	
Q9CQI3	GMFB_MOUSE	Glia maturation factor beta	1	16,20	
Q07968	F13B_MOUSE	Coagulation factor XIII B chain	2	1,49	
O88593	PGRP1_MOUSE	Peptidoglycan recognition protein 1	1	6,59	
Q9R1Q9	VAS1_MOUSE	V-type proton ATPase subunit S1	1	3,89	
Q9D733	GP2_MOUSE	Pancreatic secretory granule membrane major glycoprotein GP2	1	2,26	
Q9CQM5	TXD17_MOUSE	Thioredoxin domain-containing protein 17	1	7,32	
Q62009	POSTN_MOUSE	Periostin	1	1,67	
Q3TA59	JMJD8_MOUSE	JmjC domain-containing protein 8	1	4,80	
P35459	LY6D_MOUSE	Lymphocyte antigen 6D	1	11,02	
P26339	CMGA_MOUSE	Chromogranin-A	1	4,10	
P01878	IGHA_MOUSE	Ig alpha chain C region	1	4,36	
P01636	KV5A4_MOUSE	Ig kappa chain V-V region MOPC 149	1	12,04	
P57096	PSCA_MOUSE	Prostate stem cell antigen	1	8,13	
Q62165	DAG1_MOUSE	Dystroglycan	1	1,79	
P52480	KPYM_MOUSE	Pyruvate kinase PKM	1	2,07	

USC UNIVERSIDADE DE SANTIAGO DE COMPOSTELA

Q9Z1R3	APOM_MOUSE	Apolipoprotein M	1	3,68
Q60854	SPB6_MOUSE	Serpin B6	1	2,65
Q9D0L8	MCES_MOUSE	mRNA cap guanine-N7 methyltransferase	1	1,72
P68373	TBA1C_MOUSE	Tubulin alpha-1C chain	1	3,34
P09036	ISK1_MOUSE	Serine protease inhibitor Kazal-type 1	1	8,75
Q9WTS2	FUT8_MOUSE	Alpha-(1,6)-fucosyltransferase	1	1,04
Q8K419	LEG4_MOUSE	Galectin-4	1	2,15
P81183	IKZF2_MOUSE	Zinc finger protein Helios	1	1,90
P16110	LEG3_MOUSE	Galectin-3	1	5,68
Q9JMK0	B4GT5_MOUSE	Beta-1,4-galactosyltransferase 5	1	2,06
P06330	HVM51_MOUSE	Ig heavy chain V region AC38 205.12	1	16,10
O09159	MA2B1_MOUSE	Lysosomal alpha-mannosidase	1	1,28
Q8VHC3	SELM_MOUSE	Selenoprotein M	1	9,66
Q8BHL4	RAI3_MOUSE	Retinoic acid-induced protein 3	1	3,65
P60843	IF4A1_MOUSE	Eukaryotic initiation factor 4A-I	1	2,46
Q8BNJ6	NETO2_MOUSE	Neuropilin and tolloid-like protein 2	1	1,33
O88312	AGR2_MOUSE	Anterior gradient protein 2 homolog	1	6,29
Q9D2G2	ODO2_MOUSE	Dihydrolipoyllysine-residue succinyltransferase component of 2-oxoglutarate dehydrogenase complex, mitochondrial	1	1,76
Q91W90	TXND5_MOUSE	Thioredoxin domain-containing protein 5	1	3,36
P16294	FA9_MOUSE	Coagulation factor IX	1	1,91

Supplementary Table 9. Protein list of all identified proteins by qualitative mass spectrometry analysis in band 1 (ExoGAG isolated fraction of control sample).

Entry Name	UniProt Name	Protein Name	Peptides(95%)	%Cov(95)	Total spectrum count
P07911	UROM_HUMAN	Uromodulin	236	63,13	745
P02768	ALBU_HUMAN	Albumin	94	69,79	665
P68871	HBB_HUMAN	Hemoglobin subunit beta	25	95,24	67
P02042	HBD_HUMAN	Hemoglobin subunit delta	18	48,98	41
Q08380	LG3BP_HUMAN	Galectin-3-binding protein	18	29,91	30
P04264	K2C1_HUMAN	Keratin, type II cytoskeletal 1	15	21,43	24
P69905	HBA_HUMAN	Hemoglobin subunit alpha	16	71,13	23
P01133	EGF_HUMAN	Pro-epidermal growth factor	12	12,01	19
P01857	IGHG1_HUMAN	Immunoglobulin heavy constant gamma 1	8	34,55	14
P05155	IC1_HUMAN	Plasma protease C1 inhibitor	8	16,80	14
P02647	APOA1_HUMAN	Apolipoprotein A-I	9	31,84	12
P13645	K1C10_HUMAN	Keratin, type I cytoskeletal 10	8	13,87	12
Q6EMK4	VASN_HUMAN	Vasorin	6	11,89	10
P02760	AMBP_HUMAN	Protein AMBP	7	19,32	8
P01859	IGHG2_HUMAN	Immunoglobulin heavy constant gamma 2	4	11,66	7
P01834	IGKC_HUMAN	Immunoglobulin kappa constant	4	79,44	7
P35527	K1C9_HUMAN	Keratin, type I cytoskeletal 9	4	7,86	7
P08473	NEP_HUMAN	Neprilysin	3	4,00	7
P01009	A1AT_HUMAN	Alpha-1-antitrypsin	5	16,99	6
P00738	HPT_HUMAN	Haptoglobin	3	8,13	6

USC DE COMPOSTELA

P15144	AMPN_HUMAN	Aminopeptidase N	4	4,55	5
P08779	K1C16_HUMAN	Keratin, type I cytoskeletal 16	4	7,82	5
P01876	IGHA1_HUMAN	Immunoglobulin heavy constant alpha 1	4	19,26	4
P63261	ACTG_HUMAN	Actin, cytoplasmic 2	2	9,07	3
P12109	CO6A1_HUMAN	Collagen alpha-1(VI) chain	3	3,79	3
P02671	FIBA_HUMAN	Fibrinogen alpha chain	2	2,54	3
P02787	TRFE_HUMAN	Serotransferrin	2	7,16	3
P01011	AACT_HUMAN	Alpha-1-antichymotrypsin	2	4,73	2
P01023	A2MG_HUMAN	Alpha-2-macroglobulin	2	2,92	2
P16070	CD44_HUMAN	CD44 antigen	2	2,56	2
P02679	FIBG_HUMAN	Fibrinogen gamma chain	2	7,73	2
P62805	H4_HUMAN	Histone H4	1	7,77	2
P0DOY3	IGLC3_HUMAN	Immunoglobulin lambda constant 3	2	23,58	2
P01833	PIGR_HUMAN	Polymeric immunoglobulin receptor	1	2,49	2
P01008	ANT3_HUMAN	Antithrombin-III	1	4,96	1
P01024	CO3_HUMAN	Complement C3	1	0,78	1
P51884	LUM_HUMAN	Lumican	1	2,37	1
P13473	LAMP2_HUMAN	Lysosome-associated membrane glycoprotein 2	1	1,95	1
Q6UXB8	PI16_HUMAN	Peptidase inhibitor 16	1	2,16	1
Q695T7	S6A19_HUMAN	Sodium-dependent neutral amino acid transporter B(0)AT1	1	1,73	1
P02766	TTHY_HUMAN	Transthyretin	1	19,05	1
P08670	VIME_HUMAN	Vimentin	1	2,15	1
P36957	ODO2_HUMAN	Dihydrolipoyllysine-residue succinyltransferase component of 2-oxoglutarate dehydrogenase complex, mitochondrial	1	1,77	
Q9BTM1	H2AJ_HUMAN	Histone H2A.J	1	6,98	
P01871	IGHM_HUMAN	Immunoglobulin heavy constant mu	1	3,31	

Supplementary Table 10. Protein list of all identified proteins by qualitative mass spectrometry analysis in band 2 (ExoGAG isolated fraction of low creatinine *PKD2* sample).

Entry Name	UniProt Name	Protein Name	Peptides(95%)	%Cov(95)	Total spectrum count
P07911	UROM_HUMAN	Uromodulin	299	68,44	1331
P02768	ALBU_HUMAN	Albumin	65	69,62	373
P68871	HBB_HUMAN	Hemoglobin subunit beta	40	95,24	112
Q08380	LG3BP_HUMAN	Galectin-3-binding protein	33	40,34	88
P02042	HBD_HUMAN	Hemoglobin subunit delta	28	57,14	71
P01133	EGF_HUMAN	Pro-epidermal growth factor	25	21,71	49
P08473	NEP_HUMAN	Neprilysin	28	40,27	47
P69905	HBA_HUMAN	Hemoglobin subunit alpha	22	71,83	40
P02760	AMBP_HUMAN	Protein AMBP	13	22,73	32
P27487	DPP4_HUMAN	Dipeptidyl peptidase 4	17	25,59	27
Q6EMK4	VASN_HUMAN	Vasorin	15	16,34	27
P54802	ANAG_HUMAN	Alpha-N-acetylglucosaminidase	17	29,34	26
P01857	IGHG1_HUMAN	Immunoglobulin heavy constant gamma 1	15	47,58	26

Q8WUM4	PDC6I_HUMAN	Programmed cell death 6-interacting protein	14	19,24	22
P00450	CERU_HUMAN	Ceruloplasmin	13	16,34	21
P01859	IGHG2_HUMAN	Immunoglobulin heavy constant gamma 2	11	28,22	21
P04264	K2C1_HUMAN	Keratin, type II cytoskeletal 1	15	22,83	21
P15144	AMPN_HUMAN	Aminopeptidase N	19	20,06	14
P98164	LRP2_HUMAN	Low-density lipoprotein receptor-related protein 2	8	1,74	12
P05155	IC1_HUMAN	Plasma protease C1 inhibitor	6	13,60	12
P01834	IGKC_HUMAN	Immunoglobulin kappa constant	5	66,36	11
P13645	K1C10_HUMAN	Keratin, type I cytoskeletal 10	7	10,27	11
P35527	K1C9_HUMAN	Keratin, type I cytoskeletal 9	7	18,78	11
P07359	GP1BA_HUMAN	Platelet glycoprotein Ib alpha chain	3	4,76	10
P01024	CO3_HUMAN	Complement C3	5	3,13	9
P63261	ACTG_HUMAN	Actin, cytoplasmic 2	5	18,13	8
P01833	PIGR_HUMAN	Polymeric immunoglobulin receptor	4	6,41	8
P01009	A1AT_HUMAN	Alpha-1-antitrypsin	4	12,44	7
P16070	CD44_HUMAN	CD44 antigen	5	5,26	7
P78385	KRT83_HUMAN	Keratin, type II cuticular Hb3	4	5,68	7
P02751	FINC_HUMAN	Fibronectin	3	1,51	6
P62805	H4_HUMAN	Histone H4	3	29,13	6
P0DOY3	IGLC3_HUMAN	Immunoglobulin lambda constant 3	5	55,66	6
P51884	LUM_HUMAN	Lumican	5	19,53	6
P02787	TRFE_HUMAN	Serotransferrin	2	3,01	6
P13727	PRG2_HUMAN	Bone marrow proteoglycan	3	13,06	5
P13473	LAMP2_HUMAN	Lysosome-associated membrane glycoprotein 2	1	1,95	5
P00738	HPT_HUMAN	Haptoglobin	4	12,32	4
Q99880	H2B1L_HUMAN	Histone H2B type 1-L	2	11,90	3
P01876	IGHA1_HUMAN	Immunoglobulin heavy constant alpha 1	4	18,70	3
Q15323	K1H1_HUMAN	Keratin, type I cuticular Ha1	3	8,41	3
P01042	KNG1_HUMAN	Kininogen-1	1	1,24	3
P11279	LAMP1_HUMAN	Lysosome-associated membrane glycoprotein 1	1	2,64	3
Q695T7	S6A19_HUMAN	Sodium-dependent neutral amino acid transporter B(0)AT1	2	3,31	3
Q9BQE3	TBA1C_HUMAN	Tubulin alpha-1C chain	1	3,34	3
P02647	APOA1_HUMAN	Apolipoprotein A-I	10	38,95	2
Q53GD3	CTL4_HUMAN	Choline transporter-like protein 4	1	1,97	2
Q9NSB4	KRT82_HUMAN	Keratin, type II cuticular Hb2	1	1,95	2
P31431	SDC4_HUMAN	Syndecan-4	2	11,11	2
P08670	VIME_HUMAN	Vimentin	2	5,15	2
P01023	A2MG_HUMAN	Alpha-2-macroglobulin	1	0,68	1
P31327	CPSM_HUMAN	Carbamoyl-phosphate synthase [ammonia], mitochondrial	1	0,73	1
P10909	CLUS_HUMAN	Clusterin	1	2,67	1
P02679	FIBG_HUMAN	Fibrinogen gamma chain	1	4,41	1
Q07075	AMPE_HUMAN	Glutamyl aminopeptidase	1	1,25	1
Q9BXP8	PAPP2_HUMAN	Pappalysin-2	1	0,50	1

P04004	VTNC_HUMAN	Vitronectin	1	3,14	1
P62269	RS18_HUMAN	40S ribosomal protein S18	1	5,26	
P12814	ACTN1_HUMAN	Alpha-actinin-1	1	1,35	
P39060	COIA1_HUMAN	Collagen alpha-1(XVIII) chain	1	0,51	
Q9BTM1	H2AJ_HUMAN	Histone H2A.J	2	12,40	
O76009	KT33A_HUMAN	Keratin, type I cuticular Ha3-I	2	4,95	
O76013	KRT36_HUMAN	Keratin, type I cuticular Ha6	2	3,21	
P19012	K1C15_HUMAN	Keratin, type I cytoskeletal 15	3	6,14	
O43451	MGA_HUMAN	Maltase-glucoamylase, intestinal	1	0,54	
Q92542	NICA_HUMAN	Nicastrin	1	1,55	
Q5VTE0	EF1A3_HUMAN	Putative elongation factor 1-alpha-like 3	1	2,38	
Q9BVA1	TBB2B_HUMAN	Tubulin beta-2B chain	1	3,15	
P62987	RL40_HUMAN	Ubiquitin-60S ribosomal protein L40	1	12,50	

Supplementary Table 11. Protein list of all identified proteins by qualitative mass spectrometry analysis in band 3 (ExoGAG isolated fraction of medium creatinine *PKD2* sample).

Entry Name	UniProt Name	Protein Name	Peptides(95%)	%Cov(95)	Total spectrum count
P07911	UROM_HUMAN	Uromodulin	205	64,69	708
P02768	ALBU_HUMAN	Albumin	52	61,58	239
P68871	HBB_HUMAN	Hemoglobin subunit beta	31	84,35	98
P02042	HBD_HUMAN	Hemoglobin subunit delta	23	71,43	59
P01857	IGHG1_HUMAN	Immunoglobulin heavy constant gamma 1	19	53,33	42
P01859	IGHG2_HUMAN	Immunoglobulin heavy constant gamma 2	17	35,58	37
P69905	HBA_HUMAN	Hemoglobin subunit alpha	17	71,83	35
Q08380	LG3BP_HUMAN	Galectin-3-binding protein	16	29,74	30
P04264	K2C1_HUMAN	Keratin, type II cytoskeletal 1	18	27,95	27
P02760	AMBP_HUMAN	Protein AMBP	14	30,40	27
P00450	CERU_HUMAN	Ceruloplasmin	20	22,91	26
P01024	CO3_HUMAN	Complement C3	20	14,13	24
Q6EMK4	VASN_HUMAN	Vasorin	11	16,34	22
P01834	IGKC_HUMAN	Immunoglobulin kappa constant	9	79,44	17
P13645	K1C10_HUMAN	Keratin, type I cytoskeletal 10	16	27,23	17
P01023	A2MG_HUMAN	Alpha-2-macroglobulin	10	8,68	15
P02647	APOA1_HUMAN	Apolipoprotein A-I	11	40,45	15
P51884	LUM_HUMAN	Lumican	10	33,43	15
P08473	NEP_HUMAN	Neprilysin	9	13,60	15
P0C0L5	CO4B_HUMAN	Complement C4-B	11	9,58	14
Q6UXB8	PI16_HUMAN	Peptidase inhibitor 16	9	23,54	14
P07359	GP1BA_HUMAN	Platelet glycoprotein Ib alpha chain	1	1,69	14
P0C0L4	CO4A_HUMAN	Complement C4-A	10	9,40	13
P15144	AMPN_HUMAN	Aminopeptidase N	9	10,75	12
P0DOY3	IGLC3_HUMAN	Immunoglobulin lambda constant 3	5	55,66	12
P05155	IC1_HUMAN	Plasma protease C1 inhibitor	5	12,40	10
P01833	PIGR_HUMAN	Polymeric immunoglobulin receptor	12	15,45	10

USC UNIVERSIDADE DE SANTIAGO DE COMPOSTELA

P02787	TRFE_HUMAN	Serotransferrin	6	9,46	10
P13646	K1C13_HUMAN	Keratin, type I cytoskeletal 13	6	12,88	8
P01009	A1AT_HUMAN	Alpha-1-antitrypsin	4	11,00	7
P00738	HPT_HUMAN	Haptoglobin	6	17,98	7
P35527	K1C9_HUMAN	Keratin, type I cytoskeletal 9	8	18,46	7
P01133	EGF_HUMAN	Pro-epidermal growth factor	4	3,48	7
P63261	ACTG_HUMAN	Actin, cytoplasmic 2	6	19,47	6
P01876	IGHA1_HUMAN	Immunoglobulin heavy constant alpha 1	5	23,51	6
P04259	K2C6B_HUMAN	Keratin, type II cytoskeletal 6B	5	9,40	6
P16070	CD44_HUMAN	CD44 antigen	3	4,18	4
Q9NPY3	C1QR1_HUMAN	Complement component C1q receptor	4	8,59	4
P10643	CO7_HUMAN	Complement component C7	4	6,17	4
P19013	K2C4_HUMAN	Keratin, type II cytoskeletal 4	3	6,18	4
P54802	ANAG_HUMAN	Alpha-N-acetylglucosaminidase	3	5,79	3
P01031	CO5_HUMAN	Complement C5	2	1,31	3
P02671	FIBA_HUMAN	Fibrinogen alpha chain	1	0,92	3
P08779	K1C16_HUMAN	Keratin, type I cytoskeletal 16	5	9,30	3
Q9BXP8	PAPP2_HUMAN	Pappalysin-2	1	0,50	3
P00747	PLMN_HUMAN	Plasminogen	1	1,98	3
P01011	AACT_HUMAN	Alpha-1-antichymotrypsin	1	2,13	2
P00915	CAH1_HUMAN	Carbonic anhydrase 1	1	3,45	2
P27487	DPP4_HUMAN	Dipeptidyl peptidase 4	2	2,22	2
P02679	FIBG_HUMAN	Fibrinogen gamma chain	2	6,18	2
P23142	FBLN1_HUMAN	Fibulin-1	1	1,71	2
Q07075	AMPE_HUMAN	Glutamyl aminopeptidase	1	1,25	2
P19823	ITIH2_HUMAN	Inter-alpha-trypsin inhibitor heavy chain H2	2	2,75	2
Q8WUM4	PDC6I_HUMAN	Programmed cell death 6-interacting protein	1	1,15	2
P02766	TTHY_HUMAN	Transthyretin	1	8,84	2
P08670	VIME_HUMAN	Vimentin	1	2,15	2
P06576	ATPB_HUMAN	ATP synthase subunit beta, mitochondrial	1	1,89	1
Q9HCU0	CD248_HUMAN	Endosialin	1	1,06	1
P06396	GELS_HUMAN	Gelsolin	1	1,66	1
P02790	HEMO_HUMAN	Hemopexin	1	2,38	1
P06310	KV230_HUMAN	Immunoglobulin kappa variable 2-30	1	10,83	1
P01700	LV147_HUMAN	Immunoglobulin lambda variable 1-47	1	11,11	1
Q14624	ITIH4_HUMAN	Inter-alpha-trypsin inhibitor heavy chain H4	1	0,97	1
P98164	LRP2_HUMAN	Low-density lipoprotein receptor-related protein 2	1	0,21	1
P13473	LAMP2_HUMAN	Lysosome-associated membrane glycoprotein 2	1	1,95	1
P04004	VTNC_HUMAN	Vitronectin	1	2,51	1
P06681	CO2_HUMAN	Complement C2	1	1,60	
P06312	KV401_HUMAN	Immunoglobulin kappa variable 4-1	1	7,44	
P62987	RL40_HUMAN	Ubiquitin-60S ribosomal protein L40	1	12,50	

USC UNIVERSIDADE DE SANTIAGO DE COMPOSTELA

Supplementary Table 12.Protein list of all identified proteins by qualitative mass spectrometry analysis in band 4 (ExoGAG isolated fraction of medium creatinine *PKD2* sample)

Entry Name	UniProt Name	Protein Name	Peptides(95%)	%Cov(95)	Total spectrum count
P02768	ALBU_HUMAN	Albumin	416	82,59	1348
P01009	A1AT_HUMAN	Alpha-1-antitrypsin	82	70,10	201
P07911	UROM_HUMAN	Uromodulin	66	31,09	173
P68871	HBB_HUMAN	Hemoglobin subunit beta	33	84,35	87
P19013	K2C4_HUMAN	Keratin, type II cytoskeletal 4	31	47,94	73
P01860	IGHG3_HUMAN	Immunoglobulin heavy constant gamma 3	30	55,44	64
P01011	AACT_HUMAN	Alpha-1-antichymotrypsin	24	34,28	51
P02042	HBD_HUMAN	Hemoglobin subunit delta	20	54,42	51
P01042	KNG1_HUMAN	Kininogen-1	28	31,37	49
P10451	OSTP_HUMAN	Osteopontin	24	55,41	47
P01857	IGHG1_HUMAN	Immunoglobulin heavy constant gamma 1	21	44,85	46
P02760	AMBP_HUMAN	Protein AMBP	28	30,68	44
P01859	IGHG2_HUMAN	Immunoglobulin heavy constant gamma 2	16	35,58	43
P01876	IGHA1_HUMAN	Immunoglobulin heavy constant alpha 1	14	40,79	40
P69905	HBA_HUMAN	Hemoglobin subunit alpha	16	71,83	35
P01019	ANGT_HUMAN	Angiotensinogen	14	28,87	34
P04264	K2C1_HUMAN	Keratin, type II cytoskeletal 1	20	30,43	34
P02787	TRFE_HUMAN	Serotransferrin	22	33,09	31
P16070	CD44_HUMAN	CD44 antigen	12	5,66	26
P01024	CO3_HUMAN	Complement C3	16	11,37	25
P13645	K1C10_HUMAN	Keratin, type I cytoskeletal 10	14	24,49	23
P51884	LUM_HUMAN	Lumican	10	33,43	23
P02538	K2C6A_HUMAN	Keratin, type II cytoskeletal 6A	12	19,68	19
P13647	K2C5_HUMAN	Keratin, type II cytoskeletal 5	16	26,95	17
P16278	BGAL_HUMAN	Beta-galactosidase	9	14,48	16
P02647	APOA1_HUMAN	Apolipoprotein A-I	8	33,33	15
P01877	IGHA2_HUMAN	Immunoglobulin heavy constant alpha 2	5	18,24	15
P05543	THBG_HUMAN	Thyroxine-binding globulin	10	27,95	15
P35527	K1C9_HUMAN	Keratin, type I cytoskeletal 9	12	20,55	14
P04004	VTNC_HUMAN	Vitronectin	9	14,44	11
P0C0L5	CO4B_HUMAN	Complement C4-B	6	3,90	10
P00751	CFAB_HUMAN	Complement factor B	8	12,43	10
P19440	GGT1_HUMAN	Glutathione hydrolase 1 proenzyme	4	8,61	9
P02790	HEMO_HUMAN	Hemopexin	7	16,45	9
P19823	ITIH2_HUMAN	Inter-alpha-trypsin inhibitor heavy chain H2	5	8,77	9
P00450	CERU_HUMAN	Ceruloplasmin	7	7,51	8
Q9Y5Y7	LYVE1_HUMAN	Lymphatic vessel endothelial hyaluronic acid receptor 1	4	9,01	8
Q6EMK4	VASN_HUMAN	Vasorin	5	9,96	8
P13727	PRG2_HUMAN	Bone marrow proteoglycan	3	17,57	7

USC UNIVERSIDADE DE SANTIAGO DE COMPOSTELA

P02748	CO9_HUMAN	Complement component C9	5	9,84	7
P08185	CBG_HUMAN	Corticosteroid-binding globulin	4	10,37	7
Q08380	LG3BP_HUMAN	Galectin-3-binding protein	6	12,82	6
P63261	ACTG_HUMAN	Actin, cytoplasmic 2	3	11,20	5
P08174	DAF_HUMAN	Complement decay-accelerating factor	2	5,51	5
P02671	FIBA_HUMAN	Fibrinogen alpha chain	2	2,43	5
Q9UBX5	FBLN5_HUMAN	Fibulin-5	4	9,15	5
P00738	HPT_HUMAN	Haptoglobin	5	16,01	5
P01834	IGKC_HUMAN	Immunoglobulin kappa constant	3	47,66	5
P15144	AMPN_HUMAN	Aminopeptidase N	4	4,14	4
P01780	HV307_HUMAN	Immunoglobulin heavy variable 3-7	3	23,93	4
P0DOY3	IGLC3_HUMAN	Immunoglobulin lambda constant 3	3	37,74	4
P02765	FETUA_HUMAN	Alpha-2-HS-glycoprotein	3	10,08	3
P01008	ANT3_HUMAN	Antithrombin-III	4	9,05	3
P18428	LBP_HUMAN	Lipopolysaccharide-binding protein	3	8,32	3
Q96PD5	PGRP2_HUMAN	N-acetylmuramoyl-L-alanine amidase	1	2,43	3
P51688	SPHM_HUMAN	N-sulphoglucosamine sulphohydrolase	2	4,78	3
P14618	KPYM_HUMAN	Pyruvate kinase PKM	2	4,14	3
P23470	PTPRG_HUMAN	Receptor-type tyrosine-protein phosphatase gamma	3	2,56	3
P81605	DCD_HUMAN	Dermcidin	2	12,73	2
P19827	ITIH1_HUMAN	Inter-alpha-trypsin inhibitor heavy chain H1	1	1,10	2
Q66K66	TM198_HUMAN	Transmembrane protein 198	1	2,50	2
P00915	CAH1_HUMAN	Carbonic anhydrase 1	1	3,45	1
P02675	FIBB_HUMAN	Fibrinogen beta chain	1	1,63	1
Q99880	H2B1L_HUMAN	Histone H2B type 1-L	1	7,14	1
P01871	IGHM_HUMAN	Immunoglobulin heavy constant mu	1	1,77	1
Q6UXB8	PI16_HUMAN	Peptidase inhibitor 16	1	2,16	1
P05155	IC1_HUMAN	Plasma protease C1 inhibitor	1	2,00	1
P19961	AMY2B_HUMAN	Alpha-amylase 2B	1	2,93	
P15291	B4GT1_HUMAN	Beta-1,4-galactosyltransferase 1	1	2,01	
P39060	COIA1_HUMAN	Collagen alpha-1(XVIII) chain	1	1,71	
P36957	ODO2_HUMAN	Dihydrolipoyllysine-residue succinyltransferase component of 2-oxoglutarate dehydrogenase complex, mitochondrial	1	1,77	
A0A0B4J1X5	HV374_HUMAN	Immunoglobulin heavy variable 3-74	4	31,62	
P0DP08	HVD82_HUMAN	Immunoglobulin heavy variable 4-38-2	1	7,69	
Q6UXS9	CASPC_HUMAN	Inactive caspase-12	1	6,16	
P02533	K1C14_HUMAN	Keratin, type I cytoskeletal 14	3	5,30	
P33908	MA1A1_HUMAN	Mannosyl-oligosaccharide 1,2-alpha-mannosidase IA	1	1,69	
Q13477	MADCA_HUMAN	Mucosal addressin cell adhesion molecule 1	1	3,93	
P04180	LCAT_HUMAN	Phosphatidylcholine-sterol acyltransferase	1	3,18	
Q96M19	CL067_HUMAN	Putative transmembrane protein encoded by LINC00477	1	4,22	
P53597	SUCA_HUMAN	Succinate--CoA ligase [ADP/GDP-forming] subunit alpha, mitochondrial	1	4,33	

USC UNIVERSIDADE DE SANTIAGO DE COMPOSTELA

P62987	RL40_HUMAN	Ubiquitin-60S ribosomal protein L40	1	12,50

Supplementary Table 13. Protein list of all identified proteins by qualitative mass spectrometry analysis in band 5 (ExoGAG isolated fraction of medium creatinine *PKD2* sample)

Entry Name	UniProt Name	Protein Name	Peptides(95%)	%Cov(95)	Total spectrum count
P01859	IGHG2_HUMAN	Immunoglobulin heavy constant gamma 2	50	55,83	210
P01857	IGHG1_HUMAN	Immunoglobulin heavy constant gamma 1	51	60,30	198
P02768	ALBU_HUMAN	Albumin	48	66,67	190
P07911	UROM_HUMAN	Uromodulin	32	23,75	85
P02760	AMBP_HUMAN	Protein AMBP	35	25,28	81
P68871	HBB_HUMAN	Hemoglobin subunit beta	22	83,67	67
P13646	K1C13_HUMAN	Keratin, type I cytoskeletal 13	31	58,95	53
P01009	A1AT_HUMAN	Alpha-1-antitrypsin	19	39,71	48
P02042	HBD_HUMAN	Hemoglobin subunit delta	16	53,74	43
P69905	HBA_HUMAN	Hemoglobin subunit alpha	11	71,13	30
P04264	K2C1_HUMAN	Keratin, type II cytoskeletal 1	16	25,47	30
P13645	K1C10_HUMAN	Keratin, type I cytoskeletal 10	17	24,83	29
Q9Y5Y7	LYVE1_HUMAN	Lymphatic vessel endothelial hyaluronic acid receptor 1	9	18,01	27
P01780	HV307_HUMAN	Immunoglobulin heavy variable 3-7	11	48,72	21
Q5VTE0	EF1A3_HUMAN	Putative elongation factor 1-alpha-like 3	1	2,38	19
P02790	HEMO_HUMAN	Hemopexin	8	18,83	17
P01019	ANGT_HUMAN	Angiotensinogen	10	21,24	16
P10451	OSTP_HUMAN	Osteopontin	6	19,11	16
P05154	IPSP_HUMAN	Plasma serine protease inhibitor	9	22,17	16
P02787	TRFE_HUMAN	Serotransferrin	9	14,90	16
P02750	A2GL_HUMAN	Leucine-rich alpha-2-glycoprotein	6	18,73	15
P08571	CD14_HUMAN	Monocyte differentiation antigen CD14	10	33,87	15
P02679	FIBG_HUMAN	Fibrinogen gamma chain	8	24,94	14
P08670	VIME_HUMAN	Vimentin	8	19,31	14
P02647	APOA1_HUMAN	Apolipoprotein A-I	6	27,34	12
P0C0L5	CO4B_HUMAN	Complement C4-B	4	2,64	11
P01024	CO3_HUMAN	Complement C3	7	5,29	10
P0DP03	HV335_HUMAN	Immunoglobulin heavy variable 3-30-5	5	32,48	9
P48668	K2C6C_HUMAN	Keratin, type II cytoskeletal 6C	7	12,77	9
P51884	LUM_HUMAN	Lumican	4	11,83	9
P02774	VTDB_HUMAN	Vitamin D-binding protein	6	14,14	9
Q9UBX5	FBLN5_HUMAN	Fibulin-5	5	12,72	8
P35527	K1C9_HUMAN	Keratin, type I cytoskeletal 9	5	9,47	8
P01042	KNG1_HUMAN	Kininogen-1	5	9,01	8
P01876	IGHA1_HUMAN	Immunoglobulin heavy constant alpha 1	7	20,40	7
P0DP01	HV108_HUMAN	Immunoglobulin heavy variable 1-8	5	19,66	7
P02765	FETUA_HUMAN	Alpha-2-HS-glycoprotein	5	15,80	6
P16070	CD44_HUMAN	CD44 antigen	4	5,26	6
P02748	CO9_HUMAN	Complement component C9	3	5,55	6

USC UNIVERSIDADE DE SANTIAGO DE COMPOSTELA

Q9UHL4	DPP2_HUMAN	Dipeptidyl peptidase 2	5	11,59	6
P00738	HPT_HUMAN	Haptoglobin	6	14,78	6
P23083	HV102_HUMAN	Immunoglobulin heavy variable 1-2	4	19,66	6
P0DP08	HVD82_HUMAN	Immunoglobulin heavy variable 4-38-2	4	21,37	6
P01834	IGKC_HUMAN	Immunoglobulin kappa constant	3	47,66	6
P13647	K2C5_HUMAN	Keratin, type II cytoskeletal 5	6	10,17	6
Q6UXB8	PI16_HUMAN	Peptidase inhibitor 16	4	9,50	6
P15309	PPAP_HUMAN	Prostatic acid phosphatase	5	15,03	6
P63261	ACTG_HUMAN	Actin, cytoplasmic 2	3	10,13	5
P04217	A1BG_HUMAN	Alpha-1B-glycoprotein	1	2,42	5
P00450	CERU_HUMAN	Ceruloplasmin	3	3,19	5
Q6UVK1	CSPG4_HUMAN	Chondroitin sulfate proteoglycan 4	3	1,46	5
P06396	GELS_HUMAN	Gelsolin	4	5,50	5
P36955	PEDF_HUMAN	Pigment epithelium-derived factor	3	8,13	5
P05155	IC1_HUMAN	Plasma protease C1 inhibitor	3	7,60	5
P00734	THRB_HUMAN	Prothrombin	5	10,93	5
P01008	ANT3_HUMAN	Antithrombin-III	3	9,48	4
P13727	PRG2_HUMAN	Bone marrow proteoglycan	3	13,51	4
P02671	FIBA_HUMAN	Fibrinogen alpha chain	1	0,92	4
P0DOY3	IGLC3_HUMAN	Immunoglobulin lambda constant 3	4	37,74	4
O14498	ISLR_HUMAN	Immunoglobulin superfamily containing leucine-rich repeat protein	2	6,31	4
Q9HCN6	GPVI_HUMAN	Platelet glycoprotein VI	2	7,96	4
P04004	VTNC_HUMAN	Vitronectin	3	7,74	4
P25705	ATPA_HUMAN	ATP synthase subunit alpha, mitochondrial	1	1,81	3
P06576	ATPB_HUMAN	ATP synthase subunit beta, mitochondrial	2	3,97	3
P15291	B4GT1_HUMAN	Beta-1,4-galactosyltransferase 1	2	5,28	3
P16444	DPEP1_HUMAN	Dipeptidase 1	1	3,16	3
Q9NQ84	GPC5C_HUMAN	G-protein coupled receptor family C group 5 member C	1	2,49	3
Q9BXP8	PAPP2_HUMAN	Pappalysin-2	3	1,95	3
P01011	AACT_HUMAN	Alpha-1-antichymotrypsin	1	2,13	2
P02749	APOH_HUMAN	Beta-2-glycoprotein 1	2	7,54	2
Q9Y646	CBPQ_HUMAN	Carboxypeptidase Q	2	4,24	2
P81605	DCD_HUMAN	Dermcidin	2	12,73	2
Q08380	LG3BP_HUMAN	Galectin-3-binding protein	2	4,27	2
P29622	KAIN_HUMAN	Kallistatin	2	4,92	2
P19013	K2C4_HUMAN	Keratin, type II cytoskeletal 4	3	5,24	2
Q9BTY2	FUCO2_HUMAN	Plasma alpha-L-fucosidase	1	2,36	2
P00751	CFAB_HUMAN	Complement factor B	1	1,44	1
P02675	FIBB_HUMAN	Fibrinogen beta chain	2	4,07	1
O43505	B4GA1_HUMAN	Beta-1,4-glucuronyltransferase 1	1	2,17	
P19012	K1C15_HUMAN	Keratin, type I cytoskeletal 15	12	18,42	
O43653	PSCA_HUMAN	Prostate stem cell antigen	1	8,13	
P07478	TRY2_HUMAN	Trypsin-2	3	8,10	
P62987	RL40_HUMAN	Ubiquitin-60S ribosomal protein L40	1	12,50	

Supplementary Table 14. Protein list of all identified proteins by qualitative mass spectrometry analysis in band 6 (ExoGAG isolated fraction of medium creatinine *PKD2* sample)

Entry Name	UniProt Name	Protein Name	Peptides(95%)	%Cov(95)	Total spectrum count
P02760	AMBP_HUMAN	Protein AMBP	291	64,20	1194
P68871	HBB_HUMAN	Hemoglobin subunit beta	41	84,35	147
P02768	ALBU_HUMAN	Albumin	45	64,53	140
P02042	HBD_HUMAN	Hemoglobin subunit delta	28	47,62	92
P07911	UROM_HUMAN	Uromodulin	37	27,03	87
P25311	ZA2G_HUMAN	Zinc-alpha-2-glycoprotein	26	60,40	62
P69905	HBA_HUMAN	Hemoglobin subunit alpha	24	71,83	60
P06727	APOA4_HUMAN	Apolipoprotein A-IV	27	59,34	55
P01860	IGHG3_HUMAN	Immunoglobulin heavy constant gamma 3	14	36,34	41
Q14624	ITIH4_HUMAN	Inter-alpha-trypsin inhibitor heavy chain H4	17	9,57	41
P01857	IGHG1_HUMAN	Immunoglobulin heavy constant gamma 1	16	51,21	40
P04264	K2C1_HUMAN	Keratin, type II cytoskeletal 1	20	28,42	38
P01859	IGHG2_HUMAN	Immunoglobulin heavy constant gamma 2	13	32,82	35
P01024	CO3_HUMAN	Complement C3	24	17,02	33
P06396	GELS_HUMAN	Gelsolin	13	17,26	32
P00738	HPT_HUMAN	Haptoglobin	19	41,63	32
P07478	TRY2_HUMAN	Trypsin-2	4	8,10	24
P10909	CLUS_HUMAN	Clusterin	18	33,18	23
P13645	K1C10_HUMAN	Keratin, type I cytoskeletal 10	17	24,32	23
P01009	A1AT_HUMAN	Alpha-1-antitrypsin	15	39,71	22
P02787	TRFE_HUMAN	Serotransferrin	11	18,62	22
P02790	HEMO_HUMAN	Hemopexin	10	25,32	20
Q12805	FBLN3_HUMAN	EGF-containing fibulin-like extracellular matrix protein 1	10	22,52	18
P02647	APOA1_HUMAN	Apolipoprotein A-I	11	39,33	17
P36955	PEDF_HUMAN	Pigment epithelium-derived factor	12	31,34	16
Q5VTE0	EF1A3_HUMAN	Putative elongation factor 1-alpha-like 3	2	4,98	16
P02750	A2GL_HUMAN	Leucine-rich alpha-2-glycoprotein	5	16,14	15
P35527	K1C9_HUMAN	Keratin, type I cytoskeletal 9	12	27,29	13
P63261	ACTG_HUMAN	Actin, cytoplasmic 2	9	36,27	12
Q07075	AMPE_HUMAN	Glutamyl aminopeptidase	8	7,42	12
P16070	CD44_HUMAN	CD44 antigen	4	5,26	11
O94919	ENDD1_HUMAN	Endonuclease domain-containing 1 protein	9	26,40	11
P04406	G3P_HUMAN	Glyceraldehyde-3-phosphate dehydrogenase	7	22,69	11
P05155	IC1_HUMAN	Plasma protease C1 inhibitor	3	7,60	10
P0C0L5	CO4B_HUMAN	Complement C4-B	6	4,30	8
P02671	FIBA_HUMAN	Fibrinogen alpha chain	7	7,97	8
P13646	K1C13_HUMAN	Keratin, type I cytoskeletal 13	5	8,95	8
P04259	K2C6B_HUMAN	Keratin, type II cytoskeletal 6B	7	12,77	8
P01011	AACT_HUMAN	Alpha-1-antichymotrypsin	5	13,48	7
P05090	APOD_HUMAN	Apolipoprotein D	4	22,75	7
P10645	CMGA_HUMAN	Chromogranin-A	1	4,16	7
P00751	CFAB_HUMAN	Complement factor B	4	7,72	7
P13647	K2C5_HUMAN	Keratin, type II cytoskeletal 5	6	10,00	7

Q12907	LMAN2_HUMAN	Vesicular integral-membrane protein VIP36	3	12,08	7
Q13510	ASAH1_HUMAN	Acid ceramidase	3	6,84	6
P02748	CO9_HUMAN	Complement component C9	4	8,41	6
P02679	FIBG_HUMAN	Fibrinogen gamma chain	3	10,15	6
P01834	IGKC_HUMAN	Immunoglobulin kappa constant	3	47,66	6
P08670	VIME_HUMAN	Vimentin	6	13,30	6
P02763	A1AG1_HUMAN	Alpha-1-acid glycoprotein 1	5	20,40	5
P04083	ANXA1_HUMAN	Annexin A1	4	14,16	5
P07355	ANXA2_HUMAN	Annexin A2	3	9,44	5
P02749	APOH_HUMAN	Beta-2-glycoprotein 1	3	8,99	5
P00450	CERU_HUMAN	Ceruloplasmin	4	4,98	5
P02675	FIBB_HUMAN	Fibrinogen beta chain	4	11,41	5
P05062	ALDOB_HUMAN	Fructose-bisphosphate aldolase B	4	15,11	5
P0DOY2	IGLC2_HUMAN	Immunoglobulin lambda constant 2	3	37,74	5
B9A064	IGLL5_HUMAN	Immunoglobulin lambda-like polypeptide 5	3	17,76	5
P08727	K1C19_HUMAN	Keratin, type I cytoskeletal 19	4	7,75	5
P01042	KNG1_HUMAN	Kininogen-1	3	5,90	5
P10451	OSTP_HUMAN	Osteopontin	2	8,28	5
P02652	APOA2_HUMAN	Apolipoprotein A-II	2	19,00	4
P39059	COFA1_HUMAN	Collagen alpha-1(XV) chain	3	2,67	4
Q9UNN8	EPCR_HUMAN	Endothelial protein C receptor	2	10,92	4
P98095	FBLN2_HUMAN	Fibulin-2	2	3,29	4
P01876	IGHA1_HUMAN	Immunoglobulin heavy constant alpha 1	4	12,18	4
Q9Y5Y7	LYVE1_HUMAN	Lymphatic vessel endothelial hyaluronic acid receptor 1	2	5,59	4
P19961	AMY2B_HUMAN	Alpha-amylase 2B	1	2,35	3
Q9UKU9	ANGL2_HUMAN	Angiopoietin-related protein 2	1	1,83	3
P13727	PRG2_HUMAN	Bone marrow proteoglycan	2	8,56	3
P31327	CPSM_HUMAN	Carbamoyl-phosphate synthase [ammonia], mitochondrial	2	1,33	3
Q9UBR2	CATZ_HUMAN	Cathepsin Z	6	21,45	3
P24855	DNAS1_HUMAN	Deoxyribonuclease-1	4	19,50	3
Q08380	LG3BP_HUMAN	Galectin-3-binding protein	2	4,61	3
P19827	ITIH1_HUMAN	Inter-alpha-trypsin inhibitor heavy chain H1	2	3,29	3
P19013	K2C4_HUMAN	Keratin, type II cytoskeletal 4	4	7,49	3
Q9BRK3	MXRA8_HUMAN	Matrix remodeling-associated protein 8	1	1,81	3
P14543	NID1_HUMAN	Nidogen-1	3	2,41	3
P41222	PTGDS_HUMAN	Prostaglandin-H2 D-isomerase	2	17,37	3
P06733	ENOA_HUMAN	Alpha-enolase	2	5,07	2
Q03154	ACY1_HUMAN	Aminoacylase-1	1	2,21	2
P15144	AMPN_HUMAN	Aminopeptidase N	2	4,03	2
P01019	ANGT_HUMAN	Angiotensinogen	1	2,68	2
P01008	ANT3_HUMAN	Antithrombin-III	1	3,02	2
P41181	AQP2_HUMAN	Aquaporin-2	1	3,69	2
P12111	CO6A3_HUMAN	Collagen alpha-3(VI) chain	1	0,25	2
Q9HCU0	CD248_HUMAN	Endosialin	2	2,38	2
Q9UBX5	FBLN5_HUMAN	Fibulin-5	1	2,46	2
P05546	HEP2_HUMAN	Heparin cofactor 2	1	1,80	2
P01624	KV315_HUMAN	Immunoglobulin kappa variable 3-15	1	7,83	2

UDC UNIVERSIDADE DA CORUÑA

P20774	MIME_HUMAN	Mimecan	1	2,69	2
P08571	CD14_HUMAN	Monocyte differentiation antigen CD14	2	7,73	2
P23470	PTPRG_HUMAN	Receptor-type tyrosine-protein phosphatase gamma	2	0,83	2
O14773	TPP1_HUMAN	Tripeptidyl-peptidase 1	2	4,97	2
P06310	KV230_HUMAN	Immunoglobulin kappa variable 2-30	1	10,83	1
P04004	VTNC_HUMAN	Vitronectin	1	3,14	1
P14550	AK1A1_HUMAN	Alcohol dehydrogenase [NADP(+)]	1	4,31	
P02765	FETUA_HUMAN	Alpha-2-HS-glycoprotein	4	10,35	
P98160	PGBM_HUMAN	Basement membrane-specific heparan sulfate proteoglycan core protein	5	1,59	
P36957	ODO2_HUMAN	Dihydrolipoyllysine-residue succinyltransferase component of 2-oxoglutarate dehydrogenase complex, mitochondrial	1	1,77	
P09467	F16P1_HUMAN	Fructose-1,6-bisphosphatase 1	1	4,73	
Q92820	GGH_HUMAN	Gamma-glutamyl hydrolase	1	4,09	
Q16769	QPCT_HUMAN	Glutaminyl-peptide cyclotransferase	1	3,88	
Q5JWF2	GNAS1_HUMAN	Guanine nucleotide-binding protein G(s) subunit alpha isoforms XLas	1	1,06	
P53990	IST1_HUMAN	IST1 homolog	1	2,47	
Q99698	LYST_HUMAN	Lysosomal-trafficking regulator	1	0,21	
P40925	MDHC_HUMAN	Malate dehydrogenase, cytoplasmic	1	3,59	
O43653	PSCA_HUMAN	Prostate stem cell antigen	2	13,82	
Q8TF72	SHRM3_HUMAN	Protein Shroom3	1	0,45	
P00734	THRB_HUMAN	Prothrombin	5	9,16	
P29508	SPB3_HUMAN	Serpin B3	2	4,10	
Q9H2M3	BHMT2_HUMAN	S-methylmethionine--homocysteine S-methyltransferase BHMT2	1	2,76	
Q5TCY1	TTBK1_HUMAN	Tau-tubulin kinase 1	1	0,61	
Q6EMK4	VASN_HUMAN	Vasorin	1	2,08	

Supplementary Table 15. Protein list of all identified proteins by qualitative mass spectrometry analysis in band 7 (ExoGAG isolated fraction of medium creatinine *PKD2* sample)

Entry Name	UniProt Name	Protein Name	Peptides(95%)	%Cov(95)	Total spectrum count
P01834	IGKC_HUMAN	Immunoglobulin kappa constant	54	92,52	134
P02760	AMBP_HUMAN	Protein AMBP	44	34,09	103
P02768	ALBU_HUMAN	Albumin	38	53,20	80
P68871	HBB_HUMAN	Hemoglobin subunit beta	33	83,67	66
P02042	HBD_HUMAN	Hemoglobin subunit delta	20	53,74	37
P01859	IGHG2_HUMAN	Immunoglobulin heavy constant gamma 2	12	28,83	24
P01857	IGHG1_HUMAN	Immunoglobulin heavy constant gamma 1	11	32,73	23
P06727	APOA4_HUMAN	Apolipoprotein A-IV	17	41,92	22
P01860	IGHG3_HUMAN	Immunoglobulin heavy constant gamma 3	11	26,26	22
P69905	HBA_HUMAN	Hemoglobin subunit alpha	12	50,70	21
P41222	PTGDS_HUMAN	Prostaglandin-H2 D-isomerase	16	41,05	20
P0DOY3	IGLC3_HUMAN	Immunoglobulin lambda constant 3	11	55,66	18

USC UNIVERSIDADE DE SANTIAGO DE COMPOSTELA

B9A064	IGLL5_HUMAN	Immunoglobulin lambda-like polypeptide 5	9	26,64	18
P01619	KV320_HUMAN	Immunoglobulin kappa variable 3-20	10	62,93	16
P05090	APOD_HUMAN	Apolipoprotein D	9	34,39	14
P07911	UROM_HUMAN	Uromodulin	14	19,69	14
P00746	CFAD_HUMAN	Complement factor D	11	41,11	13
P13645	K1C10_HUMAN	Keratin, type I cytoskeletal 10	11	17,81	13
P04264	K2C1_HUMAN	Keratin, type II cytoskeletal 1	13	19,10	13
P01009	A1AT_HUMAN	Alpha-1-antitrypsin	9	21,53	12
P04433	KV311_HUMAN	Immunoglobulin kappa variable 3-11	6	34,78	12
P07478	TRY2_HUMAN	Trypsin-2	2	8,10	11
P02647	APOA1_HUMAN	Apolipoprotein A-I	8	33,71	10
P01624	KV315_HUMAN	Immunoglobulin kappa variable 3-15	5	42,61	9
O95336	6PGL_HUMAN	6-phosphogluconolactonase	7	37,98	8
P00915	CAH1_HUMAN	Carbonic anhydrase 1	6	28,35	8
P01615	KVD28_HUMAN	Immunoglobulin kappa variable 2D-28	5	31,67	8
P06312	KV401_HUMAN	Immunoglobulin kappa variable 4-1	5	45,45	8
P35527	K1C9_HUMAN	Keratin, type I cytoskeletal 9	7	10,75	7
P36955	PEDF_HUMAN	Pigment epithelium-derived factor	6	15,31	7
P63261	ACTG_HUMAN	Actin, cytoplasmic 2	7	22,67	6
P98095	FBLN2_HUMAN	Fibulin-2	3	3,29	6
P01700	LV147_HUMAN	Immunoglobulin lambda variable 1-47	3	35,04	6
P02787	TRFE_HUMAN	Serotransferrin	6	10,17	6
P02790	HEMO_HUMAN	Hemopexin	7	14,50	5
P0DP09	KV113_HUMAN	Immunoglobulin kappa variable 1-13	4	26,50	5
Q9Y5Y7	LYVE1_HUMAN	Lymphatic vessel endothelial hyaluronic acid receptor 1	4	8,38	5
P00738	HPT_HUMAN	Haptoglobin	4	10,84	4
P13647	K2C5_HUMAN	Keratin, type II cytoskeletal 5	5	8,47	4
P02743	SAMP_HUMAN	Serum amyloid P-component	5	22,87	4
P01011	AACT_HUMAN	Alpha-1-antichymotrypsin	3	6,86	3
P55290	CAD13_HUMAN	Cadherin-13	3	4,35	3
P27797	CALR_HUMAN	Calreticulin	1	3,60	3
P06396	GELS_HUMAN	Gelsolin	3	4,60	3
P09210	GSTA2_HUMAN	Glutathione S-transferase A2	3	13,06	3
P04792	HSPB1_HUMAN	Heat shock protein beta-1	3	20,98	3
Q99972	MYOC_HUMAN	Myocilin	4	7,34	3
O75594	PGRP1_HUMAN	Peptidoglycan recognition protein 1	3	27,55	3
Q12907	LMAN2_HUMAN	Vesicular integral-membrane protein VIP36	3	8,71	3
P25311	ZA2G_HUMAN	Zinc-alpha-2-glycoprotein	3	11,41	3
Q96DA0	ZG16B_HUMAN	Zymogen granule protein 16 homolog B	3	20,67	3
Q9UKU9	ANGL2_HUMAN	Angiopoietin-related protein 2	1	2,23	2
P00918	CAH2_HUMAN	Carbonic anhydrase 2	3	10,77	2
P07451	CAH3_HUMAN	Carbonic anhydrase 3	2	10,38	2
Q07507	DERM_HUMAN	Dermatopontin	2	9,45	2
P81605	DCD_HUMAN	Dermcidin	2	12,73	2
P01876	IGHA1_HUMAN	Immunoglobulin heavy constant alpha 1	0	0,00	2

USC UNIVERSIDADE DE SANTIAGO DE COMPOSTELA

P01780	HV307_HUMAN	Immunoglobulin heavy variable 3-7	2	23,08	2
P01591	IGJ_HUMAN	Immunoglobulin J chain	1	7,55	2
Q14624	ITIH4_HUMAN	Inter-alpha-trypsin inhibitor heavy chain H4	1	1,18	2
P02750	A2GL_HUMAN	Leucine-rich alpha-2-glycoprotein	2	5,76	2
P15941	MUC1_HUMAN	Mucin-1	2	2,23	2
Q9UBR2	CATZ_HUMAN	Cathepsin Z	1	3,30	1
P39059	COFA1_HUMAN	Collagen alpha-1(XV) chain	2	1,73	1
P0C0L5	CO4B_HUMAN	Complement C4-B	1	0,52	1
O94919	ENDD1_HUMAN	Endonuclease domain-containing 1 protein	1	2,60	1
P02671	FIBA_HUMAN	Fibrinogen alpha chain	1	1,50	1
P02675	FIBB_HUMAN	Fibrinogen beta chain	2	1,63	1
P04406	G3P_HUMAN	Glyceraldehyde-3-phosphate dehydrogenase	1	4,48	1
A0A0C4DH68	KV224_HUMAN	Immunoglobulin kappa variable 2-24	1	10,83	1
P19823	ITIH2_HUMAN	Inter-alpha-trypsin inhibitor heavy chain H2	1	1,59	1
Q9BRK3	MXRA8_HUMAN	Matrix remodeling-associated protein 8	1	2,49	1
P14543	NID1_HUMAN	Nidogen-1	1	0,80	1
Q96FE7	P3IP1_HUMAN	Phosphoinositide-3-kinase-interacting protein 1	1	4,18	1
P00747	PLMN_HUMAN	Plasminogen	1	1,24	1
P00734	THRB_HUMAN	Prothrombin	1	1,45	1
P04004	VTNC_HUMAN	Vitronectin	1	2,51	1
P07858	CATB_HUMAN	Cathepsin B	1	3,25	
Q9UBX5	FBLN5_HUMAN	Fibulin-5	1	2,01	
Q14390	GGTL2_HUMAN	Glutathione hydrolase light chain 2	1	5,96	
P04211	LV743_HUMAN	Immunoglobulin lambda variable 7-43	1	7,69	
P08779	K1C16_HUMAN	Keratin, type I cytoskeletal 16	5	9,72	
P09237	MMP7_HUMAN	Matrilysin	1	3,37	
P09668	CATH_HUMAN	Pro-cathepsin H	1	2,39	
O43653	PSCA_HUMAN	Prostate stem cell antigen	1	8,13	
Q9Y279	VSIG4_HUMAN	V-set and immunoglobulin domain-containing protein 4	1	2,51	

Supplementary Table 16. Protein list of all identified proteins by qualitative mass spectrometry analysis in band 8 (ExoGAG isolated fraction of high creatinine *PKD2* sample)

Entry Name	UniProt Name	Protein Name	Peptides(95%)	%Cov(95)	Total spectrum count
P02787	TRFE_HUMAN	Serotransferrin	164	62,32	420
P02768	ALBU_HUMAN	Albumin	65	57,14	203
P00734	THRB_HUMAN	Prothrombin	41	50,00	136
P51884	LUM_HUMAN	Lumican	16	37,57	72
P04004	VTNC_HUMAN	Vitronectin	20	25,94	70
P68871	HBB_HUMAN	Hemoglobin subunit beta	19	71,43	69
P0C0L5	CO4B_HUMAN	Complement C4-B	23	13,65	56
P01024	CO3_HUMAN	Complement C3	36	23,57	54

USC UNIVERSIDADE DE SANTIAGO DE COMPOSTELA

P19827	ITIH1_HUMAN	Inter-alpha-trypsin inhibitor heavy chain H1	22	19,32	51
P07911	UROM_HUMAN	Uromodulin	21	20,94	41
P02042	HBD_HUMAN	Hemoglobin subunit delta	10	41,50	40
P02760	AMBP_HUMAN	Protein AMBP	16	19,60	38
P04217	A1BG_HUMAN	Alpha-1B-glycoprotein	15	25,05	33
P19823	ITIH2_HUMAN	Inter-alpha-trypsin inhibitor heavy chain H2	14	16,60	32
P04264	K2C1_HUMAN	Keratin, type II cytoskeletal 1	14	20,96	29
P69905	HBA_HUMAN	Hemoglobin subunit alpha	9	38,03	24
P05155	IC1_HUMAN	Plasma protease C1 inhibitor	8	19,00	21
P01871	IGHM_HUMAN	Immunoglobulin heavy constant mu	9	23,40	20
Q14520	HABP2_HUMAN	Hyaluronan-binding protein 2	8	10,54	16
Q06033	ITIH3_HUMAN	Inter-alpha-trypsin inhibitor heavy chain H3	7	8,65	14
P05154	IPSP_HUMAN	Plasma serine protease inhibitor	6	17,98	14
P01857	IGHG1_HUMAN	Immunoglobulin heavy constant gamma 1	8	27,27	12
P13645	K1C10_HUMAN	Keratin, type I cytoskeletal 10	10	15,58	12
P35527	K1C9_HUMAN	Keratin, type I cytoskeletal 9	7	11,56	11
P43652	AFAM_HUMAN	Afamin	9	15,86	9
P00450	CERU_HUMAN	Ceruloplasmin	5	7,14	8
P15311	EZRI_HUMAN	Ezrin	6	9,56	8
P02671	FIBA_HUMAN	Fibrinogen alpha chain	7	9,24	8
Q08380	LG3BP_HUMAN	Galectin-3-binding protein	4	6,84	8
P07225	PROS_HUMAN	Vitamin K-dependent protein S	6	6,95	8
P01009	A1AT_HUMAN	Alpha-1-antitrypsin	4	9,09	7
P00740	FA9_HUMAN	Coagulation factor IX	5	9,76	7
P02679	FIBG_HUMAN	Fibrinogen gamma chain	4	9,27	7
P01859	IGHG2_HUMAN	Immunoglobulin heavy constant gamma 2	5	16,56	7
P02647	APOA1_HUMAN	Apolipoprotein A-I	5	22,47	6
P02790	HEMO_HUMAN	Hemopexin	2	4,54	6
P04196	HRG_HUMAN	Histidine-rich glycoprotein	6	14,67	6
Q6UXB8	PI16_HUMAN	Peptidase inhibitor 16	3	7,13	6
P22792	CPN2_HUMAN	Carboxypeptidase N subunit 2	2	5,14	5
P01031	CO5_HUMAN	Complement C5	4	2,57	5
P05546	HEP2_HUMAN	Heparin cofactor 2	4	6,81	5
Q6UX06	OLFM4_HUMAN	Olfactomedin-4	2	5,10	5
P00747	PLMN_HUMAN	Plasminogen	5	6,30	5
P01011	AACT_HUMAN	Alpha-1-antichymotrypsin	2	4,49	4
P10909	CLUS_HUMAN	Clusterin	4	13,14	4
P01834	IGKC_HUMAN	Immunoglobulin kappa constant	2	32,71	4
Q9Y5Y7	LYVE1_HUMAN	Lymphatic vessel endothelial hyaluronic acid receptor 1	2	5,59	4
P01833	PIGR_HUMAN	Polymeric immunoglobulin receptor	1	1,18	4
P00748	FA12_HUMAN	Coagulation factor XII	2	2,60	3
P02748	CO9_HUMAN	Complement component C9	3	5,55	3
P02751	FINC_HUMAN	Fibronectin	3	1,89	3
P0DOY2	IGLC2_HUMAN	Immunoglobulin lambda constant 2	3	37,74	3
Q14624	ITIH4_HUMAN	Inter-alpha-trypsin inhibitor heavy chain H4	3	3,12	3

USC DE SANTIAGO DE COMPOSTELA

Q96PD5	PGRP2_HUMAN	N-acetylmuramoyl-L-alanine amidase	2	2,95	3
P10451	OSTP_HUMAN	Osteopontin	1	2,87	3
P16070	CD44_HUMAN	CD44 antigen	1	1,08	2
P10643	CO7_HUMAN	Complement component C7	1	1,07	2
P81605	DCD_HUMAN	Dermcidin	2	20,00	2
P02675	FIBB_HUMAN	Fibrinogen beta chain	2	3,46	2
P00738	HPT_HUMAN	Haptoglobin	2	5,42	2
P01876	IGHA1_HUMAN	Immunoglobulin heavy constant alpha 1	2	7,08	2
Q6EMK4	VASN_HUMAN	Vasorin	1	2,23	2
P63261	ACTG_HUMAN	Actin, cytoplasmic 2	1	1,87	1
P08697	A2AP_HUMAN	Alpha-2-antiplasmin	1	2,24	1
P13727	PRG2_HUMAN	Bone marrow proteoglycan	1	4,96	1
Q9NPY3	C1QR1_HUMAN	Complement component C1q receptor	1	1,69	1
Q12805	FBLN3_HUMAN	EGF-containing fibulin-like extracellular matrix protein 1	1	1,83	1
P06396	GELS_HUMAN	Gelsolin	1	1,66	1
P0DJD9	PEPA5_HUMAN	Pepsin A-5	1	2,83	1
Q9BTM1	H2AJ_HUMAN	Histone H2A.J	1	6,98	
P02533	K1C14_HUMAN	Keratin, type I cytoskeletal 14	2	3,81	
P07333	CSF1R_HUMAN	Macrophage colony-stimulating factor 1 receptor	1	1,75	
O60279	SUSD5_HUMAN	Sushi domain-containing protein 5	1	1,43	
P62987	RL40_HUMAN	Ubiquitin-60S ribosomal protein L40	1	12,50	

Supplementary Table 17. Protein list of all identified proteins by qualitative mass spectrometry analysis in band 9 (ExoGAG isolated fraction of high creatinine *PKD2* sample)

Entry Name	UniProt Name	Protein Name	Peptides(95%)	%Cov(95)	Total spectrum count
P02768	ALBU_HUMAN	Albumin	959	88,83	4293
P01009	A1AT_HUMAN	Alpha-1-antitrypsin	102	68,18	303
P04004	VTNC_HUMAN	Vitronectin	62	47,91	213
P02787	TRFE_HUMAN	Serotransferrin	55	59,74	112
P68871	HBB_HUMAN	Hemoglobin subunit beta	35	95,24	107
P19823	ITIH2_HUMAN	Inter-alpha-trypsin inhibitor heavy chain H2	30	32,66	97
P02671	FIBA_HUMAN	Fibrinogen alpha chain	37	36,26	86
P02675	FIBB_HUMAN	Fibrinogen beta chain	42	71,49	85
P02760	AMBP_HUMAN	Protein AMBP	31	25,57	76
P01011	AACT_HUMAN	Alpha-1-antichymotrypsin	24	45,86	71
P51884	LUM_HUMAN	Lumican	19	33,43	69
P02042	HBD_HUMAN	Hemoglobin subunit delta	22	63,27	66
P01024	CO3_HUMAN	Complement C3	42	33,13	64
P07911	UROM_HUMAN	Uromodulin	29	29,22	61
P02790	HEMO_HUMAN	Hemopexin	27	47,40	57
P01042	KNG1_HUMAN	Kininogen-1	25	25,31	50
P02748	CO9_HUMAN	Complement component C9	24	34,53	48
P01008	ANT3_HUMAN	Antithrombin-III	21	45,26	44

USC UNIVERSIDADE DE SANTIAGO DE COMPOSTELA

P01876	IGHA1_HUMAN	Immunoglobulin heavy constant alpha 1	19	52,41	43
P04264	K2C1_HUMAN	Keratin, type II cytoskeletal 1	16	25,62	41
P01857	IGHG1_HUMAN	Immunoglobulin heavy constant gamma 1	18	43,64	40
P01860	IGHG3_HUMAN	Immunoglobulin heavy constant gamma 3	18	38,99	37
P69905	HBA_HUMAN	Hemoglobin subunit alpha	15	71,83	36
P01019	ANGT_HUMAN	Angiotensinogen	8	21,44	27
P0C0L5	CO4B_HUMAN	Complement C4-B	17	14,68	26
P19827	ITIH1_HUMAN	Inter-alpha-trypsin inhibitor heavy chain H1	19	24,48	26
Q14520	HABP2_HUMAN	Hyaluronan-binding protein 2	8	17,68	23
P01859	IGHG2_HUMAN	Immunoglobulin heavy constant gamma 2	11	23,62	22
P07478	TRY2_HUMAN	Trypsin-2	7	8,10	22
P01861	IGHG4_HUMAN	Immunoglobulin heavy constant gamma 4	15	33,03	21
P35527	K1C9_HUMAN	Keratin, type I cytoskeletal 9	15	37,08	21
P00734	THRB_HUMAN	Prothrombin	12	19,61	20
P00740	FA9_HUMAN	Coagulation factor IX	12	29,07	19
Q08380	LG3BP_HUMAN	Galectin-3-binding protein	9	19,15	19
Q9Y5Y7	LYVE1_HUMAN	Lymphatic vessel endothelial hyaluronic acid receptor 1	5	11,49	19
P16070	CD44_HUMAN	CD44 antigen	7	5,66	17
P16278	BGAL_HUMAN	Beta-galactosidase	7	11,67	15
P04196	HRG_HUMAN	Histidine-rich glycoprotein	7	14,48	15
P01877	IGHA2_HUMAN	Immunoglobulin heavy constant alpha 2	9	27,65	15
P13645	K1C10_HUMAN	Keratin, type I cytoskeletal 10	9	16,78	15
P02765	FETUA_HUMAN	Alpha-2-HS-glycoprotein	5	20,44	14
P02647	APOA1_HUMAN	Apolipoprotein A-I	7	29,59	14
P07358	CO8B_HUMAN	Complement component C8 beta chain	9	19,97	14
P02679	FIBG_HUMAN	Fibrinogen gamma chain	7	22,08	14
P00751	CFAB_HUMAN	Complement factor B	7	11,52	12
P10451	OSTP_HUMAN	Osteopontin	5	23,25	12
P05155	IC1_HUMAN	Plasma protease C1 inhibitor	4	10,00	12
P00450	CERU_HUMAN	Ceruloplasmin	6	8,45	10
P08185	CBG_HUMAN	Corticosteroid-binding globulin	7	25,43	10
P13727	PRG2_HUMAN	Bone marrow proteoglycan	6	33,78	9
P27797	CALR_HUMAN	Calreticulin	3	9,83	9
Q9UBX5	FBLN5_HUMAN	Fibulin-5	4	9,15	8
P08697	A2AP_HUMAN	Alpha-2-antiplasmin	4	12,63	7
P05154	IPSP_HUMAN	Plasma serine protease inhibitor	5	13,55	7
Q06033	ITIH3_HUMAN	Inter-alpha-trypsin inhibitor heavy chain H3	1	1,69	6
P18428	LBP_HUMAN	Lipopolysaccharide-binding protein	4	12,27	6
Q66K66	TM198_HUMAN	Transmembrane protein 198	1	2,50	6
P04217	A1BG_HUMAN	Alpha-1B-glycoprotein	3	5,86	5
P02749	APOH_HUMAN	Beta-2-glycoprotein 1	4	19,13	5
P01834	IGKC_HUMAN	Immunoglobulin kappa constant	4	44,86	5

USC
DE SANTIAGO

P0DOY3	IGLC3_HUMAN	Immunoglobulin lambda constant 3	1	14,15	5
P05543	THBG_HUMAN	Thyroxine-binding globulin	3	11,57	5
P05546	HEP2_HUMAN	Heparin cofactor 2	1	1,40	4
P02774	VTDB_HUMAN	Vitamin D-binding protein	2	6,96	4
P10909	CLUS_HUMAN	Clusterin	2	5,12	3
P08174	DAF_HUMAN	Complement decay-accelerating factor	1	3,15	3
P00738	HPT_HUMAN	Haptoglobin	2	5,91	3
P29622	KAIN_HUMAN	Kallistatin	2	4,68	3
P0DJD9	PEPA5_HUMAN	Pepsin A-5	2	4,90	3
P22891	PROZ_HUMAN	Vitamin K-dependent protein Z	3	7,75	3
P01031	CO5_HUMAN	Complement C5	1	1,13	2
P02751	FINC_HUMAN	Fibronectin	2	1,30	2
P06396	GELS_HUMAN	Gelsolin	2	3,84	2
Q6EMK4	VASN_HUMAN	Vasorin	1	2,38	2
P00915	CAH1_HUMAN	Carbonic anhydrase 1	1	3,45	1
Q99880	H2B1L_HUMAN	Histone H2B type 1-L	1	7,14	1
P62805	H4_HUMAN	Histone H4	1	7,77	1
Q6UXB8	PI16_HUMAN	Peptidase inhibitor 16	1	2,16	1
P62269	RS18_HUMAN	40S ribosomal protein S18	1	5,26	
A0A0C4DH43	HV70D_HUMAN	Immunoglobulin heavy variable 2-70D	1	5,88	
A0A0B4J1X5	HV374_HUMAN	Immunoglobulin heavy variable 3-74	1	5,98	
P36268	GGT2_HUMAN	Inactive glutathione hydrolase 2	2	3,69	
Q13477	MADCA_HUMAN	Mucosal addressin cell adhesion molecule 1	2	9,42	
O96000	NDUBA_HUMAN	NADH dehydrogenase [ubiquinone] 1 beta subcomplex subunit 10	1	8,72	
P35241	RADI_HUMAN	Radixin	1	1,54	
O60518	RNBP6_HUMAN	Ran-binding protein 6	1	0,81	
P53597	SUCA_HUMAN	Succinate--CoA ligase [ADP/GDP-forming] subunit alpha, mitochondrial	1	4,33	
P62987	RL40_HUMAN	Ubiquitin-60S ribosomal protein L40	1	12,50	

Supplementary Table 18. Protein list of all identified proteins by qualitative mass spectrometry analysis in band 10 (ExoGAG isolated fraction of high creatinine *PKD2* sample)

Entry Name	UniProt Name	Protein Name	Peptides(95%)	%Cov(95)	Total spectrum count
P02760	AMBP_HUMAN	Protein AMBP	289	67,61	1151
P02768	ALBU_HUMAN	Albumin	144	75,53	436
P68871	HBB_HUMAN	Hemoglobin subunit beta	42	94,56	141
P02042	HBD_HUMAN	Hemoglobin subunit delta	30	61,90	93
P02679	FIBG_HUMAN	Fibrinogen gamma chain	34	51,21	86
P69905	HBA_HUMAN	Hemoglobin subunit alpha	29	75,35	82
P01024	CO3_HUMAN	Complement C3	48	38,42	73
P02671	FIBA_HUMAN	Fibrinogen alpha chain	31	33,95	70
P02675	FIBB_HUMAN	Fibrinogen beta chain	36	59,67	67
P06727	APOA4_HUMAN	Apolipoprotein A-IV	26	59,34	66

USC UNIVERSIDADE DE SANTIAGO DE COMPOSTELA

P19823	ITIH2_HUMAN	Inter-alpha-trypsin inhibitor heavy chain H2	21	20,08	53
P02787	TRFE_HUMAN	Serotransferrin	30	46,56	51
P01009	A1AT_HUMAN	Alpha-1-antitrypsin	18	50,00	46
P10909	CLUS_HUMAN	Clusterin	17	26,28	44
P01876	IGHA1_HUMAN	Immunoglobulin heavy constant alpha 1	3	9,63	42
P07911	UROM_HUMAN	Uromodulin	20	21,25	40
P04264	K2C1_HUMAN	Keratin, type II cytoskeletal 1	22	30,28	39
P00738	HPT_HUMAN	Haptoglobin	20	42,61	35
P01859	IGHG2_HUMAN	Immunoglobulin heavy constant gamma 2	12	28,83	35
P00751	CFAB_HUMAN	Complement factor B	18	15,71	33
P00734	THRB_HUMAN	Prothrombin	16	33,44	32
P07478	TRY2_HUMAN	Trypsin-2	11	8,10	32
P25311	ZA2G_HUMAN	Zinc-alpha-2-glycoprotein	18	57,05	31
P0C0L4	CO4A_HUMAN	Complement C4-A	20	15,42	28
P0C0L5	CO4B_HUMAN	Complement C4-B	20	15,14	28
P01857	IGHG1_HUMAN	Immunoglobulin heavy constant gamma 1	17	50,61	28
P04004	VTNC_HUMAN	Vitronectin	15	21,97	26
P02790	HEMO_HUMAN	Hemopexin	14	32,68	25
P19827	ITIH1_HUMAN	Inter-alpha-trypsin inhibitor heavy chain H1	13	14,27	25
P13645	K1C10_HUMAN	Keratin, type I cytoskeletal 10	16	29,11	25
Q5VTE0	EF1A3_HUMAN	Putative elongation factor 1-alpha-like 3	2	4,98	23
P02647	APOA1_HUMAN	Apolipoprotein A-I	10	41,20	18
P35527	K1C9_HUMAN	Keratin, type I cytoskeletal 9	10	21,83	15
P05090	APOD_HUMAN	Apolipoprotein D	10	31,22	13
P02748	CO9_HUMAN	Complement component C9	6	12,88	13
P06396	GELS_HUMAN	Gelsolin	8	12,53	13
P27797	CALR_HUMAN	Calreticulin	4	15,11	12
P04196	HRG_HUMAN	Histidine-rich glycoprotein	6	14,10	12
P14543	NID1_HUMAN	Nidogen-1	8	8,26	12
P0DOY3	IGLC3_HUMAN	Immunoglobulin lambda constant 3	5	55,66	11
P02763	A1AG1_HUMAN	Alpha-1-acid glycoprotein 1	7	27,86	10
P04406	G3P_HUMAN	Glyceraldehyde-3-phosphate dehydrogenase	6	18,21	10
P01871	IGHM_HUMAN	Immunoglobulin heavy constant mu	3	7,06	10
B9A064	IGLL5_HUMAN	Immunoglobulin lambda-like polypeptide 5	4	17,76	10
P01042	KNG1_HUMAN	Kininogen-1	7	9,47	10
P02774	VTDB_HUMAN	Vitamin D-binding protein	6	15,19	10
P01011	AACT_HUMAN	Alpha-1-antichymotrypsin	8	21,99	9
P36955	PEDF_HUMAN	Pigment epithelium-derived factor	8	22,25	9
P00747	PLMN_HUMAN	Plasminogen	5	8,15	9
P07355	ANXA2_HUMAN	Annexin A2	7	25,66	8
Q95604	1C17_HUMAN	HLA class I histocompatibility antigen, Cw-17 alpha chain	1	3,76	7
P05155	IC1_HUMAN	Plasma protease C1 inhibitor	4	10,00	7
P63261	ACTG_HUMAN	Actin, cytoplasmic 2	5	18,13	6

USC

Q08380	LG3BP_HUMAN	Galectin-3-binding protein	6	12,31	6
P01860	IGHG3_HUMAN	Immunoglobulin heavy constant gamma 3	15	37,40	6
P51884	LUM_HUMAN	Lumican	4	13,02	6
P01019	ANGT_HUMAN	Angiotensinogen	4	12,16	5
P00450	CERU_HUMAN	Ceruloplasmin	4	5,45	5
P00742	FA10_HUMAN	Coagulation factor X	2	6,15	5
Q12805	FBLN3_HUMAN	EGF-containing fibulin-like extracellular matrix protein 1	3	10,14	5
Q9Y5Y7	LYVE1_HUMAN	Lymphatic vessel endothelial hyaluronic acid receptor 1	5	11,80	5
P02765	FETUA_HUMAN	Alpha-2-HS-glycoprotein	3	8,45	4
P08758	ANXA5_HUMAN	Annexin A5	3	9,38	4
P31327	CPSM_HUMAN	Carbamoyl-phosphate synthase [ammonia], mitochondrial	1	0,73	4
Q9UBR2	CATZ_HUMAN	Cathepsin Z	4	16,17	4
P05546	HEP2_HUMAN	Heparin cofactor 2	5	7,82	4
Q14520	HABP2_HUMAN	Hyaluronan-binding protein 2	4	7,50	4
P02750	A2GL_HUMAN	Leucine-rich alpha-2-glycoprotein	3	7,78	4
Q12907	LMAN2_HUMAN	Vesicular integral-membrane protein VIP36	3	12,08	4
P19652	A1AG2_HUMAN	Alpha-1-acid glycoprotein 2	3	16,92	3
P04217	A1BG_HUMAN	Alpha-1B-glycoprotein	3	6,67	3
P01023	A2MG_HUMAN	Alpha-2-macroglobulin	2	1,83	3
P02652	APOA2_HUMAN	Apolipoprotein A-II	1	9,00	3
P02649	APOE_HUMAN	Apolipoprotein E	2	7,57	3
P00915	CAH1_HUMAN	Carbonic anhydrase 1	2	8,05	3
P16070	CD44_HUMAN	CD44 antigen	1	1,62	3
P00740	FA9_HUMAN	Coagulation factor IX	2	4,34	3
P39059	COFA1_HUMAN	Collagen alpha-1(XV) chain	3	2,67	3
P05156	CFAI_HUMAN	Complement factor I	2	3,09	3
P81605	DCD_HUMAN	Dermcidin	1	12,73	3
P49411	EFTU_HUMAN	Elongation factor Tu, mitochondrial	2	5,31	3
P62879	GBB2_HUMAN	Guanine nucleotide-binding protein G(I)/G(S)/G(T) subunit beta-2	2	6,18	3
Q14624	ITIH4_HUMAN	Inter-alpha-trypsin inhibitor heavy chain H4	3	4,19	3
P13647	K2C5_HUMAN	Keratin, type II cytoskeletal 5	4	6,61	3
P07195	LDHB_HUMAN	L-lactate dehydrogenase B chain	2	5,09	3
P10451	OSTP_HUMAN	Osteopontin	2	8,28	3
P41222	PTGDS_HUMAN	Prostaglandin-H2 D-isomerase	3	25,79	3
Q13510	ASAH1_HUMAN	Acid ceramidase	1	3,04	2
P01008	ANT3_HUMAN	Antithrombin-III	2	5,39	2
P02749	APOH_HUMAN	Beta-2-glycoprotein 1	2	8,99	2
P13727	PRG2_HUMAN	Bone marrow proteoglycan	1	4,96	2
Q9UBX5	FBLN5_HUMAN	Fibulin-5	1	2,01	2
P62805	H4_HUMAN	Histone H4	1	7,77	2
P06312	KV401_HUMAN	Immunoglobulin kappa variable 4-1	1	7,44	2
Q8WWA0	ITLN1_HUMAN	Intelectin-1	1	3,20	2
P32119	PRDX2_HUMAN	Peroxiredoxin-2	2	13,13	2
P19320	VCAM1_HUMAN	Vascular cell adhesion protein 1	1	2,03	2

USC UNIVERSIDADE DE SANTIAGO DE COMPOSTELA

P04083	ANXA1_HUMAN	Annexin A1	1	3,76	1
P41181	AQP2_HUMAN	Aquaporin-2	0	0,00	1
P98160	PGBM_HUMAN	Basement membrane-specific heparan sulfate proteoglycan core protein	1	0,32	1
P24855	DNAS1_HUMAN	Deoxyribonuclease-1	1	4,61	1
Q9HCU0	CD248_HUMAN	Endosialin	1	1,06	1
Q9UNN8	EPCR_HUMAN	Endothelial protein C receptor	1	3,78	1
P02751	FINC_HUMAN	Fibronectin	1	0,63	1
P01834	IGKC_HUMAN	Immunoglobulin kappa constant	5	60,75	1
Q9BQE3	TBA1C_HUMAN	Tubulin alpha-1C chain	1	2,00	1
Q6EMK4	VASN_HUMAN	Vasorin	1	2,38	1
P08670	VIME_HUMAN	Vimentin	1	2,15	1
P62258	1433E_HUMAN	14-3-3 protein epsilon	1	4,71	
P09525	ANXA4_HUMAN	Annexin A4	1	5,02	
P00966	ASSY_HUMAN	Argininosuccinate synthase	0	0,00	
P06576	ATPB_HUMAN	ATP synthase subunit beta, mitochondrial	1	1,89	
P20160	CAP7_HUMAN	Azurocidin	1	5,18	
P21810	PGS1_HUMAN	Biglycan	1	2,99	
O43633	CHM2A_HUMAN	Charged multivesicular body protein 2a	1	4,05	
P10645	CMGA_HUMAN	Chromogranin-A	1	4,16	
Q03591	FHR1_HUMAN	Complement factor H-related protein 1	1	3,33	
O76062	ERG24_HUMAN	Delta(14)-sterol reductase	1	2,63	
P36957	ODO2_HUMAN	Dihydrolipoyllysine-residue succinyltransferase component of 2-oxoglutarate dehydrogenase complex, mitochondrial	1	1,77	
Q15485	FCN2_HUMAN	Ficolin-2	1	4,47	
P09467	F16P1_HUMAN	Fructose-1,6-bisphosphatase 1	1	4,73	
O75487	GPC4_HUMAN	Glypican-4	1	2,34	
P01624	KV315_HUMAN	Immunoglobulin kappa variable 3-15	1	7,83	
P24592	IBP6_HUMAN	Insulin-like growth factor-binding protein 6	1	6,25	
P19012	K1C15_HUMAN	Keratin, type I cytoskeletal 15	4	8,11	
P61626	LYSC_HUMAN	Lysozyme C	1	8,11	
P40925	MDHC_HUMAN	Malate dehydrogenase, cytoplasmic	1	3,59	
Q8IWI9	MGAP_HUMAN	MAX gene-associated protein	1	0,40	
Q8IUH5	ZDH17_HUMAN	Palmitoyltransferase ZDHHC17	1	1,74	
O43653	PSCA_HUMAN	Prostate stem cell antigen	2	13,82	
P35241	RADI_HUMAN	Radixin	1	1,54	
Q9Y490	TLN1_HUMAN	Talin-1	1	0,59	
Q5TCY1	TTBK1_HUMAN	Tau-tubulin kinase 1	1	0,61	
O60635	TSN1_HUMAN	Tetraspanin-1	1	5,39	
Q66K66	TM198_HUMAN	Transmembrane protein 198	1	2,50	
P62987	RL40_HUMAN	Ubiquitin-60S ribosomal protein L40	1	12,50	
Q9Y279	VSIG4_HUMAN	V-set and immunoglobulin domain-containing protein 4	1	2,51	

USC UNIVERSIDADE DE SANTIAGO DE COMPOSTELA

Supplementary Table 19. Protein list of all identified proteins by qualitative mass spectrometry analysis in band 11 (ExoGAG isolated fraction of high creatinine *PKD2* sample).

Entry Name	UniProt Name	Protein Name	Peptides(95%)	%Cov(95)	Total spectrum count
P07911	UROM_HUMAN	Uromodulin	176	54,37	412
P02768	ALBU_HUMAN	Albumin	85	70,44	200
P68871	HBB_HUMAN	Hemoglobin subunit beta	37	84,35	79
P02042	HBD_HUMAN	Hemoglobin subunit delta	23	54,42	47
P02760	AMBP_HUMAN	Protein AMBP	22	30,68	45
P01857	IGHG1_HUMAN	Immunoglobulin heavy constant gamma 1	17	38,79	34
P01859	IGHG2_HUMAN	Immunoglobulin heavy constant gamma 2	15	30,98	33
P01860	IGHG3_HUMAN	Immunoglobulin heavy constant gamma 3	15	36,34	31
P01024	CO3_HUMAN	Complement C3	26	19,72	28
P02787	TRFE_HUMAN	Serotransferrin	22	31,23	27
P69905	HBA_HUMAN	Hemoglobin subunit alpha	15	71,13	25
P04264	K2C1_HUMAN	Keratin, type II cytoskeletal 1	20	32,14	22
P01023	A2MG_HUMAN	Alpha-2-macroglobulin	16	12,28	18
P13645	K1C10_HUMAN	Keratin, type I cytoskeletal 10	14	24,83	14
P00450	CERU_HUMAN	Ceruloplasmin	9	10,42	12
P01834	IGKC_HUMAN	Immunoglobulin kappa constant	7	67,29	12
P35527	K1C9_HUMAN	Keratin, type I cytoskeletal 9	10	19,42	11
P01833	PIGR_HUMAN	Polymeric immunoglobulin receptor	9	11,91	10
P0DOY3	IGLC3_HUMAN	Immunoglobulin lambda constant 3	5	55,66	8
P02647	APOA1_HUMAN	Apolipoprotein A-I	6	25,84	7
P98164	LRP2_HUMAN	Low-density lipoprotein receptor-related protein 2	4	0,92	6
P02679	FIBG_HUMAN	Fibrinogen gamma chain	5	10,60	5
P00738	HPT_HUMAN	Haptoglobin	6	15,52	5
Q6UXB8	PI16_HUMAN	Peptidase inhibitor 16	4	9,29	4
P08670	VIME_HUMAN	Vimentin	3	5,15	4
P01009	A1AT_HUMAN	Alpha-1-antitrypsin	3	9,09	3
P10643	CO7_HUMAN	Complement component C7	3	3,08	3
Q08380	LG3BP_HUMAN	Galectin-3-binding protein	2	4,27	3
P01876	IGHA1_HUMAN	Immunoglobulin heavy constant alpha 1	3	11,90	3
P13647	K2C5_HUMAN	Keratin, type II cytoskeletal 5	3	5,59	3
Q9BXP8	PAPP2_HUMAN	Pappalysin-2	3	1,51	3
P05155	IC1_HUMAN	Plasma protease C1 inhibitor	3	7,60	3
P01031	CO5_HUMAN	Complement C5	0	0,00	2
P27487	DPP4_HUMAN	Dipeptidyl peptidase 4	2	2,35	2
P02671	FIBA_HUMAN	Fibrinogen alpha chain	2	2,43	2
P63261	ACTG_HUMAN	Actin, cytoplasmic 2	1	4,80	1
P01011	AACT_HUMAN	Alpha-1-antichymotrypsin	1	2,13	1
P15144	AMPN_HUMAN	Aminopeptidase N	1	1,03	1
P00915	CAH1_HUMAN	Carbonic anhydrase 1	1	3,45	1
P0C0L5	CO4B_HUMAN	Complement C4-B	1	0,86	1
Q9NPY3	C1QR1_HUMAN	Complement component C1q receptor	1	1,69	1

P81605	DCD_HUMAN	Dermcidin	1	12,73	1
P02675	FIBB_HUMAN	Fibrinogen beta chain	1	1,63	1
P02790	HEMO_HUMAN	Hemopexin	1	2,38	1
P06310	KV230_HUMAN	Immunoglobulin kappa variable 2-30	1	10,83	1
P04433	KV311_HUMAN	Immunoglobulin kappa variable 3-11	1	7,83	1
P01624	KV315_HUMAN	Immunoglobulin kappa variable 3-15	1	7,83	1
Q9Y5Y7	LYVE1_HUMAN	Lymphatic vessel endothelial hyaluronic acid receptor 1	1	2,80	1
P11279	LAMP1_HUMAN	Lysosome-associated membrane glycoprotein 1	1	2,16	1
P13473	LAMP2_HUMAN	Lysosome-associated membrane glycoprotein 2	1	1,95	1
P00747	PLMN_HUMAN	Plasminogen	2	2,10	1
P04004	VTNC_HUMAN	Vitronectin	1	2,51	1
P08519	APOA_HUMAN	Apolipoprotein(a)	1	8,29	
Q92496	FHR4_HUMAN	Complement factor H-related protein 4	2	1,21	
Q04695	K1C17_HUMAN	Keratin, type I cytoskeletal 17	2	3,70	
P62987	RL40_HUMAN	Ubiquitin-60S ribosomal protein L40	1	12,50	

Supplementary Table 20. Protein list of all identified proteins by qualitative mass spectrometry analysis in band 12 (ExoGAG isolated fraction of high creatinine *PKD2* sample).

Entry Name	UniProt Name	Protein Name	Peptides(95%)	%Cov(95)	Total spectrum count
P02768	ALBU_HUMAN	Albumin	90	64,53	205
P01834	IGKC_HUMAN	Immunoglobulin kappa constant	65	92,52	159
P02760	AMBP_HUMAN	Protein AMBP	43	51,99	84
P01024	CO3_HUMAN	Complement C3	58	36,14	72
P68871	HBB_HUMAN	Hemoglobin subunit beta	27	82,31	58
P01859	IGHG2_HUMAN	Immunoglobulin heavy constant gamma 2	30	33,74	55
P01860	IGHG3_HUMAN	Immunoglobulin heavy constant gamma 3	28	31,83	55
P01861	IGHG4_HUMAN	Immunoglobulin heavy constant gamma 4	26	32,11	47
P00915	CAH1_HUMAN	Carbonic anhydrase 1	18	43,30	32
P02042	HBD_HUMAN	Hemoglobin subunit delta	16	52,38	32
P0DOY3	IGLC3_HUMAN	Immunoglobulin lambda constant 3	11	55,66	31
B9A064	IGLL5_HUMAN	Immunoglobulin lambda-like polypeptide 5	9	26,64	25
P41222	PTGDS_HUMAN	Prostaglandin-H2 D-isomerase	20	36,84	24
P00450	CERU_HUMAN	Ceruloplasmin	18	18,31	20
P69905	HBA_HUMAN	Hemoglobin subunit alpha	11	51,41	19
P02790	HEMO_HUMAN	Hemopexin	13	25,54	18
P01009	A1AT_HUMAN	Alpha-1-antitrypsin	10	22,97	17
P01615	KVD28_HUMAN	Immunoglobulin kappa variable 2D-28	10	50,00	17
P02671	FIBA_HUMAN	Fibrinogen alpha chain	11	14,09	16
P02787	TRFE_HUMAN	Serotransferrin	14	18,91	16
P07911	UROM_HUMAN	Uromodulin	16	21,09	16
P06310	KV230_HUMAN	Immunoglobulin kappa variable 2-30	8	31,67	15

USC UNIVERSIDADE DE SANTIAGO DE COMPOSTELA

P04264	K2C1_HUMAN	Keratin, type II cytoskeletal 1	13	20,50	15
P00738	HPT_HUMAN	Haptoglobin	14	39,41	14
P01614	KVD40_HUMAN	Immunoglobulin kappa variable 2D-40	8	36,36	14
P04433	KV311_HUMAN	Immunoglobulin kappa variable 3-11	13	41,74	14
P06312	KV401_HUMAN	Immunoglobulin kappa variable 4-1	9	51,24	12
P13645	K1C10_HUMAN	Keratin, type I cytoskeletal 10	15	22,77	12
P02679	FIBG_HUMAN	Fibrinogen gamma chain	10	20,53	11
P02647	APOA1_HUMAN	Apolipoprotein A-I	9	38,20	10
P06727	APOA4_HUMAN	Apolipoprotein A-IV	8	21,97	10
P01599	KV117_HUMAN	Immunoglobulin kappa variable 1-17	7	29,06	9
P36955	PEDF_HUMAN	Pigment epithelium-derived factor	9	18,42	9
P01780	HV307_HUMAN	Immunoglobulin heavy variable 3-7	6	40,17	7
P35527	K1C9_HUMAN	Keratin, type I cytoskeletal 9	7	12,68	7
P02743	SAMP_HUMAN	Serum amyloid P-component	7	29,15	6
P25311	ZA2G_HUMAN	Zinc-alpha-2-glycoprotein	5	22,48	6
P0C0L5	CO4B_HUMAN	Complement C4-B	6	3,50	5
P01602	KV105_HUMAN	Immunoglobulin kappa variable 1-5	4	24,79	5
Q9Y5Y7	LYVE1_HUMAN	Lymphatic vessel endothelial hyaluronic acid receptor 1	5	11,80	5
P01011	AACT_HUMAN	Alpha-1-antichymotrypsin	4	9,46	4
P06396	GELS_HUMAN	Gelsolin	4	6,90	4
Q14624	ITIH4_HUMAN	Inter-alpha-trypsin inhibitor heavy chain H4	4	6,67	4
Q96DA0	ZG16B_HUMAN	Zymogen granule protein 16 homolog B	5	28,85	4
P63261	ACTG_HUMAN	Actin, cytoplasmic 2	4	13,07	3
P02763	A1AG1_HUMAN	Alpha-1-acid glycoprotein 1	2	8,46	3
P05090	APOD_HUMAN	Apolipoprotein D	2	12,70	3
P0DP03	HV335_HUMAN	Immunoglobulin heavy variable 3-30-5	2	23,08	3
P01700	LV147_HUMAN	Immunoglobulin lambda variable 1-47	2	25,64	3
P80748	LV321_HUMAN	Immunoglobulin lambda variable 3-21	3	29,06	3
P19827	ITIH1_HUMAN	Inter-alpha-trypsin inhibitor heavy chain H1	5	6,92	3
P15941	MUC1_HUMAN	Mucin-1	3	3,59	3
P01023	A2MG_HUMAN	Alpha-2-macroglobulin	2	1,36	2
P01019	ANGT_HUMAN	Angiotensinogen	4	9,69	2
P07451	CAH3_HUMAN	Carbonic anhydrase 3	3	13,85	2
P02748	CO9_HUMAN	Complement component C9	2	4,11	2
P00746	CFAD_HUMAN	Complement factor D	2	15,42	2
P81605	DCD_HUMAN	Dermcidin	2	12,73	2
P02675	FIBB_HUMAN	Fibrinogen beta chain	3	7,13	2
A0A0C4DH69	KV109_HUMAN	Immunoglobulin kappa variable 1-9	3	26,50	2
P19823	ITIH2_HUMAN	Inter-alpha-trypsin inhibitor heavy chain H2	2	2,75	2
P02750	A2GL_HUMAN	Leucine-rich alpha-2-glycoprotein	2	5,76	2
P30041	PRDX6_HUMAN	Peroxiredoxin-6	2	8,93	2
Q96FE7	P3IP1_HUMAN	Phosphoinositide-3-kinase-interacting protein 1	2	9,89	2
P04004	VTNC_HUMAN	Vitronectin	2	5,65	2
P00918	CAH2_HUMAN	Carbonic anhydrase 2	1	3,46	1

USC UNIVERSIDADE DE SANTIAGO DE COMPOSTELA

Q9UBR2	CATZ_HUMAN	Cathepsin Z	1	3,30	1
P01031	CO5_HUMAN	Complement C5	2	1,13	1
P10643	CO7_HUMAN	Complement component C7	2	2,85	1
P98095	FBLN2_HUMAN	Fibulin-2	1	2,03	1
P04792	HSPB1_HUMAN	Heat shock protein beta-1	1	4,88	1
Q14520	HABP2_HUMAN	Hyaluronan-binding protein 2	1	1,79	1
P01876	IGHA1_HUMAN	Immunoglobulin heavy constant alpha 1	1	2,83	1
P01857	IGHG1_HUMAN	Immunoglobulin heavy constant gamma 1	35	50,30	1
P01591	IGJ_HUMAN	Immunoglobulin J chain	1	7,55	1
P01042	KNG1_HUMAN	Kininogen-1	1	1,71	1
P18428	LBP_HUMAN	Lipopolysaccharide-binding protein	1	2,29	1
O75594	PGRP1_HUMAN	Peptidoglycan recognition protein 1	1	7,65	1
P05543	THBG_HUMAN	Thyroxine-binding globulin	1	2,41	1
P15291	B4GT1_HUMAN	Beta-1,4-galactosyltransferase 1	1	2,01	
P02741	CRP_HUMAN	C-reactive protein	1	4,46	
Q9UBX5	FBLN5_HUMAN	Fibulin-5	1	2,01	
P01594	KV133_HUMAN	Immunoglobulin kappa variable 1-33	5	29,06	
P01611	KVD12_HUMAN	Immunoglobulin kappa variable 1D-12	5	29,06	
A0A0C4DH68	KV224_HUMAN	Immunoglobulin kappa variable 2-24	3	30,83	
P01624	KV315_HUMAN	Immunoglobulin kappa variable 3-15	7	41,74	
P01619	KV320_HUMAN	Immunoglobulin kappa variable 3-20	17	62,93	
A0A087WSY6	KVD15_HUMAN	Immunoglobulin kappa variable 3D-15	7	41,74	
A0A0C4DH24	KV621_HUMAN	Immunoglobulin kappa variable 6-21	1	10,53	
P04211	LV743_HUMAN	Immunoglobulin lambda variable 7-43	1	7,69	
A0A075B6I0	LV861_HUMAN	Immunoglobulin lambda variable 8-61	1	7,38	
P09237	MMP7_HUMAN	Matrilysin	1	3,37	
Q9P267	MBD5_HUMAN	Methyl-CpG-binding domain protein 5	1	0,74	
Q99972	MYOC_HUMAN	Myocilin	1	1,79	
P09668	CATH_HUMAN	Pro-cathepsin H	1	3,88	
Q58FF8	H90B2_HUMAN	Putative heat shock protein HSP 90-beta 2	1	3,15	
P61020	RAB5B_HUMAN	Ras-related protein Rab-5B	1	5,12	
Q12907	LMAN2_HUMAN	Vesicular integral-membrane protein VIP36	1	2,53	
Q9Y279	VSIG4_HUMAN	V-set and immunoglobulin domain-containing protein 4	1	2,51	

Supplementary Table 21. Protein list of all identified proteins by qualitative mass spectrometry analysis in band 4A (ExoGAG supernatant fraction of control sample).

Entry Name	UniProt Name	Protein Name	Peptides(95%)	%Cov(95)	Total spectrum count
P02768	ALBU_HUMAN	Albumin	139	70,44	273
P07477	TRY1_HUMAN	Trypsin-1	30	15,38	74
P04264	K2C1_HUMAN	Keratin, type II cytoskeletal 1	12	23,91	20
P13645	K1C10_HUMAN	Keratin, type I cytoskeletal 10	13	31,85	18
P01042	KNG1_HUMAN	Kininogen-1	12	21,89	18

P02647	APOA1_HUMAN	Apolipoprotein A-I	9	37,83	17
P35030	TRY3_HUMAN	Trypsin-3	6	12,50	17
P0DOX5	IGG1_HUMAN	Immunoglobulin gamma-1 heavy chain	9	24,50	13
P01876	IGHA1_HUMAN	Immunoglobulin heavy constant alpha 1	8	30,31	13
P01011	AACT_HUMAN	Alpha-1-antichymotrypsin	8	22,93	10
P01009	A1AT_HUMAN	Alpha-1-antitrypsin	6	16,51	10
P02763	A1AG1_HUMAN	Alpha-1-acid glycoprotein 1	5	27,36	8
P00738	HPT_HUMAN	Haptoglobin	8	24,88	8
P68871	HBB_HUMAN	Hemoglobin subunit beta	4	39,46	8
P69905	HBA_HUMAN	Hemoglobin subunit alpha	4	45,77	7
P35527	K1C9_HUMAN	Keratin, type I cytoskeletal 9	6	12,84	7
P02766	TTHY_HUMAN	Transthyretin	3	39,46	7
P01859	IGHG2_HUMAN	Immunoglobulin heavy constant gamma 2	5	20,25	6
P0DUB6	AMY1A_HUMAN	Alpha-amylase 1A	2	5,28	4
P16070	CD44_HUMAN	CD44 antigen	3	4,18	4
P31025	LCN1_HUMAN	Lipocalin-1	2	12,50	4
P0DOX7	IGK_HUMAN	Immunoglobulin kappa light chain	2	14,02	3
P13647	K2C5_HUMAN	Keratin, type II cytoskeletal 5	3	5,76	3
Q6EMK4	VASN_HUMAN	Vasorin	2	3,71	3
P61626	LYSC_HUMAN	Lysozyme C	1	8,11	2
P07911	UROM_HUMAN	Uromodulin	1	2,34	2
P02765	FETUA_HUMAN	Alpha-2-HS-glycoprotein	1	3,82	1
P02652	APOA2_HUMAN	Apolipoprotein A-II	1	10,00	1
P0DOY3	IGLC3_HUMAN	Immunoglobulin lambda constant 3	1	9,43	1
P02787	TRFE_HUMAN	Serotransferrin	1	1,58	1
P02656	APOC3_HUMAN	Apolipoprotein C-III	1	16,16	
P08174	DAF_HUMAN	Complement decay-accelerating factor	0	0,00	

Supplementary Table 22. Protein list of all identified proteins by qualitative mass spectrometry analysis in band 4D (ExoGAG supernatant fraction of high creatinine *PKD2* sample sample).

Entry Name	UniProt Name	Protein Name	Peptides(95%)	%Cov(95)	Total spectrum count
P02768	ALBU_HUMAN	Albumin	1629	87,850	5792
P02787	TRFE_HUMAN	Serotransferrin	93	65,620	203
P13645	K1C10_HUMAN	Keratin, type I cytoskeletal 10	52	51,540	118
P01011	AACT_HUMAN	Alpha-1-antichymotrypsin	42	40,430	101
P04264	K2C1_HUMAN	Keratin, type II cytoskeletal 1	33	40,840	85
P0DOX5	IGG1_HUMAN	Immunoglobulin gamma-1 heavy chain	31	46,100	80
P07478	TRY2_HUMAN	Trypsin-2	22	8,502	64
P01860	IGHG3_HUMAN	Immunoglobulin heavy constant gamma 3	16	33,950	56
P01859	IGHG2_HUMAN	Immunoglobulin heavy constant gamma 2	18	45,090	49
P01042	KNG1_HUMAN	Kininogen-1	15	24,220	34
P00738	HPT_HUMAN	Haptoglobin	11	34,240	26
P13647	K2C5_HUMAN	Keratin, type II cytoskeletal 5	11	13,050	22

USC UNIVERSIDADE DE SANTIAGO DE COMPOSTELA

P01876	IGHA1_HUMAN	Immunoglobulin heavy constant alpha 1	11	32,290	21
P02647	APOA1_HUMAN	Apolipoprotein A-I	12	46,440	20
P68871	HBB_HUMAN	Hemoglobin subunit beta	8	72,790	19
P01009	A1AT_HUMAN	Alpha-1-antitrypsin	7	17,220	16
P02766	TTHY_HUMAN	Transthyretin	7	65,310	15
P02763	A1AG1_HUMAN	Alpha-1-acid glycoprotein 1	4	23,380	13
P0DOX7	IGK_HUMAN	Immunoglobulin kappa light chain	5	39,720	12
P69905	HBA_HUMAN	Hemoglobin subunit alpha	4	36,620	11
P02652	APOA2_HUMAN	Apolipoprotein A-II	3	39,000	9
P02790	HEMO_HUMAN	Hemopexin	4	12,340	9
P35527	K1C9_HUMAN	Keratin, type I cytoskeletal 9	8	20,710	9
P02765	FETUA_HUMAN	Alpha-2-HS-glycoprotein	3	8,447	7
P0DOY3	IGLC3_HUMAN	Immunoglobulin lambda constant 3	2	23,580	7
Q66K66	TM198_HUMAN	Transmembrane protein 198	2	2,500	6
P0DOX2	IGA2_HUMAN	Immunoglobulin alpha-2 heavy chain	4	9,451	5
P31025	LCN1_HUMAN	Lipocalin-1	4	26,700	5
Q9Y5Y7	LYVE1_HUMAN	Lymphatic vessel endothelial hyaluronic acid receptor 1	3	9,006	5
P43652	AFAM_HUMAN	Afamin	6	10,020	4
P19652	A1AG2_HUMAN	Alpha-1-acid glycoprotein 2	2	12,940	4
P01780	HV307_HUMAN	Immunoglobulin heavy variable 3-7	3	30,770	4
P0DJI9	SAA2_HUMAN	Serum amyloid A-2 protein	2	24,590	4
Q13085	ACACA_HUMAN	Acetyl-CoA carboxylase 1	2	0,725	3
P01008	ANT3_HUMAN	Antithrombin-III	2	4,310	3
P61626	LYSC_HUMAN	Lysozyme C	3	22,300	3
P0DJI8	SAA1_HUMAN	Serum amyloid A-1 protein	2	27,870	3
P02749	APOH_HUMAN	Beta-2-glycoprotein 1	1	4,928	2
Q9GZZ8	LACRT_HUMAN	Extracellular glycoprotein lacritin	1	5,797	2
P14923	PLAK_HUMAN	Junction plakoglobin	2	4,832	2
P01833	PIGR_HUMAN	Polymeric immunoglobulin receptor	1	2,487	2
P02679	FIBG_HUMAN	Fibrinogen gamma chain	1	4,415	1
P02760	AMBP_HUMAN	Protein AMBP	1	2,273	1
P02656	APOC3_HUMAN	Apolipoprotein C-III	1	16,160	
P16070	CD44_HUMAN	CD44 antigen	1	1,617	
P15924	DESP_HUMAN	Desmoplakin	1	0,522	
P20930	FILA_HUMAN	Filaggrin	1	0,246	
Q08499-7	PDE4D_HUMAN	Isoform N3 of cAMP-specific 3',5'-cyclic phosphodiesterase 4D	1	3,721	
P48739	PIPNB_HUMAN	Phosphatidylinositol transfer protein beta isoform	1	6,642	
P0C6X7	R1AB_SARS	Replicase polyprotein 1ab	1	0,127	

USC UNIVERSIDADE DE SANTIAGO DE COMPOSTELA

Supplementary Table 23. Protein list of all identified proteins by qualitative mass spectrometry analysis in band 5B (ExoGAG supernatant fraction of low creatinine *PKD2* sample sample).

Entry Name	UniProt Name	Protein Name	Peptides(95%)	%Cov(95)	Total spectrum count
P02768	ALBU_HUMAN	Albumin	67	71,59	97
P01009	A1AT_HUMAN	Alpha-1-antitrypsin	12	30,14	25
P13645	K1C10_HUMAN	Keratin, type I cytoskeletal 10	18	36,47	22
P04264	K2C1_HUMAN	Keratin, type II cytoskeletal 1	12	22,67	22
P02647	APOA1_HUMAN	Apolipoprotein A-I	12	37,45	20
P0DOX5	IGG1_HUMAN	Immunoglobulin gamma-1 heavy chain	12	30,07	18
P00738	HPT_HUMAN	Haptoglobin	12	35,71	17
P35527	K1C9_HUMAN	Keratin, type I cytoskeletal 9	11	24,40	12
P02766	TTHY_HUMAN	Transthyretin	6	55,78	12
P68871	HBB_HUMAN	Hemoglobin subunit beta	8	67,35	11
P02763	A1AG1_HUMAN	Alpha-1-acid glycoprotein 1	5	27,36	10
P69905	HBA_HUMAN	Hemoglobin subunit alpha	5	57,04	10
P01834	IGKC_HUMAN	Immunoglobulin kappa constant	5	79,44	9
P01859	IGHG2_HUMAN	Immunoglobulin heavy constant gamma 2	6	22,39	8
P31025	LCN1_HUMAN	Lipocalin-1	4	26,14	5
P02749	APOH_HUMAN	Beta-2-glycoprotein 1	4	17,39	4
P13647	K2C5_HUMAN	Keratin, type II cytoskeletal 5	3	5,59	4
P0DOY3	IGLC3_HUMAN	Immunoglobulin lambda constant 3	3	30,19	3
P61626	LYSC_HUMAN	Lysozyme C	2	14,19	3
P07911	UROM_HUMAN	Uromodulin	3	5,00	3
P01011	AACT_HUMAN	Alpha-1-antichymotrypsin	2	4,73	2
P02652	APOA2_HUMAN	Apolipoprotein A-II	2	10,00	2
P16070	CD44_HUMAN	CD44 antigen	2	2,97	2
P02790	HEMO_HUMAN	Hemopexin	2	9,74	2
P01876	IGHA1_HUMAN	Immunoglobulin heavy constant alpha 1	2	7,65	2
P0DJI8	SAA1_HUMAN	Serum amyloid A-1 protein	3	29,51	2
P0DJI9	SAA2_HUMAN	Serum amyloid A-2 protein	3	26,23	2
P02765	FETUA_HUMAN	Alpha-2-HS-glycoprotein	1	3,82	1
P12273	PIP_HUMAN	Prolactin-inducible protein	1	8,22	1
P35030	TRY3_HUMAN	Trypsin-3	1	4,28	1
P02656	APOC3_HUMAN	Apolipoprotein C-III	1	16,16	
Q04695	K1C17_HUMAN	Keratin, type I cytoskeletal 17	2	3,70	
O75556	SG2A1_HUMAN	Mammaglobin-B	1	12,63	
Q6EMK4	VASN_HUMAN	Vasorin	1	2,23	

Supplementary Table 24. Protein list of all identified proteins by qualitative mass spectrometry analysis in band 5D (ExoGAG supernatant fraction of high creatinine *PKD2* sample sample).

Entry Name	UniProt Name	Protein Name	Peptides(95%)	%Cov(95)	Total spectrum count
P02768	ALBU_HUMAN	Albumin	408	83,09	1145
P0DOX5	IGG1_HUMAN	Immunoglobulin gamma-1 heavy chain	101	58,80	294

USC UNIVERSIDADE DE SANTIAGO DE COMPOSTELA

P01859	IGHG2_HUMAN	Immunoglobulin heavy constant gamma 2	57	61,96	234
P01861	IGHG4_HUMAN	Immunoglobulin heavy constant gamma 4	54	53,82	154
P02787	TRFE_HUMAN	Serotransferrin	64	66,05	146
P02774	VTDB_HUMAN	Vitamin D-binding protein	62	70,89	117
P02763	A1AG1_HUMAN	Alpha-1-acid glycoprotein 1	25	45,27	69
P04264	K2C1_HUMAN	Keratin, type II cytoskeletal 1	32	39,13	61
P01009	A1AT_HUMAN	Alpha-1-antitrypsin	24	45,69	54
P35527	K1C9_HUMAN	Keratin, type I cytoskeletal 9	22	45,43	38
P13645	K1C10_HUMAN	Keratin, type I cytoskeletal 10	21	41,10	34
P19652	A1AG2_HUMAN	Alpha-1-acid glycoprotein 2	11	30,35	31
P02749	APOH_HUMAN	Beta-2-glycoprotein 1	16	51,59	30
P02765	FETUA_HUMAN	Alpha-2-HS-glycoprotein	17	26,43	27
P68871	HBB_HUMAN	Hemoglobin subunit beta	11	93,20	22
P02647	APOA1_HUMAN	Apolipoprotein A-I	12	46,07	21
P01011	AACT_HUMAN	Alpha-1-antichymotrypsin	10	23,88	20
P01876	IGHA1_HUMAN	Immunoglobulin heavy constant alpha 1	13	34,84	19
P00738	HPT_HUMAN	Haptoglobin	16	39,41	18
P01042	KNG1_HUMAN	Kininogen-1	10	16,30	16
P01764	HV323_HUMAN	Immunoglobulin heavy variable 3-23	8	41,03	15
P69905	HBA_HUMAN	Hemoglobin subunit alpha	7	57,04	13
P01780	HV307_HUMAN	Immunoglobulin heavy variable 3-7	6	42,74	13
P01834	IGKC_HUMAN	Immunoglobulin kappa constant	6	79,44	12
P01833	PIGR_HUMAN	Polymeric immunoglobulin receptor	5	10,73	11
P13647	K2C5_HUMAN	Keratin, type II cytoskeletal 5	8	13,22	10
P02766	TTHY_HUMAN	Transthyretin	6	64,63	10
P01782	HV309_HUMAN	Immunoglobulin heavy variable 3-9	3	29,66	9
P02790	HEMO_HUMAN	Hemopexin	4	14,50	8
A0A0J9YX35	HV64D_HUMAN	Immunoglobulin heavy variable 3-64D	4	31,62	8
P0DOY3	IGLC3_HUMAN	Immunoglobulin lambda constant 3	3	37,74	7
A0A0C4DH38	HV551_HUMAN	Immunoglobulin heavy variable 5-51	5	29,06	6
P31025	LCN1_HUMAN	Lipocalin-1	4	22,16	6
Q9Y5Y7	LYVE1_HUMAN	Lymphatic vessel endothelial hyaluronic acid receptor 1	3	9,01	6
P01008	ANT3_HUMAN	Antithrombin-III	3	7,97	5
P02652	APOA2_HUMAN	Apolipoprotein A-II	4	39,00	5
P02533	K1C14_HUMAN	Keratin, type I cytoskeletal 14	4	7,20	5
P15586	GNS_HUMAN	N-acetylglucosamine-6-sulfatase	2	3,80	4
P02760	AMBP_HUMAN	Protein AMBP	2	5,40	4
Q8TF72	SHRM3_HUMAN	Protein Shroom3	1	0,45	4
Q9Y646	CBPQ_HUMAN	Carboxypeptidase Q	2	4,24	3
P23083	HV102_HUMAN	Immunoglobulin heavy variable 1-2	2	17,09	3
P01742	HV169_HUMAN	Immunoglobulin heavy variable 1-69	3	23,08	3
Q6EMK4	VASN_HUMAN	Vasorin	1	2,23	3
P43652	AFAM_HUMAN	Afamin	3	5,51	2
P02654	APOC1_HUMAN	Apolipoprotein C-I	1	8,43	2
P61626	LYSC_HUMAN	Lysozyme C	2	14,19	2

USC UNIVERSIDADE DE SANTIAGO DE COMPOSTELA

P0DJI8	SAA1_HUMAN	Serum amyloid A-1 protein	3	33,61	2
P02675	FIBB_HUMAN	Fibrinogen beta chain	1	1,63	1
P05109	S10A8_HUMAN	Protein S100-A8	1	11,83	1
P25311	ZA2G_HUMAN	Zinc-alpha-2-glycoprotein	1	4,03	1
Q9H6S0	YTDC2_HUMAN	3'-5' RNA helicase YTHDC2	1	0,42	
P02656	APOC3_HUMAN	Apolipoprotein C-III	1	16,16	
P05156	CFAI_HUMAN	Complement factor I	2	3,26	
P0DP08	HVD82_HUMAN	Immunoglobulin heavy variable 4-38-2	5	21,37	
O75556	SG2A1_HUMAN	Mammaglobin-B	1	12,63	
P35030	TRY3_HUMAN	Trypsin-3	1	2,63	
P04004	VTNC_HUMAN	Vitronectin	1	2,51	

Supplementary Table 25. Protein list of all identified proteins by qualitative mass spectrometry analysis in band 6B (ExoGAG supernatant fraction of low creatinine *PKD2* sample sample).

Entry Name	UniProt Name	Protein Name	Peptides(95%)	%Cov(95)	Total spectrum count
P02768	ALBU_HUMAN	Albumin	203	76,03	323
P04264	K2C1_HUMAN	Keratin, type II cytoskeletal 1	92	44,57	151
P13645	K1C10_HUMAN	Keratin, type I cytoskeletal 10	92	52,40	147
P07478	TRY2_HUMAN	Trypsin-2	44	8,10	95
P02763	A1AG1_HUMAN	Alpha-1-acid glycoprotein 1	20	41,29	39
P35527	K1C9_HUMAN	Keratin, type I cytoskeletal 9	20	34,99	29
P02647	APOA1_HUMAN	Apolipoprotein A-I	19	49,06	26
P01009	A1AT_HUMAN	Alpha-1-antitrypsin	15	37,32	24
P00738	HPT_HUMAN	Haptoglobin	18	48,03	23
P02766	TTHY_HUMAN	Transthyretin	11	69,39	23
P13647	K2C5_HUMAN	Keratin, type II cytoskeletal 5	18	17,97	22
P68871	HBB_HUMAN	Hemoglobin subunit beta	12	85,03	21
P0DOX5	IGG1_HUMAN	Immunoglobulin gamma-1 heavy chain	11	28,51	20
P19652	A1AG2_HUMAN	Alpha-1-acid glycoprotein 2	8	21,89	16
P69905	HBA_HUMAN	Hemoglobin subunit alpha	7	63,38	16
P0DJD9	PEPA5_HUMAN	Pepsin A-5	8	9,54	14
P0DOX7	IGK_HUMAN	Immunoglobulin kappa light chain	6	30,37	12
P30740	ILEU_HUMAN	Leukocyte elastase inhibitor	9	29,55	12
P02533	K1C14_HUMAN	Keratin, type I cytoskeletal 14	8	19,49	9
P01876	IGHA1_HUMAN	Immunoglobulin heavy constant alpha 1	7	26,91	8
P01859	IGHG2_HUMAN	Immunoglobulin heavy constant gamma 2	5	20,25	8
P02788	TRFL_HUMAN	Lactotransferrin	6	8,59	8
P0DJI8	SAA1_HUMAN	Serum amyloid A-1 protein	7	68,03	8
P25311	ZA2G_HUMAN	Zinc-alpha-2-glycoprotein	7	31,54	8
P02749	APOH_HUMAN	Beta-2-glycoprotein 1	5	20,87	6
P02790	HEMO_HUMAN	Hemopexin	5	16,88	6
P31025	LCN1_HUMAN	Lipocalin-1	3	12,50	6
P61626	LYSC_HUMAN	Lysozyme C	4	41,22	6
P05154	IPSP_HUMAN	Plasma serine protease inhibitor	7	17,73	6

USC UNIVERSIDADE DE SANTIAGO DE COMPOSTELA

P02787	TRFE_HUMAN	Serotransferrin	5	6,73	6
P01011	AACT_HUMAN	Alpha-1-antichymotrypsin	3	6,62	4
P02765	FETUA_HUMAN	Alpha-2-HS-glycoprotein	4	11,17	4
P02652	APOA2_HUMAN	Apolipoprotein A-II	3	37,00	4
Q9GZZ8	LACRT_HUMAN	Extracellular glycoprotein lacritin	3	16,67	4
P0DOY3	IGLC3_HUMAN	Immunoglobulin lambda constant 3	4	44,34	4
Q8N1N4	K2C78_HUMAN	Keratin, type II cytoskeletal 78	4	5,77	4
P16070	CD44_HUMAN	CD44 antigen	2	2,97	3
P12273	PIP_HUMAN	Prolactin-inducible protein	3	15,07	3
P02760	AMBP_HUMAN	Protein AMBP	3	8,81	3
P07911	UROM_HUMAN	Uromodulin	5	7,50	3
P10909	CLUS_HUMAN	Clusterin	2	7,57	2
P01619	KV320_HUMAN	Immunoglobulin kappa variable 3-20	2	21,55	2
O95968	SG1D1_HUMAN	Secretoglobin family 1D member 1	2	36,67	2
P02675	FIBB_HUMAN	Fibrinogen beta chain	1	1,63	1
P10153	RNAS2_HUMAN	Non-secretory ribonuclease	1	8,70	1
P01833	PIGR_HUMAN	Polymeric immunoglobulin receptor	1	2,09	1
P05109	S10A8_HUMAN	Protein S100-A8	1	11,83	1
Q13867	BLMH_HUMAN	Bleomycin hydrolase	1	2,42	
P01040	CYTA_HUMAN	Cystatin-A	1	12,24	
Q5D862	FILA2_HUMAN	Filaggrin-2	1	0,46	
Q7Z794	K2C1B_HUMAN	Keratin, type II cytoskeletal 1b	16	16,44	
Q16378	PROL4_HUMAN	Proline-rich protein 4	1	11,19	
P06702	S10A9_HUMAN	Protein S100-A9	1	13,16	
Q29RF7	PDS5A_HUMAN	Sister chromatid cohesion protein PDS5 homolog A	1	0,90	
Q5T750	XP32_HUMAN	Skin-specific protein 32	1	3,20	

Supplementary Table 26. Protein list of all identified proteins by qualitative mass spectrometry analysis in band 6C (ExoGAG supernatant fraction of medium creatinine *PKD2* sample sample).

Entry Name	UniProt Name	Protein Name	Peptides(95%)	%Cov(95)	Total spectrum count
P02768	ALBU_HUMAN	Albumin	450	79,80	742
P25311	ZA2G_HUMAN	Zinc-alpha-2-glycoprotein	82	67,11	145
P07478	TRY2_HUMAN	Trypsin-2	50	9,72	90
P02787	TRFE_HUMAN	Serotransferrin	58	62,46	89
P02763	A1AG1_HUMAN	Alpha-1-acid glycoprotein 1	52	50,75	84
P00738	HPT_HUMAN	Haptoglobin	49	62,56	77
P19652	A1AG2_HUMAN	Alpha-1-acid glycoprotein 2	32	49,75	56
P04264	K2C1_HUMAN	Keratin, type II cytoskeletal 1	24	35,56	37
P13645	K1C10_HUMAN	Keratin, type I cytoskeletal 10	23	39,04	31
P01009	A1AT_HUMAN	Alpha-1-antitrypsin	16	39,71	25
P02647	APOA1_HUMAN	Apolipoprotein A-I	13	47,19	24
P68871	HBB_HUMAN	Hemoglobin subunit beta	11	85,03	23
P04217	A1BG_HUMAN	Alpha-1B-glycoprotein	13	32,53	22
P01859	IGHG2_HUMAN	Immunoglobulin heavy constant gamma 2	13	31,29	20

US UNIVERSITAT DE DE

P02766	TTHY_HUMAN	Transthyretin	8	65,31	20
P02750	A2GL_HUMAN	Leucine-rich alpha-2-glycoprotein	11	33,14	17
P69905	HBA_HUMAN	Hemoglobin subunit alpha	7	62,68	13
P0DOX5	IGG1_HUMAN	Immunoglobulin gamma-1 heavy chain	10	26,73	13
P06396	GELS_HUMAN	Gelsolin	9	11,25	11
P05154	IPSP_HUMAN	Plasma serine protease inhibitor	8	22,66	11
P07911	UROM_HUMAN	Uromodulin	8	13,12	10
P0DOX7	IGK_HUMAN	Immunoglobulin kappa light chain	6	31,78	9
P35527	K1C9_HUMAN	Keratin, type I cytoskeletal 9	7	15,41	8
P31025	LCN1_HUMAN	Lipocalin-1	6	29,55	8
P02654	APOC1_HUMAN	Apolipoprotein C-I	4	36,14	7
P11117	PPAL_HUMAN	Lysosomal acid phosphatase	5	10,64	6
P61626	LYSC_HUMAN	Lysozyme C	4	41,22	6
P0DJD8	PEPA3_HUMAN	Pepsin A-3	6	10,57	6
P0DJI8	SAA1_HUMAN	Serum amyloid A-1 protein	4	35,25	6
P02652	APOA2_HUMAN	Apolipoprotein A-II	3	39,00	5
P0DJI9	SAA2_HUMAN	Serum amyloid A-2 protein	4	18,85	5
P01011	AACT_HUMAN	Alpha-1-antichymotrypsin	3	10,87	4
P16070	CD44_HUMAN	CD44 antigen	2	2,97	4
P10909	CLUS_HUMAN	Clusterin	3	8,91	4
Q9GZZ8	LACRT_HUMAN	Extracellular glycoprotein lacritin	3	22,46	4
P02790	HEMO_HUMAN	Hemopexin	4	11,26	4
P01876	IGHA1_HUMAN	Immunoglobulin heavy constant alpha 1	5	17,28	4
P0DOY2	IGLC2_HUMAN	Immunoglobulin lambda constant 2	3	37,74	4
Q7Z794	K2C1B_HUMAN	Keratin, type II cytoskeletal 1b	4	5,36	4
P13647	K2C5_HUMAN	Keratin, type II cytoskeletal 5	4	6,78	4
P15586	GNS_HUMAN	N-acetylglucosamine-6-sulfatase	3	5,25	4
Q8IYS5	OSCAR_HUMAN	Osteoclast-associated immunoglobulin-like receptor	3	14,18	4
Q07075	AMPE_HUMAN	Glutamyl aminopeptidase	2	2,19	3
P10153	RNAS2_HUMAN	Non-secretory ribonuclease	2	9,32	3
P12273	PIP_HUMAN	Prolactin-inducible protein	3	15,07	3
P02760	AMBP_HUMAN	Protein AMBP	2	5,40	3
P17050	NAGAB_HUMAN	Alpha-N-acetylgalactosaminidase	2	5,11	2
P02749	APOH_HUMAN	Beta-2-glycoprotein 1	2	10,72	2
P08185	CBG_HUMAN	Corticosteroid-binding globulin	2	6,42	2
Q01459	DIAC_HUMAN	Di-N-acetylchitobiase	2	7,79	2
P01042	KNG1_HUMAN	Kininogen-1	2	4,66	2
Q16378	PROL4_HUMAN	Proline-rich protein 4	2	17,16	2
O95968	SG1D1_HUMAN	Secretoglobin family 1D member 1	2	36,67	2
P35542	SAA4_HUMAN	Serum amyloid A-4 protein	3	21,54	2
Q66K66	TM198_HUMAN	Transmembrane protein 198	1	2,50	2
P02765	FETUA_HUMAN	Alpha-2-HS-glycoprotein	3	7,36	1
P06280	AGAL_HUMAN	Alpha-galactosidase A	1	4,20	
P02655	APOC2_HUMAN	Apolipoprotein C-II	1	10,89	
P02656	APOC3_HUMAN	Apolipoprotein C-III	1	16,16	

USC UNIVERSIDADE DE SANTIAGO DE COMPOSTELA

P05090	APOD_HUMAN	Apolipoprotein D	1	5,82
Q9UNN8	EPCR_HUMAN	Endothelial protein C receptor	1	3,78
P02671	FIBA_HUMAN	Fibrinogen alpha chain	1	1,50
Q5D862	FILA2_HUMAN	Filaggrin-2	1	0,46
Q16769	QPCT_HUMAN	Glutaminyl-peptide cyclotransferase	1	3,88
P06870	KLK1_HUMAN	Kallikrein-1	1	4,96
P19012	K1C15_HUMAN	Keratin, type I cytoskeletal 15	3	5,04
P02788	TRFL_HUMAN	Lactotransferrin	2	2,68
P13473	LAMP2_HUMAN	Lysosome-associated membrane glycoprotein 2	1	1,95
O75556	SG2A1_HUMAN	Mammaglobin-B	1	12,63
Q13421	MSLN_HUMAN	Mesothelin	1	2,22
P05109	S10A8_HUMAN	Protein S100-A8	1	11,83
P06702	S10A9_HUMAN	Protein S100-A9	1	13,16

Supplementary Table 27. Protein list of all identified proteins by qualitative mass spectrometry analysis in band 7D (ExoGAG supernatant fraction of high creatinine *PKD2* sample sample).

Entry Name	UniProt Name	Protein Name	Peptides(95%)	%Cov(95)	Total spectrum count
P02768	ALBU_HUMAN	Albumin	417	83,25	1090
P02760	AMBP_HUMAN	Protein AMBP	186	53,41	508
P02787	TRFE_HUMAN	Serotransferrin	62	57,74	126
P0DOX5	IGG1_HUMAN	Immunoglobulin gamma-1 heavy chain	35	37,42	93
P07478	TRY2_HUMAN	Trypsin-2	32	15,79	90
P04264	K2C1_HUMAN	Keratin, type II cytoskeletal 1	40	38,20	77
P01859	IGHG2_HUMAN	Immunoglobulin heavy constant gamma 2	27	41,41	64
P01860	IGHG3_HUMAN	Immunoglobulin heavy constant gamma 3	25	35,54	57
P00738	HPT_HUMAN	Haptoglobin	26	60,34	52
P35527	K1C9_HUMAN	Keratin, type I cytoskeletal 9	26	43,02	47
P02763	A1AG1_HUMAN	Alpha-1-acid glycoprotein 1	20	75,62	43
P00751	CFAB_HUMAN	Complement factor B	22	15,45	37
P0DOX8	IGL1_HUMAN	Immunoglobulin lambda-1 light chain	15	25,93	37
P25311	ZA2G_HUMAN	Zinc-alpha-2-glycoprotein	25	49,33	37
P05090	APOD_HUMAN	Apolipoprotein D	11	31,22	36
P02774	VTDB_HUMAN	Vitamin D-binding protein	17	35,86	34
P13645	K1C10_HUMAN	Keratin, type I cytoskeletal 10	19	30,82	33
P0DOY3	IGLC3_HUMAN	Immunoglobulin lambda constant 3	17	62,26	31
P19652	A1AG2_HUMAN	Alpha-1-acid glycoprotein 2	12	44,28	29
P02647	APOA1_HUMAN	Apolipoprotein A-I	15	50,19	29
P01834	IGKC_HUMAN	Immunoglobulin kappa constant	11	87,85	25
P01009	A1AT_HUMAN	Alpha-1-antitrypsin	12	30,62	24
P68871	HBB_HUMAN	Hemoglobin subunit beta	14	93,20	21
P01042	KNG1_HUMAN	Kininogen-1	14	17,24	21
P02790	HEMO_HUMAN	Hemopexin	9	28,79	17
P69905	HBA_HUMAN	Hemoglobin subunit alpha	6	57,04	14
P01011	AACT_HUMAN	Alpha-1-antichymotrypsin	7	18,68	12

USC UNIVERSIDAD DE CANTABRIA

P41222	PTGDS_HUMAN	Prostaglandin-H2 D-isomerase	9	38,95	12
P01871	IGHM_HUMAN	Immunoglobulin heavy constant mu	4	10,15	11
P0C0L5	CO4B_HUMAN	Complement C4-B	4	1,89	10
P02766	TTHY_HUMAN	Transthyretin	6	64,63	9
P00747	PLMN_HUMAN	Plasminogen	4	6,79	8
P24592	IBP6_HUMAN	Insulin-like growth factor-binding protein 6	1	6,25	7
P13647	K2C5_HUMAN	Keratin, type II cytoskeletal 5	7	10,68	7
P61626	LYSC_HUMAN	Lysozyme C	3	33,11	7
P02652	APOA2_HUMAN	Apolipoprotein A-II	3	21,00	6
P06396	GELS_HUMAN	Gelsolin	5	7,29	6
P31025	LCN1_HUMAN	Lipocalin-1	4	22,16	6
P01876	IGHA1_HUMAN	Immunoglobulin heavy constant alpha 1	4	11,33	5
P01780	HV307_HUMAN	Immunoglobulin heavy variable 3-7	4	33,33	5
Q14624	ITIH4_HUMAN	Inter-alpha-trypsin inhibitor heavy chain H4	4	5,16	5
P02533	K1C14_HUMAN	Keratin, type I cytoskeletal 14	4	6,78	5
P08571	CD14_HUMAN	Monocyte differentiation antigen CD14	2	9,87	5
P01833	PIGR_HUMAN	Polymeric immunoglobulin receptor	2	3,27	5
P04217	A1BG_HUMAN	Alpha-1B-glycoprotein	2	7,27	4
Q9GZZ8	LACRT_HUMAN	Extracellular glycoprotein lacritin	3	16,67	4
P02675	FIBB_HUMAN	Fibrinogen beta chain	2	5,29	4
P01764	HV323_HUMAN	Immunoglobulin heavy variable 3-23	4	35,04	4
P0DJI8	SAA1_HUMAN	Serum amyloid A-1 protein	4	42,62	4
P02679	FIBG_HUMAN	Fibrinogen gamma chain	1	3,31	3
P04216	THY1_HUMAN	Thy-1 membrane glycoprotein	2	14,91	3
P02765	FETUA_HUMAN	Alpha-2-HS-glycoprotein	2	5,72	2
P01024	CO3_HUMAN	Complement C3	2	1,20	2
P01619	KV320_HUMAN	Immunoglobulin kappa variable 3-20	3	35,34	2
P06312	KV401_HUMAN	Immunoglobulin kappa variable 4-1	3	28,93	2
P15586	GNS_HUMAN	N-acetylglucosamine-6-sulfatase	1	2,17	2
P06310	KV230_HUMAN	Immunoglobulin kappa variable 2-30	1	10,83	1
O95968	SG1D1_HUMAN	Secretoglobin family 1D member 1	1	12,22	1
P02656	APOC3_HUMAN	Apolipoprotein C-III	1	16,16	
P10909	CLUS_HUMAN	Clusterin	6	17,37	

Supplementary Table 28. Protein list of all identified proteins by qualitative mass spectrometry analysis in band 9B (ExoGAG supernatant fraction of low creatinine *PKD2* sample sample).

Entry Name	UniProt Name	Protein Name	Peptides(95%)	%Cov(95)	Total spectrum count
P02768	ALBU_HUMAN	Albumin	45	56,81	83
P04264	K2C1_HUMAN	Keratin, type II cytoskeletal 1	23	34,16	34
P00738	HPT_HUMAN	Haptoglobin	20	42,36	31
P68871	HBB_HUMAN	Hemoglobin subunit beta	12	93,20	30
P13645	K1C10_HUMAN	Keratin, type I cytoskeletal 10	17	33,39	28
P02766	TTHY_HUMAN	Transthyretin	11	69,39	27

USC UNIVERSIDADE DE SANTIAGO DE COMPOSTELA

P02647	APOA1_HUMAN	Apolipoprotein A-I	16	53,18	26
P02760	AMBP_HUMAN	Protein AMBP	8	17,33	20
P01009	A1AT_HUMAN	Alpha-1-antitrypsin	12	35,65	19
P0DOX5	IGG1_HUMAN	Immunoglobulin gamma-1 heavy chain	11	24,28	17
P01834	IGKC_HUMAN	Immunoglobulin kappa constant	7	79,44	17
P69905	HBA_HUMAN	Hemoglobin subunit alpha	7	64,08	15
P35527	K1C9_HUMAN	Keratin, type I cytoskeletal 9	12	27,13	14
P80188	NGAL_HUMAN	Neutrophil gelatinase-associated lipocalin	10	60,10	13
P31025	LCN1_HUMAN	Lipocalin-1	6	26,70	12
P0DJI8	SAA1_HUMAN	Serum amyloid A-1 protein	6	52,46	11
P02763	A1AG1_HUMAN	Alpha-1-acid glycoprotein 1	5	27,36	10
P0DJI9	SAA2_HUMAN	Serum amyloid A-2 protein	6	36,07	10
P01859	IGHG2_HUMAN	Immunoglobulin heavy constant gamma 2	7	22,39	8
P01042	KNG1_HUMAN	Kininogen-1	5	7,45	8
P25311	ZA2G_HUMAN	Zinc-alpha-2-glycoprotein	5	17,11	8
P02652	APOA2_HUMAN	Apolipoprotein A-II	3	39,00	7
P02654	APOC1_HUMAN	Apolipoprotein C-I	4	36,14	7
P98160	PGBM_HUMAN	Basement membrane-specific heparan sulfate proteoglycan core protein	4	0,98	7
P08779	K1C16_HUMAN	Keratin, type I cytoskeletal 16	5	12,26	6
P48668	K2C6C_HUMAN	Keratin, type II cytoskeletal 6C	6	12,06	6
P12273	PIP_HUMAN	Prolactin-inducible protein	4	36,30	6
P01871	IGHM_HUMAN	Immunoglobulin heavy constant mu	2	3,53	5
P0DOY3	IGLC3_HUMAN	Immunoglobulin lambda constant 3	5	44,34	5
P61626	LYSC_HUMAN	Lysozyme C	4	41,22	5
P10153	RNAS2_HUMAN	Non-secretory ribonuclease	2	9,32	5
Q9GZZ8	LACRT_HUMAN	Extracellular glycoprotein lacritin	3	16,67	4
P13647	K2C5_HUMAN	Keratin, type II cytoskeletal 5	4	6,95	4
P01011	AACT_HUMAN	Alpha-1-antichymotrypsin	1	2,13	3
P13646	K1C13_HUMAN	Keratin, type I cytoskeletal 13	2	4,80	3
O95968	SG1D1_HUMAN	Secretoglobin family 1D member 1	2	36,67	3
P02787	TRFE_HUMAN	Serotransferrin	2	3,73	3
P02655	APOC2_HUMAN	Apolipoprotein C-II	2	19,80	2
P13987	CD59_HUMAN	CD59 glycoprotein	10	25,00	2
P17900	SAP3_HUMAN	Ganglioside GM2 activator	2	9,33	2
P41222	PTGDS_HUMAN	Prostaglandin-H2 D-isomerase	2	8,42	2
P05109	S10A8_HUMAN	Protein S100-A8	2	23,66	2
P35030	TRY3_HUMAN	Trypsin-3	2	6,91	2
P10909	CLUS_HUMAN	Clusterin	1	5,12	1
P02790	HEMO_HUMAN	Hemopexin	1	2,38	1
P07911	UROM_HUMAN	Uromodulin	4	6,72	1
P02656	APOC3_HUMAN	Apolipoprotein C-III	1	16,16	
Q86WR0	CCD25_HUMAN	Coiled-coil domain-containing protein 25	1	4,33	
P02042	HBD_HUMAN	Hemoglobin subunit delta	6	46,26	
P06310	KV230_HUMAN	Immunoglobulin kappa variable 2-30	1	10,83	

USC UNIVERSIDADE DE SANTIAGO DE COMPOSTELA

P04433	KV311_HUMAN	Immunoglobulin kappa variable 3-11	1	7,83
P01619	KV320_HUMAN	Immunoglobulin kappa variable 3-20	1	13,79
O75556	SG2A1_HUMAN	Mammaglobin-B	1	12,63
P0DJD9	PEPA5_HUMAN	Pepsin A-5	1	2,83
P02775	CXCL7_HUMAN	Platelet basic protein	1	7,81
Q16378	PROL4_HUMAN	Proline-rich protein 4	1	11,19
P06702	S10A9_HUMAN	Protein S100-A9	1	13,16
P02753	RET4_HUMAN	Retinol-binding protein 4	1	4,98
Q8WVN6	SCTM1_HUMAN	Secreted and transmembrane protein 1	1	7,66
P35542	SAA4_HUMAN	Serum amyloid A-4 protein	1	6,92

Supplementary Table 29. Protein list of all identified proteins by qualitative mass spectrometry analysis in band 9D (ExoGAG supernatant fraction of high creatinine *PKD2* sample sample).

Entry Name	UniProt Name	Protein Name	Peptides(95%)	%Cov(95)	Total spectrum count
P02768	ALBU_HUMAN	Albumin	287	81,77	766
P02787	TRFE_HUMAN	Serotransferrin	50	44,41	101
P07477	TRY1_HUMAN	Trypsin-1	25	11,74	99
P00738	HPT_HUMAN	Haptoglobin	38	64,78	92
P02753	RET4_HUMAN	Retinol-binding protein 4	29	41,29	87
P0DOX5	IGG1_HUMAN	Immunoglobulin gamma-1 heavy chain	26	41,43	75
P01834	IGKC_HUMAN	Immunoglobulin kappa constant	23	88,79	68
P0DOX7	IGK_HUMAN	Immunoglobulin kappa light chain	24	47,20	68
P98160	PGBM_HUMAN	Basement membrane-specific heparan sulfate proteoglycan core protein	33	3,69	60
P01859	IGHG2_HUMAN	Immunoglobulin heavy constant gamma 2	18	28,83	60
P02647	APOA1_HUMAN	Apolipoprotein A-I	30	67,79	51
P01009	A1AT_HUMAN	Alpha-1-antitrypsin	20	47,85	49
P02760	AMBP_HUMAN	Protein AMBP	25	47,16	45
P04264	K2C1_HUMAN	Keratin, type II cytoskeletal 1	25	33,39	43
P25311	ZA2G_HUMAN	Zinc-alpha-2-glycoprotein	18	41,95	31
P68871	HBB_HUMAN	Hemoglobin subunit beta	12	82,31	30
P0DOX8	IGL1_HUMAN	Immunoglobulin lambda-1 light chain	8	34,26	29
P35527	K1C9_HUMAN	Keratin, type I cytoskeletal 9	19	34,51	28
P13645	K1C10_HUMAN	Keratin, type I cytoskeletal 10	17	26,88	27
P69905	HBA_HUMAN	Hemoglobin subunit alpha	10	68,31	22
P0DOY3	IGLC3_HUMAN	Immunoglobulin lambda constant 3	9	69,81	22
P80188	NGAL_HUMAN	Neutrophil gelatinase-associated lipocalin	9	45,96	21
P41222	PTGDS_HUMAN	Prostaglandin-H2 D-isomerase	14	42,63	21
P02763	A1AG1_HUMAN	Alpha-1-acid glycoprotein 1	10	45,27	20
P01011	AACT_HUMAN	Alpha-1-antichymotrypsin	10	22,93	19
P17900	SAP3_HUMAN	Ganglioside GM2 activator	7	34,72	18
P02042	HBD_HUMAN	Hemoglobin subunit delta	8	52,38	17
P01042	KNG1_HUMAN	Kininogen-1	6	11,02	14
P02766	TTHY_HUMAN	Transthyretin	7	53,06	14

USC UNIVERSIDADE DE SANTIAGO DE COMPOSTELA

P02790	HEMO_HUMAN	Hemopexin	7	21,21	13
P31025	LCN1_HUMAN	Lipocalin-1	10	34,66	13
P19652	A1AG2_HUMAN	Alpha-1-acid glycoprotein 2	4	17,41	11
P55290	CAD13_HUMAN	Cadherin-13	4	6,59	9
P02679	FIBG_HUMAN	Fibrinogen gamma chain	6	17,66	9
P05451	REG1A_HUMAN	Lithostathine-1-alpha	4	27,71	9
P02652	APOA2_HUMAN	Apolipoprotein A-II	6	21,00	8
P02654	APOC1_HUMAN	Apolipoprotein C-I	4	33,73	8
P02675	FIBB_HUMAN	Fibrinogen beta chain	5	15,27	8
P01876	IGHA1_HUMAN	Immunoglobulin heavy constant alpha 1	7	22,38	8
P61626	LYSC_HUMAN	Lysozyme C	5	46,62	8
P0C0L5	CO4B_HUMAN	Complement C4-B	2	1,20	7
P07360	CO8G_HUMAN	Complement component C8 gamma chain	4	25,74	7
Q9GZZ8	LACRT_HUMAN	Extracellular glycoprotein lacritin	4	19,57	7
P02671	FIBA_HUMAN	Fibrinogen alpha chain	5	6,47	7
P48668	K2C6C_HUMAN	Keratin, type II cytoskeletal 6C	6	10,46	7
P0DJI8	SAA1_HUMAN	Serum amyloid A-1 protein	6	51,64	7
P0DJI9	SAA2_HUMAN	Serum amyloid A-2 protein	7	35,25	7
P01024	CO3_HUMAN	Complement C3	1	0,96	6
P22352	GPX3_HUMAN	Glutathione peroxidase 3	5	28,32	6
P01780	HV307_HUMAN	Immunoglobulin heavy variable 3-7	5	42,74	6
P04217	A1BG_HUMAN	Alpha-1B-glycoprotein	2	4,65	5
P13647	K2C5_HUMAN	Keratin, type II cytoskeletal 5	4	6,61	5
P02788	TRFL_HUMAN	Lactotransferrin	2	3,94	5
P00450	CERU_HUMAN	Ceruloplasmin	2	2,07	4
A0A0C4DH69	KV109_HUMAN	Immunoglobulin kappa variable 1-9	4	34,19	4
P01619	KV320_HUMAN	Immunoglobulin kappa variable 3-20	5	48,28	4
Q14624	ITIH4_HUMAN	Inter-alpha-trypsin inhibitor heavy chain H4	2	2,26	4
P02533	K1C14_HUMAN	Keratin, type I cytoskeletal 14	4	7,20	4
Q16378	PROL4_HUMAN	Proline-rich protein 4	1	5,97	4
P00734	THRB_HUMAN	Prothrombin	2	4,66	4
P02774	VTDB_HUMAN	Vitamin D-binding protein	2	3,80	4
P01008	ANT3_HUMAN	Antithrombin-III	1	3,02	3
P06727	APOA4_HUMAN	Apolipoprotein A-IV	2	5,56	3
P02655	APOC2_HUMAN	Apolipoprotein C-II	2	19,80	3
P07339	CATD_HUMAN	Cathepsin D	1	2,43	3
P10909	CLUS_HUMAN	Clusterin	2	8,91	3
P53634	CATC_HUMAN	Dipeptidyl peptidase 1	3	4,32	3
P06312	KV401_HUMAN	Immunoglobulin kappa variable 4-1	2	23,14	3
P01700	LV147_HUMAN	Immunoglobulin lambda variable 1-47	2	25,64	3
P61916	NPC2_HUMAN	NPC intracellular cholesterol transporter 2	1	5,96	3
P07998	RNAS1_HUMAN	Ribonuclease pancreatic	3	24,36	3
P35542	SAA4_HUMAN	Serum amyloid A-4 protein	2	14,62	3
P02765	FETUA_HUMAN	Alpha-2-HS-glycoprotein	3	8,45	2
P06396	GELS_HUMAN	Gelsolin	2	2,69	2

USC UNIVERSIDADE DE SANTIAGO DE COMPOSTELA

P01591	IGJ_HUMAN	Immunoglobulin J chain	2	12,58	2
P06310	KV230_HUMAN	Immunoglobulin kappa variable 2-30	2	10,83	2
A0A075B6I0	LV861_HUMAN	Immunoglobulin lambda variable 8-61	2	13,11	2
P05155	IC1_HUMAN	Plasma protease C1 inhibitor	2	5,60	2
P05109	S10A8_HUMAN	Protein S100-A8	2	23,66	2
O95968	SG1D1_HUMAN	Secretoglobin family 1D member 1	2	12,22	2
P05090	APOD_HUMAN	Apolipoprotein D	1	5,82	1
P00751	CFAB_HUMAN	Complement factor B	1	1,18	1
A0A0C4DH68	KV224_HUMAN	Immunoglobulin kappa variable 2-24	1	10,83	1
P80748	LV321_HUMAN	Immunoglobulin lambda variable 3-21	1	13,68	1
P07911	UROM_HUMAN	Uromodulin	2	2,50	1
P02656	APOC3_HUMAN	Apolipoprotein C-III	1	16,16	
P54253	ATX1_HUMAN	Ataxin-1	1	0,98	
Q9UIF8	BAZ2B_HUMAN	Bromodomain adjacent to zinc finger domain protein 2B	1	0,28	
P13987	CD59_HUMAN	CD59 glycoprotein	7	25,00	
Q9NS71	GKN1_HUMAN	Gastrokine-1	1	8,04	
P01594	KV133_HUMAN	Immunoglobulin kappa variable 1-33	2	29,06	
P04432	KVD39_HUMAN	Immunoglobulin kappa variable 1D-39	3	34,19	
P0DOX6	IGM_HUMAN	Immunoglobulin mu heavy chain	4	7,99	
O00468-6	AGRIN_HUMAN	Isoform 6 of Agrin	6	3,52	
O75556	SG2A1_HUMAN	Mammaglobin-B	1	12,63	
Q9Y4C0	NRX3A_HUMAN	Neurexin-3	1	0,43	
Q9WC28	POLN_HEVHY	Non-structural polyprotein pORF1	1	0,41	
O75594	PGRP1_HUMAN	Peptidoglycan recognition protein 1	1	7,65	
Q06830	PRDX1_HUMAN	Peroxiredoxin-1	1	5,53	
P12273	PIP_HUMAN	Prolactin-inducible protein	3	24,66	
Q8TC56	FA71B_HUMAN	Protein FAM71B	1	1,16	
Q8WVN6	SCTM1_HUMAN	Secreted and transmembrane protein 1	1	7,66	

Supplementary Table 30. Summary of results of ExoGAG and Ultracentrifugation isolation mass spectrometry sequencing. Total proteins identified in ExoGAG and Ultracentrifugation samples as well as common proteins for all ExoGAG or Ultracentrifugation samples are described. Uniprot Name is used as identifier.

Proteins identified in ExoGAG samples	Proteins identified in UC samples	ExoGAG Proteins shared by all samples	UC Proteins shared by all samples
1433B_HUMAN	1433B_HUMAN	1433E_HUMAN	1433B_HUMAN
1433E_HUMAN	1433E_HUMAN	1433Z_HUMAN	1433E_HUMAN
1433G_HUMAN	1433F_HUMAN	4F2_HUMAN	1433Z_HUMAN
1433S_HUMAN	1433G_HUMAN	6PGL_HUMAN	6PGD_HUMAN
1433T_HUMAN	1433S_HUMAN	A1AG1_HUMAN	6PGL_HUMAN
1433Z_HUMAN	1433T_HUMAN	A1AT_HUMAN	A1AT_HUMAN
2AAA_HUMAN	1433Z_HUMAN	A1BG_HUMAN	A2MG_HUMAN
4F2_HUMAN	2AAA_HUMAN	A2AP_HUMAN	AATC_HUMAN
6PGD_HUMAN	4F2_HUMAN	A2GL_HUMAN	ABHEB_HUMAN
6PGL_HUMAN	6PGD_HUMAN	A2MG_HUMAN	ABI1_HUMAN
A1AG1_HUMAN	6PGL_HUMAN	A4_PANTR	ACE_HUMAN
A1AG2_HUMAN	A1AG1_HUMAN	AACT_HUMAN	ACOC_HUMAN

A1AT_HUMAN	A1AG2_HUMAN	ACE_HUMAN	ACTG_HUMAN
A1BG_HUMAN	A1AT_HUMAN	ACTG_HUMAN	ACTN4_HUMAN
A2AP_HUMAN	A1BG_HUMAN	ACY1_HUMAN	ACY1_HUMAN
A2GL_HUMAN	A2GL_HUMAN	AGAL_HUMAN	ADSV_HUMAN
A2MG_HUMAN	A2MG_HUMAN	AGRIN_HUMAN	AK1A1_HUMAN
A2ML1_HUMAN	AAAT_HUMAN	AK1A1_HUMAN	AL1A1_HUMAN
A4_PANTR	AACT_HUMAN	AL1A1_HUMAN	AL3B1_HUMAN
AACT_HUMAN	AATC_HUMAN	ALBU_HUMAN	AL9A1_HUMAN
AATC_HUMAN	AATM_HUMAN	ALS_HUMAN	ALBU_HUMAN
AATM_HUMAN	ABHDA_HUMAN	AMBP_HUMAN	ALDOA_HUMAN
ABHDA_HUMAN	ABHEB_HUMAN	AMPE_HUMAN	ALDOB_HUMAN
ABHEB_HUMAN	ABI1_HUMAN	AMPN_HUMAN	ALDR_HUMAN
ABLM2_HUMAN	ABR_HUMAN	AMYP_HUMAN	AMBP_HUMAN
ACE_HUMAN	ACBP_HUMAN	ANAG_HUMAN	AMPB_HUMAN
ACE2_HUMAN	ACE_HUMAN	ANGL2_HUMAN	AMPE_HUMAN
ACOC_HUMAN	ACE2_HUMAN	ANGT_HUMAN	AMPN_HUMAN
ACPH_HUMAN	ACOC_HUMAN	ANT3_HUMAN	ANX11_HUMAN
ACTG_HUMAN	ACOT1_HUMAN	ANX11_HUMAN	ANXA2_HUMAN
ACTN1_HUMAN	ACPH_HUMAN	ANXA4_HUMAN	ANXA3_HUMAN
ACTN3_HUMAN	ACSL4_HUMAN	ANXA5_HUMAN	ANXA4_HUMAN
ACTN4_HUMAN	ACTB_HUMAN	ANXA7_HUMAN	ANXA5_HUMAN
ACTS_HUMAN	ACTBL_HUMAN	APLP2_HUMAN	ANXA6_HUMAN
ACY1_HUMAN	ACTG_HUMAN	APOA_HUMAN	ANXA7_HUMAN
ADAS_HUMAN	ACTN1_HUMAN	APOA1_HUMAN	APOA1_HUMAN
ADH6_HUMAN	ACTN2_HUMAN	APOA2_HUMAN	APOA2_HUMAN
ADHX_HUMAN	ACTN3_HUMAN	APOA4_HUMAN	APOC1_HUMAN
ADT2_HUMAN	ACTN4_HUMAN	APOC1_HUMAN	APOD_HUMAN
ADT3_HUMAN	ACTS_HUMAN	APOD_HUMAN	APT_HUMAN
AFAM_HUMAN	ACTZ_HUMAN	APOE_HUMAN	AQP1_HUMAN
AGAL_HUMAN	ACY1_HUMAN	AQP2_HUMAN	AQP2_HUMAN
AGRF5_HUMAN	ADAS_HUMAN	ASAH1_HUMAN	ARL3_HUMAN
AGRG1_HUMAN	ADH1G_HUMAN	AT1B1_HUMAN	ARRD1_HUMAN
AGRIN_HUMAN	ADHX_HUMAN	B4GA1_HUMAN	ASSY_HUMAN
AGRL1_HUMAN	ADRO_HUMAN	B4GT1_HUMAN	AT1A1_HUMAN
AHNK_HUMAN	ADSV_HUMAN	BGAL_HUMAN	AT1B1_HUMAN
AIFM1_HUMAN	ADT1_HUMAN	BHMT1_HUMAN	ATPA_HUMAN
AK1A1_HUMAN	ADT2_HUMAN	BROX_HUMAN	ATPB_HUMAN
AK1C1_HUMAN	ADT3_HUMAN	BTD_HUMAN	BAIP2_HUMAN
AK1C3_HUMAN	AHNK_HUMAN	C1RL_HUMAN	BASP1_HUMAN
AL1A1_HUMAN	AIDA_HUMAN	CAB39_HUMAN	BDH2_HUMAN
AL1L1_HUMAN	AIFM1_HUMAN	CAD13_HUMAN	BHMT1_HUMAN
AL7A1_HUMAN	AK1A1_HUMAN	CADM1_HUMAN	BI2L1_HUMAN
AL9A1_HUMAN	AK1C1_HUMAN	CADM4_HUMAN	BLVRB_HUMAN
ALAT1_HUMAN	AK1C3_HUMAN	CAH2_HUMAN	BROX_HUMAN
ALBU_HUMAN	AKA12_HUMAN	CALB1_HUMAN	BST1_HUMAN
ALDOA_HUMAN	AL1A1_HUMAN	CAN7_HUMAN	CAB39_HUMAN
ALDOB_HUMAN	AL1L1_HUMAN	CATD_HUMAN	CAH2_HUMAN
ALDR_HUMAN	AL3B1_HUMAN	CATZ_HUMAN	CALB1_HUMAN
ALS_HUMAN	AL7A1_HUMAN	CBG_HUMAN	CAN1_HUMAN
AMBP_HUMAN	AL9A1_HUMAN	CBPE_HUMAN	CAN5_HUMAN
AMD_HUMAN	ALBU_HUMAN	CBPM_HUMAN	CAN7_HUMAN
AMPE_HUMAN	ALDH2_HUMAN	CBPQ_HUMAN	CAPG_HUMAN
AMPL_HUMAN	ALDOA_HUMAN	CBR1_HUMAN	CAPZB_HUMAN
AMPN_HUMAN	ALDOB_HUMAN	CD14_HUMAN	CAYP1_HUMAN
AMY1A_HUMAN	ALDR_HUMAN	CD248_HUMAN	CAZA2_HUMAN

AMY2B_HUMAN	AMBP_HUMAN	CD44_HUMAN	CB39L_HUMAN
AMYP_HUMAN	AMPB_HUMAN	CD59_HUMAN	CBPM_HUMAN
ANAG_HUMAN	AMPD1_HUMAN	CD63_HUMAN	CBR1_HUMAN
ANGL1_HUMAN	AMPE_HUMAN	CD9_HUMAN	CD2AP_HUMAN
ANGL2_HUMAN	AMPL_HUMAN	CEL_HUMAN	CD59_HUMAN
ANGT_HUMAN	AMPN_HUMAN	CERU_HUMAN	CD9_HUMAN
ANO6_HUMAN	AN13B_HUMAN	CETP_HUMAN	CDC42_HUMAN
ANPRC_HUMAN	ANCHR_HUMAN	CFAB_HUMAN	CEAM1_HUMAN
ANT3_HUMAN	ANO6_HUMAN	CFAI_HUMAN	CHM1A_HUMAN
ANTR1_HUMAN	ANT3_HUMAN	CHM1B_HUMAN	CHM1B_HUMAN
ANX10_HUMAN	ANX11_HUMAN	CHM2A_HUMAN	CHM2A_HUMAN
ANX11_HUMAN	ANX13_HUMAN	CHM4B_HUMAN	CHM2B_HUMAN
ANXA1_HUMAN	ANXA1_HUMAN	CHMP5_HUMAN	CHM4A_HUMAN
ANXA2_HUMAN	ANXA2_HUMAN	CILP2_HUMAN	CHM4B_HUMAN
ANXA4_HUMAN	ANXA3_HUMAN	CLC14_HUMAN	CHMP3_HUMAN
ANXA5_HUMAN	ANXA4_HUMAN	CLM9_HUMAN	CHMP5_HUMAN
ANXA6_HUMAN	ANXA5_HUMAN	CLUS_HUMAN	CHMP6_HUMAN
ANXA7_HUMAN	ANXA6_HUMAN	CN37_HUMAN	CLH1_HUMAN
AOC1_HUMAN	ANXA7_HUMAN	CNDP2_HUMAN	CLIC1_HUMAN
APLP2_HUMAN	ANXA9_HUMAN	CNTN1_HUMAN	CN37_HUMAN
APOA_HUMAN	AOXA_HUMAN	CO3_HUMAN	CNDP2_HUMAN
APOA1_HUMAN	AP1B1_HUMAN	CO4B_HUMAN	CPNE3_HUMAN
APOA2_HUMAN	AP1G1_HUMAN	CO6A1_HUMAN	CPNE8_HUMAN
APOA4_HUMAN	AP2A1_HUMAN	CO6A3_HUMAN	CR1_HUMAN
APOB_HUMAN	AP2A2_HUMAN	CO9_HUMAN	CRYL1_HUMAN
APOC1_HUMAN	AP2B1_HUMAN	COFA1_HUMAN	CTDS1_HUMAN
APOC2_HUMAN	AP2M1_HUMAN	CPN2_HUMAN	CTL2_HUMAN
APOC3_HUMAN	APOA1_HUMAN	CPNE3_HUMAN	CTL4_HUMAN
APOD_HUMAN	APOA2_HUMAN	CPNE8_HUMAN	CYBR1_HUMAN
APOE_HUMAN	APOA4_HUMAN	CPVL_HUMAN	CYFP1_HUMAN
APOH_HUMAN	APOB_HUMAN	CSF1_HUMAN	CYRIB_HUMAN
APOM_HUMAN	APOC1_HUMAN	CSPG4_HUMAN	DAF_HUMAN
APT_HUMAN	APOC2_HUMAN	CTL2_HUMAN	DPEP1_HUMAN
AQP1_HUMAN	APOC3_HUMAN	CTL4_HUMAN	DPP4_HUMAN
AQP2_HUMAN	APOD_HUMAN	CUBN_HUMAN	EF1A3_HUMAN
AQP7_HUMAN	APOE_HUMAN	DDAH2_HUMAN	EHD1_HUMAN
ARF5_HUMAN	APOH_HUMAN	DERM_HUMAN	EHD4_HUMAN
ARGAL_HUMAN	APOM_HUMAN	DNAS1_HUMAN	ENOA_HUMAN
ARGI1_HUMAN	APT_HUMAN	DPEP1_HUMAN	EPS8_HUMAN
ARK72_HUMAN	AQP1_HUMAN	DPP2_HUMAN	ES8L1_HUMAN
ARK73_HUMAN	AQP2_HUMAN	DPP4_HUMAN	ES8L2_HUMAN
ARK74_HUMAN	AQP7_HUMAN	DSC2_HUMAN	EZRI_HUMAN
ARL15_HUMAN	AR13B_HUMAN	EF1A3_HUMAN	FLOT1_HUMAN
ARL3_HUMAN	ARC1A_HUMAN	EGF_HUMAN	FLOT2_HUMAN
ARLY_HUMAN	ARC1B_HUMAN	ENDD1_HUMAN	FRK_HUMAN
ARMT1_HUMAN	ARF1_HUMAN	ENOA_HUMAN	G3P_HUMAN
ARP2_HUMAN	ARF4_HUMAN	EPCR_HUMAN	G6PI_HUMAN
ARP3_HUMAN	ARF5_HUMAN	EPS8_HUMAN	GBB1_HUMAN
ARPC2_HUMAN	ARF6_HUMAN	EZRI_HUMAN	GBB2_HUMAN
ARRD1_HUMAN	ARGAL_HUMAN	FA11_HUMAN	GDIB_HUMAN
ARSA_HUMAN	ARK72_HUMAN	FA12_HUMAN	GDIR1_HUMAN
ARSB_HUMAN	ARK73_HUMAN	FAM3C_HUMAN	GELS_HUMAN
ARSF_HUMAN	ARL15_HUMAN	FAT4_HUMAN	GGT1_HUMAN
ASAH1_HUMAN	ARL3_HUMAN	FBLN3_HUMAN	GLTP_HUMAN
ASM_HUMAN	ARL6_HUMAN	FBLN4_HUMAN	GNA11_HUMAN

ASM3B_HUMAN	ARL8B_HUMAN	FBLN5_HUMAN	GNA13_HUMAN
ASSY_HUMAN	ARLY_HUMAN	FCN2_HUMAN	GNAI1_HUMAN
AT1A1_HUMAN	ARMC9_HUMAN	FETUA_HUMAN	GNAI2_HUMAN
AT1B1_HUMAN	ARMT1_HUMAN	FIBA_HUMAN	GNAI3_HUMAN
AT2A1_HUMAN	ARP2_HUMAN	FIBG_HUMAN	GNAQ_HUMAN
AT2A2_HUMAN	ARP3_HUMAN	FINC_HUMAN	GPC5B_HUMAN
AT8B3_HUMAN	ARP3B_HUMAN	FREM2_HUMAN	GPC5C_HUMAN
ATL2_HUMAN	ARP5L_HUMAN	G3P_HUMAN	GPDA_HUMAN
ATPA_HUMAN	ARPC2_HUMAN	GAS6_HUMAN	GPX4_HUMAN
ATPB_HUMAN	ARPC3_HUMAN	GBB2_HUMAN	GSTM3_HUMAN
ATRN_HUMAN	ARPC4_HUMAN	GELS_HUMAN	GSTO1_HUMAN
AXA2L_HUMAN	ARPC5_HUMAN	GGH_HUMAN	GSTP1_HUMAN
B2MG_HUMAN	ARRD1_HUMAN	GGT1_HUMAN	GTR5_HUMAN
B3GN2_HUMAN	ARSF_HUMAN	GNAS1_HUMAN	HBB_HUMAN
B3GN8_HUMAN	ASAH1_HUMAN	GPC1_HUMAN	HEBP1_HUMAN
B4GA1_HUMAN	ASC_HUMAN	GPC3_HUMAN	HPT_HUMAN
B4GT1_HUMAN	ASM3B_HUMAN	GPC4_HUMAN	HS71B_HUMAN
BAP31_HUMAN	ASSY_HUMAN	GPC5B_HUMAN	HS90A_HUMAN
BCAM_HUMAN	AT12A_HUMAN	GPC5C_HUMAN	HS90B_HUMAN
BDH2_HUMAN	AT1A1_HUMAN	GPVI_HUMAN	HSP72_HUMAN
BGAL_HUMAN	AT1B1_HUMAN	GPX3_HUMAN	HSP7C_HUMAN
BGLR_HUMAN	AT2A1_HUMAN	GSTM3_HUMAN	HSPB1_HUMAN
BHMT1_HUMAN	AT2A2_HUMAN	GTR5_HUMAN	HYES_HUMAN
BHMT2_HUMAN	AT8B1_HUMAN	HBB_HUMAN	IDHC_HUMAN
BI2L1_HUMAN	ATNG_HUMAN	HEMO_HUMAN	IGG1_HUMAN
BIEA_HUMAN	ATPA_HUMAN	HPT_HUMAN	IGHA1_HUMAN
BIP_HUMAN	ATPB_HUMAN	HS71B_HUMAN	IGHG2_HUMAN
BLMH_HUMAN	ATRN_HUMAN	HS90A_HUMAN	IGHM_HUMAN
BLVRB_HUMAN	B2MG_HUMAN	HSP7C_HUMAN	IGK_HUMAN
BODG_HUMAN	B4_VACCC	HSPB1_HUMAN	ILEU_HUMAN
BPIB1_HUMAN	BAIP2_HUMAN	HV307_HUMAN	IPYR_HUMAN
BROX_HUMAN	BAP31_HUMAN	HYAL1_HUMAN	IQGA1_HUMAN
BST1_HUMAN	BARD1_HUMAN	I18BP_HUMAN	IST1_HUMAN
BT2A2_HUMAN	BASI_HUMAN	IC1_HUMAN	ITA3_HUMAN
BT3A2_HUMAN	BASP1_HUMAN	ICOSL_HUMAN	ITAV_HUMAN
BTD_HUMAN	BCAM_HUMAN	IDHC_HUMAN	ITB1_HUMAN
C1QB_HUMAN	BCAS1_HUMAN	IF6_HUMAN	K1C10_HUMAN
C1QBP_HUMAN	BCR_HUMAN	IGG1_HUMAN	K1C16_HUMAN
C1QC_HUMAN	BDH2_HUMAN	IGHA1_HUMAN	K1C9_HUMAN
C1R_HUMAN	BGAL_HUMAN	IGHG2_HUMAN	K2C1_HUMAN
C1RL_HUMAN	BHMT1_HUMAN	IGHM_HUMAN	K2C5_HUMAN
C1TC_HUMAN	BI2L1_HUMAN	IGJ_HUMAN	KAD1_HUMAN
C1TM_HUMAN	BIEA_HUMAN	IGK_HUMAN	KCRB_HUMAN
CA2D1_HUMAN	BIP_HUMAN	IGKC_HUMAN	KCY_HUMAN
CAB39_HUMAN	BLVRB_HUMAN	IGL1_HUMAN	KIF12_HUMAN
CAB45_HUMAN	BODG_HUMAN	IGLC3_HUMAN	KNG1_HUMAN
CAD11_HUMAN	BPNT1_HUMAN	IPSP_HUMAN	KPYM_HUMAN
CAD13_HUMAN	BROX_HUMAN	ISLR_HUMAN	LAMP1_HUMAN
CAD16_HUMAN	BST1_HUMAN	IST1_HUMAN	LAMP2_HUMAN
CAD19_HUMAN	BST2_HUMAN	ITIH4_HUMAN	LDHA_HUMAN
CADH1_HUMAN	BT3A2_HUMAN	K1C10_HUMAN	LDHB_HUMAN
CADH6_HUMAN	C1QBP_HUMAN	K1C14_HUMAN	LEG3_HUMAN
CADM1_HUMAN	C1TC_HUMAN	K1C9_HUMAN	LFG3_HUMAN
CADM4_HUMAN	C1TM_HUMAN	K2C1_HUMAN	LG3BP_HUMAN
CAH1_HUMAN	C2D1A_HUMAN	K2C5_HUMAN	LGUL_HUMAN

CAH12_HUMAN	C2D1B_HUMAN	KAIN_HUMAN	LIN7C_HUMAN
CAH2_HUMAN	CA2D1_HUMAN	KLK1_HUMAN	LRP2_HUMAN
CALB1_HUMAN	CAAS1_HUMAN	KNG1_HUMAN	LYPA1_HUMAN
CALR_HUMAN	CAB39_HUMAN	KV311_HUMAN	MAL2_HUMAN
CALX_HUMAN	CAH2_HUMAN	KV320_HUMAN	MDHC_HUMAN
CAN1_HUMAN	CAH3_HUMAN	KV401_HUMAN	MDR1_HUMAN
CAN7_HUMAN	CAH4_HUMAN	KVD28_HUMAN	MERL_HUMAN
CAN8_HUMAN	CALB1_HUMAN	LAMP1_HUMAN	MGA_HUMAN
CAND1_HUMAN	CALM3_HUMAN	LAMP2_HUMAN	MINY1_HUMAN
CANT1_HUMAN	CALR_HUMAN	LCAT_HUMAN	MITD1_HUMAN
CAP1_HUMAN	CALX_HUMAN	LDHB_HUMAN	MOB1A_HUMAN
CAP7_HUMAN	CAN1_HUMAN	LEG3_HUMAN	MOES_HUMAN
CAPG_HUMAN	CAN2_HUMAN	LG3BP_HUMAN	MUC1_HUMAN
CAPZB_HUMAN	CAN5_HUMAN	LMAN2_HUMAN	MYH9_HUMAN
CATB_HUMAN	CAN6_HUMAN	LRC15_HUMAN	MYO1C_HUMAN
CATC_HUMAN	CAN7_HUMAN	LRP2_HUMAN	MYO1D_HUMAN
CATD_HUMAN	CAN8_HUMAN	LRRN4_HUMAN	NAPSA_HUMAN
CATH_HUMAN	CAND1_HUMAN	LUM_HUMAN	NCKP1_HUMAN
CATO_HUMAN	CAP1_HUMAN	LV147_HUMAN	NEP_HUMAN
CATS_HUMAN	CAPG_HUMAN	LYAG_HUMAN	NHRF1_HUMAN
CATZ_HUMAN	CAPZB_HUMAN	LYAM1_HUMAN	NHRF3_HUMAN
CAZA2_HUMAN	CARL1_HUMAN	MA1A1_HUMAN	NIBA2_HUMAN
CBG_HUMAN	CASQ1_HUMAN	MASP2_HUMAN	OLFM4_HUMAN
CBPE_HUMAN	CATA_HUMAN	MDHC_HUMAN	PA1B2_HUMAN
CBPM_HUMAN	CATD_HUMAN	MDR1_HUMAN	PARK7_HUMAN
CBPN_HUMAN	CAYP1_HUMAN	MFAP4_HUMAN	PDC10_HUMAN
CBPQ_HUMAN	CAZA1_HUMAN	MOES_HUMAN	PDC6I_HUMAN
CBR1_HUMAN	CAZA2_HUMAN	MUC1_HUMAN	PDCD6_HUMAN
CCD25_HUMAN	CB39L_HUMAN	MXRA8_HUMAN	PEBP1_HUMAN
CD14_HUMAN	CBPM_HUMAN	NAGAB_HUMAN	PEF1_HUMAN
CD248_HUMAN	CBPQ_HUMAN	NAPSA_HUMAN	PEPD_HUMAN
CD27_HUMAN	CBR1_HUMAN	NECT2_HUMAN	PEPL_HUMAN
CD2AP_HUMAN	CC186_HUMAN	NECT4_HUMAN	PGAM1_HUMAN
CD34_HUMAN	CC50A_HUMAN	NEO1_HUMAN	PGDH_HUMAN
CD44_HUMAN	CC50B_HUMAN	NEP_HUMAN	PGK1_HUMAN
CD59_HUMAN	CCD57_HUMAN	NEUR1_HUMAN	PGM1_HUMAN
CD63_HUMAN	CCM2_HUMAN	NEUS_HUMAN	PLCD1_HUMAN
CD7_HUMAN	CCNY_HUMAN	NID1_HUMAN	PLST_HUMAN
CD81_HUMAN	CCYL1_HUMAN	NUCB1_HUMAN	PNPH_HUMAN
CD9_HUMAN	CD14_HUMAN	OLFM4_HUMAN	PODXL_HUMAN
CDC42_HUMAN	CD2AP_HUMAN	OSCAR_HUMAN	PPAL_HUMAN
CDHR2_HUMAN	CD44_HUMAN	OSTP_HUMAN	PRDX1_HUMAN
CDHR5_HUMAN	CD47_HUMAN	PAPP2_HUMAN	PRDX2_HUMAN
CEAM1_HUMAN	CD59_HUMAN	PCDGK_HUMAN	PRDX6_HUMAN
CEAM5_HUMAN	CD63_HUMAN	PDC6I_HUMAN	PROM1_HUMAN
CEAM8_HUMAN	CD81_HUMAN	PDCD6_HUMAN	PROM2_HUMAN
CEL_HUMAN	CD82_HUMAN	PEBP1_HUMAN	PRSS8_HUMAN
CERS6_HUMAN	CD9_HUMAN	PEDF_HUMAN	PSA_HUMAN
CERU_HUMAN	CDC42_HUMAN	PEF1_HUMAN	PSCA_HUMAN
CETP_HUMAN	CDHR2_HUMAN	PGBM_HUMAN	PTGR1_HUMAN
CFAB_HUMAN	CDHR5_HUMAN	PGK1_HUMAN	PTN13_HUMAN
CFAD_HUMAN	CE104_HUMAN	PGRP1_HUMAN	PTPRJ_HUMAN
CFAH_HUMAN	CEAM1_HUMAN	PGRP2_HUMAN	PTPRO_HUMAN
CFAI_HUMAN	CEAM5_HUMAN	PGS1_HUMAN	RAB10_HUMAN
CGL_HUMAN	CEAM6_HUMAN	PIGR_HUMAN	RAB13_HUMAN

CH10_HUMAN	CEAM7_HUMAN	PLD3_HUMAN	RAB14_HUMAN
CH60_HUMAN	CEAM8_HUMAN	PODXL_HUMAN	RAB1A_HUMAN
CHM1A_HUMAN	CERS6_HUMAN	PPAL_HUMAN	RAB25_HUMAN
CHM1B_HUMAN	CERU_HUMAN	PPAP_HUMAN	RAB5C_HUMAN
CHM2A_HUMAN	CFA58_HUMAN	PPGB_HUMAN	RAB7A_HUMAN
CHM2B_HUMAN	CFAB_HUMAN	PPT2_HUMAN	RAC1_HUMAN
CHM4B_HUMAN	CH10_HUMAN	PRDX1_HUMAN	RADI_HUMAN
CHM4C_HUMAN	CH60_HUMAN	PRDX2_HUMAN	RAI3_HUMAN
CHMP3_HUMAN	CHM1A_HUMAN	PRDX6_HUMAN	RALA_HUMAN
CHMP5_HUMAN	CHM1B_HUMAN	PRG2_HUMAN	RALB_HUMAN
CHMP6_HUMAN	CHM2A_HUMAN	PROM1_HUMAN	RAP1A_HUMAN
CHODL_HUMAN	CHM2B_HUMAN	PROM2_HUMAN	RAP1B_HUMAN
CILP2_HUMAN	CHM4A_HUMAN	PROZ_HUMAN	RAP2B_HUMAN
CISY_HUMAN	CHM4B_HUMAN	PRSS8_HUMAN	RASK_HUMAN
CK054_HUMAN	CHM4C_HUMAN	PTGDS_HUMAN	RB11B_HUMAN
CLC14_HUMAN	CHMP3_HUMAN	PTPRG_HUMAN	RB27B_HUMAN
CLH1_HUMAN	CHMP5_HUMAN	PTPRJ_HUMAN	RHCG_HUMAN
CLIC1_HUMAN	CHMP6_HUMAN	QPCT_HUMAN	RHG18_HUMAN
CLIC4_HUMAN	CHP1_HUMAN	R4RL2_HUMAN	RINI_HUMAN
CLM8_HUMAN	CHSP1_HUMAN	RAB10_HUMAN	RL40_HUMAN
CLM9_HUMAN	CIB1_HUMAN	RAC1_HUMAN	RRAS_HUMAN
CLMP_HUMAN	CILK1_HUMAN	RAP1A_HUMAN	S12A1_HUMAN
CLN3_HUMAN	CING_HUMAN	RB11B_HUMAN	S12A3_HUMAN
CLN5_HUMAN	CISY_HUMAN	RENR_HUMAN	S13A2_HUMAN
CLRN3_HUMAN	CK052_HUMAN	RET4_HUMAN	S26A4_HUMAN
CLTRN_HUMAN	CK054_HUMAN	RHCG_HUMAN	S36A2_HUMAN
CLUS_HUMAN	CLCA4_HUMAN	RISC_HUMAN	S6A19_HUMAN
CM046_HUMAN	CLD19_HUMAN	RL40_HUMAN	SAHH_HUMAN
CMBL_HUMAN	CLD6_HUMAN	RNAS2_HUMAN	SBP1_HUMAN
CMGA_HUMAN	CLH1_HUMAN	ROBO4_HUMAN	SC5AA_HUMAN
CN37_HUMAN	CLIC1_HUMAN	S12A1_HUMAN	SCRB2_HUMAN
CNDP1_HUMAN	CLIC3_HUMAN	S12A3_HUMAN	SDCB1_HUMAN
CNDP2_HUMAN	CLIC4_HUMAN	SAMP_HUMAN	SERA_HUMAN
CNTFR_HUMAN	CLIC5_HUMAN	SCTM1_HUMAN	SLK_HUMAN
CNTN1_HUMAN	CLIC6_HUMAN	SDC4_HUMAN	SNAA_HUMAN
CO2_HUMAN	CLN3_HUMAN	SDCB1_HUMAN	SNF8_HUMAN
CO3_HUMAN	CLPX_HUMAN	SLIK1_HUMAN	SNP23_HUMAN
CO4A_HUMAN	CLRN3_HUMAN	SODE_HUMAN	SNX18_HUMAN
CO4A2_HUMAN	CLTRN_HUMAN	SORL_HUMAN	SORCN_HUMAN
CO4B_HUMAN	CLUS_HUMAN	SPRL1_HUMAN	SRC_HUMAN
CO5_HUMAN	CMBL_HUMAN	SUSD2_HUMAN	STABP_HUMAN
CO6A1_HUMAN	CN37_HUMAN	SYPL1_HUMAN	STK24_HUMAN
CO6A3_HUMAN	CNDP2_HUMAN	TBA1C_HUMAN	STOM_HUMAN
CO7_HUMAN	CO3_HUMAN	TENX_HUMAN	STX3_HUMAN
CO8G_HUMAN	CO4B_HUMAN	TETN_HUMAN	STXB2_HUMAN
CO9_HUMAN	CO6A1_HUMAN	THBG_HUMAN	TBA4A_HUMAN
COCA1_HUMAN	CO6A3_HUMAN	THRB_HUMAN	THY1_HUMAN
COFA1_HUMAN	COASY_HUMAN	THY1_HUMAN	TMPS2_HUMAN
COIA1_HUMAN	COF1_HUMAN	TPIS_HUMAN	TOLIP_HUMAN
COMP_HUMAN	COIA1_HUMAN	TRFE_HUMAN	TPIS_HUMAN
COPB2_HUMAN	COMT_HUMAN	TRFM_HUMAN	TRFE_HUMAN
CPN2_HUMAN	COR1B_HUMAN	TRHDE_HUMAN	TRFL_HUMAN
CPNE3_HUMAN	CPNE1_HUMAN	TRY1_HUMAN	TRFM_HUMAN
CPNE4_HUMAN	CPNE2_HUMAN	TS101_HUMAN	TRY1_HUMAN
CPNE5_HUMAN	CPNE3_HUMAN	TSN1_HUMAN	TS101_HUMAN

CPNE7_HUMAN
CPNE8_HUMAN
CPSM_HUMAN
CPVL_HUMAN
CPXM2_HUMAN
CR1_HUMAN
CRAC1_HUMAN
CREG1_HUMAN
CRNN_HUMAN
CRP_HUMAN
CRUM2_HUMAN
CRYAB_HUMAN
CRYL1_HUMAN
CRYM_HUMAN
CSF1_HUMAN
CSF1R_HUMAN
CSPG2_HUMAN
CSPG4_HUMAN
CTL2_HUMAN
CTL4_HUMAN
CUBN_HUMAN
CUTA_HUMAN
CXCL7_HUMAN
CYBR1_HUMAN
CYFP1_HUMAN
CYTA_HUMAN
CYTC_HUMAN
CYTN_HUMAN
CYTS_HUMAN
DAF_HUMAN
DAG1_HUMAN
DCD_HUMAN
DCXR_HUMAN
DDAH1_HUMAN
DDAH2_HUMAN
DDC_HUMAN
DDR1_HUMAN
DEF3_HUMAN
DERM_HUMAN
DESP_HUMAN
DHB4_HUMAN
DHPR_HUMAN
DHSO_HUMAN
DLK1_HUMAN
DMA_HUMAN
DMB_HUMAN
DMBT1_HUMAN
DNAS1_HUMAN
DNJC3_HUMAN
DNPH1_HUMAN
DNS2A_HUMAN
DPEP1_HUMAN
DPP2_HUMAN
DPP4_HUMAN
DPP6_HUMAN

CPNE4_HUMAN
CPNE5_HUMAN
CPNE7_HUMAN
CPNE8_HUMAN
CPNS1_HUMAN
CPPED_HUMAN
CPSM_HUMAN
CR1_HUMAN
CREG1_HUMAN
CRIM1_HUMAN
CRIP2_HUMAN
CRK_HUMAN
CRKL_HUMAN
CRNN_HUMAN
CRP_HUMAN
CRTP1_HUMAN
CRUM2_HUMAN
CRUM3_HUMAN
CRYAB_HUMAN
CRYL1_HUMAN
CRYM_HUMAN
CSPP1_HUMAN
CSRP1_HUMAN
CTDS1_HUMAN
CTDSL_HUMAN
CTL1_HUMAN
CTL2_HUMAN
CTL4_HUMAN
CUBN_HUMAN
CXCL7_HUMAN
CYBR1_HUMAN
CYFP1_HUMAN
CYFP2_HUMAN
CYRIB_HUMAN
CYS1_HUMAN
CYTA_HUMAN
CYTB_HUMAN
CYTC_HUMAN
CYTM1_HUMAN
CYTN_HUMAN
CYTS_HUMAN
DAB2_HUMAN
DAF_HUMAN
DAG1_HUMAN
DCD_HUMAN
DCDC2_HUMAN
DCHS_HUMAN
DCTN2_HUMAN
DCXR_HUMAN
DDAH1_HUMAN
DDAH2_HUMAN
DDC_HUMAN
DDX3X_HUMAN
DDX46_HUMAN
DEF3_HUMAN

UEVLD_HUMAN
UFO_HUMAN
UROM_HUMAN
VAS1_HUMAN
VASN_HUMAN
VATA_HUMAN
VMO1_HUMAN
VP37D_HUMAN
VPS4A_HUMAN
VPS4B_HUMAN
VTA1_HUMAN
VTDB_HUMAN
VTNC_HUMAN
XPP2_HUMAN
ZA2G_HUMAN
ZG16B_HUMAN

TSN1_HUMAN
UBA1_HUMAN
UBXN6_HUMAN
UCHL1_HUMAN
UEVLD_HUMAN
ULK3_HUMAN
UPK1A_HUMAN
UPK3A_HUMAN
UROM_HUMAN
VA0D1_HUMAN
VA0D2_HUMAN
VAT1_HUMAN
VATA_HUMAN
VATB1_HUMAN
VATB2_HUMAN
VATC1_HUMAN
VATD_HUMAN
VATE1_HUMAN
VATH_HUMAN
VP37B_HUMAN
VP37D_HUMAN
VPP4_HUMAN
VPS25_HUMAN
VPS28_HUMAN
VPS4A_HUMAN
VPS4B_HUMAN
VTA1_HUMAN
WDR1_HUMAN
XPP2_HUMAN
XRP2_HUMAN
YES_HUMAN

DSC2_HUMAN
DSC3_HUMAN
DSG4_HUMAN
DYST_HUMAN
E1BS_ADE02
EAA3_HUMAN
ECHA_HUMAN
ECHB_HUMAN
ECHD1_HUMAN
EF1A3_HUMAN
EF1G_HUMAN
EF2_HUMAN
EFNA1_HUMAN
EFTU_HUMAN
EGF_HUMAN
EHD1_HUMAN
ELFN1_HUMAN
ENDD1_HUMAN
ENOA_HUMAN
ENPL_HUMAN
ENPP6_HUMAN
EPCR_HUMAN
EPHB3_HUMAN
EPHB4_HUMAN
EPS8_HUMAN
ERD22_HUMAN
ERO1A_HUMAN
ERP44_HUMAN
ES8L2_HUMAN
ESTD_HUMAN
ETFA_HUMAN
EVPL_HUMAN
EXTL2_HUMAN
EZRI_HUMAN
F10A1_HUMAN
F10A5_HUMAN
F151A_HUMAN
F16P1_HUMAN
F16P2_HUMAN
FA10_HUMAN
FA11_HUMAN
FA12_HUMAN
FA9_HUMAN
FAKD4_HUMAN
FAM3B_HUMAN
FAM3C_HUMAN
FANCI_HUMAN
FAT4_HUMAN
FBLN1_HUMAN
FBLN2_HUMAN
FBLN3_HUMAN
FBLN4_HUMAN
FBLN5_HUMAN
FBLN7_HUMAN
FBN1_HUMAN
DEN2D_HUMAN
DESM_HUMAN
DESP_HUMAN
DEST_HUMAN
DHB4_HUMAN
DHPR_HUMAN
DHSO_HUMAN
DIAP1_HUMAN
DIP2A_HUMAN
DIP2B_HUMAN
DMA_HUMAN
DMB_HUMAN
DMBT1_HUMAN
DMXL1_HUMAN
DNJA1_HUMAN
DNJC5_HUMAN
DNJC8_HUMAN
DNPH1_HUMAN
DOCK9_HUMAN
DOP2_HUMAN
DOPD_HUMAN
DPEP1_HUMAN
DPP3_HUMAN
DPP4_HUMAN
DPP6_PANTR
DRA_HUMAN
DUS3_HUMAN
DYHC1_HUMAN
DYN2_HUMAN
DYN3_HUMAN
DYST_HUMAN
E1BS_ADE02
ECHA_HUMAN
ECHB_HUMAN
EF1A1_HUMAN
EF1A2_HUMAN
EF1A3_HUMAN
EF2_HUMAN
EFNB1_HUMAN
EFR3A_HUMAN
EFTU_HUMAN
EGF_HUMAN
EHD1_HUMAN
EHD4_HUMAN
EMAL2_HUMAN
ENOA_HUMAN
ENOB_HUMAN
ENPL_HUMAN
ENPP6_HUMAN
ENTP3_HUMAN
ENTP8_HUMAN
EPN1_HUMAN
EPN3_HUMAN
EPS8_HUMAN
ES8L1_HUMAN

FCER2_HUMAN
FCG3A_HUMAN
FCGBP_HUMAN
FCN2_HUMAN
FDSCP_HUMAN
FETUA_HUMAN
FGFR2_HUMAN
FGFR4_HUMAN
FHR4_HUMAN
FIBA_HUMAN
FIBB_HUMAN
FIBG_HUMAN
FILA_HUMAN
FILA2_HUMAN
FINC_HUMAN
FLNC_HUMAN
FLOT1_HUMAN
FLRT2_HUMAN
FMOD_HUMAN
FOLR1_HUMAN
FREM2_HUMAN
FRIL_HUMAN
FSTL1_HUMAN
FTCD_HUMAN
FUCO_HUMAN
FUCO2_HUMAN
G3P_HUMAN
G6PI_HUMAN
GALC_HUMAN
GALK1_HUMAN
GALNS_HUMAN
GANAB_HUMAN
GANP_HUMAN
GAS1_HUMAN
GAS6_HUMAN
GBB1_HUMAN
GBB2_HUMAN
GBB4_HUMAN
GDIB_HUMAN
GELS_HUMAN
GGA1_HUMAN
GGH_HUMAN
GGT1_HUMAN
GGT2_HUMAN
GGT6_HUMAN
GGTL2_HUMAN
GINM1_HUMAN
GLCM_HUMAN
GLO2_HUMAN
GLOD4_HUMAN
GLPK_HUMAN
GLT18_HUMAN
GLU2B_HUMAN
GLYC_HUMAN
GLYM_HUMAN
ES8L2_HUMAN
ESTD_HUMAN
ETFA_HUMAN
EVPL_HUMAN
EXOC1_HUMAN
EXOC2_HUMAN
EXOC3_HUMAN
EXOC5_HUMAN
EXOC7_HUMAN
EXOC8_HUMAN
EZRI_HUMAN
F10A1_HUMAN
F10A5_HUMAN
F151A_HUMAN
F16P1_HUMAN
F16P2_HUMAN
F262_HUMAN
FAAA_HUMAN
FABPH_HUMAN
FABPL_HUMAN
FAKD4_HUMAN
FAS_HUMAN
FBAS1_HUMAN
FBX50_HUMAN
FCL_HUMAN
FETUA_HUMAN
FHL1_HUMAN
FIBA_HUMAN
FIBB_HUMAN
FIBG_HUMAN
FILA2_HUMAN
FKB15_HUMAN
FKB1A_HUMAN
FKBP4_HUMAN
FLNB_HUMAN
FLNC_HUMAN
FLOT1_HUMAN
FLOT2_HUMAN
FRIL_HUMAN
FRK_HUMAN
FTCD_HUMAN
G3P_HUMAN
G6PI_HUMAN
GALK1_HUMAN
GALM_HUMAN
GANAB_HUMAN
GANP_HUMAN
GARS_HUMAN
GBB1_HUMAN
GBB2_HUMAN
GBB4_HUMAN
GBG12_HUMAN
GBG5_HUMAN
GBG7_HUMAN
GDE_HUMAN

GMPR2_HUMAN
GNA11_HUMAN
GNA12_HUMAN
GNA13_HUMAN
GNAI1_HUMAN
GNAI2_HUMAN
GNAI3_HUMAN
GNAQ_HUMAN
GNAS1_HUMAN
GNAS2_HUMAN
GNPI1_HUMAN
GNS_HUMAN
GOLM1_HUMAN
GP180_HUMAN
GP1BA_HUMAN
GPC1_HUMAN
GPC3_HUMAN
GPC4_HUMAN
GPC5B_HUMAN
GPC5C_HUMAN
GPC6_HUMAN
GPDA_HUMAN
GPNMB_HUMAN
GPV_HUMAN
GPVI_HUMAN
GPX3_HUMAN
GRAN_HUMAN
GRHPR_HUMAN
GRP75_HUMAN
GSHB_HUMAN
GSLG1_HUMAN
GSTA1_HUMAN
GSTA2_HUMAN
GSTA5_HUMAN
GSTM1_HUMAN
GSTM2_HUMAN
GSTM3_HUMAN
GSTM5_HUMAN
GSTO1_HUMAN
GSTP1_HUMAN
GSTT1_HUMAN
GTR5_HUMAN
GUAD_HUMAN
H13_HUMAN
H2AJ_HUMAN
H2B1M_HUMAN
H32_HUMAN
H4_HUMAN
HAVR2_HUMAN
HBA_HUMAN
HBB_HUMAN
HBD_HUMAN
HBG2_HUMAN
HCD2_HUMAN
HCDH_HUMAN
GDIA_PANTR
GDIB_HUMAN
GDIR1_HUMAN
GDIR2_HUMAN
GELS_HUMAN
GET3_HUMAN
GFPT1_HUMAN
GGACT_HUMAN
GGCT_HUMAN
GGH_HUMAN
GGT1_HUMAN
GGT2_HUMAN
GGTL2_HUMAN
GIPC1_HUMAN
GLGB_HUMAN
GLO2_HUMAN
GLOD4_HUMAN
GLRX1_HUMAN
GLTP_HUMAN
GLYC_HUMAN
GLYM_HUMAN
GMDS_HUMAN
GNA1_HUMAN
GNA11_HUMAN
GNA13_HUMAN
GNA14_HUMAN
GNAI1_HUMAN
GNAI2_HUMAN
GNAI3_HUMAN
GNAO_HUMAN
GNAQ_HUMAN
GNAS1_HUMAN
GNAS2_HUMAN
GNAZ_HUMAN
GNPI1_HUMAN
GPC5B_HUMAN
GPC5C_HUMAN
GPD1L_HUMAN
GPDA_HUMAN
GPX4_HUMAN
GRAN_HUMAN
GRB2_HUMAN
GRB7_HUMAN
GRHPR_HUMAN
GRP75_HUMAN
GSH1_HUMAN
GSHB_HUMAN
GSHR_HUMAN
GSTA1_HUMAN
GSTA2_HUMAN
GSTM1_HUMAN
GSTM2_HUMAN
GSTM3_HUMAN
GSTO1_HUMAN
GSTP1_HUMAN

HECW2_HUMAN
HEM2_HUMAN
HEMO_HUMAN
HEP2_HUMAN
HEXA_HUMAN
HEXB_HUMAN
HGD_HUMAN
HGFA_HUMAN
HLAA_HUMAN
HLAE_HUMAN
HMCN1_HUMAN
HNRPK_HUMAN
HPPD_HUMAN
HPT_HUMAN
HRG_HUMAN
HS71B_HUMAN
HS71L_HUMAN
HS90A_HUMAN
HS90B_HUMAN
HSP72_HUMAN
HSP7C_HUMAN
HSPB1_HUMAN
HTRA1_HUMAN
HV102_HUMAN
HV307_HUMAN
HV311_HUMAN
HV315_HUMAN
HV323_HUMAN
HV335_HUMAN
HV349_HUMAN
HV372_HUMAN
HV374_HUMAN
HV428_HUMAN
HV551_HUMAN
HV601_HUMAN
HVC05_HUMAN
HVD82_HUMAN
HYAL1_HUMAN
HYES_HUMAN
HYOU1_HUMAN
I18BP_HUMAN
IBP2_HUMAN
IBP3_HUMAN
IBP7_HUMAN
IC1_HUMAN
ICAM2_HUMAN
ICOSL_HUMAN
IDHC_HUMAN
IDUA_HUMAN
IF4A2_HUMAN
IF6_HUMAN
IGA2_HUMAN
IGE_HUMAN
IGG1_HUMAN
IGHA1_HUMAN
GSTT1_HUMAN
GTR2_HUMAN
GTR5_HUMAN
GXLT2_HUMAN
H12_HUMAN
H2AJ_HUMAN
H2B1M_HUMAN
H32_HUMAN
H4_HUMAN
H90B2_HUMAN
HBA_HUMAN
HBB_HUMAN
HBD_HUMAN
HBE_HUMAN
HCD2_HUMAN
HCDH_HUMAN
HDHD2_HUMAN
HEBP1_HUMAN
HEBP2_HUMAN
HEM2_HUMAN
HEMO_HUMAN
HGD_HUMAN
HGS_HUMAN
HINT3_HUMAN
HLAA_HUMAN
HLAH_HUMAN
HNMT_HUMAN
HNRPK_HUMAN
HOME1_HUMAN
HORN_HUMAN
HPCA_HUMAN
HPPD_HUMAN
HPRT_HUMAN
HPT_HUMAN
HS105_HUMAN
HS12A_HUMAN
HS71B_HUMAN
HS71L_HUMAN
HS90A_HUMAN
HS90B_HUMAN
HSP72_HUMAN
HSP74_HUMAN
HSP7C_HUMAN
HSPB1_HUMAN
HTAI2_HUMAN
HVC05_HUMAN
HYES_HUMAN
HYOU1_HUMAN
I5P1_HUMAN
IC1_HUMAN
IDHC_HUMAN
IDHP_HUMAN
IF172_HUMAN
IF4A2_HUMAN
IF4G1_HUMAN

IGHA2_HUMAN
IGHG2_HUMAN
IGHG3_HUMAN
IGHG4_HUMAN
IGHM_HUMAN
IGJ_HUMAN
IGK_HUMAN
IGKC_HUMAN
IGL1_HUMAN
IGLC2_HUMAN
IGLC3_HUMAN
IGLL1_HUMAN
IGM_HUMAN
ILEU_HUMAN
IPSP_HUMAN
IQEC2_HUMAN
IQGA1_HUMAN
IQGA3_HUMAN
ISLR_HUMAN
IST1_HUMAN
ITA3_HUMAN
ITAV_HUMAN
ITB1_HUMAN
ITIH1_HUMAN
ITIH2_HUMAN
ITIH3_HUMAN
ITIH4_HUMAN
ITIH5_HUMAN
ITLN1_HUMAN
ITM2B_HUMAN
JMJD8_HUMAN
JUNB_HUMAN
K1549_HUMAN
K1C10_HUMAN
K1C13_HUMAN
K1C14_HUMAN
K1C15_HUMAN
K1C16_HUMAN
K1C17_HUMAN
K1C19_HUMAN
K1C9_HUMAN
K1H1_HUMAN
K1H2_HUMAN
K22E_HUMAN
K2C1_HUMAN
K2C4_HUMAN
K2C5_HUMAN
K2C6A_HUMAN
K2C6B_HUMAN
K2C6C_HUMAN
K2C78_HUMAN
K2C8_HUMAN
KAIN_HUMAN
KCRB_HUMAN
KHK_HUMAN
IF4H_HUMAN
IF5AL_HUMAN
IFT27_HUMAN
IGA2_HUMAN
IGG1_HUMAN
IGHA1_HUMAN
IGHA2_HUMAN
IGHG2_HUMAN
IGHM_HUMAN
IGJ_HUMAN
IGK_HUMAN
IGKC_HUMAN
IGL1_HUMAN
IGLC2_HUMAN
IGLC3_HUMAN
IGSF8_HUMAN
IL18_HUMAN
ILEU_HUMAN
IMB1_HUMAN
IMPA1_HUMAN
IMPA2_HUMAN
INADL_HUMAN
INP5E_HUMAN
IPSP_HUMAN
IPYR_HUMAN
IQGA1_HUMAN
IQGA2_HUMAN
ISOC1_HUMAN
IST1_HUMAN
ITA1_HUMAN
ITA3_HUMAN
ITAV_HUMAN
ITB1_HUMAN
ITB3_HUMAN
ITB5_HUMAN
ITB8_HUMAN
ITBP1_HUMAN
ITCH_HUMAN
ITIH1_HUMAN
ITM2B_HUMAN
JIP4_HUMAN
K1C10_HUMAN
K1C13_HUMAN
K1C14_HUMAN
K1C15_HUMAN
K1C16_HUMAN
K1C17_HUMAN
K1C19_HUMAN
K1C9_HUMAN
K1H1_HUMAN
K2C1_HUMAN
K2C5_HUMAN
K2C6A_HUMAN
K2C6B_HUMAN
K2C6C_HUMAN

KIF12_HUMAN
KLK1_HUMAN
KLK3_HUMAN
KLKB1_HUMAN
KLOT_HUMAN
KNG1_HUMAN
KPYM_HUMAN
KPYR_HUMAN
KR111_HUMAN
KR87P_HUMAN
KRA21_HUMAN
KRT35_HUMAN
KRT36_HUMAN
KRT81_HUMAN
KRT82_HUMAN
KRT83_HUMAN
KRT85_HUMAN
KT33B_HUMAN
KV105_HUMAN
KV109_HUMAN
KV116_HUMAN
KV117_HUMAN
KV133_HUMAN
KV224_HUMAN
KV229_HUMAN
KV230_HUMAN
KV311_HUMAN
KV315_HUMAN
KV320_HUMAN
KV37_HUMAN
KV401_HUMAN
KVD15_HUMAN
KVD16_HUMAN
KVD20_HUMAN
KVD28_HUMAN
KVD39_HUMAN
L1CAM_HUMAN
LACRT_HUMAN
LAIR1_HUMAN
LAIR2_HUMAN
LAMP1_HUMAN
LAMP2_HUMAN
LAP2A_HUMAN
LAR4B_HUMAN
LBP_HUMAN
LCAT_HUMAN
LCN1_HUMAN
LDHA_HUMAN
LDHB_HUMAN
LEG3_HUMAN
LFG3_HUMAN
LG3BP_HUMAN
LHPP_HUMAN
LICH_HUMAN
LIPL_HUMAN
K2C78_HUMAN
K2C8_HUMAN
KAD1_HUMAN
KALRN_HUMAN
KAP0_HUMAN
KAP2_HUMAN
KAPCA_HUMAN
KAPCB_HUMAN
KC1G3_HUMAN
KCD12_HUMAN
KCRB_HUMAN
KCRM_HUMAN
KCRS_HUMAN
KCTD3_HUMAN
KCY_HUMAN
KDM7A_HUMAN
KHK_HUMAN
KIF12_HUMAN
KIF27_HUMAN
KIF3A_HUMAN
KIF3B_HUMAN
KIF5A_HUMAN
KIFA3_HUMAN
KINH_HUMAN
KLH41_HUMAN
KLK3_HUMAN
KMT5B_HUMAN
KNG1_HUMAN
KPCA_HUMAN
KPCD_HUMAN
KPCE_HUMAN
KPCI_HUMAN
KPCZ_HUMAN
KPYM_HUMAN
KRIT1_HUMAN
KRT81_HUMAN
KRT82_HUMAN
KRT85_HUMAN
KSYK_HUMAN
KV127_HUMAN
KV133_HUMAN
KV230_HUMAN
KV311_HUMAN
KV315_HUMAN
KV320_HUMAN
KV401_HUMAN
KVD28_HUMAN
KVD40_HUMAN
LACRT_HUMAN
LAMP1_HUMAN
LAMP2_HUMAN
LANC1_HUMAN
LANC2_HUMAN
LAP2A_HUMAN
LASP1_HUMAN

LITAF_HUMAN	LCK_HUMAN
LMAN2_HUMAN	LCN1_HUMAN
LMNA_HUMAN	LDHA_HUMAN
LPPRC_HUMAN	LDHB_HUMAN
LRC15_HUMAN	LEG3_HUMAN
LRC59_HUMAN	LEG4_HUMAN
LRP2_HUMAN	LEG8_HUMAN
LRP4_HUMAN	LFG3_HUMAN
LRRN4_HUMAN	LG3BP_HUMAN
LTBP2_HUMAN	LGUL_HUMAN
LTP_HHV11	LHPP_HUMAN
LUM_HUMAN	LIN7C_HUMAN
LV147_HUMAN	LITAF_HUMAN
LV151_HUMAN	LKHA4_HUMAN
LV208_HUMAN	LMAN2_HUMAN
LV211_HUMAN	LMBD1_HUMAN
LV214_HUMAN	LMTK2_HUMAN
LV310_HUMAN	LPPRC_HUMAN
LV319_HUMAN	LRC57_HUMAN
LV321_HUMAN	LRC59_HUMAN
LV460_HUMAN	LRC8A_HUMAN
LV469_HUMAN	LRP2_HUMAN
LV657_HUMAN	LTOR1_HUMAN
LV743_HUMAN	LV147_HUMAN
LV861_HUMAN	LV321_HUMAN
LY75_HUMAN	LXN_HUMAN
LYAG_HUMAN	LYN_HUMAN
LYAM1_HUMAN	LYNX1_HUMAN
LYNX1_HUMAN	LYPA1_HUMAN
LYPA1_HUMAN	LYPL1_HUMAN
LYSC_HUMAN	LYSC_HUMAN
LYST_HUMAN	MA1A1_HUMAN
LYVE1_HUMAN	MAL2_HUMAN
MA1A1_HUMAN	MARCS_HUMAN
MA1C1_HUMAN	MASP2_HUMAN
MA2A1_HUMAN	MATK_HUMAN
MA2A2_HUMAN	MB12A_HUMAN
MA2B1_HUMAN	MB12B_HUMAN
MA2B2_HUMAN	MDHC_HUMAN
MABP1_HUMAN	MDHM_HUMAN
MADCA_HUMAN	MDR1_HUMAN
MAL2_HUMAN	MEAK7_HUMAN
MALR1_HUMAN	MED23_HUMAN
MAMC2_HUMAN	MEMO1_HUMAN
MASP2_HUMAN	MERL_HUMAN
MB12A_HUMAN	MET_HUMAN
MBTP1_HUMAN	METK1_HUMAN
MDHC_HUMAN	MFGM_HUMAN
MDHM_HUMAN	MGA_HUMAN
MDR1_HUMAN	MIF_HUMAN
MEGF8_HUMAN	MINY1_HUMAN
METK2_HUMAN	MIPO1_HUMAN
MFAP4_HUMAN	MITD1_HUMAN
MFGM_HUMAN	MK01_HUMAN
MGA_HUMAN	MKRN2_HUMAN

USC UNIVERSIDAD DE CONCEPCIÓN

MGAL_HUMAN
MGAT1_HUMAN
MGT5A_HUMAN
MINP1_HUMAN
MITD1_HUMAN
MLEC_HUMAN
MMP7_HUMAN
MMP9_HUMAN
MMRN2_HUMAN
MOB1A_HUMAN
MOES_HUMAN
MOT12_HUMAN
MPPB_HUMAN
MPRI_HUMAN
MRO2A_HUMAN
MSLN_HUMAN
MUC1_HUMAN
MUC18_HUMAN
MUC20_HUMAN
MUC5B_HUMAN
MVP_HUMAN
MXRA5_HUMAN
MXRA8_HUMAN
MY18B_HUMAN
MYH1_HUMAN
MYH2_HUMAN
MYH4_HUMAN
MYH7_HUMAN
MYH8_HUMAN
MYH9_HUMAN
MYO1C_HUMAN
MYOC_HUMAN
MYOM2_HUMAN
MYPC2_HUMAN
NAAA_HUMAN
NADC_HUMAN
NAGAB_HUMAN
NAPSA_HUMAN
NCAM1_HUMAN
NCHL1_HUMAN
NDUS1_HUMAN
NECT2_HUMAN
NECT4_HUMAN
NEGR1_HUMAN
NEO1_HUMAN
NEP_HUMAN
NEUR1_HUMAN
NEUS_HUMAN
NGAL_HUMAN
NHLC3_HUMAN
NHRF1_HUMAN
NHRF3_HUMAN
NICA_HUMAN
NID1_HUMAN
NIT2_HUMAN
ML12A_HUMAN
MLRS_HUMAN
MOB1A_HUMAN
MOES_HUMAN
MOT5_HUMAN
MP2K1_HUMAN
MPP5_HUMAN
MPPB_HUMAN
MRCKB_HUMAN
MRP_HUMAN
MRP8_HUMAN
MSRA_HUMAN
MSTRO_HUMAN
MTPN_HUMAN
MUC1_HUMAN
MUC4_HUMAN
MVP_HUMAN
MXRA8_HUMAN
MYADM_HUMAN
MYH1_HUMAN
MYH10_HUMAN
MYH2_HUMAN
MYH4_HUMAN
MYH6_HUMAN
MYH7_HUMAN
MYH8_HUMAN
MYH9_HUMAN
MYL1_HUMAN
MYL6_HUMAN
MYO1B_HUMAN
MYO1C_HUMAN
MYO1D_HUMAN
MYO1E_HUMAN
MYO5B_HUMAN
MYO6_HUMAN
MYOF_HUMAN
MYOM1_HUMAN
MYOM2_HUMAN
MYPC1_HUMAN
MYPC2_HUMAN
NAGK_HUMAN
NAPSA_HUMAN
NBEL2_HUMAN
NCKP1_HUMAN
NDKB_HUMAN
NDRG1_HUMAN
NDUS1_HUMAN
NEBL_HUMAN
NEBU_HUMAN
NECT2_HUMAN
NED4L_HUMAN
NEP_HUMAN
NFASC_HUMAN
NHRF1_HUMAN
NHRF2_HUMAN

NOL6_HUMAN	NHRF3_HUMAN
NPC2_HUMAN	NIBA2_HUMAN
NQO2_HUMAN	NICA_HUMAN
NRP1_HUMAN	NIT2_HUMAN
NSDHL_HUMAN	NNRE_HUMAN
NSF_HUMAN	NPHN_HUMAN
NT5C_HUMAN	NPS3A_HUMAN
NUCB1_HUMAN	NPT2C_HUMAN
NUCB2_HUMAN	NRAM2_HUMAN
NUCL_HUMAN	NSDHL_HUMAN
NXF2_HUMAN	NSF_HUMAN
OAF_HUMAN	NUCL_HUMAN
OAT_HUMAN	OAT_HUMAN
ODP2_HUMAN	OBSCN_HUMAN
ODPB_HUMAN	ODO2_HUMAN
OGFD3_HUMAN	ODP2_HUMAN
OLFM4_HUMAN	ODPB_HUMAN
OMD_HUMAN	OLA1_HUMAN
OSCAR_HUMAN	OLFM4_HUMAN
OSTP_HUMAN	OSTF1_HUMAN
OTUB1_HUMAN	OTUB1_HUMAN
P210L_HUMAN	OXSR1_HUMAN
P3IP1_HUMAN	P2RX4_HUMAN
P5CR2_HUMAN	P5CR2_HUMAN
P5CS_HUMAN	P5CS_HUMAN
PA1B2_HUMAN	PA1B2_HUMAN
PADC1_HUMAN	PA1B3_HUMAN
PAG15_HUMAN	PACN2_HUMAN
PAPP2_HUMAN	PACN3_HUMAN
PARK7_HUMAN	PACS1_HUMAN
PBLD_HUMAN	PADI3_HUMAN
PCBP2_HUMAN	PAK4_HUMAN
PCD16_HUMAN	PAR6B_HUMAN
PCDGK_HUMAN	PARK7_HUMAN
PCDH1_HUMAN	PARVA_HUMAN
PCKGC_HUMAN	PBLD_HUMAN
PCP_HUMAN	PCBP1_HUMAN
PCX3_HUMAN	PCBP2_HUMAN
PCYOX_HUMAN	PCDGC_HUMAN
PD1L2_HUMAN	PCKGC_HUMAN
PDC10_HUMAN	PCX3_HUMAN
PDC6I_HUMAN	PCYOX_HUMAN
PDCD6_HUMAN	PDC10_HUMAN
PDE4D_HUMAN	PDC6I_HUMAN
PDGFD_HUMAN	PDCD6_HUMAN
PDIA1_HUMAN	PDE4D_HUMAN
PDIA2_HUMAN	PDE8A_HUMAN
PDIA3_HUMAN	PDIA1_HUMAN
PDIA4_HUMAN	PDIA3_HUMAN
PDIA6_HUMAN	PDIA4_HUMAN
PEBP1_HUMAN	PDIA6_HUMAN
PEDF_HUMAN	PDLI5_HUMAN
PEF1_HUMAN	PDXK_HUMAN
PEPA3_HUMAN	PDZ1I_HUMAN
PEPA5_HUMAN	PEBP1_HUMAN

PEPD_HUMAN	PEF1_HUMAN
PEPL_HUMAN	PEPA5_HUMAN
PF4V_HUMAN	PEPD_HUMAN
PFKAL_HUMAN	PEPL_HUMAN
PGAM1_HUMAN	PERM_HUMAN
PGAM4_HUMAN	PF4V_HUMAN
PGBM_HUMAN	PFKAL_HUMAN
PGCA_HUMAN	PFKAM_HUMAN
PGDH_HUMAN	PGAM1_HUMAN
PGFRB_HUMAN	PGAM2_HUMAN
PGK1_HUMAN	PGDH_HUMAN
PGM1_HUMAN	PGFRB_HUMAN
PGRP1_HUMAN	PGK1_HUMAN
PGRP2_HUMAN	PGM1_HUMAN
PGS1_HUMAN	PGM2_HUMAN
PGS2_HUMAN	PGRP1_HUMAN
PH4H_HUMAN	PHAR4_HUMAN
PHB_HUMAN	PHB_HUMAN
PIGR_HUMAN	PHS_HUMAN
PIP_HUMAN	PI42C_HUMAN
PKHD1_HUMAN	PI4KA_HUMAN
PLAK_HUMAN	PICAL_HUMAN
PLBL2_HUMAN	PIGR_HUMAN
PLCA_HUMAN	PIP_HUMAN
PLD3_HUMAN	PIPNA_HUMAN
PLDX1_HUMAN	PIWL3_HUMAN
PLF4_HUMAN	PKD2_HUMAN
PLMN_HUMAN	PKHA1_HUMAN
PLOD3_HUMAN	PKHB2_HUMAN
PLS1_HUMAN	PKN2_HUMAN
PLSI_HUMAN	PLA2R_HUMAN
PLST_HUMAN	PLCA_HUMAN
PMGT1_HUMAN	PLCB3_HUMAN
PNCB_HUMAN	PLCB4_HUMAN
PNPH_HUMAN	PLCD1_HUMAN
PNPO_HUMAN	PLCG2_HUMAN
PODO_HUMAN	PLD3_HUMAN
PODXL_HUMAN	PLLP_HUMAN
PON1_HUMAN	PLPP1_HUMAN
PPAL_HUMAN	PLS1_HUMAN
PPAP_HUMAN	PLS4_HUMAN
PPGB_HUMAN	PLSI_HUMAN
PPIA_HUMAN	PLST_HUMAN
PPIB_HUMAN	PLXB2_HUMAN
PPIC_HUMAN	PMVK_HUMAN
PPT2_HUMAN	PNCB_HUMAN
PRDX1_HUMAN	PNPH_HUMAN
PRDX2_HUMAN	PNPO_HUMAN
PRDX3_HUMAN	PODO_HUMAN
PRDX4_HUMAN	PODXL_HUMAN
PRDX5_HUMAN	POTEE_HUMAN
PRDX6_HUMAN	PP1B_HUMAN
PRG2_HUMAN	PP1R7_HUMAN
PROC_HUMAN	PP2AA_HUMAN
PROL4_HUMAN	PPAC_HUMAN

PROM1_HUMAN	PPAL_HUMAN
PROM2_HUMAN	PPAP_HUMAN
PROS_HUMAN	PPBI_HUMAN
PROZ_HUMAN	PPBT_HUMAN
PRSS8_HUMAN	PPCE_HUMAN
PRTN3_HUMAN	PPIA_HUMAN
PSA_HUMAN	PPIB_HUMAN
PSA1_HUMAN	PRDX1_HUMAN
PSA3_HUMAN	PRDX2_HUMAN
PSA4_HUMAN	PRDX3_HUMAN
PSA6_HUMAN	PRDX4_HUMAN
PSA7_HUMAN	PRDX5_HUMAN
PSB2_HUMAN	PRDX6_HUMAN
PSB5_HUMAN	PRG2_HUMAN
PSB8_HUMAN	PROF1_HUMAN
PSCA_HUMAN	PROF2_HUMAN
PSD1_HUMAN	PROL4_HUMAN
PTCD3_HUMAN	PROM1_HUMAN
PTER_HUMAN	PROM2_HUMAN
PTGDS_HUMAN	PRSS8_HUMAN
PTGR1_HUMAN	PRVA_HUMAN
PTN13_HUMAN	PSA_HUMAN
PTPRG_HUMAN	PSA3_HUMAN
PTPRJ_HUMAN	PSA4_HUMAN
PTPRK_HUMAN	PSA6_HUMAN
PTPRO_HUMAN	PSA7_HUMAN
PTPRS_HUMAN	PSB2_HUMAN
PTPRZ_HUMAN	PSB6_HUMAN
PVR_HUMAN	PSCA_HUMAN
PYGM_HUMAN	PSMD2_HUMAN
PZP_HUMAN	PSMD9_HUMAN
QCR1_HUMAN	PSME1_HUMAN
QOR_HUMAN	PTCD3_HUMAN
QPCT_HUMAN	PTER_HUMAN
QSOX1_HUMAN	PTGDS_HUMAN
R4RL2_HUMAN	PTGR1_HUMAN
RAB10_HUMAN	PTGR2_HUMAN
RAB14_HUMAN	PTH1R_HUMAN
RAB1A_HUMAN	PTN11_HUMAN
RAB1B_HUMAN	PTN13_HUMAN
RAB21_HUMAN	PTN23_HUMAN
RAB25_HUMAN	PTN6_HUMAN
RAB4A_HUMAN	PTPA_HUMAN
RAB4B_HUMAN	PTPRB_HUMAN
RAB5A_HUMAN	PTPRJ_HUMAN
RAB5B_HUMAN	PTPRO_HUMAN
RAB5C_HUMAN	PTTG_HUMAN
RAB7A_HUMAN	PUR9_HUMAN
RAB8A_HUMAN	PXL2B_HUMAN
RAC1_HUMAN	PYGB_HUMAN
RADI_HUMAN	PYGM_HUMAN
RAI3_HUMAN	PZP_HUMAN
RALA_HUMAN	QCR1_HUMAN
RALB_HUMAN	QOR_HUMAN
RAN_HUMAN	RAB10_HUMAN

RAP1A_HUMAN
RAP1B_HUMAN
RAP2B_HUMAN
RASH_HUMAN
RASK_HUMAN
RB11B_HUMAN
RBM22_HUMAN
RENBP_HUMAN
RENR_HUMAN
RET4_HUMAN
RHCG_HUMAN
RHOA_HUMAN
RHOV_HUMAN
RINI_HUMAN
RISC_HUMAN
RL17_HUMAN
RL40_HUMAN
RLA0_HUMAN
RLA2_HUMAN
RNAS1_HUMAN
RNAS2_HUMAN
RNT2_HUMAN
ROBO4_HUMAN
ROR1_HUMAN
RPN1_HUMAN
RRAS_HUMAN
RRAS2_HUMAN
RS16_HUMAN
RSSA_HUMAN
S10A6_HUMAN
S10A8_HUMAN
S10A9_HUMAN
S12A1_HUMAN
S12A3_HUMAN
S13A2_HUMAN
S17A5_HUMAN
S22A2_HUMAN
S22A6_HUMAN
S22A8_HUMAN
S22AC_HUMAN
S23A1_HUMAN
S26A4_HUMAN
S36A2_HUMAN
S4A4_HUMAN
S4A8_HUMAN
S6A19_HUMAN
SAA1_HUMAN
SAA2_HUMAN
SAA4_HUMAN
SAHH_HUMAN
SAMP_HUMAN
SAP_HUMAN
SAP3_HUMAN
SBP1_HUMAN
SC5A2_HUMAN
RAB12_HUMAN
RAB13_HUMAN
RAB14_HUMAN
RAB17_HUMAN
RAB18_HUMAN
RAB19_HUMAN
RAB1A_HUMAN
RAB1B_HUMAN
RAB21_HUMAN
RAB23_HUMAN
RAB25_HUMAN
RAB2A_HUMAN
RAB2B_HUMAN
RAB35_HUMAN
RAB3A_HUMAN
RAB3C_HUMAN
RAB4B_HUMAN
RAB5A_HUMAN
RAB5B_HUMAN
RAB5C_HUMAN
RAB6A_HUMAN
RAB6B_HUMAN
RAB7A_HUMAN
RAB7L_HUMAN
RAB8A_HUMAN
RAB8B_HUMAN
RABP2_HUMAN
RAC1_HUMAN
RADI_HUMAN
RAGP1_HUMAN
RAI3_HUMAN
RALA_HUMAN
RALB_HUMAN
RAN_HUMAN
RAP1A_HUMAN
RAP1B_HUMAN
RAP2B_HUMAN
RASH_HUMAN
RASK_HUMAN
RASL1_HUMAN
RASM_HUMAN
RASN_HUMAN
RB11B_HUMAN
RB22A_HUMAN
RB27A_HUMAN
RB27B_HUMAN
RD23B_HUMAN
RET4_HUMAN
RFIP1_HUMAN
RHBT3_HUMAN
RHCG_HUMAN
RHG01_HUMAN
RHG05_HUMAN
RHG12_HUMAN
RHG18_HUMAN

SC5AA_HUMAN
SC5AC_HUMAN
SCP2_HUMAN
SCRB2_HUMAN
SCTM1_HUMAN
SDC1_HUMAN
SDC2_HUMAN
SDC4_HUMAN
SDCB1_HUMAN
SDF2L_HUMAN
SEM5A_HUMAN
SEM6D_HUMAN
SEPP1_HUMAN
SERA_HUMAN
SFRP1_HUMAN
SG1D1_HUMAN
SG2A1_HUMAN
SHAN1_HUMAN
SHBG_HUMAN
SHC1_HUMAN
SHRM3_HUMAN
SIA10_HUMAN
SIA4C_HUMAN
SIAE_HUMAN
SIM24_HUMAN
SIRBL_HUMAN
SLAF5_HUMAN
SLC31_HUMAN
SLIK1_HUMAN
SLK_HUMAN
SMO_HUMAN
SND1_HUMAN
SNP23_HUMAN
SODE_HUMAN
SORCN_HUMAN
SORL_HUMAN
SORT_HUMAN
SOST_HUMAN
SPB12_HUMAN
SPB13_HUMAN
SPB3_HUMAN
SPB4_HUMAN
SPB5_HUMAN
SPHM_HUMAN
SPIT1_HUMAN
SPRL1_HUMAN
SPRR3_HUMAN
SPRY4_HUMAN
SSBP_HUMAN
ST134_HUMAN
STC1_HUMAN
STK24_HUMAN
STK26_HUMAN
STML3_HUMAN
STOM_HUMAN
RHOA_HUMAN
RHOC_HUMAN
RHOF_HUMAN
RHOG_HUMAN
RHOV_HUMAN
RHPN2_HUMAN
RIDA_HUMAN
RINI_HUMAN
RIPR1_HUMAN
RL17_HUMAN
RL40_HUMAN
RLA0_HUMAN
RNAS2_HUMAN
RNB_HHV1M
RP1_HUMAN
RPGF3_HUMAN
RPN1_HUMAN
RRAS_HUMAN
RRAS2_HUMAN
RSU1_HUMAN
RT18C_HUMAN
S100P_HUMAN
S10A6_HUMAN
S10A7_HUMAN
S10A8_HUMAN
S10A9_HUMAN
S10AB_HUMAN
S10AE_HUMAN
S10AG_HUMAN
S12A1_HUMAN
S12A3_HUMAN
S13A2_HUMAN
S15A2_HUMAN
S17A5_HUMAN
S22A2_HUMAN
S22A6_HUMAN
S22A8_HUMAN
S22AC_HUMAN
S23A1_HUMAN
S26A4_HUMAN
S36A2_HUMAN
S4A4_HUMAN
S6A19_HUMAN
SAA1_HUMAN
SAA2_HUMAN
SAA4_HUMAN
SAHH_HUMAN
SAHH2_HUMAN
SAHH3_HUMAN
SAM50_HUMAN
SAMP_HUMAN
SARG_HUMAN
SBDS_HUMAN
SBP1_HUMAN
SC5A1_HUMAN

SUSD2_HUMAN	SC5A2_HUMAN
SVEP1_HUMAN	SC5A9_HUMAN
SYIM_HUMAN	SC5AA_HUMAN
SYPL1_HUMAN	SC5AC_HUMAN
TARSH_HUMAN	SCAM2_HUMAN
TBA1B_HUMAN	SCP2_HUMAN
TBA1C_HUMAN	SCRB2_HUMAN
TBA4A_HUMAN	SCRN1_HUMAN
TBB2B_HUMAN	SCTM1_HUMAN
TBB4B_HUMAN	SDC1_HUMAN
TBB5_HUMAN	SDCB1_HUMAN
TBB6_HUMAN	SDCB2_HUMAN
TBCD1_HUMAN	SDF2L_HUMAN
TCPB_HUMAN	SEM5A_HUMAN
TCPD_HUMAN	SEP11_HUMAN
TCPG_HUMAN	SEPT2_HUMAN
TCPZ_HUMAN	SEPT6_HUMAN
TENA_HUMAN	SERA_HUMAN
TENX_HUMAN	SERC5_HUMAN
TERA_HUMAN	SG1D1_HUMAN
TETN_HUMAN	SG2A1_HUMAN
TGBR3_HUMAN	SH24A_HUMAN
THBG_HUMAN	SH3B4_HUMAN
THRB_HUMAN	SH3G1_HUMAN
THTM_HUMAN	SH3G2_HUMAN
THY1_HUMAN	SHAN2_HUMAN
TICN1_HUMAN	SHLB2_HUMAN
TICN2_HUMAN	SHPS1_HUMAN
TIG1_HUMAN	SHRM3_HUMAN
TIP_HUMAN	SIM22_HUMAN
TITIN_HUMAN	SIM24_HUMAN
TKFC_HUMAN	SLC31_HUMAN
TKT_HUMAN	SLF1_HUMAN
TLN1_HUMAN	SLK_HUMAN
TLR10_HUMAN	SMAD2_HUMAN
TM11D_HUMAN	SMAD5_HUMAN
TMPS2_HUMAN	SMIM5_HUMAN
TNG6_HUMAN	SMO_HUMAN
TNIK_HUMAN	SMUF1_HUMAN
TOLIP_HUMAN	SNAA_HUMAN
TPIS_HUMAN	SNAG_HUMAN
TPM1_HUMAN	SND1_HUMAN
TPM2_HUMAN	SNF8_HUMAN
TPM3_HUMAN	SNP23_HUMAN
TPM4_HUMAN	SNX18_HUMAN
TPMT_HUMAN	SNX2_HUMAN
TPP1_PANTR	SNX6_HUMAN
TRAP1_HUMAN	SNX9_HUMAN
TRBM_HUMAN	SO4C1_HUMAN
TREA_HUMAN	SODC_HUMAN
TRFE_HUMAN	SODM_HUMAN
TRFL_HUMAN	SORCN_HUMAN
TRFM_HUMAN	SPAST_HUMAN
TRHDE_HUMAN	SPB3_HUMAN
TRIPB_HUMAN	SPB4_HUMAN

TRY1_HUMAN	SPB6_HUMAN
TRY2_HUMAN	SPP2A_HUMAN
TRY3_HUMAN	SPP2B_HUMAN
TS101_HUMAN	SPRE_HUMAN
TSN1_HUMAN	SPRR3_HUMAN
TSN3_HUMAN	SPRY4_HUMAN
TSN8_HUMAN	SRC_HUMAN
TSP1_HUMAN	SRC8_HUMAN
TTC38_HUMAN	SRSF8_HUMAN
TTHY_HUMAN	SSBP_HUMAN
TTL11_HUMAN	SSH3_HUMAN
TTYH3_HUMAN	ST134_HUMAN
TWF1_HUMAN	ST1A1_HUMAN
TXND5_HUMAN	STABP_HUMAN
TYPH_HUMAN	STK10_HUMAN
UBA1_HUMAN	STK11_HUMAN
UCHL1_HUMAN	STK24_HUMAN
UEVLD_HUMAN	STK25_HUMAN
UFO_HUMAN	STK26_HUMAN
UGDH_HUMAN	STOM_HUMAN
UGPA_HUMAN	STRAB_HUMAN
ULK3_HUMAN	STX3_HUMAN
UPK1A_HUMAN	STX7_HUMAN
UPK1B_HUMAN	STXB2_HUMAN
UPK3A_HUMAN	STXB3_HUMAN
UROK_HUMAN	STXB4_HUMAN
UROM_HUMAN	SUMO4_HUMAN
US02_HCMVT	SUSD2_HUMAN
VAS1_HUMAN	SYIM_HUMAN
VASN_HUMAN	SYNC_HUMAN
VAT1_HUMAN	SYPL1_HUMAN
VATA_HUMAN	SYSC_HUMAN
VATB1_HUMAN	SYTC_HUMAN
VATC1_HUMAN	SYTL2_HUMAN
VATC2_HUMAN	SYUG_HUMAN
VATE1_HUMAN	TAGL2_HUMAN
VATH_HUMAN	TAOK1_HUMAN
VDAC1_HUMAN	TAOK2_HUMAN
VDAC3_HUMAN	TAOK3_HUMAN
VMO1_HUMAN	TB10A_HUMAN
VNN1_HUMAN	TBA1B_HUMAN
VP13D_HUMAN	TBA1C_HUMAN
VP37C_HUMAN	TBA4A_HUMAN
VP37D_HUMAN	TBB2B_HUMAN
VPP4_HUMAN	TBB4B_HUMAN
VPS28_HUMAN	TBB5_HUMAN
VPS4A_HUMAN	TBC24_HUMAN
VPS4B_HUMAN	TBCA_HUMAN
VSIG4_HUMAN	TCAF1_HUMAN
VSIG8_HUMAN	TCPA_HUMAN
VTA1_HUMAN	TCPB_HUMAN
VTDB_HUMAN	TCPD_HUMAN
VTNC_HUMAN	TCPG_HUMAN
WDFY4_HUMAN	TCPH_HUMAN
WDR1_HUMAN	TCPQ_HUMAN

USC UNIVERSIDAD DE SANTIAGO DE COMPOSTELA

WDR87_HUMAN	TCPZ_HUMAN
WFDC2_HUMAN	TCTP_HUMAN
X3CL1_HUMAN	TENA_HUMAN
XPP2_HUMAN	TERA_HUMAN
XYLT2_HUMAN	TFG_HUMAN
YTDC2_HUMAN	TGBR3_HUMAN
ZA2G_HUMAN	TGM4_HUMAN
ZG16B_HUMAN	TGRM1_HUMAN

USC
UNIVERSIDADE
DE SANTIAGO
DE COMPOSTELA

ANNEXES

USC
UNIVERSIDADE
DE SANTIAGO
DE COMPOSTELA

USC
UNIVERSIDADE
DE SANTIAGO
DE COMPOSTELA

ANNEX 1: AUTHORISATION OF THE BIOETHICS COMMITTEE FOR HUMAN AND EXPERIMENTAL ANIMAL STUDIES

1.1 BIOETHICS COMMITTEE AUTHORIZATION FOR HUMAN STUDIES

Secretaría Técnica
Comité Autonómico de Ética da Investigación de Galicia
Secretaría Xeral. Consellería de Sanidade
Edificio Administrativo San Lázaro
15703 SANTIAGO DE COMPOSTELA
Tel: 881546425. Correo-e: ceic@sergas.es

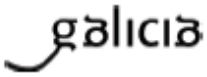

DICTAMEN DEL COMITÉ DE ÉTICA DE LA INVESTIGACIÓN DE SANTIAGO-LUGO

Cristina Márquez Riveras, Secretaria del Comité de Ética de la Investigación de Santiago-Lugo,

CERTIFICA:

Que este Comité evaluó en su reunión del día 22/01/19 el estudio:

Título: Acción estratégica en Galicia_2.0 para la Enfermedad Renal Hereditaria: Diagnóstico Genético y establecimiento de un registro gallego de pacientes, una medida de prevención coste/eficiente
Versión:
Promotor/a:Miguel Ángel García González
Investigador/a: Miguel Ángel García González; Jesús Calviño
Código de Registro:2018/611

Y que este Comité, tomando en consideración la pertinencia del estudio, el conocimiento disponible, los requisitos legales aplicables y los Procedimientos Normalizados de Trabajo del Comité, emite un dictamen **FAVORABLE** para la realización del citado estudio.

USC UNIVERSIDADE DE SANTIAGO DE COMPOSTELA

Documento firmado digitalmente por:
Márquez Riveras, Cristina: 31/01/2019 10:39
SAOC-Z4G4-BOAH-OFHK-6M15-4892-7577-549

XUNTA DE GALICIA
CONSELLERÍA DE SANIDADE
Secretaría Xeral Técnica

galicia

Y HACE CONSTAR QUE:

1.- El Comité Territorial de Ética de la Investigación de Santiago-Lugo cumple tanto en su composición como en sus PNTs los requisitos legales vigentes.

2.- La composición actual del Comité Territorial de Ética de la Investigación de Santiago-Lugo es:

- **Juan Manuel Vázquez Lago (Presidente).** Médico especialista en Medicina Preventiva y Salud Pública. Área de Gestión Integrada de Santiago.
- **Pilar Rodríguez Ledo (Vicepresidenta).** Médico especialista en Medicina Familiar y Comunitaria. Área de Gestión Integrada de Lugo.
- **Cristina Márquez Riveras (Secretaria).** Enfermera. Dirección Xeral de Saúde Pública.
- **Lorenzo Armenteros del Olmo (Secretario Suplente).** Médico especialista en Medicina Familiar y Comunitaria. Área de Gestión Integrada de Lugo.
- **Francisco Campos Pérez.** Biólogo. Fundación Instituto de Investigación Sanitaria de Santiago de Compostela.
- **Rosana Castelo Domínguez.** Farmacéutica de Atención Primaria. Área de Gestión Integrada de Santiago.
- **Ricardo García Martínez.** Licenciado en Derecho. Área de Gestión Integrada de Lugo.
- **Jaime Gulín Dávila.** Farmacéutico especialista en Farmacia Hospitalaria. Área de Gestión Integrada de Lugo.
- **María Jesús Lamas Díaz.** Farmacéutica especialista en Farmacia Hospitalaria. Área de Gestión Integrada de Santiago.
- **Guillermo José Prada Ramallal** Médico especialista en Farmacología Clínica. Área de Gestión Integrada de Santiago. Fundación Instituto de Investigación Sanitaria de Santiago de Compostela.
- **Carlos Rodríguez Moreno.** Médico especialista en Farmacología Clínica. Área de Gestión Integrada de Santiago.
- **Sandra Vidal Martínez.** Enfermera. Área de Gestión Integrada de Santiago
- **Rafael Carlos Vidal Pérez.** Médico especialista en Cardiología. Área de Gestión Integrada de Lugo.

Para que conste donde proceda, y a petición de quien proceda, en Santiago de Compostela,

La Secretaria del Comité Territorial de Ética de la Investigación de Santiago Lugo,

Cristina Márquez Riveras

Documento firmado digitalmente por:
Márquez Riveras, Cristina: 31/01/2019 10:39
SAOC-Z4G4-BOAH-OFHK-6M15-4892-7577-549

USC UNIVERSIDADE DE SANTIAGO DE COMPOSTELA

1.2 BIOETHICS COMMITTEE AUTHORIZATION FOR STUDIES ON EXPERIMENTAL ANIMALS

XUNTA DE GALICIA
CONSELLERÍA DO MEDIO RURAL

Xefatura Territorial
8ª de Gandaría
Edificio administrativo Monelos, 4º andar
Rúa Vicente Ferrer, Nº 2
15008 A Coruña
Tfno.: 981 184 565, fax.: 981 184 653
Correo electrónico: servizo.gandaria.a.coruna@xunta.gal

galicia

RESOLUCIÓN DE AUTORIZACIÓN DE PROXECTO DE EXPERIMENTACIÓN ANIMAL

Expediente núm.: 15010/2020/002
Data de Inicio: 5.2.2020
Persoa Interesada: Miguel Ángel García González
Procedemento: resolución de autorización
Forma de Inicio: solicitude da persoa interesada

ANTECEDENTES

A persoa interesada presentou con data 4.2.2020 unha solicitude para a realización do proxecto de experimentación animal (entrada no Rexistro Electrónico da Xunta de Galicia 2019/239412), cuxos datos se detallan a continuación:

Denominación do proxecto: *Modelos experimentais para o estudo da enfermidade poliquística renal (PKD)*
Nome do centro usuario: Animalario do CIMUS
Persoa responsable do proxecto: Miguel Ángel García González
Establecemento onde se realizarán os procedementos do proxecto (ou lugar xeográfico no caso de traballos de campo): Centro de Investigación en Medicina Molecular e Enfermidades Crónicas e a Universidade de Santiago de Compostela

Clasificación do proxecto : Tipo I ☐ Tipo II ☒ Tipo III ☐

CONSIDERACIÓNS LEGAIS E TÉCNICAS

1 O Real decreto 53/2013, de 1 de febreiro (BOE 34, do 8 de febreiro), polo que se establecen as normas básicas aplicables para a protección dos animais utilizados en experimentación e outros fins científicos, incluíndo a docencias, establece no seu artigo 33 as condicións de autorizacións dos proxectos con animais de experimentación.

2 O artigo 88 da Lei 39/2015, de 1 de outubro, do procedemento administrativo común das administracións públicas (BOE 236, do 2 de outubro de 2015) establece que a resolución que poña fin o procedemento decidirá todas as cuestións expostas polos interesados e aquelas outras derivadas deste.

CVE: 0JIEDoi2g
Verificación: https://sede.xunta.gal/csv

Xacobeo 2021

USC UNIVERSIDADE DE SANTIAGO DE COMPOSTELA

XUNTA DE GALICIA
CONSELLERÍA DO MEDIO RURAL

Xefatura Territorial
8ª de Gandaría
Edificio administrativo Monelos, 4º andar
Rúa Vicente Ferrer, Nº 2
15008 A Coruña
Tfno.: 981 184 565, fax.: 981 184 653
Correo electrónico: servizo.gandaria.a.coruna@xunta.gal

galicia

3 O Servizo de Gandaría da Coruña revisou a documentación achegada na solicitude e o resultado favorable da avaliación do proxecto realizada polo órgano habilitado, a Sección de Experimentación Animal do Comité de Bioética da Universidade de Santiago de Compostela.

Esta xefatura territorial é competente para ditar unha resolución, de conformidade co Decreto 149/2018, do 5 de decembro, polo que se establece a estrutura orgánica da Consellería do Medio Rural e se modifica parcialmente o Decreto 177/2016, do 15 de decembro, polo que se fixa a estrutura orgánica da Vicepresidencia e das consellerías da Xunta de Galicia (DOG 235, do 11 de novembro).

De acordo con todo o indicado, RESOLVO:

1 Autorizar o proxecto solicitado.

2 O proxecto non precisa someterse a unha avaliación retrospectiva.

3 A autorización deste proxecto terá unha duración de cinco anos e unha vez transcorrido este tempo deberá ser renovada.

A citada autorización é unicamente válida nas condicións que figuran no expediente. Ante calquera cambio significativo no proxecto que poida ter efectos negativos sobre o benestar dos animais, deberá solicitar a confirmación da autorización ao Servizo Provincial de Gandaría.

Esta autorización poderá ser suspendida no caso de que o proxecto non se leve a cabo de acordo coas condicións de autorización e retirala, previo expediente tramitado ao que se lle dará audiencia.

Contra a presente resolución, que non pon fin á vía administrativa, poderá interpoñer un recurso de alzada ante o conselleiro de Medio Rural. O prazo comezará a contar dende o día seguinte ao da recepción desta resolución. Todo isto, segundo o disposto nos artigos 121 e 122 da citada Lei 39/2015.

Mediante este escrito notificaselle a Miguel Ángel García González esta resolución segundo o esixido no artigo 40.1 da antedita Lei 39/2015.

Asinado por LOPEZ LOPEZ, MONICA
Cargo/s: Xefa Territorial
Data e hora: 07/10/2020 13:29:27

CVE: RJEDoc319
Verificación: https://sede.xunta.gal/cve

Xacobeo 2021

USC UNIVERSIDADE DE SANTIAGO DE COMPOSTELA

USC
UNIVERSIDADE
DE SANTIAGO
DE COMPOSTELA

USC
UNIVERSIDADE
DE SANTIAGO
DE COMPOSTELA

Polycystic kidney disease (PKD) is a group of monogenic disorders resulting in renal cyst development, which cause chronic renal disease (CKD), and other organs, as liver, may be affected. Although several molecular pathways were discovered, the key mechanism remains unclear with no efficient therapy. PKD monitoring progression is based on the measurement of low specificity and sensitivity parameters which are unable to predict disease evolution.
Hence, the main objectives of this work are studying cystogenesis-related signaling pathways for new therapeutic strategies and the development of a new diagnostic tool that allow to anticipate disease progression by characterizing the glycoprotein and vesicular fraction. In conclusion, the present thesis expands the knowledge about pathophysiology and biomarkers in PKD.